UNITED STATES

DEPARTMENT OF THE INTERIOR

GEOLOGICAL SURVEY

Office of Earthquake Studies

PROCEEDINGS OF

CONFERENCE VII

STRESS AND STRAIN MEASUREMENTS

RELATED TO EARTHQUAKE PREDICTION

Convened Under Auspices of

NATIONAL EARTHQUAKE HAZARDS REDUCTION PROGRAM

7-9 September, 1978

OPEN-FILE REPORT 79-370

Menlo Park, California

1978

CONFERENCES TO DATE

Conference I	Abnormal Animal Behavior Prior to Earthquakes, I
Conference II	Experimental Studies of Rock Friction with Application to Earthquake Prediction
Conference III	Fault Mechanics and Its Relation to Earthquake Prediction
Conference IV	Use of Volunteers in the Earthquake Hazards Reduction Program
Conference V	Connumicating Earthquake Hazard Reduction Information
Conference VI	Methodology for Identifying Seismic Gaps and Soon-To Break Gaps
Conference VII	Stress and Strain Measurements Related to Earthquake Prediction

UNITED STATES

DEPARTMENT OF THE INTERIOR

GEOLOGICAL SURVEY

Office of Earthquake Studies

PROCEEDINGS OF

CONFERENCE VII

STRESS AND STRAIN MEASUREMENTS

RELATED TO EARTHQUAKE PREDICTON

Convened Under Auspices of

NATIONAL EARTHQUAKE HAZARDS REDUCTION PROGRAM

7 - 9 September 1978

Co-Organizers

Bruce R. Clark
Leighton and Associates Inc.
Irvine, California 92714

J.H. Pfluke
United States Geological Survey
Office of Earthquake Studies
Menlo Park, California 94025

Convener

Jack F. Evernden
United States Geological Survey
Office of Earthquake Studies
Menlo Park, California 94025

OPEN-FILE REPORT 79-370

This report is preliminary and has not been edited or reviewed for conformity with Geological Survey standards and nomenclature

Menlo Park, California

1978

CONTENTS

INTRODUCTION

The seventh conference in the continuing series under the Earthquake Hazards Reduction Program was held in Carmel, California on September 7 - 9, 1978. The theme of the conference was "Stress and Strain Measurements Related to Earthquake Prediction". In the planning of this meeting, it was the intention of the program coordinators to create a forum whereby the experts in the endeavor of collecting and interpreting slow rate of geologic stress-strain data could communicate and could provide their accumulated data to all of us. Therefore, the intent was to put forward as much data as possible, to discuss noise levels, origin of the noise, modes of eliminating noise, expected signal amplitudes, and to discuss the credibility of reported earthquake precursory "signals". In the session planning, four topics of discussion were outlined. They were:

1) Observations from tiltmeter networks

2) Methods of Stress determination

3) Long baseline surveying techniques (geodesy, gravity, etc.)

4) Electromagnetic methods of stress-strain determination

It is the nature of an exploratory conference such as this that the emphasis of the discussion deviates substantially from that which was planned. This conference was no exception. The actual topics of discussion can be categorized as follows:

1) Measurements with Kinemetrics bubble-level tiltmeter. Discussion on the problems of instrument installation by far outweighed discussions on tectonic interpretation of the data, there being very few signals and very much noise to discuss.

2) Stress-strain measurement by means other than tilt or electromagnetic techniques.

3) Instrument construction and new instrument design. The fact that this topic captured a substantial proportion of the discussion emphasizes that there is an underlying dissatisfaction with many of our current techniques for measuring tectonic stress-strain.

4) Long baseline techniques. Discussions of topics 3) and 4) proceeded more or less as planned. Topics in 4) included:

   a) geodetic strain determination by leveling; and

   b) astronomical techniques, all components of strain, and gravity measurements as a means of determining uplift.

5) Electromagnetic techniques for hopefully detecting changes in sensitivity associated with tectonic stress-strain. These discussions also proceeded as planned.

The collection of papers herewith presented are those that were given at the conference with two exceptions. The paper by Logan is included as it is pertinent to a critical point that arose in discussions (see Summary). A good deal of discussion of this matter followed the papers on hydrofracing and overcoring. A paper by Tanake is included because in reports current Chinese ideas on stress-strain phenomena prior to earthquakes. The paper was distributed to all participants prior to the meeting with the intent of soliciting critical comments. The basic conclusion is that we do not know how to accomodate some of their reputed signals into a physical model. The critical question and one not addressed by Tanake is the false alarm rate in limited data. The papers are presented in alphabetical order by author, as is our usual procedure.

At this conference there was not time for the usual prepared oral summary by the conferees that had taken place as a conclusion to the previous meetings. Therefore, J.F. Evernden wrote a summary designed to bring some of the controversies present in discussion at the meeting into clear focus for the readers of this volume. That summary was distributed to all participants. Their comments, either on the meeting or on Evernden's summary, follow this summary at the end of the volume.

Some Remarks on the Base Length of Tilt and Strain Measurements

Jon Berger and Frank Wyatt

Institute of Geophysics and Planetary Physics
Scripps Institution of Oceanography
University of California, San Diego
La Jolla, California 92093

Introduction

Mathematically, the deformation of the crustal rocks may be characterized in terms of the spatial derivatives of displacements. There are nine such independent derivatives in general.

Whether we use data from a geodetic network, strainmeter or tiltmeter, we are only making approximations to these quantities. (We will exclude gravimeters in this discussion as they measure changes in the force of gravity and it is an interpretation of this data to recover the crustal deformation quantities.) We note that the units of our observations are all dimensionless quantities and further assert that in most reasonable models of crustal deformations, including earthquake dislocations, these quantities are all on the same order of magnitude.

Typically, the available data sets consist of various combinations of these quantities as a function of time at a particular place. The task is to try to make geophysical sense out of such data--a task at which the geophysical community has not been eminently successful.

As with any measurement of a physical quantity, the scientist must answer two questions about the data before he can proceed with the interpretation:

1. What is the accuracy of the measurements?
2. What are the noise levels?

The first question is usually straightforward to answer, based on instrumental considerations, but often accuracy (or resolution) is taken to imply noise levels which, in fact, are totally independent. Noise is a term used to encompass many things from the random electronic fluctuations

in amplifiers, to the effects of cultural inputs. An operational definition might simply be: Noise consists of those signals in which we are not interested and which mask those in which we are interested. We are interested in signals of tectonic and seismic origin. We are usually not interested in signals of meteorological origin.

The deformations we wish to study are four-dimensional quantities varying in space and time but we can limit ourselves to portions of 4-D spectrum in which we are interested. Generally, the study of non-elastically propagating deformations are confined to periods of minutes and longer and spatial dimensions of say 60 m and longer. Thus our area of interest in the ω , k space may be represented in graphic fashion in Figure 1.

Clearly, the first task to perform is to fill in the labeled area in Figure 1 with the "normal background" spectrum, the noise background, out of which our signals must project to be observable. Unfortunately, this has not been done yet so we are still left to speculate on what is "normal" and what is "abnormal" or what constitutes an anomaly.

We have some rough idea of the size of some of the constituents of this spectral picture. Table 1 suggests some estimates. In this table seasonal, thermal and topographic deformations, although confined to the near surface (<1 km depth) are clearly a source of noise in tectonic studies.

Our studies at Piñon Flat Observatory (PFO) over the past few years have provided some insight into the questions of near surface deformations on a scale of approximately 10 km and less. The strainmeters measure deformations on a base of 732 m, a borehole tiltmeter array measures deformations on the base length of 1 m, or less, and the results of the USGS Geodimeter arrays in this area provide us with a picture of the larger scale deformations.

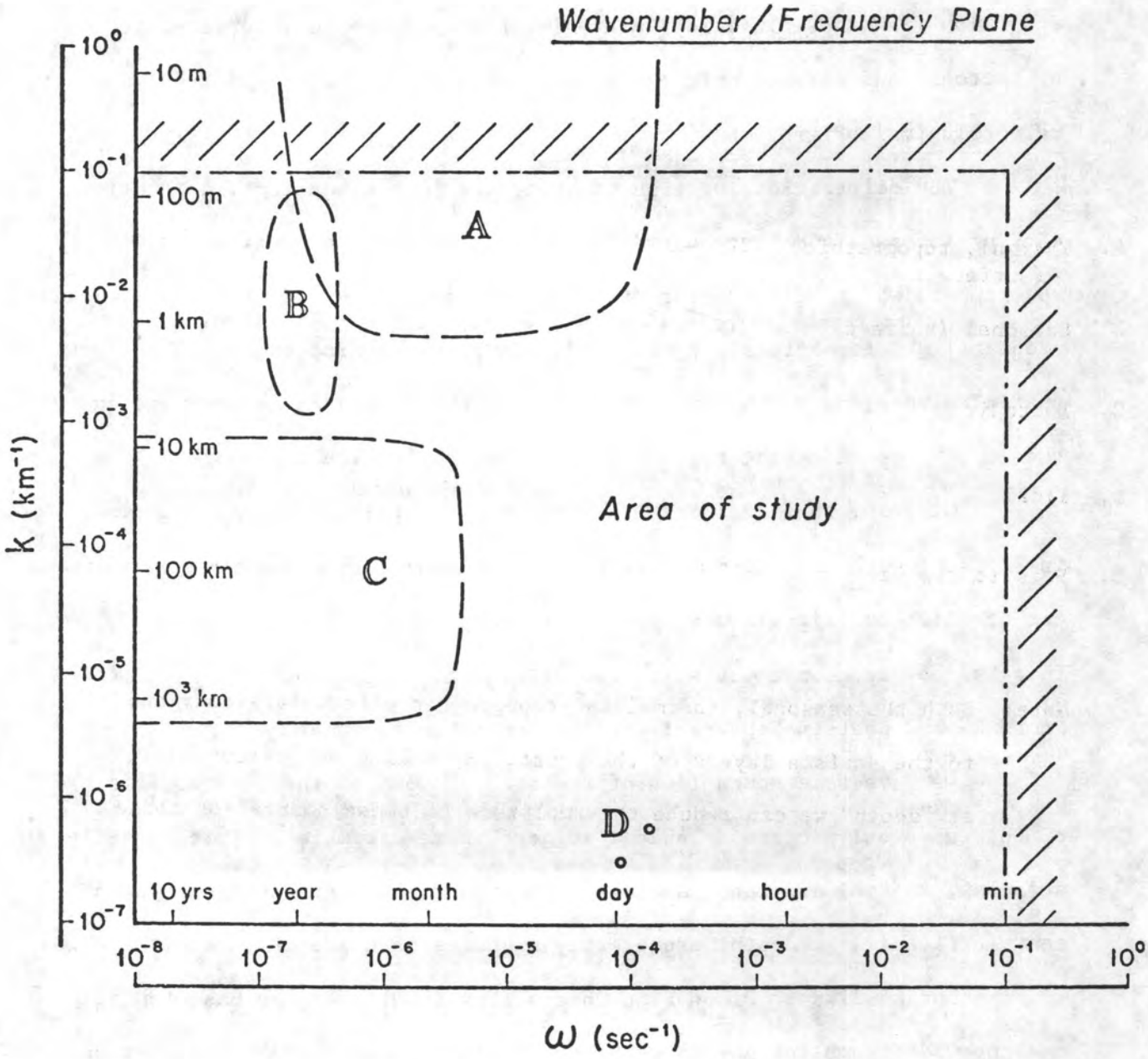
Wavenumber / Frequency Plane
10 m
100 m
1 km
10 km
100 km
10³ km
A
B
C
D
Area of study
k (km⁻¹)
10 yrs
year
month
day
hour
min
ω (sec⁻¹)

Figure 1.

TABLE 1

Some Crustal Deformation Signals

	Source	Amplitude $\frac{\Delta \ell}{\ell}$, Rad	Wavelength	Period
A.	Thermal, topographic (surface)	10^{-7}-10^{-5}	1 cm-1 km	Day - Year
B.	Seasonal (surface)	10^{-6}	1 km	Year
C.	Tectonic	10^{-8}-10^{-7}	10-10^{3} km	Month - Year
D.	Tidal	10^{-8}	Whole earth	Daily
E.	Seismic dislocation	10^{-8}	1-10 km	Discontinuous

Note: Both the seasonal, thermal and topographic effects are confined to the surface layers of the crust. By making our measurements at "depth" we can reduce the amplitude of these sources of noise.

The Horse Canyon Earthquake Story

A good example of the utility of establishing "normal background" deformations before suggesting the existence of a true anomaly was the observations made near the epicenter of the Horse Canyon earthquake.

On 2 August 1975 a magnitude 4.8 earthquake occurred at the upper end of Horse Canyon (33° 31.44'N, 116° 33.48'W) along the main branch of the San Jacinto Fault. This was north of the break of the 1969 Clark Lake earthquake ($m_L \geq 6.3$) which marks the southern end of the seismicity gap noted by Thatcher and Hanks (1973). The epicentral distance to PFO was 13 km and the depth was estimated at 12 km. Excellent records were obtained from the CIT strong motion network (one of the stations is at PFO) and an analysis of their spectra by Hartzell and Brune (1978) gave a moment of 6.0-8.0 x 10^{22} dyne-cm, a high stress drop of 225 bars and a small source dimension of 0.5 km. Analysis of the surface waves recorded at WWSSN stations gives a moment of 3.0-4.0 x 10^{23} dyne-cm, five times larger than the moment estimated from the strong motion records (which are predominantly one second or shorter period energy). The distribution of aftershocks for the Anza earthquake is estimated to cover a 2 km by 2 km square area (Kanamori, 1977). This is a significantly larger area than the fault area estimated by the above dislocation model.

It is possible to explain these discrepancies in moment and fault area in terms of a two stage rupture process. An initial dislocation of 27 cm may have occurred over a small area of about 0.8 sq. km, probably associated with an asperity on the fault, and with a high stress drop of approximately 225 bars. Following this initial break, motion may have continued over a much larger and expanding fault plane. This process is

consistent with the larger distribution of aftershocks and the larger moment estimated from 20 to 30 sec surface waves. The average stress drop over the larger 4 km^2 area would be about 90 bars. In any event, this was the closest $m_L \geq 4$ earthquake recorded at PFO during its operation and hence we had considerable interest in examining our records closely to see if we could detect any precursive activity or any evidence of post-seismic slip. Further, the USGS had tiltmeters operating at Table Mountain, virtually at the epicenter and in the town of Anza. A report of a tilt precursor by Myren and Johnson (1975) further stimulated our interest.

Figure 2 top panel shows the Table Mountain and Anza tilts with their hypocentral distances on the right. On the same scale, the bottom panel shows the PFO strains for the same period. There is no signal evident on either the Anza tiltmeters or the PFO strainmeters that could be termed a precursor to the earthquake. Indeed the only instrument that produces anomalous records is the Table Mountain tiltmeter.

Figure 3 shows the Anza tilts and the PFO strains blown up by a factor of 10. The nearly vertical lines in the top panel are the Table Mountain records. Note also the difference in noise levels on the tiltmeters and the strainmeters. To get a better idea of the noise on the strain records Figure 4 expands the amplitude scale of the strain by 10 again to clearly show the earth tides. Even at tidal amplitudes (2×10^{-8}) we see no evidence of a precursor. Figure 5 shows a section of a typical record expanded in both scales to give an indication of short period noise. Thus, if one scrutinizes the strain records in detail there are no evident fluctuations in the general trend of the records not associated with a heavy local rainfall.

Figure 6 shows the gravity and tilt data for four months before the event to two months after. The top panel is produced by removing the

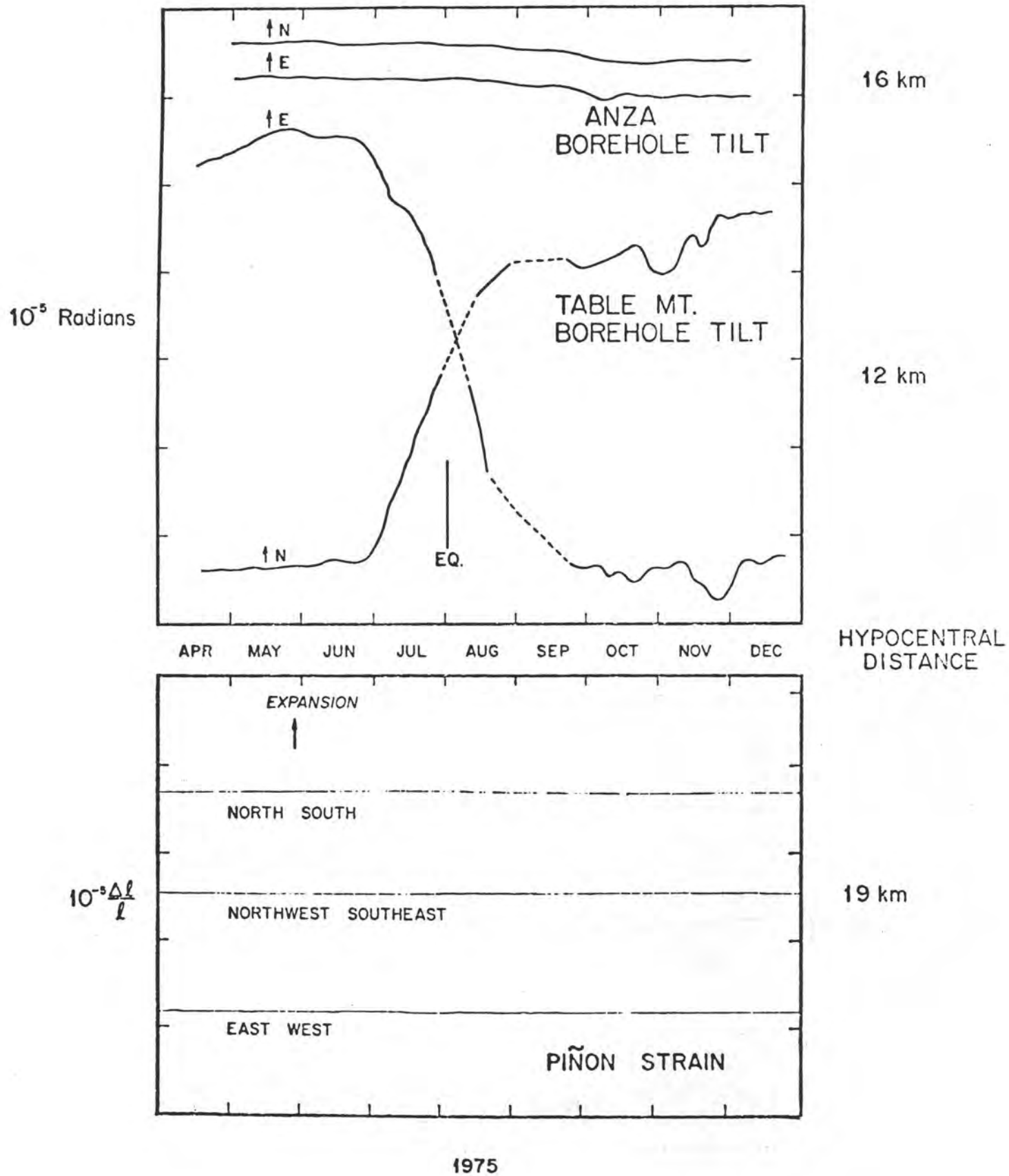
N
E
16 km
E
ANZA
BOREHOLE TILT
10^{-5} Radians
TABLE MT.
BOREHOLE TILT
12 km
N
EQ.
APR
MAY
JUN
JUL
AUG
SEP
OCT
NOV
DEC
HYPOCENTRAL
DISTANCE
EXPANSION
NORTH SOUTH
$10^{-5}\frac{\Delta l}{l}$
19 km
NORTHWEST SOUTHEAST
EAST WEST
PIÑON STRAIN
1975

Figure 2.

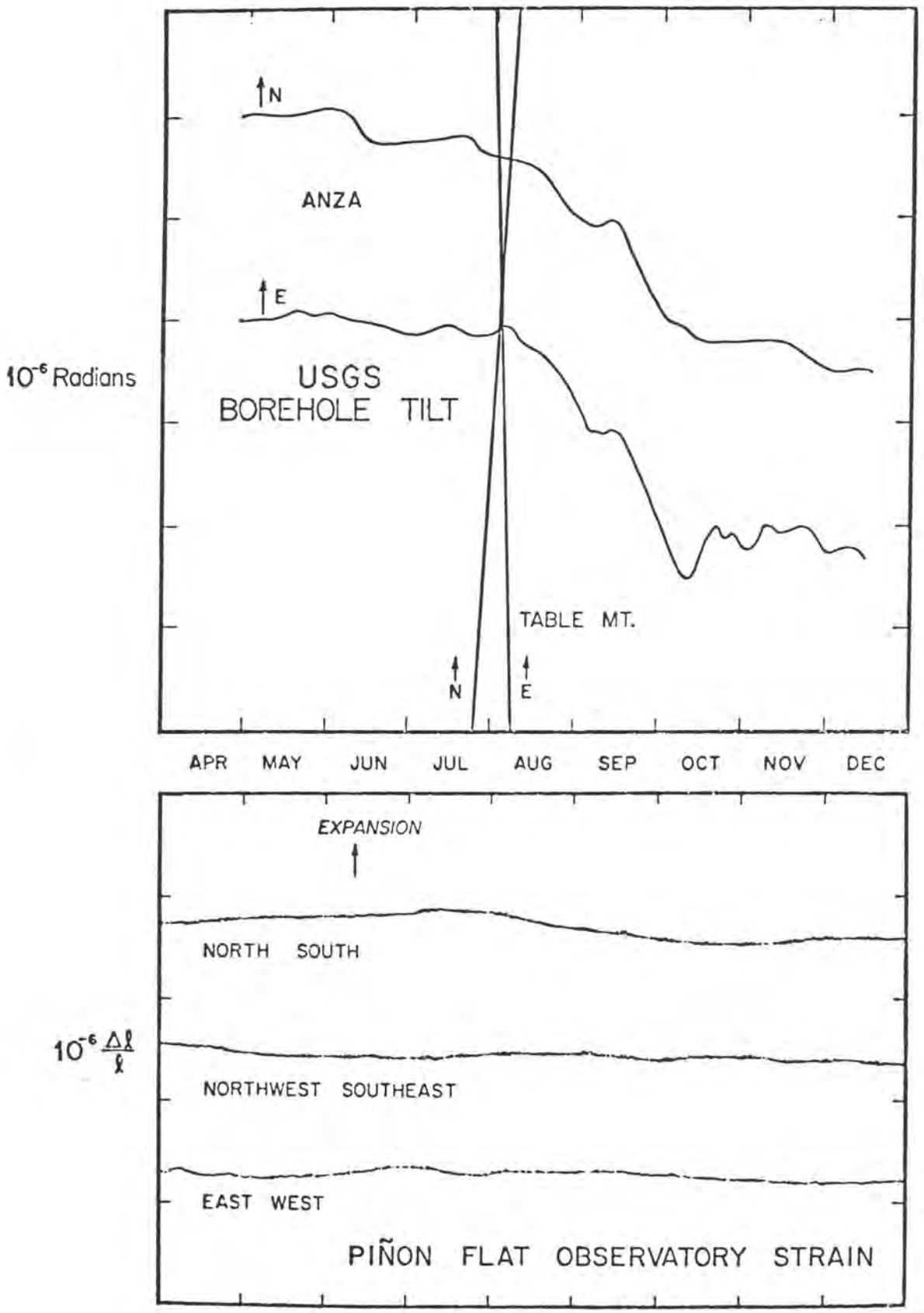
N
ANZA
E
10^{-6} Radians
USGS
BOREHOLE TILT
TABLE MT.
N
E
APR
MAY
JUN
JUL
AUG
SEP
OCT
NOV
DEC
EXPANSION
NORTH SOUTH
$10^{-6} \frac{\Delta l}{l}$
NORTHWEST SOUTHEAST
EAST WEST
PIÑON FLAT OBSERVATORY STRAIN
1975

Figure 3.

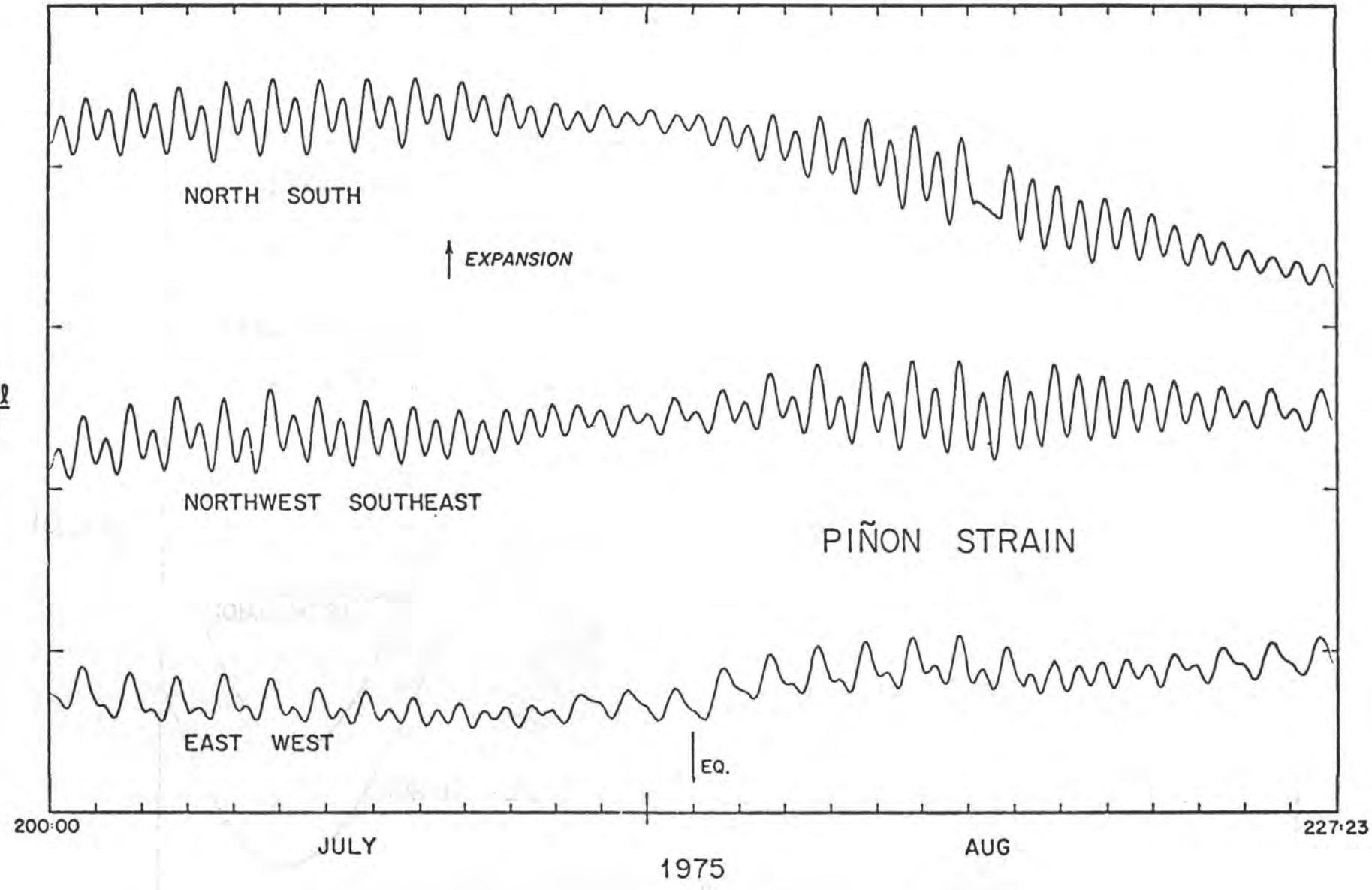
NORTH SOUTH
EXPANSION
NORTHWEST SOUTHEAST
PIÑON STRAIN
EAST WEST
EQ.
200:00
JULY
1975
AUG
227:23
$10^{-7}\frac{\Delta l}{l}$

Figure 4.

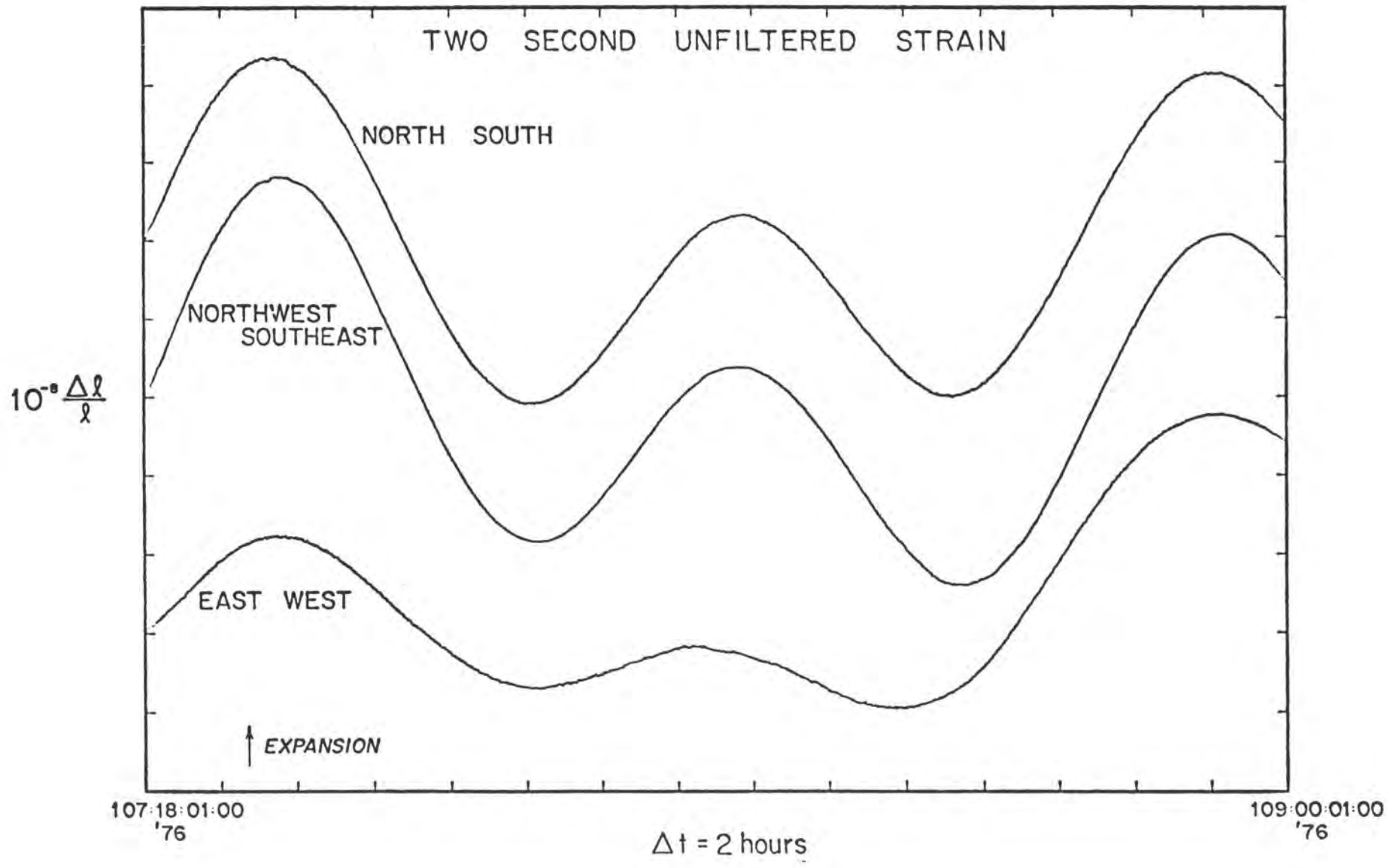
TWO SECOND UNFILTERED STRAIN
NORTH SOUTH
NORTHWEST
SOUTHEAST
EAST WEST
EXPANSION
$10^{-6}\frac{\Delta\ell}{\ell}$
107:18:01:00
'76
109:00:01:00
'76
Δt = 2 hours

Figure 5.

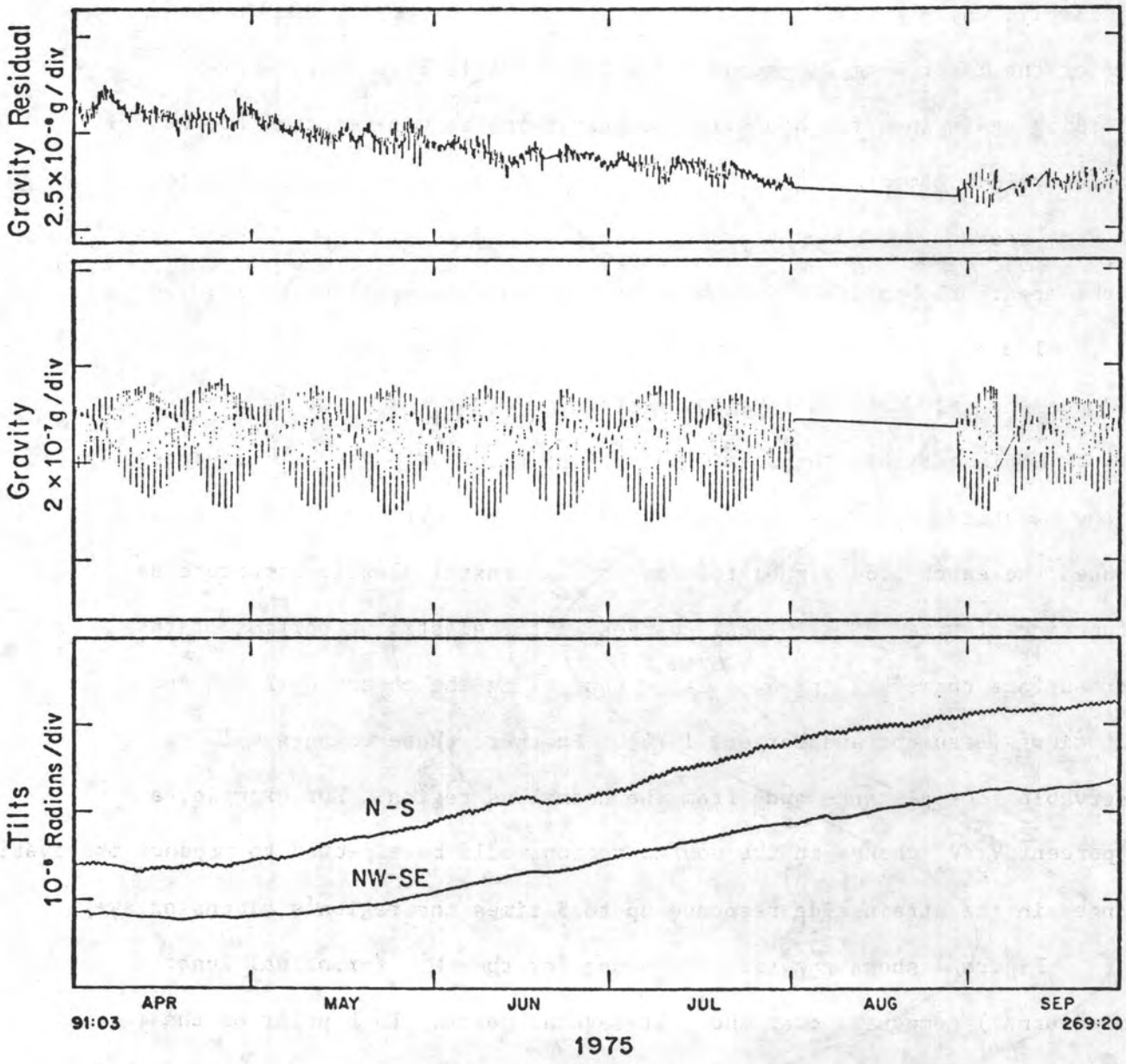
Gravity Residual
2.5×10⁻⁸g/div
Gravity
2×10⁻⁷g/div
Tilts
10⁻⁸ Radians/div
N-S
NW-SE
APR
MAY
JUN
JUL
AUG
SEP
91:03
269:20
1975

Figure 6.

tides from the observed record. The exact time of the Horse Canyon earthquake is marked by the data gap in the gravity record. Due to the high local accelerations experienced, the ball, normally leviated in a superconducting magnetic field, struck the sides of its container so hard that it went "normal" and lost its superconducting properties at the point of contact. (Similarly, the strainmeters were interrupted by the earthquake due to a loss of the laser beam alignment. However, in this case, they were recording again in a few hours.) The gravity meter was returned to the lab for refurbishment, a partial rebuilding and was at room temperature for some weeks. We do not attach any geophysical significance, therefore, to the apparent change in drift rate once it was in operation again.

Two pier tilt records are shown in the bottom panel. No clear evidence for anomalous tilts either before or after the event is seen.

To investigate the possibility of some sort of systematic changes in the elastic properties which are predicted by the theories of dilatancy, we used the earth tide signal to monitor the crustal elastic structure as a function of time. Small local changes in the elastic properties of the near surface rocks will produce large changes in the observed strain and tilt tides (Beaumont and Berger, 1974). Further, these changes will be observable some distance away from the anomalous region. For example, a 10 percent V_p/V_s change in the source region would be expected to produce observable changes in the strain tide response up to 5 times the region's dimension away.

Figure 7 shows the tidal response for the M_2 (principal lunar semi-diurnal) component over the past several years. Each point on the plots represents an independent 29 day estimate of the response. The dashed lines are the fluctuations in the response we expect due to the normal background earth noise in this band. It is clear that over the period

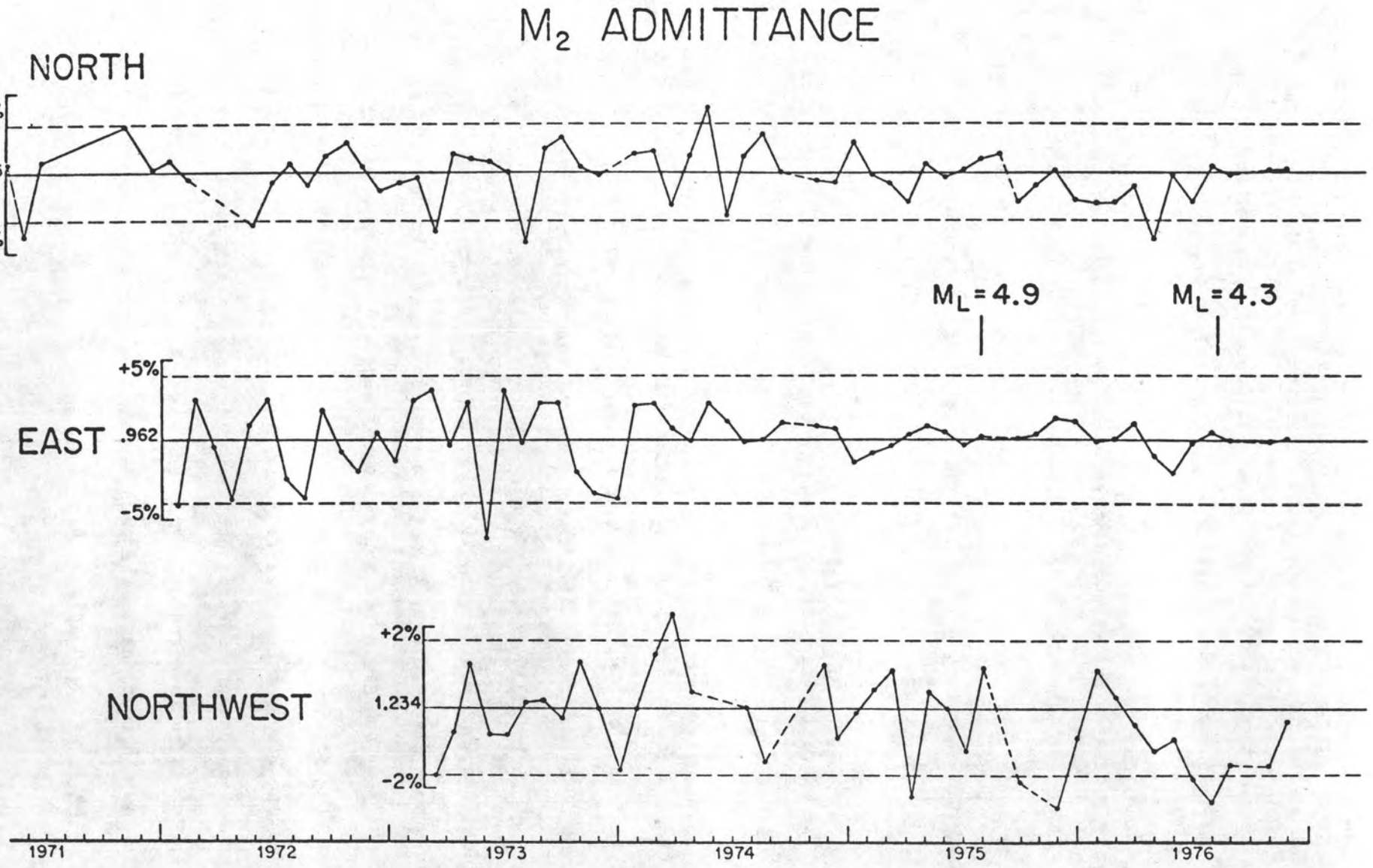
M2 ADMITTANCE
NORTH
+2%
.895
-2%
ML = 4.9
ML = 4.3
+5%
EAST
.962
-5%
+2%
NORTHWEST
1.234
-2%
1971
1972
1973
1974
1975
1976

Figure 7.

of time just prior to the Horse Canyon earthquake there were no detectable changes in the earth's tidal response.

What can we conclude from this set of observations:

1. "Anomaly" observed at Table Mountain tiltmeter Δ = 12 km
2. No "anomaly" observed at Anza tiltmeter Δ = 16 km
3. No "anomaly" observed at PFO on many instruments Δ = 19 km

We could conclude that the earthquake-produced anomaly was somehow directed at the Table Mountain instrument above. One can argue about the rheological properties of the fault zone, exact hypocentral depth, and various models of preseismic deformation. Many models can explain the data. Or we could conclude that the tiltmeters are responding only to very local deformations that are not indicative of a larger deformation. The former conclusion requires some complicated models and some mental gymnastics while the latter rests on the simple observation that the tiltmeters are very small and buried very shallowly.

Our conclusions are that the Table Mountain tilts are artifacts of local origin and have nothing to do with the subsequent earthquake. We cannot prove this, but the weight of evidence would seem to indicate that if some precursive slip had taken place, associated with an earthquake 12 km deep, some signal would be seen at Anza and PFO.

Direct Comparison of Short-Base Tilt and Long-Base Strain

The questions that arose when analyzing the Horse Canyon earthquake data were examples of the larger questions that have arisen whenever such short base tilt data is compared with long base data. It has been observed that short base instruments (~ 1 m) produce signals in general which are considerably bigger (i.e. order of magnitude or more) than those of long (> 1 km) base instruments. Why is this? We have conducted an experiment at PFO over the past year utilizing 732 m strainmeters and an array of short base borehole tiltmeters (Kinemetrics TM-1B). Figure 8 shows a plan view of the observatory. The tiltmeters are emplaced at sites α, β, γ, and δ ranging in separation from 10 m to 750 m. Great care was exercised in planting the instruments to avoid obvious sources of thermal and mechanical stability. The scheme is illustrated in Figure 9. For each site, a hole 1.1 m in diameter was drilled to a depth of approximately 3 meters. Inserted into the hole was a thin walled 91 cm diameter corrugated tube. Finally a smaller 12 cm diameter hole was drilled out the bottom of the larger hole, to an overall depth of nearly 5 meters. The sensor package was inserted into the smaller hole and maintained within 10^{-5} radians of vertical while fine silica sand was compacted around the sensor. Many layers of insulation fill the larger hole in an effort to isolate the instrument from surface temperature variations.

The nature of the surface layers at PFO (decomposed granite) allows direct emplacement of the sensor and packing into the surrounding material. This procedure should represent an improvement over the method of installing the package inside an outer water-tight tubing. If we are hoping to detect tilts of 10^{-7} radians faithfully (i.e., or displacements of 10^{-7} meters on

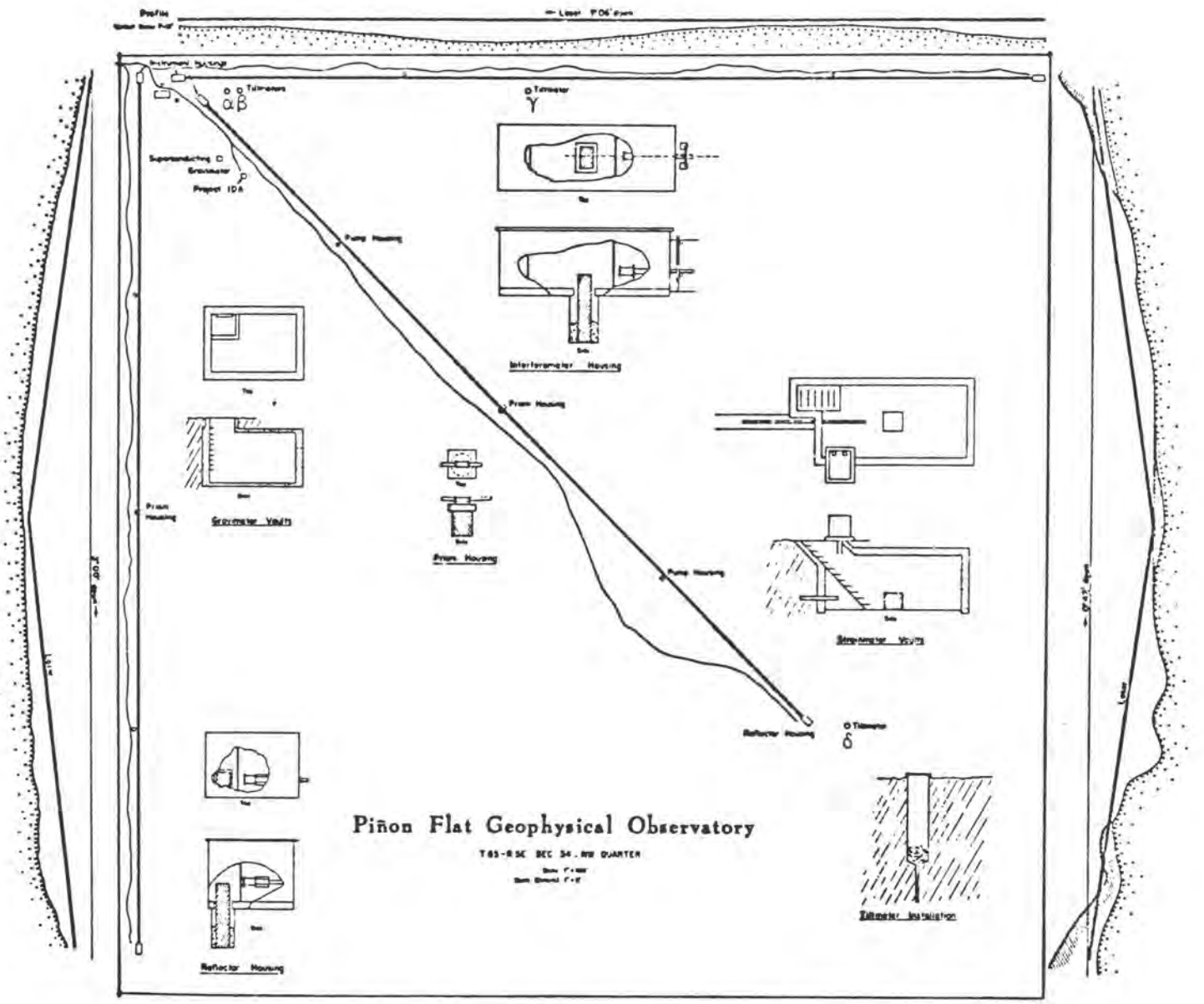
Piñon Flat Geophysical Observatory
Tiltmeters
αβ
Tiltmeter
γ
Superconducting Gravimeter
Project IDA
Pump Housing
Interferometer Housing
Prism Housing
Gravimeter Vaults
Prism Housing
Pump Housing
Reflector Housing
Tiltmeter
δ
Reflector Housing
Tiltmeter Installation

Figure 8.

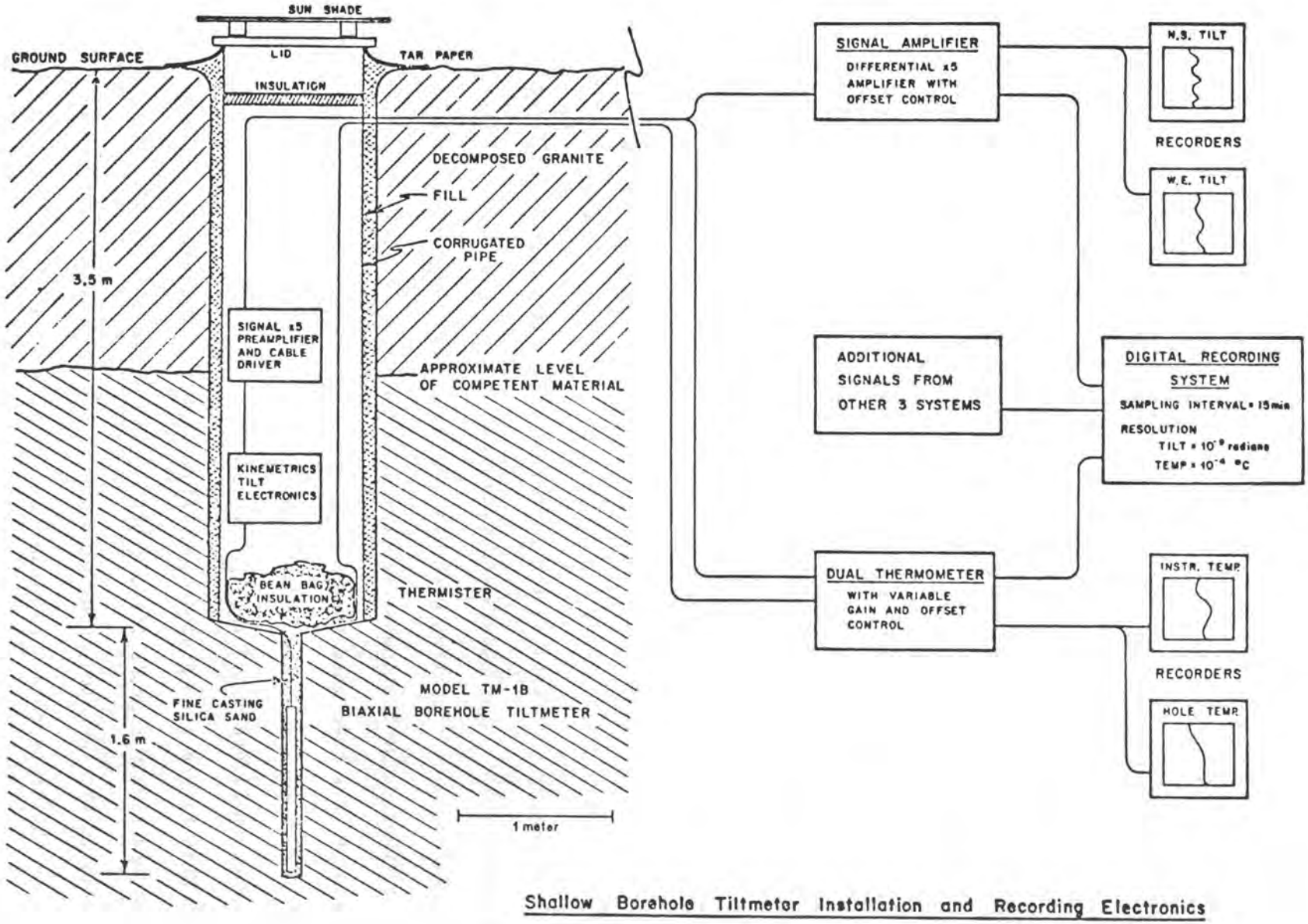

Shallow Borehole Tiltmeter Installation and Recording Electronics

Figure 9.

a 1 meter base line), it is essential to minimize the number of interfaces between the sensor and the surroundings.

Figure 10 shows the data collected to date. It is worth recalling that α and β refer to the two tiltmeters 10 meters apart (see Figure 9). The secular tilt signals over the period illustrated are given in Table 2. From this table and Figure 10 it is obvious that even the tiltmeters 10 meters apart do not produce correlated secular tilt signals. Figure 11 shows a comparison of the short base line N-S tilts and the long base line strains for the same period. Note that the strain is plotted on a scale 10 times more sensitive than the tilt. In Figure 12 we show the tilt vector as a function of time over the same period. It can be seen that α and β tilt vectors are nearly in opposite direction and offer no indication of a general trend one way or another.

The apparent large differences in the tidal signatures of the α and β instruments are indications of thermal contamination. Indeed, spectral analysis reveals that M_2, the principal lunar semidiurnal signal, is nearly identical on the instruments but diurnal and semidiurnal temperature effects contaminate the records.

Numerous difficulties with the commercial tiltmeter electronics have interrupted the continuous recordings. The erroneous signals observed might easily have been interpreted as local ground movement were it not for the close spacing of the instruments. An example of such noise is illustrated in Figure 13 on the α_{WE} record.

This figure also graphically illustrates the difference between the tilt and strain signals for a short section of record. Note that the tilt scale is 10 times less sensitive than the strain scale. The seismic signals on the tiltmeters seem to be correlated but the rest of the tilt signals are difficult to interpret, to say the least.

Table 2

Shallow Bore Hole Tilt Observations

60:00 to 278:00 1977

(units 10^{-6} radians)

	Instrument			
North-South	α	β	γ	δ
Rate of drift/year	11.5	-26.4	-12.0	-13.2
Maximum deviation from linear drift	5.6	5.7	17.5	5.5
West-East				
Rate of drift/year	-11.2	-20.4	-18.0	19.2
Maximum deviation from linear drift	4.6	11.7	11.7	9.0

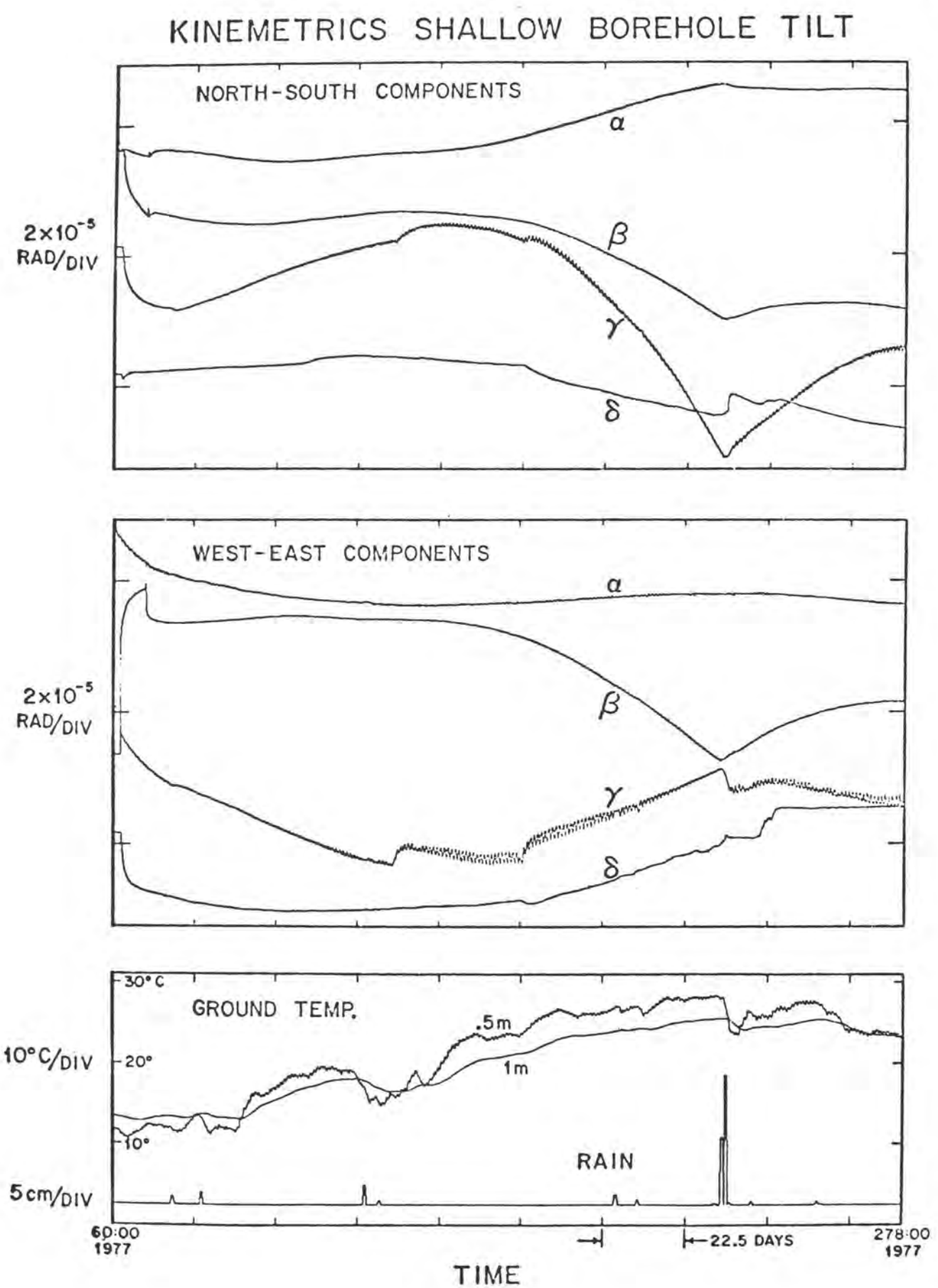
KINEMETRICS SHALLOW BOREHOLE TILT
NORTH-SOUTH COMPONENTS
α
β
γ
δ
2×10⁻⁵ RAD/DIV
WEST-EAST COMPONENTS
α
β
γ
δ
2×10⁻⁵ RAD/DIV
30° C
GROUND TEMP.
.5m
1m
20°
10°
10°C/DIV
RAIN
5cm/DIV
60:00 1977
22.5 DAYS
278:00 1977
TIME

Figure 10.

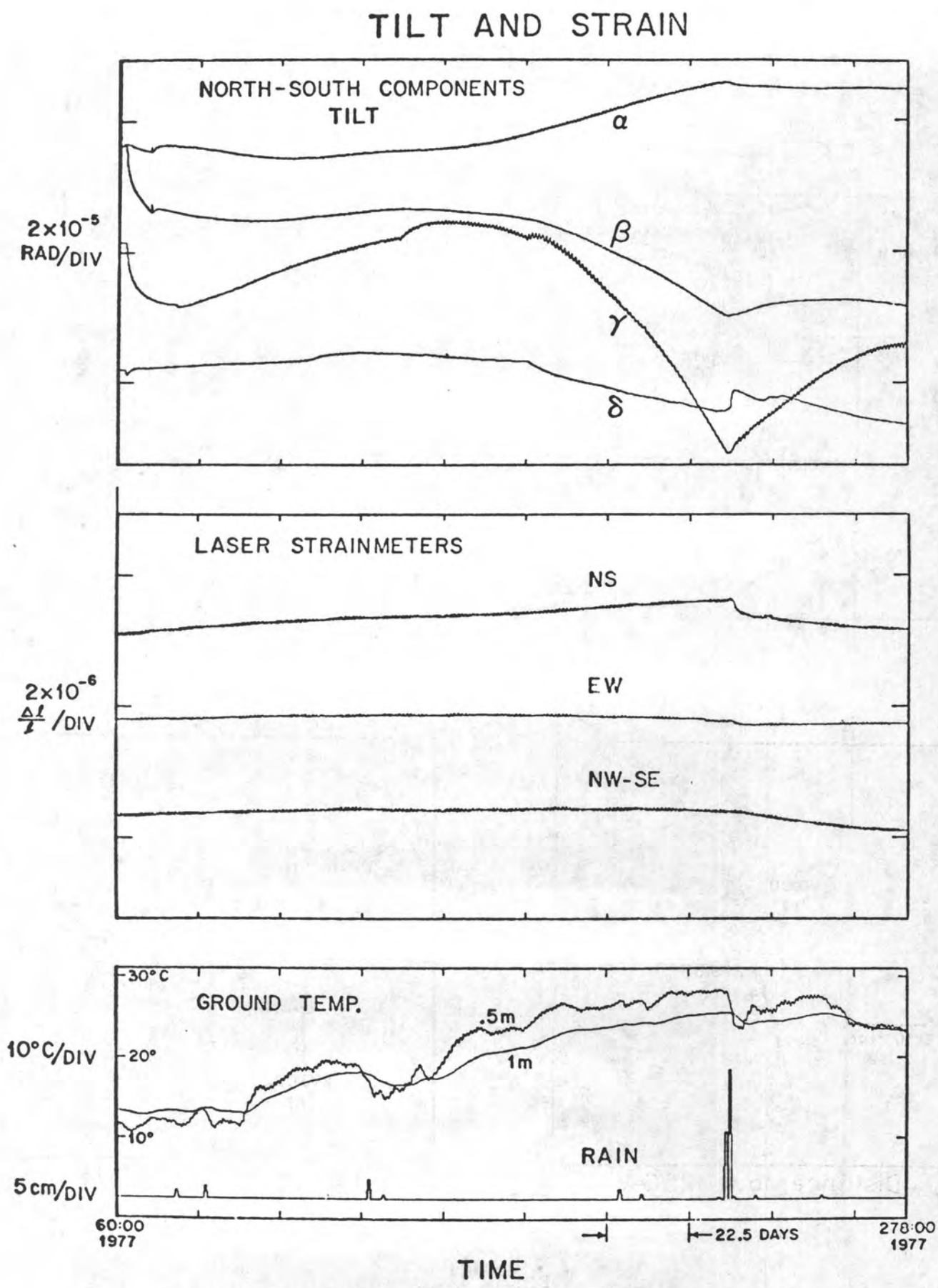
TILT AND STRAIN
NORTH-SOUTH COMPONENTS
TILT
α
β
γ
δ
2×10⁻⁵
RAD/DIV
LASER STRAINMETERS
NS
EW
NW-SE
2×10⁻⁶
Δl/l /DIV
30°C
GROUND TEMP.
.5m
1m
20°
10°
10°C/DIV
RAIN
5cm/DIV
60:00
1977
22.5 DAYS
278:00
1977
TIME

Figure 11.

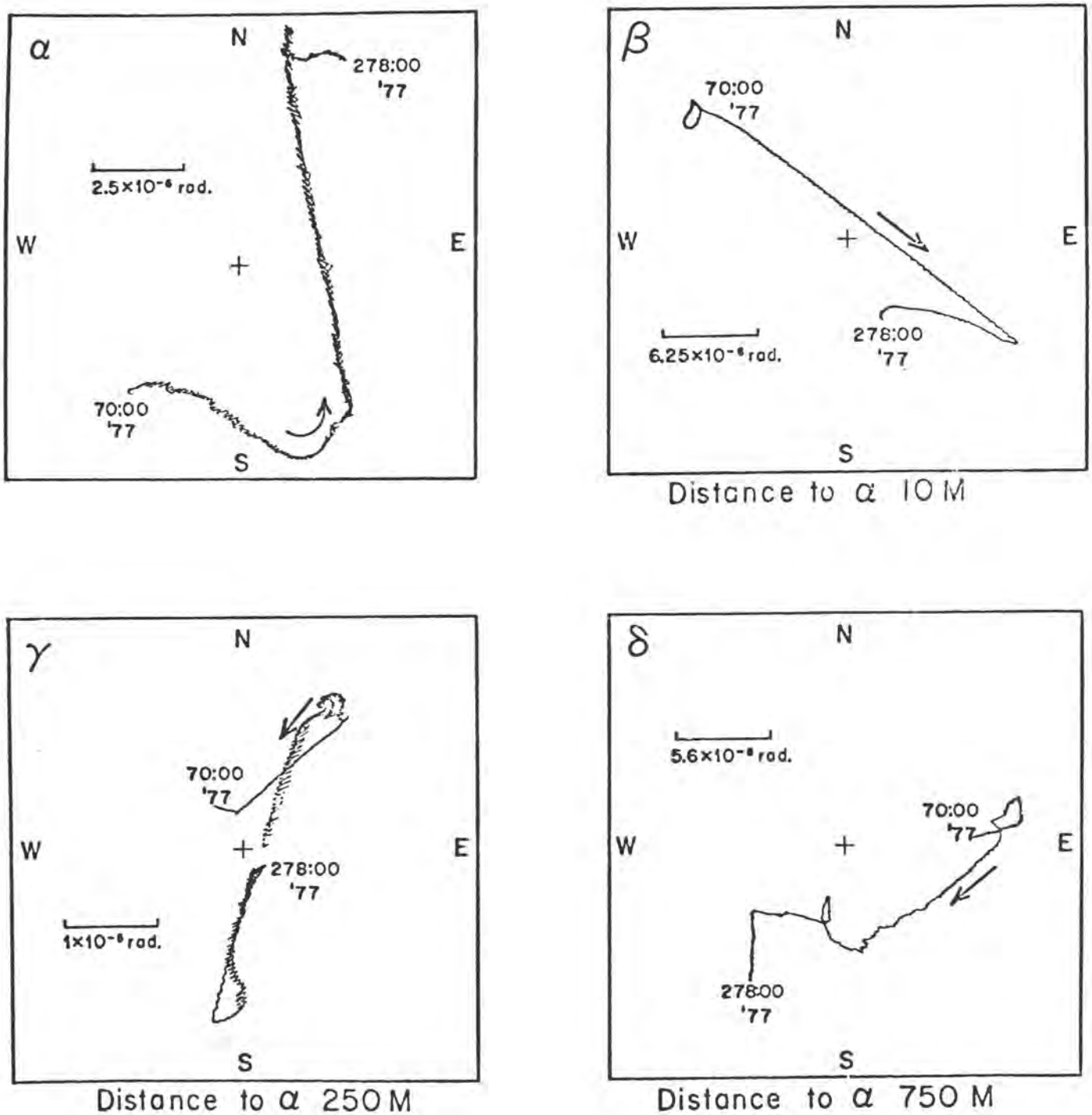
KINEMETRICS SHALLOW BOREHOLE TILTS
α
N
278:00
'77
2.5×10⁻⁶ rad.
W
E
70:00
'77
S
β
N
70:00
'77
W
E
6.25×10⁻⁶ rad.
278:00
'77
S
Distance to α 10 M
γ
N
70:00
'77
W
E
278:00
'77
1×10⁻⁶ rad.
S
Distance to α 250 M
δ
N
5.6×10⁻⁶ rad.
70:00
'77
W
E
278:00
'77
S
Distance to α 750 M

Figure 12.

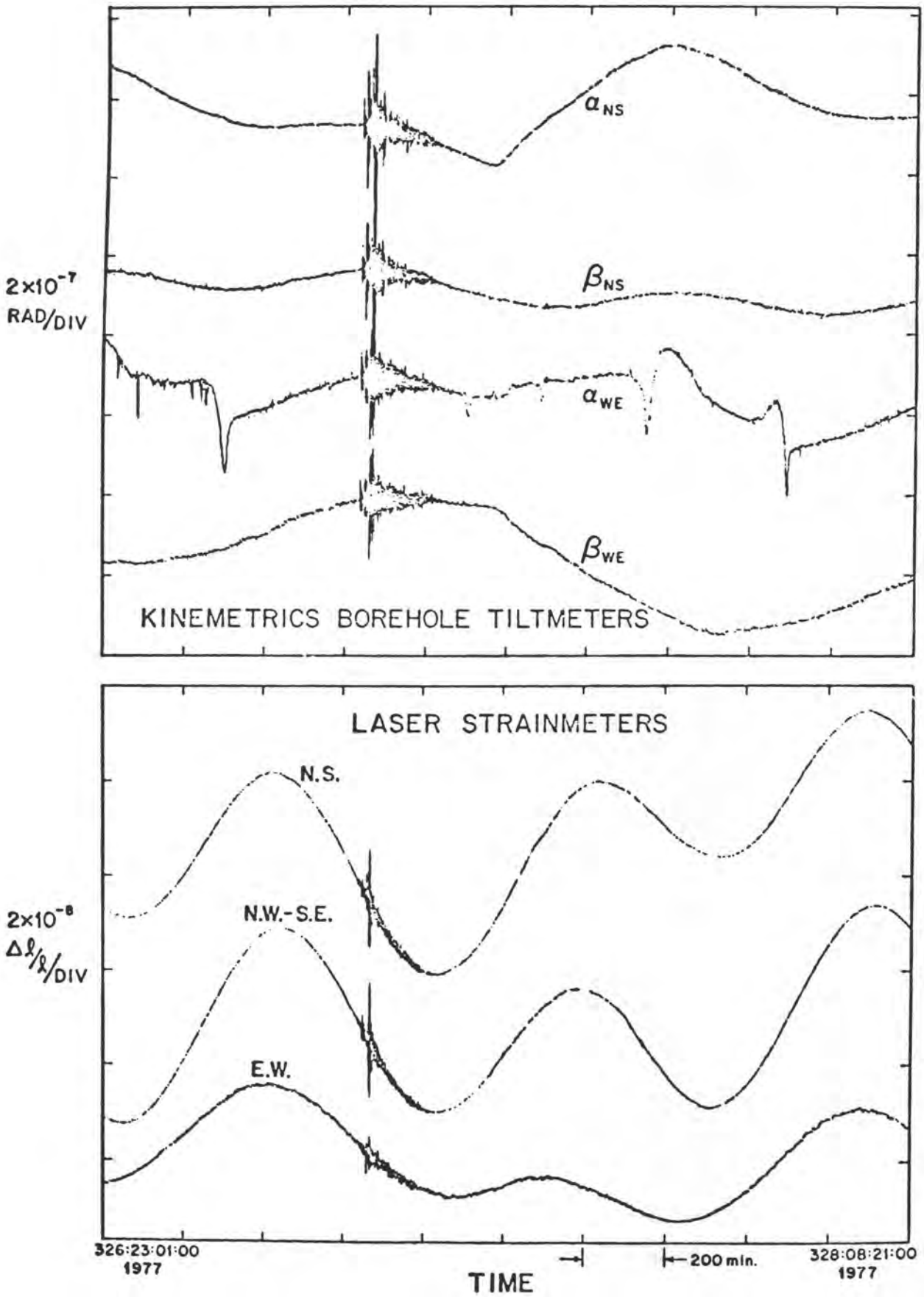
α_{NS}
β_{NS}
α_{WE}
β_{WE}
2×10^{-7}
RAD/DIV
KINEMETRICS BOREHOLE TILTMETERS
LASER STRAINMETERS
N.S.
N.W.-S.E.
E.W.
2×10^{-8}
$\Delta\ell/\ell$/DIV
326:23:01:00
1977
200 min.
328:08:21:00
1977
TIME

Figure 13.

To check the correlation of signals on the tiltmeters at seismic frequencies (in the absence of earthquakes) we performed a cross-spectral analysis of 3 hrs. of data from α and β instruments; N-S components. Figure 14 shows the results. There is fairly high coherence over the microseismic energy peak near 8 seconds but for the longer periods, where the true background noise is low, the coherence drops rapidly to a value not significantly different from zero. Since the wavelengths associated with seismic signals are so much longer than the 10 m separation of the instruments, we must conclude that we are observing instrument noise only.

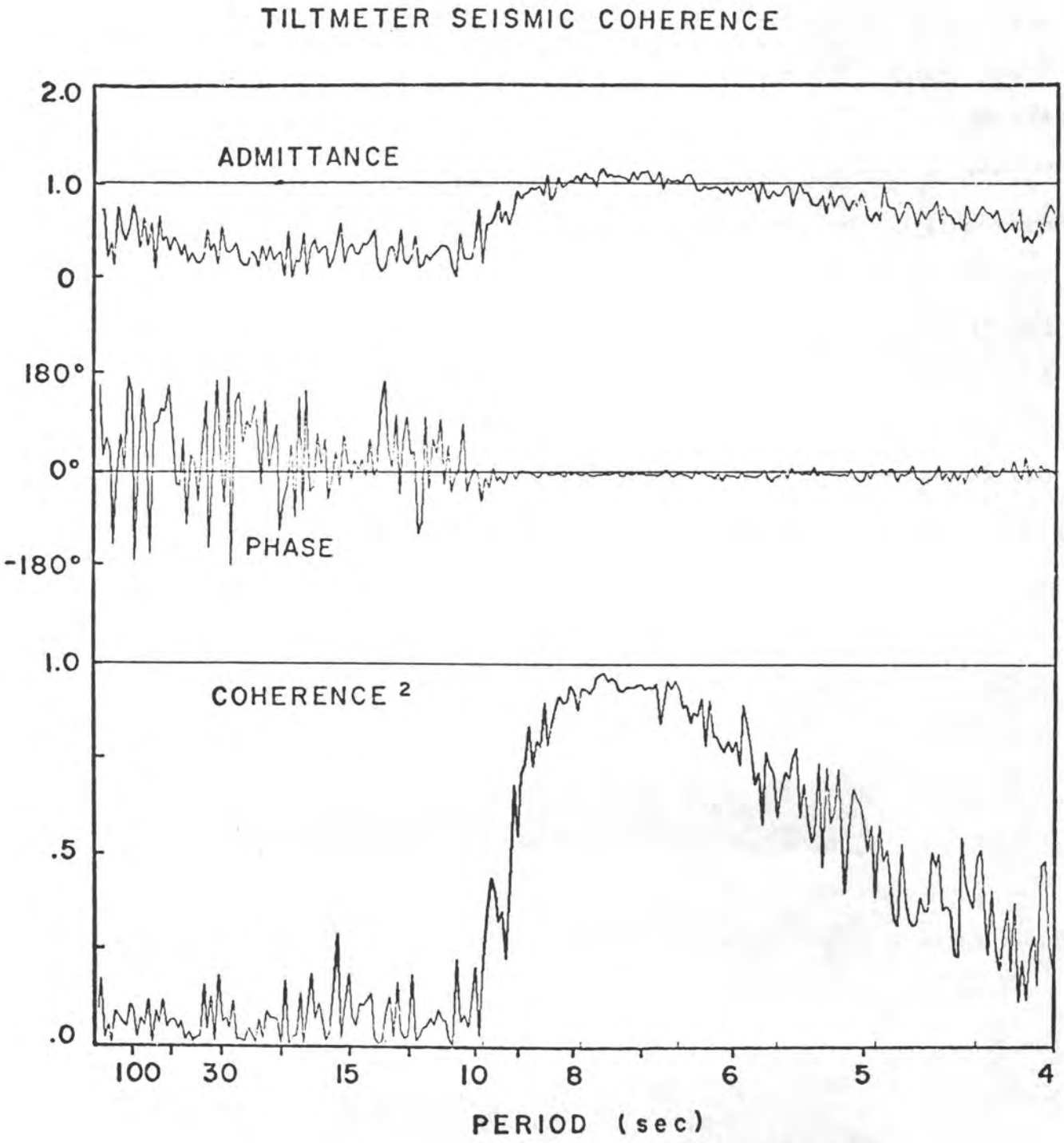
TILTMETER SEISMIC COHERENCE
2.0
ADMITTANCE
1.0
0
180°
0°
-180°
PHASE
1.0
COHERENCE ²
.5
.0
100
30
15
10
8
6
5
4
PERIOD (sec)

Figure 14.

Conclusions

The results of the Horse Canyon earthquake observations and the direct comparisons carried out at PFO indicate that the wavelength spectrum of crustal deformations is decidedly "red." In the temporal domain, it is well known that most geophysical quantities exhibit what has been termed the "infrared catastrophe." That is, the noise levels rise exponentially towards decreased frequencies. In the spatial domain, it appears the same thing occurs; as the wavelength decreases the noise increases and perhaps we should not be surprised. If the spectrum of ground displacement may be modelled by random noise (white in the spatial domain), then the spatial derivatives of this (what we usually measure) may be expected to show a similar rise in power towards low wavelength.

In the case of the short base tiltmeters installed at PFO, if we look at a multi-decade spectrum of the tilt signal and compare it with that of the strainmeters (Figure 15) we observe that the tilt spectrum is at least two orders of magnitude larger. We can only conclude from this that over the period range of this study, 1 second to 1 month, we are observing nothing but "instrument" noise on these short base tiltmeters.

Now some of this noise can be attributed to electronic noise or other noise of purely instrumental origin especially at the shorter periods. But at the longer periods we believe that what we are seeing is a consequence of the base length rather than the instrument. (A tilt of 10^{-7} radians is a displacement of 10 Å on a 1 cm base!) We suspect that shallow buried strainmeters a few cm in length would produce similarly useless data. It is certainly true that the longer base strainmeters are orders of magnitude quieter.

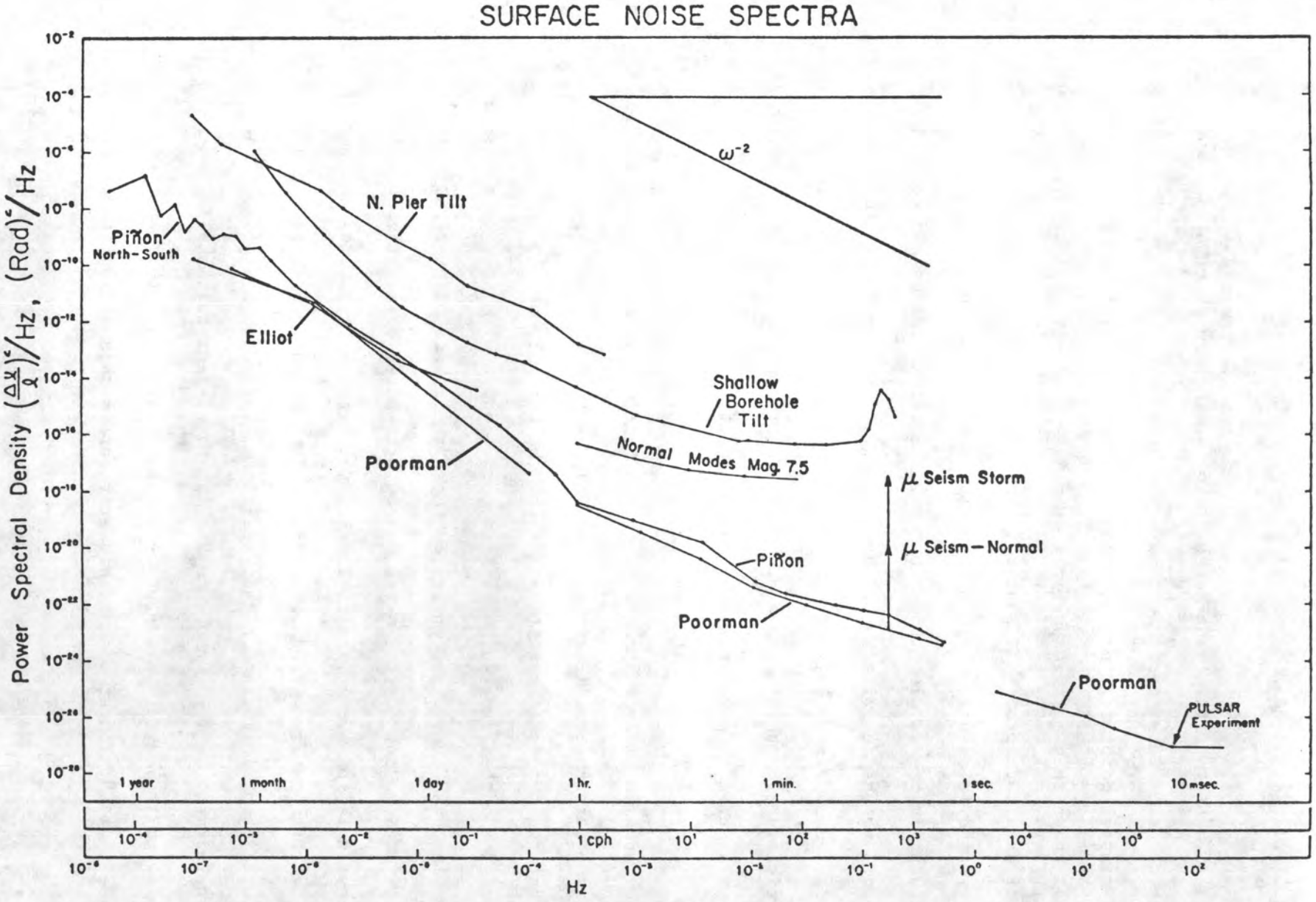
SURFACE NOISE SPECTRA
Power Spectral Density $(\frac{\Delta\alpha}{\alpha})^2/Hz$, $(Rad)^2/Hz$
ω^{-2}
N. Pier Tilt
Pinon
North-South
Elliot
Shallow
Borehole
Tilt
Normal Modes Mag. 7.5
Poorman
μ Seism Storm
μ Seism—Normal
Pinon
Poorman
Poorman
PULSAR
Experiment
1 year
1 month
1 day
1 hr.
1 min.
1 sec.
10 msec.
1 cph
Hz

Figure 15.

It is also true that Michelson's (1914) original long base tiltmeter produced exceptionally "quiet" data.

As many studies have shown (Berger and Beaumont, 1976; Harrison, 1976), the coupling of one spatial derivative to another due to inhomogeneities in the material can be a large source of "noise." Further, we should not be surprised that measurements on the sub-meter scale length fail to produce data relevant to the deep rooted tectonic and seismic processes in which we are interested.

Finally, if we had planned to use many short base instruments as an array, employing multichannel processing techniques to improve the signal to noise ratio, then the instruments would have to be emplaced densely enough so that each instrument exhibits some coherence with its nearest neighbors. Using the long base length observations at PFO as an upper limit to the low frequency tectonic signals in the region, the signal to noise ratio of the short base instruments is estimated to be 1/50. This result suggests that an array of 2500 instruments would be necessary to monitor a region in which uniform deformation was occurring. Hence the study of an area 100 km^2, commensurate with a fault dimension of 10 km, would require an instrument separation of 200 m--a dense network indeed!

References

Beaumont, C. and J. Berger (1974). Earthquake prediction: Modification of the earth tide tilts and strains by dilatancy, *Geophys. J. Roy. astr. Soc.*, 39, 111-121.

Berger, J. and C. Beaumont (1976). An analysis of tidal strain observations from the United States of America: II. The inhomogeneous tide, *Bull. Seism. Soc. Am.*, 65, 1821-1846.

Harrison, J. C. (1976). Cavity and topographic effects in tilt and strain measurements, *J. Geophys. Res.*, 81, 319-336.

Hartzell, S. H. and J. N. Brune (1978). The Horse Canyon earthquake of August 2, 1975 - Two stage stress release process in a strike-slip earthquake, *Bull. Seism. Soc. Am.*, submitted.

Kanamori, H. (1977). 2 August 1975 Anza earthquake, *U.S. Geologic Survey Open File Report.*

Michelson, A. A. (1914). Preliminary results of measurements of the rigidity of the Earth, *The Astrophysical Journal*, 39, 105-138.

Myren, G. D. and M. J. S. Johnson (1975). Preliminary results from a tiltmeter array around the Los Angeles basin and along the San Jacinto fault, *EOS*, 56, 1059.

Thatcher, W. and T. C. Hanks (1973). Proceedings of the conference on tectonic problems of the San Andreas fault system, *Geological Sciences XIII*, Stanford University, 12.

Tilt Measurements on a Small Tropical Island

ROGER BILHAM AND JOHN BEAVAN

Lamont-Doherty Geological Observatory of Columbia University,

Palisades, New York 10964

ABSTRACT

Tilt measurements have been made on the Caribbean Island of Anegada (18°44'N, 64°25'W) using precision levelling, sea-level measurements and an array of borehole tiltmeters. The tiltmeter measurements after two years of undisturbed operation indicate a tilt rate of approximately a microradian per month, whereas the precision levelling indicates that the island is stable to within a microradian per year (1976-1978). Variations in sea level appear to affect the tiltmeters coherently, although tidal tilts vary significantly over 400 m distances.

INTRODUCTION

There has been much discussion concerning the fidelity of short-baseline tiltmeters installed near the Earth's surface because there are no published results that can be considered totally beyond suspicion. That is, redundancy and duplication of tiltmeters is rare and coherence of tilt signals is frequently poor even over distances of kilometers. Long-term measurements of tilt do not agree with absolute measurements using independent methods such as levelling. Tiltmeters respond to rainfall, changes in subsurface hydrology and surface temperature and it is usually difficult to exclude some or all of these noise sources as a possible source of observed signals.

Moreover, the generation of tilts can occur through the interaction of local elastic inhomogeneity and applied strainfields. Hence, tilt amplitudes and phases can be distorted even if instruments are of adequately good fidelity. These secondary problems cannot be studied systematically without first demonstrating tiltfield coherence.

It was decided, therefore, that six of the Kinemetrics borehole instruments would be installed sufficiently close to each other to examine the wavelengths of surface tilt and that additional, different tiltmeters and measurements would be introduced to provide an independent evaluation of the real tilt of the area.

LOCATION OF THE EXPERIMENT

The experiment was set up on Anegada in the British Virgin Islands (Figure 1). The Virgin Islands have not experienced a major earthquake in the last 500 years of recorded history but there is reason to believe that a major earthquake may be overdue because regions to the west and south have experienced earthquakes with magnitudes greater than 7. An alternative explanation of the gap in significant seismic energy release may be that strain energy is released in the form of creep or as "slow" or "silent" earthquakes with a large component of long-period energy (minutes to days) and relatively little high frequency energy. The installation of strainmeters or tiltmeters was considered to be a possible means to provide an insight into the two alternative tectonic mechanisms or others that might be involved. Anegada was chosen to site the array since it is essentially horizontal, low-lying, and surrounded by a shallow shelf. Approximately four microearthquakes a day are detected by the Lamont-Doherty Caribbean Seismic Network and there is about one magnitude 4 earthquake a month. The residents on Anegada feel one or two earthquakes a year, which appear to be centered about 20 km to the NW of the island.

GEOGRAPHY OF ANEGADA REGION

Anegada Island measures approximately 16 km east-west by 3 km north-south. The central and eastern parts of the island are surfaced by partly recrystallized coral reef, calcarenites and calcareous sand which nowhere attain a height of more than 9 m above mean sea level. The western part of the island is a layer of sand which thickens westward to a maximum of 10 m depth and which rarely exceeds 2 m above sea level except in the form of wind-blown dunes. The western area has a series of salt ponds that drain poorly to the sea. The eastern part of the island consists of interleaved horizontal layers of calcarenite and coral with a vertical spacing of about 1 m between layers. Borehole information does not exist below 20 m.

The island is fringed by coral reefs. To the north the shelf drops steeply toward the Puerto Rico trench and to the east to the Anegada trough. To the south and west the sea floor is uniformly shallow (about 10 m) across to the islands of St. Thomas and Tortolla. Three or four submerged terraces with a vertical spacing of 3-4 m have been identified to the south of Anegada and *Howard* [1970] argues that this signifies stages of geological uplift.

In 1797 Anegada was marked by *Captain Waring* [1797] on a map as the "drowned island" being "almost entirely covered at spring tide". This "drowning" may have referred to the western half of the island which is now at least 50 cm above the highest tide. If we assume that no other process is operating, the difference between Captain Waring's map and the present implies an emergence of approximately 1 to 3 mm/year. A more probable mechanism is that the present surface is the product of sedimentation. The rapid erosion and rebuilding of the westerly tip of Anegada occurs presently during storm conditions although it is clearly restricted by the reef. According to admiralty charts made in 1890 and more recently, shallowing of the sea floor to the south by about 1 m has occurred. This is interpreted as sediment influx and although it is clear that sediment transport from east to west occurs, it is uncertain where such quantities of sand come from.

Studies by *Schomburgk* [1832] and by developers more recently show large quantities of fresh water underlying the island. The general porosity of the island was revealed by two experiments we performed in 1976. A series of wells up to 90 m from the beach at the west end encountered brackish water right up to the beach with a periodic modulation of height caused by the 30 cm sea tide. The amplitude of the periodic effect fell off rapidly to about 30% of the tidal amplitude in the first 10 m and then less than 5% for the next 100 m. A well 1.5 km from the coast shows a 5 cm tide.

TILTMETERS

In 1976 we installed six Kinemetrics tiltmeters in boreholes in a 2 km array along the island. Our intention was to examine the nature of island tilt noise and the suitability of using borehole tiltmeters in island-arc deformation studies. Operating problems in the first two years of installation encouraged us to reduce the array dimensions to a more modest array of three instruments (numbered 2, 3, and 4 on Figure 4). The details of our initial installation are to be found in the Final Report to USGS contract 14-08-0001-G371. An important feature of the tiltmeter installation is that the tiltmeters were encased in sand-filled

7.5 cm diameter, 3 m long aluminum tubes before being lowered into 15 cm diameter, 3 m auger holes in the coral. The tiltmeter electronics are augmented by a servo-system for maintaining the tiltmeters close to zero output, by a local recording system, and by a centrally located satellite transmitter (DCP). Each installation is covered by a 1 m high mound of white sand canopied by an elevated sheet roof to minimize the direct effects of sun and rain. The installation method successfully reduces thermal contamination of the tilt data to an acceptable level (see Figure 2).

The local chart recorder at each tiltmeter is multiplexed to monitor the x and y tilt channels and the output from a thermistor thermometer positioned within the electronics unit. The chart is advanced at a rate of approximately 5 cm per day. The tilt data are dominated at high frequencies (3-6s) by microseismic tilt that has its origin in surf action on the surrounding reefs. The microseismic noise varies in amplitude from .1 to .3 microradians according to surf conditions. The telemetered data are smoothed with a 20s filter to attenuate the microseismic energy, sampled every six hours on six channels and transmitted twice daily.

During the first two years of operation the signals from the six tiltmeters were greater than 10^{-5} radians per month in random directions. By 1978 the drift rate had reduced to approximately 10^{-6} radians in a month. The observed decay in the drift rate is presumably due to settling of the instrument and may be an elastic adjustment of the borehole tiltmeter casing in response to installation stresses [*Stauder and Morrissey*, 1978].

We present two figures illsutrating recent data. In Figure 2, synchronous data from tiltmeters 2 and 3 are shown. The x and y channels of tiltmeter 2 show a clear semidiurnal tide with a peak-to-peak amplitude of 1-2 microradians. The y channel of tiltmeter 3 shows a diurnal thermal signal with an amplitude of 4 microradians and the x channel suggests a semidiurnal tide with an amplitude of less than 0.5 microradians. The microseismic tilt amplitude is approximately the same amplitude on 2x, 2y, and 3y but is about half that on channel 2x. Three teleseismic earthquakes confirm that the calibration of 2y and 3y are within 20% of each other in that surface wave magnitudes recorded by each are similar. We view the tiltmeter 2 data with suspicion since the tidal amplitudes are larger than we might expect from tidal loading and may be the result of direct influence of semidiurnal variations of hydraulic pressure [*Van der Kamp*, 1973]. Tiltmeter 2 is the deepest operating tiltmeter and is less than 1 m above mean sea level. Curiously, 1976 data from this instrument showed a dominant diurnal thermal variation although its absence in recent data may be the result of an improved surface cover. On the other 5 tiltmeters the maximum semidiurnal tide peak-to-peak amplitude has not exceeded 0.5 microradians. The thermal signal apparent on the tilt data varies in amplitude from 1 to 5 microradians. Much of this signal is the direct effect of temperature on the electronics unit.

SEA-LEVEL MEASUREMENTS

A number of measurements of mean sea level are being made on the island and other nearby islands [Figure 1 and *Bilham*, 1977]. On Anegada we are currently operating three sea-level monitors: at the west end, on the NE coast, and in a water well near the center of the island. The latter instrument shows a 5 cm tide and longer period oscillations that closely follow sea-level variations monitored by the other gauges. The two coastal sea-level monitors are installed on the beach and monitor the water table rather than sea level. This experimental arrangement was adopted in order to avoid a direct connection to the sea that we have found vulnerable to vandalism and erosion. The arrangement appears to be effective on Anegada since all three gauges track each other (Figure 3). Long-period changes of sea level are detected by the tiltmeters and can account for some of the inflections in tilt rate observed by the array. Rainfall does not have any obvious effect on either the sea level or tiltmeter data.

DISCUSSION

The tidal tilt of Anegada observed by borehole tiltmeters appears to vary over a relatively short distance (400 m) by a factor of four. The maximum measured value for daily tilt (2 μrad) is sufficiently large to disturb precise geodetic levelling surveys of the island, although the data we present do not appear to be seriously disturbed. This may be due to fortuitous timing of the outward and return surveys used to derive a mean value for the line or it may be due to a systematic error in the tiltmeter measurements. We intend to process the levelling data more carefully to remove the known tilt tide.

An error analysis on the numerical values obtained for each adjacent pair of levelling pins provides a surprisingly low cumulative error estimate; ± 0.6 mm in 2.5 km. This is approximately three times smaller than the maximum permissible error required in normal precision levelling although it has been attained by other investigators [e.g., *Schellens*, 1965]. An earthquake (M_S = 5) occurred on 15 Oct. 1976, 20 km to the NW of Anegada. The tiltmeter array was inoperative at the time but the levelling line showed no change ($\pm 2 \times 10^{-7}$) when it was resurveyed nine days later. Over a period of two years there appears to be a suggestion of a tilt up to the NE amounting to 0.5 microradians. Since this value is barely above the estimated measurement precision and we are not yet certain of the influence of tilt tides on the island, we do not place much confidence on its significance.

In Figure 3 we plot data obtained via satellite between March and July 1978 together with rainfall and sea-level data. Tiltmeter 2 behaves erratically and eventually fails when its negative power line is severed by a goat. Tiltmeters 3 and 4 show an interesting correspondence with sea level. Inflections in tilt and sea level occur at similar times. The sea-level data follow each other for the period plotted but the tiltmeter data have different trends on all channels.

PRECISION SURVEYING

A 2.5 km levelling line was laid out in 1976 consisting of 38 bench-marks in an approximately E-W line along the tiltmeter array. In 1977 the line was extended to the north. Brass levelling pins were cemented into the coral surface at intervals of 40-100 m, although the majority were spaced at 70 m intervals. Cairns were constructed to locate the mid-points of every measurement pair to within 50 cm. We used matched invar rods and a Zeiss Ni2 level with optical micrometer for the measurements. A reading precision of 0.1 mm can be obtained with this equipment.

The levelling line has been measured five times in two years (Figure 4). We adopted standard first-order levelling procedures for the measurements with one addition; where the outgoing and return levelling measurements for an adjacent pair of bench-marks differed by more than 0.3 mm they were repeated the following day. Normally such errors were attributable to a dust particle on one or another of the bench-marks during a previous measurement. The closure errors for the five outward and return levelling runs vary between 0.3 mm and 1.4 mm, that is, within the 1.6 mm error defined as "first order levelling" [e.g., *Bomford*, 1971]. In most cases the errors were less than the ± .6 mm we estimated as the cumulative reading error for the line.

The island tilt tide may be a significant source of systematic error since it has a measured daily peak-to-peak amplitude of up to 2×10^{-6} radians. Surveying was usually done over a period of six hours in the morning and two in the early evening. The whole line was usually surveyed over a period of two days. Consider two extreme possibilities. In a period of six hours the tilt tide could tilt the surface from + 1 μrad to - 1 μrad or it could tilt from zero, ± 1 μrad to zero. In the first instance, a cumulative tilt of 2 μrad would be measured; in the second instance, no tilt would be measured. Note that none of our measurements result in more than a 1 μrad tilt for the whole line but that there are slopes within the line that may be the result of tidal changes of tilt during the measurements. We plan to try to correct the levelling data for the island tilt tide using the borehole tiltmeter measurements.

The long-term tilt rate ($\sim 10^{-6}$ rad/month) seen by the tiltmeters even after two years from installation is approximately an order of magnitude larger than that established by precision levelling. Some inflections in the tilt rate can be accounted for by sea-level variations around and under the island. The levelling data indicate that it may be possible to install a long baseline tiltmeter on the surface between two selected levelling pins to obtain a stability of at least 10^{-6} radians per year. This would represent a significant improvement in the continuous monitoring of surface tilt on the island.

We have observed nothing suggestive of a "slow" earthquake on the data though this may have occurred during the numerous occasions when the tiltmeters were inoperative. The seismograph network operated by this observatory has revealed a complex pattern of earthquakes with magnitudes from -1 to 5 in the Anegada region [*Murphy et al.*, 1978]. Our measurements do not clarify the mechanism of plate collision in this corner of the Caribbean. A longer span of data may help and so would continuous tilt measurements of improved fidelity.

Acknowledgments. We would like to thank the Geophysics Applications Group of NASA, Captain Ira Smith, Earle Vanterpool, and George Anthony Smith for help in various aspects of this study. The work has been supported by USGS contracts 14-08-0001-G286, G290, and G371 and by NASA contract NSG 5072. Linearity tests on the tiltmeters in Ogdensburg Seismic Observatory were made possible by NSF contract EAR 77 04856.

REFERENCES

Bilham, R., A sea-level recorder for tectonic studies, *Geophys. J. Roy. astron. Soc., 48,* 307-314, 1977.

Bilham, R. G., and A. Murphy, Analysis of data from several tiltmeter arrays, *Final Rept.,* USGS contract 14-08-0001-G371, 1978.

Bomford, G., *Geodesy,* pp. 731, Third Edition, Clarendon Press, Oxford, 1971.

Howard, J., Reconnaissance geology of Anegada Island, *Caribbean Res. Inst. Spec. Publ. No. 1,* pp. 1-16, 1970.

Murphy, A. J., W. McCann, and A. Frankel, Anomalous microearthquake activity in the northeast Caribbean: Potential precursors to two moderate-sized earthquakes (abstract), *EOS, Trans. Amer. Geophys. Union, 59,* 8, 1978.

Schellens, D. F., Design and application of automatic levels, *Can. Surveyor, 19,* 2, 1965.

Schomburgk, R. H., Remarks on Anegada, *Roy. Geograph. Soc. Jour., 2,* 152-170, 1832.

Stauder, W., and S. T. Morrissey, Tiltmeter array in New Madrid, *Semi-Annual Tech. Rept. No. 3,* USGS contract 14-08-0001-15848, May 19, 1978.

Van der Kamp, G. S. J. P., Periodic flow of groundwater, *Publ. Ph.D. Thesis,* Free Univ. of Amsterdam, Editions Rodopi N. V., Amsterdam, 1973.

Waring, J., West Indian Atlas, Map of the Virgin Islands, Laurie and Whittle, London, 1797.

FIGURE CAPTIONS

Figure 1. Anegada is the most northerly of the Virgin Islands group. The location of tide gauges and mean sea-level monitors is indicated by a dot.

Figure 2. Copy of typical tiltmeter records from instruments 2 and 3. The tiltmeters were visited on 16 and 19 March 1978 between which times they were minimally insulated from surface temperature variations. The lowest trace on each record is the temperature record. An intermittent fault develops on 2x on 24 March. Teleseismic arrivals are indicated by arrows. A semi-diurnal tide is recorded by tiltmeter 2. Tiltmeter 3 shows a large diurnal thermal signal on the y channel and a small semi-diurnal signal after insulation 19 March on the x channel. The calibration on each record is the same (14 microradians full-scale, 20°C full-scale).

Figure 3. Satellite telemetered data from three tiltmeters. 2x and 2y are disabled by a goat on 30 May and the remaining records are interrupted by the launch of Landsat 4 in late June. The instruments were visited on June 26. The rainfall and daily mean values of sea level are plotted to the beginning of May. Note that inflections of sea level recorded by the three Anegada sea level monitors can be identified on the tiltmeter data. The lowest sea-level trace is obtained from an inland well near the tiltmeters (see Figure 4).

Figure 4. Profile along the Anegada levelling line. The top figure is the topography (vertical exaggeration x 100) with the locations (2-6) of borehole tiltmeters. Data (trace 36 in Figure 3) from a water-level monitor located at position 1 follow mean sea-level data monitored on the coast. The lower figures show the cumulative differences between subsequent levellings and the original (May 1976) levelling.

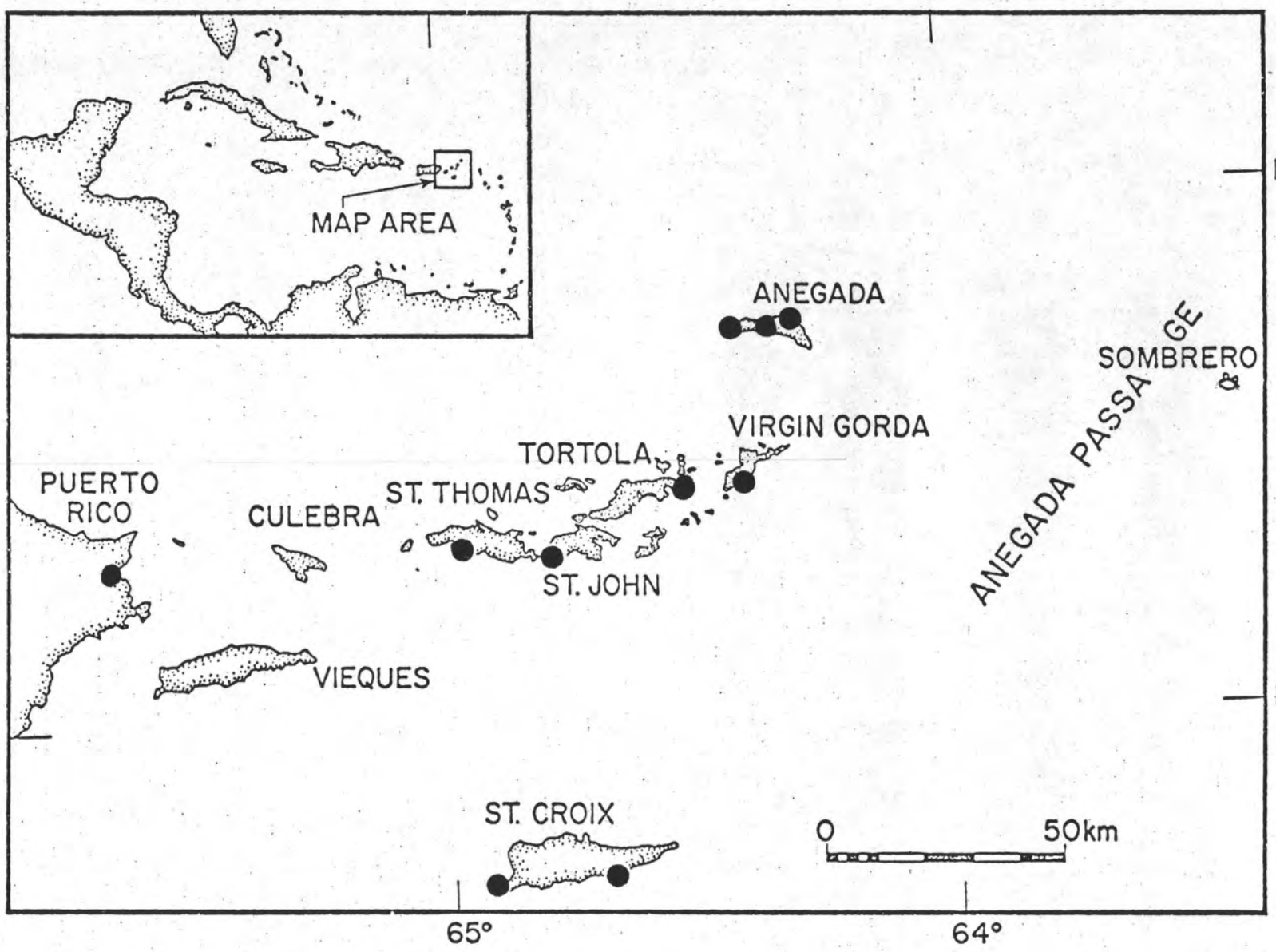
MAP AREA
ANEGADA
SOMBRERO
ANEGADA PASSAGE
VIRGIN GORDA
TORTOLA
ST. THOMAS
PUERTO RICO
CULEBRA
ST. JOHN
VIEQUES
ST. CROIX
0
50km
19°
18°
65°
64°

Figure 1

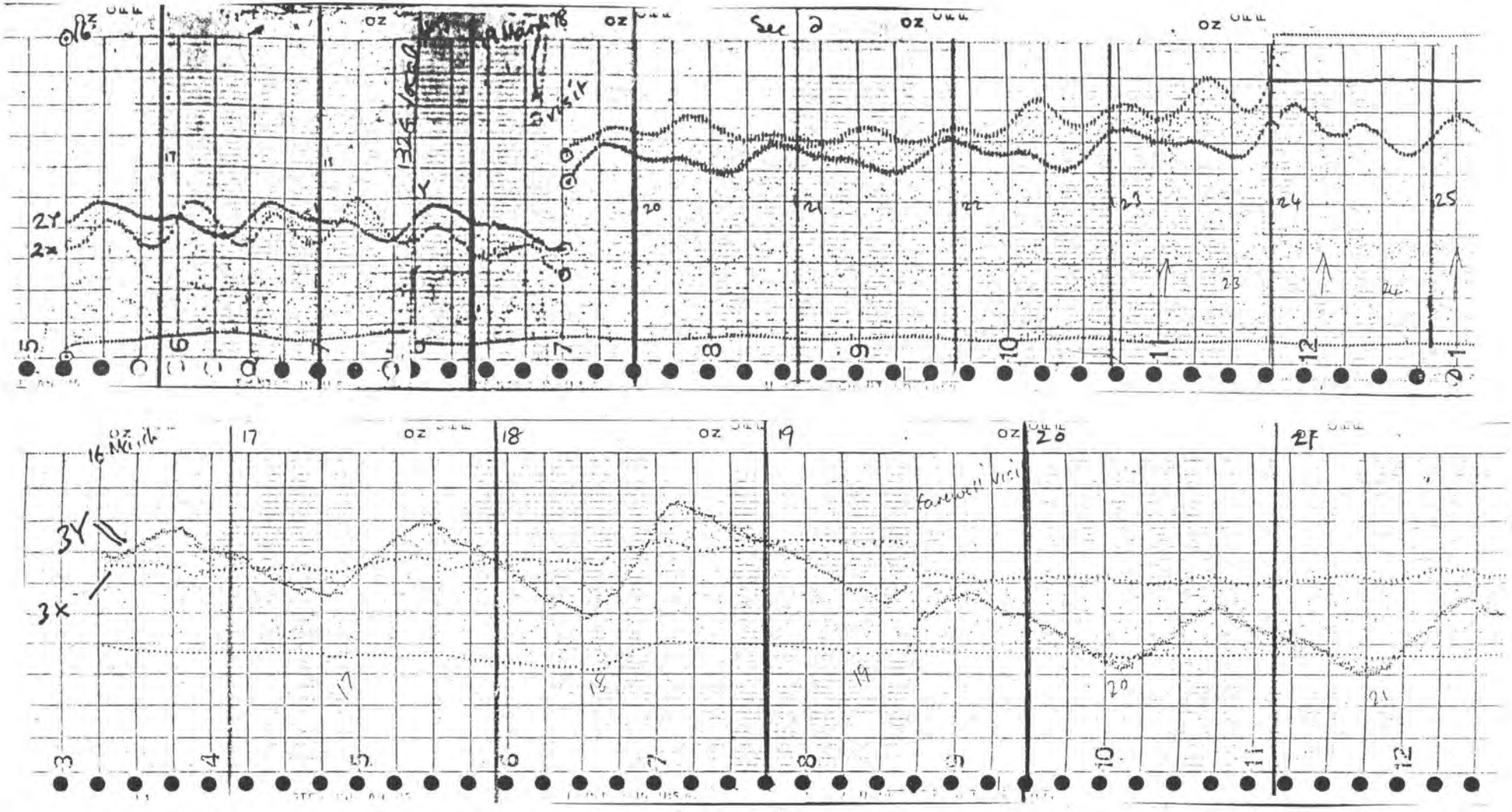

Figure 2

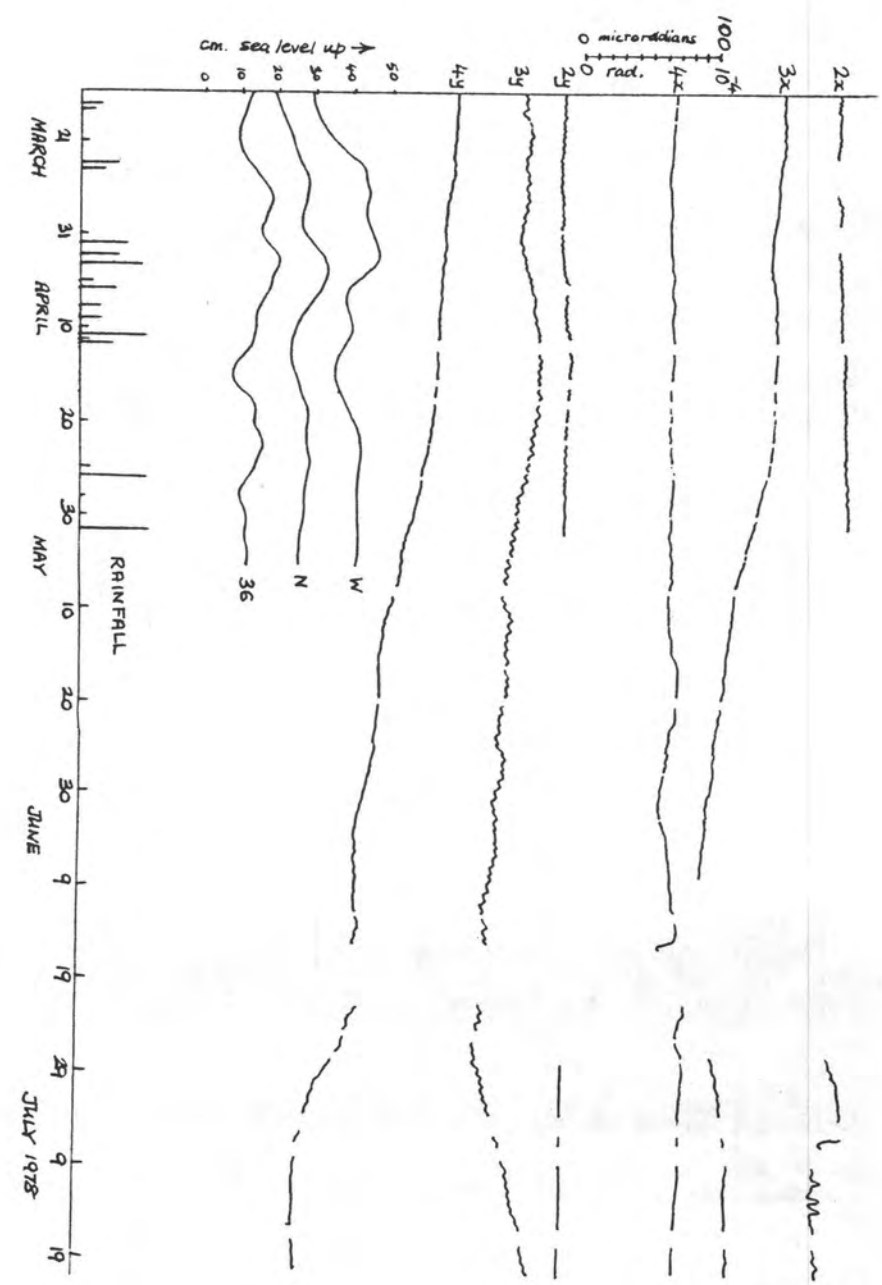
2x
3x
4x
2y
3y
4y
100 10⁻⁴ rad.
0 microradians
cm. sea level up
0
10
20
30
40
50
36
N
W
RAINFALL
21 MARCH
31
10 APRIL
20
30
10 MAY
20
30
9 JUNE
19
29
9 JULY 1978
19

Figure 3

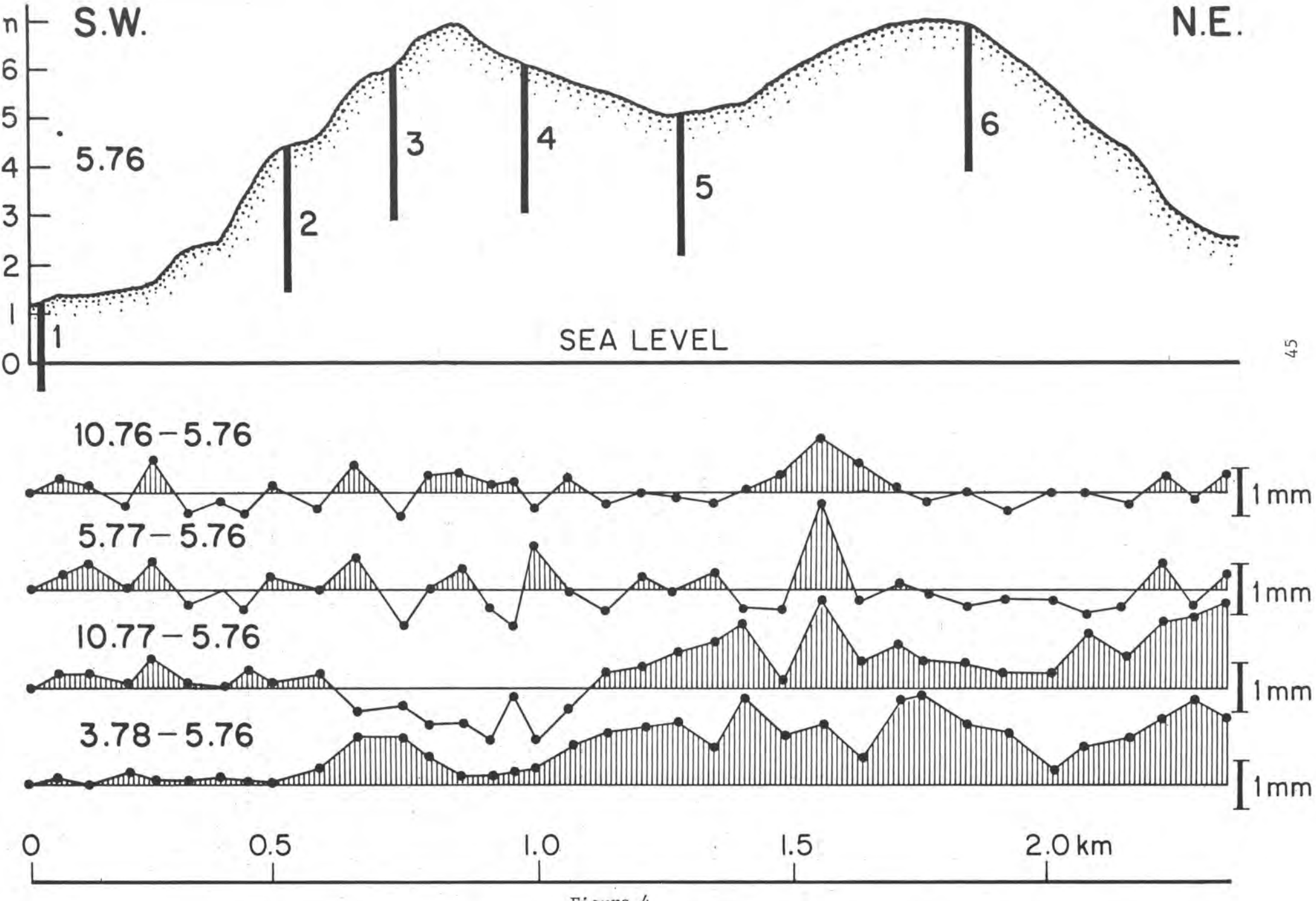
S.W.
N.E.
m
6
5
4
3
2
1
0
5.76
1
2
3
4
5
6
SEA LEVEL
10.76 – 5.76
5.77 – 5.76
10.77 – 5.76
3.78 – 5.76
1 mm
1 mm
1 mm
1 mm
0
0.5
1.0
1.5
2.0 km

Figure 4

A Stable Long Baseline Fluid Tiltmeter for Tectonic Studies

RICHARD PLUMB, ROGER BILHAM, AND JOHN BEAVAN

Lamont-Doherty Geological Observatory of Columbia University

Palisades, New York 10964

ABSTRACT

By improving aspects of *Michelson and Gale's* [1919] water-tube tiltmeter we have constructed a tiltmeter that at long periods is substantially more stable than existing instruments. The 239 m half-filled water pipe tiltmeter has a resolution of 4×10^{-9} radians and a monitoring range of 10^{-4} radians. Our experiments indicate that the construction of longer instruments is not constrained by instrumental limitations but by the space available; resolution, stability and the time constant increase with length. The use of a half-filled water pipe effectively reduces thermally-induced noise in the 239 m tiltmeter to the order of 10^{-7} radians in the presence of 10°C variations. The end reservoirs of a half-filled pipe tiltmeter respond virtually independently to end-mount instability, enabling certain noise signals to be recognized and removed from the data. A comparison of tidal amplitudes obtained from each end of the tiltmeter reveals a 10% discrepancy that can be explained by periodic short-wavelength flexure of the local surface. An important application for the instrument is in the study of secular-tectonic deformation since initial tests indicate that an instrumental stability much better than 10^{-7} radians/month can be obtained. An earthquake (m_b = 2.9) 5 km from the tiltmeter resulted in no observable surface tilt.

1. *Introduction*

Where long baseline tiltmeters have operated side-by-side with horizontal pendulums or other short-baseline instruments (< 2 m) it has been observed that in general the longer instruments provide a more accurate indication of changes of surface tilt [e.g., *Takahasi*, 1931a; *Hagiwara and Yamada*, 1947; *Hagiwara and Rikitaki*, 1950; *Davis et al.*, 1977; *Horsfall*, 1978]. Data from tiltmeters with baselines exceeding 10 m not only appear less contaminated by variations in atmospheric conditions and subsurface hydrology but also more closely resemble secular tilt data measured independently by geodetic levelling [*Kasahara*, 1973]. The enhanced signal-to-noise ratio gained through increased length is attributable to the suppression of locally-generated surface noise with wavelengths shorter than the instrument length. Locally-generated surface noise includes apparent tilts caused by end mount movements relative to the average surface as well as

Lamont-Doherty Geological Observatory Contribution Number 0000.

tilts generated by wind and pressure [*Haubrich and MacKenzie*, 1965; *Ziolkowski*, 1973; *Zschau*, 1977], hydrologically induced tilts [*Herbst*, 1976; *Wood and King*, 1977], thermoelastic tilts [*Harrison and Herbst*, 1977] and the effects of elastic and topographic inhomogeneities [*Harrison*, 1976; *McHugh and Johnston*, 1977]. It is important to note that the continuum spectrum of tilt noise generated by atmospheric loading [e.g., *Warburton and Goodkind*, 1977] is not itself the limiting noise source in tectonic studies. More important are the non-stationary temporal and spatial characteristics of atmospherically induced tilt noise. Thus a single shower of rain in a desert location can dramatically reduce the effective signal-to-noise ratio of a surface instrument.

Though it is generally accepted that at least some surface noise can be attenuated by increasing the measurement baseline, it is not at all clear whether there is an optimum length beyond which little improvement in signal-to-noise can be gained. Experiments with arrays of surface borehole tiltmeters indicate that surface tilt noise for periods greater than a few hours is incoherent over distances less than a kilometer [e.g., *Bilham and Beavan*, 1978; *Wyatt and Berger*, 1978; *Stauder and Morrissey*, 1978]. It seems reasonable to assume that the longer the instrument the greater the improvement in signal-to-noise ratio. The single exception is in the study of tectonic signals that are themselves of short wavelength, for example, the study of propagating displacements near active faults.

The construction of a long baseline fluid tiltmeter is not technically difficult and there are numerous reports in the literature [e.g., see *Horsfall*, 1978 for early references: *Michelson*, 1914; *Michelson and Gale*, 1919; *Takahasi*, 1931a, 1931b; *Haalck*, 1932; *Egedal*, 1947; *Hagiwara and Yamada*, 1947; *Hagiwara and Rikitake*, 1950; *Crumrie and Palmer*, 1951; *Eto*, 1966; *Kukkamäki*, 1966; *Kääriäinen*, 1973; *Kasahara*, 1973; *Bower*, 1973; *Earthquake Res. Inst.*, 1973; *Weber and Erdelyi*, 1976; *Bower and Courtier*, 1978]. The fundamental instrumental problem is that without considerable care, thermally-induced noise can be excessive in very long instruments. The subject of thermally induced errors is treated by *Hugget et al.* [1976] and by *Beavan and Bilham* [1977]. The use of a half-filled horizontal fluid tube by *Michelson and Gale* [1919] resulted in an instrument that was essentially insensitive to thermal variations except at the ends. We have adopted this arrangement and describe the instrument in some detail below.

2. *The Michelson Gale tiltmeter applied to tectonic studies*

In 1919 Michelson and Gale reported the successful operation of two 165 m long water-pipe tiltmeters designed to monitor the solid Earth tide. The instruments consisted of buried horizontal 15 cm diameter pipes, half-filled with water, that were terminated by optical interferometers at each end for monitoring water height (Figure 1). The recording of optical fringes was achieved photographically but since the film was advanced slowly, vibra-

tion of the ground caused loss of data. To inhibit vibration-induced ripples in the end measurement interferometers a shallow water depth was used, which resulted in a somewhat limited measurement range (< 1 mm of water height).

There are several advantages to be gained from using a half-filled tube configuration for tectonic tilt measurements where stability and precision are required:

1) Uniform thermal changes caused an identical change of water height at each end. Although temperature differences between the two ends induce thermal errors there is an exact relationship between temperature variation and water height at each end. This can be arranged to be small using an optical transducer (see Appendix). Residual thermal effects on the instrument can be eliminated if a record of temperature at each end is maintained.

2) A half-filled fluid pipe eliminates the effects of thermal variations along the pipe if the period of these variations is much longer than the time of transmission of surface waves along the pipe.

3) The water surface area in a half-filled pipe can be made considerably larger than the area of the end measurement reservoirs. When the ratio of these two quantities is large, it results in a *decoupling effect* between the two ends such that the two end measurement transducers can respond virtually independently of each other. For example, if an artificial 2.5 mm vertical movement of a 10 cm diameter end reservoir were to occur at one end of a 250 m long tiltmeter, it would result in only a 1 μm change in height of the water in a 75 mm diameter pipe and remote end-reservoir. If, however, the ground tilted by 2×10^{-5} radians, it would produce a 2.5 mm water level change of opposite sign in each end reservoir. Thus, to a large extent real tilts can be separated from apparent tilts caused by end mount instability.

4) It is particularly relevant to the study of tectonic signals where instrument fidelity is important that a long baseline tiltmeter offers two independent methods for verifying the indicated instrumental tilt. First, in the event of a temporary instrumental malfunction the instrument can be arranged to provide an absolute measurement of relative height between the two ends in order that the tilt datum is not lost (see Section 7 below). Most continuously recording tiltmeters and strainmeters do not have this capacity and lose their datum should a break in the record occur. Second, the relative height between the two end-mounts can be checked to 10^{-6} radians precision using conventional optical levelling. Advanced optical levelling techniques [*Schellens*, 1965; *Gagnon et al.*, 1978] and hydrostatic levelling methods [*Hagiwara*, 1947; *Eaton*, 1959] enable verification with a precision of 10^{-7} radians.

Compared with alternative fluid arrangements [*Beavan and Bilham*, 1977] there are two principal disadvantages to the half-filled pipe configuration. The first is that the tube must be installed horizontal to within at least the vertical dimension of the pipe. In practice a cylindrical pipe must be

emplaced to within a quarter of the pipe diameter along its length in order to approach the theoretical dynamic response, although this is not difficult given a nominally horizontal surface. For example, if transparent connectors are used to join pipe sections the pipe can be levelled to millimeter precision by inspection. The second disadvantage is that the response time is slow compared to filled fluid-tube tiltmeters. The response time is limited by the propagation velocity of a surface wave (approximately 0.5 m/s). We believe that these objections are of limited importance in an instrument intended for monitoring long-term variations in surface tilt (hours to decades). The principal advantage of the half-filled tube is that it is primarily a tiltmeter of unquestionable instrumental stability. The limit to the usefulness of the instrument in applications demanding extreme stability is to be found in the attachment of the instrument to the Earth's surface. This is a weakness common to all surface deformation monitors that can be reduced but not eliminated by increasing the instrument baseline.

3. *Instrument design*

We have made a number of improvements to the water-tube tiltmeter described by *Michelson and Gale* [1919] in order to increase the dynamic range and convenience of the system. Instead of iron pipes we have used 75 mm I.D. polyvinyl chloride (PVC) to contain the fluid since the coefficient of expansion of PVC is close to that of water. Although other fluids could have been used (kerosene was used in a prototype) the quantities required argue for an easily available, inexpensive liquid. The 239 m instrument required 540 liters of water. The fluid tube is terminated at each end by an interferometric transducer unit with a digital readout to monitor fluid height changes. The end reservoirs (10 cm I.D.) are coupled to the fluid pipe by flexible tubes (Figure 2). In order to suppress rapid fluid flow into the end unit a short length of capillary tube is inserted in the lower flexible tube. The time constant for filling or emptying the end reservoir is given by

$$\tau = 8\nu\ell a^2 \, r^{-4} g^{-1} \; s$$

where ν is the kinematic viscosity of water (.01 $cm^2 s^{-1}$), ℓ and 2r are the length and internal diameter of the capillary tube, 2a is the diameter of the reservoir, and g is the acceleration due to gravity. An 8 cm length of 2 mm diameter capillary provides a 3 minute time constant in our instrument.

Each end measurement unit consists of an approximately equal-arm Michelson interferometer. Cube corners are used as alignment-free reflectors and a helium/neon laser as an emission source (Figure 2). The lower cube corner is submerged beneath the water surface such that a fringe is produced for a change in surface height

$$d = \lambda/2(\mu-1) = 954 \text{ nm}$$

where λ = 6328Å (helium/neon laser) and μ = 1.3317, the refractive index of water at 20°C. Note that the fringe position is independent of emission wavelength when the optical path difference in the two interferometer arms is zero. The maximum path difference allowable in the present design is 5 cm, hence an emission stability of $10^{-6}\lambda$ is required to reduce errors to within 10% of a fringe. This stability is easily attained by He/Ne gas lasers [*Jaseja et al.*, 1963]. These also provide a convenient collimated beam of light, although other emission sources could be used. The use of a submerged cube-corner reflector reduces one of the minor problems described by *Michelson and Gale* [1919], namely the loss of fringes caused by surface ripples (see Figure 3).

The interferometer is simple to align even when poor quality optical components are used. It was found advantageous to introduce a glass wedge in one optical path of the interferometer in order to establish parallel fringes with a 10 mm line spacing. The fringes are observed by a double-photodiode that provides a suitable quadrature signal to a reversible counter (Figure 4). The signal is displayed as a four-digit number corresponding to fringe position. In addition to a direct digital output the two least significant digits are converted to an analogue signal for chart display. The analogue output is useful in that it automatically maintains a chart record on-scale at earth tide sensitivity over the entire measurement range. The water surface height at each end is monitored together with the water temperature in each end reservoir. Atmospheric pressure and the electrical difference between the two water height outputs provide a further two channels of data.

No attempt has been made to subdivide the fringes to obtain greater resolution. The existing fringe-counting system provides a tilt resolution of approximately 10^{-9} radians in a 1 km instrument (10^{-6}/L radians for a tiltmeter of length L meters). We consider this to be adequate for tectonic studies. The instrumental output is linear over a 5 cm water height range and is accurate to better than 1%, being limited by the accuracy with which the refractive index of the water is known.

Surface tension effects in the tiltmeter are important only in the end reservoirs. The brass end units are coated with nylon to prevent corrosion and to provide a clean internal surface. The theoretical capillary elevation at the center of the 10 cm I.D. end reservoir can be estimated from Rayleigh's formula for a wide cylinder [*Rayleigh*, 1915].

$$r/a - \log_e a/H = .8381 + .2798\ a/r + \tfrac{1}{2} \log_e r/a$$

where $a = \sqrt{T/g\rho}$ and T is the surface tension, r the tube radius, H the capillary rise at the center, ρ the fluid density and g the acceleration due to gravity. For water in a 10 cm diameter cylinder H = 25 nm, a value that is insignificant compared to the magnitude of a fringe. However, the surface tension effects in a tiltmeter are complicated by *adhesion tension* at the solid fluid boundary. Adhesion tension varies with the rate of movement of the fluid across the solid and its value also depends on whether the

fluid is advancing or receding. Adhesion tension results in undesirable stick-slip motion of the water boundary, particularly when the motions are slow. To eliminate adhesion tension effects we have introduced porous filters to line the internal surfaces of the end reservoirs. The filters (Whatman cellulose extraction filters) absorb water to the top of the end reservoir. The water in the reservoir no longer "sees" the solid boundary and instead forms a zero-angle of contact meniscus against the filter. The adhesion-tension becomes vanishingly small and as a result, stick-slip motion of the water surface no longer occurs. Stick-slip events with magnitudes of between 4 μm and 12 μm were observed to occur before introducing the filters.

4. *Thermal effects*

An important advantage of the half-filled tube tiltmeter is that thermally-induced errors in the instrument are small in this configuration. The residual thermal effects can be made smaller by careful design in the geometry of the optical transducer and still further reduced by subsequent processing using the temperature record. The instrumental insensitivity to thermal variations is such that it is conceivable that the instrument can be installed on the surface with relatively modest thermal insulation. The unprocessed data from the 239 m tiltmeter at Suffern contain a temperature signal of about ten nanoradians per centigrade degree.

Temperature variations affect the tiltmeter in the following ways:

Uniform thermal variations affecting the whole instrument give rise to a symmetrical change in fluid height at each end. The height variation is made suitably small even in the presence of large temperature changes by matching the container coefficient of volume expansion to that of the fluid, e.g., PVC (21-24 x 10^{-5}/°C), water (21 x 10^{-5}/°C). Temperature *differences* between the two ends cause an apparent change in the height of the fluid in each end reservoir and a change in the refractive index of the fluid. The two effects can be arranged to result in a zero composite thermal coefficient by choosing the correct combination of water depth and depth of water above the submerged cube corner (see Appendix). This combination was not used in the prototype instrument but exact compensation for temperature differences between the two end reservoirs can nevertheless be achieved if the end temperatures are monitored and the absolute fluid depth is known. Temperature *variations along the fluid pipe* result in changes of fluid volume and pipe dimensions and may cause convection cells to be set up in the fluid. A brief discussion of the effects of convection is to be found in *Egedal* [1947]. In some circumstances a travelling wave can be initiated that travels

to the two end reservoirs at different times, resulting in an apparent tilt. The condition that this should not occur is that the initiating temperature disturbance should have a time-constant long compared to the propagation time of surface waves along the pipe. Measurements of surface wave velocities in half-filled water pipes indicate velocities of the order of 0.5 m/s, hence for a 240 m tiltmeter a thermal time constant greater than 10 minutes is necessary. We estimate that the thermal time constant for a 75 mm diameter half-filled pipe is 30 minutes in the absence of convection.

A secondary effect of spatial and temporal temperature variations along the fluid pipe is to cause pressure variations in the water-saturated air space above the fluid and additionally, to change the vapor pressure distribution. Rapid variations in the spatial temperature distribution along the pipe can contribute significantly to the instrument noise level unless the cross-sectional area of the air space is made uniform and sufficiently large to allow adequate flow. A single constriction away from the ends of a long tiltmeter, such as can be formed by allowing the half-filled tube to dip more than a quarter of a pipe diameter from horizontal, effectively divides the air space into two large gas volumes whose tendency to equilibrate is approximately proportional to the square of the cross-sectional area of the constriction. If, by accident, the constriction is made very small, effusion will dominate and the free fluid surface will depart from an equipotential surface as a result of pressure differences P_1, P_2 generated by temperature differences T_1, T_2 where

$$\frac{P_1}{P_2} = \sqrt{\frac{T_1}{T_2}}$$

[see, for example, *Champion and Davy*, 1958] resulting in an enormous dependence on temperature which we have estimated as up to 10^{-5} radians per °C in the 239 m tiltmeter. Clearly constrictions must be avoided.

5. *Experimental operation*

The tiltmeter has been tested at two locations: in Ogdensburg Seismic Observatory, New Jersey under constant temperature conditions and in an active warehouse at the Western Electric Ramapo Materials Management Center, Suffern, New York (Figure 5). The Ogdensburg instrument was 60 m long and was operated for a period of 10 months and the Suffern instrument is 239 m long and has operated since February 1978. In both cases data have been interrupted by experimental modifications to the instrument.

The 60 m Ogdensburg tiltmeter was installed parallel to the N48.5°E quartz tube strainmeter [*Major et al.*, 1964] and used the same NE concrete mount. The SW mount consisted of a temporary steel structure bolted to the concrete

floor and of sufficient elevation to compensate for the 1:100 gradient of the tunnel floor. The tube was aligned using an optical level and a laser beam, and was fastened horizontally to an existing wall using pipe straps. Water was pumped into the tube from an underground pool. In order to check instrument performance, a device to pump small amounts of water in and out of the center of the pipe was installed. This consisted of a vertical 6 mm I.D. plastic tube that could be driven remotely up or down 10 cm and whose ends were connected to the top and bottom of the pipe. The amplitude of the resulting water height change in the 60 m pipe and end units was approximately 6 μm, corresponding to 6 fringes on the two electronic outputs.

During the period of operation the tiltmeter was dismantled twice to examine the quality of the water surface. Dust particles, a minor amount of organic growth, and a decline in laser emission intensity caused a slow degradation of the fringe pattern that was corrected electronically every three weeks. One electronic unit was damaged by an electrical storm. The time constant of the 60 m tiltmeter was measured to be approximately 100s, its sensitivity 1.6×10^{-8} radians per fringe and its range approximately 1.5×10^{-4} radians. As a result of the relatively low sensitivity of the 60 m tiltmeter, the earth tide has a peak to peak amplitude of less than ten fringes on the data shown in Figures 6 and 7. It is to be noted that the long-term signal in the data is less than 10^{-8} radians/month.

There were two noise sources in the Ogdensburg tiltmeter that gave rise to sudden offsets in the data (Figure 8a,b). Under normal circumstances neither surface waves from large earthquakes (M_S 8, Δ = 130) nor vibrations from local explosions (10 kg at 200 m) gave rise to offsets in the record, although incorrect electronic adjustment can cause the up-down counter to miscount. The stability of the Ogdensburg site was such that the combined effect of constant temperature, low fluid loss, low drift and small tidal signal caused the water surface boundary at each end to remain at the same level for extended periods. The adhesion tension (discussed in Section 3 above) between the nylon coating and the water prevented the boundary layer from moving except at irregular intervals of between two weeks and two months; in between these sudden movements, when usually only part of the circumferential surface boundary would move, the water surface would strain as an elastic membrane. The amplitudes of the stick-slip events varied from 4 μm to 12 μm and clearly the tilt data between these events were subject to at least this margin of error. The introduction of a cellulose porous lining to the end reservoirs eliminated this effect in the Suffern installation.

The second source of noise at the Ogdensburg site was identified as originating in the floor beneath the temporary, steel end-mount. The observatory is sealed by double-pressure doors from atmospheric changes with periods less than about 4 hours. On opening the pressure-tight section for inspection, rapid pressure changes are introduced if a recent large change in atmospheric pressure has occurred. It was found that occasionally the

SW mount would respond with rapid vertical movements of up to 25 μm, although the NE end mount would be unaffected. The rapid vertical movement was followed by an exponential decay to its original level (Figure 8b). We believe that these movements are caused by fluid movements beneath the floor in response to air pressure changes. This identification of end-mount instability is a good illustration of the *decoupling effect* inherent in the half-filled fluid tube instrument. In a filled tube instrument (without an auxiliary, large surface area reservoir [e.g., *Eto*, 1966]) the same transient would be indistinguishable from a symmetrical tilt signal.

The Suffern tiltmeter is installed on the floor and against the northern wall of a $10^5 m^2$ warehouse operated by Western Electric, Inc. The site is less than 2 km SE of the Ramapo fault, a 180 km NE/SW trending fault system that is associated with minor seismicity [*Aggarwal and Sykes*, 1978]. The warehouse has a concrete slab floor that is flat to within 2 cm in 330 m. The two end mounts have been bolted to the reinforced-concrete wall foundations that extend to a depth of 2.5 m in unconsolidated sediments. The plastic pipe rests on the concrete floor and is continuous except where it passes two of the building's emergency exits. These were by-passed by terminating the half-filled pipe on either side of the doors and by running short flexible tubes beneath the concrete floor. It was subsequently realized that the original air tube was too narrow (6 mm) and was the reason for considerable thermally induced noise at one end until it was replaced by a 25 mm I.D. tube. At one point the fluid pipe is offset horizontally through a fire wall inside the building. Thermal insulation is placed around the end ten meters of pipe and around the end reservoirs to reduce convection effects near the ends. The remainder of the pipe is unprotected and subject to temperatures between 5 and 20°C. Thermal variations along the pipe result from air currents forced into the building through unsealed joints.

The time taken for a surface wave to travel from one end of the 239 m pipe to the other was measured to be 7.5 minutes. The surface wave arrival is characterized by a sudden increase in water height and a sequence of secondary arrivals caused by reflections at the emergency-exit, bypass tubes. To smooth the wave arrivals, short capillary tubes introduce a 3 minute time-constant between the end reservoirs and the pipe. The sensitivity of the 239 m tiltmeter is 3.99×10^{-9} radians per fringe and its range approximately 4×10^{-5} radians. Representative data are shown in Figures 9 and 10.

The interferometer optics has required dusting twice in five months and we have found it advisable to fine adjust the prototype electronics every two to four weeks. Chemical and biological contamination has occurred in the end reservoir where the laser beam enters the water. The water remains transparent though a translucent film appears on the surface of the submerged corner cube. It appears that the interferometer fringe pattern is degraded sufficiently after about 3 months at 16°C to make it worthwhile to clean the reflector surface. At lower temperatures the degradation appears to be slower.

6. *Data*

Ogdensburg

Six weeks of the 60 m Ogdensburg tiltmeter data are shown in Figure 7. The plot is based on hourly values read from the strip chart records. The values have been smoothed with a zero-phase low-pass Butterworth filter having a 6 db point at 6 c/d and a roll-off of 48 db/octave. The SW end data are considerably more noisy than the NE end and reflect the poor stability of the concrete floor mount compared to the NE strainmeter end mount.

The NE end data show an offset on day 345 that is caused by adhesion tension of the water surface. Two similar events are apparent on the SW end data. Tides are visible on the instrument despite adhesion tension because the transducer is at the center of the end reservoir, some 5 cm from the adhering surface. The water at the center of the reservoir moves to follow the equipotential surface and this movement is resisted by elastic forces in the water surface. Only when the equipotential surface has moved sufficiently far are the forces great enough to break the adhering surface, and when this occurs a sudden offset is seen in the data. Usually the whole adhering surface does not break at once; a typical break is 5 cm, some 15% of the end reservoir circumference, which gives rise to an offset in the data of some 4 μm. This reason for the offsets in the Ogdensburg record was not realised until the instrument was reinstalled at Suffern where the water height changes in the end reservoirs were some four times larger and adhesion jumps occurred several times per tidal cycle. Thus the tilt record in Figure 7 has been plotted with the events removed from the data, though they have not been removed from the individual water-level plots. Clearly, however, the adhesion tension events represent part of the long-term signal in the data.

The NE end operated almost continuously for 10 months with very little long-term signal (for example, Figure 7), while the SW end, which suffered damage from an electrical storm and was out of action for some months, showed considerable long-period variations. This gives another example of how the decoupling effect between the ends can be used to recognize and correct for end-mount instability. It is not possible unambiguously to separate real tilt from apparent tilt (due to end-mount instability) simply from the water-level records at each end. However, in the case where one end gives a virtually straight line record while the other shows large variations, it is strongly suggestive that the variations are due to end-mount movements rather than to real tilt. In the case of the Ogdensburg data we assume from the flatness of the NE end record that there was little or no water loss during the experiment, and we hence estimate from the combined end records that the net tilt over ten months was a few tenths of a microradian.

Suffern

The data collected from Suffern between 1 March and 22 July 1978 are plotted in Figure 10. This figure is based on hourly values read from strip charts; no subsequent filtering has been applied to the data. The first part of the tilt and water level records is heavily contaminated by thermally induced noise caused by a constriction in the air path. On day 105 this was corrected and the signal-to-noise ratio improves dramatically. The gaps in the data are principally due to recorder malfunctions. Close examination of the tidal signal shows that the character of the tides is somewhat different on the east and west end transducers. The reason for this is that the true tidal signals are 180° out of phase at the two ends, whereas diurnal temperature changes cause signals that are approximately in phase. There are also longer period variations in the water-level data, some of which correlate clearly with the temperature or pressure records.

An important observation is that the amplitude of ground noise at approximately 10 minute periods is seldom more than one fringe and is usually less than a tenth of this amplitude. Thus given a least count of one fringe, a sampling interval of one minute is adequate to provide unbiased data. The exception is for large distant earthquakes with significant seismic energy at periods greater than 5 minutes.

Because of the close matching of expansion coefficients of PVC and water, uniform temperature changes along the pipe give rise to a change of water height in each end reservoir of less than 0.5 μm/°C. Temperature variations at the ends are far more important, resulting in water height changes of up to 4 μm/°C, depending on the design of the reservoir (see Appendix). Furthermore, if the temperature varies differently, or if the water depth is different at each end then the water height changes will be different, resulting in an apparent tilt; temperature variations along the pipe give rise to identical water height changes at each end. It is therefore desirable to correct the two water level records separately for temperature effects before combining them to give the tilt. Note that in Figure 10 no corrections have been made to the data.

During the $4\frac{1}{2}$ months of operation the water level at the east end has fallen approximately 100 μm while that at the west end has risen 65 μm, resulting in a net tilt up to the east of 6.9×10^{-7} radians. As we discuss below, some of this may be apparent tilt due to end-mount instability. Over the four months the mean temperature has risen by 10°C, which we estimate should cause a rise of 40 μm in water level in each end. In fact, the apparent mean water level has fallen by about 18 μm. This discrepancy may be due to plastic deformation of the PVC pipe, to minor leakage of water or of water vapor, to end-mount instability, or to thermal

bending of the floor of the building. It should be noted that the overall water level changes quoted above are subject to some uncertainty due to the gaps in the data; the prototype instrument has not yet been provided with a means for checking absolute water height. It is, however, clear from the above that there are no important leaks in the instrument.

A local earthquake (m_b = 2.9) occurs on day 181 with an aftershock (m_b = 2.0) four hours later. The events were located 7 km to the southwest of the tiltmeter and at a depth of 5 km. There is no clear correlation of tilt with the earthquake and the record shows no change in character before or after the earthquake, although there is a persistent tilt down to the west starting 20 days before and lasting until a few days afterward. There was no tilt offset at the time of the event.

In the remainder of this discussion of data analysis we use only the data from day 110 onwards, after the constriction was removed from the air path. Rather than estimate the temperature effect on the water level data by direct calculation of the expected height change (see Appendix), we have calculated a non-causal least-squares Wiener filter using the water level time series as desired output and the temperature series as input [see *Beavan and Goulty*, 1977]. Figure 11 shows the water level data after removal of the temperature effects and of a least-squares best fit straight line. 36% of the energy in the east end water level series was predicted from the temperature record using a filter of length ± 1½ days, and this was not significantly improved by using a longer filter. In contrast, the west end required a filter of length ± 3 days, and 30% of the energy in the series was predicted. This difference in response time between the west and east ends clearly cannot be associated with direct temperature effects on the instrument. We feel that the long filters required reflect local movement of the end mounts, particularly the west end, in response to ground temperature changes. As mentioned earlier, the end mounts are attached to the concrete foundations of the building, which are pilings 2.5 m deep in unconsolidated sediments and land fill. When more data become available an examination will be made of whether the water level-temperature filters remain stable with time.

Cross-spectral analysis [see method "B" of *Beavan and Goulty*, 1977] between the east end temperature and water level records gives a coherence of about 50% at 1 c/d with an admittance of 1.2×10^{-8} rad/°C and a phase lag of 25°. At the west end the corresponding figures are 50%, 0.8×10^{-8} rad/°C and 110°. The significant difference in phase response is due to there being a tidal signal at 1 c/d as well as a temperature signal.

It is of interest that the temperature traces at the two ends are significantly different. Cross-spectral analysis shows that at periods longer than two days the coherence between the temperature records is about 90% and the admittance about unity with zero phase. At 1 c/d the coherence estimate is 97% and the west end temperature is about 50% larger than and has a 20° (1¼ hour) phase lead over the east. At higher harmonics of 1 c/d

the coherence is lower, but the admittance appears to decrease somewhat, with the west end retaining a small phase lead. These differences are presumably due to a shadow effect. The coherence between the temperature-corrected tilt record (the difference between the two traces in Figure 11) and the pressure is small, though there is some coherence between the individual water levels and pressure. A Wiener filter using the temperature-corrected east water level as desired output and the pressure as input extracted a further 30% of noise energy from the record, and a similar result was obtained for the west end.

An interesting result was obtained by comparing the amplitude of water height variations at each end at tidal periods. Curiously, the data indicate that although the phases are exactly 180° apart the east amplitude is approximately 10% larger than the west at the M_2 frequency. This suggests that the local surface is not planar but has a periodic curvature of short wavelength. Such curvature could be introduced by strain-tilt coupling or tilt-tilt coupling given reasonable surface inhomogeneity [*Harrison*, 1976].

We have calculated the admittance between the observed tilt and the solid earth tilt tide by cross-spectral analysis and the results are given in Table 1. No estimate of ocean load tide has yet been made. We used the raw tilt data (Figure 10) for these calculations rather than the temperature-corrected tilt, since the application of the Wiener filters removes a significant length from the ends of the records and we require as long a data length as possible to get good resolution of the tides. However, the gaps in the data were filled in by Wiener filtering from the solid earth tide series as gaps can lead to serious errors in admittance estimates [*Beavan and Goulty*, 1977]. We give the power spectrum of the data in Figure 12a; thermal contamination is evident in the spectral peaks at 3, 4, 5, and 6 c/d. No coherence was obtained at the O_1 tidal frequency and the phase of -179° at the K_1P_1 frequency is presumably a reflection of the thermal signal dominating the tide.

As discussed earlier, it is not possible unambiguously to separate true tilt from apparent tilt caused by end-mount instability simply from the two water level records; some further constraint is needed to effect such a separation. An approach we have experimented with is to attempt to extract only those parts of the two water level records which are coherent with each other, and to assume that non-coherent parts are due to end-mount instability. This is done by generating a Wiener filter using the east end as desired output and the west end as input, then filtering the west end time series to give that part of the east end series coherent with the west end. Then the process is repeated with east and west reversed. The results of this calculation are shown in Figure 13, where we have used the raw water level data of Figure 10 and Wiener filters of length ± 6 days. Note that all the plots in Figure 13 have had a least-squares best fit straight line removed. This is a necessary prerequisite to cal-

culating a Wiener filter so we are fundamentally unable to extract any information about persistent tilt trends by this method. We plot the power spectrum of the tilt (Figure 13g) generated by this method in Figure 12b; the resolution is worse than in Figure 12a because of the shorter data length due to the application of the Wiener filter. The reduction in noise level at all frequencies is striking.

7. *Discussion*

The quality of the tiltmeter data from the 239 m instrument is good when it is remembered that the instrument is in an area of industrial activity and is exposed to surface temperature variations. Movements of surface loads occur near the ends of the instrument (on one occasion a fork-lift truck punctured the fluid-tube) without noticeably affecting the tilt signal; however, there are significant thermal effects in the data. That thermally induced noise can be effectively reduced is demonstrated by the improved quality of the processed data from the east end of the tiltmeter. That the residual noise is not entirely of instrumental origin can be deduced from the poorer quality of the data from the west end even after measured temperature and pressure variations have been accounted for. It is probable that the upper layers of the ground in the vicinity of the tiltmeter end mounts contribute to the observed long-period signal in the data. Clearly, improvements to the data quality could be achieved by providing improved thermal stability for the fluid tube (for example by shallow burial) and by referencing the end measurement points to presumably more stable subsurface strata. In certain applications, for example in volcanic studies, the present noise level may be acceptable. In such cases an above-ground installation might be considered with a nominally insulated fluid-tube resting horizontally on supports between carefully located end-measurement points.

The optical interferometer system for monitoring fluid height is accurate, linear, relatively insensitive to temperature effects and has the attraction of providing a direct digital output without requiring calibration. These qualities are ideally matched to the transducer requirements of a fluid-tube tiltmeter. However, in its present form the system requires regular weekly supervision to assure a reliable output. Minor improvements to the electronics to automatically compensate for fringe degradation would render such maintenance unnecessary. Organic growth in the fluid and contamination of the water surface can be inhibited by suitable additives. Power consumption could be reduced using a pulsed laser or an alternate emission source.

A major advantage can be gained by relating the indicated fringe value to the absolute depth of the water since the instrument can then be used to indicate the relative height difference between the two ends

even when recording failures occur. We considered using the interferometer to measure the absolute water depth in each end reservoir by counting fringes as the reservoir filled from an initial empty state. Unfortunately, we have found no satisfactory way to monitor the thickness of the initial surge of water as it crossed the submerged cube-corner. Micrometers have been used in other water-tube tiltmeters to determine the instantaneous water height. A repeatability of better than 3 μm is usually claimed by driving a submerged micrometer toward the water surface [*Eaton*, 1959]. A more convenient arrangement that we have tested experimentally is to drive a micrometer toward the surface from above. A high impedance switch closes when the resistive path to the water surface reduces below 20 MΩ. In our tests we have photographed the stainless-steel micrometer pointer several microseconds after the closure and find that the water surface has not yet moved to form a meniscus. The repeatability of these measurements is of the order of 1 μm, though it is extremely critical of surface contamination of the micrometer pointer. The measurement cannot be repeated immediately afterwards, as a film of water changes the surface properties of the pointer, resulting in discrepancies of tens of μm. An automatic device to obtain readings spaced 1 minute apart showed good repeatability since in this time the surface film had time to evaporate. We have noted earlier that 1 minute samples could provide unbiased data from the Suffern instrument for all but the largest earthquakes.

Acknowledgments. We wish to thank Western Electric Inc. for permission to site the tiltmeter in their Materials Management Center at Suffern, New York. Martin Berry designed the fringe counting electronics. Merrill Conner and Daniel Grob have assisted in maintenance of the instruments at Ogdensburg and at Suffern. April Hooper helped with the reading of the strip-chart data. The design and building of the tiltmeter has been funded by the National Science Foundation, Geophysics Program, under contract EAR 76 03957. Funds for the maintenance of the Suffern installation are being provided by New York State Energy Research and Development Authority Phase 5.

TABLE 1. Comparison of observed tilt with solid earth tilt tide. The 2160 hours of data were broken into 4 blocks of 540 hours each for estimating the coherence.

	K_1P_1	M_2	S_2K_2
Frequency of measurement c/d	1.022	1.911	2.000
Coherence	.81	.995	.95
Modulus of admittance	1.00	1.53	1.36
Phase (lag) of admittance	-179°	-13°	-4°

APPENDIX

Temperature Compensation in the Water Level Transducers

We refer to Figure 14 and define the following quantities:

α	Thermal expansion coefficient of reservoir material at 20°C. 1.9×10^{-5}/°C for brass	
γ	Thermal expansion coefficient of fluid at 20°C.	21×10^{-5}/°C for water.
μ	Refractive index of fluid at 20°C.	1.3317 at 6328Å for water.
β	Thermal coefficient of μ	-8.0×10^{-5}/°C for water.
T	Temperature difference from 20°C.	

At 20°C in the absence of tilt the optical path length measured from the half silvered mirror along the horizontal arm of the interferometer is $2c'$. In the vertical arm it is $2c + 2(\mu - 1)z$. Hence the optical path difference is

$$2(c - c') + 2(\mu - 1)z.$$

We ignore the path through the glass of the cube-corners as we assume this is independent of temperature.

If the water level changes by δh due to a true tilt of the ground, and the temperature changes from 20°C, the optical path length in the horizontal arm is $2c'(1 + \alpha T)$. In the vertical arm, it is

$$2\{c(1+\alpha T) + [\mu(1+\beta T) - 1][(z+d)(1+(\gamma-2\alpha)T) - d(1+\alpha T) + \delta h]\}$$

The apparent height change in the reservoir from the initial position is given by the optical path difference divided by $2(\mu-1)$. This is

$$\delta h + \frac{(c-c')\alpha T}{\mu-1} + (\gamma-2\alpha + \frac{\mu\beta}{\mu-1})\, Tz + (\gamma-3\alpha)\, Td$$

Hence an initial step in reducing thermal effects is to make the interferometer equal arm, $c = c'$.

Assuming this has been done, the height change is

$$\delta h + [(\gamma-2\alpha + \frac{\mu\beta}{\mu-1})z + (\gamma-3\alpha)d]\ T$$

and the temperature coefficient of the reservoir is given by the quantity in square brackets. Because the expansion coefficient and the thermal coefficient of refractive index of water are of opposite sign, this can be arranged to be close to zero by suitable choice of z and d. Using the numerical values above, the water height change becomes

$$\delta h + [-49.3z + 15.3d] \times 10^{-5}\ T$$

Hence z should be about 0.3d for optimal compensation of temperature effects within the end reservoirs. We note that it is possible to modify the temperature coefficient simply by adjusting the arm length difference, c-c'.

REFERENCES

Aggarwal, Y. P., and L. R. Sykes, Earthquakes, faults, and nuclear power plants in southern New York and northern New Jersey, *Science, 200*, 425-429, 1978.

Beavan, J., and R. Bilham, Thermally induced errors in fluid tube tiltmeters, *J. Geophys. Res., 82*, 5699-5704, 1977.

Beavan, R. J., and N. R. Goulty, Earth strain observations made with the Cambridge laser strainmeter, *Geophys. J. Roy. astron. Soc., 48*, 293-305, 1977.

Bilham, R., and J. Beavan, Tilt measurement on a small tropical island, *Conf. Meas. Ground Strain Phenomena rel. to Earthq. Prediction*, Carmel, Sept. 1978.

Bower, D. R., A sensitive water-level tiltmeter, *Phil. Trans. Roy. Soc. Lond., Ser. A-274*, 223-226, 1973.

Bower, D. R., and N. Courtier, Long-baseline tilt observations in a mine near Ottawa, *Canadian Geophys. Union Meeting*, London, Ontario, May 13-17, 1978.

Champion, F. C., and N. Davy, *Properties of Matter*, pp. 1-334, Blackie and Son, Glasgow, 1958.

Crumrie, K. C., and J. E. Palmer, Hydrostatic level for elevation surveying, *Geophysics, 16*, 486-493, 1951.

Davis, P., K. Evans, J. Horsfall, and G. King, Long baseline tilt and strain measurement, *1977 Recent Crystal Movement Symposium*, Stanford, Ca., Aug. 1977.

Earthquake Research Institute, Technical Division, Construction of a float type water-tube tiltmeter, *Bull. Earthq. Res. Inst., 9*, pp. 1-8, 1973. (in Japanese)

Eaton, J. P., A portable water tube tiltmeter, *Bull. Seismol. Soc. Amer., 49*, 301-306, 1959.

Egedal, J., On the application of the hydrostatic method to levelling and to determination of vertical movements in the Earth's crust, *Danish Meteor. Inst. Publ. 10*, 1-64, 1947.

Eto, T., A recording water tube tiltmeter, *Bull. Dis. Prev. Res. Inst., 15,* 21-59, 1966.

Gagnon, P., J. Jobin, and R. Sanchez, Evaluation and monitoring of long-term tilting of the crust by geometric levelling (abstract), *Canadian Geophys. Union,* London, Ontario, May 15-17, 1978.

Haalck, H., Ein quecksilberneigungsmesser von hoher empfindlichkeit, *Z. Geophysik, 8,* 256-271, 1932.

Hagiwara, T., Observations of changes in the inclination of the Earth's surface at Mt. Tsukuba, *Bull. Earthq. Res. Inst., Tokyo Univ., 25,* 27-32, 1947.

Hagiwara, T., and J. Yamada, Changes in inclination of the Earth's surface observed with the water tube tiltmeter, *Earthq. Res. Inst. Spec. Publ. 5,* 179-185, 1947.

Hagiwara, T., and T. Rikitake, Observation of the deformation of the Earth's surface in the vicinity of the epicenters of the Imaichi earthquake, *Bull. Earthq. Res. Inst., Tokyo Univ., 4,* 435-441, 1950.

Harrison, J. C., Cavity and topographic effects in tilt and strain measurement, *J. Geophys. Res., 81,* 319-328, 1976.

Harrison, J. C., and K. Herbst, Thermoelastic strains and tilts revisited, *Geophys. Res. Lett., 4,* 535-537, 1977.

Haubrich, R. A., and G. S. MacKenzie, Earth noise, 5 to 500 millicycles per second, 2. Reaction of Earth to oceans and atmosphere, *J. Geophys. Res., 70,* 1429-1440, 1965.

Herbst, K., Interpretation von Neigungsmessungen im Periodenbereich oberhalb der Gezeiten, Ph.D. thesis, Technischen Universität Clausthal, 1976.

Horsfall, J. A. C., Ph.D. thesis, Univ. Cambridge, U. K., 1978.

Huggett, G. R., L. E. Slater, and G. Pavlis, Precision levelling with a two-fluid tiltmeter, *Geophys. Res. Lett., 3,* 754-756, 1976.

Jaseja, T. S., A. Javan, and C. H. Townes, Frequency stability of He/Ne masers and measurements of lengths, *Phys. Rev. Lett., 10,* 5, 165-167, 1963.

Kääriäinen, J., Über die 50m lange rohrlibelle zur untersuchung der neigung der erdkruste, *Finnish Geod. Inst. Rept. ISBN 951-711-002-2,* Helsinki, 1973.

Kasahara, K., Tiltmeter observation in complement with precise levelling, *J. Geod. Soc. Japan, 19,* 93-99, 1973, (in Japanese).

Kükkamaki, T. J., Recording of the secular land tilting with pipe level, Proc. 2nd Intl. Conf. Recent Crustal Movements, Aulanko, Finland, Aug. 3-7, 1965, *Annales Acad. Scient. Fennicae, Ser. A-III,* Helsinki, 1966.

Major, M. W., G. H. Sutton, J. Oliver, and R. Metsger, On elastic strain of the Earth in the period range 5 seconds to 100 hours, *Bull. Seismol. Soc. Amer., 54,* 295-346, 1964.

McHugh, S., and M. J. S. Johnston, An analysis of coseismic tilt changes from an array in central California, *J. Geophys. Res., 82,* 5692-5698, 1977.

Michelson, A. A., Preliminary results of measurements of the rigidity of the Earth, *Astrophys. J., 39,* 105-138, 1914.

Michelson, A. A., and H. G. Gale, The rigidity of the Earth, *Astrophys. J., 50,* 330-345, 1919.

Rayleigh, L., On the theory of the capillary tube, *Proc. Roy. Soc. Lond., Ser. A-92,* 184-195, 1915.

Schellens, D. F., Design and application of automatic levels, *Can. Surveyor, 20,* 16-22, 1965.

Sorrels, G. G., J. A. McDonald, Z. A. Der, and E. Herrin, Earth motion caused by local atmospheric pressure changes, *Geophys. J. Roy. astron. Soc., 26,* 83-98, 1971.

Stauder, W., and S. T. Morrissey, Tiltmeter array in New Madrid, *Semi-Annual Tech. Rept. No. 3,* USGS Contract 14-08-0001-15848, 1978.

Takahasi, R., Preliminary report on the observation of the tilting of the Earth's crust with a pair of water pipes, *Bull. Earthq. Res. Inst., 8,* 143-152, 1931a.

Takahasi, R., Tilting motion of the Earth's crust observed at Kawana, *Bull. Earthq. Res. Inst., 9,* 1931b.

Warburton, R. J., and J. M. Goodkind, Barometric pressure variations and gravity, *Geophys. J. Roy. astron. Soc., 48,* 281-292, 1977.

Weber, J. R., and M. Erdelyi, Ice and ocean tilt measurements in the Beaufort Sea, *J. Glaciol., 17,* 61-71, 1976.

Wood, M. D., and N. E. King, Relation between earthquakes, weather, and soil tilt, *Science, 197,* 4299, 154-156, 1977.

Wyatt, F., and J. Berger, Correlations of short based tilt measurements and long base strain measurements (abstract), *EOS, Trans. Amer. Geophys. Union, 59,* 4, 1978.

Yamada, J., A water-tube tiltmeter and its application to crustal movement studies, *Earthq. Res. Inst. Rept. 10,* 1-147, 1973 (in Japanese).

Ziolkowski, A. M., Prediction and suppression of long-period nonpropagating seismic noise, *Bull. Seismol. Soc. Amer., 63,* 937-958, 1973.

Zschau, J., Air pressure induced tilt in porous media, in *Proc. 8th Intl. Symp. Earth Tides,* Bonn, 1977.

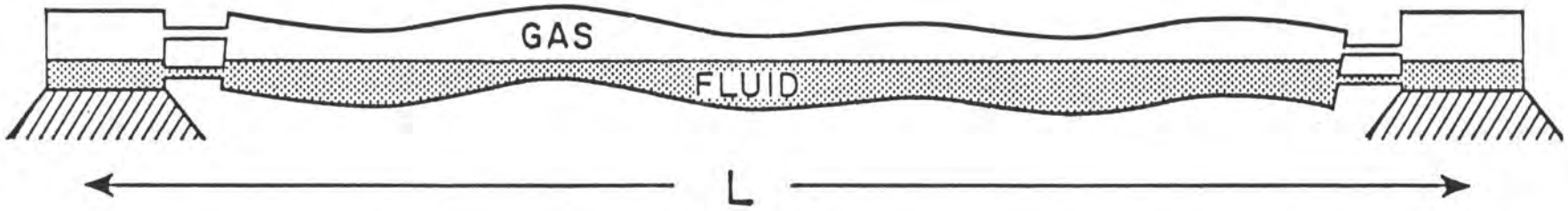

Figure 1. Schematic arrangement of the half-filled fluid tube tiltmeter; the baseline, L, can be many hundreds of meters. The water surface is continuous between the two end measurement reservoirs. Ground tilt, T, causes an equal and opposite change of water level, δh, at each end where $T = \frac{2\delta h}{L}$.

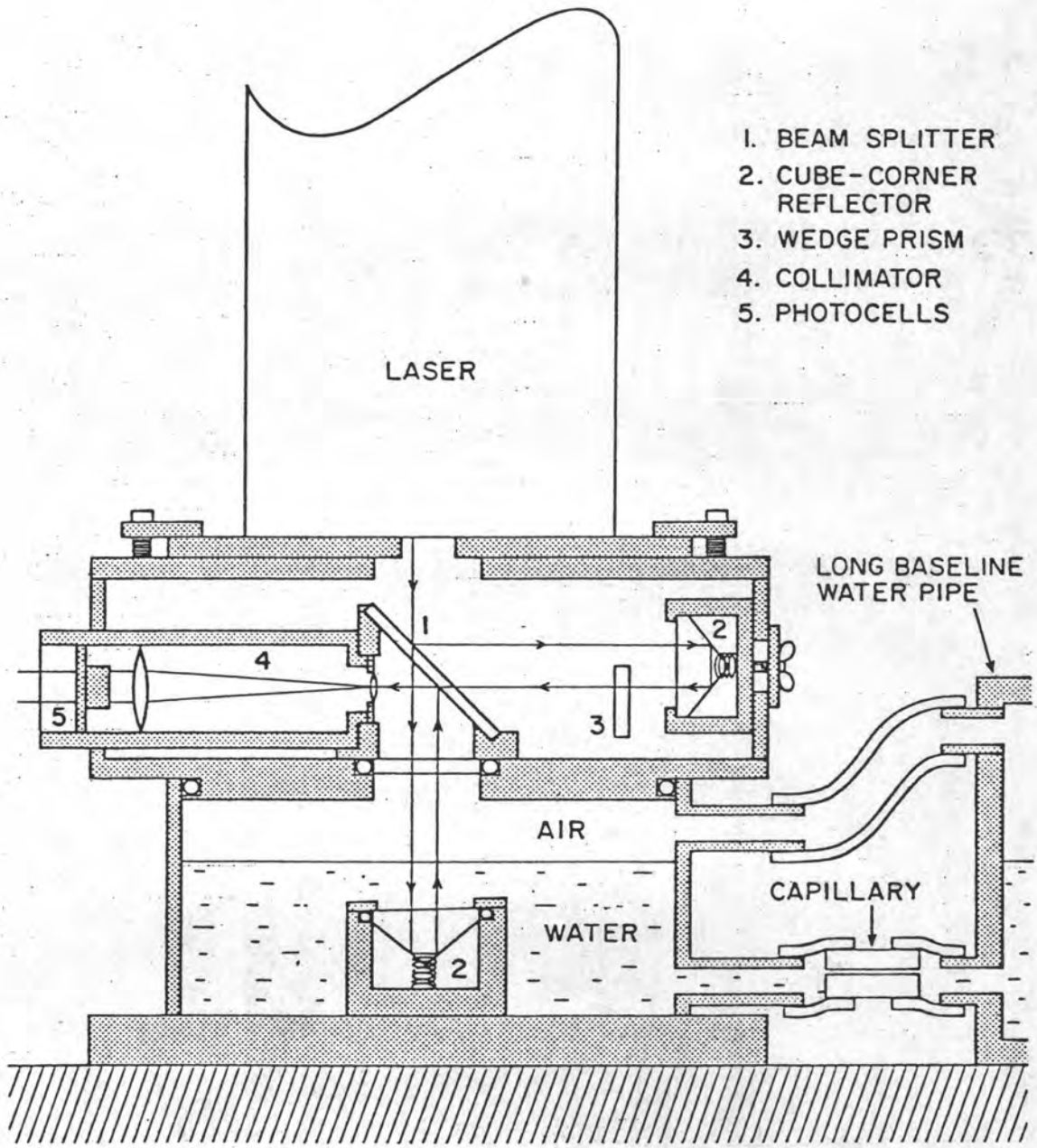

Figure 2. Cross-section of one of the two equal-arm Michelson-interferometer water-depth transducers. The uncollimated light from a He/Ne gas laser is split by semi-reflector (1) into a vertical and horizontal beam. The transmitted vertical beam passes through a window into the pressure-tight 10 cm diameter reservoir and reflects from a submerged 2.5 cm cube corner. Variations in water-level change the optical path length and result in fringe movements upon recombination with the horizontal beam. The visible fringes are converted from circular to parallel using a wedge (3) and collimated (4) to produce a 1 cm fringe spacing that is observed by the twin photocell (5). The laser can be replaced without additional alignment and due to the small physical size of the system high quality optics are not essential. The units are made of brass and lined internally with nylon.

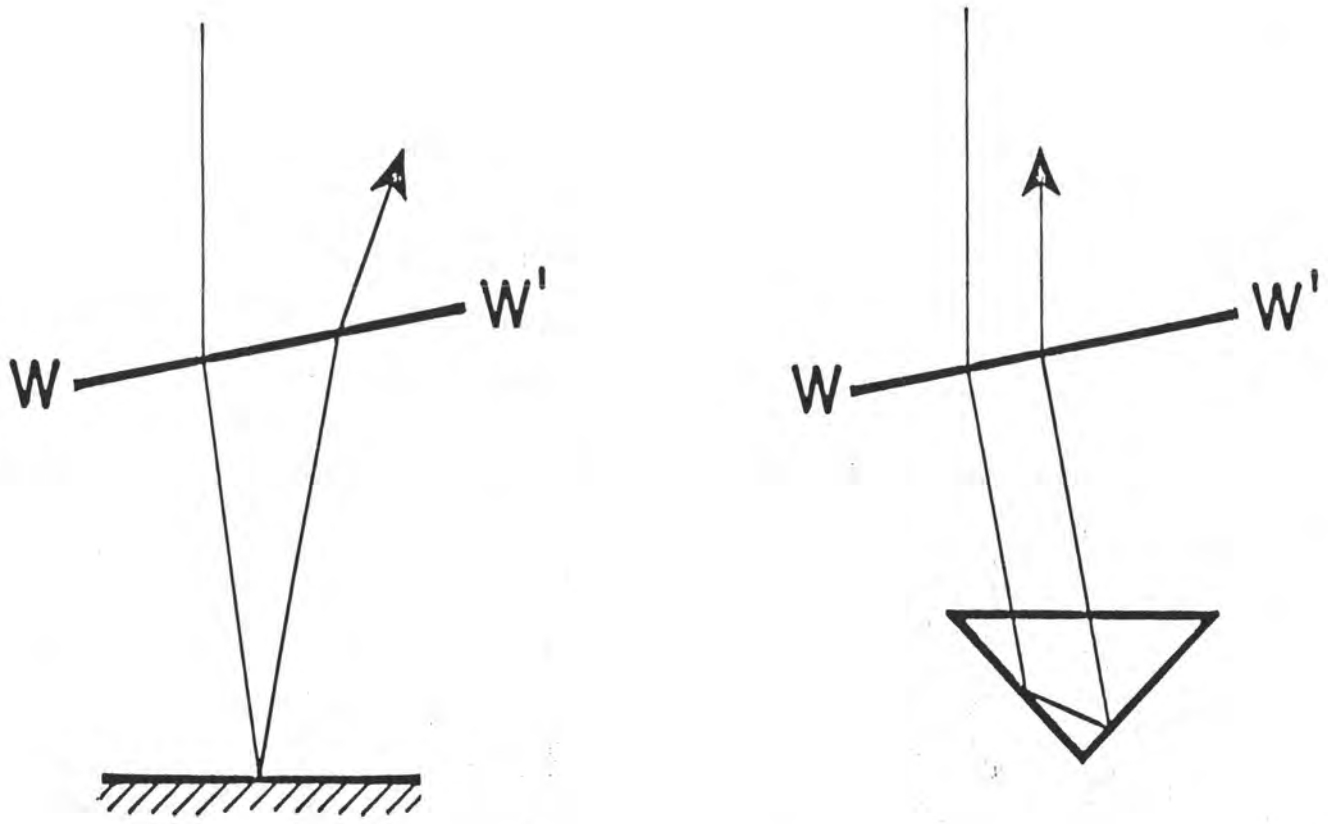

Figure 3. There are several advantages to be gained through the use of a cube-corner subsurface reflector compared to the plane-mirror used by *Michelson and Gale* [1919]. The return beam from a plane mirror diverges from the original beam if the water-surface, WW', slopes. This hinders alignment, can cause loss of fringes in the presence of waves and limits the allowable water depth. A cube-corner will return the beam parallel to the outgoing beam unless the water surface is curved, for example by large-amplitude, short-wavelength ripples.

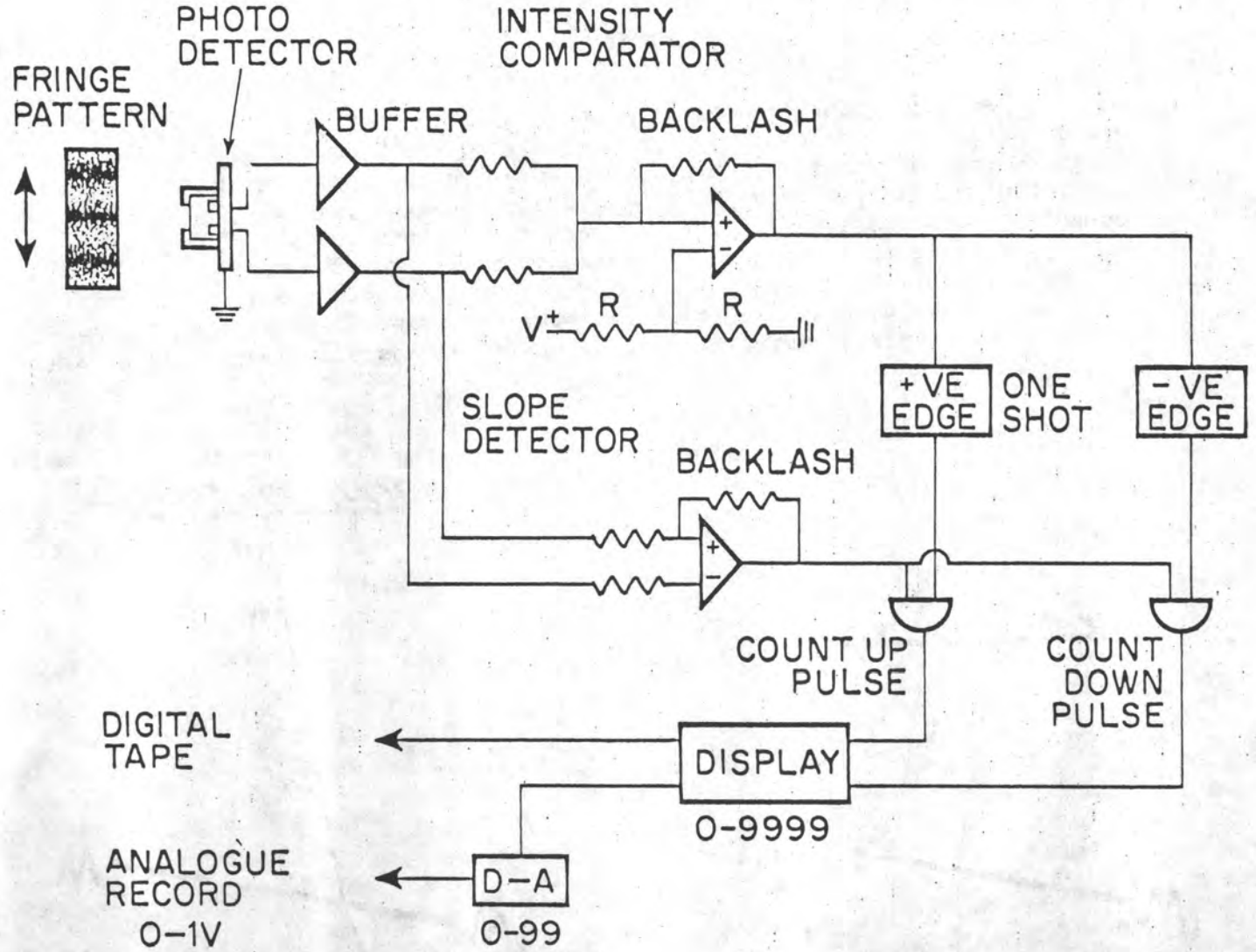

Figure 4. Schematic electronics of the water level transducer. The complete system, including laser and display requires 40 W of electrical power at 120V. A standby 12V battery and inverter provide 10 hours of emergency power in case of line failure. Each fringe corresponds to 954 nm; the display range to 9.54 nm and the analogue output to 95.4 μm full-scale. The transducer has a range that is limited mechanically to approximately ± 25 mm. The maximum fringe count rate is approximately 1 KHz, corresponding to a water elevation velocity greater than 5 cm per minute.

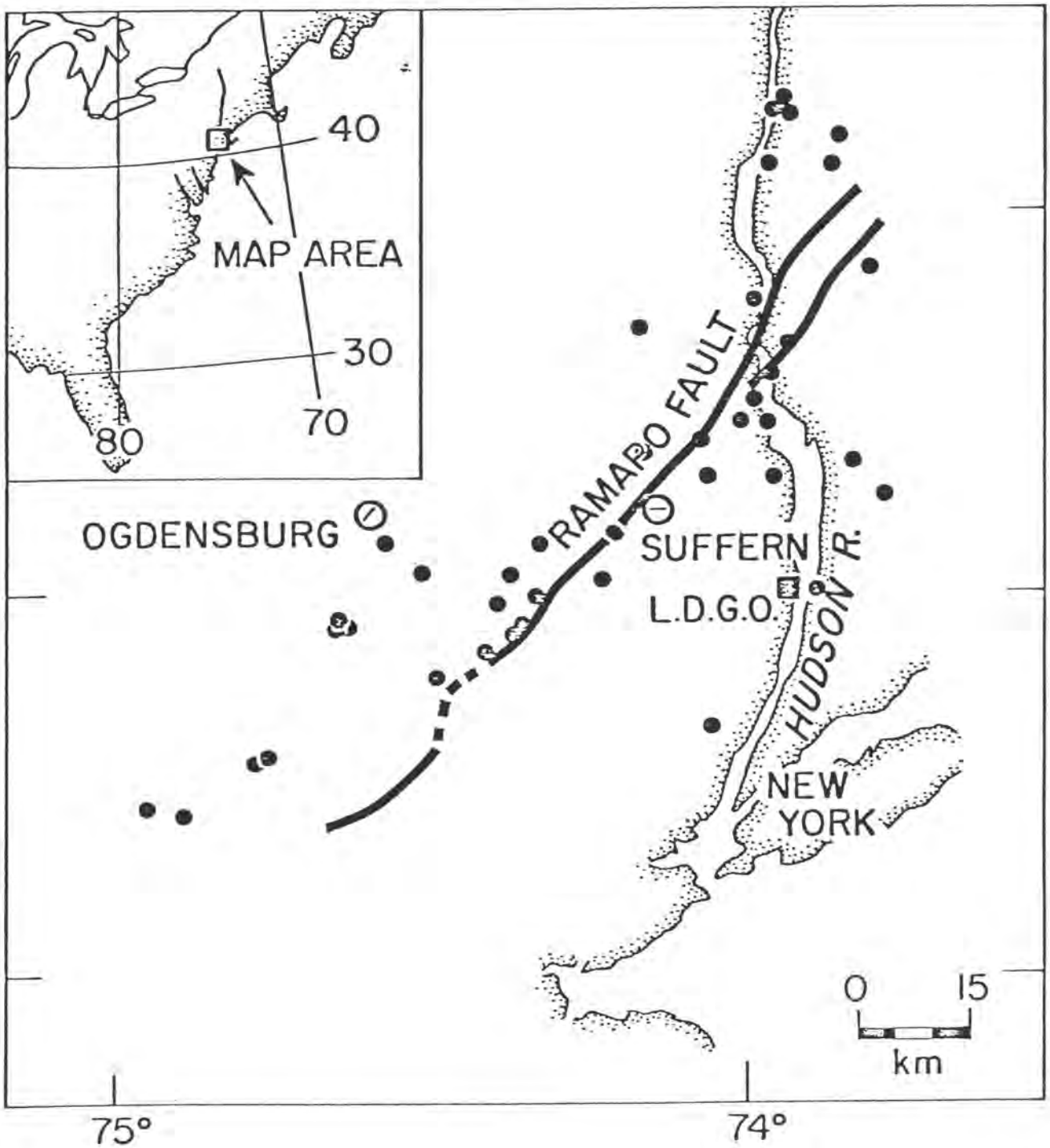

Figure 5. Map showing location and orientation of the two tiltmeter test sites at Ogdensburg, NJ and Suffern, NY. The map is taken from *Aggarwal and Sykes* [1978], with additional epicenter locations, and includes all instrumentally detected earthquakes near the Ramapo fault system between 1962 and July 1978. An earthquake, m_b = 2.9, occurred on June 30, 1978 on the Ramapo fault 5 km deep and 7 km SW of the 239 m Suffern tiltmeter. The latitude, longitude and azimuth of Ogdensburg and Suffern are, respectively: 41.088°N, 74.596°W, N48.5°E and 41.115°N, 74.125°W, N106°E.

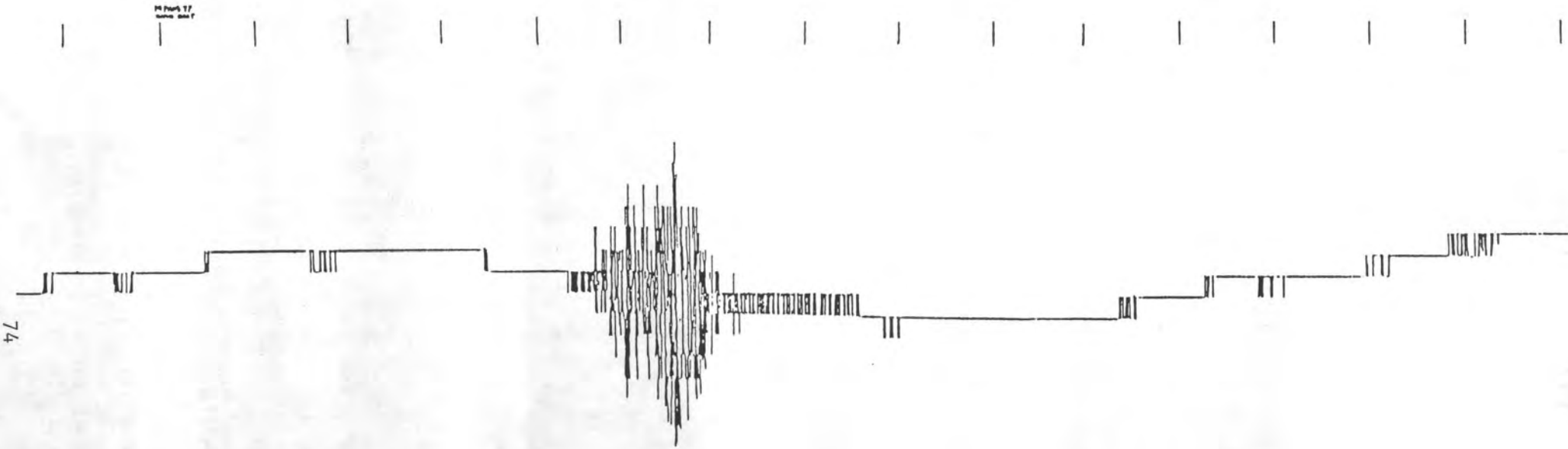

Figure 6. The Sumbawo earthquake, Indonesia (M_S = 7.9) of 1977 Aug. 19 recorded at Ogdensburg Observatory. The SW end of the 60 m tiltmeter was not operating at the time. The tilt signal on this record corresponds to 3.2 x 10^{-8} radians per fringe. The earthquake is superimposed on a tilt tide with an amplitude of approximately four fringes. Time marks occur at hourly intervals. The unfamiliar coda shape is the result of the 3 minute time constant hydraulic filter.

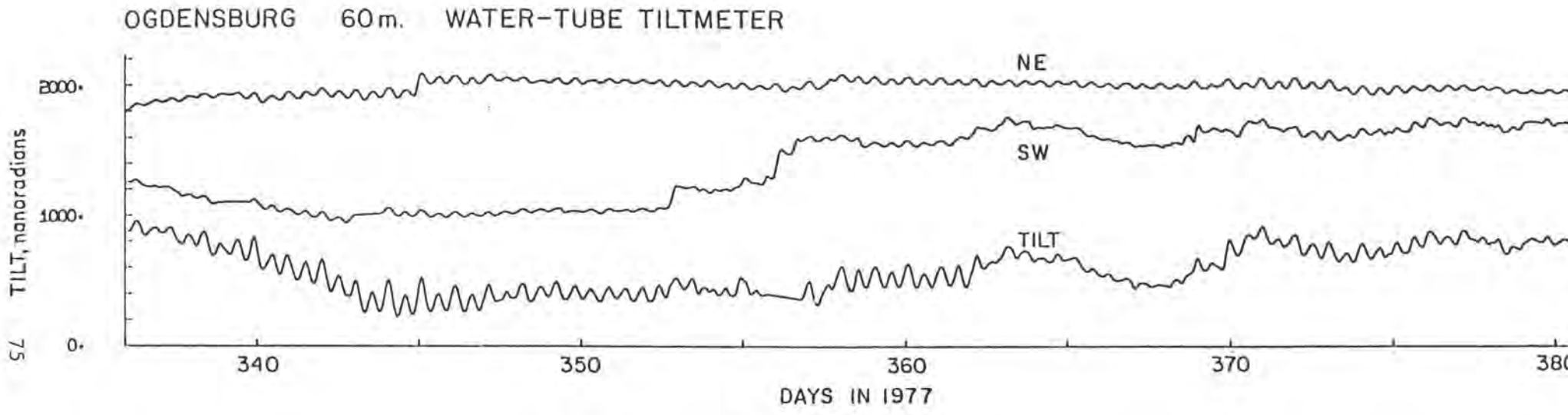

Figure 7. Six weeks of Ogdensburg tilt data collected between 1 Dec. 1977 and 15 Jan. 1978. The data were read from strip charts (Figure 6), then twice passed through a 2-pole Butterworth filter with 3 db point at 6 c/d, once forwards and once backwards, resulting in a zero phase filter with a roll off of 48 db/octave above 6 c/d. The SW end has been plotted with reverse polarity so that the tides appear in phase on the two end level records. Note the adhesion tension events on the NE end near day 345 and on the SW end near days 353 and 356. These have been removed from the tilt record.

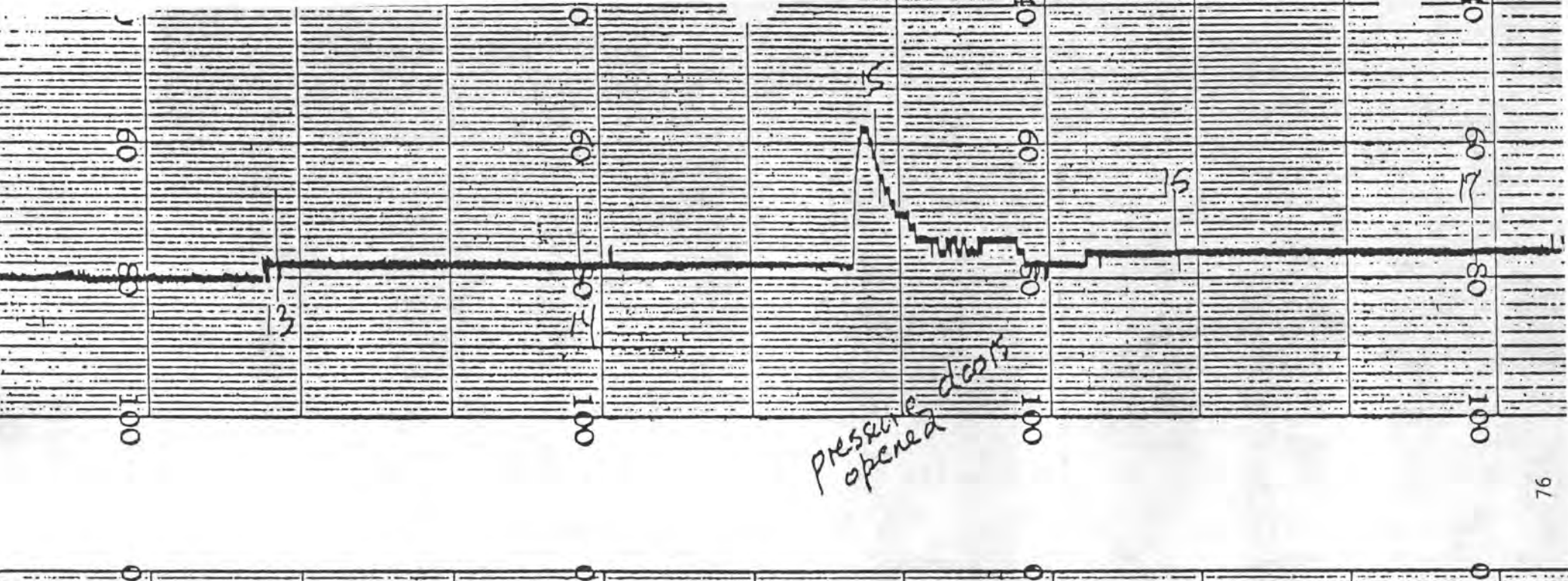

Figure 8b. Rapid pressure changes in Ogdensburg Observatory caused instability on the SW end mount. In this case the end mount rose 104 μm within 3 minutes of opening the pressure tight section of the Observatory and recovered its original position after one hour.

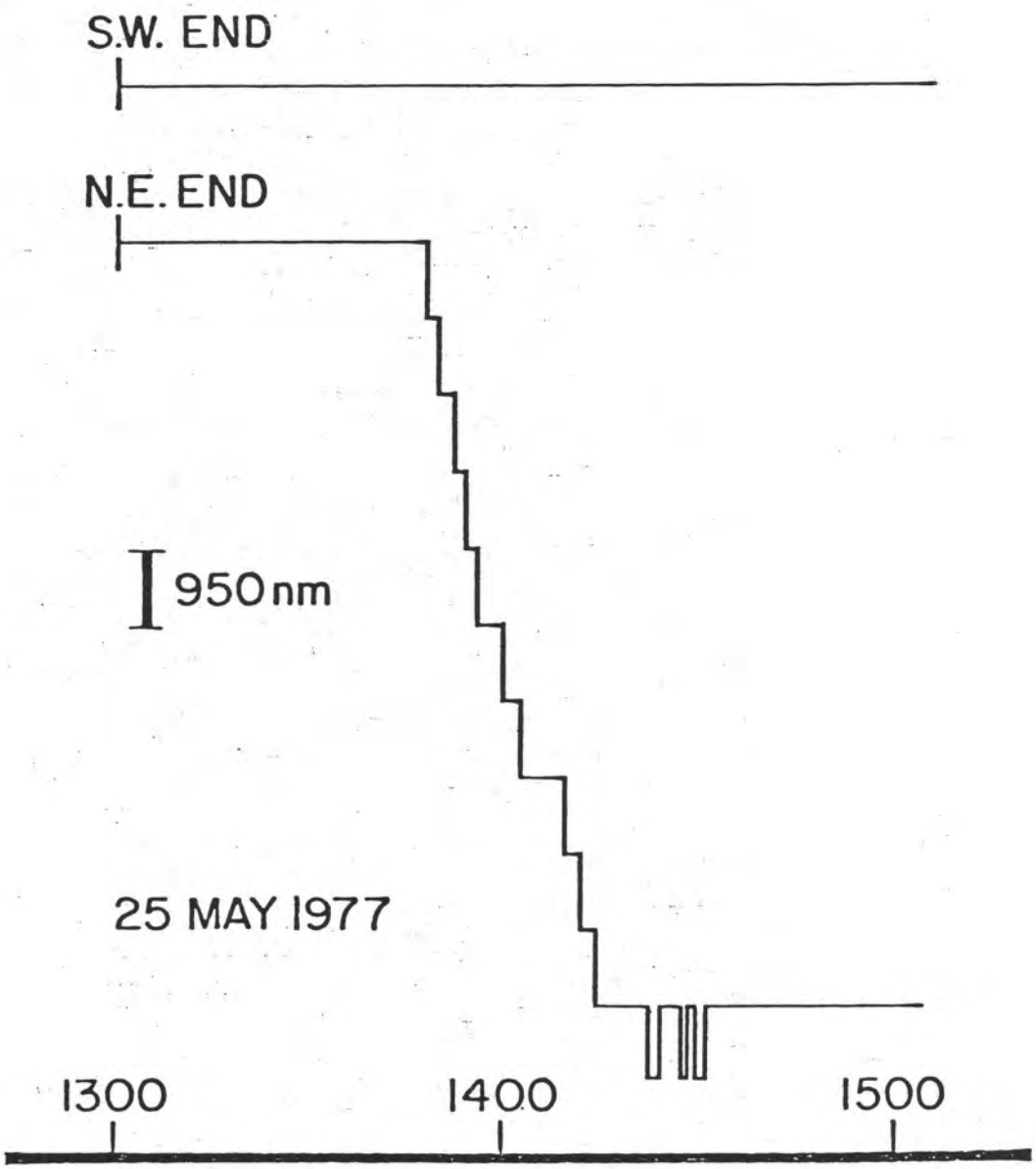

Figure 8a. Puzzling offsets occurred at infrequent intervals in the Ogdensburg tilt data. The offset shown resulted in a 9.5 μm increment in the data over a period of 30 minutes. The jumps were identified as adhesion tension effects equivalent to "stiction" in mechanical systems. The effects were eliminated in the 239 m Suffern tiltmeter by lining the end reservoirs with porous filters.

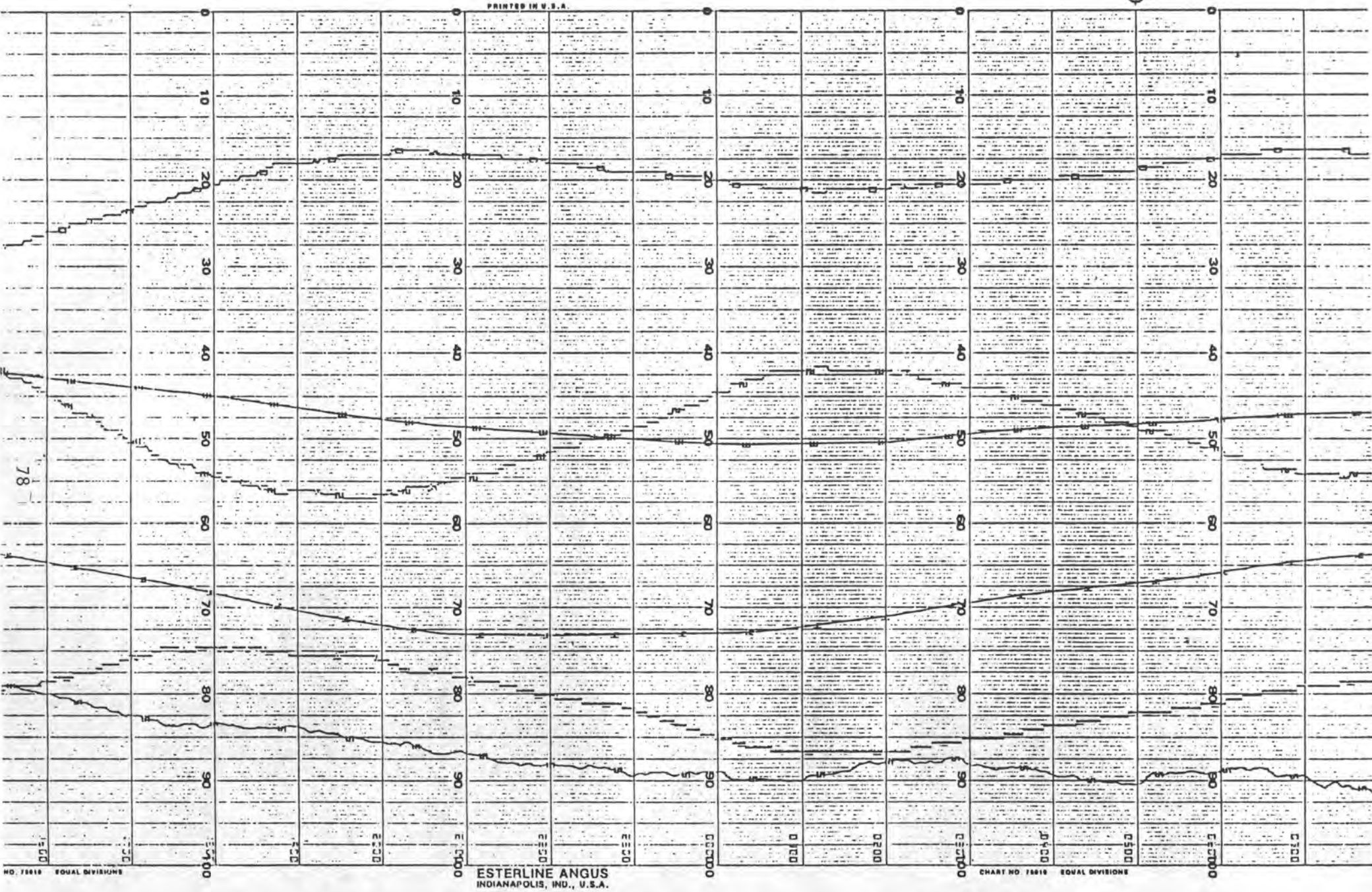

Figure 9. A sample of strip chart data from the Suffern installation. Channel 0 is east end water level, 1 is west end, 2 is tilt, 3 is east end temperature, 4 is west temperature and 5 is atmospheric pressure. Note the incremental nature of the water level and tilt traces. Each step corresponds

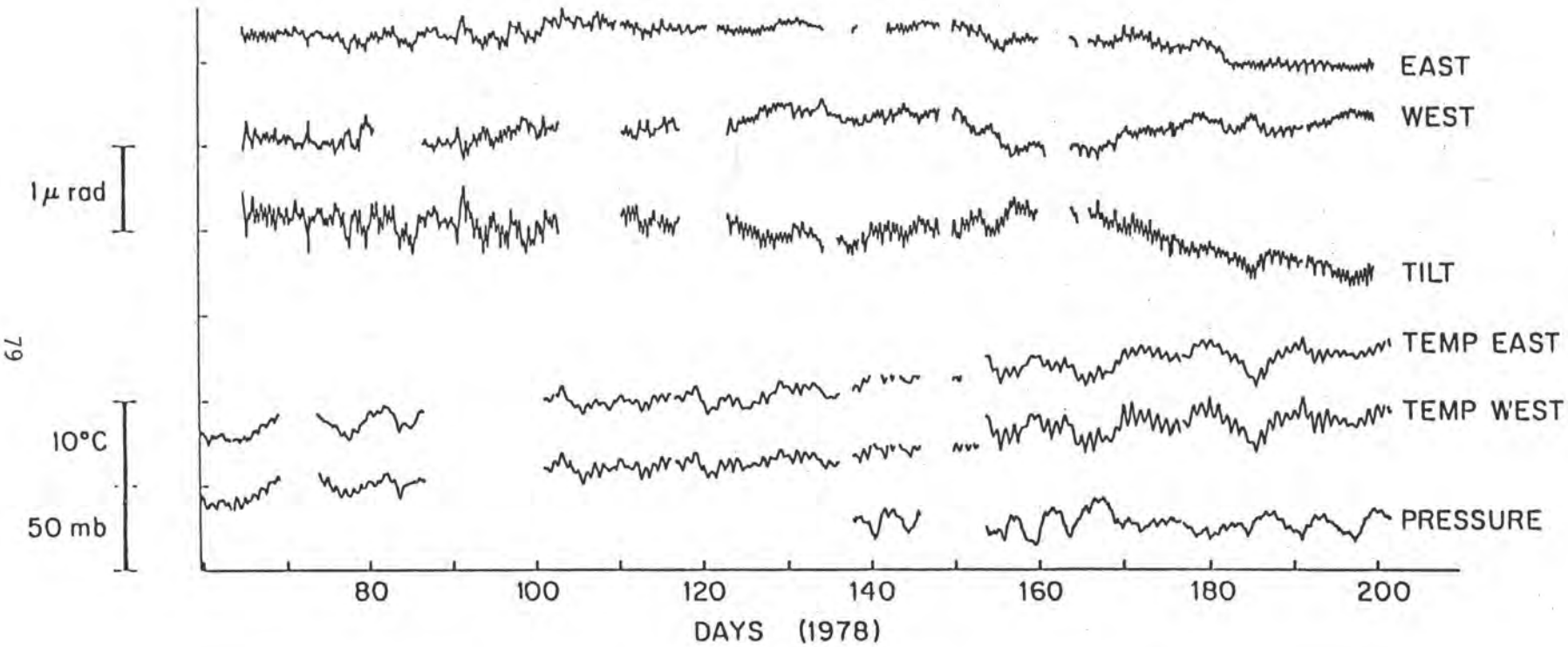

Figure 10. Twenty weeks of data from the Suffern installation between 1 Mar. and 22 Jul. 1978. The data have been read from strip chart records similar to that in Figure 9. The water levels are plotted on the same scale as the tilt by dividing them by the length of the tiltmeter. Gaps are due principally to recorder malfunctions. Note the noisy water level and tilt data prior to day 105 when a constriction in the air path was cleared. Note also some events which correlate between the water level and temperature or pressure records.

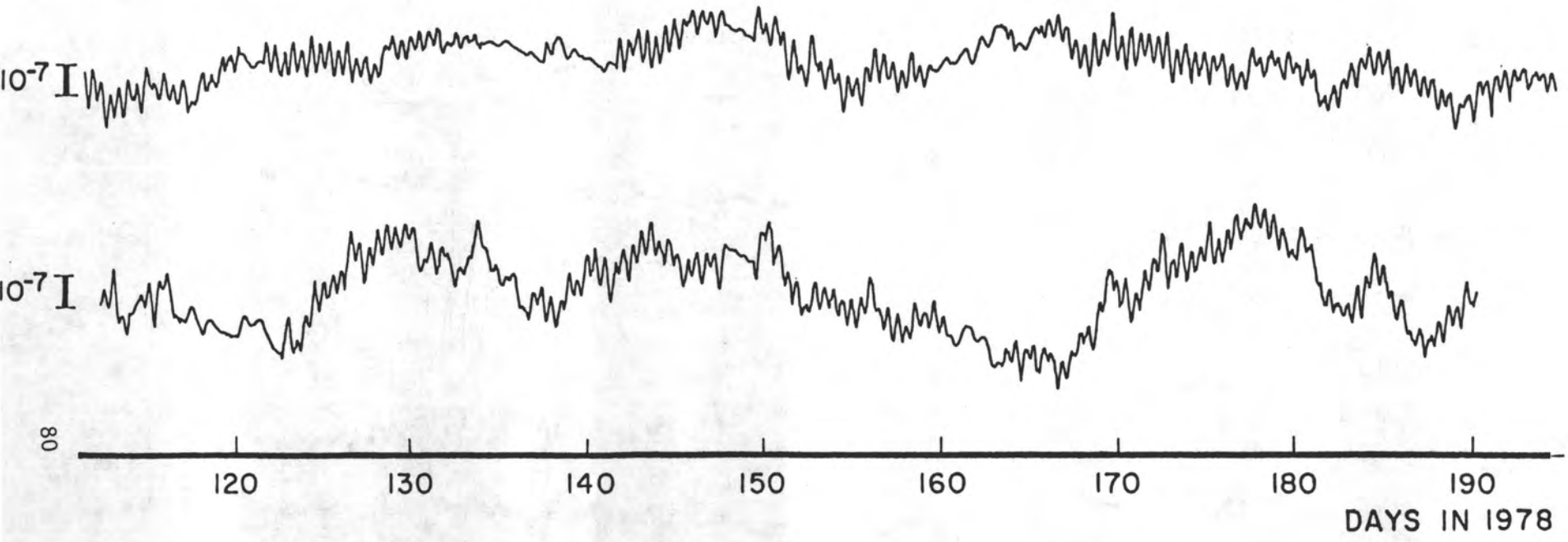

Figure 11. The Suffern end level records after processing using the measured temperature. Note that a straight line has been removed from both records (see Figure 13 for a detrended plot of part of the raw water level data).

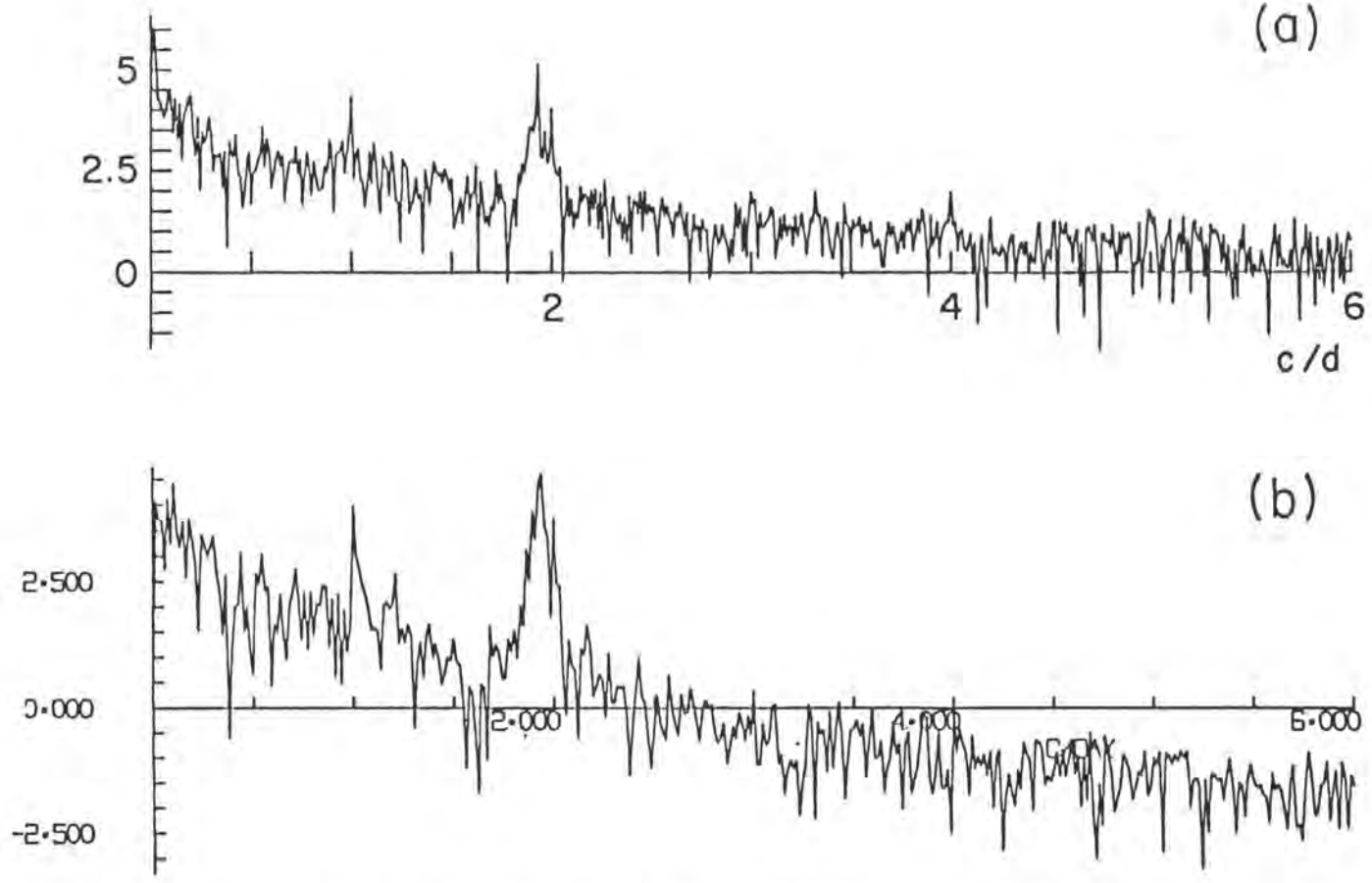

Figure 12a. The log of the power spectrum of 2160 hours of Suffern tilt data [see method "A" of *Beavan and Goulty*, 1977]. The tilt data used are those in Figure 10 except that gaps have been filled by Wiener filtering using the calculated solid earth tilt tide as input. The vertical axis is $\log_{10}$ ("tilt power" per c/d) where "tilt power" = ½ (tilt amplitude in nanoradians)^2.

Figure 12b. The log of the power spectrum of 1584 hours of Suffern tilt data after processing to extract only those parts of the signal coherent between the two ends (see Figure 13). The data span is shorter than in Figure 12a because the ends of the data are truncated during application of the Wiener filter (see text). Note the significant decrease in noise level at all frequencies.

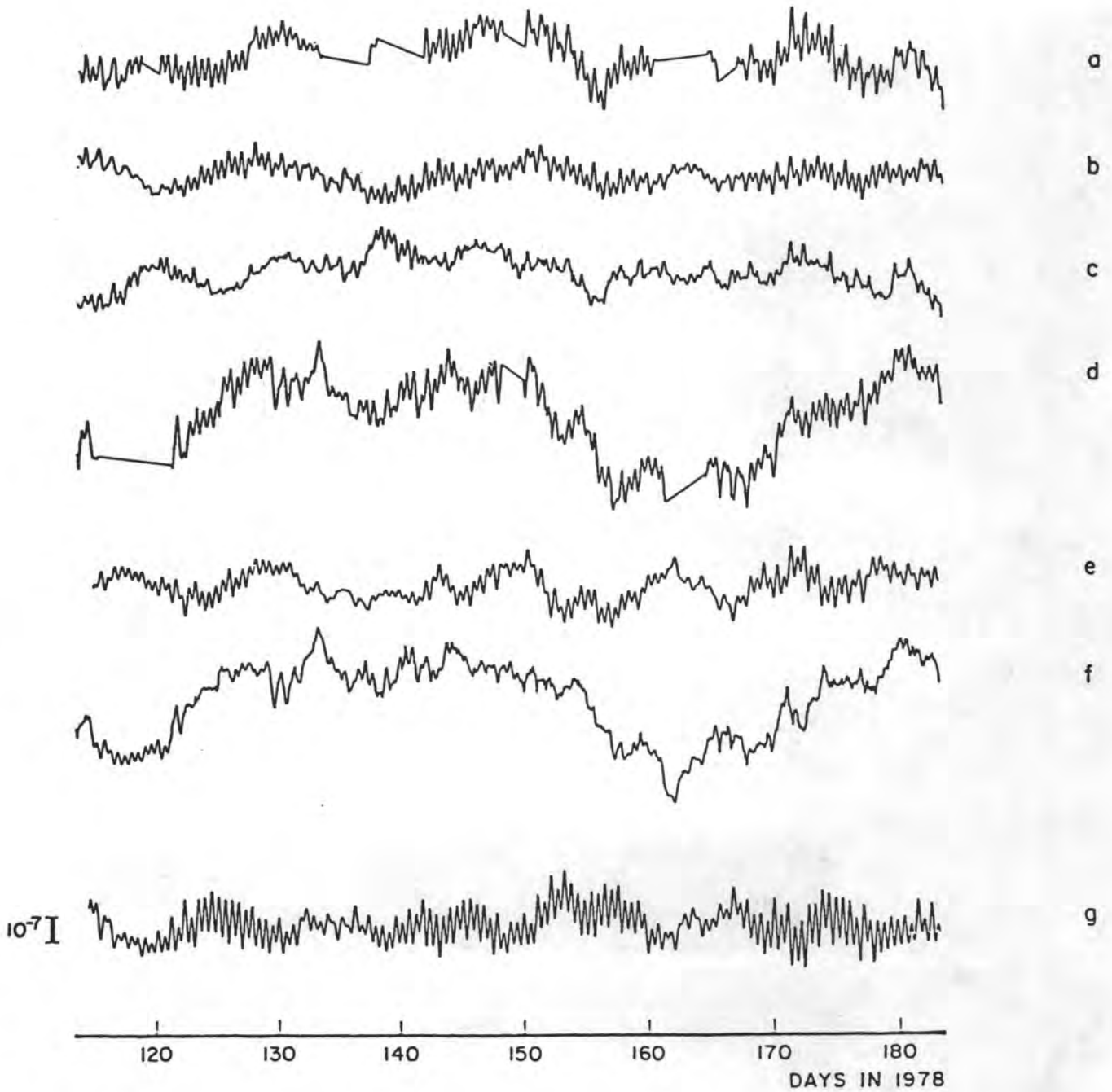

Figure 13. The use of Wiener filtering to extract the coherent parts of the end level records. All records have been detrended by the removal of a least-squares best fit straight line. (a) and (d) are the east and west end level raw data. (b) is that part of the east end record coherent with the west end, (e) is that part of the west end record coherent with the east end. (c) and (f) are the residuals, that is, the difference between the raw data and the coherent data. (g) is the tilt calculated as the difference between (b) and (e). The spectrum of (g) is shown in Figure 12b.

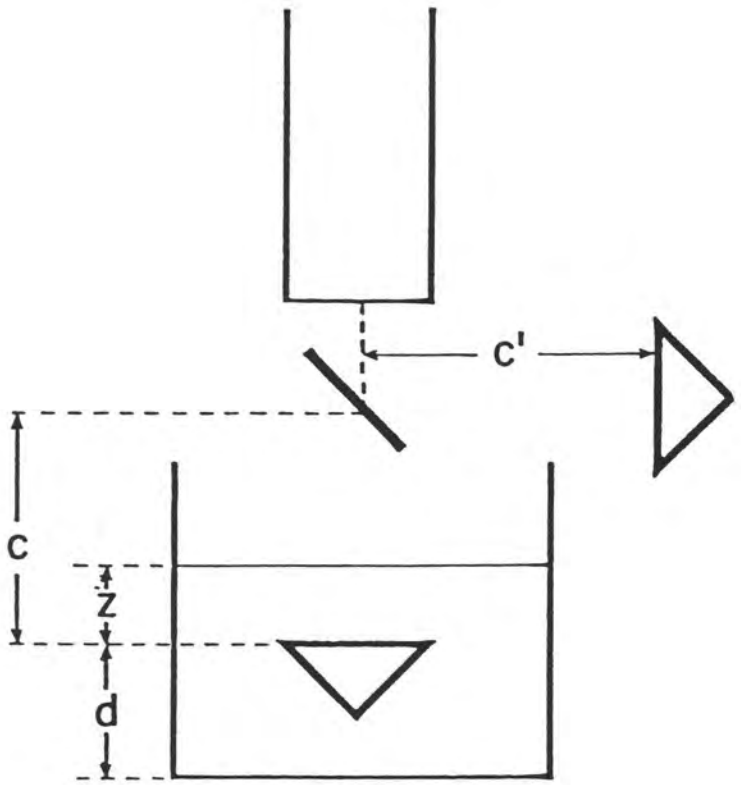

Figure 14

Progress in Monitoring Stress Changes near Active Faults in Southern California

Bruce R. Clark
Leighton and Associates, Inc.
17975 Sky Park Circle
Irvine, California 92714

ABSTRACT

Results obtained from the last year of recording stress levels in the stressmeter net around Palmdale indicate that local horizontal stresses are changing in a reasonably systematic way. In a six-month period from November 1977 through April 1978, three of the sites showed an increase in compressive stress in the northeast-southwest direction. The fourth site, near Valyermo coincides with the area of the earthquake swarm of 1976-77 and showed an increase in stresses in all directions. The fifth site, southeast of the earthquake swarm was extremely quiet.

The lack of major earthquake activity in the net has made it difficult to establish that the instruments are measuring real tectonic stress changes. However, indirect arguments suggest the data are real. The changes are consistent at three widely spaced sites, they do not correspond to any instrument drift patterns in laboratory tests, and they are not consistent with any predicted non-tectonic effects.

If the changes are real and are caused by tectonic changes at depth, then the magnitude of the changes we see supports the contention that at least for short-term fluctuations, the coupling between tectonic stresses at depth and near the ground surface is quite good. Consequently the near-surface measurements have potential application as an independent measure of at least local seismic stress drops. More important, the prognosis for use of the instrumentation for detecting stress precursors to earthquakes is very favorable. We appear to be measuring at approximately the correct sensitivity and the noise level is low.

INTRODUCTION

A full year of data is now available from the Stress Monitoring Project and it is possible to begin to assess the effectiveness of the Project. In this summary I will concentrate on the critical questions of the reality of the data, whether the results indicate good vertical coupling in the near surface rocks, their application to the seismic stress drop and the prognosis for stress monitoring as an earthquake prediction tool. I will review the general stress change patterns only briefly as this is the topic of another paper already submitted for publication.

The stress monitoring project consists of an ongoing program of measurements of change in stress levels at five different sites near active faults in southern California. A total of 20 IRAD vibrating-wire "stressmeters" (Hawkes and Hooker, 1974, Sellers, 1977) is installed at present in seven boreholes. Only two gauges could be installed in an initial attempt at Lytle Creek, but this site will be upgraded in the next few months. The stressmeters are actually rigid inclusion strain gauges, but they deserve to be thought of as stress-measuring devices. Since they have a considerably higher elastic modulus than the surrounding rock, they measure the stress required to hold a borehole open. Thus, even though the actual measurement is of a small strain in the stressmeter body, the gauge can be calibrated accurately in the lab and conversion of the reading to an actual stress value is straightforward (Sellers, 1977).

The stressmeters were wedged into an EX borehole (Figure 1) and pre-stressed to some level between .5 and 5MPa (75 and 750 psi) at our sites. After an initial relaxation phase, which is mostly a function of the degree of weathering and/or fracturing of the host rock, the gauges began to read a steady-state stress level. Further changes in this level should be a response of the gauge to externally applied stresses. The instruments give only the change in stress level from an initial pre-stressed level, not an absolute value of the stress. Each unit is unidirectional, and measures only normal stress, so three gauges in different orientations in a plane are required to define the principal stress components in that plane. In our study only horizontal stress components are measured, since we are within 20m of the ground surface and the vertical component should not change significantly.

The gauges are currently being read manually at approximately biweekly intervals and the data reduced and stored in our computer facility. I have reproduced the data in both tabular (Table I) and graphical form (Figures 2-8). It is this information on which the analysis below is based.

ANALYSIS OF RESULTS

The results are grouped graphically in the figures to show the behavior of the gauges at each site together. Since the gauges are oriented in different azimuthal directions, a short-term fluctuation affecting all gauges is likely to be the result of some environmental factor such as temperature rather than tectonic stress. Although the instruments are temperature-compensated, the rocks are not, so a local temperature fluctuation would change the stress as felt by the gauges. However, very few of the fluctuations observed actually affect all gauges in a similar manner, a strong argument that the instruments are buried deeply enough not to be sensing any short-term thermal effects. Seasonal effects are another matter and will receive further consideration when data have been collected over an interval long enough to analyze.

Three of the 20 original gauges have ceased functioning and will soon be replaced. A few others have been working intermittently (see graphs) and are still providing useful data although the plan is to replace these as well in the near future. The other gauges are yielding data of excellent quality directly from field readings by a technician.

The results generated to date are extemely interesting. My preliminary conclusion is that most of the area is experiencing an increased compressive stress in the northeast-southwest quadrants at the rate of approximately .1 MPa (1 bar) in a six-month period (Figure 9). This pattern is not uniform, particularly along the San Andreas fault. The stress appears to be building up at Elizabeth Lake but being relieved at Valyermo and remaining unchanged at Lytle Creek. This could be the surface expression of a small zone of stress relief in the vicinity of the Valyermo site, with an associated increase in stress to the northwest and no change to the southeast. During much of 1977, the Valyermo area was affected by an unusually high level of seismic activity (McNally and Kanamori, 1978) and the area might have become de-stressed at depth as a result of the earthquakes. We did not obtain any useful data until after the earthquakes had essentially stopped, but since that time all components of the stresses have decreased, perhaps as a delayed response to the changes at depth.

Stressmeter Readings as Actual Stress Changes

The most fundamental question is whether the data we are collecting accurately reflect changes in the externally applied stress field at the point at which instruments are located. There is no simple kind of control station which can be held at zero change and against which the individual field gauges can be rechecked. Once the gauges are set in place, they can not be returned to an unloaded state and checked for drift. They can only be monitored through time. Individual gauges could be drifting in some uniform way, the contact between the cylinder and the borehole wall could be progressively deteriorating, or temperatures could be changing systematically.

Because I have a relatively large number of gauges in operation, I think it is possible to make a fairly strong case that the data are real and are measuring precisely what we intend to measure. First, the changes that are occurring are remarkably consistent. Until the last couple months, only the north-south gauges at several different sites showed a net increase in stress level. Had these changes been due to instrument drift the probability of only the north-south gauges drifting in the positive direction would be very low. Gauges that have been stressed in the laboratory for similar periods show essentially no drift (Hawkes, pers. comm.). I have had a gauge under dead-weight load in my laboratory for nearly two months with similar results. While I cannot rule out instrument drift in each individual stressmeter, I have circumstantial evidence that drift is not a factor in this type of instrument.

The variation in response of the three gauges in each hole is strong evidence that we are not observing an "environmental" phenomenon such as temperature change or progressive changes in the character of the stressmeter - wall rock contact. These should affect each gauge in at least the same direction if not the same amount. If the Valyermo (Figure 6) results were the only ones available for analysis, this environmental effect would indeed be a distinct possibility. However, the results at Elizabeth Lake (Figures 4 and 5) or San Antonio Dam (Figure 8) cannot be interpreted as a logical result of environmental effects.

I conclude that although the data cannot be proven to be accurately measuring the changes in tectonic stress, we can eliminate the logical alternatives. A major stress perturbation such as a moderate to large earthquake within the net should produce a distinct offset in the data. We now have ample background data to be able to "calibrate" the instruments with that type of stress change if it should occur. These results have not yet been correlated with surface groundstrain measurements in the area. The stress data suggest that a significant northeast-southwest compression has occurred since last November in both the Elizabeth Lake area and the southern San Gabriel front. These changes should be reflected as near-surface crustal shortening and should be correlated with data from long-baseline strain measuring instruments when they become available.

Vertical Coupling

A major unanswered question about stress measurements in general is whether they are representative of stress conditions at depth. Some success has been reported for correlation of surface stress measurements with deeper readings (Raleigh et al., 1972) and with earthquake focal mechanisms (de la Cruz and Raleigh, 1971; Sbar et al., 1977). Usually only the general stress directions can be correlated, and the relative magnitudes of principal stress are only poorly known. But this at least provides hope that the surface stresses reflect conditions at depth.

Changes of stress levels are probably more closely coupled vertically than absolute stress values, since the absolute stress field has had a long time to relax near the ground surface. We might expect short-term perturbations of the stress field not to be damped by relaxation. However, the absolute values of horizontal stresses are much smaller at the ground surface then at depth, and the real question is whether stress-change components are transmitted without alteration or reorientation over vertical distances as much as several kilometers. If even the relative stress-change components in the horizontal directions were transmitted to the surface without major alterations, then the near-surface data would be very useful. Precursory events might be recognized as distinct changes in either magnitude or orientation.

One reason for installing multiple sets of gauges at the same location was to see if the gauges at two different depths near each other would record the same changes. In general this experiment met with mixed results. The two stations in question are Buck Canyon and Elizabeth Lake.

The Buck Canyon gauges which failed are in critical orientations, so it is difficult to compare the results (Figures 2 and 3). In terms of long-term behavior the gauges correlate reasonably well. Both N30°W units show long periods of stress decrease followed by an increase in stress level since March or April. The other two gauges in the deep hole either failed completely (N75°W) or are operating intermittently (N15°E). Both of these gauges will be replaced soon and I would like to withhold any conclusions about behavior there until we have better data. The N15°E gauge does not correlate well with its counterpart in the shallow hole.

At Elizabeth Lake we have a bad gauge at N45°W in the shallow hole, but the other two sets of gauges contain some very encouraging results (Figures 4 and 5). First, the north-south units are the only two that have increased since their initial relaxing phase. The deep hole stressmeter had some problems for a while but is now operating again. Second, the east-west units look very similar, even to the extent that both recorded an unusual drop in March. In general we can conclude that the readings to date at the two depths are very similar.

The results to date indicate rather large changes observable at the ground surface - as much as .1MPa (one bar) in 6 months. This is at least the proper order of magnitude for the stress buildup that would be postulated from recurrence intervals along the San Andreas fault. Using a recurrence interval of 200 years (Sieh, 1978) and a local stress drop of as much as 50 MPa (Aki, 1977) at depth, we could develop local average stress buildups as great as .25 MPa per year. If the surface changes are a highly attenuated version of stress changes at depth, then conditions at depth would have to change very rapidly indeed. At the moment I tend to believe that changes in the deep stress conditions must be transmitted to the surface with little attenuation. A preliminary comparison with integrated data, such as long-baseline strain measurements, would be extremely helpful.

The ultimate test of this vertical coupling problem is to monitor with gauges much deeper in the earth, up to a kilometer or more below the ground surface. This requires a different type of installation, but there is no major technological barrier to such a deep installation. Thus the limited data to date encourage cautious optimism that the near-surface stress changes do reflect similar conditions at greater depth.

The Seismic Stress Drop

Considerable thought has gone into the significance of the theoretically-derived seismic stress drop (e.g., Aki, 1977). The problem is that stress drops derived from seismic moments are an order of magnitude smaller than the stress drops that might be predicted from laboratory rock mechanics. It is logical to infer that the seismically determined stress drop is an average over large areas of the fault, but local stress drops at "asperities" are much higher.

One of the objectives of the stress monitoring experiments is to obtain an independent measure of the stress change during an earthquake. The entire stress pattern is highly dependent on the specific dislocation model used and it is unlikely that the relatively data-poor net we have at present will allow for a unique determination of the source mechanism. However, if the coupling between deep and shallow stress conditions is as good as hoped and the dislocation mechanism is reasonably simple, then a few point measurements of actual stress drops, even if they are very near the ground surface, will considerably constrain the range of appropriate models. When combined with integrative strain measurements such as leveling, triangulation, and long-baseline interferometry the stress measurements should be very helpful in modeling the source mechanism when data from earthquakes within the net become available.

Stress Monitoring for Earthquake Precursors

No significant earthquakes have occurred within the net since serious data recording began. One earthquake occurred in August, 1977 (Mb=4.4) several kilometors away from the Buck Canyon site. There was no obvious effect on the instruments at that site. However, this was still a time of relaxation at Buck Canyon and any signal could easily have been lost in the large changes still being recorded there.

From a theoretical standpoint, the type of precursory signal to be expected is not obvious. Again the signal depends heavily on the source mechanism which itself is not well known. If a constant strain-rate model with dilatancy is correct, then at most locations the stress level might be expected to drop before final failure as dilatancy weakens the rock, in a manner analogous to the constant strain rate laboratory experiment. However, the mechanism is undoubtedly complex on a regional scale, and local stress levels could rise. Unlike long-baseline type measurements, these point measurements do not integrate an effect. They are much more analogous to the surface tiltmeters which display a precursory change, but not in a consistent direction (Johnston and Mortensen, 1976).

The stressmeters in their present configuration may not be sensitive enough to detect precursory information . The one stress precursor that has been recorded (Swolfs et al., 1977) was for a large rock burst and was on the order of .001 MPa (10 mb). Since the sensitivity of our units is approximately .01 MPa (100 Mb), that precursor would have escaped detection. However, the noise level in the data is quite low. In view of the fact that we are detecting apparent changes of the ambient field, chances are excellent that for moderate earthquakes we are monitoring at the proper sensitivity.

Future Directions

The sites have just recently been upgraded to a telemetry system that allows us to record readings at any interval from a few seconds to 10 hours. The units are currently being recorded at one hour intervals. We thus will be able to determine the details of short-period changes in stress although none of that data has been processed yet. In addition to providing a nearly continuous measure of stress changes in the area, the system is designed to continue collecting and recording data even if electricity and telephone service were cut off by a large earthquake. Two types of recording devices are being used: digital cassette units and integrated circuit memory chips. The digital cassettes run until the batteries fail after AC power is cut off, and the data are stored permanently on tape. The memory chips will hold the recorded data until the large storage batteries at the site fail. They are intended to operate for periods as long as two months, although the memory will be filled under normal conditions in about two weeks. The memory chips are part of a system of Telemetry Interface Modules developed by Caltech for remote sites at which AC power is not available. These units run on battery power for extended periods of time, yet can telemeter data back to a central site via voice-grade telephone lines.

The major future directions for the program are an increased density of stations along active faults in southern California, and eventual development of a deep borehole stress monitoring package. An increased number of stations will be placed along the San Andreas fault to improve our understanding of the variations in stress buildup between Elizabeth Lake and Lytle Creek. As it becomes appropriate, the net can easily be expanded to other faults in the area as well. The deep borehole package is an important tool for future deep drilling efforts in active fault zones. The basic design has been completed but funds are not yet available for the laboratory prototype and the necessary testing. The eventual goal is to be able to monitor stresses directly at depths approaching the earthquake source itself.

REFERENCES

Aki, K., 1977, A Quantitative Model for Stress in a Seismic Region as a Basis for Earthquake Prediction: USGS OFR - 78-380, p. 7 - 32.

de la Cruz, R. V., and Raleigh, C. B., 1972, Absolute Stress Measurements at the Rangely Anticline, Northwestern Colorado: Int. J. Rock Mech Min. Sci. v. 9, p. 625 - 634.

Hawkes, I., and Hooker, V. E., 1974, The Vibrating Wire Stressmeter: Proc. 3rd ISRM symp., Denver, Colo., v. II-A, p. 439 - 444.

Johnston, M. J. S., and Mortensen, C. E., 1974, Tilt Precursors before Earthquakes on the San Andreas Fault, California: Science, v. 186, p. 1031 - 1034.

McNally, K., Kanamori, H., Pechmann, J. C., and Fuis, G., 1978, Earthquake Swarm along the San Andreas Fault near Palmdale, Southern California, 1976-1977: Science, in press.

Raleigh, C. B., Healy, J. H., and Bredehoeft, J. D., 1972, Faulting and Crustal Stress at Rangeley, Colorado: Am. Geoph. Union Monograph 16, p. 275 - 284.

Sbar, M. L., Engelder, T., Plumb, R., and Marshak, S., 1978, Stress Pattern near the San Andreas Fault, Palmdale California from Near Surface in situ Measurements: Jour. Geoph. Res., in press.

Sellers, J. B., 1977, The Measurement of Stress Changes in Rock Using the Vibrating Wire Stressmeter: in Kovari, ed., Field Measurements in Rock Mechanics, Balkema, Rotterdam, p. 275 - 288.

Sieh, K., 1978, Earthquake Recurrence Intervals, San Andreas fault, Palmdale, California: California Geology, v. 31, p. 143 - 145.

Swolfs, H., and Brechtel, C. E., 1977, The Direct Measurement of Long-Term Stress Variations in Rock: Proc 18th Symp. Rock Mech. p. 4C51 - 3.

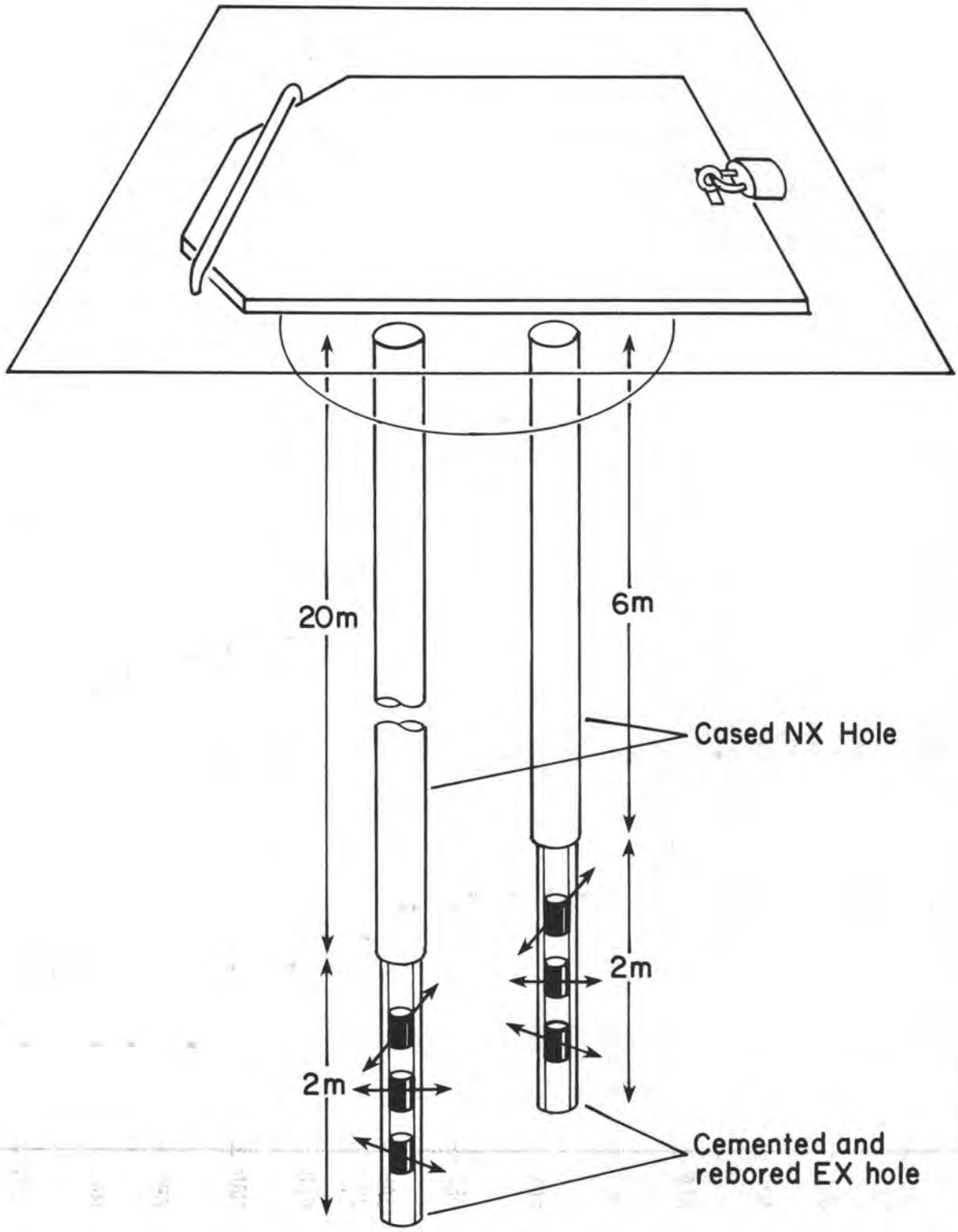

Figure 1 Schematic view of a two-hole installation showing location of stress-meter units in the hole and relative orientation of sensing wires.

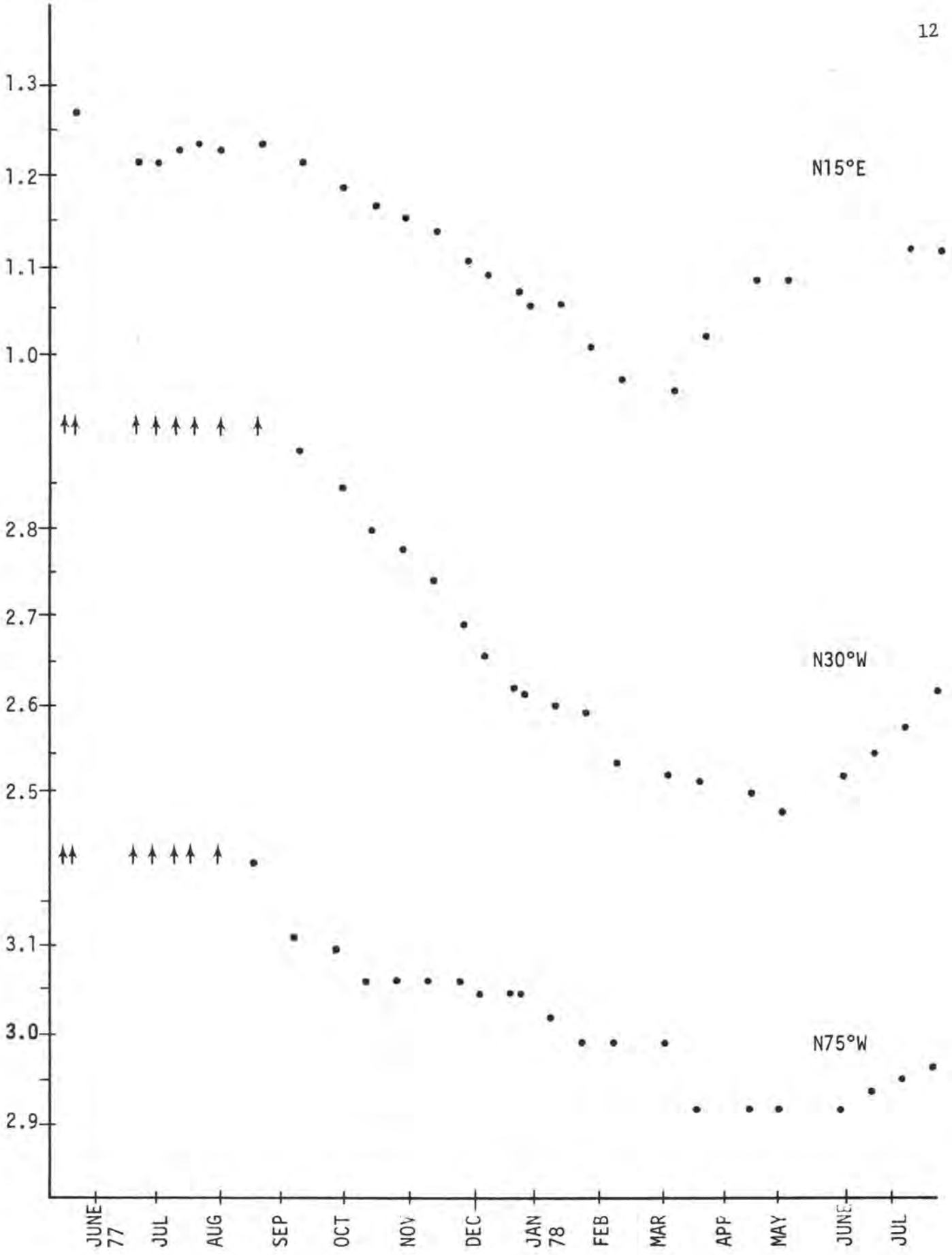

Figure 2 Changes in stress levels recorded in shallow hole at Buck Canyon since recording began in May, 1977.

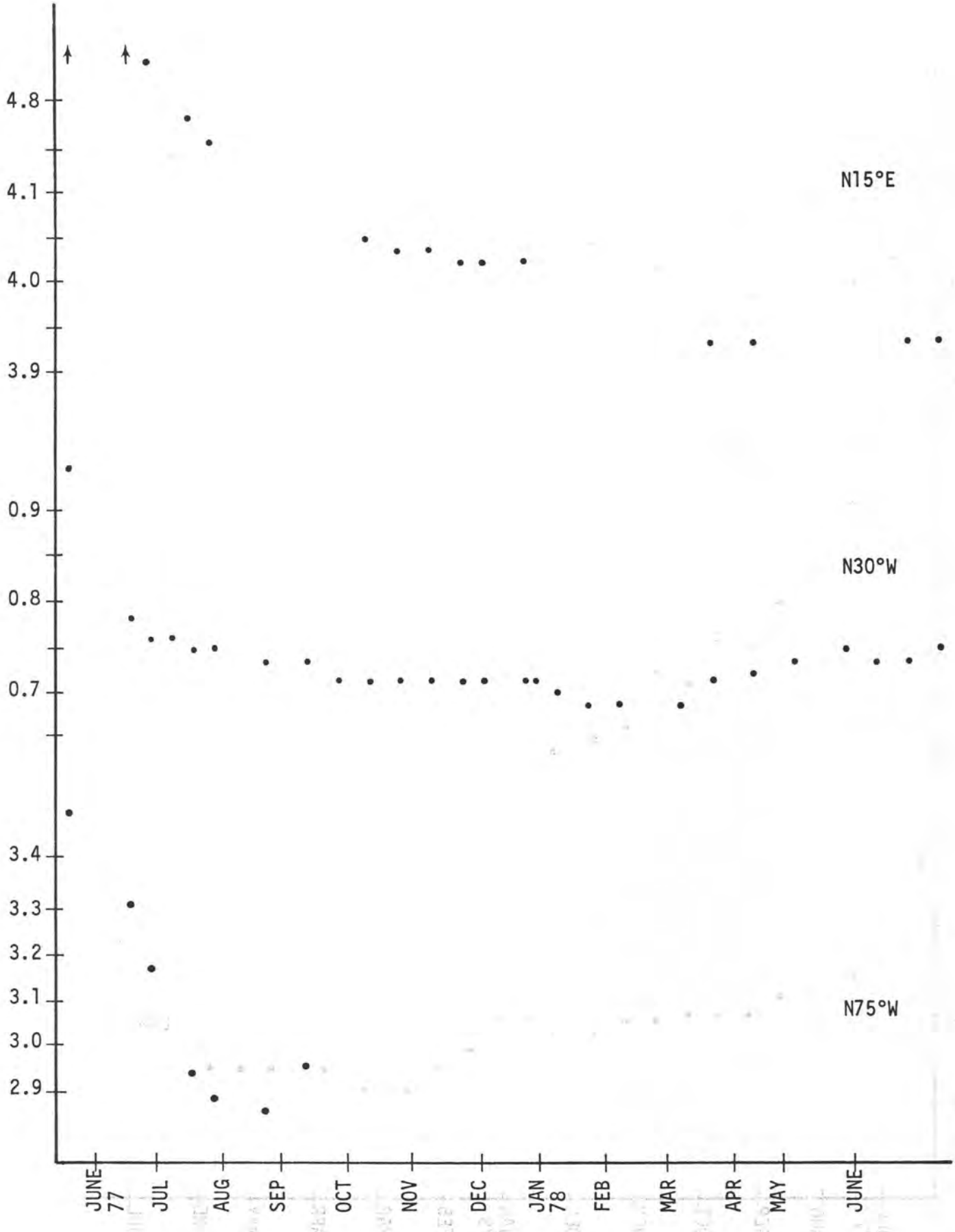

Figure 3 Changes in stress levels recorded in deep hole at Buck Canyon since recording began in May, 1977.

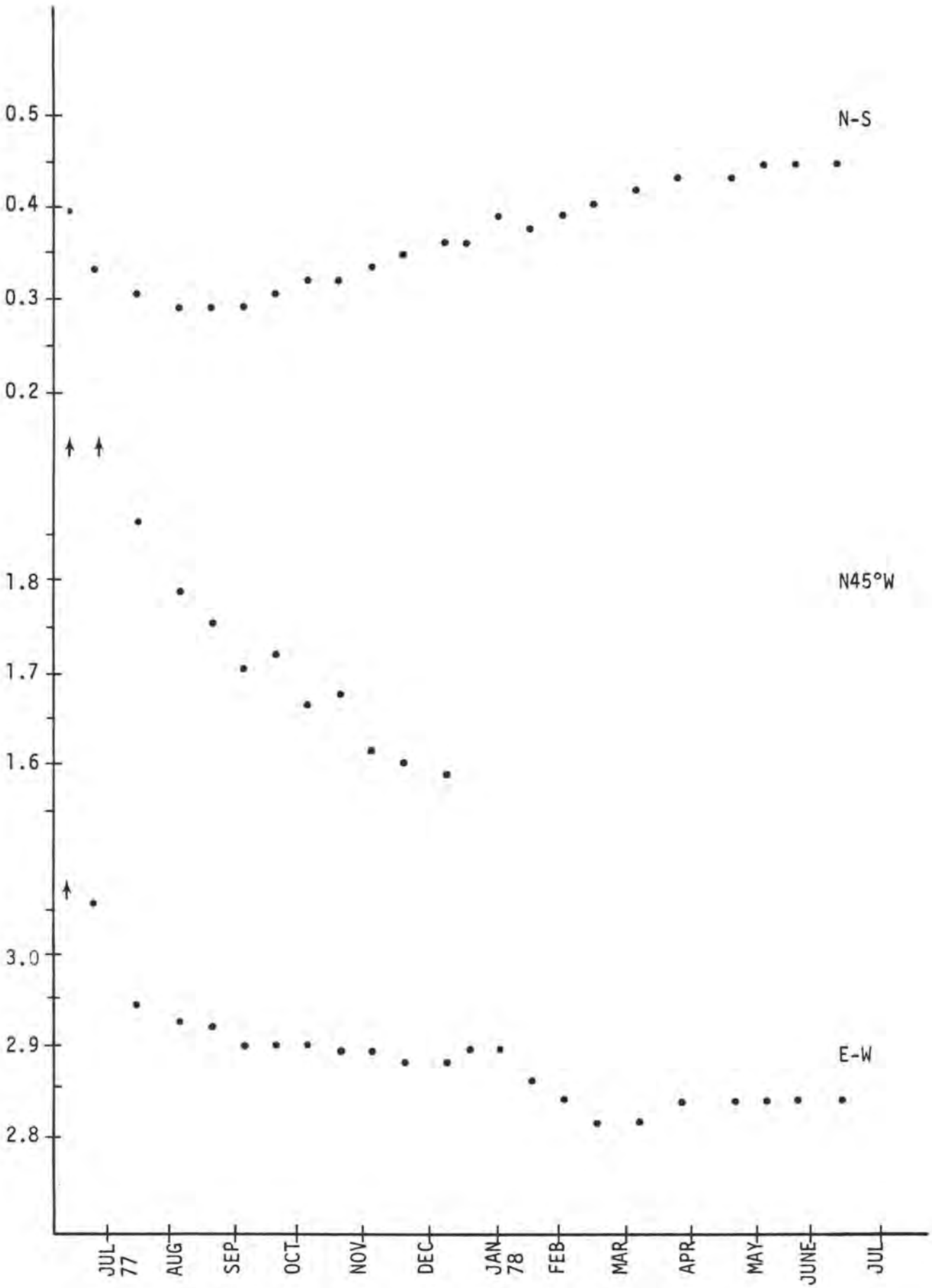

Figure 4 Changes in stress levels recorded in shallow hole at Elizabeth Lake since recording began in July, 1977.

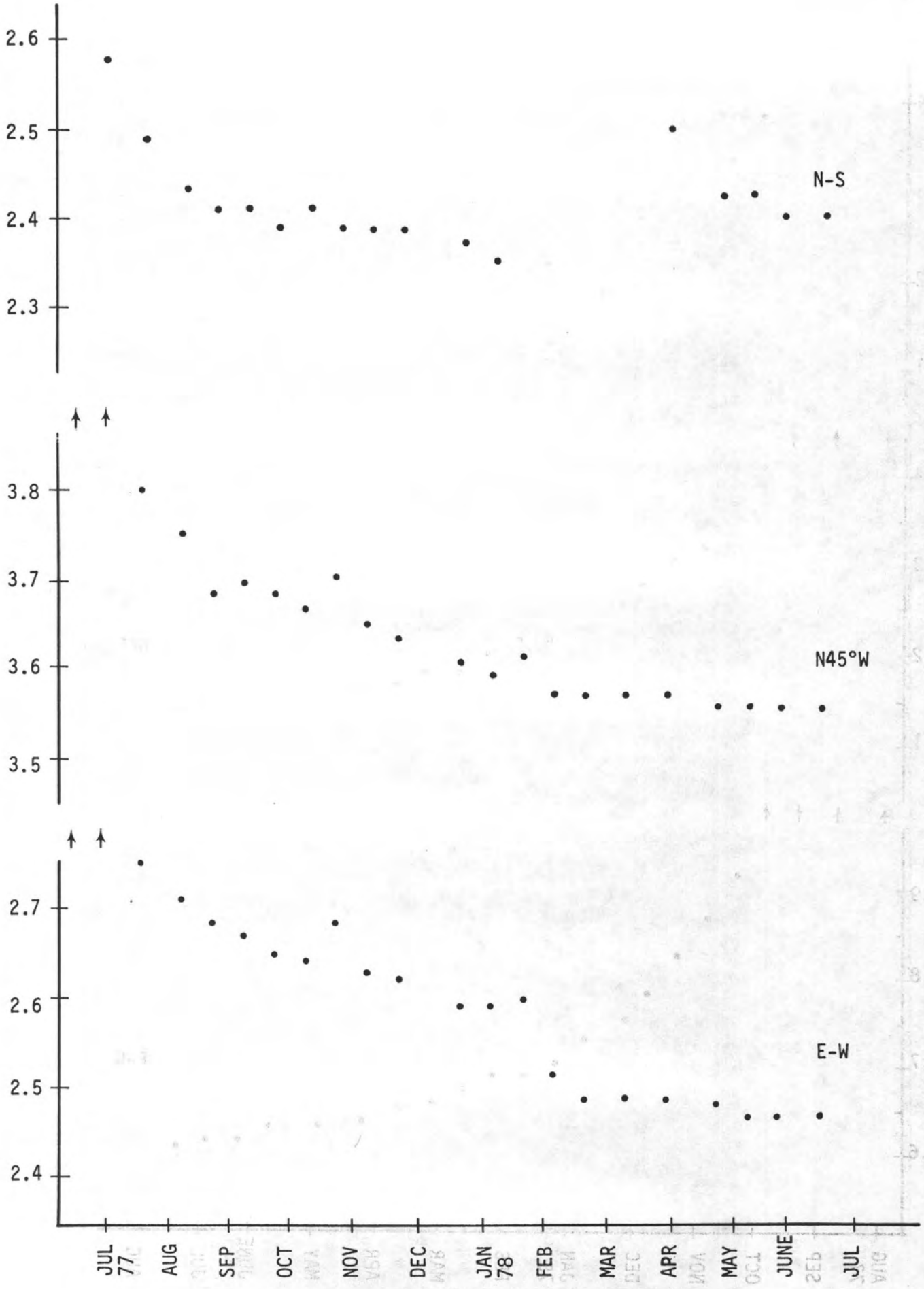

Figure 5 Changes in stress levels recorded in deep hole at Elizabeth Lake since recording began in July, 1977.

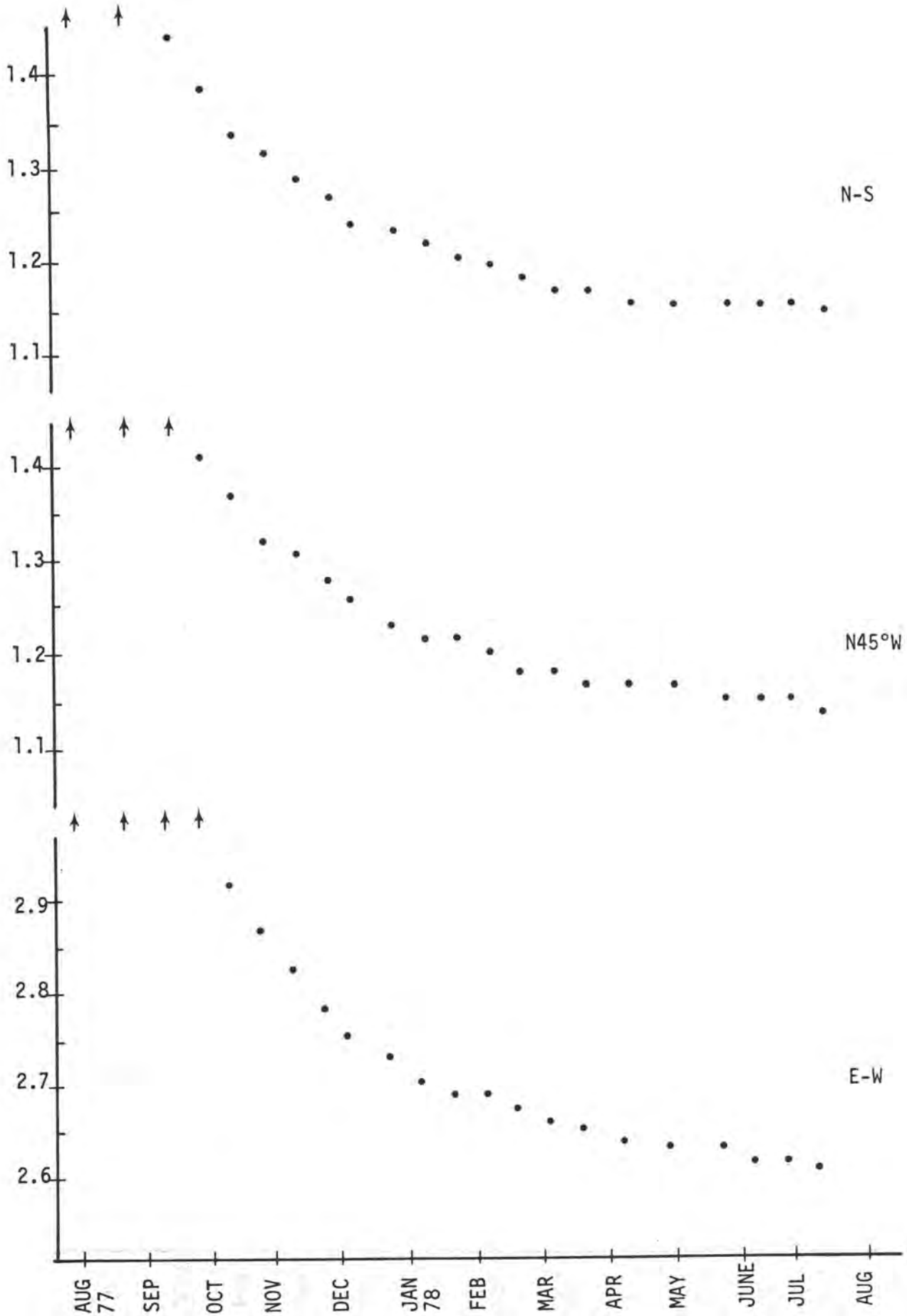

Figure 6 Changes in stress levels recorded at Valyermo since recording began in July, 1977.

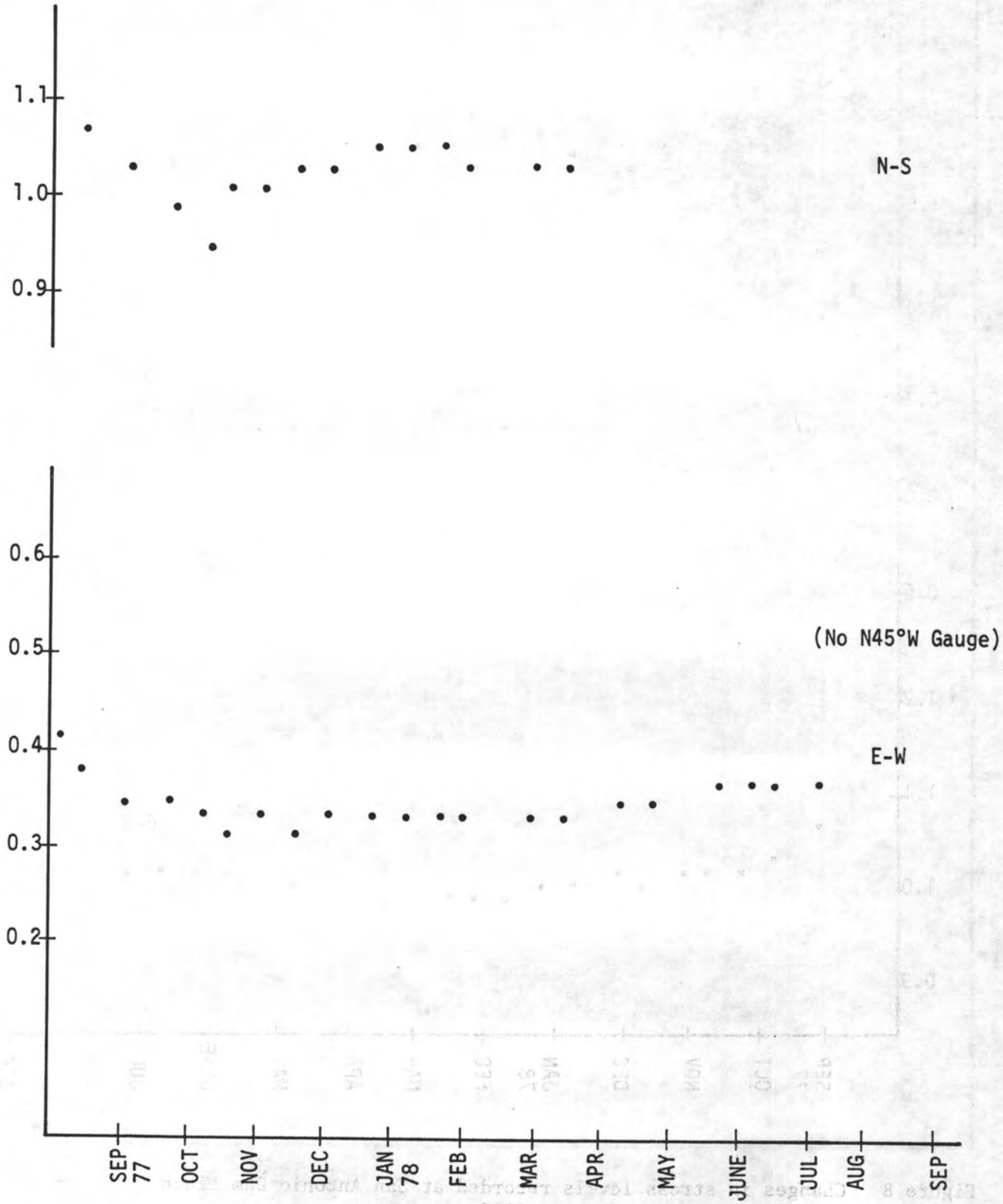

Figure 7 Changes in stress levels recorded at Lytle Creek since recording began in August, 1977.

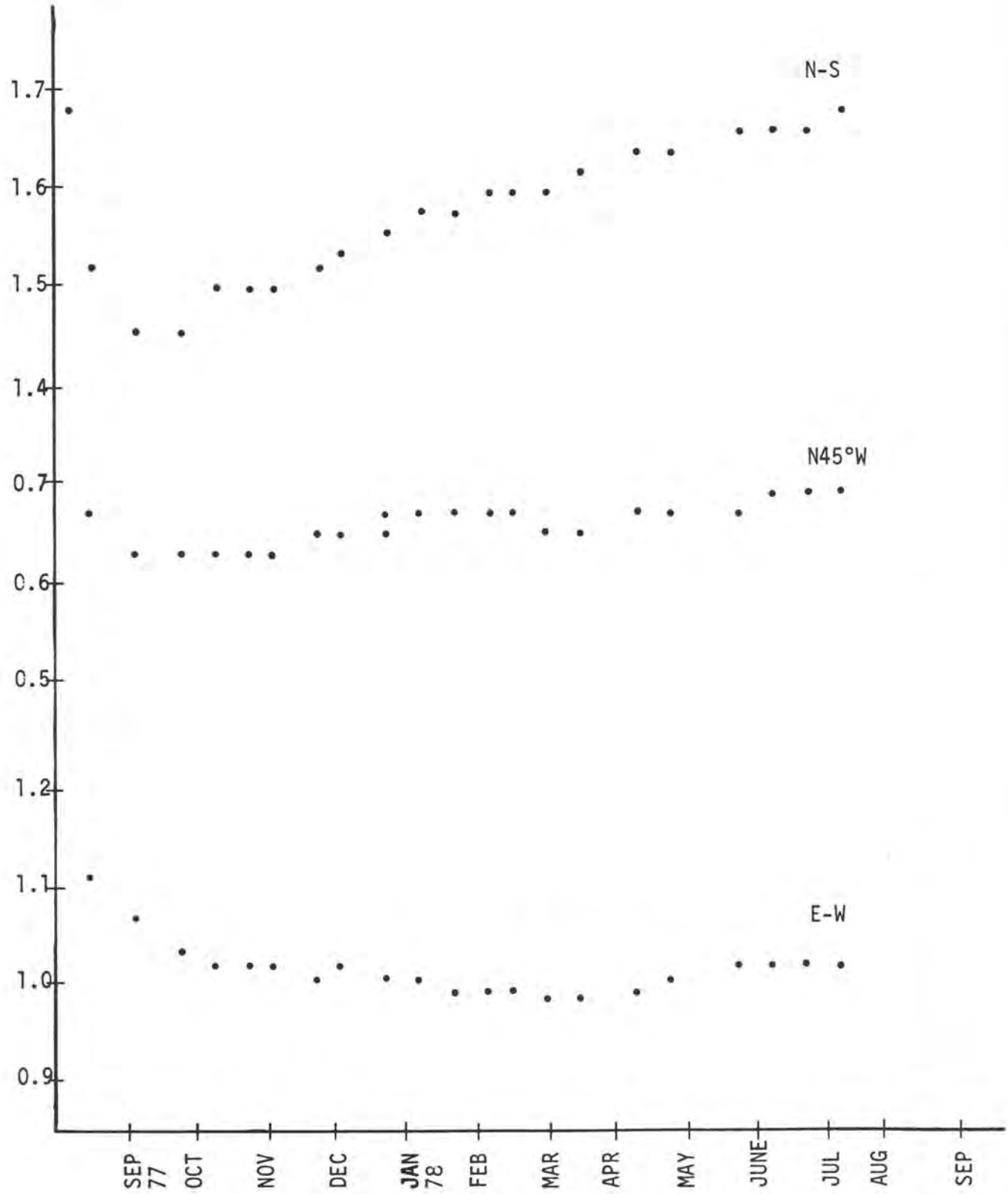

Figure 8 Changes in stress levels recorded at San Antonio Dam since recording began in August, 1977.

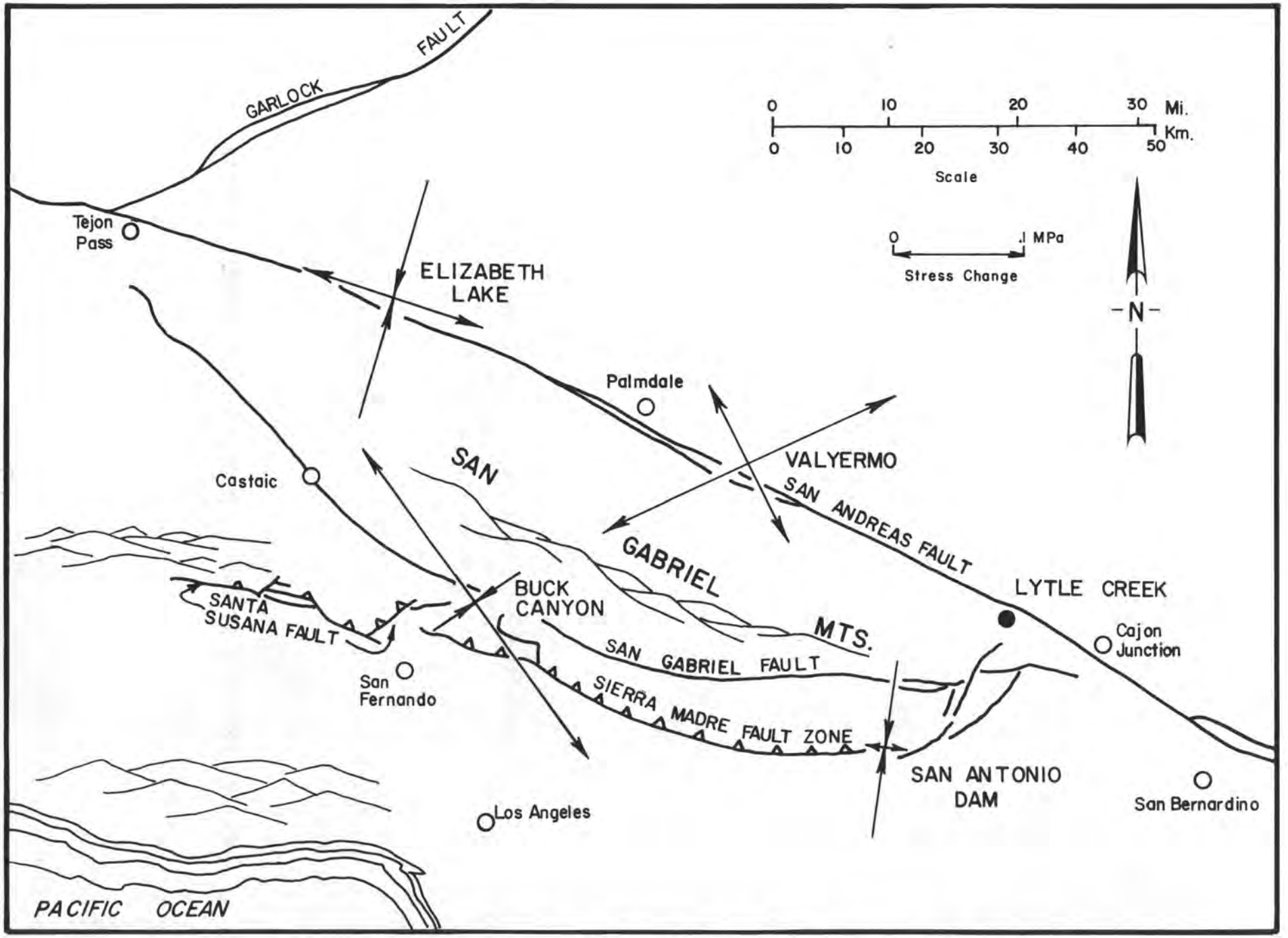

Figure 9 Map showing changes of horizontal principal stresses during period of October 16, 1977 - April 24, 1978. General pattern is one of NE-SW compression, but there are anomalies, such as Valyermo and

TOTAL FIELD MEASUREMENTS ON THE SAN ANDREAS FAULT NEAR GORMAN, CALIFORNIA

by

C. A. SEARLS
R. L. McPHERRON*
D. D. JACKSON
P. J. COLEMAN, JR.*

Department of Earth and Space Sciences
University of California
Los Angeles, CA 90024

*Also Institute of Geophysics and Planetary Physics

PAPER PRESENTED AT CARMEL CONFERENCE ON PALMDALE BULGE
AUGUST 1978

INTRODUCTION

It has long been believed that changes in the magnetic field accompanied earthquakes. As the magnetometer has been improved, the magnetic change associated with earthquakes decreased in amplitude until it appeared to be nonexistent. The idea has been subject to reexamination following experimental verification of the piezomagnetic properties of rocks. Shamsi and Stacey (1969), using a screw-type dislocation model for the fault, demonstrated two important characteristics of stress induced magnetic anomalies. First, the magnetic perturbation shows a linear proportionality to the stress sensitivity. Consequently, a higher magnetization implies a larger perturbation. Second, the perturbation is roughly antisymmetric across the fault plane and decays rather rapidly away from the fault trace (fig. 1). The absolute value of these perturbations is considerably larger for the individual components than for the total field. This is because a total field instrument measures only the perturbation component along the ambient field, while much of the predicted field change lies perpendicular to the ambient field.

Using the results of piezomagnetic lab experiments people began looking more systematically for magnetic changes resulting from tectonic stress (Rikitake, 1975; Johnston et al., 1975, 1976; Wyss, 1975). The two most promising attempts at correlating magnetic change and tectonic stress changes were the magnetic changes associated with the 1975 Thanksgiving Day

earthquake near Hollister (M = 5.2) and two earthquakes (M = 5) on the Garlock Fault in June of 1974 (Johnston et al., 1975). The Thanksgiving Day earthquake showed a possible precursor at one of the seven USGS Magnetic Observatories stretched along the San Andreas Fault near Hollister. The magnetic changes associated with the earthquakes along the Garlock fault also occurred at only one station, but since the experiment involved reoccupying a linear array of fixed survey points, the presence of precursory activity could not be determined.

These observations demonstrate that continuous recording is necessary to detect any precursory activity and that indeed as indicated by theory the geographical extent is small (less than 10 km), at least for magnitude five earthquakes. In order to locate the source of the anomaly and effectively remove the magnetic changes from all external sources (so as to see the small signal) a two-dimensional array is required. To take advantage of the linear relationship of the anomaly to magnetization, the array should also be located within or near a region of large magnetic susceptibility.

With these considerations in mind, we plan to establish five continuously recording magnetic observatories in the northwestern San Gabriel Mountains near Gorman (fig. 2). The observatories form a two-dimensional array adjacent to a magnetic high in the vicinity of the junction of the San Andreas and Garlock Faults (fig. 3).

INSTRUMENTATION

Each observatory in the Gorman array includes a Geometrics 816 proton precession magnetometer, supported by a UCLA designed system controller and Memodyne Model 201 cassette recording system (fig. 4). The data cassettes are returned to UCLA on a monthly basis for playback and analysis. After an initial check-out to determine the performance of each instrument over the previous recording interval, the data are transferred via a Hewlett-Packard 21MX minicomputer to an IBM 360/91 data file. Tectomagnetic analyses are then performed on this data set.

The magnetometers are equipped with a special high stability crystal oscillator that functions both as a frequency standard for the magnetometer field reading and as the timing clock for the system controller. Following the work of Johnston et al. (1973), the scaling of the instrument has been modified to provide 1/4 gamma resolution. Also, the power for the light emitting diode display was disconnected so as to reduce power consumption.

The timing circuit uses the 2.857 Mhz oscillator signal to provide time programming for the other circuits in the system. The primary functions are to initiate, once per minute, a sample sequence in the magnetometer and to step the data recorder.

The data line from the magnetometer carries the precession frequency which has been multiplied by 64 in the magnetometer's phase-locked loop. This frequency is counted in the data count block that is gated by the 1472 millisecond count enable signal.

At completeion of the count enable period, the data are parallel transferred from the data counter and the frame counter to the shift register. A short time later the data in the shift registers are clocked serially into the cassette recorder. The frame count totals the number of 1-minute read sequences starting at 0, when the system is intialized, and can total 2^{16} before recycling to zero. Each 16 bit word recorded by the cassette is followed by a four bit word gap. The data are further blocked by inserting a record gap of 16 blank bits between blocks of 128 data points.

The data cassettes are read using a Memodyne Cassette Reader which has been interfaced to a Hewlett-Packard 21 MX minicomputer (fig. 5). The Hewlett-Packard data handling software provides us the capability of printing either the raw data or converted field values, scaling the time and field data and making printer plots of 2^N point averages, and evaluating the data noting the location of any obvious errors in the frame count or field values. In addition, the raw data can be written to an IBM compatible tape for further analysis using a larger computer.

In developing and installing these observatories we encountered a number of problems. Most of these problems have been corrected. There remain, however, a few unsolved problems relating to the final installation of the observatory.

The problems encountered with the magnetometer portion of the observatory stemmed primarily from insufficient documentation of the Geometrics 816 Magnetometer and the changes necessary

to have the instruments operate consistently at 1/4 γ resolution. In addition, there were some bad solder joints on the sensor connectors and a few of the instruments had very noisy input transistors. The magnetometers also occasionally produce intermittent sections of obviously bad data. The cause of this problem has been extremely difficult to diagnose as our laboratory has a very high level of magnetic noise. The noise level of the laboratory is such that any signal put into the magnetometer large enough to be observed above the noise is also large enough that the phase locked loop is no longer marginal and the instrument does not fail.

The recording units received did not meet the manufacturer's specifications. To read the cassette tapes (including the test tape), it was necessary to lengthen the word and record gaps. This seemed to alleviate the problem for a while; however, continued operations appears to degrade the performance even farther requiring substantial relaxation of the reader gap specifications to permit reading the tapes without read errors. Also, moisture over the period of a month caused rusting and failure of several drive capstans.

The system controllers operate well when run for short intervals of time. When running for a long period of time, however, the frame counter occasionally drops the second count bit as it writes on the cassette tape. This causes only every fourth count to be correct. This problem is again difficult to solve since we have not yet been successful in causing this failure in the laboratory.

The large volumes of water associated with the heavy rains early in 1978 caused problems with the observatory installations including in some cases collapse of the fiberglass pits. This problem has demonstrated the need for stronger pits as well as the importance of geological considerations in site selection.

INSTRUMENT TESTS

The first information required for processing and understanding total field magnetic data is information on how well the instruments track each other given an identical input signal. To this end we initiated a closely spaced array test.

This test consisted of installing four complete observatories within 100 m of one another. The observatories were then run continuously for a period of three weeks. The data collected were transferred to an IBM compatible tape. The time information was edited and the data from the four observatories were merged into a single file in parallel format. The obviously bad data were deleted and an array average was calculated. Residuals from this average were calculated for each observatory and histograms of these residuals were plotted. With the exception of one observatory the histograms showed a 2α confidence interval of $\pm$ 1 γ about the mean. This is quite good considering the noisy city environment of the test. The bad instrument was not working properly at the time and has since been modified.

The final step in the operation involved installing the observatories in their final field configuration in the vicinity

of the San Andreas Fault. The sites are all in isolated locations where they cannot be easily observed from raods. Drainage was also an important consideration.

The instruments are installed in fiberglass pits 2 feet in diameter and 6 feet deep which are buried in the ground. The magnetometer and system controller sit on an instrumentation shelf. The instrumentation rests on the equipment rack which holds the ten 1,000 ampere hour carbon air cells that provide power for the observatory. The sensor is installed inside a 4 in. by 8 in. redwood post to hide it from view. This post is the only portion of the observatory that is obvious when the observatory is left unattended.

DATA ANALYSIS

Fig. 6 shows 15 minute averages of the raw magnetometer data from the closely spaced array test. During this 22 day test only Station 1 worked properly. The instrument in Station 5 showed an extremely high percentage of bad data with the bad points occurring when the magnetic field has a value near the upper edge of the magnetometer's operational range. To some extent, Station 2 exhibits the same behavior, only for low field values. The settings on these two magnetometers were the same. This suggests that a single setting, at least in a moderately noisy environment, may not be able to accommodate the daily dynamic range of the earth's magnetic field unless the circumstances are fortuitous, as in the case of Station 1.

The high percentage of bad data required the development of a new procedure for editing the data. The procedure used to edit the data consisted of breaking the time series into a number of segments, establishing the statistics for these segments, and subsequently flagging all points outside a statistically selected range. To accomplish this the data in a given interval are first flagged if they fall outside an expected range and then sorted in ascending order. Using the number of unflagged data points in the time interval, the lower, median and upper quartiles are determined. All points falling outside the range 2.5* (quartile-median) about the median are flagged. The flagged points in the interval are then removed by linearly interpolating between neighboring unflagged points. This editor worked quite well in most cases, but it fails when more than 50% of the points in any one interval are bad (fig. 7, Station 5).

After editing the data and creating an array mean, the residuals for each station were calculated. Fig. 8 shows the array mean and residuals for the closely spaced array test. The noise in these residuals is less than 4 γ, peak to peak, with the exception of Station 3. The gaps and large spikes in the data are a result of the noise in Station 5 contaminating the array average. The addition of Station 2 on June 22 caused the observation base line shift. The large variation near the end of the record is artificial and results from the data editor's interpolating nonexistent data. Histograms of the residuals (fig. 9) also show contamination of the average, this time with the random 3 γ steps of Station 3. These statistics demonstrate the importance of using an uncontaminated array mean.

The first data from the Liebre Mountain array (figs. 10, 11) show a much quieter magnetic environment and consequently a smaller number of bad data points (about 100 points/day maximum). Histograms of the residuals (fig. 12) show two peaks each separated by 2 γ. The residuals for quiet time indicate that Station 1 has two fixed states separated by 2 γ. During the magnetis torm at the end of the record there is also an apparent time dependence of the residual. This may result from induction effects causing variable station differences. The two states observed at Station 1 may be caused by the system controller as the 2 γ difference could be caused by dropping the same bit in the field counter as was dropped in the frame count. The dispersion of the peaks about their mean values is 0.36 γ which may be taken as the accuracy of the two station residual. This result demonstrates that the dispersion for a particular station is roughly one half gamma for the one minute raw data.

SUMMARY AND CONCLUSIONS

A two-dimensional array of total field magnetometers is being established along the San Andreas Fault in the vicinity of Gorman, California. Currently three magnetometers have been installed and are continuously recording variations in the earth's field. Two additional instruments will be installed in the near future. Deployment has progressed in three phases; initial system development and checkout; a closely spaced array test, and installation of observatories along the fault. Experience

obtained in each phase of this work shows that considerable care is required to obtain meaningful data for use in earthquake prediction.

In the first phase of this project five Geometrics proton precession magnetometers were modified for one quarter gamma resolution measurements and interfaced with a Memodyne digital cassette recorder. While the magnetometer modifications are simple in principal, we have found it difficult to make them work reliably for long intervals of time. The main problem seems to be weak proton precession signals which cause the detector to lose lock and count erratically. Optimization of the magnetometer signal to noise ratio has been extremely difficult in the noisy environment of our UCLA laboratory.

The Memodyne digital cassette recorders have been another source of difficulty. A major problem encountered in this component is the inability of the cassette reader to distinguish between bit, word and record gaps. Variations between various recorders and within a single recorder as environmental conditions change exceed the tolerances of the reader as originally manufactured. We have found it necessary to increase the relative size of both word and record gaps to reliably retrieve recorded data.

In addition to these problems, we are still plagued by system controller problems of unknown origin. The symptom of this problem is a failure of certain bits in the frame counter which distorts the recorded time information. The problem only occurs occasionally after long intervals of time and disappears with a system restart. Data are recoverable but only with additional programming effort.

In the second phase of this project we performed a closely spaced array test. Four instruments were placed in close proximity and continuously monitored the earth's field for a three-week interval. Data from this test were processed in the same manner as data to be acquired on the San Andreas Fault. This test revealed additional problems with the magnetometers and showed the sensitivity of the final data to malfunctions in any one instrument.

One major conclusion from this test is that when the magnetometers have a poor signal-to-noise ratio, they produce occasional erratic readings in certain portions of their dynamic range. Another conclusion is that at least one of the magnetometers experiences random step function offsets of $\pm$ 4 γ. The cause has not been identified.

Another conclusion from this test is the necessity for careful editing of the input data. A single bad value in an hour of data can bias the array mean sufficiently to perturb station residuals by noticeable amounts. Unfortunately, when the magnetometer signal-to-noise ratio is not optimized, more than 50% of the data can be bad by amounts exceed 1000 γ. In these circumstances, even very sophisticated editing programs fail.

In the third phase of the project we have installed three of five planned observatories on the San Andreas Fault. Two weeks of data recorded at these observatories have been received and processed. These data show that most of the problems encountered in the two initial phases have been eliminated. The raw data are extremely good and after editing no bad data are apparent.

REFERENCES

Johnston, M. J. S., G. P. Myren, N. W. O'Hara and T. H. Rogers (1975) A possible seismomagnetic observation on the Garlock Fault, California: Bull. Seis. Soc. Amer. 65:1129.

Johnston, M. J. S., B. E. Smith and Mueller (1976) Tectonic magnetic experiments and observations in western U.S.A.: Unpublished manuscript, 1976.

Johnston, M. J. S., B. E. Smith, J. R. Johnston, and F. J. Williams (1973) A search for tectonomagnetic effects in California and western Nevada, Proceedings of the Conference on Tectonic Problems of the San Andreas Fault System, edited by R. L. Kovach and A. Nur: Stanford Univ. Publ. Geol. Sci. 13:225-238.

Rikitake, T. (1975) Earthquake precursors: Bull. Seis. Soc. Amer. 65:1133-1162.

Shamsi, S. and P. Stacey (1969) Dislocation models and seismomagnetic calculations for California 1906 and Alaska 1964 earthquakes: Bull. Seis. Soc. Amer. 59:1435-1448.

Wyss, M. (1975) A search for precursors to the Sitka, 1972, earthquake: sea level, magnetic field, and P-residuals: Pure Appl. Geophys. 113:297-309.

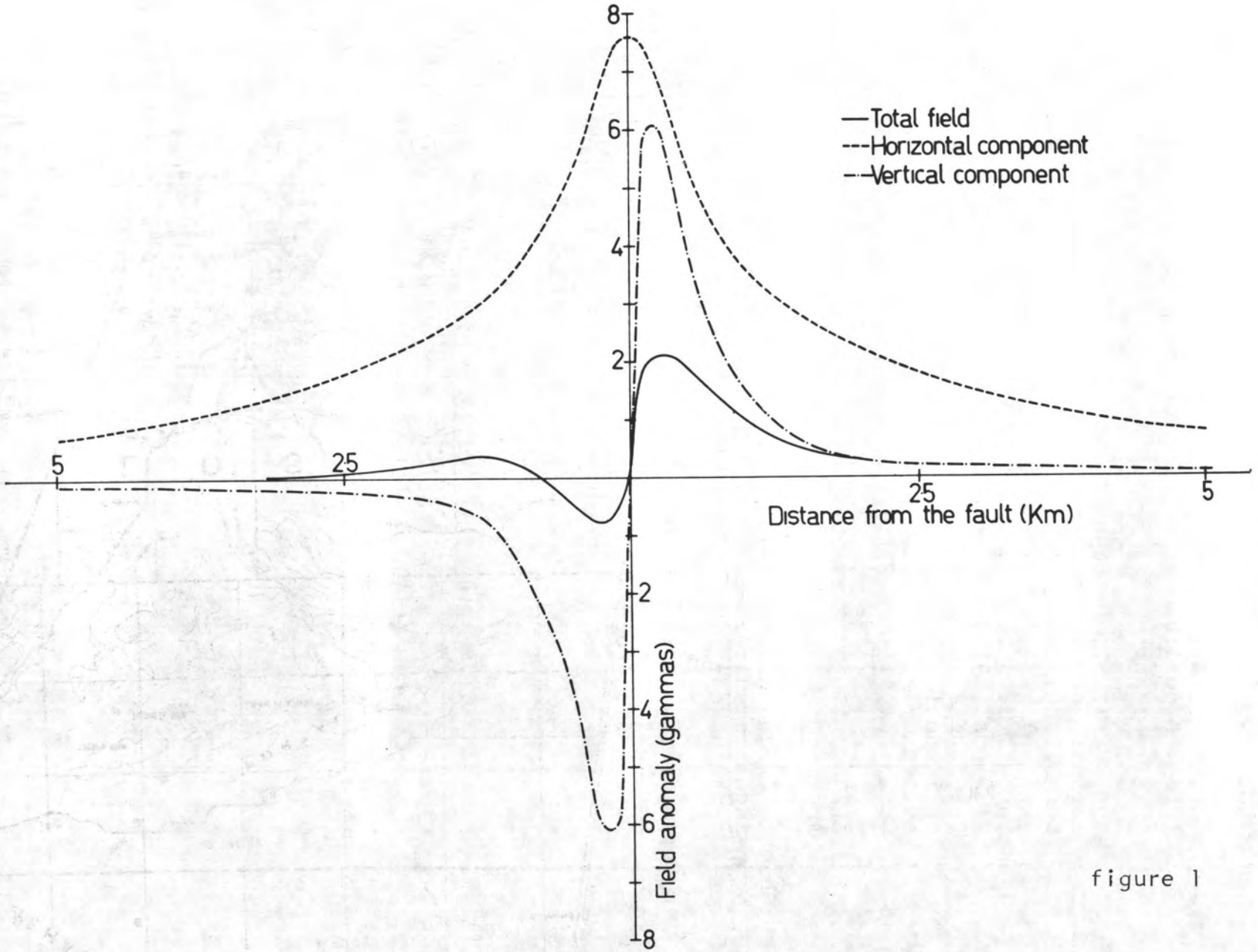
8
6
4
2
—Total field
---Horizontal component
-·-Vertical component
5
25
25
5
Distance from the fault (Km)
2
4
6
8
Field anomaly (gammas)

figure 1

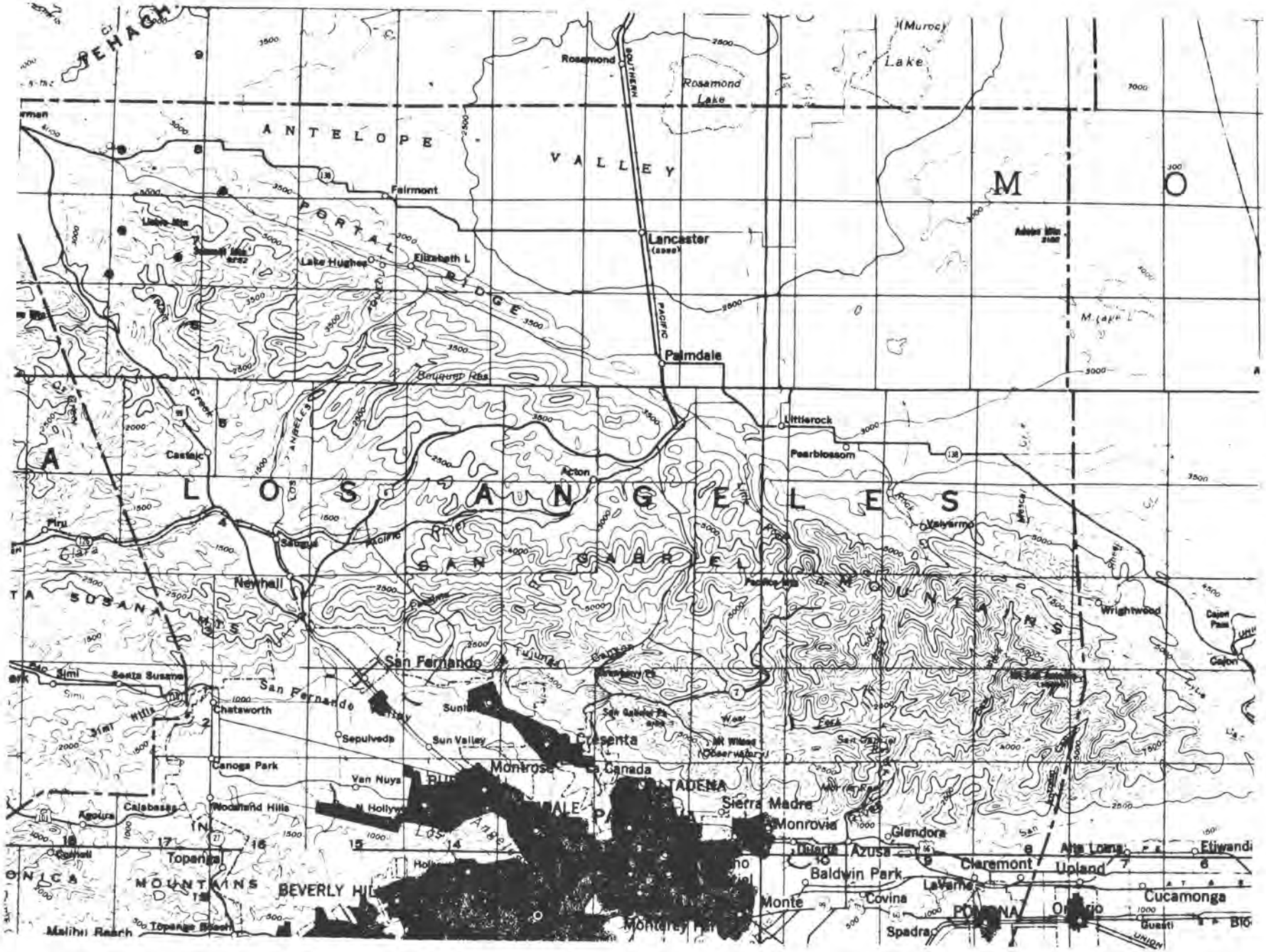
ANTELOPE VALLEY
Rosamond
Rosamond Lake
Lake
Fairmont
Lancaster
Palmdale
Lake Hughes
Elizabeth L
PORTAL RIDGE
PACIFIC
Littlerock
Pearblossom
Acton
Castaic
Piru
Saugus
Newhall
SAN GABRIEL MOUNTAINS
Wrightwood
Cajon Pass
Valyermo
San Fernando
Santa Susana
Simi
Chatsworth
Sepulveda
Sun Valley
Crescenta
Canada
Monrose
Canoga Park
Van Nuys
Woodland Hills
Calabasas
Agoura
Topanga
MONTAINS
BEVERLY HILLS
Malibu Beach
Topanga Beach
Sierra Madre
Monrovia
Glendora
Azusa
Baldwin Park
Claremont
Upland
Covina
Monte
Spadra
Cucamonga
Ontario
Alta Loma
Etiwanda

figure 2

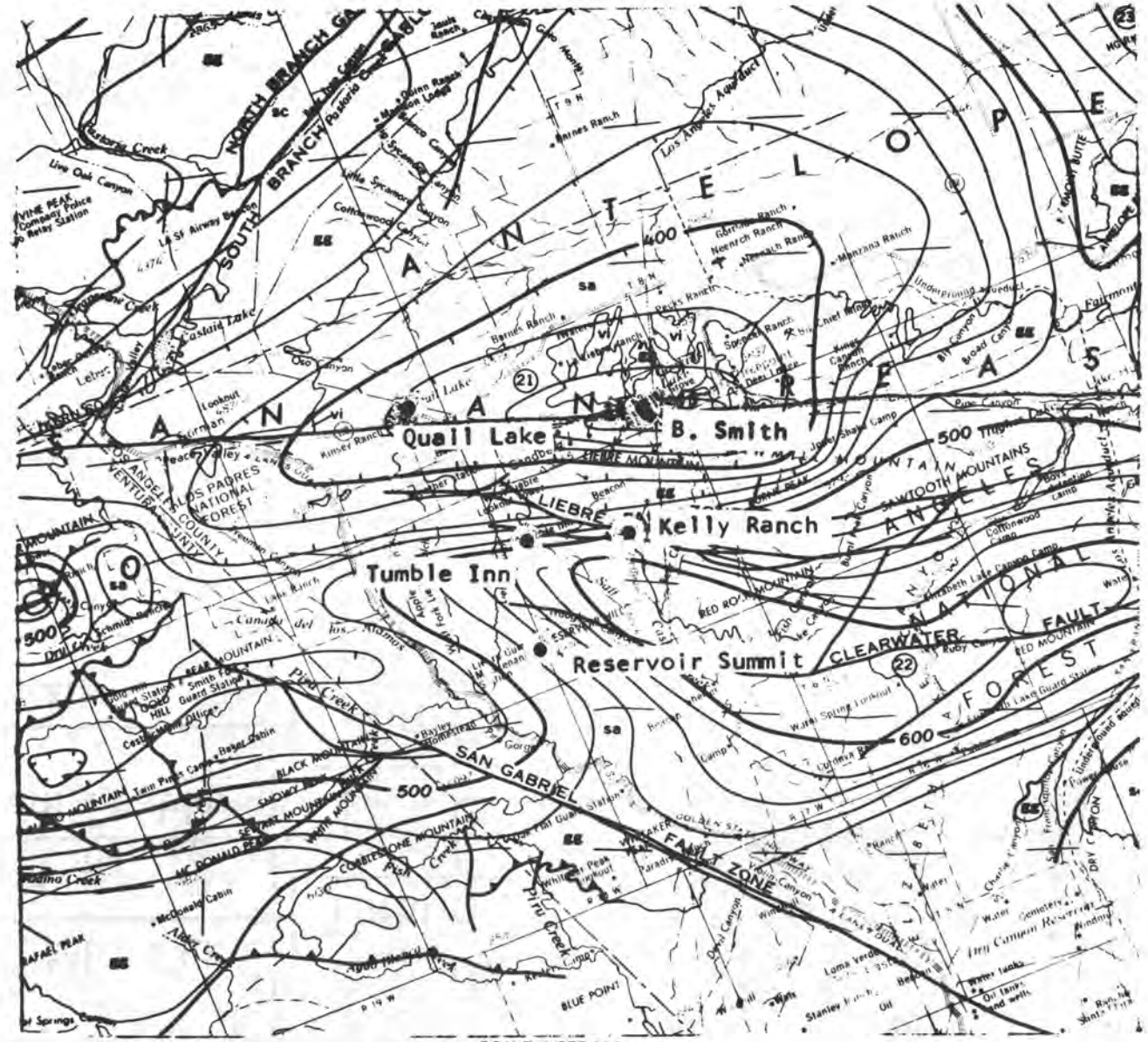
ANTELOPE
VALLEY
ANGELES
NATIONAL
FOREST
Quail Lake
B. Smith
Kelly Ranch
Tumble Inn
Reservoir Summit
SAN GABRIEL
FAULT ZONE
FAULT
CLEARWATER
SAWTOOH MOUNTAINS
LIEBRE
SCALE 1:250 000
25 MILES
25 KILOMETERS

figure 3

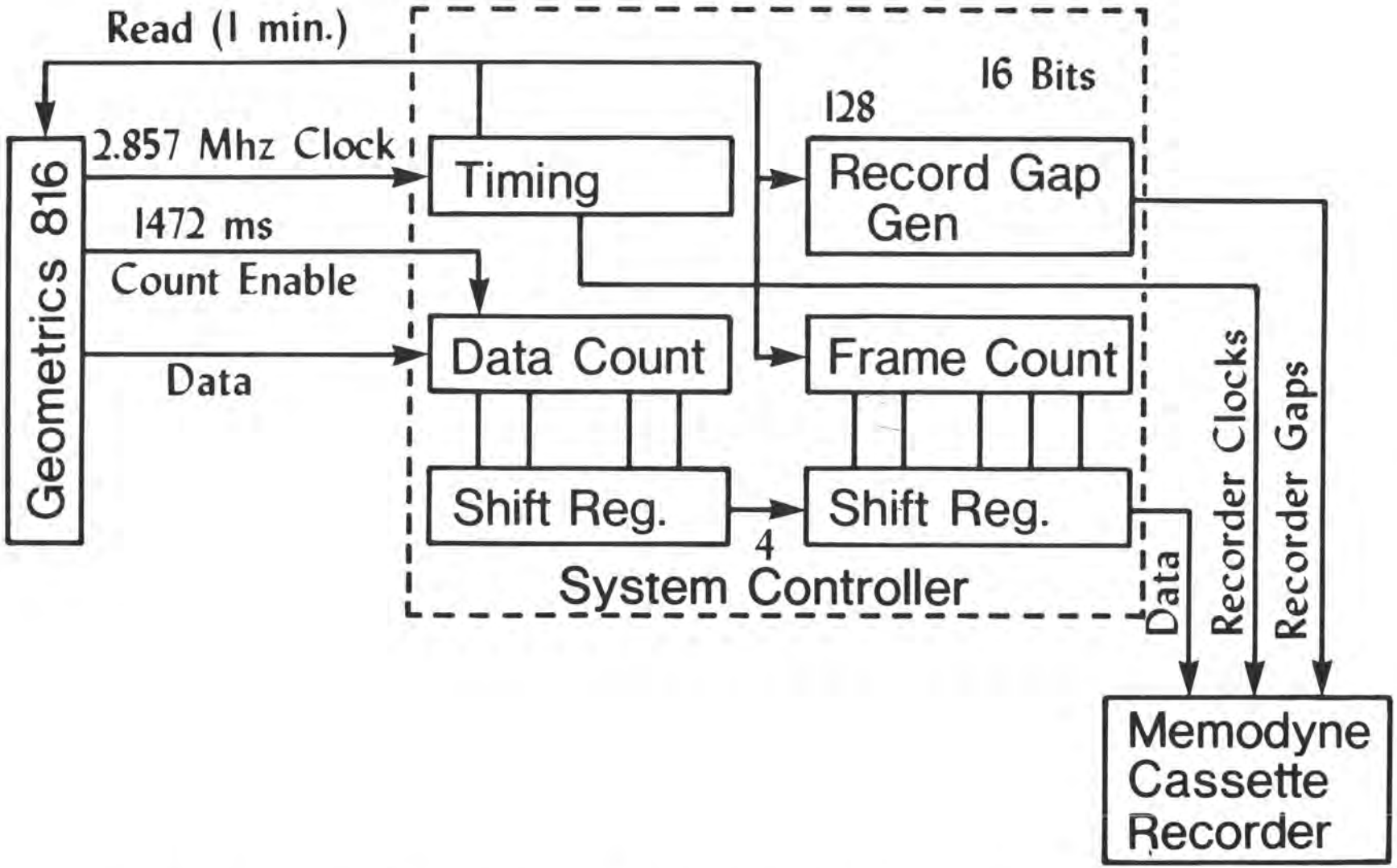

MAGNETOMETER RECORDING SYSTEM

figure 4

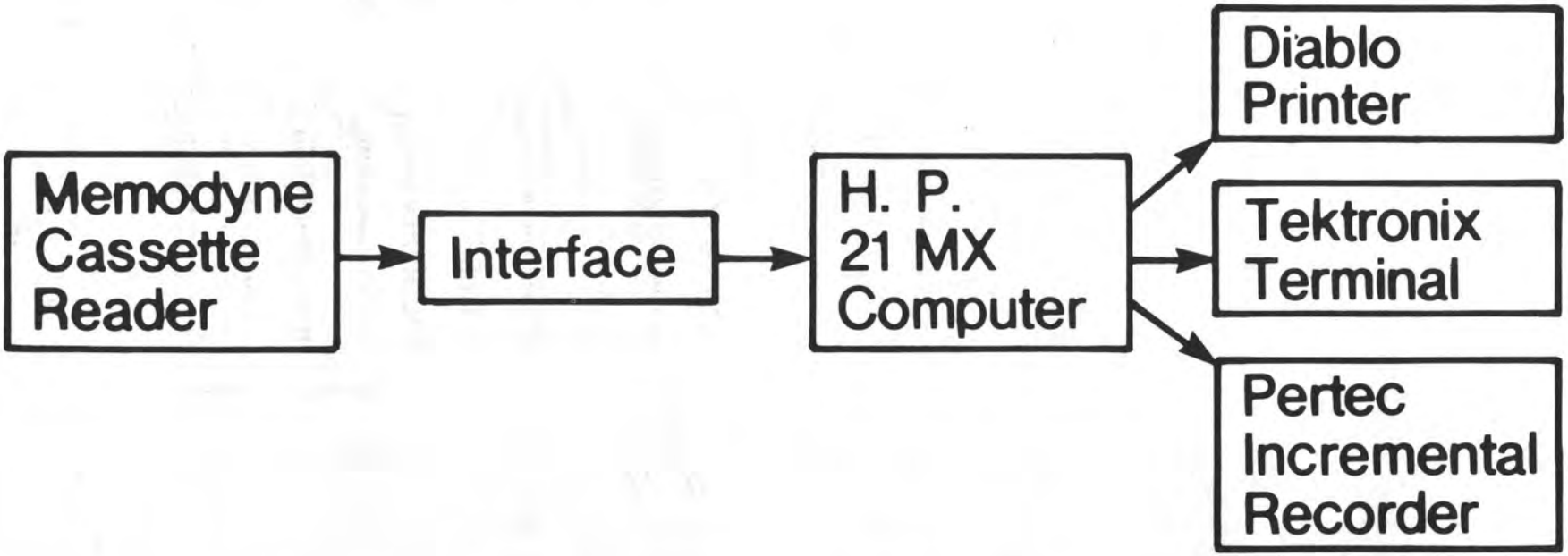

PLAYBACK SYSTEM

figure 5

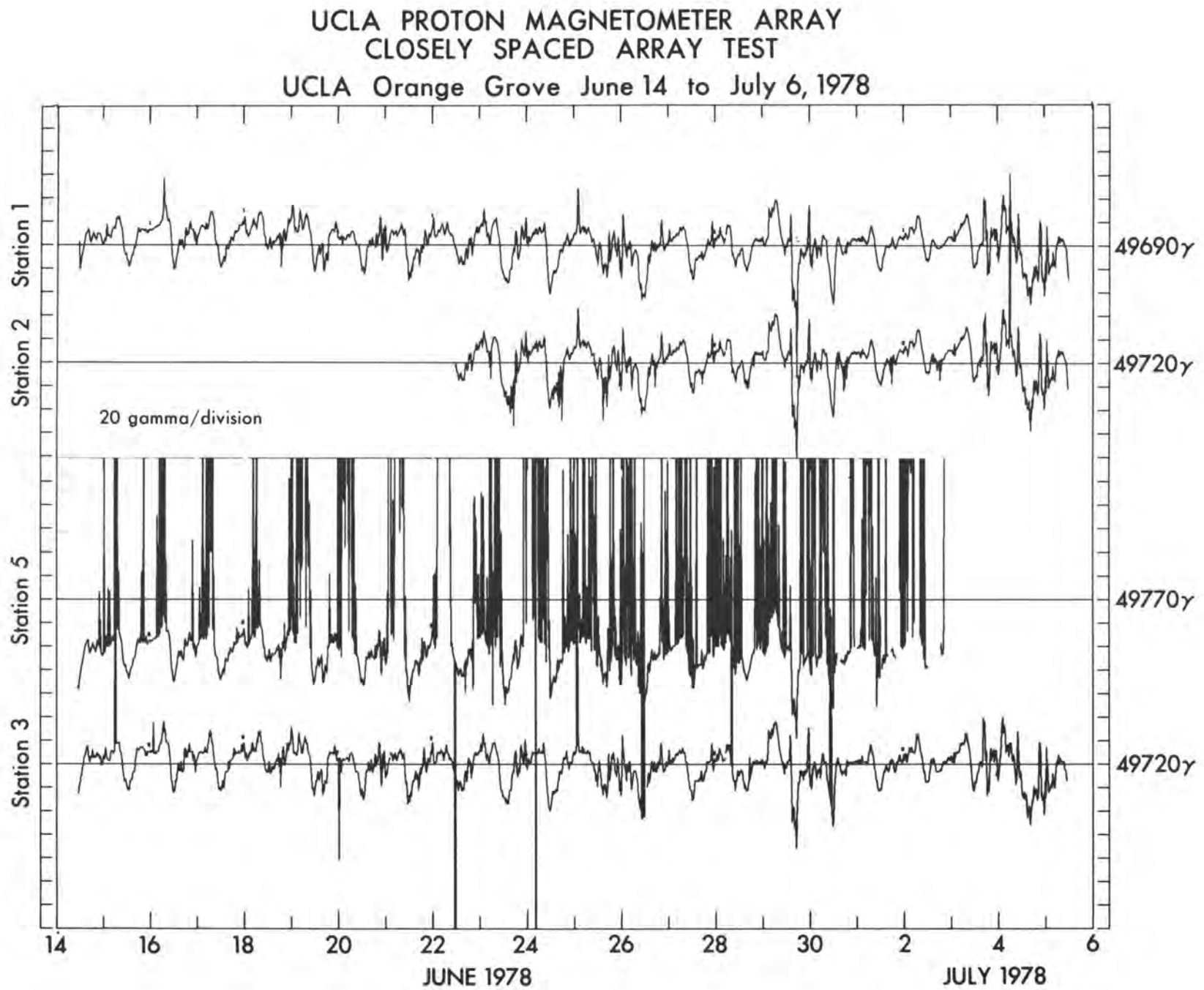
UCLA PROTON MAGNETOMETER ARRAY
CLOSELY SPACED ARRAY TEST
UCLA Orange Grove June 14 to July 6, 1978
Station 1
Station 2
Station 5
Station 3
20 gamma/division
49690γ
49720γ
49770γ
49720γ
14
16
18
20
22
24
26
28
30
2
4
6
JUNE 1978
JULY 1978

figure 6

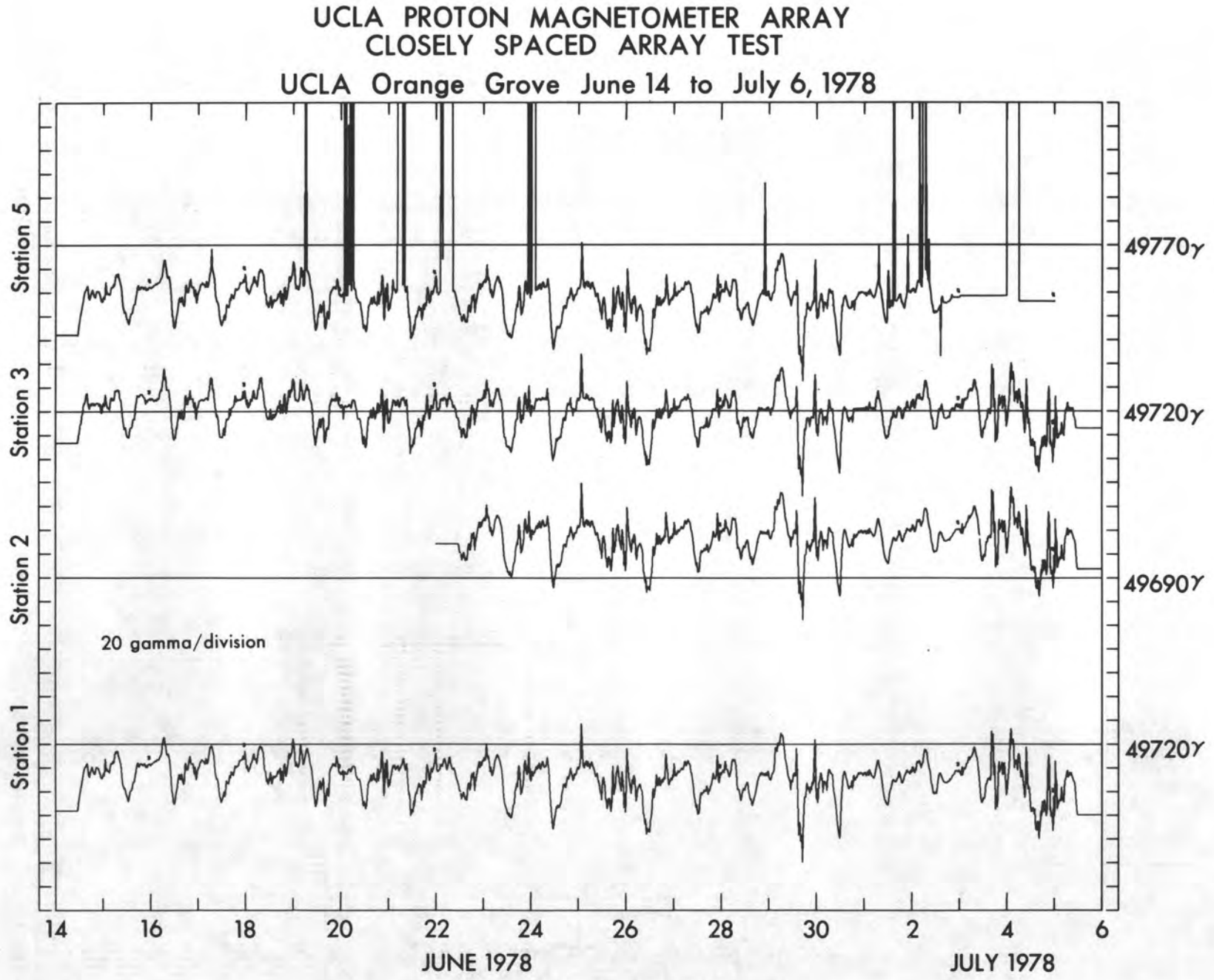
UCLA PROTON MAGNETOMETER ARRAY
CLOSELY SPACED ARRAY TEST
UCLA Orange Grove June 14 to July 6, 1978
Station 5
Station 3
Station 2
Station 1
49770γ
49720γ
49690γ
49720γ
20 gamma/division
14
16
18
20
22
24
26
28
30
2
4
6
JUNE 1978
JULY 1978

figure 7

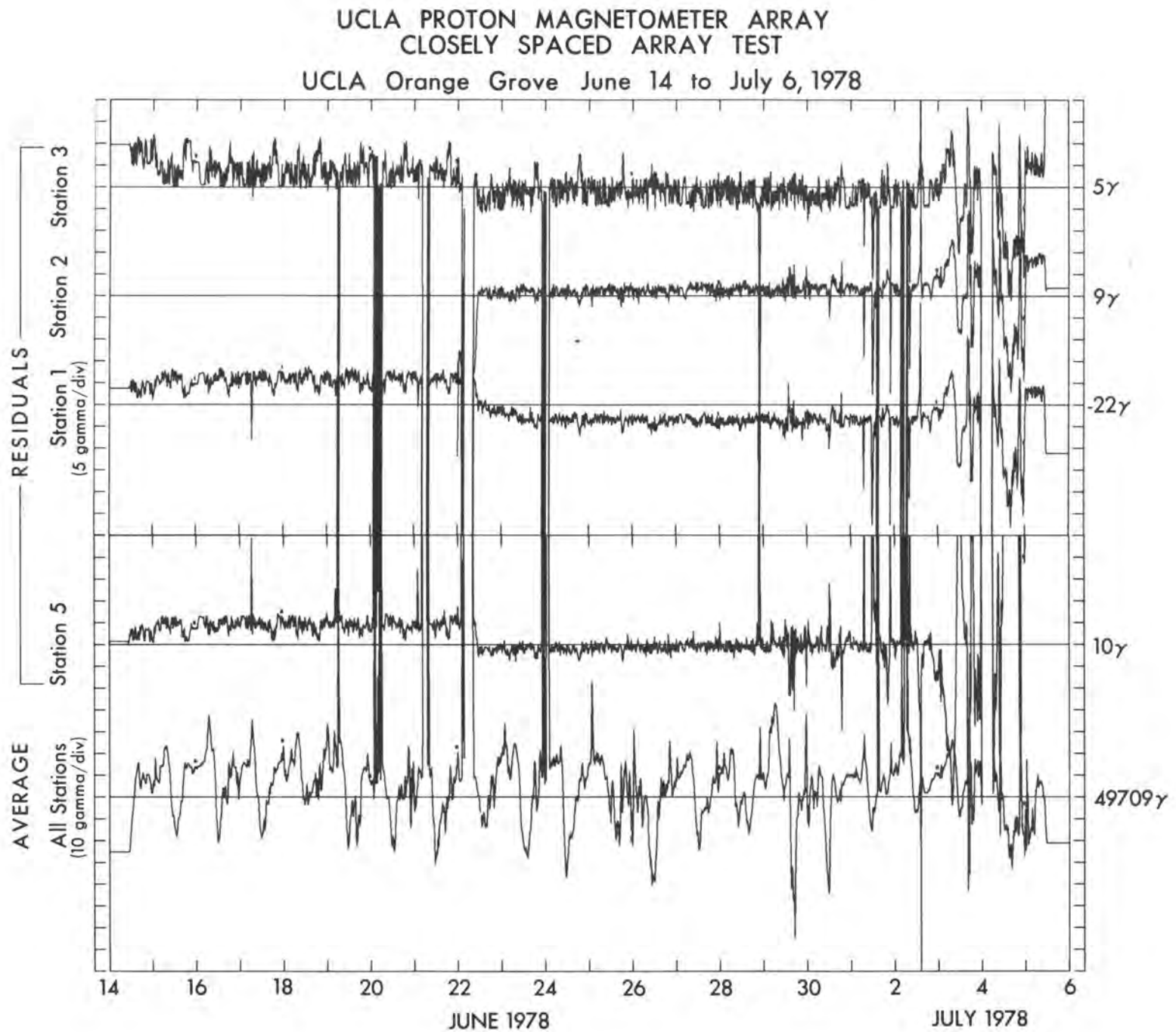
UCLA PROTON MAGNETOMETER ARRAY
CLOSELY SPACED ARRAY TEST
UCLA Orange Grove June 14 to July 6, 1978
RESIDUALS
Station 3
Station 2
Station 1
(5 gamma/div)
Station 5
AVERAGE
All Stations
(10 gamma/div)
5γ
9γ
-22γ
10γ
49709γ
14
16
18
20
22
24
26
28
30
2
4
6
JUNE 1978
JULY 1978

figure 8

UCLA MAGNETOMETER ARRAY
CLOSELY SPACED ARRAY TEST
UCLA Orange Grove June 14 to July 6,1978

Distribution of Station Residuals with Respect to Array Average

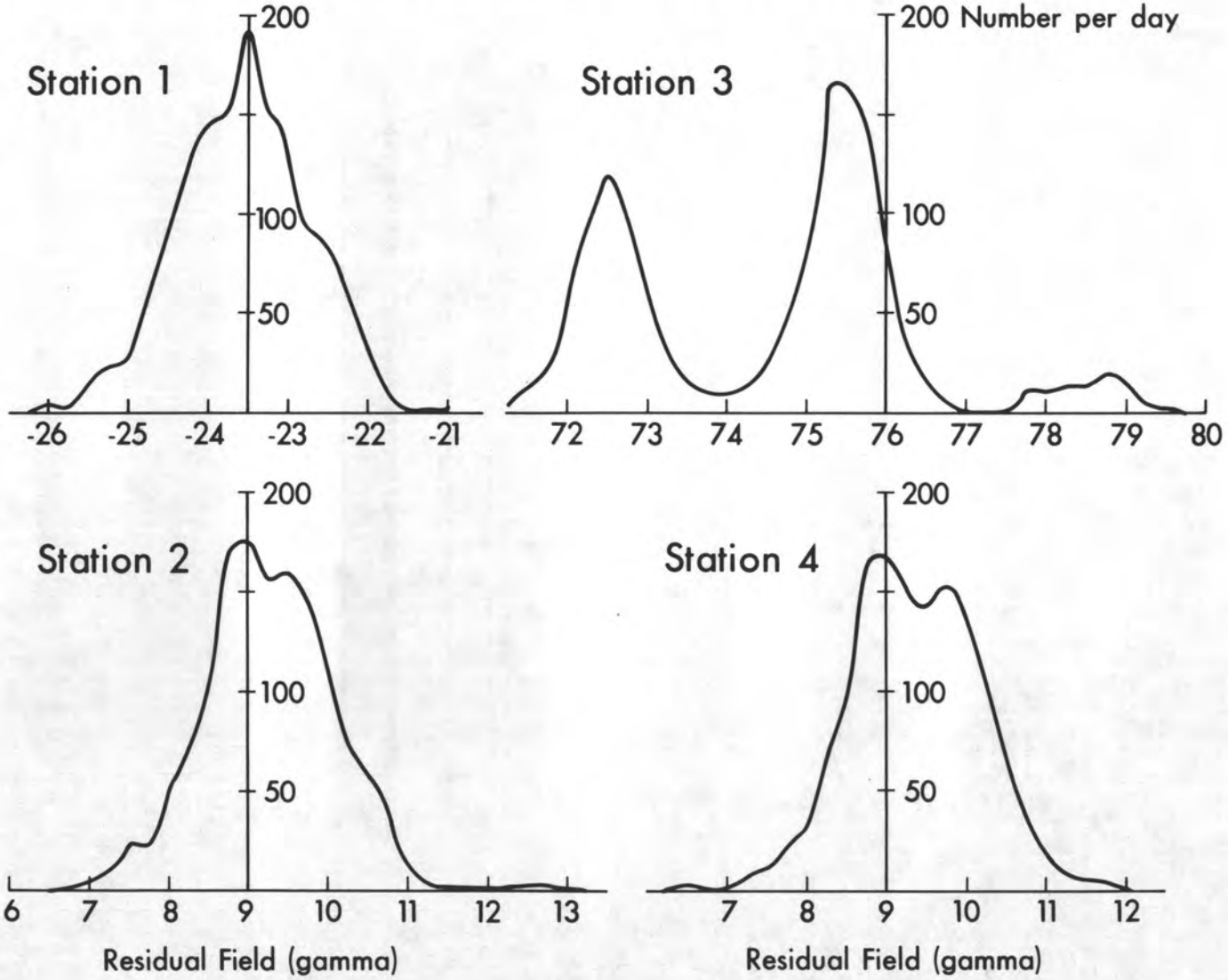

figure 9

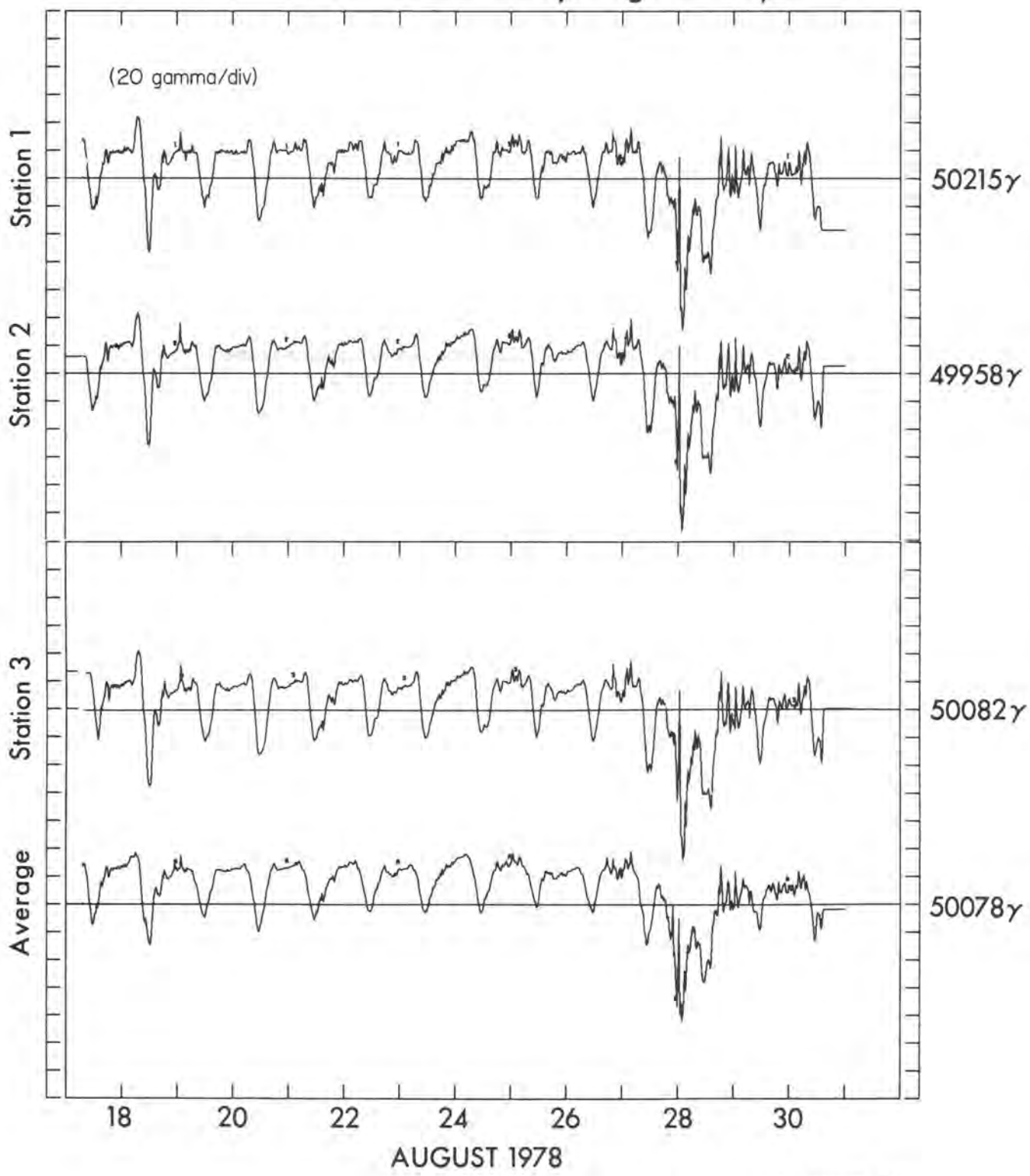
UCLA PROTON MAGNETOMETER ARRAY
PALMDALE BULGE OBSERVATIONS
Liebre Mountain and Vicinity August 17-31, 1978
(20 gamma/div)
Station 1
Station 2
Station 3
Average
50215γ
49958γ
50082γ
50078γ
18
20
22
24
26
28
30
AUGUST 1978

figure 1C

Two Station Array Mean and Station 1 Residual

Palmdale Bulge Data

Aug 17 - Aug 30, 1978

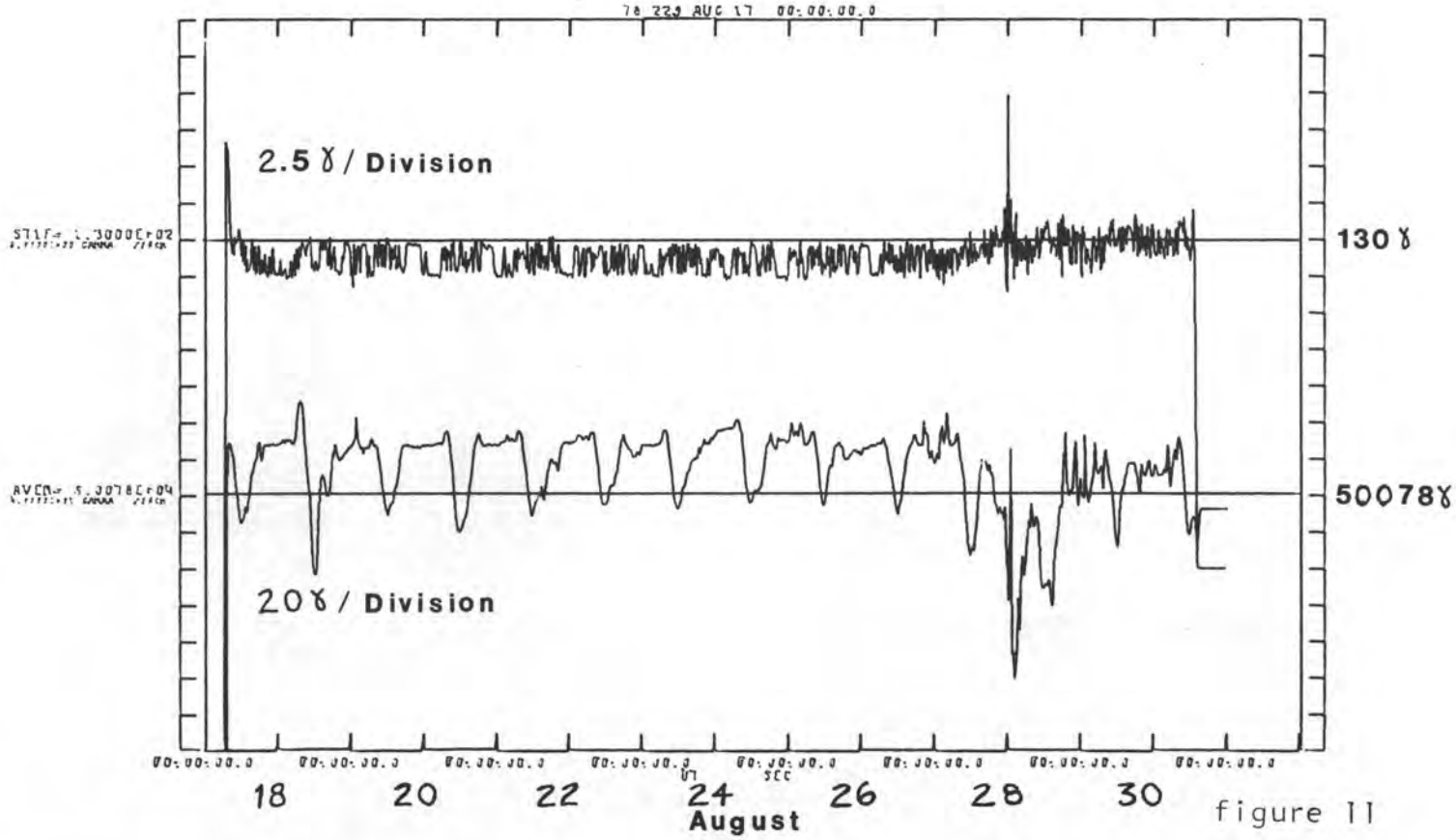

figure 11

HISTOGRAM OF ONE MINUTE RESIDUALS

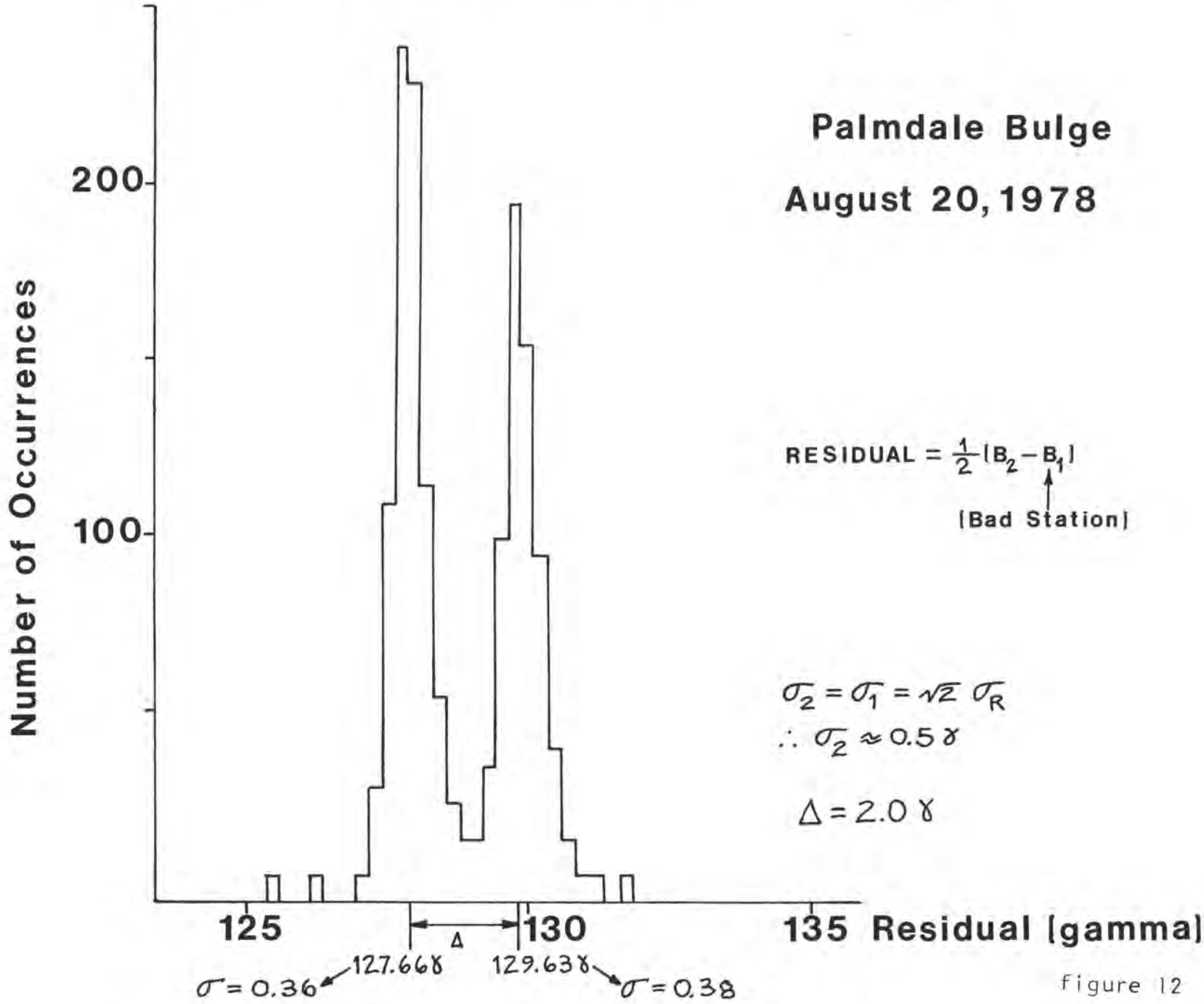

figure 12

Principles of VLBI Applied to Geodesy

Charles C. Counselman III and Irwin I. Shapiro

Dept. of Earth and Planetary Sciences

Massachusetts Institute of Technology

Cambridge, Mass., U.S.A.

Abstract

We discuss the principles underlying the determination of baseline vectors from very-long-baseline interferometric observations of radio sources. We also describe the limitations on achievable accuracy and, very briefly, some of the results obtained and plans for the future.

November 1978

lines from the cental oscillator to the two antennas' mixers, and the phase delays of the two sets of receiving electronics, are equal; any differences not accounted for will introduce errors in the observed interferometric phase. In current practice, these phase errors can be reduced to the level of 1° at a frequency of 5 GHz, or the equivalent of 0.2 mm of path-length error, for a 5-km baseline interferometer (Ryle & Elsmore 1973, and Elsmore & Ryle 1976).

In VLBI, a direct electrical connection between antennas is not maintained. Rather, the LO signal used for the RF to IF conversion at each antenna is derived from an independent frequency standard (see Figure 2). At each site the IF signal is tape-recorded with a reference time base derived from the same standard. Tapes recorded simultaneously at the two antenna sites are later replayed at a processing station where the reproduced signals are cross-correlated to determine the interferometric phase and related observables.

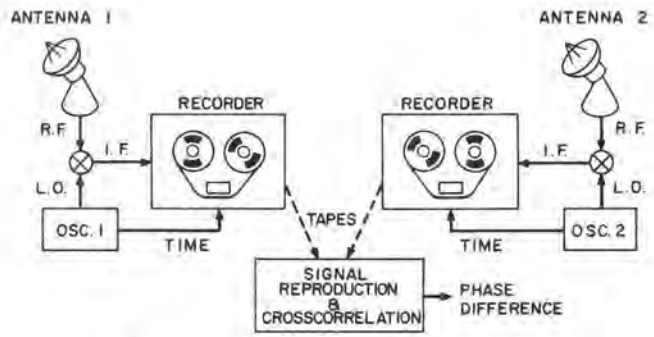

Figure 2 Very-long-baseline interferometer.

The advantage of substituting independent frequency standards and tape recorders for real-time signal transmission links is an economic one: Once the need for a real-time connection between the ends of the baseline is eliminated, baseline lengths of thousands of kilometers become practical. At present, the main disadvantages of VLBI for geodetic applications are that: (a) the IF bandwidth limitation set by the tape recorders may be more stringent than the corresponding limitation of a real-time transmission medium, and (b) very high stabilities are demanded of the frequency standards.

The effect of limiting the recorded bandwidth in VLBI is only to reduce the signal-to-noise- ratio (SNR) of the observations and therefore to raise the lower limit on the flux density of the radio sources that may be decteced with the interferometer. The state of the art of frequency standards is improving with sufficient

I. Introduction

A marriage of convenience has been consummated between the disparate fields of geodesy and radio astronomy. The radio technique of very-long-baseline interferometry (VLBI) promises to have a profound effect on studies of the Earth. Whether such promises will be fulfilled remains to be seen.

In this paper, we will outline the basic principles involved in applications of VLBI to geodesy, discuss some of the important factors limiting the accuracy of the technique, and describe briefly some recent geodetic results. Minor deviations from the truth will occasionally be allowed to accompany explanations so as to emphasize the main points without adding the confusion that usually accompanies too many qualifications.

II. Basic Principles

Interferometry is certainly not new nor is radio interferometry. What is new is the technique of very-long-baseline interferometry, the use of widely separated radio antennas in an interferometric mode. To understand the distinction between conventional and very-long-baseline radio interferometry, we first describe each briefly, emphasizing the contrast. We then discuss, in turn, the basic observable, its information content, and the limitations on the accuracy of its determination.

1. Interferometry Equipment

Figure 1 shows, in simplified form, a typical conventional interferometer with two antenna-receiver systems. At each antenna the radio-interferometry (RF) signal received from the source being observed is converted to a lower, "intermediate" frequency (IF) by mixing with a local-oscillator (LO) signal. The LO signals are supplied to the mixers at both antennas via transmission lines from the centrally located oscillator. The IF signals are carried by similar lines back to the central station where the interferometric phase, equal to the difference between the RF signal phases, is determined by cross-correlation of the two IF signals. Ideally, the electrical path lengths of the transmission

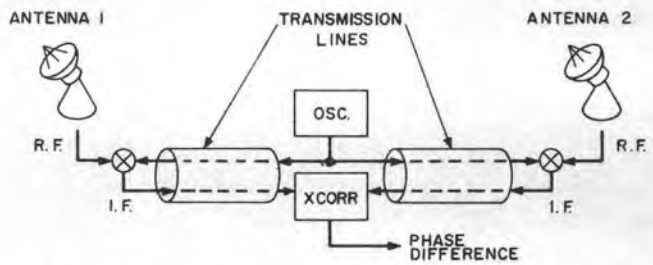

Figure 1 Conventional, connected-element radio interferometer.

rapidity that instabilities of the standards will not pose the limit on the geodetic accuracy achievable with VLBI.

The parameters of a typical very-long-baseline interferometer are presented in Table 1. Various tradeoffs exist, based on the fact that the SNR is given by:

$$\frac{S}{N} \approx \left(\frac{(A_1 \varepsilon_1)(A_2 \varepsilon_2) B \tau}{T_{s1} T_{s2}} \right)^{1/2} F \qquad (1)$$

where A_i, ε_i, T_{si} are, respectively, the antenna area, its efficiency, and the system temperature at site i (i=1,2); B is the bandwidth of the tape recording; τ is the integration time; and F is the correlated flux density (that fraction of the total flux density from the source that "survives" cross correlation). As an illustration of possible tradeoffs, note that an increase in bandwidth to 56 MHz, as will be achieved in our new Mark III system*, could be accompanied by a decrease in the diameter of one of the antennas to about 4 m with essentially no overall loss of sensitivity.

Table 1

Parameters for a Typical Very-Long-Baseline Radio Interferometer

Antenna diameter (each site)	25 m
Antenna efficiency (each site)	50 %
System noise temperature (each site)	100 K
Recorder bandwidth	2 MHz
Integration time	300 sec
Signal-to-noise ratio for source with 1 Jy correlated flux density	~25

Note: 1 Jy = 10^{-26} w/m^2-Hz.

*A prototype of this new system, developed by our group, was tested for the first time, successfully, in September 1977. The system is scheduled for operational use on several antennas by early 1979.

2. Time-Delay Observable

What actually do we seek from the data? Primarily, we wish to determine the difference Δt in the times of arrival at each antenna of the same wave front from a celestial (point) source of radio radiation. The source is usually sufficiently far away so that the wave fronts can be considered to be plane at the Earth. (For certain applications, where, for example, the source is an earth satellite, spherical wave fronts must be considered.) The error in determining Δt is essentially independent of the length, d, of the baseline separating the two antennas. This simple fact is the key to the potential usefulness of this technique for geodetic applications: a determination of the difference between two antennas 1 km apart with an error of the order of a centimeter would not be so terribly impressive. But the fact that this error can be kept almost this low even for antennas separated by intercontinental distances is the impressive feature of the technique.

The arrival-time difference Δt is deduced by computing the cross-correlation function between the two recordings of the signals received at the respective antennas. The value of the time-offset argument for which the cross-correlation function is maximized is a good estimate of Δt. However, if the bandwidth of the recording is infinitesimal compared to the center frequency of the band of radio signals that are received, then we can determine Δt only modulo λ/c, where λ is the wavelength of the essentially monochromatic radiation. That is, the cross-correlation will have essentially equal maxima for many values of Δt, each of which differs from the other by λ/c. Thus, if propagation is through a non-dispersive medium, which we shall here assume for expository purposes, we may suppress the difference between phase and group delays and write

$$c\Delta t = n\lambda + \delta\lambda; \quad 0 \leqslant \delta\lambda < \lambda$$

$$2\pi f\Delta t = 2\pi n + \phi; \quad f = c/\lambda; \; 0 \leqslant \phi < 2\pi,$$

where n (a positive or negative integer) would be essentially indeterminate from this nearly single-frequency measurement. This, ambiguous, observable Δt is, in reality, the phase delay.

In practice, one does not record only a single frequency. But, if the bandwidth Δf of the recording is only narrow instead of infinitesimal, we are not helped much. We will still be plagued by ambiguities which, however, will not be essentially infinite in number. Rather, the ambiguities will spread only over a time offset interval of the order of $(\Delta f)^{-1}$. The cross-correlation in the noise-free case as a function of the difference, $\delta\Delta t$, between the actual and true offset is proportional to

$$\frac{\sin\,(2\pi\Delta f\delta\Delta t)}{\delta\Delta t}\,(\cos\,2\pi f\delta\Delta t)\ ,$$

where the first term provides the 'sin x/x' envelope that restricts the ambiguities (maxima of cos $2\pi f\delta\Delta t$) to lie in a region of approximate extent $(\Delta f)^{-1}$.

Suppose, however, that the only restriction on the experiment is that samples of the incoming signal can be recorded at a rate no higher than a prescribed maximum. That is, we would not be restricted to sampling the signal only over a single band of extent Δf; we could, for example, sample several distinct parts of the spectrum with the total of the sampled bandwidths being Δf. What then would be the optimum strategy to minimize the error in the determination of Δt? An efficient scheme, called bandwidth synthesis (see, for example, Whitney et al. 1976), involves the sampling of several narrow bands distributed throughout an extremely wide band. From the relation

$$2\pi f\Delta t = 2\pi n + \phi$$

it follows that

$$\Delta t = \frac{1}{2\pi}\,\frac{d\phi}{df}\ .$$

The delay sought, then, is simply the slope of the curve of phase vs. (angular) frequency: at a given instant, the cross-correlation will have a maximum at a different phase, but at the same time offset, for each different frequency. Therefore, if we sample the ϕ vs. f curve over a very wide band we can determine the slope and, hence, Δt very accurately. This observable is, in reality, the group delay. The standard error $\sigma(\Delta t)$ in this estimation of Δt is

$$\sigma(\Delta t) \cong \frac{\sigma(\phi)}{2\pi(f_{max} - f_{min})}\ ,$$

where $f_{max} - f_{min}$ is the synthesized bandwidth and $\sigma(\phi)$ is related to the uncertainty in the estimation of ϕ from each of the separate narrow bands. These latter must be distributed so as to insure no ambiguity. (The satisfaction of this criterion will depend on the achievable signal-to-noise ratio.) One useful scheme is to distribute the frequencies in a geometric progression, $f_1,\ldots,f_n$. The phase vs. frequency between the closely spaced f_1 and f_2 can

be determined unambiguously with the aid of the slopes determined from the finite, non-zero bandwidth, Δf. The more accurate slope resulting from this connection can then be used to extend the connection to f_3, etc. The actual analysis of the data proceeds in a different, optimal fashion, but the description given here contains the essential ideas. A more precise formula for the uncertainty $\sigma(\Delta t)$ in the estimate of Δt from application of the bandwidth synthesis technique is:

$$\sigma(\tau) \simeq 3.2\times10^{3}\left(\frac{T_{s1}T_{s2}}{N}\right)^{1/2} \frac{1}{D_1 D_2 (\varepsilon_1\varepsilon_2)^{1/2} F \Delta f_{sp}} \text{ sec}$$

where, in addition to the quantities defined earlier, we introduced $D_i (i=1,2)$ for the antenna diameter, in meters, Δf_{sp} for the spanned bandwidth, in Hertz, and N for the number of tape recorded and cross-correlated samples, dimensionless. The quantities T_s and F are expressed in °K and Janskys, respectively. For the Mark III system with $D_i \simeq 25$ m, $T_i = 100$°K, $\varepsilon_i = 0.5 (i=1,2)$, and $\Delta f_{sp} = 400$ MHz, we find $\sigma(t) \simeq 0.05$ nsec for a 100-second observation of 1 Jy source.

For typical values of SNR, synthesized bandwidths of 400 MHz can be spanned unambiguously with six narrow bands or "windows". The signals in the separate windows can be sampled sequentially, or simultaneously; in the latter case the instantaneous recorded bandwidth would be divided equally among the separate windows. For this type of bandwidth synthesis to work, it is of course essential that strict account be kept of the instrumental phase relations for the different frequencies. A suitable phase-calibration scheme has been developed for this purpose. If the overall system is properly calibrated, and the signal-to-noise ratio sufficiently high, it is possible to eliminate entirely the phase-delay or 'fringe ambiguity' so that the error in Δt can be reduced to $\sigma(\phi)/f$, i.e. to the time-equivalent of a fraction of a wavelength. For observations made with $\sigma(\Delta t)$ below about 0.1 nsec ($\approx$3 cm), the useful interpretation of Δt is limited by the Earth's atmosphere, as discussed in Subsection 4.

3. Information Content of Observable

What in fact can we deduce from measurements of Δt? A single (instantaneous) measurement, involving two antennas, suffices in essence to locate the radiation source on the surface of a cone whose axis is the intersite vector, $\vec{d}$, and whose half-angle, θ, is determined by $c\Delta t$ and the intersite distance:

$$\cos\theta = \frac{c\Delta t}{d} .$$

This result, though perhaps interesting, does not help much by itself. However, with a series of measurements, we can infer not only the vector $\vec{d}$ but also the direction to the source, any proper motion of the source, variations in the motion of the Earth's crust with respect to its axis of rotation, the motion of this axis with respect to a stellar reference frame, etc. The procedure is based largely on the 'bootstrap principle' and its success is based on the following fact: the theoretical expression for Δt is a function of the source direction, the antenna locations, the time of day, the model atmosphere employed, etc. By parameterizing this theoretical expression in terms of the (a priori partially unknown) source direction, antenna locations, etc. and by making a sufficiently large number of observations of each of a number of celestial radio sources, we can estimate the 'best-fit' values for these parameters from, say, a weighted-least-squares analysis. All effects are incorporated that affect the time-dependence of the location of the antenna sites with respect to the sources. The extraction from the delay observables of estimates of the relevant quantities is thus a complicated, but routine, exercise in parameter estimation. Each effect under consideration introduces a characteristic time variation in the Δt observable which allows the corresponding parameters to be estimated unambiguously. Of course, nonzero correlations between the parameters cause the standard deviations of the parameter estimates to be increased.

As an illustration of the extraction method, let us consider a very simple example in which the Earth is assumed rigid, with a known and constant rotation vector, and the source positions are assumed fixed in space. Then the unknowns comprise three for the intersite vector $\vec{d}$, two for the direction $\vec{e}_o$ in space of each observed radio source, and one each for the error in initial clock epoch and rate synchronization. By assuming that the axis direction and rate of the Earth's rotation are known, the coordinate system in terms of which $\vec{d}$ and $\vec{e}_o$ are to be expressed is only partially defined. The origin of longitude in the Earth's equatorial plane remains arbitrary but can be specified, for example, by choosing the longitude of one of the sources to be zero. Hence, for observations of n sources, there will be a total of 2n+4 unknowns to be determined. For each source, the time dependence of Δt will then be (if we ignore aberration and other corrections):

$$\Delta t(t) = \frac{1}{c}\vec{d}\cdot\vec{e}_o + \delta t_o^c + \delta \dot{t}_o^c \cdot t$$

$$= \alpha + \beta \sin \Omega t + \gamma \cos \Omega t + \delta \dot{t}_o^c \cdot t,$$

where δt_o^c and $\delta \dot{t}_o^c$ are the initial clock epoch and rate synchronization errors; α, β, and γ are constants; and Ω is the Earth's

spin angular velocity. The dot product $\vec{d}\cdot\hat{e}_o$ represents, of course, the component of the intersite vector along the direction to the source. The constant α contains δt_o^c and the (constant) component of $\vec{d}\cdot\hat{e}_o$ along the Earth's axis of rotation. The constants β and γ are the coefficients of the (sinusoidally changing) components of $\vec{d}\cdot\hat{e}_o$ along two orthogonal directions in the Earth's equatorial plane. Hence arbitrarily large numbers of measurements of Δt for a single source can determine no more than four constants (α, β, γ, δt_o^c); the remainder of the measurements will be redundant. To determine $\vec{d}$ at least three observations must be made of at least n*-1 sources and four observations of an additional source, where n* is the smallest integer that satisfies the equation

$$3n^* + 1 \geqslant 2n^* + 4 \ ,$$

the left side giving the number of 'knowns' and the right the number of 'unknowns'. (Note that the average slope of $\Delta t(t)$ will be the same for observations of every source; hence this slope, δt_o^c, can be determined from observations of a single source.) Clearly, $n^* = 3$. Of course, once the source directions $\hat{e}_o$ have been determined to the required accuracy, or if three or more antennas are involved, a few observations of each of two sources will provide the necessary data.

In the above discussion we assumed, for simplicity, that the difference in the distance of a given source from each antenna site remained constant during a single observation. In fact, the sites move differentially with respect to the source causing Δt to vary and thereby giving rise to the 'fringe rate'. The a priori rate is, of course, taken into account in the data processing; the residual rate is estimated along with the residual Δt and is useful in the deduction of geophysical and astronomical information. Accurate estimates of fringe rate (error $\lesssim$ 0.001 Hz) can also be useful in relating the fringe phases from separate tape recordings, taken sequentially, of signals from a given source. A concise mathematical discussion of the algorithms used for the analysis of the interferometry data is given in part by Whitney et al. (1976) and in part by Shapiro (1976).

The example we have been discussing so far is, of course, simplified in other ways as well. In reality, many other effects must be included in the theoretical model of $\Delta t(t)$, as indicated above. This is at once a disadvantage -- because it means that there are more unknown parameters to be solved for, requiring more measurements to be included in the solution -- and an advantage -- because it means that there are many more things to be learned from VLBI measurements than just station and source positions. Perhaps the most natural way to list quantities of geodetic interest for which VLBI is a useful measuring tool is to list facts of life which are contrary to the simplifying assumptions made in the preceding

example. For example, the Earth's rotation is uniform neither in rate nor in direction, neither with respect to the Earth's "crust", which is not rigid, nor with respect to the "fixed" stars, which are not even "fixed" relative to one another.

Does all of this mean that VLBI is useless? The answer is no, because each of the pertinent assumptions is an excellent one for the short times, on the order of hours, required to make a useful series of VLBI measurements. The Earth's rotation may be described relative to a celestial "fixed" coordinate system by 3 angles: 2 giving the direction of the pole; and the third, the angle of rotation about the polar axis. Variations in the celestial coordinates of the pole are caused principally by torques exerted on the Earth's equatorial bulge by the Sun and Moon. Variations in the spin rate may be caused by changes in the moment of inertia and by dissipation of energy by the tides which the Moon and Sun raise in the fluid and solid Earth. There are also important spin-rate variations believed to be due to variations in atmospheric circulation, core-mantle interaction, and other causes. The position of the pole shifts relative to the crust in a complicated manner reflecting not only lunar and solar forces and the Earth's nonrigid inelastic nature, but possibly also displacements of the crust associated with earthquakes and other tectonic activity.

It is impractical even to mention all of the phenomena that have been suggested as being associated with the Earth's rotation. But, in principle, the application of VLBI is straightforward. Motion of the Earth's pole relative to distant celestial objects would appear as a variation in the coordinates of those objects if the pole were used to define the celestial coordinate system. Likewise, variations in rotation about the pole would appear to shift all the station longitudes relative to the source longitudes. Alternatively (and more reasonably) one may define the celestial coordinate system in terms of a set of distant reference objects, such as quasars, which are believed to have negligible angular motions, and then use VLBI observations to solve for the position of the pole and the rotation angle. Motion of the pole relative to the crust would appear as variation of the intersite baseline vectors, expressed in coordinates measured relative to the instantaneous pole. Instead, one may adopt a set of geodetic coordinates fixed to the crust (insofar as this is possible) and solve for the coordinates of the pole.

The Earth's crust, of course, is not rigid. The solid Earth undergoes tidal deformations as a direct result of lunar and solar forces and also due to loading by oceanic tides. These effects are modeled theoretically and are included in our calculation of site locations in the analysis of VLBI data. It has also been possible to determine important parameters of the solid-Earth tide, which has an amplitude reaching 20 cm in some places. Such determinations, together with measurements of long-term

changes in the Earth's spin rate, will yield important information not only on the interior of the Earth but also on the changes which tidal dissipation is producing in the Moon's orbit about the Earth. More exciting to residents of some places on the Earth's crust is the possibility of using VLBI to measure motions of crustal blocks both long-term and long-range, as associated with sea-floor spreading and continental drift, and short-term and possibly short-range, as with strains close to active faults. Motions near faults associated with single earthquakes may exceed tens of centimeters, and average rates for crustal block motions over millions of years are believed to range up to about 15 cm/yr. The prospect of using VLBI measurements to aid in the development of methods for earthquake prediction and for direct measurement of plate motions is an enticing one.

4. Limitations

There are many influences on the measurements of Δt that affect the interpretation of these data, as we just discussed. Such influences can be divided into two classes: those that are of geophysical interest and those that can be viewed as unwanted 'noise'. Here we consider only the latter which in effect govern the measurement 'errors' and establish the limitations of the technique. We discuss, in turn, the effects of the neutral atmosphere, charged particles, frequency standards, and antenna flexure.

The total delay introduced by the neutral atmosphere in the zenith direction is equivalent to the time taken by a radio wave to traverse about 2.5 m in vacuum. The main difficulty in accounting for the atmospheric delay -- the most important error source -- is caused by the variability of the water-vapor content. With the use of model atmospheres and surface measurements of temperature, pressure, and humidity at each site, the uncertainty in the electrical path length through the atmosphere can be reduced to about the 3 cm level for the zenith direction. The use of special techniques may allow the uncertainty to be reduced much further. A particularly promising method employs water-vapor radiometers to monitor the sky brightness temperature along the line-of-sight to the object being observed. A linear (statistical) relation between sky brightness temperatures at and near the 22.235 GHz resonance line of water vapor, and the electrical path length of the water vapor in the atmosphere, has been determined semi-empirically (see, for examples, Moran and Penfield 1976, and Winn et al. 1976). These studies indicate that the zenith-direction uncertainty in the atmospheric delay can be deduced to ~1 cm by use of the radiometric and surface meteorological data.

The ionosphere, in particular, and the plasma between source and observing site, in general, cause an important change in the delay. Fortunately, the index of refraction, n, of a plasma depends strongly on frequency ($n^2-1 \approx \text{const}/f^2$) so that by making simultaneous measurements at two widely separated frequencies, the plasma effects can be deduced and subtracted. The residual

error, due in part to the slightly different paths followed by waves of different frequency, can be reduced to well under 1 cm.

The frequency standards serve two functions: (i) to provide sufficient phase stability to insure that the signals recorded separately at each site can be cross-correlated without significant loss of coherence. For this purpose, rubidium standards are adequate since their short-term stability is about 5×10^{-13}. A hydrogen maser, operating within presently advertised specifications (long-term stability 7×10^{-15}), serves this function admirably. (ii) to keep time with sufficient accuracy to ensure that the clock offset and rate errors remain constant -- within the accuracy otherwise achievable -- over the interval required for the determination of the 'instantaneous' vector between the interferometer sites. If this interval were about 8 hr it would lead to a corresponding change in clock offset error of ~0.2 nanosec, or equivalently, to about a 6 cm error in distance. The use of redundant observations, however, allows the more frequent estimation of the characteristics of the relative clock drifts. Thus, the errors introduced by the long-term drifts in the frequency standards can be rendered virtually harmless. Differencing techniques (Shapiro et al. 1974, and Robertson 1975) can also be employed for this same purpose: The delays from neighboring observations of different sources can be differenced; the resultant differenced observables are thereby freed from the effects of long-term clock drifts.

Changes with antenna orientation and temperature in the effective distance to the feed could introduce systematic errors in the geophysical interpretations of the Δt data. Fortunately, these effects can be accounted for with sufficient accuracy even for large antennas [see Rogers et al. (1978)] for an extended discussion]. For smaller, portable antennas, the effects will be even less.

Thus, if hydrogen-maser frequency standards are used and measurements made simultaneously in two widely separated frequency bands, the main source of error is caused by atmospheric variations which may produce an uncertainty of a few centimeters in intercontinental or transcontinental distance determinations.

III. Results

We mention here, very briefly, some VLBI results obtained by our group*. Descriptions of results obtained by the group at the Jet Propulsion Laboratory are given by Thomas et al. (1976) and Ong et al. (1976).

---

*This group contains members primarily from the Goddard Space Flight Center, the Haystack Observatory, the Massachusetts Institute of Technology, and the National Geodetic Survey.

1. Short Baseline

We conducted a series of 11 separate radio interferometric experiments between the Haystack and Westford antennas, 1.24 km apart. The results (Rogers et al. 1978) for the vector baseline were repeatable at about the 5 mm level in each component, even though not all of the instrumental calibration equipment was available for the measurements. A further experiment, carried out in May 1977 with full calibration, yielded results which agreed within ~2 mm with the mean of the prior measurements for each component of the baseline vector.

2. Long Baseline

We undertook a series of VLBI experiments between the 37-m diameter antenna of the Haystack Observatory in Massachusetts and the 40-m diameter antenna of the Owens Valley Radio Observatory in California (Robertson et al. 1978). Ten experiments were made between September 1976 and June 1977. Each spanned from 15 to 36 hours in which from 150 to 300 separate, three-minute, observations were made. The data from each session were first analyzed separately, and the following parameters were estimated: the vector components of the baseline, the epoch and rate offsets of the clock at Owens Valley relative to those at Haystack, the zenith electrical path length of the atmosphere at each site, and the right ascension and declination of each source, with one right ascension held fixed to define the origin of right ascension. To test the consistency of the results, the repeatability of the estimates of baseline length were examined. Baseline lengths were selected for examination because the values of the direction components of the baseline vector were affected by errors in the values used for the pole direction and for UT.1; similarly, the estimated values for the source coordinates were affected by errors in the formulas used for precession and nutation, although the arclengths between sources are free from such errors. The root-weighted-mean-square scatter about the weighted mean (hereinafter "RMS scatter" or "repeatability") of these baseline length values was 7 cm, or, expressed as a fraction of the 3900 km baseline, about 2 parts in 10^8. The values of the source coordinates from these solutions had an RMS scatter of 0".015 or less, except for the declinations of the low-declination sources for which our observations have less sensitivity. The values for these coordinates appear to be somewhat more accurate than our previously published results (Clark et al. 1976).

To examine how the repeatability of the baseline results might have been affected by the prior availability of sufficiently accurate values for the source coordinates, we obtained new solutions with each source coordinate fixed at the weighted mean of its values from the 10 separate solutions, thereby reducing the number of parameters estimated in each solution from about 30 to about 10. We would expect the RMS scatter to be reduced, provided that any systematic errors affecting the data and the model

were sufficiently benign. The RMS scatter was indeed reduced, to about 3 cm, and the mean itself, as one might expect, changed little, by only 1.5 cm. These results indicate that at present VLBI can be used at least to determine lengths of transcontinental baselines with a repeatability of about 3 cm.

IV. Future Prospects

After our Mark III system is in full operation we may anticipate more definitive results and, perhaps, even a reliable measurement of plate motions.

Further in the future, it may be possible to monitor regional strain accumulation very accurately with a simple system based on satellite signals. We describe here briefly the main characteristics of this system which we are developing (Counselman and Shapiro 1978): The measurement uncertainties should range from the millimeter to the centimeter level for baseline lengths ranging from a few to a few hundred kilometers. Each terminal would have no moving parts, could be packaged in a volume of less than 0.1 m^3, and could operate unattended. These units would receive radio signals from simple, low-power (<10 w), transmitters on Earth-orbiting satellites. The baselines between units could be determined virtually instantaneously and monitored continuously as long as at least four satellites were visible simultaneously. Initial signal acquisition would require under one minute; thereafter less than a second of signal integration, and the collection of about 2 kilobits of data from each receiving unit, would be required for the determination of a baseline. This system could therefore be used to monitor the regional accumulation and release of strain preceding, following, and even during earthquakes. These units could be deployed in arrays of various dimensions and densities. Their use could also include monitoring variations in transcontinental and intercontinental baselines, but with reduced accuracy. Comparisons with other systems proposed for extensive measurements of regional baseline vectors appear to favor this interferometric approach.

Acknowledgement

Much of the material presented here was adapted, with the permission of the publishers, from Shapiro and Knight (1970) and Counselman (1973 and 1976). Figures 1 and 2 are from Counselman (1976).

References

Clark, T. A. et al. 1976. Astron. J. 81: 599-603.

Counselman, C. C. 1973. Proc. IEEE (Special Issue on Radio and Radar Astronomy) 61: 1225-1230.

Counselman, C. C. 1976. Ann. Rev. Astron. and Astrophys. 14: 197-214.

Counselman, C. C. and I. I. Shapiro. 1978. Proceedings of the Ninth GEOP Conference, in press.

Elsmore, B., and M. Ryle. 1976. MNRAS 174: 411-423.

Moran, J. M. and H. Penfield. 1976. Final Report, Contract NAS5-20975.

Ong, K. M. et al. 1976. J. Geophys. Res. 81: 3587-3593.

Robertson, D. S. 1975. Ph.D. Thesis, M.I.T., Cambridge, Mass.

Robertson, D. S. et al. 1978. In Proceedings of IAU Symposium No. 82, in press.

Rogers, A. E. E. et al. 1978. J. Geophys. Res. 83: 325-334.

Ryle, M. and B. Elsmore. 1973. MNRAS 164: 223-242.

Shapiro, I. I. 1976. In Methods of Experimental Physics, ed. by M. L. Meeks, Vol. 12C (Radio Measurements), New York: Academic Press, Chap. 5. 6 , pp. 261-276.

Shapiro, I. I. and C. A. Knight. 1970. In Earthquake Displacement Fields and the Rotation of the Earth, ed. by A. Beck Dordrecht: D. Reidel, pp. 284-301.

Shapiro, I. I. et al. 1974. Science 186: 920-922.

Thomas, J. B. et al. 1976. J. Geophys. Res. 81: 995-1005.

Whitney, A. R. et al. 1976. Radio Science 11: 421-432.

Winn, F. B. et al. 1976. Deep Space Network Progr. Rep. 42-32, Jet Propul. Lab., Pasadena, Calif.

A Comparison of Three Strain Relaxation Techniques in Western New York

TERRY ENGELDER

Lamont-Doherty Geological Observatory
of Columbia University
Palisades, New York 10964

MARC. L. SBAR

Department of Geosciences
University of Arizona
Tucson, Arizona 85721

ABSTRACT

Overcoring techniques including surface overcoring, the doorstopper and the U.S.B.M. borehole deformation gauge were compared to investigate the influence of residual strain on stress measurements. The techniques were applied in western New York State where the rock contains a residual maximum compressive strain oriented N to NNW. This trend is normal to the ENE applied compressive stress documented using hydrofracture measurements and focal mechanisms in the northeastern United States. Surface overcoring is most sensitive to the residual strain as indicated by a N to NNW maximum expansion. Maximum expansion from the U.S.B.M. borehole deformation gauge was closer to the ENE applied compressive stress than the other two techniques. The doorstopper seemed to detect a combination of the residual strain measured with surface overcoring and the applied stress associated with the borehole deformation gauge measurements.

INTRODUCTION

The magnitude and orientation of tectonic stress* in the crust is a subject of debate in solid earth geophysics. Within continental plates the tectonic stress field appears to have the same orientation over areas of as much as 10^6 km^2 [Sbar and Sykes, 1973; Haimson, 1977]. On the scale of continents, the tectonic stress field does vary in orientation [Street, Herrmann, and Nuttli, 1974; Sbar and Sykes, 1977]. Ideas concerning magnitude and ori-

*We define tectonic stress as that stress which causes earthquakes. Tectonic stress may have more than one component including boundary loading and residual stresses.

entation of the tectonic stress field come from fault-plane solutions of earthquakes, hydrofracture measurements, in situ strain relief measurements, and observations of Quaternary and historic crustal deformation. Part of the debate concerning tectonic stress stems from the lack of understanding of just what each of these techniques is measuring.

We have conducted a program of strain relaxation measurements on carefully selected surface outcrops for the purpose of trying to use strain relaxation to measure the tectonic stress field. The development of near-surface strain relaxation techniques is important because they are inexpensive compared with techniques requiring deep boreholes. Using near-surface techniques, many measurements can be made over short periods of time. However, strain relaxation measurements are still poorly understood because the orientation of the strain relaxation is influenced by the fabric of the rock, residual strain, and weathering.

To date we have shown that strain relaxation measurements in the northeastern United States are influenced by a microcrack fabric, and a residual strain. Near Barre, Vermont, the relaxation of microcracks clearly controlled the orientation of strain relaxation, thus masking the relief of crustal stresses [Engelder, Sbar, and Kranz, 1977]. Strain relaxation in western New York included a component of residual strain which we attribute to a NNW compression which occurred during the folding of the Appalachian Mountains [Engelder, 1978b]. Near Alexandria Bay, New York, we argued that a tectonic stress was measured in Cambrian sandstone based on 1) a correlation between the orientation of a post-glacial pop-up and strain relaxation, and 2) the small magnitude of residual strain as indicated by double overcoring.

We measured strain relaxation in the northeastern United States where information on the tectonic stress field comes primarily from the orientation of earthquake fault-plane solutions [Sbar and Sykes, 1977]. In brief, areas of Ohio, New York and southeastern Canada have fault-plane solutions showing a ENE-trending maximum compressive stress. This trend for the orientation of fault-plane solutions does not extend to New England, southern New York, New Jersey, or Delaware.

BACKGROUND

All overcoring techniques record a strain relaxation which is an approximate measure of the rock stress when multiplied by the appropriate moduli. The reason overcoring is never a perfect measure of rock stress is that during strain relaxation the mechanical properties of the rock change by nonrecoverable processes such as the opening of microcracks and relaxation of residual strain. These nonrecoverable changes make it difficult to assess the in situ moduli of the rocks. Such nonrecoverable changes are manifest in the reduced seismic velocities in rock bodies that have been

strain relieved and then reloaded to the original state of strain [Pratt et al., 1975]. The literature contains little information on the effect of these nonrecoverable changes on different overcoring techniques. To discover the effect of nonrecoverable changes, we attempted a suite of experiments in western New York to compare overcoring techniques using: the U. S. Bureau of Mines borehole deformation gauge, strain gauges bonded directly to the end of a borehole (the doorstopper), and strain gauges bonded to outcrop surfaces.

The derivation of absolute stress from strain relaxation data should give a direct comparison of the three overcoring techniques. We are not sure, however, that the standard techniques for deriving moduli for cores taken by the three techniques give comparable data on in situ moduli. This uncertainty is reinforced by the fact that one technique requires that a hole be drilled beyond the measurement point in the rock, whereas the other two are measured on rock undisturbed below the point of the measurement. Presumably the extent to which a residual strain is disturbed and, thus, nonrecoverable changes occur depends on the position of the end of the initial borehole relative to the plane of the measurement. In the standard moduli tests there is no way to account for the way various overcoring techniques affect the residual strain of the rock prior to the overcore or changes in residual strain during overcoring.

Our hypothesis is that there are inherent differences in the strain relaxations measured by three different overcoring techniques. To check this hypothesis we assumed that the effect of nonrecoverable changes on overcoring would be easier to assess if we concerned ourselves only with differences in orientation of strain relaxation among various overcoring techniques. Thus, from this point on in the paper we discuss strain relaxation without attempting to assign values for stress.

We chose western New York for our overcoring experiments because of the unambiguous difference in orientation between the compression causing the late Paleozoic deformation of the rocks of western New York [Engelder and Engelder, 1977] and the present-day maximum compressive stress [Sbar and Sykes, 1973; Haimson, 1977]. The later stress occurs in the area west of the Appalachian Valley and Ridge province where fault-plane solutions generally have ENE P-axes. This is equivalent to an ENE maximum compressive stress, an orientation which is obtained repeatedly using hydrofracture measurements. Thus, ENE is the assumed orientation for the maximum compressive stress from applied loads caused by present earth processes on the scale of continents.

In western New York, ENE was not always the orientation of the maximum compressive stress caused by earth processes on the scale of continents. Lightly deformed fossils throughout western New York indicate the presence of a late Paleozoic NNW maximum compressive stress within the folded portion of the Appalachian plateau [Engelder and Engelder, 1977]. The fossils record as much as 20% layer-parallel shortening normal to the fold axes on the Appalachian plateau. Two mechanisms for fossil distortion are intragranular deformation by the mechanical twinning of calcite and pressure solu-

tion along solution cleavage planes [Engelder, 1978a]. Intragranular deformation accounts for 1-5% layer-parallel shortening, whereas pressure solution accounts for 4-18% layer-parallel shortening. Layer-parallel shortening of less than 2% also extends NNW of the outermost fold as mapped by Wedel [1932] where strain recorded by the calcite twinning decreases with an increase in distance from the last fold [Engelder, 1978b]. The orientation of maximum shortening on the outer limits of the Appalachian plateau is shown in Figure 1 for the intragranular deformation of calcite. Total fossil distortion including dissolution shows the same orientation for maximum compressive strain [Engelder and Engelder, 1977] which in general is normal to the fold axes mapped by Wedel [1932].

The deformed fossils are found only as far north as Wedel mapped folds. Farther north at the outcrops marked LRY and MED (Figure 1) the rocks contain both a residual and a permanent strain imposed during transmission of tectonic stresses during the development of the Appalachian foreland fold and thrust belt to the southeast. By a residual strain, we mean any self-equilibrating recoverable strain that remains in rocks even after external forces and moments are removed. Incipient deformation at the leading edge of the central Appalachian foreland fold and thrust belt includes: 1) residual strain which is recoverable upon overcoring; 2) an elastic distortion of quartz grains which is detected by X-ray techniques; 3) a plastic deformation by mechanical twinning of calcite; and 4) a N to NNW shortening by solution cleavage. This very early stage of deformation imprints a small ($\sim$ 5%) velocity anisotropy on the mechanical properties of some rocks. A gradual decrease in NNW-directed compressional strain recorded in the mechanical twinning of calcite links the incipient deformation to more strongly deformed portions of the Appalachian plateau.

Based on the preceding data, we assume that overcoring stress measurements yielding a maximum compressive stress oriented ENE are sensitive to or have detected the present stress field, whereas those measurements showing a N to NNW maximum compressive stress are sensitive to or detect a residual stress imprinted during the late Paleozoic Appalachian compression.

SURFACE OVERCORING

During the summer of 1975 we measured the recoverable *in situ* strain of some rocks in western New York (Figure 2). This was accomplished by cutting 15 cm cores from bedrock and monitoring the strain change at the surface of the outcrop caused by freeing the core. Details of this technique are given in Engelder and Sbar [1976, 1977] and Engelder et al. [1977]. Briefly, measurements were made as far away as possible from vertical fractures on outcrops with the least weathering. We bonded three-component rosettes, a compensation gauge, and temperature sensor to surfaces ground flat and horizontal at each site. One rosette was overcored per day with either a 15.2 cm (6 inches) or 7.6 cm (3 inches) diamond core barrel; all holes were vertical.

The biaxial strain change during relief of a core of rock was determined by taking the difference in resistance of the gauges in a rosette before and after overcoring. The thermal drift of the other rosettes and the temperature sensor are used to subtract the effect of thermal drift on the overcored rosette. Using this technique, we are able to measure strain to $\pm 1 \times 10^{-5}$; 1 με equals a strain of 1×10^{-6}.

Sites in the vicinity of the Clarendon-Linden fault were selected for strain relaxation measurements (Figures 1 and 2). With the exception of a site labelled MON all were inside or on benches of stone quarries. In the formations described above we wished to sample outcrops between the intersections with the surface of the three branches of the Clarendon-Linden fault and at a distance from the fault system. Our experiment was designed to compare the variation in magnitude and orientation of strain relaxation among stratigraphic units and to measure the effect of the Clarendon-Linden fault on the in situ strain. Small earthquakes had been triggered along the fault by fluid injection near Dale, New York [Fletcher and Sykes, 1977]. A fault-plane solution from these earthquakes indicated a N80°W compressive stress and it was of interest to compare this stress orientation with that detected at the surface.

Maximum expansion following the initial overcore of both the Grimsby sandstone and Onondaga limestone was generally toward the NNW (Figure 2). In strain-relief work the maximum expansion corresponds to the maximum compressive strain in the plane of the measurement prior to overcoring. The magnitude of the maximum expansion varied from the maximum of about 200 με in the Grimsby sandstone to a minimum of 50 με in the Onondaga limestone. Variation in orientation differed from outcrop to outcrop with LRY and PIL producing the most repeatable data. It may be of signficance to note that both of these outcrops are farthest from the Clarendon-Linden fault system.

To test for residual strain a 7.6 cm overcore was placed inside some 15 cm cores [Friedman, 1972; Swolfs et al., 1974; Engelder and Sbar, 1976]. Of 6 double overcores within Grimsby sandstone, the maximum expansion was oriented no more than 31° from a north-south trend with an average orientation slightly west of north (Figure 2). This includes measurements for samples from both within the Clarendon-Linden fault zone and adjacent to it. Measurement of relaxation following double overcoring of the Onondaga limestone failed because of strain gauge failure in one case and the breaking of a core in another case. In general the orientation of maximum expansion for the 7.6 cm overcore correlated with the orientation of the maximum expansion following the initial overcore.

THE DOORSTOPPER

Downhole strain relaxation measurements included the use of a strain cell built at Lamont-Doherty Geological Observatory and similar to one

described by Stephenson and Murray [1970] and Leeman [1971]. The popular name for this strain cell is the "doorstopper". We report doorstopper measurements along the San Andreas fault in Sbar et al. [1978] and Engelder et al. [1978].

Briefly, our doorstopper consists of a hard plastic cylinder which contains a low modulus plastic (Dow-Corning RTV and Silguard). At the base of the RTV is a strain-gauge rosette consisting of three foil-resistance strain gauges along radii spaced 120° apart. A thermal compensation gauge, consisting of a strain gauge bonded to a wafer of Barre granite, is embedded in the Silguard above the RTV. The resistance of this gauge is balanced against that of the active components of the rosette using an AC resistance bridge. The thermal compensation gauge is necessary to minimize the thermal effect of drilling water on the strain readings. To further reduce this effect, we let the water flow before overcoring until the readings stabilized.

The strain gauge rosette is exposed at the end of the doorstopper and is epoxied to the flattened bottom of a borehole. When bonded, each gauge covers an area of 21 mm^2 between 1 and 8 mm, as measured from the center of the core along a radius. We used a NW oversize diamond drill bit (79 mm outer diameter), which produced a 55 mm core, for drilling both the initial hole and the overcore. Our technique differs from standard doorstopper methods in that we run a cable from the doorstopper through the drill string to our strain indicator to allow readings during overcoring. Thus, we were able to recover data even if the core broke before the drilling was completed. We calculated the maximum and minimum principal strains (ε_1 and ε_2, respectively) and their orientation from the strain observed on the three gauges of the rosette.

Maximum expansion following overcoring of the doorstopper in Grimsby sandstone was generally NE or clockwise from the maximum expansion recorded by surface overcoring (Figures 2 and 3). The magnitudes of the principal strains were larger for the doorstopper than for surface overcoring. For overcoring doorstoppers within the Onondaga limestone the difference in orientation between the doorstopper and the surface overcore was not so clear. Two of three measurements had about the same orientation for maximum expansion (Figures 2 and 3), whereas the third, showing the largest strain relaxation, was oriented WNW or counterclockwise from the surface overcore.

U.S.B.M. BOREHOLE DEFORMATION GAUGE

We measured strain relaxation using a three-component borehole deformation gauge designed by the U. S. Bureau of Mines and built by Roger Arms and Machine Company of Grand Junction, Colorado. The measurement consists

of drilling a 37.7 mm hole with an EW diamond coring bit, placing the borehole deformation gauge in this EW-hole, and then overcoring the gauge with a 152.4 mm (6"-diameter) masonry bit. Details for this technique are given in Hooker and Bickel [1974].

Maximum expansion on overcoring of the borehole deformation gauge was oriented NE for the Grimsby sandstone and almost E-W for the Onondaga limestone (Figure 3). For both rocks the tensor average for maximum expansion of the borehole deformation gauge was closer to the present trend for the maximum principal stress than the doorstopper measurement (Figures 4 and 5).

DISCUSSION

Repeated tests indicate that the precision of the strain relaxation measurement is seldom better than 20% in magnitude and ± 10° in orientation. Our surface overcoring measurements at LRY and PIL conform to these standards (Figure 2). The data from many outcrops yield more scatter in magnitude and orientation. Our doorstopper and borehole deformation gauge measurements show variations of as much as 50% in magnitude and ± 25° in orientation. Greiner and Illies [1977] show an outcrop variation in orientation of maximum expansion between ± 6° and ± 19° using the doorstopper technique. Smith's [1977] tables of various measurements by the borehole deformation gauge made in New York State show an outcrop variation in orientation of maximum expansion between ± 10° and ± 25°.

Our explanation for the differences in orientation between the strain relaxation measured by the three techniques is quite simple yet difficult to prove. Surface overcoring is most sensitive to residual strains, whereas the borehole deformation gauge is apparently not as sensitive to the same residual strain. This seems reasonable because the drilling of an EW hole in which to place the borehole deformation gauge is more likely to disturb or relieve a residual strain. In both the Onondaga limestone and Grimsby sandstone the borehole deformation gauge yielded a maximum expansion in an orientation close to the present maximum compressive stress (Figures 4 and 5). We suspect that drilling for the doorstopper is less likely to disturb the residual strain in the rock under the gauge and is more likely to sense both a residual strain and the present compressive stress. Likewise, we also expect that the present compressive stress is least likely to be found at the surface of an outcrop.

The relative orientations for the tensor averages of maximum expansions obtained using three strain relaxation techniques conforms with other information we have on the Grimsby sandstone and Onondaga limestone (Figures 4 and 5). Both rocks have been subjected to a late Paleozoic compression oriented slightly west of north, as indicated by twinned calcite. This compression has printed a seismic anisotropy of 5-10% which can be mea-

sured over distances of 30-60 m using a Bison seismograph. Cores of Grimsby sandstone show a 3-5% anisotropy of the same orientation (i.e., maximum P-wave velocity is slightly west of north). Quartz grains of the Grimsby sandstone contain an elastic residual strain indicative of a NW compression which Engelder [1978b] attributes to the same late Paleozoic compression. Orientations of the tensor averages for strain relaxation from surface overcoring conform with this late Paleozoic compression. Because relaxation of double overcores is also of this late Paleozoic trend, we must conclude that the strain relaxation of surface cores is the recovery of residual strain. The mechanism for recovery of the residual strain, however, is not clear. We can't attribute the mechanism to the opening of microcracks as was the case for Barre granite [Engelder et al., 1977].

The quarry floor at outcrop LRY in Onondaga limestone contains many extension fractures and post-excavation pop-ups (Figure 4). Both are oriented for a maximum principal stress at about 280°, which is the orientation for the tensor average of our borehole deformation gauge measurements in the Onondaga. Pop-ups have been interpreted as indicating the orientation of an ambient or present maximum compressive stress [Sbar and Sykes, 1973; Engelder et al., 1977]. The correlation between the pop-ups and the borehole deformation gauge re-enforces our notion that the gauge senses an ambient rather than residual stress and that pop-ups are indicative of a modern rather than a residual stress.

In the Grimsby sandstone both the doorstopper and borehole deformation gauge measurements showed a maximum expansion close to the present ENE maximum compressive stress as defined by Sbar and Sykes [1973]. Smith [1977], however, notes three other sets of measurements by the borehole deformation gauge in western New York give maximum principal stresses that conform more closely with measurements in the Onondaga limestone (Rochester, NY - 291°; Sterling, NY - 312° and Somerset, NY - 333°).

CONCLUSIONS

We conclude that there is a distinct difference among the strain relaxations detected by surface overcoring, the doorstopper, and the borehole deformation gauge. Surface overcoring is most sensitive to residual strain, whereas the borehole deformation gauge seems to detect a maximum expansion that conforms with that orientation of the maximum compressive stress indicated by fault-plane solutions in the northeastern United States.

ACKNOWLEDGEMENTS

This work was supported by the U. S. Nuclear Regulatory Commission and the New York State Energy Research and Development Authority. We thank Niagara Stone, Concrete Materials Inc., and Leroy Lime and Crushed Stone for permission to use their quarries for our experiment. Lynn Sykes and Chris Scholz provided a critique of this paper.

REFERENCES

Engelder, T., Penetrative deformation within the décollement sheets of the Appalachian plateau, western New York, Am. J. Sci., 1978a, in press.

Engelder, T., The nature of deformation within the outer limits of the central Appalachian foreland fold and thrust belt in New York State, Tectonophysics, 1978b, in press.

Engelder, T., and R. Engelder, Fossil distortion and décollement tectonics on the Appalachian plateau, Geology, 5, 457-460, 1977.

Engelder, T., and M. L. Sbar, Evidence for uniform strain orientation in the Potsdam sandstone, northern New York, from in situ measurements, J. Geophys. Res., 81, 3013-3017, 1976.

Engelder, T., and M. L. Sbar, The relationship between in situ strain and outcrop fractures in the Potsdam sandstone, Alexandria Bay, New York, Pure Appl. Geophys., 115, 41-55, 1977.

Engelder, T., M. L. Sbar, and R. Kranz, Strain relaxation of Barre granite: residual strain attributed to opening of microfractures, Pure Appl. Geophys., 115, 27-40, 1977.

Engelder, T., M. L. Sbar, S. Marshak, and R. Plumb, Near-surface in situ stress pattern adjacent to the San Andreas fault, Palmdale, California, 19th U. S. Symposium on Rock Mechanics, p. 95-100, Stateline Nevada, 1978.

Fletcher, J. B., and L. R. Sykes, Earthquakes related to hydraulic mining and natural seismic activity in western New York State, J. Geophys. Res., 82, 3767-3780, 1977.

Friedman, M., Residual elastic strain in rocks, Tectonophysics, 15, 297-330, 1972.

Greiner, G., and J. H. Illies, Central Europe: active or residual tectonic stresses, Pure Appl. Geophys., 115, 11-26, 1977.

Haimson, B. C., Hydrofracturing stress measurements - method, results and interpretations, Synopsis Joint General Assemblies IASPEI and IAVCEI, Durham, England, 1977.

Hooker, V. E., and D. L. Bickel, Overcoring equipment and techniques used in rock stress determination, U. S. Bureau Mines IC 8618, 32 p., 1974.

Leeman, E. R., The CSIR 'doorstopper' and triaxial rock stress measuring instruments, Rock Mechanics, 3, 25-50, 1971.

Pratt, H. R., H. S. Swolfs, and A. D. Black, The effect of in situ stress state on seismic velocity and elastic modulus, EOS, 56, 449, 1975.

Sbar, M. L., and L. Sykes, Contemporary compressive stress and seismicity in eastern North America: an example of intraplate tectonics, Geol. Soc. Am. Bull., 84, 1861-1882, 1973.

Sbar, M. L., and L. R. Sykes, Seismicity and lithospheric stress in New York and adjacent areas, J. Geophys. Res., 82, 5771-5786, 1977.

Sbar, M. L., T. Engelder, R. Plumb, and S. Marshak, Near-surface in situ stress pattern near the San Andreas fault, Palmdale, California, J. Geophys. Res., 83, 1978, submitted.

Smith, A. C., In situ rock stresses and small anticlinal features in eastern North America, Masters Thesis, Cornell Univ., Ithaca, New York, 136 p., 1977.

Stephenson, B. R., and K. J. Murray, Application of the strain rosette relief method to measure principal stress throughout a mine, Int. J. Rock Mech. Min. Sci., 7, 1-22, 1970.

Street, R. L., R. B. Herrmann, and O. W. Nuttli, Earthquake mechanics in the central United States, Science, 184, 1285-1287, 1974.

Swolfs, H. S., J. Handin, and H. R. Pratt, Field measurements of residual strain in granitic rock masses, Advances in Rock Mechanics, Proc. 3rd Cong. ISRM, II, 563-568, 1974.

Van Tyne, A. M., Clarendon-Linden structure, western New York, New York State Geol. Surv. Open File Report, 1975.

Wedel, A. A., Geologic structure of the Devonian strata of south-central New York, New York State Museum Bull., 294, 74 p., 1932.

FIGURE CAPTIONS

Figure 1. The general tectonics of western New York State. Solid curved lines are anticlinal axes mapped by Wedel [1932]. Dotted lines locate the Clarendon-Linden fault system mapped by Van Tyne [1975]. Squares and circles with three letter labels are sample localities for this study and triangles for that of Engelder [1978]. The orientation of horizontal maximum compressive strain measured using mechanical twins in calcite is shown for most localities.

Figure 2. Geology and in situ strain in the vicinity of Brockport and Batavia, New York. Six sample sites are labelled. The magnitude and orientation of the strain relieved by the initial overcore are indicated by dark lines. The magnitude and orientation of the strain relieved by a double overcore are indicated by light lines. Solid lines represent expansion and dashed lines represent contractions. The long axis of the ellipse is oriented in the direction of maximum expansion (minimum contraction) where contraction took place along both axes. The magnitude of relieved strain is represented by a scale in microstrain ($\mu\varepsilon$).

Figure 3. The orientation of maximum expansion versus depth for three overcoring techniques applied in western New York State.

Figure 4. The orientation of tensor averages for maximum expansion of surface overcoring, doorstopper, and U.S.B.M. borehole deformation gauge for Onondaga limestone.

Figure 5. The orientation of tensor averages for maximum expansion of surface overcoring, doorstopper, and U.S.B.M. borehole deformation gauge for Grimsby sandstone.

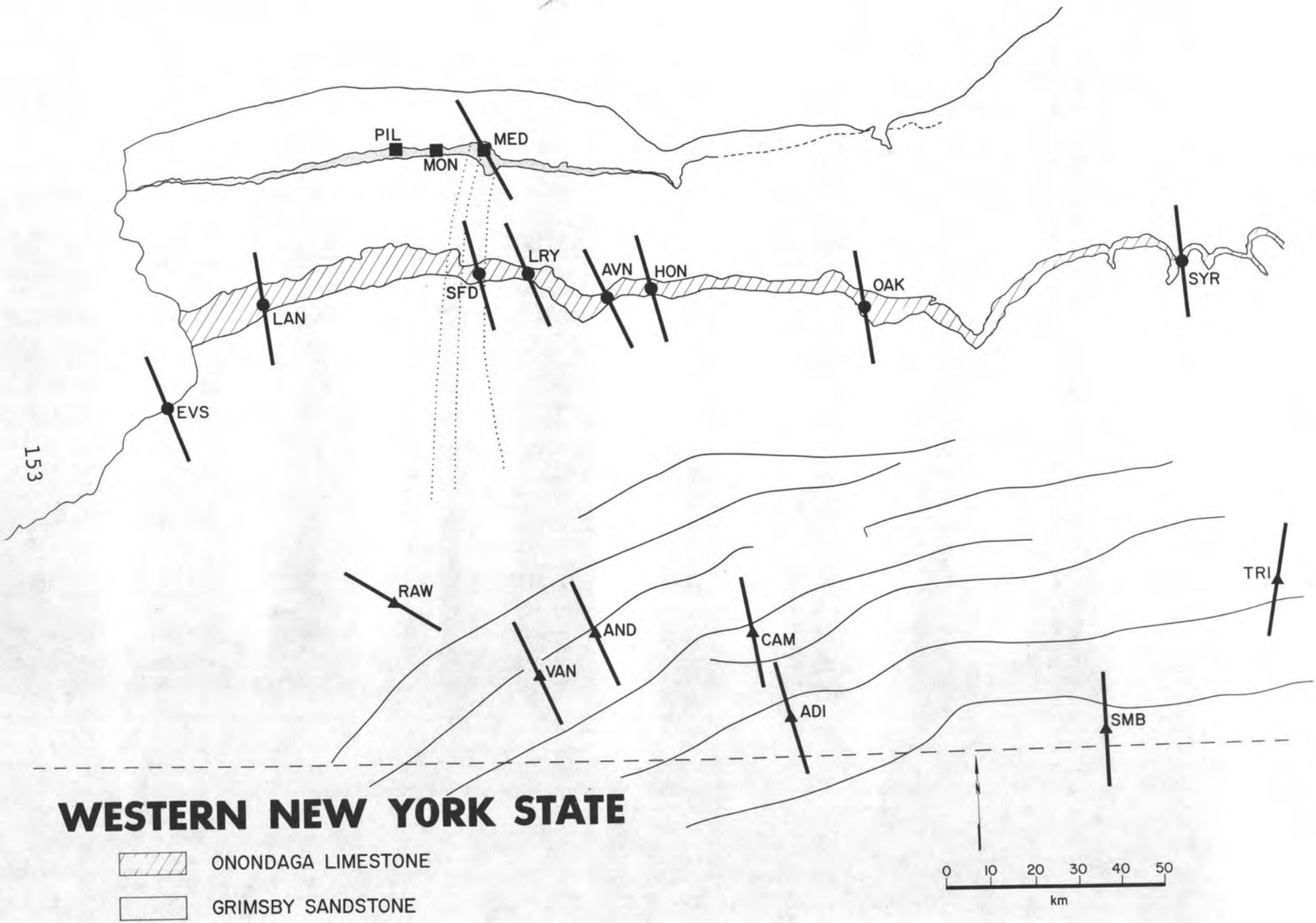
PIL
MON
MED
LAN
SFD
LRY
AVN
HON
OAK
SYR
EVS
RAW
VAN
AND
CAM
ADI
SMB
TRI
WESTERN NEW YORK STATE
ONONDAGA LIMESTONE
GRIMSBY SANDSTONE
0 10 20 30 40 50
km

Figure 1

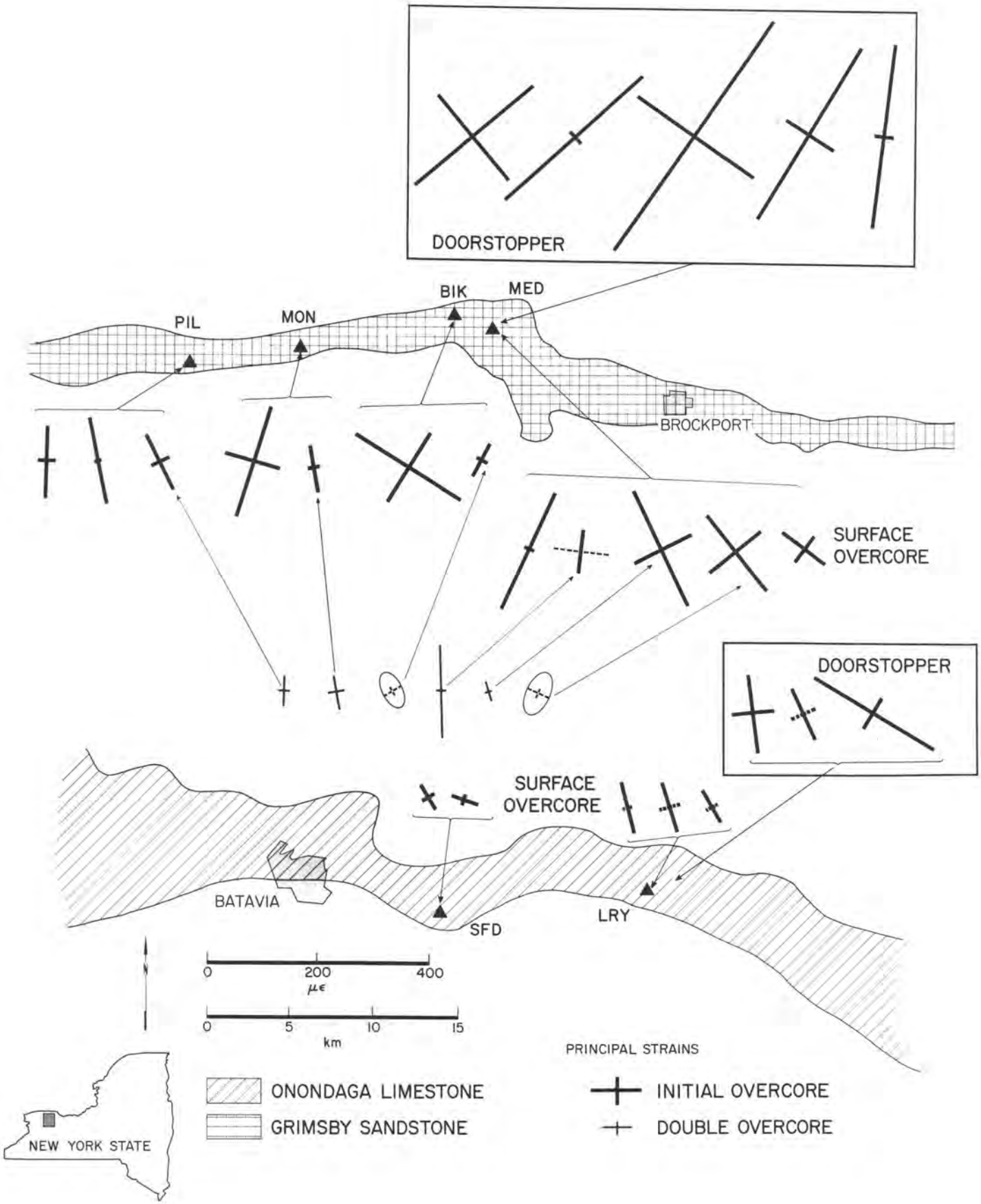
DOORSTOPPER
BIK
MED
PIL
MON
BROCKPORT
SURFACE
OVERCORE
DOORSTOPPER
SURFACE
OVERCORE
BATAVIA
SFD
LRY
0
200
400
με
0
5
10
15
km
PRINCIPAL STRAINS
NEW YORK STATE
ONONDAGA LIMESTONE
GRIMSBY SANDSTONE
INITIAL OVERCORE
DOUBLE OVERCORE

Figure 2

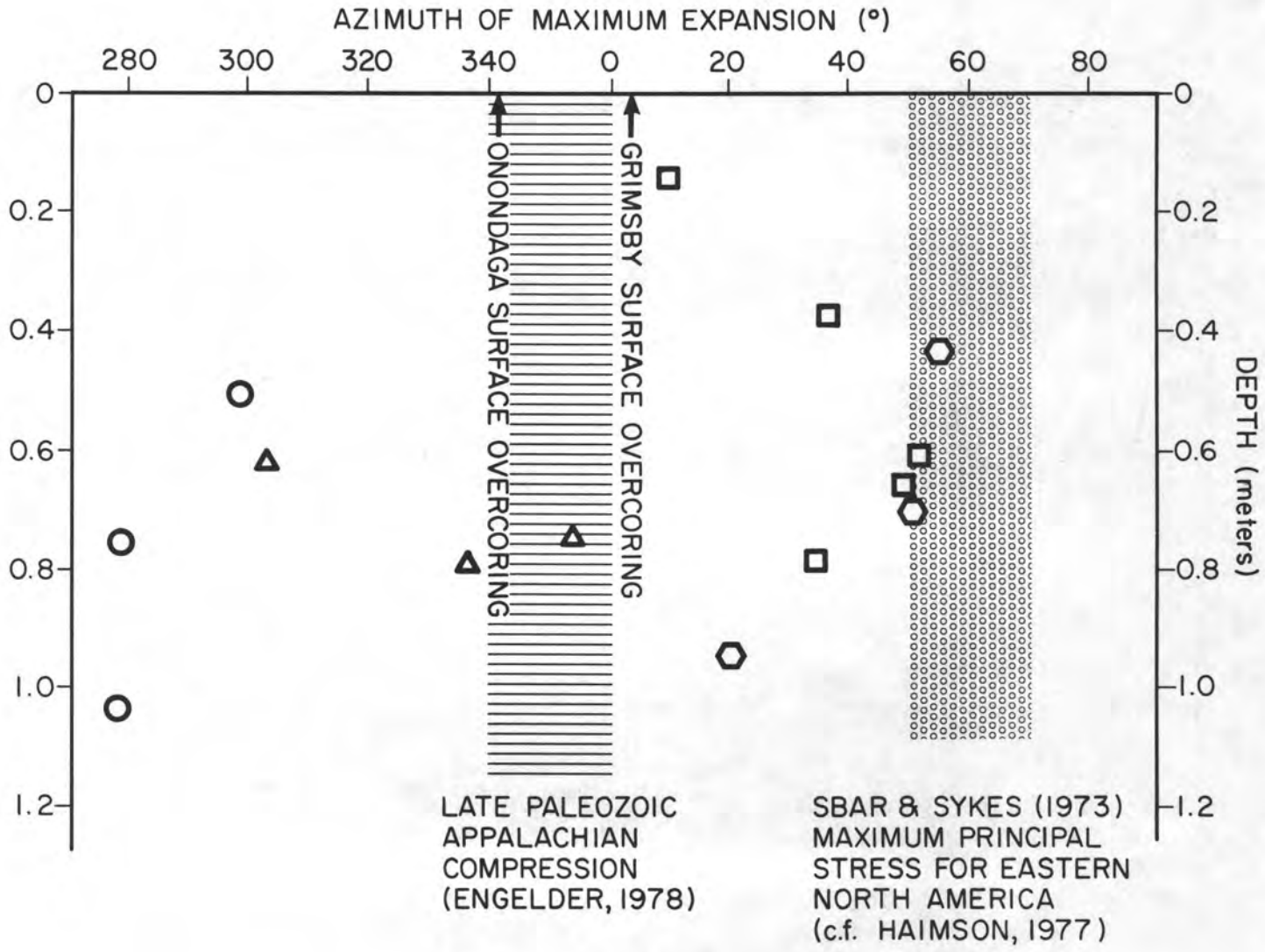

□ — GRIMSBY SANDSTONE: DOORSTOPPER

⬡ — GRIMSBY SANDSTONE: U.S.B.M. BOREHOLE DEFORMATION GAUGE

△ — ONONDAGA LIMESTONE: DOORSTOPPER

○ — ONONDAGA LIMESTONE: U.S.B.M. BOREHOLE DEFORMATION GAUGE

Figure 3

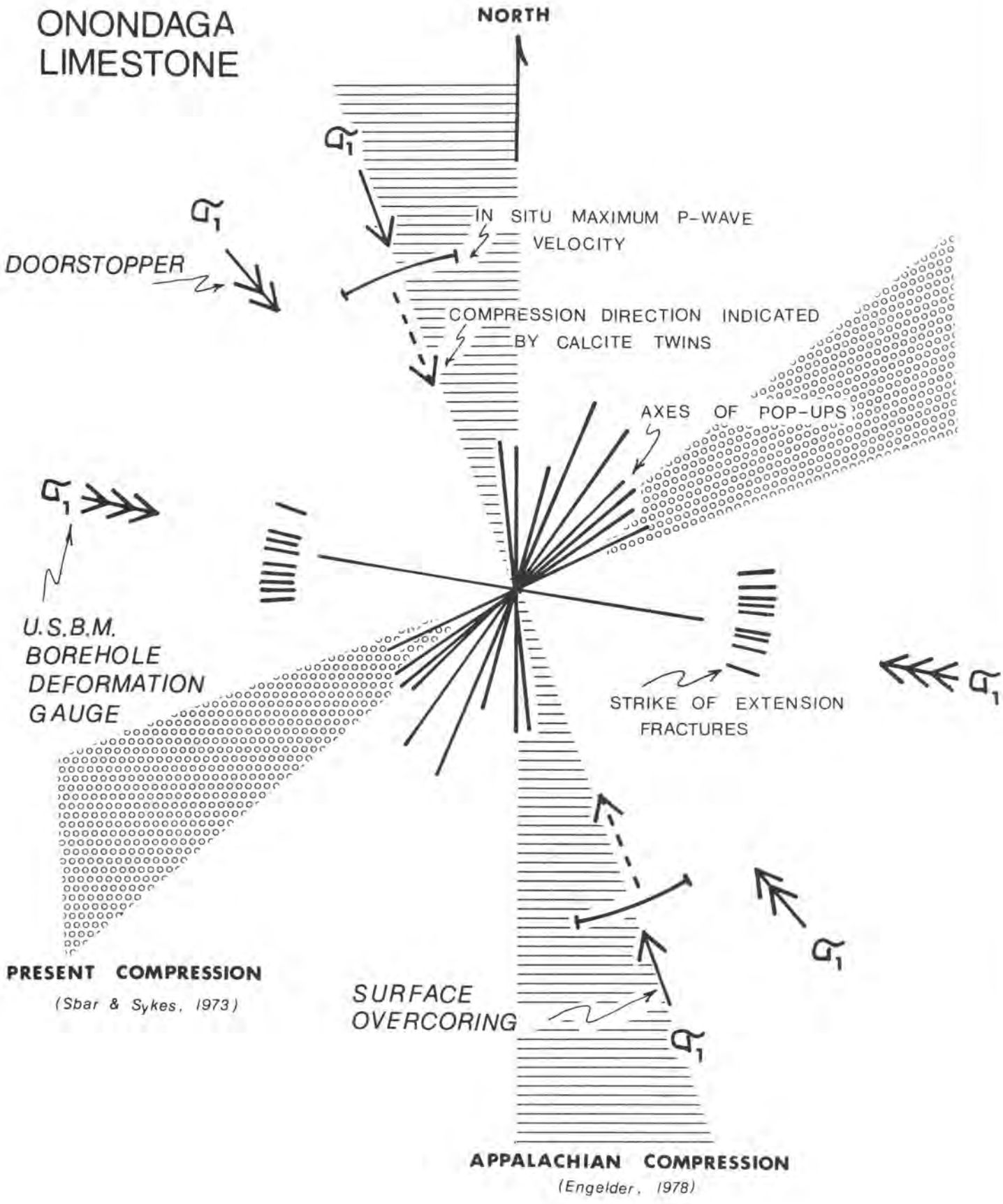
ONONDAGA LIMESTONE
NORTH
σ_1
IN SITU MAXIMUM P-WAVE VELOCITY
DOORSTOPPER
COMPRESSION DIRECTION INDICATED BY CALCITE TWINS
AXES OF POP-UPS
U.S.B.M. BOREHOLE DEFORMATION GAUGE
STRIKE OF EXTENSION FRACTURES
PRESENT COMPRESSION
(Sbar & Sykes, 1973)
SURFACE OVERCORING
APPALACHIAN COMPRESSION
(Engelder, 1978)

Figure 4 156

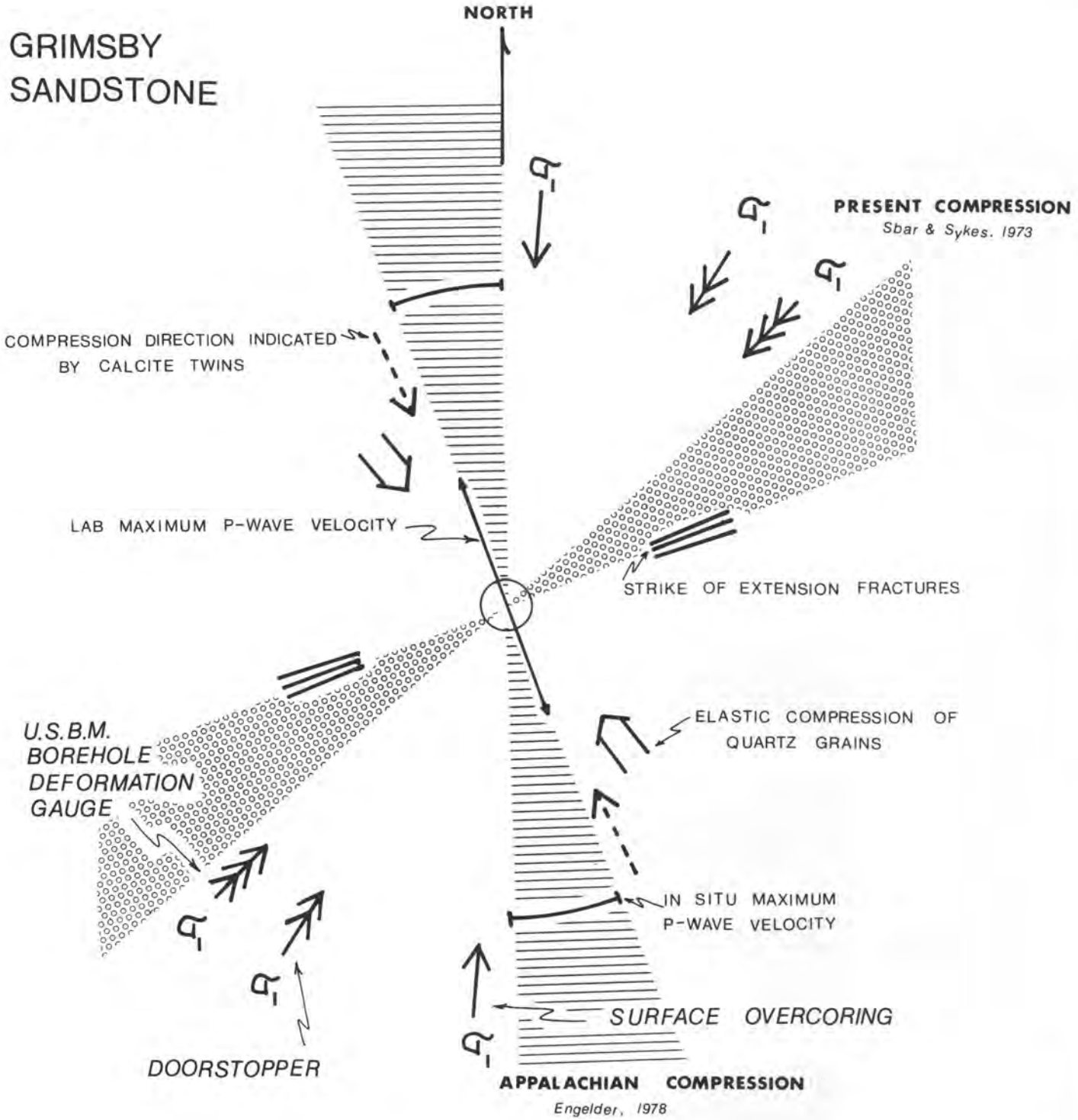
GRIMSBY
SANDSTONE
NORTH
PRESENT COMPRESSION
Sbar & Sykes. 1973
COMPRESSION DIRECTION INDICATED
BY CALCITE TWINS
LAB MAXIMUM P-WAVE VELOCITY
STRIKE OF EXTENSION FRACTURES
ELASTIC COMPRESSION OF
QUARTZ GRAINS
U.S.B.M.
BOREHOLE
DEFORMATION
GAUGE
IN SITU MAXIMUM
P-WAVE VELOCITY
SURFACE OVERCORING
DOORSTOPPER
APPALACHIAN COMPRESSION
Engelder, 1978

Figure 5

PERIODIC HIGH PRECISION GRAVITY OBSERVATIONS IN SOUTHERN CALIFORNIA

John D. Fett
Earth Science & Engineering, Inc.
Hemet, California

Earth Science & Engineering has established two networks of permanent gravity stations in southern California. Establishment of the first network commenced in late 1975 and it is observed semiannually in January and July. The network has been expanded to approximately 130 stations. It consists of permanent bench marks widely spaced along eight lines normal to the major fault zones. A small portion of the area influenced by the San Andreas Fault is covered by the network and a major portion of the area influenced by the San Jacinto Fault and Elsinore Fault are covered.

The second network was established in October of 1976 and it is monitored monthly. It consists of 86 stations along seven lines crossing and approximately normal to the San Andreas Fault.

The goal of the research is to help develop an economical and reliable method for monitoring elevation or density changes that might be precursors to earthquakes. Early observations (Fett, 1976), supported by the more recent observations, indicate multiple precision gravity observations spaced 5 kilometers along lines may be performed with one-twentieth to one-thirtieth the manpower as first order level.

Gravity at a particular location is dependent upon the elevation at the location. If the elevation changes, the gravity will change at a rate of about 0.06 milligal per foot of change. Conventional LaCoste and Romberg Model G gravimeters have been successfully used in subsidence studies (Strange and Carroll, 1974) and for studies of earthquake-related ground deformation (Oliver et at, 1975). With care such studies have yielded a precision of about $\pm$ 15 cm. This precision has been improved by use of "Microgal" LaCoste and Romberg Model D gravimeters. Careful and repetitive use of these improved instruments appears to permit elevation change determination to about $\pm$ 5 cm or better provided care is taken with station selection, instrument transportation and care, tidal corrections and program planning. Experience gained during the first year of the semiannual program allowed the monthly program to be designed and implemented more efficiently.

To minimize errors, almost all stations were located along paved roads. Vehicles with soft suspension are utilized. The elevations of the stations and especially the base stations were kept similar to each other where feasible.

Care was exercised to avoid station locations that had traffic noise or the likelihood of frequent winds. Where practical, local base stations were located near the center of lines to minimize the time between base observations and thus reduce error from irregular meter drift and barometric related gravity change (Warburton and Goodkind, 1977). Station locations were avoided near potential mass changes such as rapid gullying, deposition or ground water change.

Multiple gravity observations are made to statistically improve the data. Observations are made with two LaCoste and Romberg Model D "Microgal" gravimeters (D-3 and D-19). For each set of observations at least two ties are made with each of the gravimeters. Each line has a local base station. The local stations are tied to the local base and the local bases are tied to the master base station in Hemet. Semiannually the master base is tied to the U. S. G. S. master base stations in Riverside and Palmdale and to the California Institute of Technology base in Pasadena.

The longevity of stations has been good. Four stations have been lost due to highway widening or maintenance for an annual loss rate of about 1/2 %.

Because of the inaccuracies of the five-scale calibration of the gravimeters, the results of one meter must be compared against the results of the same meter obtained at an earlier time. Two gravimeters are utilized to provide continuity, should one instrument be modified during periodic cleaning and repair or an instrument lost. A distinct advantage of the Model D gravimeter is its ability to be reranged. As the meters drift, every week or two they are reranged to return to the original position of the main nulling screw.

A byproduct of this program and the U. S. G. S. program is a network of well documented gravity base stations throughout southern California that may be utilized by commercial and research workers for having their gravity observations on a common datum. To improve the accuracy of the gravity values at the network of stations in this program, the U. S. G. S. program and any other interested program, Earth Science & Engineering has established a fine-scale gravimeter calibration range that covers most gravity values in the southern United States as well as southern California. Stations are located at 10 milligal intervals from 979,568.9 to 979,296.4. The range is compact, located within a single tectonic block, and along a readily accessable paved highway. It is close to the Pinyon Flat recording cryogenic gravimeter to facilitate accurate tidal and barometric gravity corrections.

Another by-product of this program is the verification of a new technique to determine aquifer specific yield by measuring with a gravimeter the increased or decreased mass of ground water and observing the rise or fall of the water table in an observation well. To determine the magnitude of errors that could

be caused by poor station site selection in a program to measure gravity changes due to tectonic factors, a few stations in the semiannual network were established atop ground water basins that were undergoing subsidence or significant fluctuations in water table.

One station, ESE-032, is atop a small groundwater subbasin that had a 99 foot rise in the water table. The gravity increased about 185 microgals, implying an aquifer specific yield of 0.15. This is close to the amount estimated in a ground water investigation of the area (Bean, 1955) and is probably more accurate than that previous estimate. The data are presented on Figure 1.

Relative to the main gravity base in Hemet, gravity at the local base (C1) northwest of Palm Springs increased about 30 microgals in April of 1978. This increase above a relatively flat seventeen month baseline was consistent with all eight ties performed in early April. The increase became greater in May (about 45 microgals) and remained at that level in early June and early July. On July 5th a magnitude 3.8 earthquake occured at 33° 53' North, 116° 30' West (C.I.T., personal communication). The local base (C1) is at 33° 53.92' North, 116° 37.36 West; seven miles west of the epicenter. Subsequently gravity decreased to about 25 microgals above the baseline.

Several minor refinements have been made in the use of LaCoste and Romberg gravimeters for periodic gravity observations. As this program progresses, further refinements are being sought to increase the precision and accuracy.

References:

Bean, R. T., Geology of San Jacinto and Elsinore Basins: Calif. State Water Resources Board, Bull. 15, Appendix B, June 1955

Fett, John D., Precise periodic gravity observations to economically monitor vertical crustal deformation: Abstract (Paper G20A) American Geophysical Union Fall meeting, San Francisco, 1976

Oliver, H.W., S.O. Robbins, R.B. Grannell, R.W. Alewine and Shawn Biehler, Surface and subsurface movements determined by remeasuring gravity: Chap. 10 (pp. 195-211), in San Fernando earthquake of Feb. 9, 1971, G. B. Oakshott (Ed.), Calif. Div. Mines and Geology Bull. 196, 1976

Strange, W.E., and D.G. Carroll, The relation of gravity change and elevation change in sedimentary basins (Abs.) EOE, Vol. 56, No. 12, p. 1105, 1974

Warburton, R. and J. Goodkind, The influence of barometric pressure variations on gravity: Geophys. J. Roy. Astron. Soc, Vol. 48, pp. 281-292, 1977

FIGURE 1 Gravity Change in the Cienega Subbasin of San Jacinto Basin

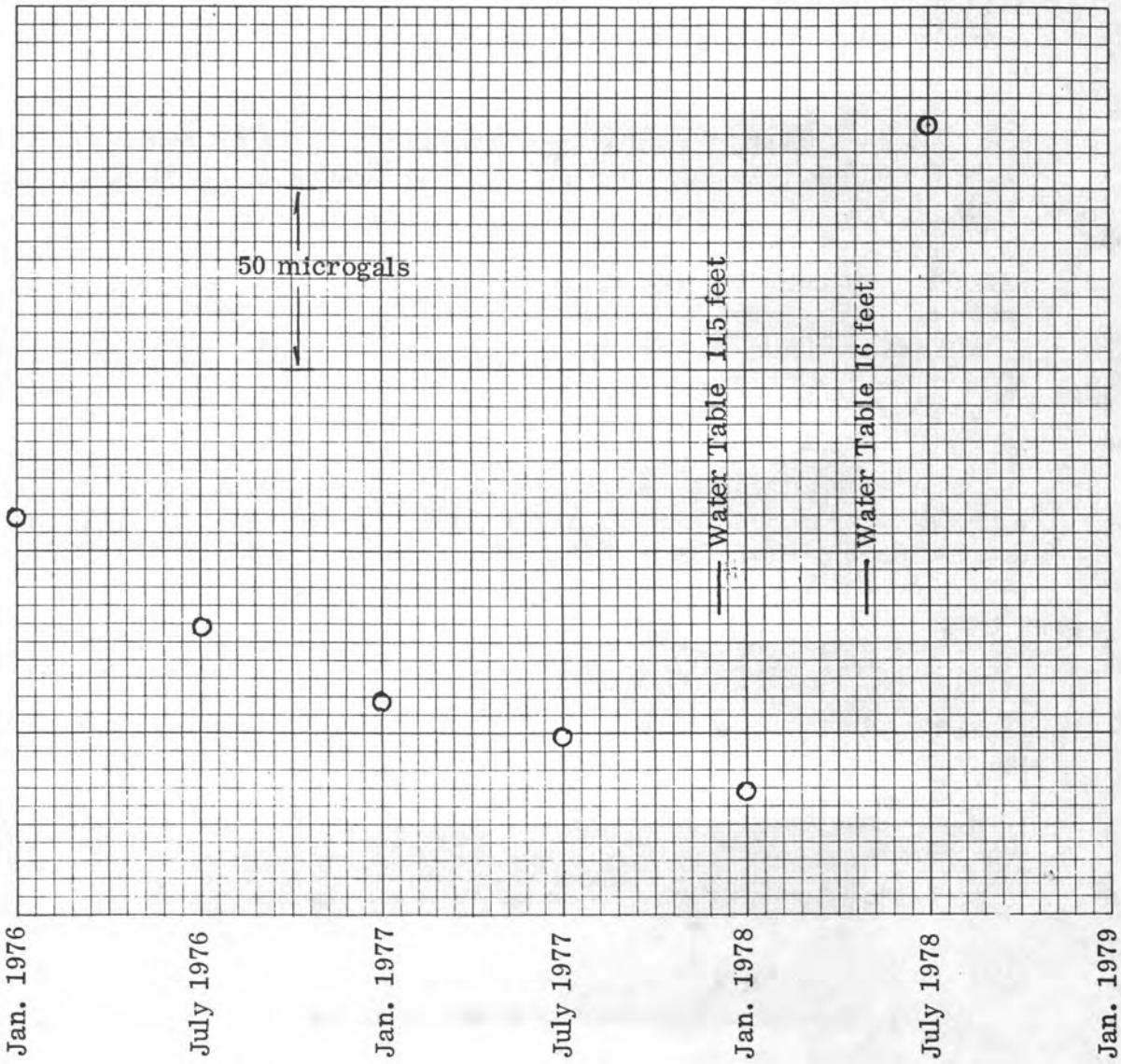

Tiltmeter Results from Adak

J. C. Harrison, J. M. DeMay and C. Meertens
Cooperative Institute for Research in Environmental Sciences
University of Colorado/NOAA
Boulder, Colorado 80309

We have been measuring tilt on Adak since the summer of 1975 in an attempt to establish a correlation between the occurrence of earthquakes and a supposed precursory tilting of the ground. The problem is twofold: firstly, to establish the nature and size of the assumed precursory tilts, and secondly, to devise a way of installing and operating a network of tiltmeters capable of observing these tilts under the constraints imposed by the Aleutian conditions. USGS experience in California is of little help in predicting the character of precursory tilts in the Aleutians, because the tectonic setting is very different - a subduction zone rather than a strike-slip fault. The Aleutian conditions mean that, away from the immediate vicinity of the Adak townsite, sites are only accessible by helicopter, the instruments must be capable of unattended operation on batteries for one year, and the information must be telemetered in to Adak Observatory. So far we have only worked in the vicinity of the Adak townsite, but the ultimate requirement to cut the umbilical "hard wire" cord and move out to remote sites has played an important role in governing the techniques employed.

Our work can be considered in three phases. From May 1975 to February 1976 when it was hit by lightning, we ran a Hughes tiltmeter in the Adak seismic vault. Such sites are notoriously poor, but it seemed worthwhile to make the attempt to get some handle on the size of precursory tilts before starting Phase II in the summer of 1976. Vault temperature was monitored and corrected for, and the attempt turned out better than might have been expected. We were blessed with a magnitude 5 earthquake at 63 km range the day before the lightning strike. Figure 1 shows the tilts recorded for 11 days before the earthquake and the tilt on February 19 invites discussion as a possible precursor. However, there is a daily periodicity in the tilt, presumably due to the daily solar heating of the outside of the vault. The long and short period tilts were separated and the short period component (1 cycle/day and shorter) is plotted day by day in Figure 2. The tilting on February 19 is then seen to have the character of the normal daily solar induced tilt, albeit somewhat more pronounced. The long period tilts for 6 months before the earthquake are shown in Figures 3 and 4. There is a reversal in tilt on both components three months before the earthquake. On the other hand, this could well be part of a normal annual cycle to be expected in such a site. This first phase thus proved inconclusive but did suggest that there are no easy answers and that we must look to better than 1 μrad short term stability and 10 μrad seasonal stability to do any good.

Phase II started in the summer of 1976 and continued through summer 1978. Kinemetrics bubble tiltmeters were modified and installed by Sean-Thomas Morrissey as described by him in a companion paper (Morrissey and Stauder, this volume). The holes were dug with a soil auger which limited the depth of installation to the soil layer. Some of the early data from two instruments about 10 meters apart at the west site are shown in Figure 5 together with daily rainfall. We have periods of relatively

uniform tilt separated by large disturbances which correlate with heavy rainfall. Sometimes the tilt and trend recover after a rainfall disturbance, sometimes the trend appears to recover but with an offset. The y (west-east) channels appear to track reasonably well both in general character of the rainfall effects and between rain storms. The x (north-south) channels do not, the north installation at the west site showing smaller rainfall disturbances although the south installation is more stable in the fine intervals.

Thus, as one might expect, meteorological effects appear as the number one enemy when operating at such a shallow depth, with rainfall as the most important cause of disturbance during this period. The important questions are: what is the mechanism for these rainfall-induced tilts; do the tiltmeters return to their initial states following rainfall so that we may ignore the disturbances and join the periods of fine weather tilt together; is the fine weather tilt of geophysical interest or merely the soil drying out; can we predict the rainfall effects given past rainfall and thus remove them from the record; can we reduce the meteorological effects to the point where we can live with them?

We can answer these questions to some extent. The rainfall mechanisms are complex consisting of (1) loading of the soil due to added weight of water, (2) differential pressures caused by rain penetrating more easily in some places than in others, and (3) changes in the elastic constants of the soil due to changing water content. They may be expected to depend on the large scale topography of a site and the small scale details of each installation and its immediate surrounds. Their behavior with depth may be expected to depend greatly on the local geology, being small at depth where impermeable beds block the downward movement of water or where the water moves in a uniform manner through permeable beds. They will be large in heterogeneous materials at depths to which water penetrates and are, for instance, quite large in fractured greywacke at 50 feet depth (Herbst, 1976). In a general way stresses due to loading and differential water pressures are deforming the subsurface material, thus these effects will be reduced as the rigidity of the subsurface material increases. In addition the more competent material is likely to behave elastically, whereas soil may exhibit inelastic non-reversible behavior. Attempts by Herbst at predicting rainfall effects were only partially successful because the response depends markedly on the state of the ground at the time of rainfall; a given amount of rain can have quite different effects depending on whether it follows a long dry spell or a wet period. Accurate prediction of the rainfall effects is therefore likely to be difficult and it is important that reinstallation of the tiltmeters in the summer of 1978 appears to have reduced these effects very markedly.

The tilt records proceeded in much the way sampled by Figure 5 until late February 1977 when, as shown in Figure 6, a large daily signal suddenly appeared on the records (especially prominently on the west-south tiltmeter), together with a suggestion of a correlation of tilt with atmospheric pressure. A look at the temperatures during this period suggests that we are dealing with a freeze-thaw effect. Interestingly this period is followed by a period of very large tilt excursions, Figure 7, in which two channels are sharing a very large correlation with atmospheric pressure, a correlation which is only evident during this period. The influence of atmospheric pressure on tilt measurements has been developed by Zschau (in press). Figure 8 from his study shows that pressure dependencies of the magnitude observed in Figure 7 (50 mas or 0.25 μrad per millibar) are

possible in unconsolidated materials. Porous materials show very different compressibilities depending on whether or not air is allowed to penetrate into the pores; a mattress with an impermeable cover is greatly compressed by a change in external air pressure whereas if the pressure is allowed to penetrate into the interior only the metal of the springs is compressed, and this is a very small effect. It appears that this effect is being seen here: the frozen ground surface is sealing the interior and introducing a large pressure coefficient which is not normally present.

Figure 9 shows data from November-December 1977, which is very similar in general character to that in Figure 5. We have smooth behavior and low tilt rates in fine intervals and disturbances associated with periods of heavy rainfall. Net tilts in the x and y directions, as observed at the north and south installations of the west site over a period of 150 days, are also indicated. These are of the order of 5 μrad, but the net tilts on the two instruments are in opposite directions in both components suggesting that we cannot obtain any geophysically important tilt information from the Phase II installations. However, the most interesting feature of this plot is the behavior of the south installation already described by Sean-Thomas Morrissey (Morrissey and Stauder, this volume). The meteorological disturbances are much subdued and the long term tilt indication over the 150 day period is only 1 μrad; this period began shortly after the installation of the tiltmeter and, if a longer settling in period had been allowed, the net drift would have been even less. The tiltmeter was, in fact, very shallow, at only one meter depth, but was installed in rocky glacial rubble rather than soil. This order of magnitude improvement can probably be ascribed to the more competent nature of the material in which the tiltmeters are installed and to the other changes in technique described by Morrissey. During the summer of 1978 all the tiltmeters including that at the south side were reinstalled in the broken rock layer beneath the soil using the new technique. A gasoline powered rock breaker/drill was used in the excavation. Initial results, Figure 10, are most encouraging and we have high hopes that Phase III will bring us stabilities of the order of 1 μrad/year, at which point we may hope to see tilts of geophysical importance.

Finally, we would like to mention the development at CIRES under sponsorship by the Air Force Geophysical Laboratories and NSF of a deeper borehole tiltmeter. The instrument is contained in a 2 meter long cylindrical capsule 8.9 cm (3 1/2") in external diameter. Tilt is sensed with two single-axis simple pendulums 5 cm in length on a mounting plate (Figure 11) which can be leveled by means of two screws driven by motors controlled from the surface. Four of these tiltmeters are under construction and will be installed in boreholes at Boulder, Colorado, at depths of 20, 50, 100 and 200 feet in order to study the attenuation of meteorological influences with depth. It would be most interesting to study the behavior of a Kinemetrics bubble tiltmeter in an Adak-type installation at the same site.

References

Herbst, K., Interpretation von Neigungsmessungen im Periodenbereich oberhalb der Gezeiten, Ph.D. thesis, Technical University of Clausthal, 1976.

Zschau, J., Air pressure induced tilt in porous media, Proceedings of the 8th International Symposium on Earth Tides, Bonn, 1977, in press.

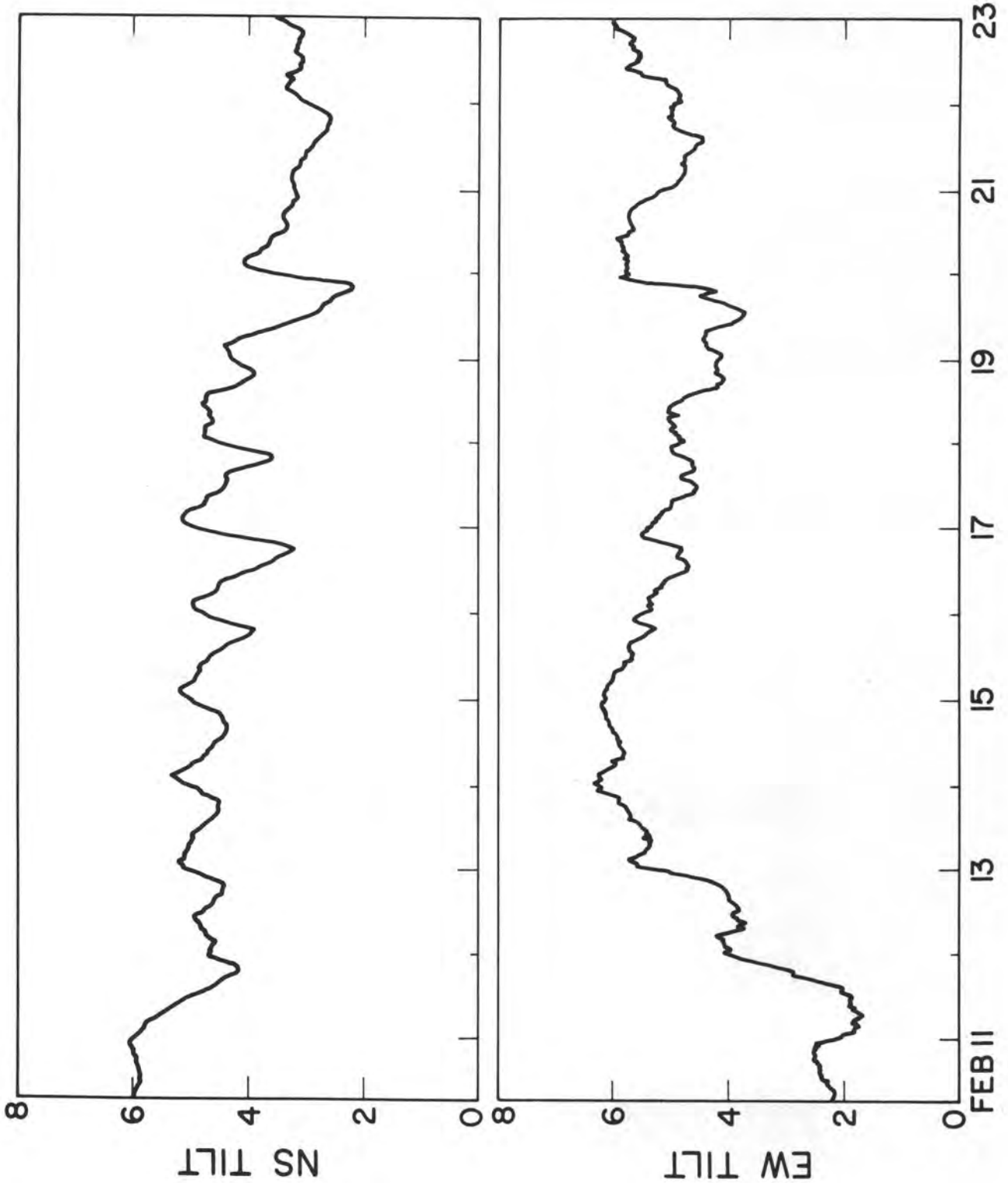
NS TILT
EW TILT
8
6
4
2
0
FEB 11
13
15
17
19
21
23

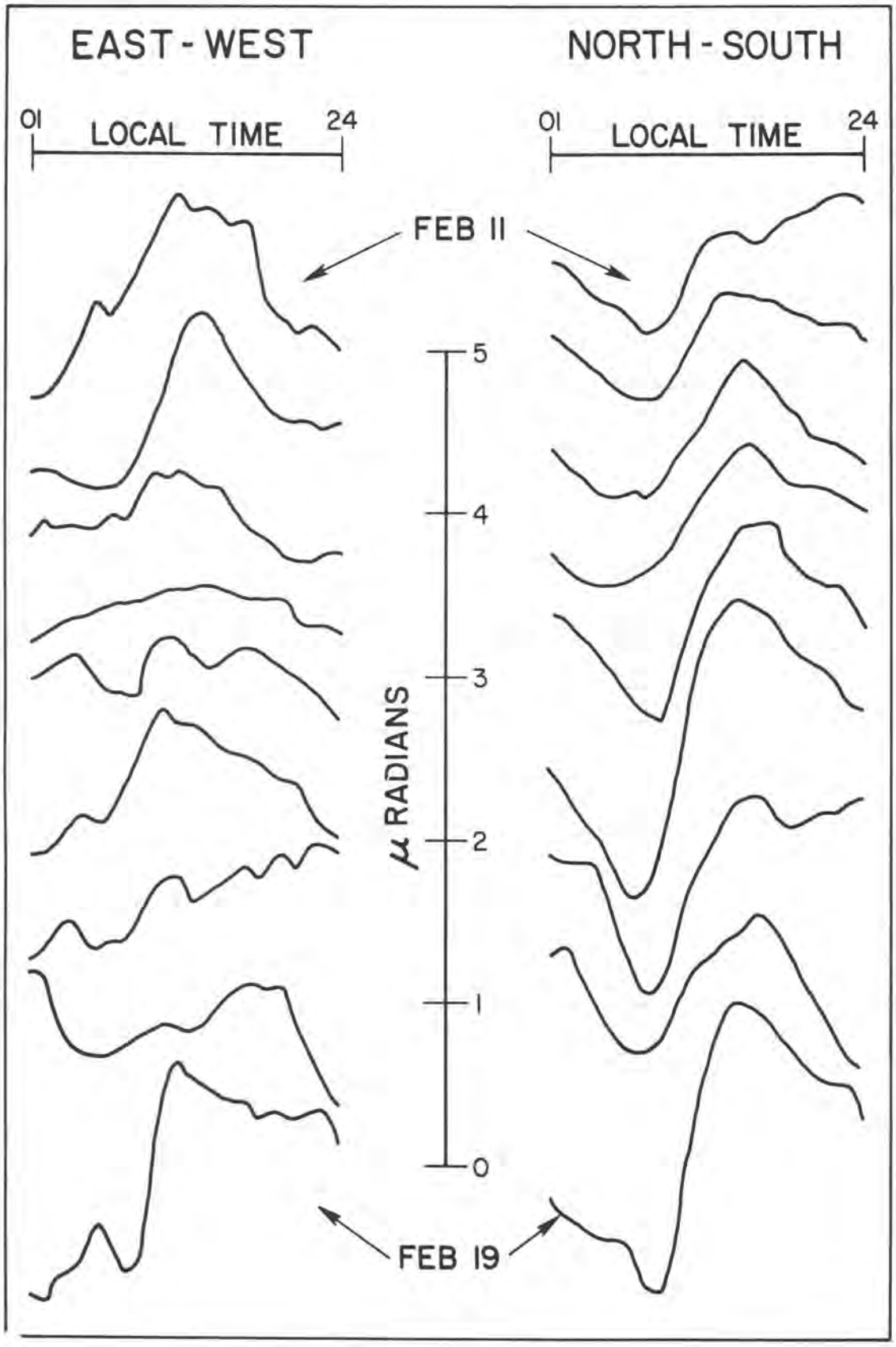
EAST - WEST
NORTH - SOUTH
01
LOCAL TIME
24
01
LOCAL TIME
24
FEB 11
5
4
3
2
1
0
μ RADIANS
FEB 19

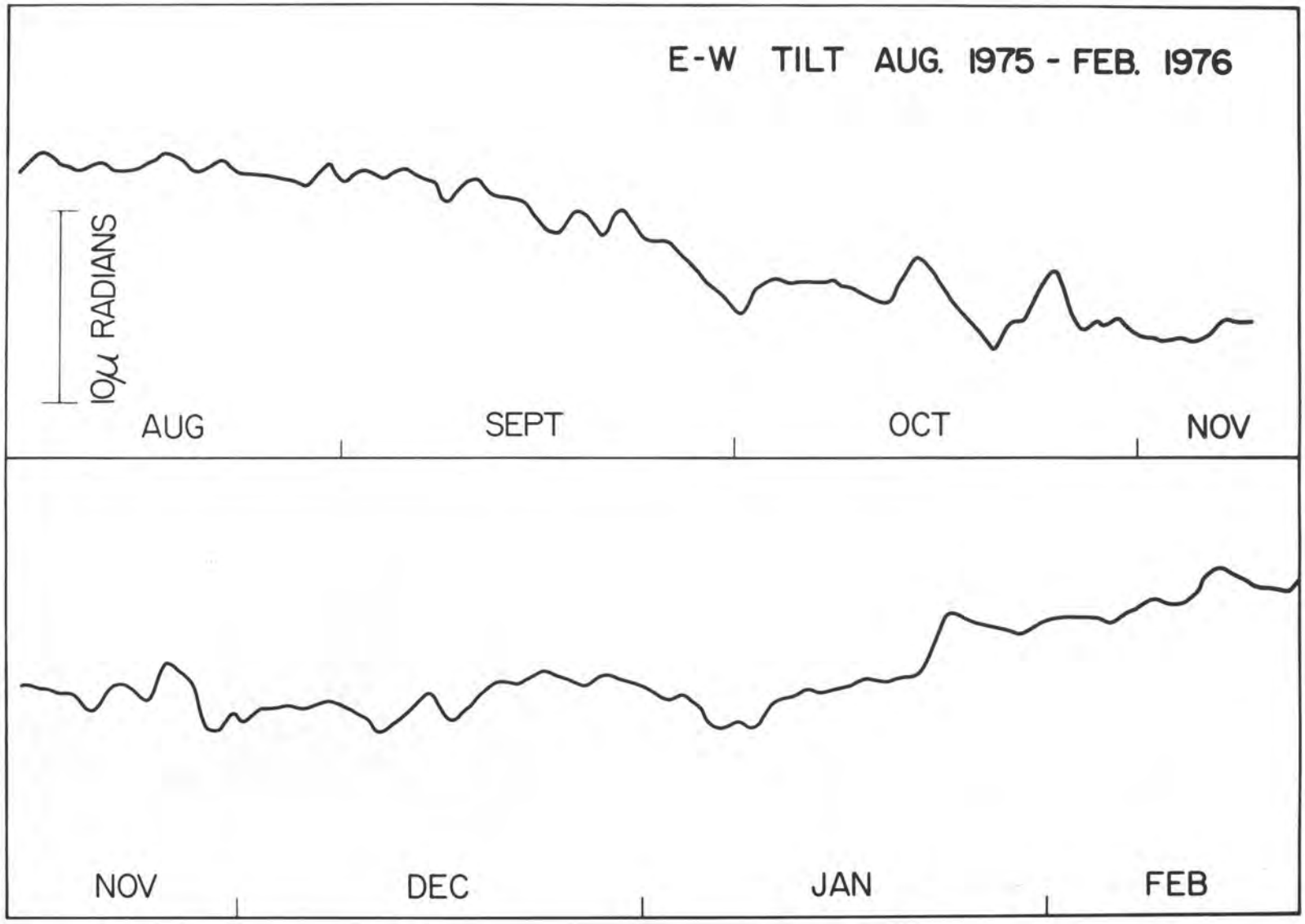
E-W TILT AUG. 1975 - FEB. 1976
10μ RADIANS
AUG
SEPT
OCT
NOV
NOV
DEC
JAN
FEB

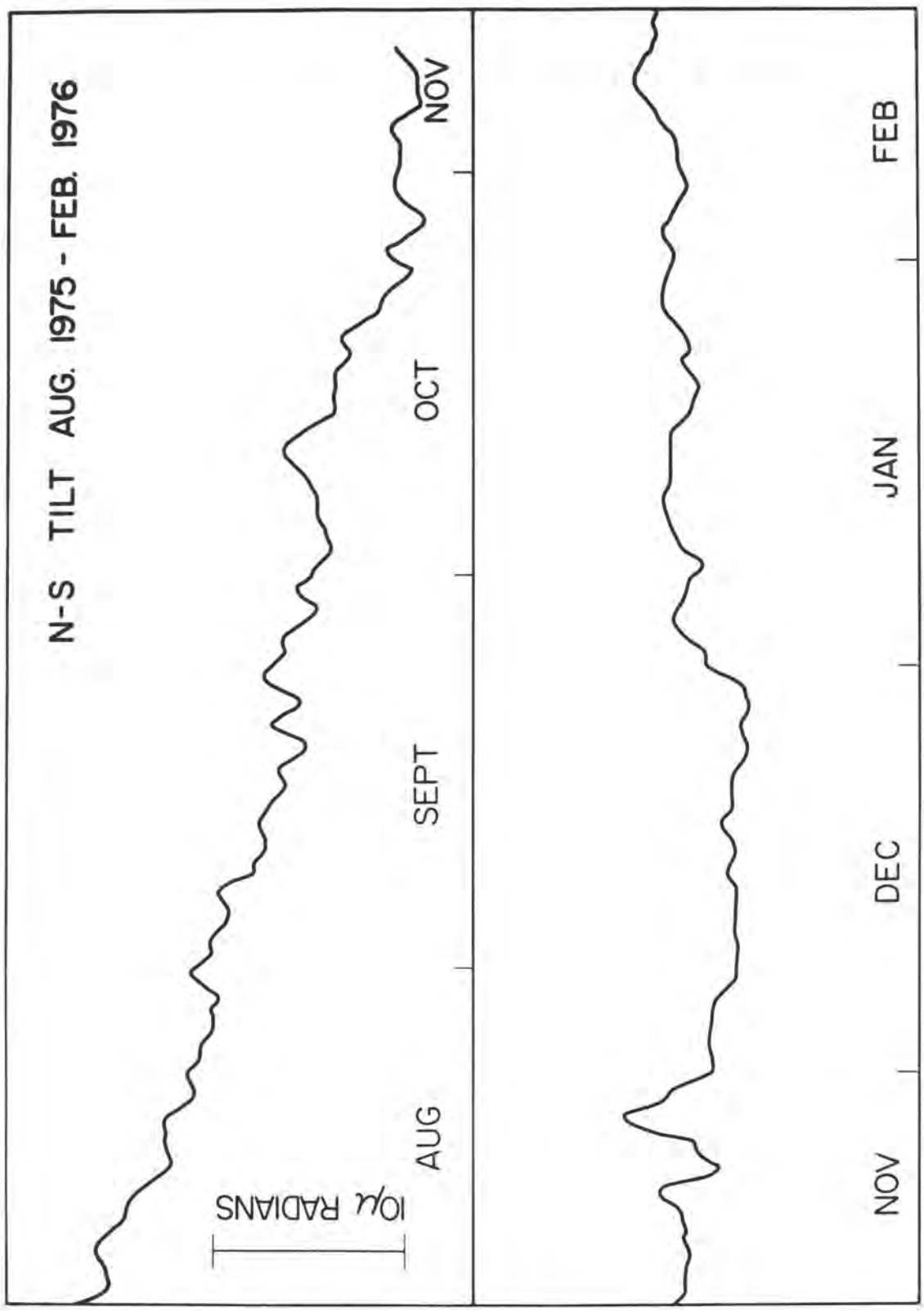
N-S TILT AUG. 1975 - FEB. 1976
AUG
SEPT
OCT
NOV
10μ RADIANS
NOV
DEC
JAN
FEB

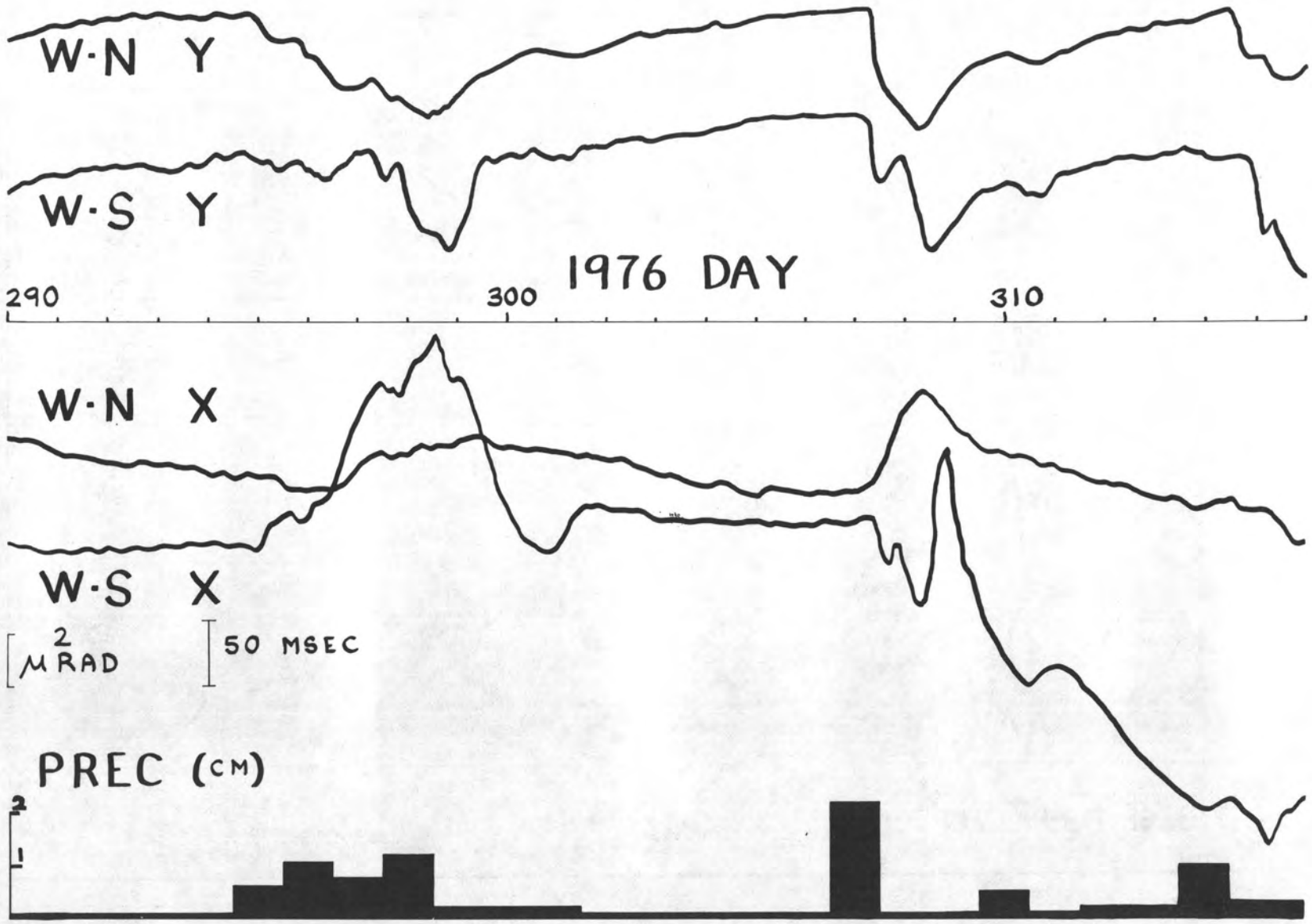
W·N Y
W·S Y
290
300
1976 DAY
310
W·N X
W·S X
2
μRAD
50 MSEC
PREC (CM)
2
1

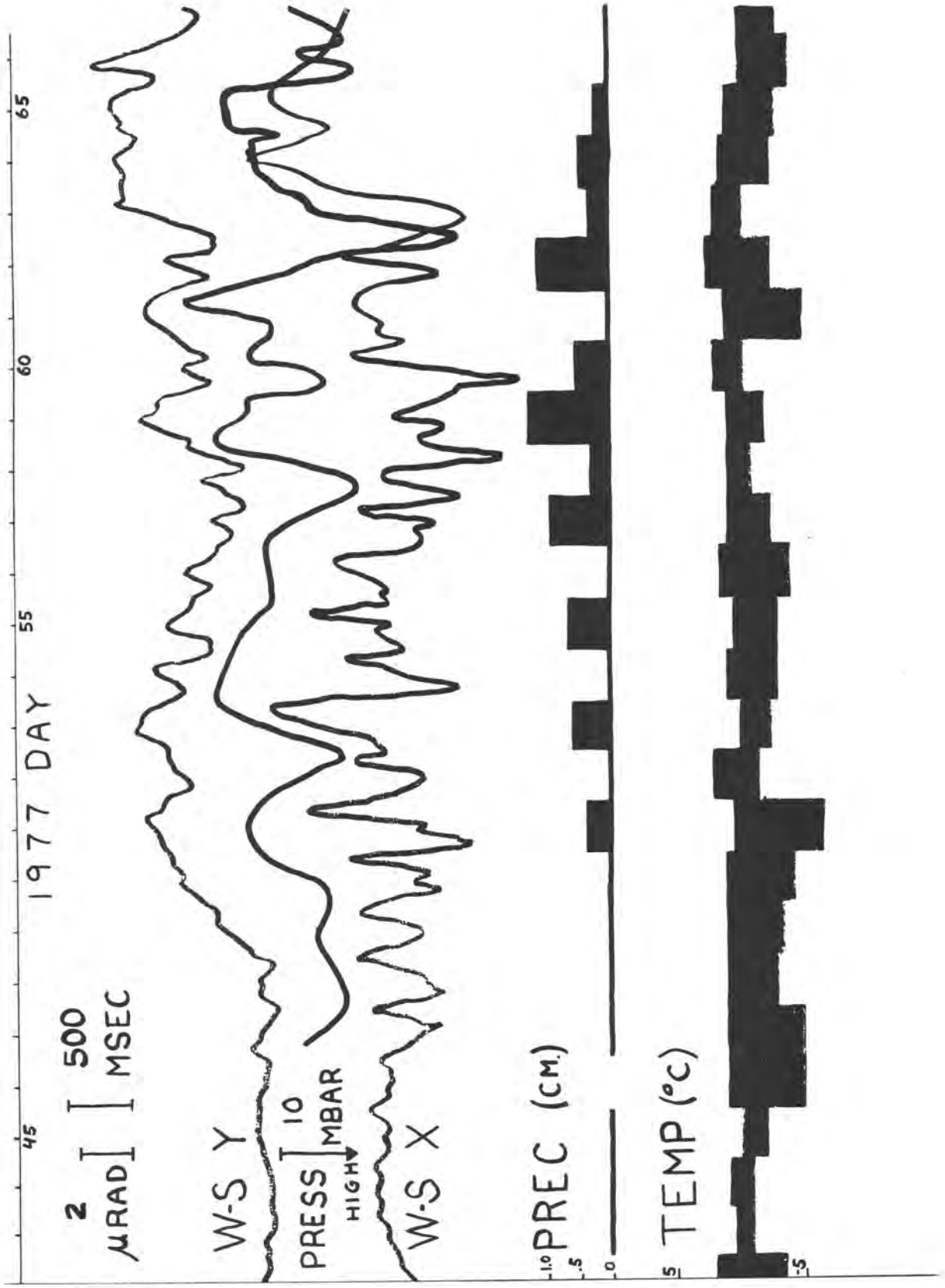
45
1977 DAY
55
60
65
2
μRAD
500
MSEC
W-S Y
PRESS
10
MBAR
HIGH
W-S X
1.0
PREC (CM.)
.5
0
5
TEMP (°C)
-5

1977 DAYS
70
75
80
85
90
95
WS (y)
2 μ RAD
500 msec
WN (y)
WN (x)
LOW
10 MBAR
HIGH
PRES.

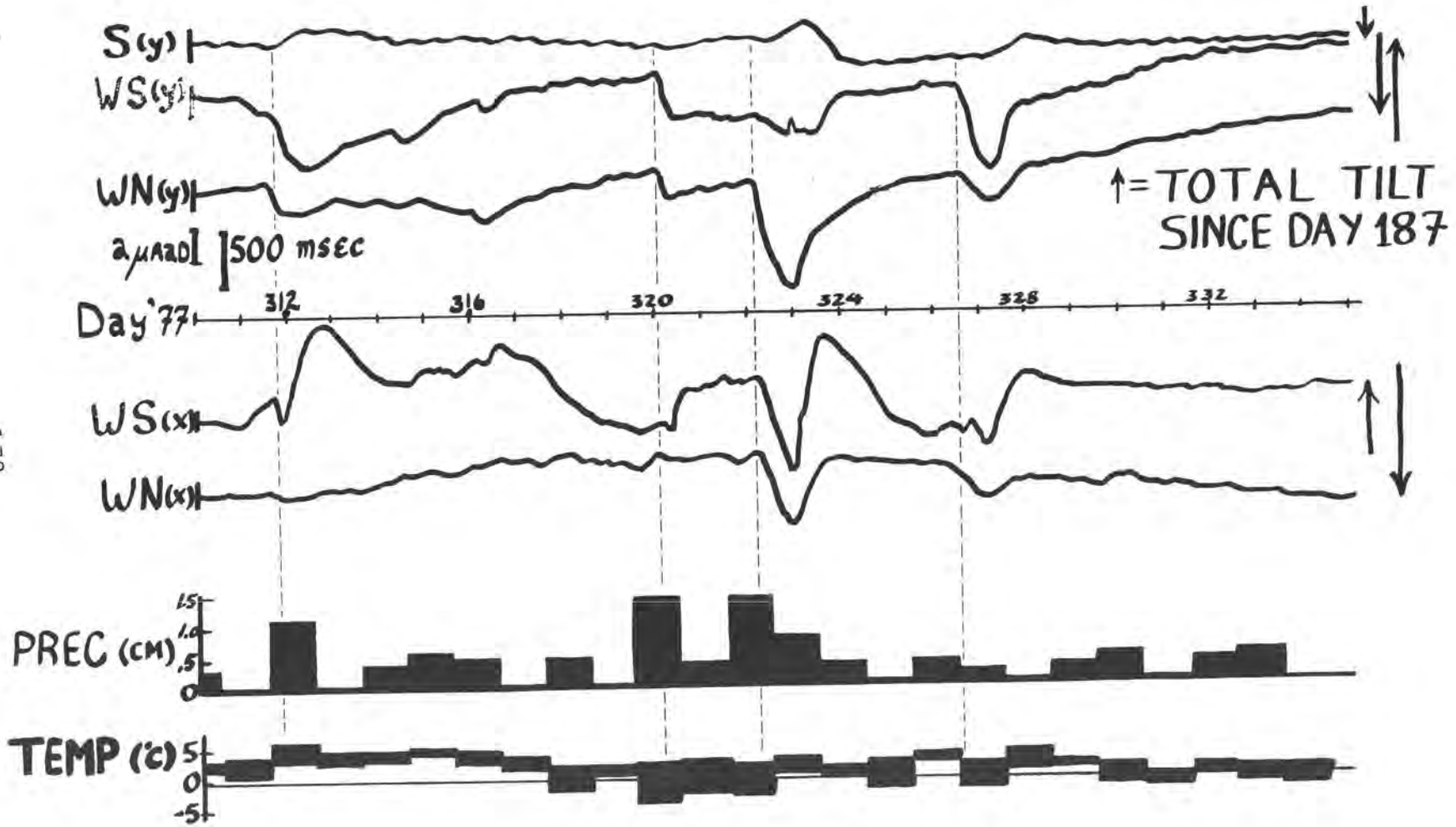
S(y)
WS(y)
WN(y)
a μ rad
500 msec
↑=TOTAL TILT
SINCE DAY 187
Day '77
312
316
320
324
328
332
WS(x)
WN(x)
PREC (CM)
1.5
1.0
.5
0
TEMP (°C)
5
0
-5

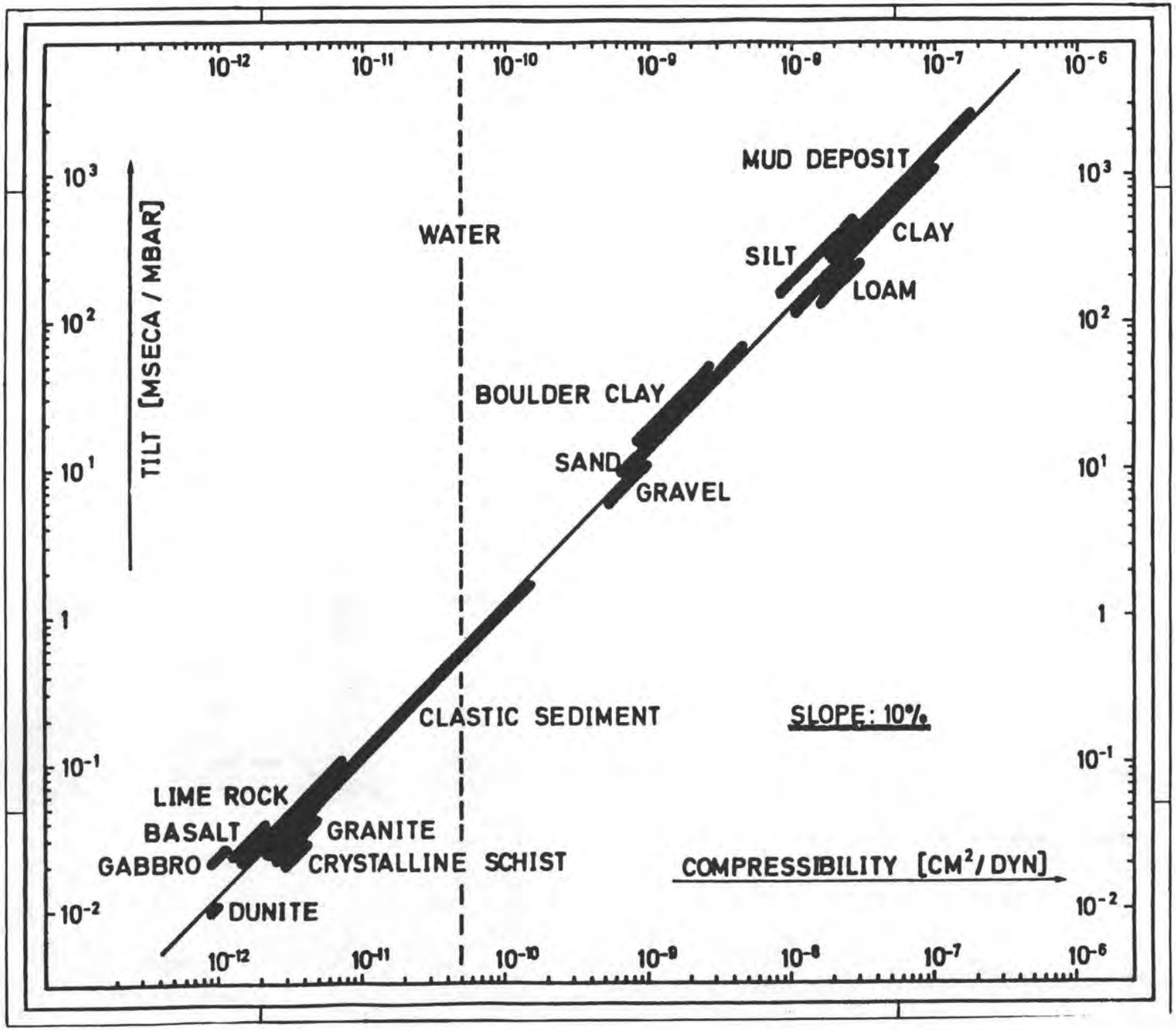
TILT [MSECA / MBAR]
COMPRESSIBILITY [CM²/ DYN]
WATER
CLASTIC SEDIMENT
SLOPE: 10%
MUD DEPOSIT
SILT
CLAY
LOAM
BOULDER CLAY
SAND
GRAVEL
LIME ROCK
BASALT
GRANITE
GABBRO
CRYSTALLINE SCHIST
DUNITE

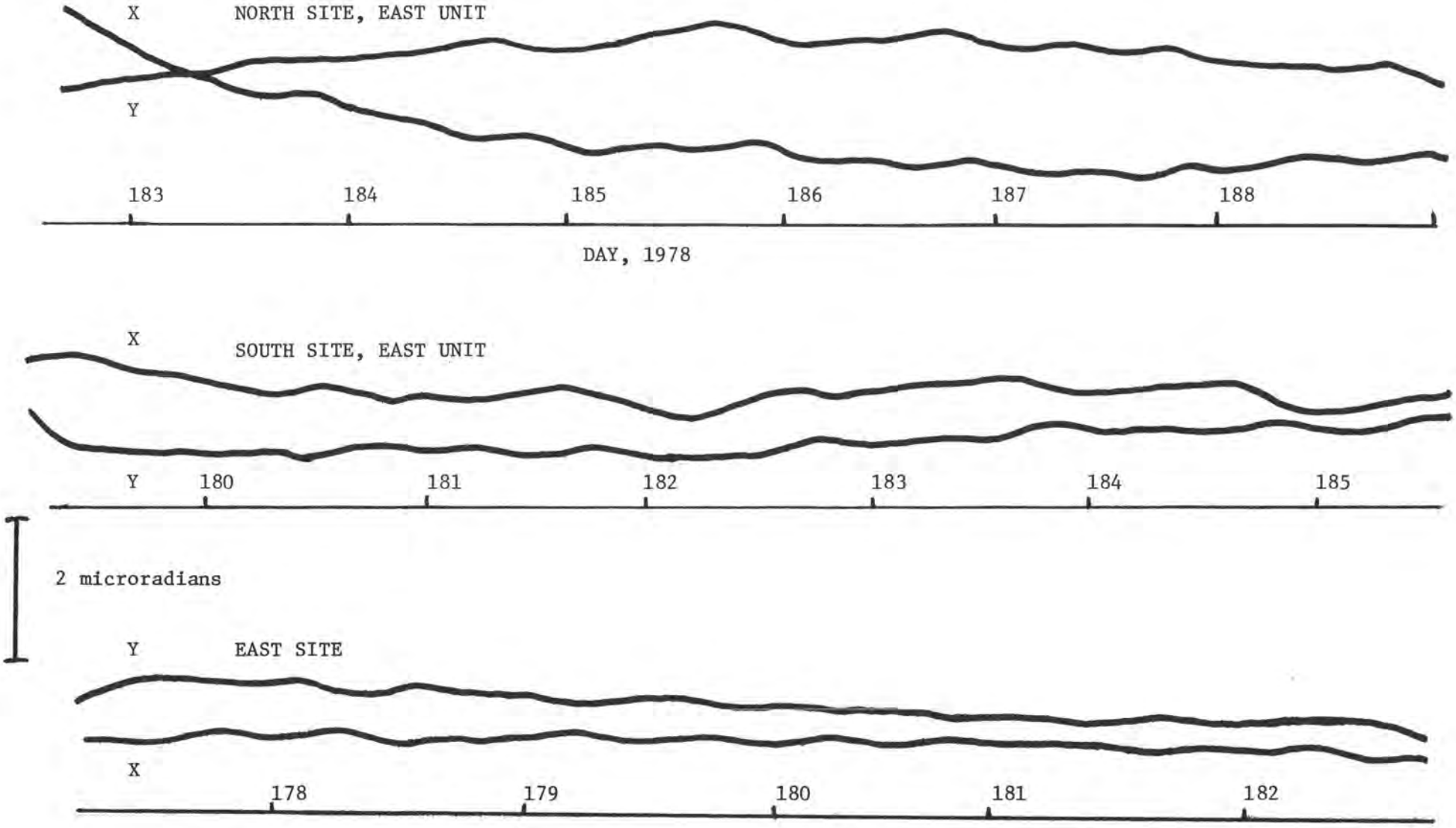

RECORD FROM THREE ADAK TILTMETERS STARTING EIGHT HOURS AFTER INSTALLATION

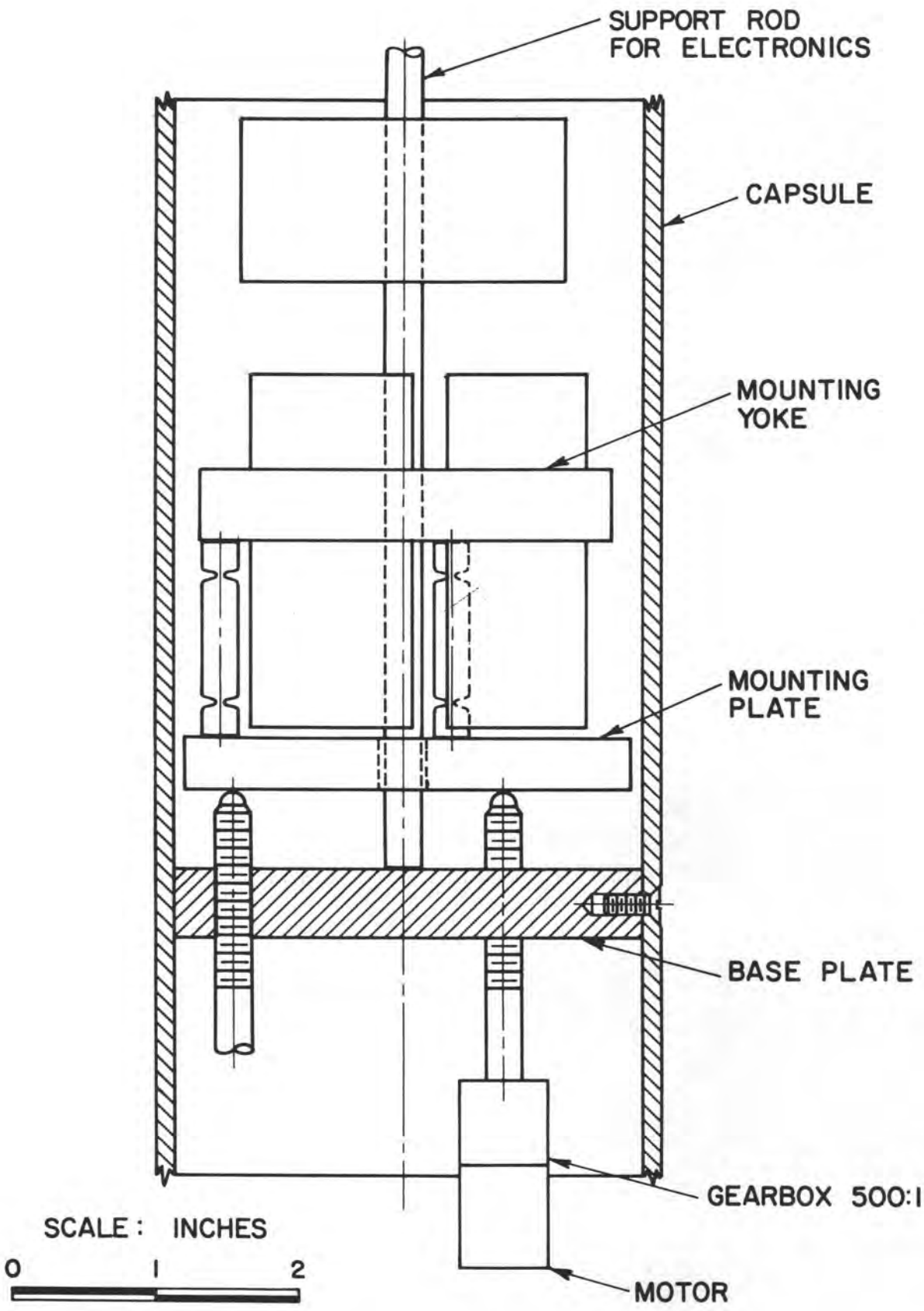
SUPPORT ROD
FOR ELECTRONICS
CAPSULE
MOUNTING
YOKE
MOUNTING
PLATE
BASE PLATE
GEARBOX 500:1
MOTOR
SCALE : INCHES
0
1
2

MEASUREMENTS OF TILT IN THE NEW HEBRIDES ISLAND ARC

by

Bryan L. Isacks[1], George Hade[1], Rene Campillo[2], Michael Bevis[1], Douglas Chinn[1], Jacques Dubois[3], Jacques Recy[2], and Jean-Luc Saos[4]

1. Dept. of Geological Sciences
   Cornell University
   Ithaca, New York 14853 USA

2. Office de la Recherche Scientifique et Technique Outre-Mer
   Boite Postale A-5
   Noumea, New Caledonia

3. Office de la Recherche Scientifique et Technique Outre-Mer
   24 Rue Bayard
   75008 Paris, France

4. Direction des Ressources Minerales des Nouvelles Hebrides
   Boite Postale 637
   Port Vila, New Hebrides

INTRODUCTION

The New Hebrides island arc, part of a seismically active zone of lithosphere subduction, has several features which make it an attractive area to "catch" a large earthquake. The shallow seismicity associated with the boundary between the convergent plates is characterized by the frequent occurrence of clusters of moderately large earthquakes rather than by the infrequent occurrence of great earthquakes such as in the seismic zones of Chile, the Kuriles, and Kamchatka. In the central New Hebrides, islands accessible to instrumentation are located unusually close to the zone of thrust faulting where the major shallow earthquakes are generated. To take advantage of these and other favorable factors, Cornell University and the French Office de la Recherche Scientifique et Technique Outre-Mer (ORSTOM) are working with agencies of the New Hebrides government, the Direction des Ressources Minerales and the Service Topographique, in a program of earthquake studies which includes monitoring tilt in the central region of the New Hebrides.

The New Hebrides is an area where field conditions do not favor sophisticated instrumentation requiring constant and special attention. Thus the bubble-level borehole tiltmeters developed by the U.S. Geological Survey (USGS) and built by Kinemetrics seemed a reasonable choice, although we felt from the beginning that the extremely short baseline of the instrument would be a problem in respect to long term stability. Accordingly, a leveling technique was adapted to cover the long term effects and to measure tilt over a significant baseline. In August 1975 measurements of tilt began with the installation and leveling of two arrays of bench marks. These arrays have dimensions of the order of a kilometer and have been releveled at intervals of approximately 6 months during a nearly three year period. In July and August of 1976 a network of tiltmeters of the borehole, bubble-level type commenced operation and now includes eight stations. The releveling results and the tiltmeter recordings comprise the data discussed in this paper.

So far the central New Hebrides has been remarkably quiet. No earthquakes with magnitudes (mb) greater than 5.4 have occurred within the network, while two events with magnitudes (Ms) of 6.5 and 6.9 occurred about 140 km north and 350 km south of the network, respectively. No clear and unambiguous signals have been associated with the earthquake sources. Co-seismic offsets, changes in slope, and exponentially decaying offsets are observed, but the data suggest that these are effects near the stations of the large amplitude seismic waves. However, the search for possible pre- or post-seismic signals reveal characteristics of the noise levels and sensitivity of the monitoring system. In addition, evidence is found for a tilt signal of marginal significance that may be related to a time-space migration of seismicity in the central region. This signal is produced by the leveling method, but some evidence for it is found in the tiltmeter recordings.

MONITORING TILT IN THE CENTRAL NEW HEBRIDES

Tiltmeter Network

Ten tiltmeters were obtained from Kinemetrics through the USGS in the Spring of 1976. One was eventually found to be defective (the bubble lost its liquid) and eight have been installed in the central New Hebrides. These units have nominal outputs of 40 millivolts per microradian and are recorded with Rustrak strip chart recorders at sensitivities all within 50% of about 2 mm/microradian. Chart speeds are 0.5 in/hr. Beginning in the latter part of 1977 tilt has also been recorded on a second Rustrak recorder operating at chart speeds of 1-2 in/day. Rainfall at the site is also recorded on the slow speed Rustraks.

The locations of the stations were chosen as a compromise among several factors. Necessary conditions included topographic and subsurface characteristics thought to be favorable to instrumental performance and reasonable accessibility. Fortunately, these two factors turn out to be positively correlated in the New Hebrides. The flat coral terraces, the best terrain for tiltmeters, are also favored as locations for coconut plantations, and have thus been cleared and are reasonably accessible. Additional factors in the locations included nearness to the zone of shallow earthquakes, coverage of a large area of the seismic zone to increase the chances of catching an event, and spacing between stations which provide some possibility of correlations among the recordings.

The resulting locations are shown in Figure 1. The relationship of these locations to the main zone of earthquake generation is shown in Figure 2. The islands south of Efate are located too far east of the shallow zone of earthquakes to be useful sites. The Torres Islands, located north of Santo Island and close to the shallow earthquake zone, are relatively inaccessible but are still possible sites for future stations if sufficient logistic support can be managed. The west coast of Santo Island is also difficult logistically.

The stations are located on level and well-drained terrain with a water table well below the three-meter depth of the tiltmeter borehole. Clay-rich soils were avoided, particularly the dense, sticky clays developed in the volcanic ash deposited on the older, high coral terraces. Five of the sites are located on relatively young uplifted coral terraces, two in soil, and one in sand. In the last case (Southwest Bay) the tiltmeter site was built up into a broad circular mound around the tiltmeter enclosure in order to keep the bottom of the borehole casing well above the ground water level. The sites on coral terraces are in semi-consolidated coral material which at some sites could be broken easily with a pickaxe or shovel but at other sites required a jackhammer. This material is generally very well drained and contains no clay. The older terraces at Port Olry and Malapoa are covered with a near-surface layer of clay soil, but the borehole and lower part of the enclosure are completely within the clay free coral material.

The installation procedure is basically similar to that developed by the USGS, but was modified to provide additional protection against moisture. Aged iron pipes with six inch diameters were used to case the holes and were sealed at the bottom and capped at the top to keep moisture away from the tiltmeter tube. Cleaned, sieved and oven-dried coral sand was used to pack the tiltmeter tubes within the iron pipe casing. The sand was packed by tapping the iron pipe while monitoring the tiltmeter output and mechanically centering the tube for zero outputs on both channels. The iron pipe is itself initially set into the borehole with sandy backfill from the excavation. After completion, one can move about in the enclosure right next to the top of the iron pipe casing without causing more than a few tenths of a microradian disturbance.

The fiberglass enclosure was buried above the cased sand-packed tiltmeter tube as shown in Figure 3. Styrofoam sheet planks cut into circular forms were installed in the enclosure to provide thermal insulation. The fiberglass tops were fitted with rubber gaskets and bolted down to the enclosure to prevent any moisture leakage. Condensation is minimized by placing a styrofoam plank very close to the top of the enclosure. A polyethylene sheet is fitted over the pipe and sealed to it and to the bottom of the fiberglass enclosure to exclude water vapor entering the enclosure from the bottom.

The recording system, housed in a second enclosure, is shown in Figure 4. The records obtained from the tiltmeter stations are summarized in Figure 5. Many of the record gaps were due to problems with the Rustrak recorders. Modifications to the recording system and the addition of a second Rustrak (as shown in Figure 4) has significantly improved the continuity of the recordings obtained.

Tilt Determined By First Order Releveling of Benchmark Arrays

During July-October 1975, two networks of benchmarks were established near the sites where the Devil's Point and Ratard tiltmeter stations are now operating. These networks are shown in Figure 6. The Devil's Point tiltmeter was located near but not within the original leveling network. The network was expanded in 1976 to include the tiltmeter by the addition of a small array of four benchmarks installed around the tiltmeter (PD 6-9 in Figure 6). In 1977, three more benchmarks were added to strengthen the array in the north-south direction.

Each benchmark consists of a marine-grade stainless steel rod (3/8" or 1/2" diameter) about 0.5 to 1 m long embedded in a buried concrete pier. The dimensions and shape of the pier vary but occupy a volume of approximately 0.15 cubic meters. Typically, the pier is poured into a hole excavated in semi-consolidated coral deposits. It is then reinforced and is further anchored by rods driven into the ground before the concrete is poured. The stainless steel rod upon which the leveling staff is placed is attached to cross-pieces and embedded in the pier. It has its upper end filed to a smooth rounded surface. The upper end is protected with a plastic pipe and a cap.

The leveling is done by standard first order techniques. Zeiss Ni-1 self-leveling instruments and Wild invar rods with 1 cm gradations and steel rod supports are used. The initial leveling of the Ratard array in 1975 was done with foot plates as turning points, but all subsequent levelings of both arrays were done with permanently installed turning points. These are galvanized pipes driven into the ground or set into concrete on rocky terrain. The permanent turning points significantly reduce closure errors and increase the speed and ease of the leveling work. The leveling of an array takes about three to four days. Since 1975 each array has been leveled 6 times, with intervals between levelings varying between about 1 to 11 months. Since 1976 the intervals have been between 5 and 8 months.

Both the Devil's Point and Ratard arrays include small clusters of three or four benchmarks spaced close enough together to be leveled with one central instrument setup. The spacings between the benchmarks are typically about 70 m. The purpose of the small arrays is to check benchmark stability and to provide a means to determine large tilts very rapidly. As shown in Figure 7a, the relative movements of two benchmarks as determined for two successive levelings, are mostly within the noise levels of the leveling technique. The small Ratard array R-1, 2, and 3 shows a grouping of values between 0.3 and 0.5 mm which are slightly larger than the errors expected from the closures(0.1-0.3mm). For a given pair of benchmarks these movements oscillate between plus and minus values for successive levelings so that little or no net movement has accumulated. These fluctuations are mostly small, however, and do not indicate a serious problem of benchmark stability. The Devil's Point benchmarks appear to be more stable, especially R 6,7,8 and 9.

The errors in determining movements between the more widely spaced benchmarks of the entire array are indicated by the closures obtained in the double run lines between two benchmarks. The closure is taken as the difference between the relative elevations determined by the forward and backward runs between two benchmarks. Of the closures thus far obtained, 75% are less than 1 mm, 93% less than 2 mm, and all are less than 3 mm. The closures depend on the length of the lines, which vary from about 350 to 900 m. In Figure 7b, a histogram of the closures is given in terms of the equivalent tilt, i.e. the tilt calculated by dividing the closure by the length of the line. This histogram gives an indication that sensitivity of the method could be about 1-2 microradians. Tilt change in time is determined by subtracting the results of successive levelings, which increases the error, and by combining the redundant results of the several lines in a given array to determine two components of tilt, which reduces the error. The determinations of tilt changes described in a later section of this paper indicate that the resolution of the leveling method is close to 1-2 microradians.

TILTMETER PERFORMANCE: ENVIRONMENTAL AND INSTRUMENTAL NOISE

The processing of the Rustrak records includes detailed examination of the original records, digitization of the records at intervals of 1 hour, and computer re-plotting of the data with several different time scales. At the most compressed time scale a low-pass filter is applied to the data to remove tidal oscillations. The filtered plots are then composited into a single record for each component after electronic offsets, etc. are removed. Otherwise, further processing into tilt vectors, derivatives, etc. is avoided. We feel that the interpretations at this stage are best done as close to the original data as possible.

The data is illustrated in plots with several time scales in Figures 8 to 10. These plots show the general character of the data as well as give examples of several types of noise signals that have been identified.

Periodic Noise: Tidal Loading and Diurnal Thermal Oscillations

Signals with tidal periodicities are clearly recorded at Malapoa, Devil's Point, Lamap, and Ratard, which are all located at distances less than 1 km from the nearest coastline. Tidal signals are barely perceptible or not recorded at Olry, Sarmet, Southwest Bay and Tukutuk. Olry and Sarmet are located at distances of 1.5 to 2 km from the coast. The last two are located on narrow strips of land nearly halfway between two nearby coastlines, and are thus in positions where the loading effect on tilt would tend to cancel out. These facts, in addition to detailed calculations of the loading of the ocean tides at Malapoa and Devil's Point (Marthelot et al., in preparation), show that the tidal signals observed on the records are probably largely due to the load of the ocean tides as applied within a distance of a kilometer or less of the station. Marthelot et al. show that the effect can be explained by a Boussinesq-type model which is modified to include a low rigidity near-surface layer. Malapoa, located only 100 m from the nearest coast, is most affected by the low-rigidity layer and records a very large tilt of 3.5 microradians per meter of water load (see Figures 9d-e). Devil's Point, located 700 m from the shore, records only 0.5 microradians per meter of water load(also Figures 9d-e), while the more distant stations from the coast record smaller signals. The estimate of the thickness of the low rigidity layer obtained by Marthelot et al. is 0.5 to 1 km.

These tidal signals are quite useful in monitoring instrument performance and sensitivity. In one case, analysis of the tidal signal led to the detection of an error in instrument polarity. However, at Malapoa the effect is so large that the tilt recorded there may be significantly coupled to variations in sea level and thus to vertical tectonic motions. Data from a tide gauge operating across the bay from the station can be used to separate the tilt from the loading effects. Both instruments record a 25 minute seiche in the bay at about the same amplitudes relative to the tidal signal.

Several of the stations have recorded a strong diurnal oscillation

which is inferred to be a thermal effect. At Southwest Bay the effect seems to be a thermoelastic response of the small mound of earth around the tiltmemeter. The oscillations can be significantly reduced by covering the mound and nearby area with coconut fronds. This treatment works well at Southwest Bay, Ratard and Lamap, but has had less success at Sarmet and Tukutuk. The cause of the oscillations at those two stations is not clear. The amplitudes have "spontaneously" decreased to a reasonable level at Sarmet, while Tukutuk has not changed since the inception of recording. Tukutuk is sited in a very level area. It is not clear why there should be a thermoelastic effect there larger than at several of the other stations. The effect continued unchanged after replacement of the tiltmeter electronics and continued to be associated with only one of the components. The oscillation may be due to a very thermally sensitive component within the borehole unit itself.

Rainfall Effects

Rainfall is one of the most important sources of noise on the tiltmeter records. The susceptibility of the tiltmeters to rainfall, however, varies quite remarkably. Devil's Point shows virtually no effect at all. Other stations, such as Malapoa, Southwest Bay, and Olry, show characteristic signals of up to about 4 microradians associated with the heaviest rainfalls (which can be 10-20 cm within a day) but are not otherwise seriously affected. The signals are exponential-like steps, in the case of Olry and Southwest Bay, and unipolar transient waveforms approximated by the function T*exp(-T/To), in the case of Malapoa. The time constants involved are about one day. Long period effects with time constants of the order of 10 days are also visible at Malapoa, but these are small. At Ratard a long period bay-like disturbance with time constants of the order of 10 days is associated with heavy rainfall. The susceptibility seems to be somewhat worse than the aforementioned stations. The bay-like signals account for much of the character of the filtered record shown in Figure 10b. The worst stations in terms of rainfall effects are Lamap and Sarmet. Both short and long period effects can be large, i.e. tens of microradians. The records have been repeatedly driven offscale and several times the tiltmeter tube itself had to be reset in order to recenter the instrument. However, during relatively dry periods the instruments operate at reasonable noise levels.

The rainfall effects are most likely related to the various factors affecting runoff and percolation of rainwater in the immediate vicinity of the tiltmeter installation, and to possible dilatant effects on clay material. The two worst sites, Lamap and Sarmet, are both sited in brown soil which is not entirely clay free, while at the other sites the iron tube is buried in clay free and fairly well-drained porous coral material (or sand in the case of Southwest Bay). In respect to rainfall, Devil's Point is the best station and has the most level local topography. It is speculated that the varying responses among the moderate to good stations depends upon heterogeneities in the percolation of rainwater near the installation. The unipolar transient signals may represent a localized loading effect due to temporary concentration of water within the non-uniform porosity of the coral

rock, while the steps represent a kind of settling of the iron tube or the surrounding area as a result of the flow of water. This complexity of response could account for the puzzling occurrence of rainfall steps on different components at different times at Olry, as illustrated by the steps during December 1976 and June 1977.

Long Period Noise

Figure 10 shows the tiltmeter data filtered and plotted at the most compressed time scale. Over the 20 month period sampled, the records show an overall drift of as little as several microradians to as much as several tens of microradians in the case of the Devil's Point ENE component. In some cases the two components show some correlations while in others they do not. The Devil's Point record, for example, shows a large drift during the first half of the period on the ENE component which does not appear on the other component, while the second half of the record is dominated by a large bay-like excursion apparent on both components. It is interesting that the bay-like excursion with a similar period and phase is observed also on the Malapoa ENE component (see also Figure 11).

The results of releveling the Devil's Point benchmark array, however, do not show the large excursions indicated by the tiltmeter (see Figure 11). The results from the large array and from the small four point array surrounding the tiltmeter (PD 6,7,8,and 9) both do not yield the large tilt excursions shown by the Devil's Point tiltmeter. Neither array shows a tilt change greater than about 2 microradians between successive levelings. Thus the large tiltmeter drifts must be instrumental in origin or reflect tilting over dimensions significantly smaller than the 70 meter dimension of the small array surrounding the tiltmeter. An instrumental problem is suggested where there is no correlation between the two components, as in the case of the large drift on Devil's Point ENE at the end of 1976. Replacement of the electronics and experiments with recording with a resistive network in place of the tiltmeter sensor at Devil's Point have shown that the large drift of the ENE component is not due to defective components external to the tiltmeter tube. On the other hand, the large bay-like excursion seen during the second half of the Devil's Point record and also at Malapoa may be a seasonal effect on the sites.

EARTHQUAKES MONITORED BY THE TILTMETERS

The earthquake activity for a period during which the tiltmeters operated is shown in Figure 12. Since the inception of tilt measurements in August 1975, no shallow earthquake with a body-wave magnitude greater than 5.4 has occurred in the central New Hebrides. Three events recorded at Olry, one event at Ratard and two events at Devil's Point and Malapoa had magnitudes (mb) between 5.0 and 5.4 and were located at (straight-line) distances from the hypocenters to the stations of between 30 and 65 km. In the entire arc, the largest event occurred on August 2, 1976 about 350 km south of the tiltmeter stations on Efate island. This event has a thrust-type focal mechanism, and a

magnitude (Ms) of 6.9. On September 4, 1977 a magnitude (Ms) 6.5 event occurred north of Santo island about 140 km from the nearest tiltmeter on Santo (Olry). These events are probably too far away from the tiltmeter stations to produce any strong effects.

Nevertheless, the data are examined for these events as well as the largest of the earthquakes which occurred within the network of observations. The data are plotted with three different time scales in Figures 8-10. The copies of the original records cover periods from minutes to nearly one day (Figure 8). Time-compressed plots of unfiltered data cover periods from several hours to about one month (Figure 9), and plots of filtered data which cover periods from about several days to nearly two years (Figure 10). The leveling data are also plotted with the long time base in Figures 11 and 15.

The tiltmeter data show two characteristic signals which can be clearly associated with the occurrence of earthquakes, or rather with the passage of seismic waves. The first is a simple offset in the trace which has been recorded for both local and more distant regional events. The second type of signal is an exponential recovery following a co-seismic offset. Most of the local events produce an exponentially decaying signal with a time constant appropriate to the overloading of the electronic low-pass filters in the system. However, the larger events sometimes produce a signal with a significantly longer time constant, of the order of 10 minutes, which cannot be explained as an electronic effect (see Figure 8). These signals are quite similar to the "tilt impulses" described by McHugh and Johnston (1977) for the central California tiltmeter network. The New Hebrides results are similar also in respect to the lack of consistency and regularity in the observations. This is illustrated, for example, in Figures 8c-e by the recordings of events by the Devil's Point and Malapoa tiltmeters. These stations are located only 11 km apart and 55 to 70 km from the sources. A step is recorded by Devil's Point but not the Malapoa tiltmeter in one case, but in another the reverse is true for an "impulse". These data support the conclusion that the signals are effects of the passage of the large amplitude seismic waves at or near the tiltmeter rather than effects near the source.

Rapid changes in drift rate, seen as corners or kinks in the tilt-meter plots, sometimes occur near the times of local events. The most remarkable case is recorded at Ratard for the large earthquake of September 4, 1977 located 217 km north of the station (see Figure 10b). The coincidence of the change in drift rate and the earthquake is quite close. However, the Olry tiltmeter, located about 77 km closer to event, shows no similar change in drift rate (see Figure 10a). Changes in drift rate can be seen at Ratard for the earthquakes of December 6, 1976 and February 5, 1977 (Figure 9a), but are not evident for local events recorded by Olry (Figures 9b-c). Changes in drift rate are also recorded at Malapoa and Devil's Point. Both stations record a change in the same sense on the ENE components near the time of the November 9, 1976 event, although the change is small and the timing resolution poor (see Figure 9d). A remarkable change in drift rate on the ENE component of Devil's Point begins about one day after the October 10, 1976 event (see Figure 10e). This change is correllatable with much smaller but

resolvable changes on the SSE component of Devil's Point as well as on the ENE component of Malapoa (see Figure 10d). In general, the leveling data do not support the large drift rates seen on the Ratard and Devil's Point tiltmeter records. This evidence, in addition to the lack of correlation between Olry and Ratard for the September 4 event, suggest that the changes in drift rate may again be site or instrumental effects of the large amplitude seismic waves reaching the stations.

Further examination of the records reveals no other signals which can be clearly associated with the earthquakes. The bay-like signals recorded at Ratard that appear to be associated with the earthquakes of December 1976 and February 1977 (see Figure 9a) are probably associated with rainfall. At that time the nearest rain gauge operated 17 km away. However, similar signals have been observed since then which are clearly related to local rainfall as recorded at the site. In general, the search for effects related to the earthquakes has demonstrated to us the absolute necessity for having rainfall recorded continuously at the station along with the tilt.

TILT RECORDED BY RELEVELING: A REAL SIGNAL AT RATARD?

In Figure 13 the releveling results are shown in terms of changes of relative elevations between two benchmarks as a function of time. The tilt change is obtained by dividing the elevation change by the length of the line. Thus each line measures the component of tilt in the direction of the line, and the array can be thought of as a multi-component tiltmeter. This method of presentation remains close to the original data and also yields a plot directly comparable to a tiltmeter recording. Coherence of the "records" of two independent but nearly parallel lines is a good test that a real tilt is being observed. In Figure 13 the lines are grouped accordingly.

The Devil's Point array shows relative stability, with a suggestion of small drift in the sense of a tilt downwards to the WNW or towards the trench. These results, if not merely errors of measurement, indicate a rate of about one microradian per year. The drift appears on both the lines PD6-PD1 and PD4-PD5. As mentioned above, the leveling results do not substantiate the large excursions exhibited by the tiltmeter.

The Ratard results indicate what appears to be a real tilt signal which is coherent over the dimensions of the array. The signal is marginal in the sense that it is represented by a single releveling. This tilt occurs between the August 1976 and April 1977 relevelings and is approximately recovered in the next interval terminated by the October 1977 releveling. The relationship of the measurements along individual lines to the overall tilt is shown in a simple graphical form in Figure 14.

The dashed lines in Figure 14 give an approximate eyeball fit to the data. In addition, a least squares procedure was used to calculate the tilt. In this calculation the tilt is taken as the slope of a plane

which best fits the data on changes in the relative elevations of benchmarks. In double-run levelings of four benchmarks, for example, six lines can be measured and yield 12 data on changes in relative elevations of the six pairs of benchmarks.

For the Ratard array the least squares solutions yield tilt changes with magnitudes of 0.8, 3.5, 3.5 and 0.4 microradians, respectively, for the four successive intervals covered by the relevelings during the period 1975-1977. The same analysis applied to the results from the Devil's Point array yields magnitudes of tilt all less than 1.5 microradians for all successive intervals. In the case of the October, 1977 to April, 1978 interval, at Ratard, where all 6 lines were measured in both levelings, the 12 data yield an estimate of 3.5 $\pm$ 2.9 microradians, where the plus/minus value is the 95% confidence interval. This estimate, in addition to the consistently low magnitudes of tilt for the first and last interval at Ratard aand for all the intervals at Devil's Point, suggest that the tilt signals illustrated in Figures 13 and 14 represent real tilt signals which are coherent over the dimensions of the Ratard array.

The tilt is 3.5 microradians downward toward the southeast during the first interval, July 1976-April 1977, and then is approximately recovered during the following interval, April 1977-October 1977, with a tilt of 3.5 microradians downward toward the NNW. The tilt directions are approximately parallel to the strike of the island arc and subduction zone.

The tilt determined along one of the lines approximately parallel to the estimated tilt excursion is plotted together with the appropriate tiltmeter component in Figure 15. The average trend of the SSE component of Ratard is approximately linear during two periods: (1) December 1976 to the rainfall signal of April 1977, and (2) May 1977 to the middle of August 1977. If these two trends are extrapolated throughout the period covered by the three levelings in 1976 and 1977, i.e. if the rapid drifts prior to December 1976 and after August 1977 and the rainfall signal of April 1977 are eliminated, then the agreement between the leveling and the tiltmeter data is excellent. This is encouraging, but the tiltmeter data alone would be considerably uncertain.

The pattern of seismicity in the region around the Ratard leveling array reveals an interesting feature possibly related to the tilt event. The seismicity in the New Hebrides is in general characterized by a strong degree of clustering in time and space. The pattern of occurrence near the Ratard array during the three year period is shown in Figure 15. A cluster occurs first in Malekula. After this the two relatively isolated events located close to the Ratard array occur in December 1976 and February 1977. Then in the Spring and Summer of 1977 a cluster occurs in northern Santo. Finally, the large event of September 4, 1977 occurs north of Santo. The tilt excursion inferred from the releveling data could thus be related to the northward progression of seismicity. One can speculate that a propagating stress pulse, perhaps of the type discussed by Elsasser (1969) and others, passed northward along the strike of the arc and produced the tilt

excursion.

The small arrays at Ratard apparently do not have the resolution to detect the signal. The closure errors of 0.1-0.2 mm for a given leveling of the small arrays imply a tilt error of 1.4-2.8 microradians. The elevation changes between successive levelings are somewhat larger than this, as discussed in a previous section, (see Figure 7a), and yield tilt changes with magnitudes up to 5-6 microradians. However, the tilts do not agree with those determined for the larger array either in magnitude or direction. Although these results could be interpreted as an indication of small wavelength irregularities in the tilt field, it is more likely that larger tilts determined by the small arrays arise from errors in measurements or small movements of the benchmarks. All that is required to produce tilts of observed amounts is an additional few tenths of a millimeter above that indicated by the closures.

The data indicate that the resolution of the large arrays approaches 1-2 microradians, while that of the small triangular arrays of Ratard and the one at Devil's Point is probably not better than about 5 microradians. The small four-point array around the Devil's Point tiltmeter, however, seems quite stable and has a resolution approaching that of the larger arrays.

CONCLUSIONS

The bubble-level borehole tiltmeters are relatively noisy instruments which appear best adapted to monitor in the short period part of the spectrum of transient deformations. As illustrated by the original records, the noise levels are small in the range of periods between minutes and hours, and the sensitivity in this range can approach 0.1 microradians. Rainfall signals are an important source of noise at periods of hours to weeks, but the rainfall transients are fairly easy to identify. However, rainfall must be monitored at the site. At periods of days to weeks, the sensitivity is probably of the order of a microradian at the better stations where rainfall effects are not too serious and are carefully monitored. At longer periods the sensitivity decreases to probably the order of 10 microradians although certain components of certain stations may have significantly better sensitivity. In general, as period increases the performance of the instrument is degraded by long period effects of rainfall, instrumental noise, and possibly other effects in the siting (which are poorly understood), in addition to the problems of maintaining an accurate baseline for the complex electronic recording system over a long period of time. In contrast, with the leveling technique a sensitivity of the order of a microradian is preserved at long periods. In retrospect, the leveling system has provided the best data on tilt so far in the New Hebrides.

Although the leveling method could be applied at weekly intervals, for example, practical considerations limit it to longer intervals. More frequent levelings will be made temporarily after a large earthquake. Nevertheless, there is a gap in the measurements provided by the tiltmeters and the leveling. The gap includes approximately the range

of periods between days and months in which the tiltmeter records show increasing noise but which is too short to be easily covered by the leveling method. We think that the best way to cover this gap is with a long-baseline liquid level tiltmeter. This type of instrument is simple and in our opinion has the best chance to achieve long term stability and sensitivity. We are now installing a system of about 100 meters length near the Devil's Point site. The terrain is flat enough to use a half filled, buried tube (Beavan and Bilham, 1977), so that thermal problems will be minimized. A simple sensing technique will be used to obtain a sensitivity of 0.1 microradians.

Acknowledgements. This program has benefited significantly from the interests and efforts of surveyors of the Service Topographique, in particular from the efforts of the Chef de Service, M. Gely and Mr. Peter Horla. Important contributions to the program were made by J. Laurent (Direction des Ressources Minerales, New Hebrides), C. Stephens, J. York, M. Barazangi, R. Cardwell (all at Cornell), B. Pontoise, G. Reichenfeld, and R. Decourt (all at ORSTOM, Noumea).

REFERENCES

Beaven, J. and R. Bilham, 1977, Thermally induced errors in fluid tube tiltmeters, J. Geophys. Res., 82, 5699.

Elsasser, W., 1969, Convection and stress propagation in the upper mantle, in The Application of Modern Physics to the Earth and Planetary Interiors, S.K. Runcorn, ed., John Wiley, New York, 223.

Marthelot, Jean-Michel, E. Coudert, B.L. Isacks, and J. Dubois, 1979, Local tidal loading tilts in the New Hebrides island arc, (in preparation)

McHugh, S. and M. Johnston, 1977, An analysis of coseismic tilt changes from and array in central California, J. Geophys. Res., 82, 5692.

FIGURE CAPTIONS

Figure 1. Presently operating network in the New Hebrides. Most of the seismograph stations shown were parts of temporary networks operated for periods of 1-2 months. The heavy line with filled triangles shows the trace of the zone of thrust fault contact between the subducted oceanic plate to the west and the island arc, as inferred from seismic studies.

Figure 2. Vertical cross section through New Hebrides Subduction Zone showing locations of tiltmeter stations. The dotted area shows the most active zone of thrust type earthquakes along the convergent plate boundary.

Figure 3. Tiltmeter installation.

Figure 4. Tiltmeter recording system in use now. The digital recorder is still under development. The original system included only Rustrak B.

Figure 5. Tiltmeter records obtained and analyzed for this paper. The stations have continued to produce records through to the present. The gaps in records are due mainly to recording problems, primarily paper jams or records running out.

Figure 6. Map view of Devil's Point and Ratard bench mark arrays. The elevation variations within the arrays vary from tens of centimeters to about 5 meters. See Figure 1 for the locations of these arrays in the New Hebrides. Both are located on young coral terraces.

Figure 7a. Histograms of changes in relative elevations between pairs of bench marks within the small arrays in the Ratard and Devil's Point arrays. These are changes between successive relevelings.

Figure 7b. Histogram of closure errors expressed in terms of microradians of tilt. These data are for the long lines within the Ratard and Devil's Point arrays.

Figure 8a. Ratard tiltmeter records for two earthquakes. The distances given are straight line distances between hypocenter and station. The vertical lines indicate half hour intervals. The vertical scale for this and following records is close to about 2 Rustrak units/microradian or 25 microradians full scale. Top: Dec. 6, 1976, depth=29 km, distance=38 km, mb=4.8. Bottom: Feb. 5, 1977, depth=39 km, distance=34 km, mb=5.2, Ms=4.6. In this figure, the solid trace is the ENE component (down on the record equals tilt downward to the ENE) and the dashed component is the SSE component (down on the record equals tilt downward to the SSE).

Figure 8b. Olry records of three earthquakes. Top: May 21, 1977, depth=35 km, distance=46 km, mb=5.2, Ms=4.6. Middle: June 18, 1977, depth=37 km, distance=51 km, mb=5.4, Ms=4.8. Bottom: Aug. 25, 1977, depth=35 km, distance=40 km, mb=5.1. The signal about 7 to 4 hours before the June 18 event is seen at other times without earthquakes and is probably an effect of rainfall. In Figures 8b-8e, the solid trace is the ENE component (up on the record equals tilt downwards to the ENE) and the dashed trace is the SSE component (up on the record equals tilt downward to the SSE). This applies to all records except Ratard which has the opposite polarity.

Figure 8c. Devils's Point records for four earthquakes. The same earthquakes as recorded by Malapoa are shown in Figure 8d. Top: Oct. 10, 1976, depth=22 km, distance=63 km, mb=4.8. Upper Middle: Nov. 9, 1976, depth=32 km, distance=55 km, mb=5.0. Lower Middle: Dec. 14, 1976, depth=68 km, distance=68 km, mb=4.9. Bottom: May 16, 1977, depth=30 km, distance=54 km, mb=5.1, Ms=5.3.

Figure 8d. Malapoa records for the same four earthquakes as shown for Devil's Point in Figure 8c. Note the large exponentially decaying signal following the Dec. 14 event. Top: Oct. 10, 1976, depth=22 km, distance=70 km, mb=4.8. Upper Middle: Nov. 9, 1976, depth=32 km, distance=55 km, mb=5.0. Lower Middle: Dec. 14, 1976, depth=68 km, distance=70 km, mb=4.9. Bottom: May 16, 1977, depth=30 km, distance=61 km, mb=5.1, Ms=5.3.

Figure 8e. Large regional earthquakes (both shallow depth) as recorded by the nearest stations. The upper two records at Devil's Point and Malapoa show the Aug. 2, 1976 (Ms=7.0) event located south of Efate Island and the lower two for Olry and Ratard show the Sept. 4, 1977 (mb=6.0, Ms=6.5) event located north of Santo Island. Top: Devil's Point, Aug. 2, 1976, distance=350 km. Upper Middle: Malapoa, Aug. 2, 1976, distance=350 km. Lower Middle: Olry, Sept. 4, 1976, distance=150 km. Bottom: Ratard, Sept. 4, 1976, distance=215 km.

Figure 9a. In this and in Figures 9b through 9e the tiltmeter data are unfiltered and plotted on the same time scale. The plots are made from hourly digitizations. The rainfall data, given in daily totals, are taken from a rain gauge located 17 km from the Ratard tiltmeter. In Figures 9 and 10 the distance is the straight line distance between the hypocenter and the station.

Figure 9b. Olry records for earthquakes in the Spring of 1977. The large offsets occurring at the end of March in the upper plot are the effects of a magnitude (mb) 5.7 intermediate-depth earthquake (depth=109 km) located northeast of Santo. The rainfall data are obtained from a Catholic Mission located about 3 km from the station.

Figure 9c. Ratard and Olry records for the large Sept. 4, 1977 event located north of Santo (see also Figure 8e). Again rainfall data are taken from a gauge located 17 km from the tiltmeter. The large offsets associated with the Sept. 4 event are removed but the amount of offset is noted in the figure.

Figure 9d. Devil's Point and Malapoa records for an event in Nov. 1976. A small rainfall transient is illustrated on the left side of the Malapoa records. The rain data for both plots are taken from the Port Vila rain gauge located about 2 km from Malapoa and about 13 km from Devil's Point.

Figure 9e. Devil's Point and Malapoa records for the May 16, 1977 event. The downturning of the Malapoa traces following the earthquake is believed to be due to failure of the lead-acid storage batteries being used at the station prior to the Summer of 1977. The rainfall data are from the same source as described for Figure 9d.

Figure 10a. This and Figures 10b-10f are all plotted on the same time scale. The data have been filtered by taking a running 12 hour average of the hourly digitizations of the Rustrak records. Note the step-like transients associated with rainfall in January and June of 1977. The baseline was preserved through the gap in recording in Oct.-Dec. 1977. Rainfall data are taken from a gauge at a distance of about 3 km from the station. The data are given as daily totals in mm according to the scale on the lower left hand side of the figure.

Figure 10b. Filtered data for the Ratard station. Rainfall data are taken from a gauge located 17 km from the station, and are given as daily totals in mm, as indicated by the scale on the lower left hand side of the figure. No rain data are available for March and April 1978.

Figure 10c. Filtered data for Southwest Bay. The rainfall data are taken from the nearest raingauge located at Lamap, a distance of 40 km on the other side of the island. Hence the correlations are very uncertain. The step-like transient in June 1977 associated with the heavy rainfall at Lamap is confirmed by later rainfall data recorded at the Southwest Bay site.

Figure 10d. Filtered data for Malapoa. The rain data are taken from the raingauge in Port Vila located 2 km away from the station.

Figure 10e. Filtered data from Devil's Point. The rainfall data are taken from Port Vila, 13 km from the station. The baseline was not lost through the gap in records during February-April 1977. The dotted segment there is shown to identify the traces on the left of the gap.

Figure 10f. Filtered data from the station at Tukutuk. The station commenced operation in late September 1977. The large oscillations on the SSE component accompany a large diurnal signal of unknown origin. Rainfall data from Port Vila.

Figure 11. Comparison of leveling data at Devil's Point and tiltmeter data. See Figure 6 for locations of observations. The leveling results are shown with the same scale of tilt as for the tiltmeters. See Figure 13.

Figure 12. Earthquakes located by the PDE for the period August 1976 - December 1977. The tiltmeter stations are shown by triangles and are identified in Figure 1. Only shallow earthquakes are shown.

Figure 13. Leveling results summarized for each pair of bench marks in the Santo and Efate arrays. The locations of the bench marks are shown in Figure 6. Circles are unadjusted values (average of foreward and backward runs) and triangles are adjusted values.

Figure 14. Tilt change along lines between two bench marks plotted as a function of azimuth of the line. The intervals over which the tilt change is computed are shown in the figure. The dashed line is the variation in tilt if the tilt is uniform and coherent over the array, and is a graphical fit to the data. The estimated tilt is 4 microradians along the azimuth of the maximum of the dashed line, or about southwest and northeast, respectively.

Figure 15. Comparison of leveling data and tiltmeter data for Ratard, as in Figure 11. See also Figures 6 and 13. The seismicity data is taken from the listing of the PDE for the period concerned, and the areas covered shown in the figure.

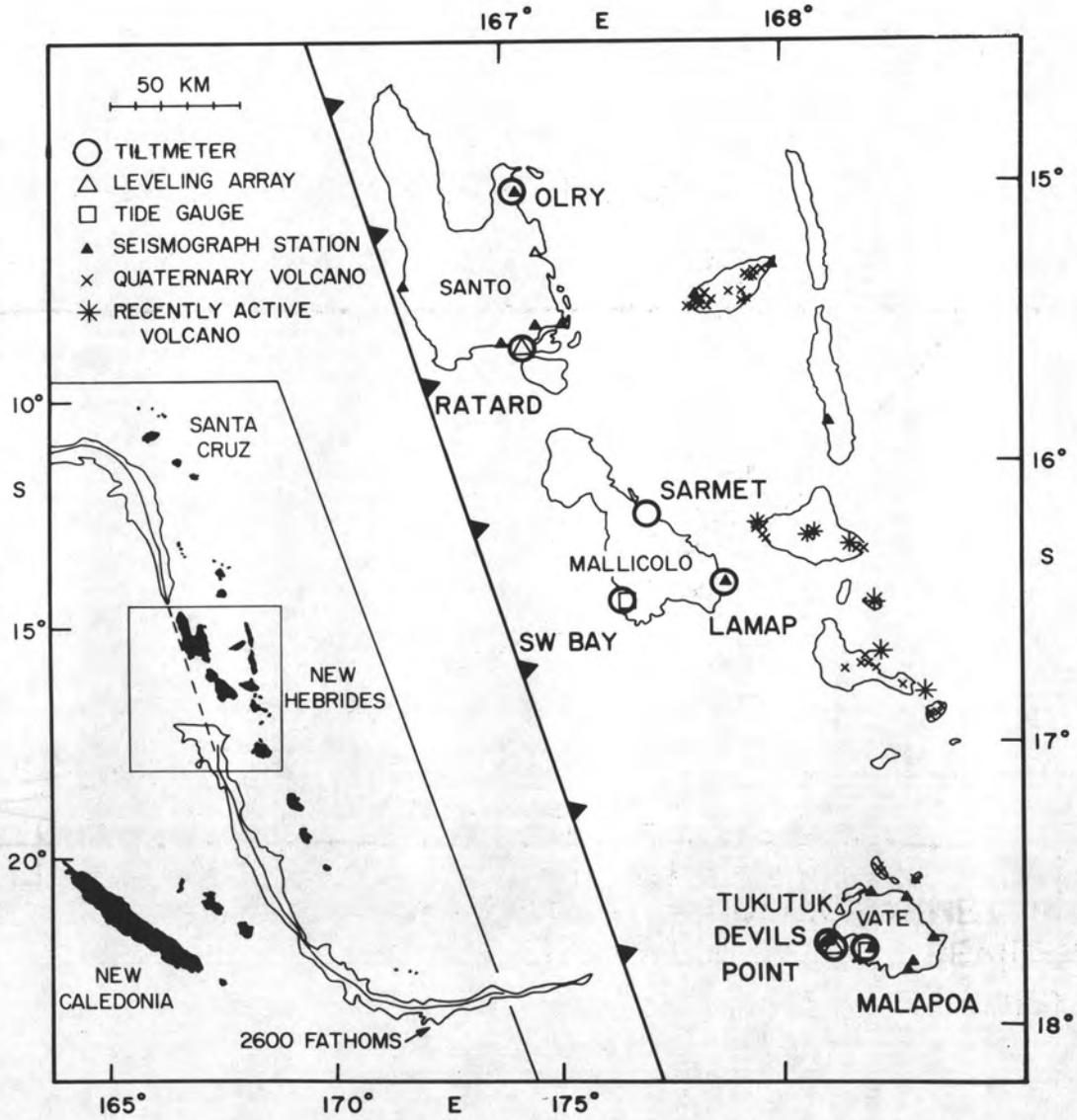
167° E
168°
50 KM
TILTMETER
LEVELING ARRAY
TIDE GAUGE
SEISMOGRAPH STATION
QUATERNARY VOLCANO
RECENTLY ACTIVE VOLCANO
OLRY
SANTO
RATARD
SARMET
MALLICOLO
LAMAP
SW BAY
SANTA CRUZ
NEW HEBRIDES
NEW CALEDONIA
2600 FATHOMS
TUKUTUK
VATE
DEVILS POINT
MALAPOA
10° S
15° S
20°
15°
16°
17°
18°
165°
170° E
175°

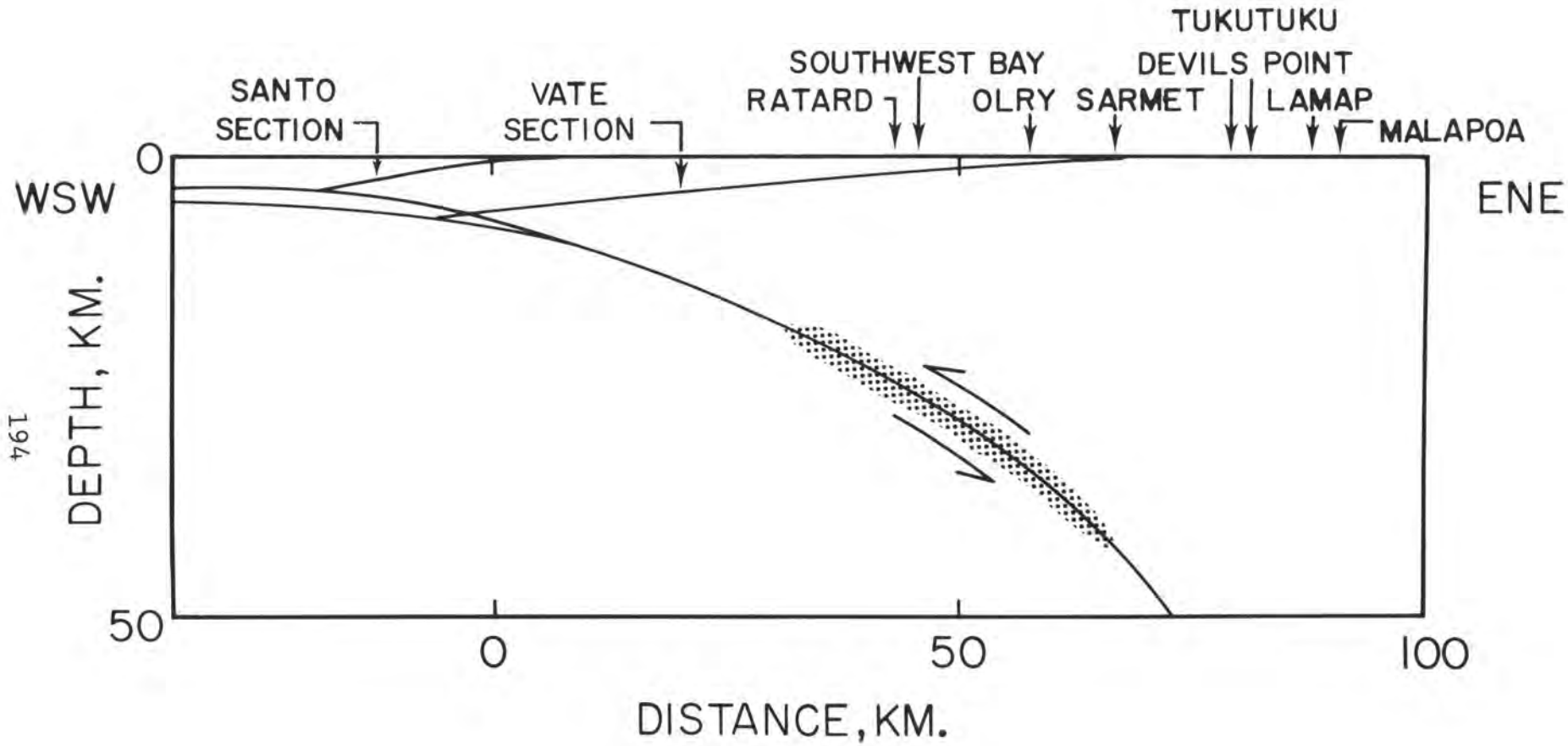
SANTO SECTION
VATE SECTION
RATARD
SOUTHWEST BAY
OLRY
SARMET
TUKUTUKU
DEVILS POINT
LAMAP
MALAPOA
WSW
ENE
0
50
DEPTH, KM.
0
50
100
DISTANCE, KM.

194

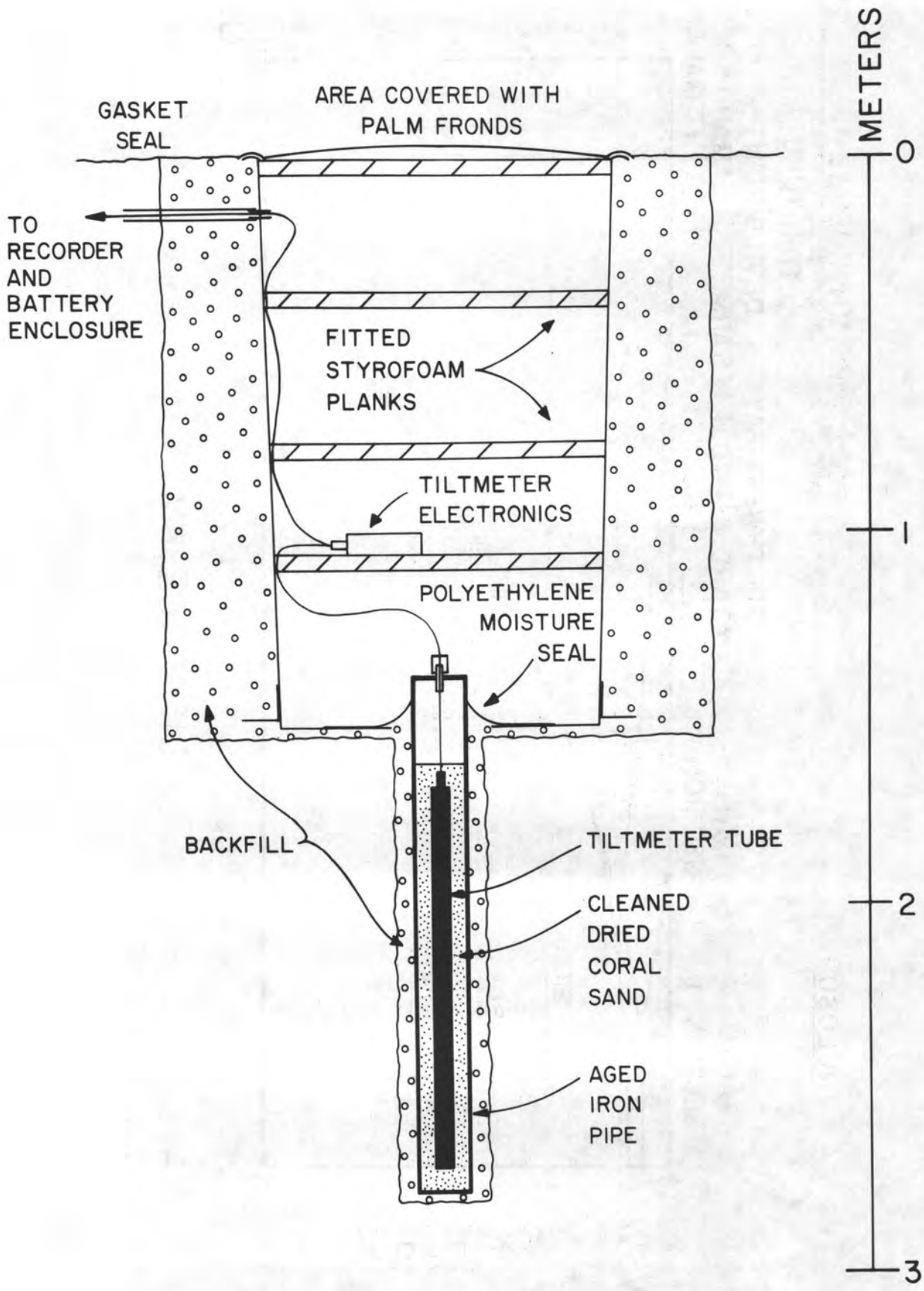
GASKET SEAL
AREA COVERED WITH PALM FRONDS
TO RECORDER AND BATTERY ENCLOSURE
FITTED STYROFOAM PLANKS
TILTMETER ELECTRONICS
POLYETHYLENE MOISTURE SEAL
BACKFILL
TILTMETER TUBE
CLEANED DRIED CORAL SAND
AGED IRON PIPE
METERS
0
1
2
3

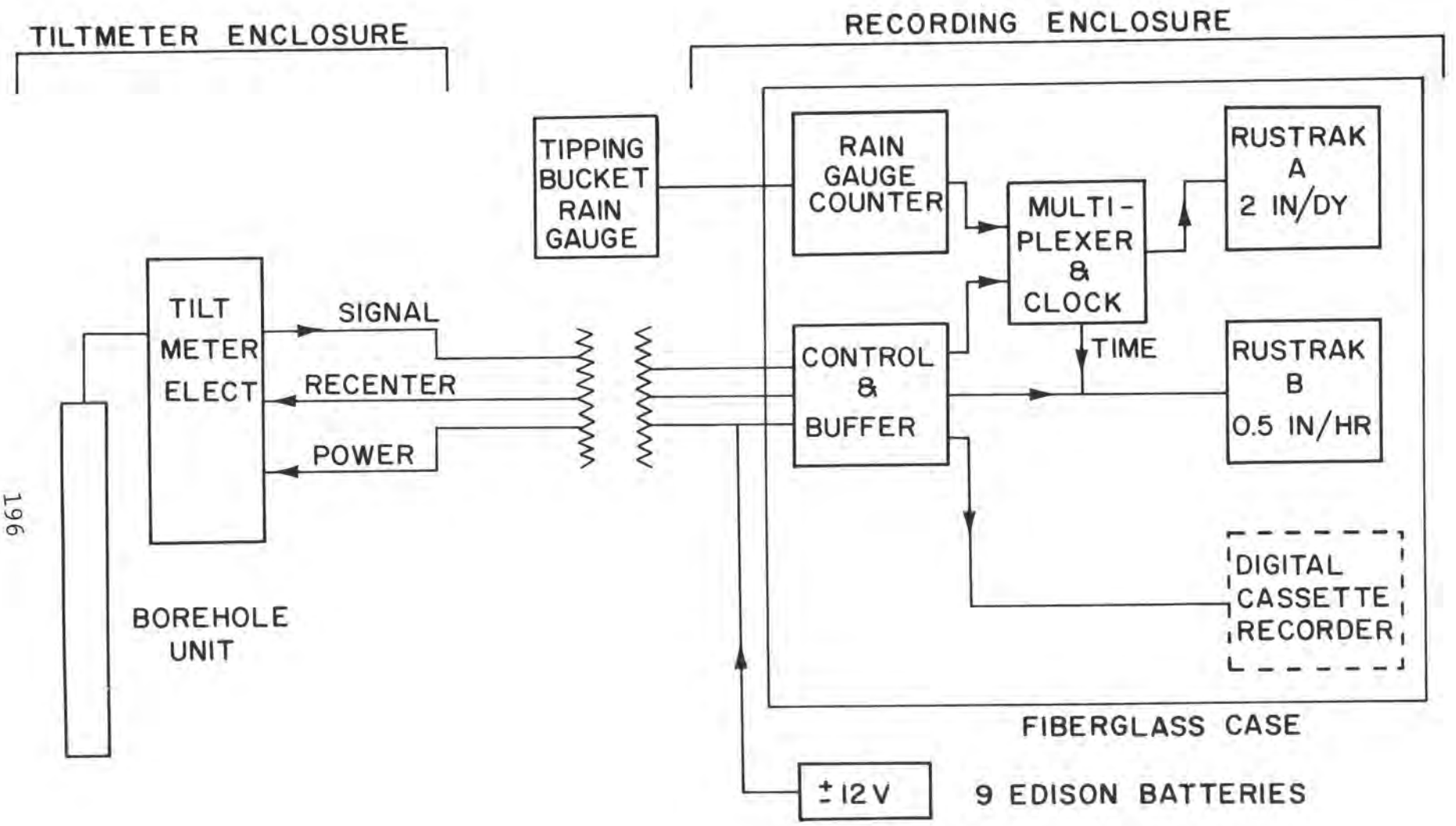
TILTMETER ENCLOSURE
RECORDING ENCLOSURE
TIPPING BUCKET RAIN GAUGE
RAIN GAUGE COUNTER
MULTI-PLEXER & CLOCK
RUSTRAK A 2 IN/DY
TILT METER ELECT
SIGNAL
RECENTER
POWER
CONTROL & BUFFER
TIME
RUSTRAK B 0.5 IN/HR
DIGITAL CASSETTE RECORDER
BOREHOLE UNIT
FIBERGLASS CASE
±12V
9 EDISON BATTERIES

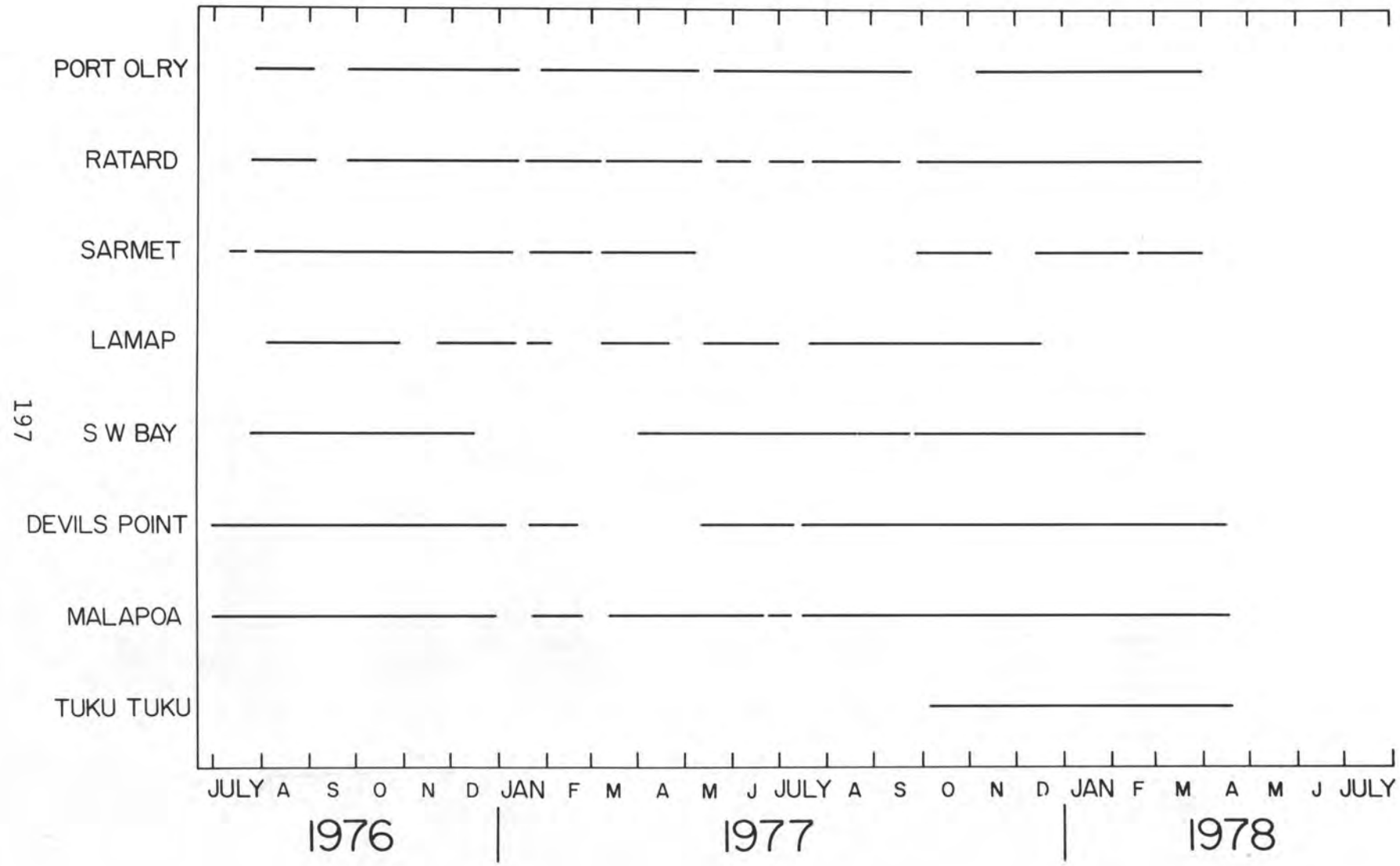
PORT OLRY
RATARD
SARMET
LAMAP
S W BAY
DEVILS POINT
MALAPOA
TUKU TUKU
JULY A S O N D JAN F M A M J JULY A S O N D JAN F M A M J JULY
1976
1977
1978

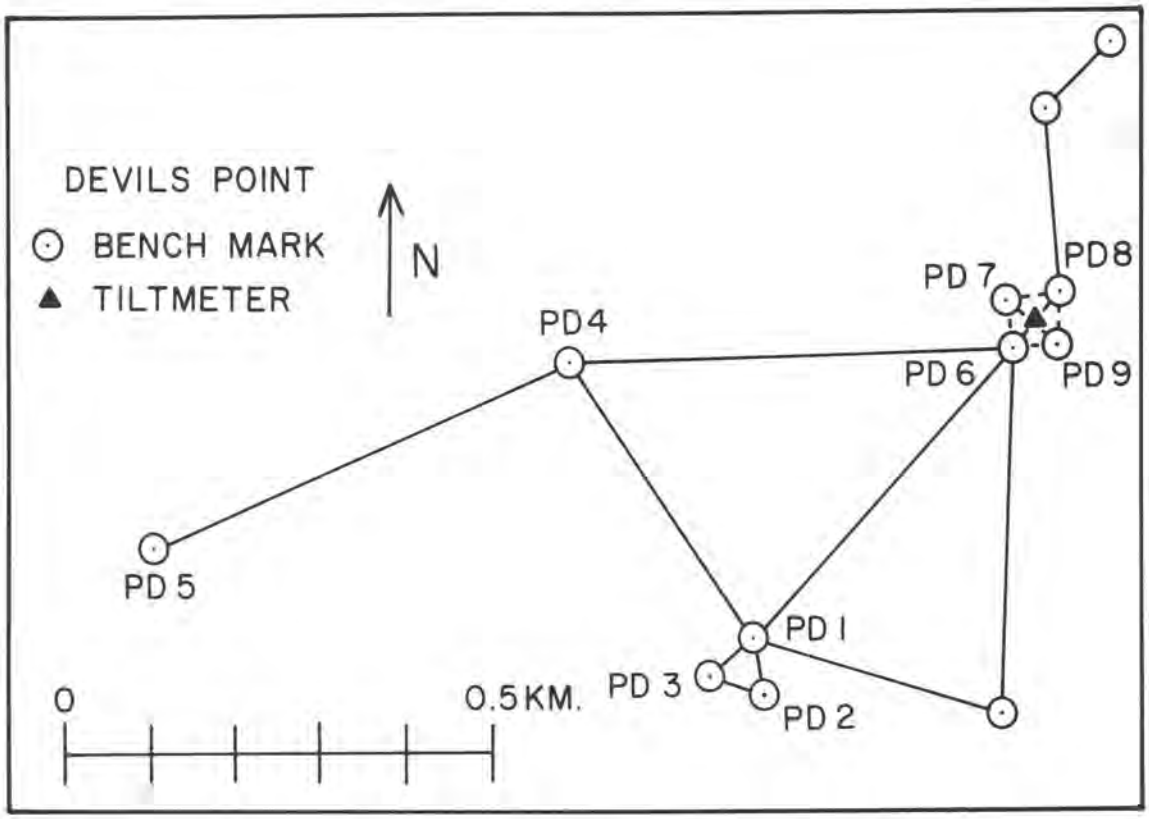
DEVILS POINT
BENCH MARK
TILTMETER
N
PD 7
PD8
PD4
PD 6
PD 9
PD 5
PD 1
PD 3
PD 2
0
0.5KM.

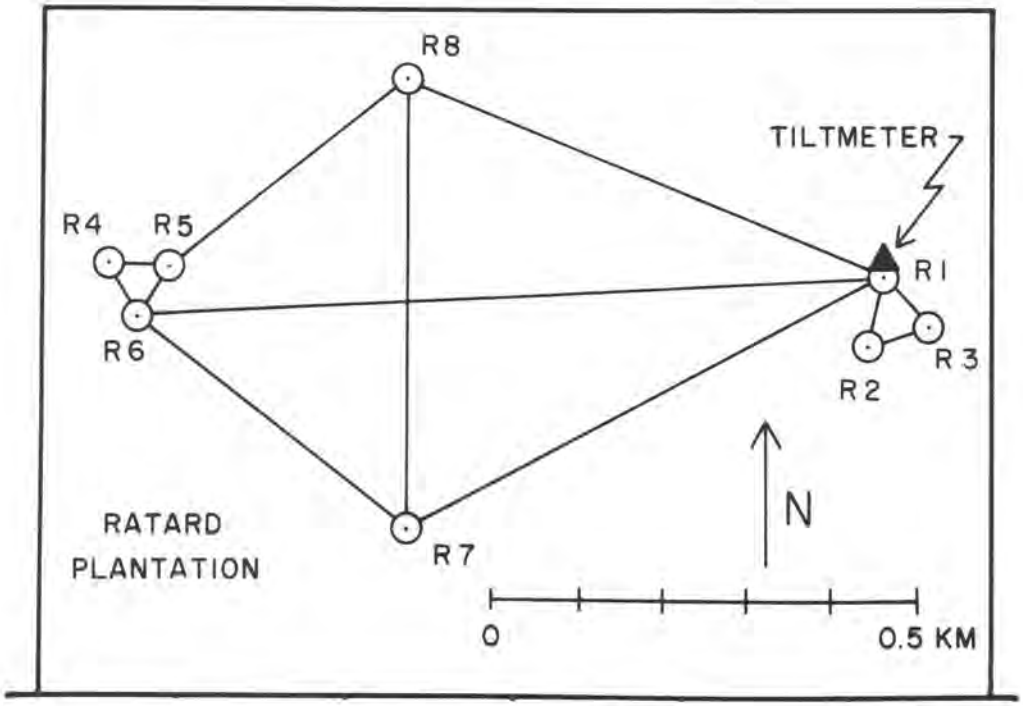
R8
TILTMETER
R4
R5
R1
R6
R2
R3
N
RATARD
PLANTATION
R7
0
0.5 KM

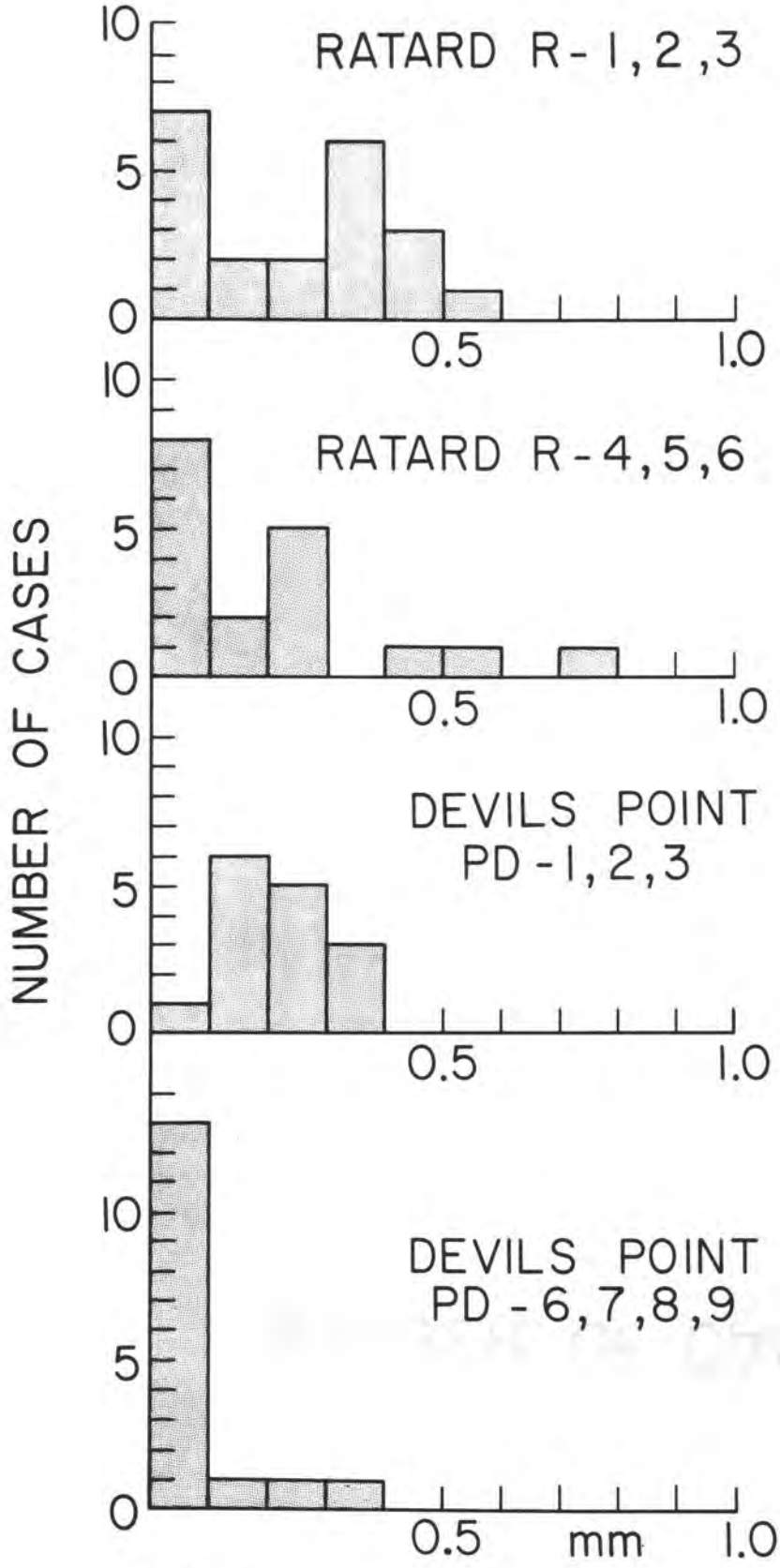
RATARD R-1,2,3
RATARD R-4,5,6
DEVILS POINT
PD-1,2,3
DEVILS POINT
PD-6,7,8,9
NUMBER OF CASES
0
5
10
0.5
1.0
mm
APPARENT CHANGE IN ELEVATION
BETWEEN PAIRS OF BENCHMARKS

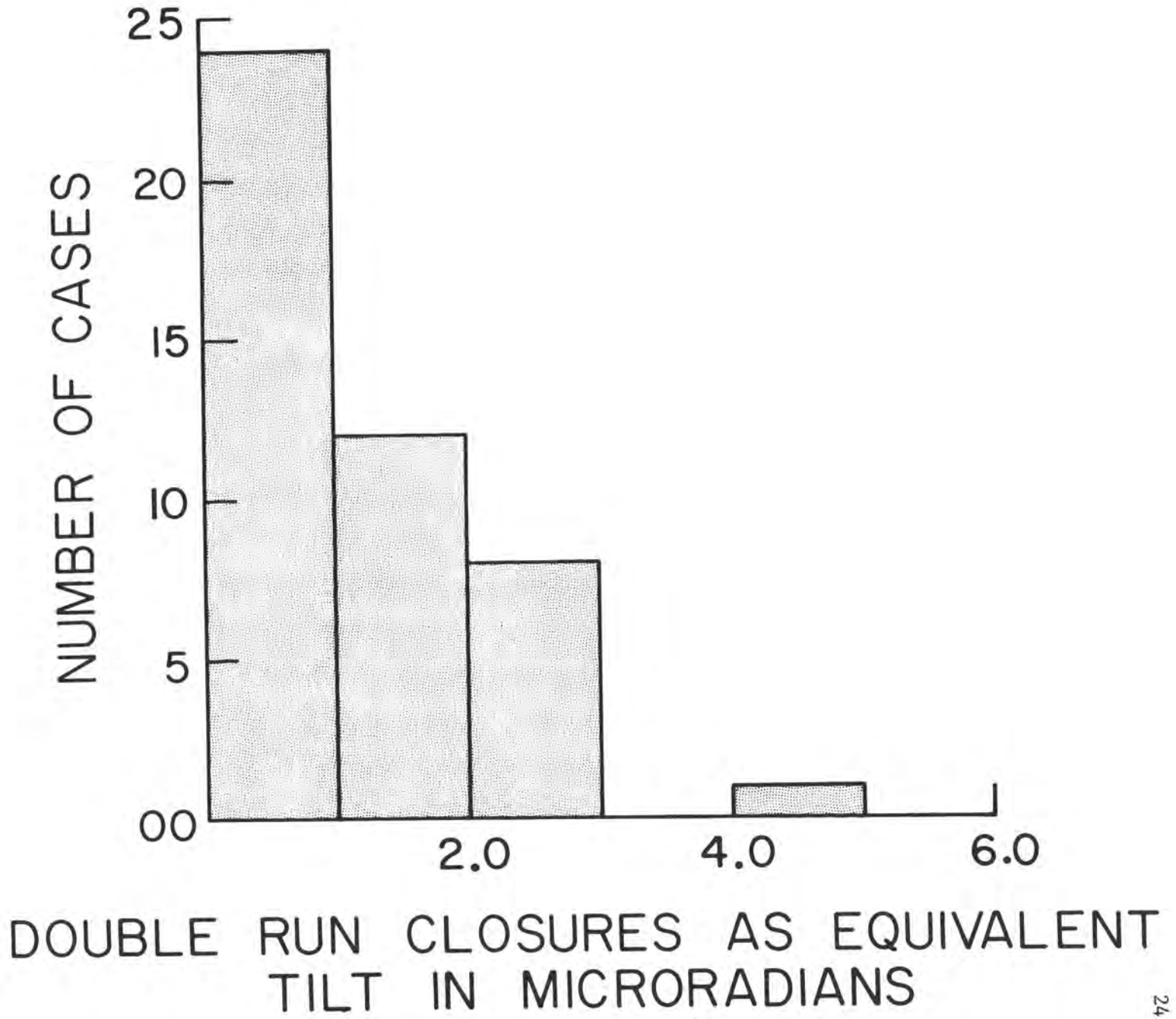
25
20
15
10
5
00
NUMBER OF CASES
2.0
4.0
6.0
DOUBLE RUN CLOSURES AS EQUIVALENT
TILT IN MICRORADIANS

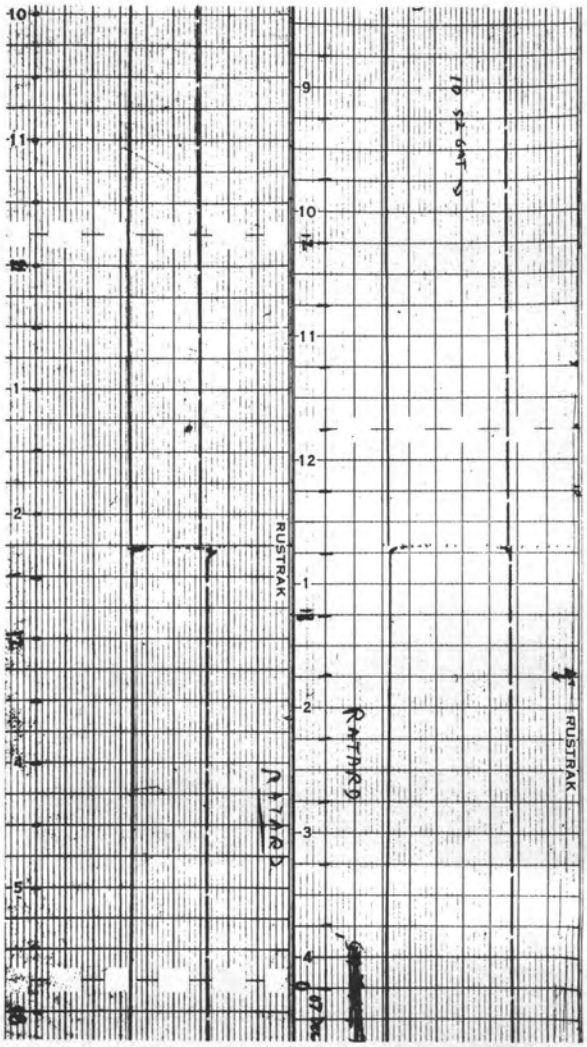
RUSTRAK
RUSTRAK

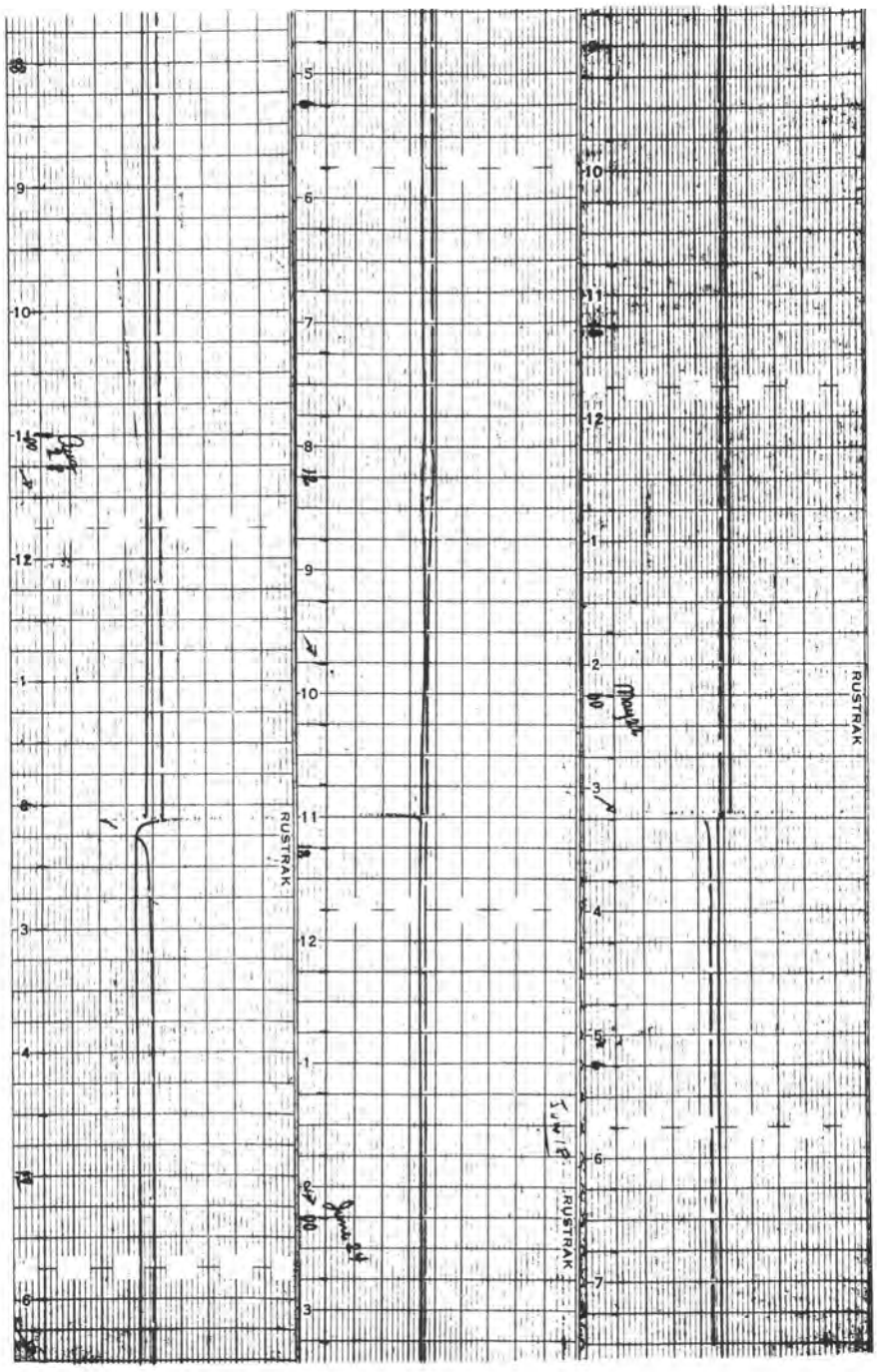
RUSTRAK
RUSTRAK
RUSTRAK

RUSTRAK
Nov 9
Oct 10

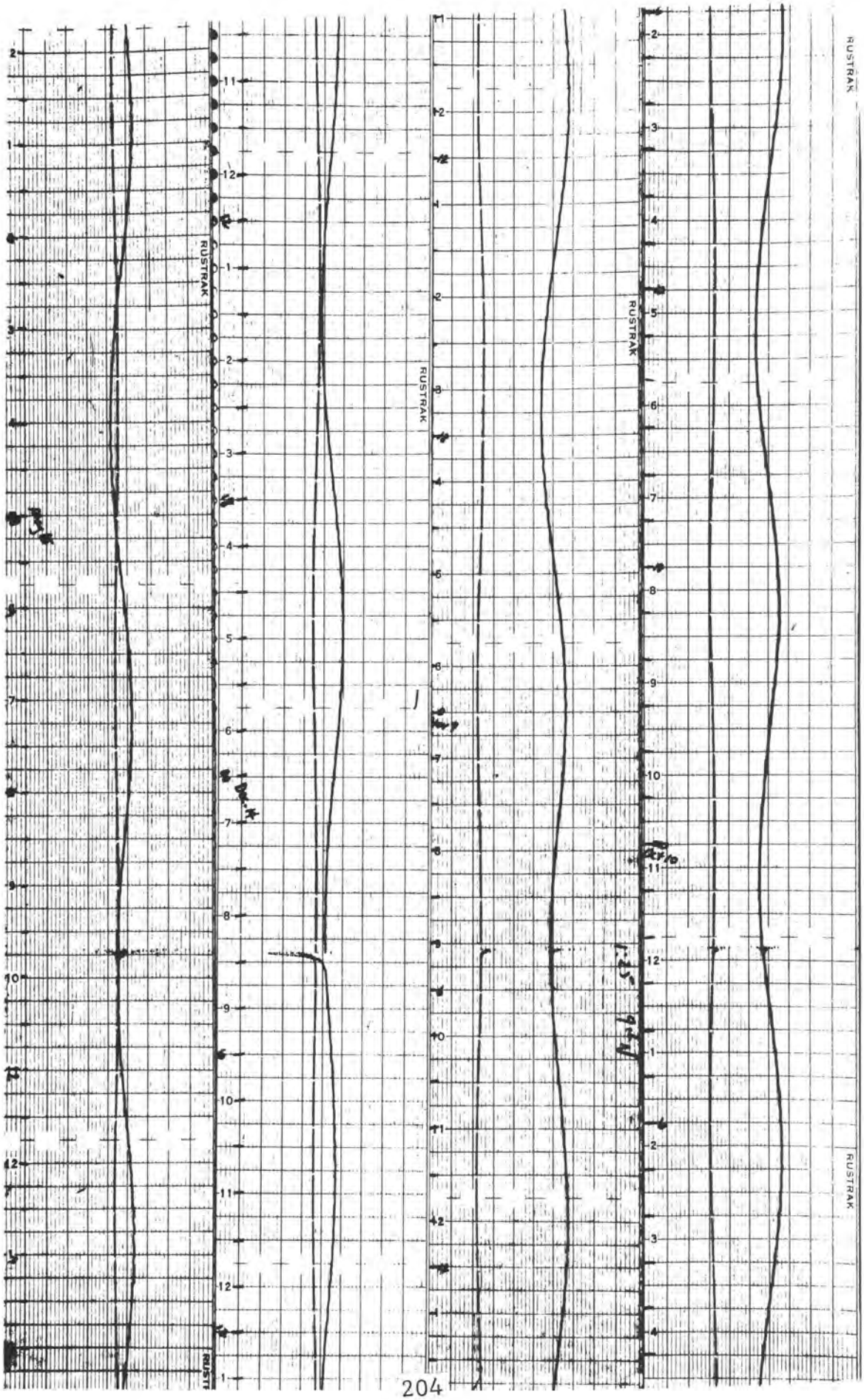
RUSTRAK
RUSTRAK
RUSTRAK
RUSTRAK

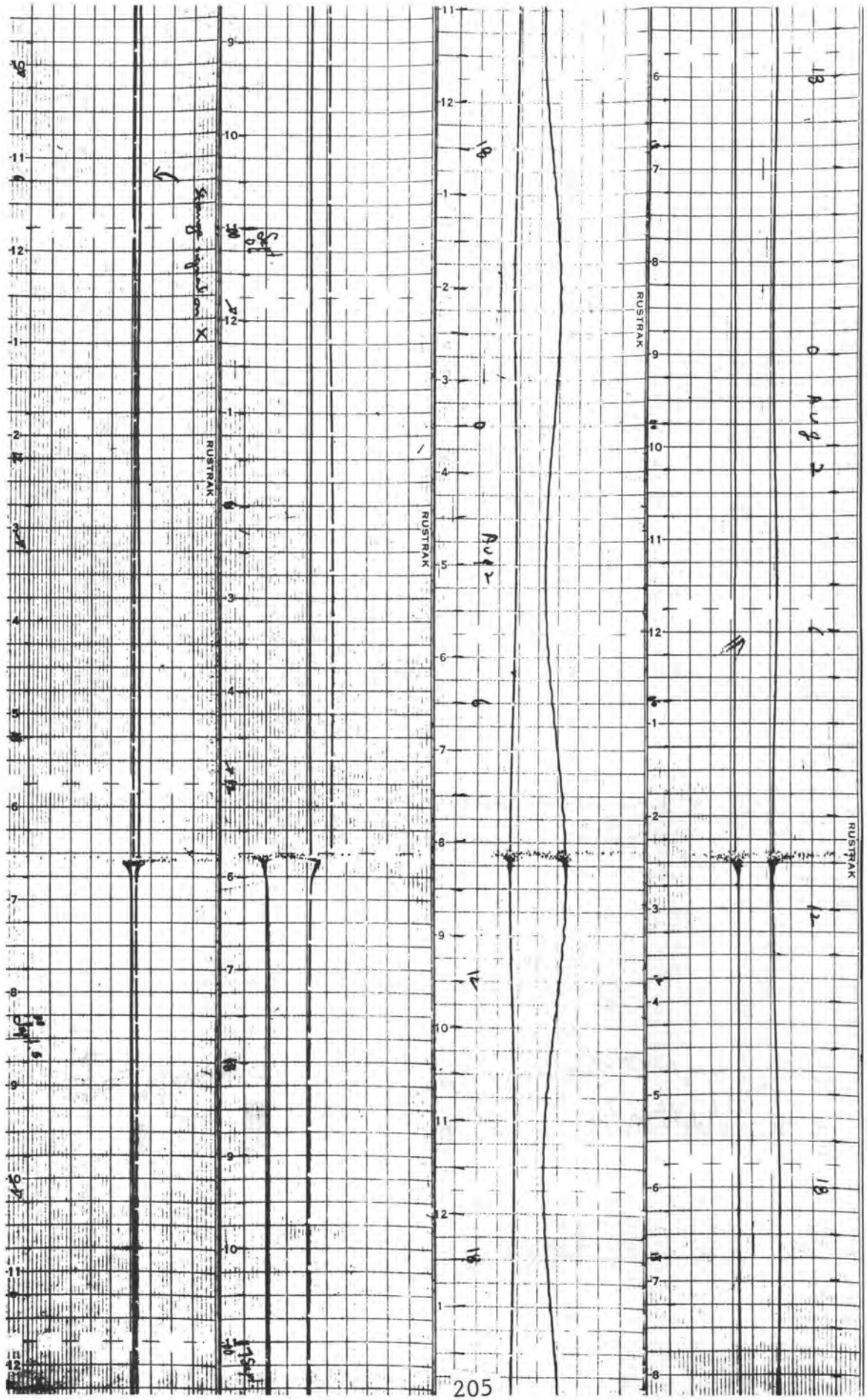
RUSTRAK
RUSTRAK
RUSTRAK

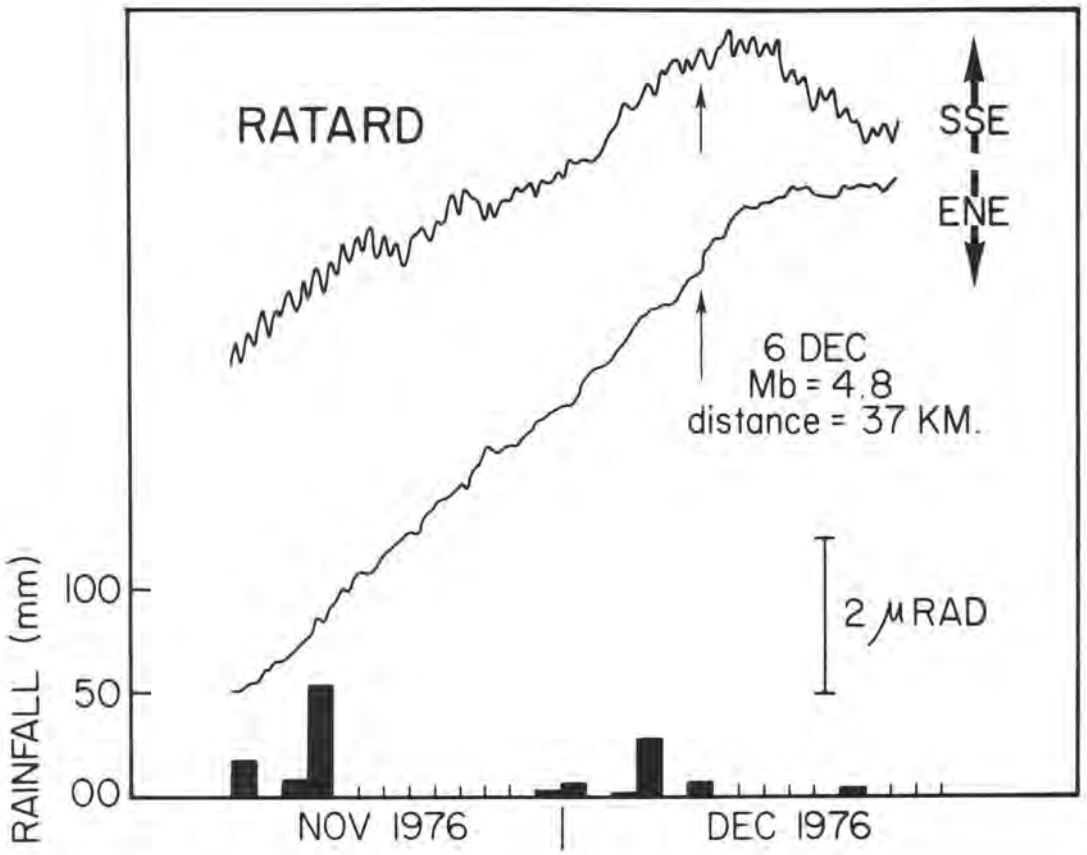
RATARD
SSE
ENE
6 DEC
Mb = 4.8
distance = 37 KM.
2 μ RAD
RAINFALL (mm)
100
50
00
NOV 1976
DEC 1976

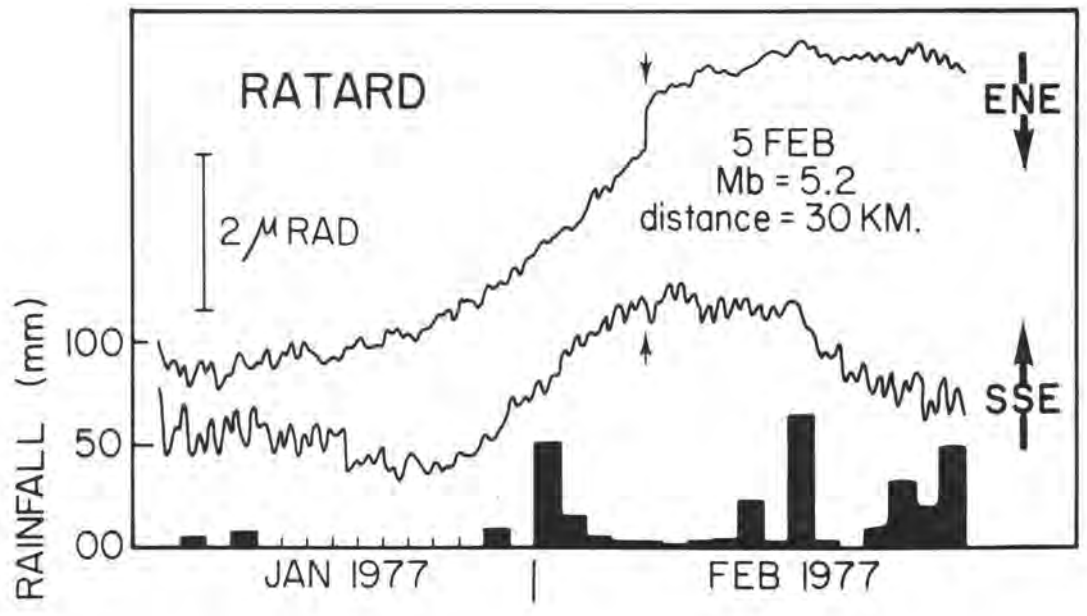
RATARD
ENE
5 FEB
Mb = 5.2
distance = 30 KM.
2 μ RAD
SSE
RAINFALL (mm)
100
50
00
JAN 1977
FEB 1977

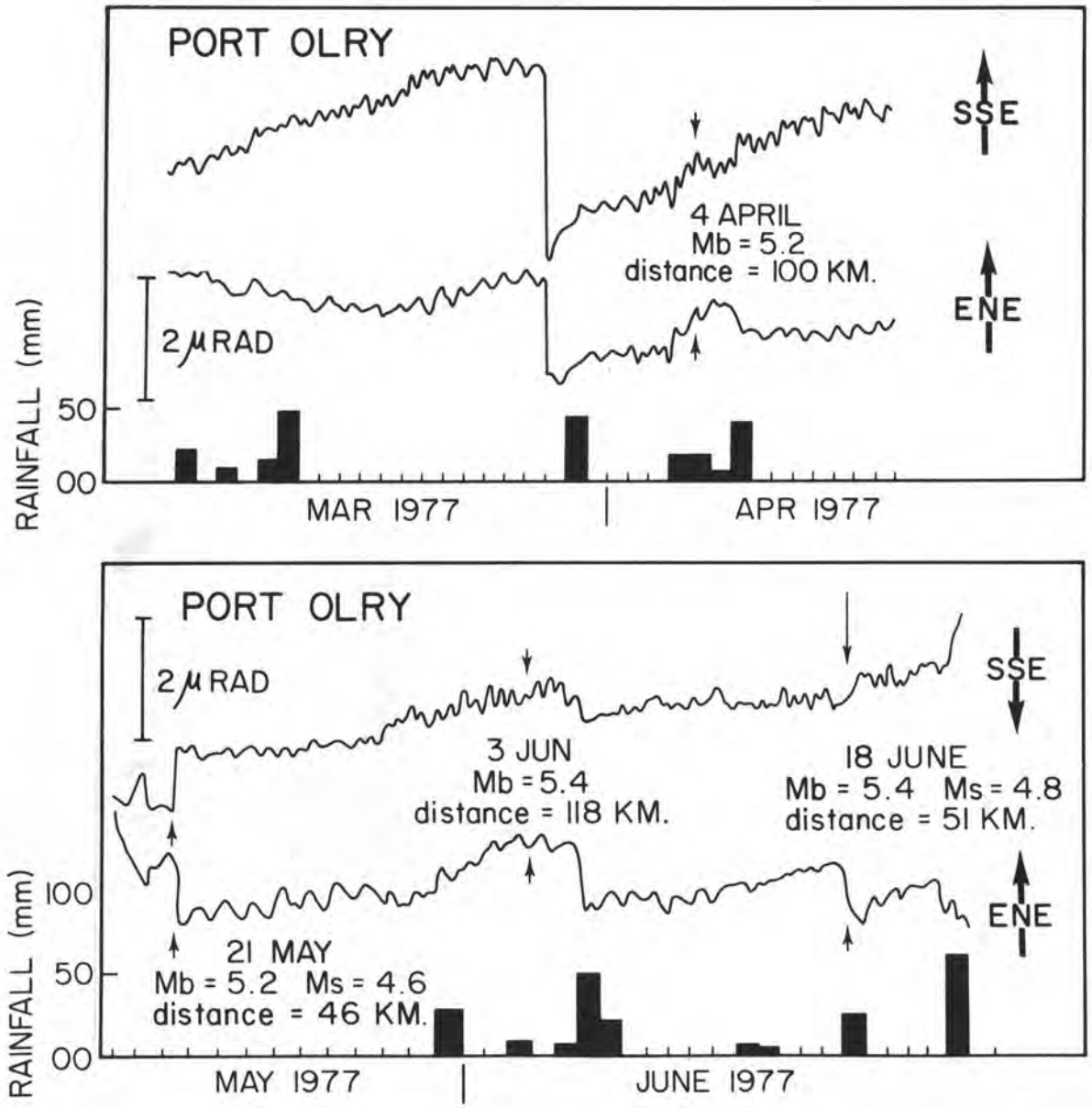
PORT OLRY
SSE
4 APRIL
Mb = 5.2
distance = 100 KM.
ENE
2 μ RAD
RAINFALL (mm)
50
00
MAR 1977
APR 1977
PORT OLRY
2 μ RAD
SSE
3 JUN
Mb = 5.4
distance = 118 KM.
18 JUNE
Mb = 5.4 Ms = 4.8
distance = 51 KM.
ENE
21 MAY
Mb = 5.2 Ms = 4.6
distance = 46 KM.
RAINFALL (mm)
100
50
00
MAY 1977
JUNE 1977

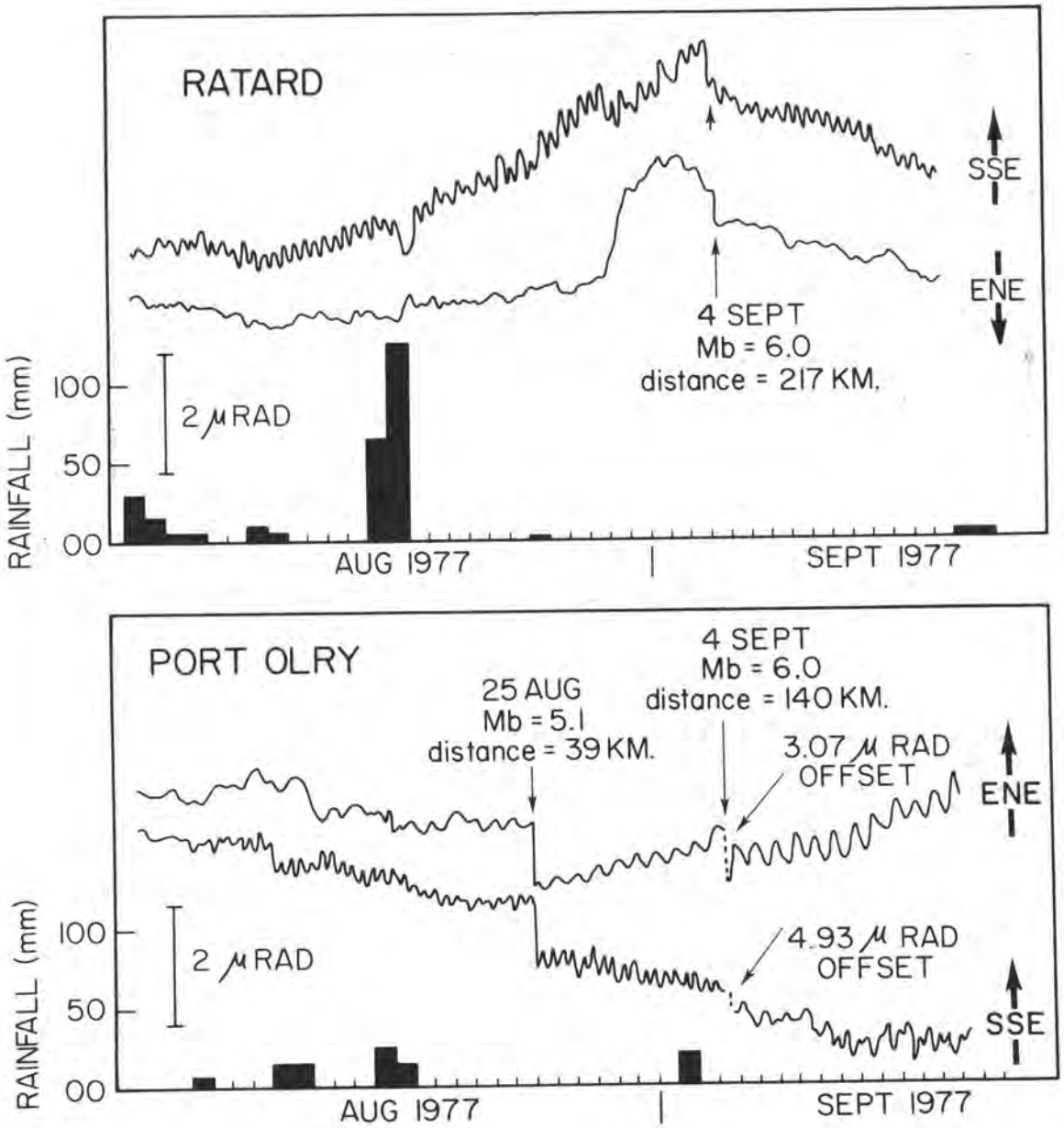
RATARD
SSE
ENE
4 SEPT
Mb = 6.0
distance = 217 KM.
2 μ RAD
RAINFALL (mm)
100
50
00
AUG 1977
SEPT 1977
PORT OLRY
4 SEPT
Mb = 6.0
distance = 140 KM.
25 AUG
Mb = 5.1
distance = 39 KM.
3.07 μ RAD
OFFSET
ENE
2 μ RAD
4.93 μ RAD
OFFSET
SSE
RAINFALL (mm)
100
50
00
AUG 1977
SEPT 1977

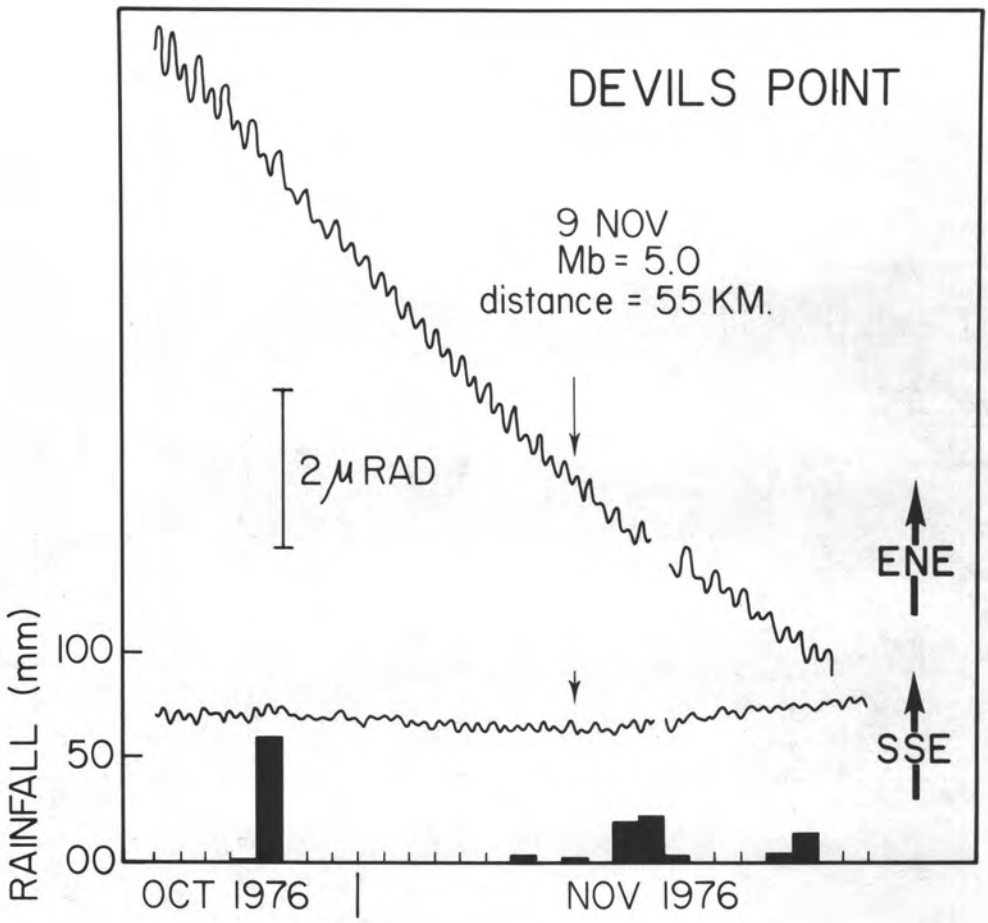
DEVILS POINT
9 NOV
Mb = 5.0
distance = 55 KM.
2 μ RAD
ENE
SSE
RAINFALL (mm)
100
50
00
OCT 1976
NOV 1976

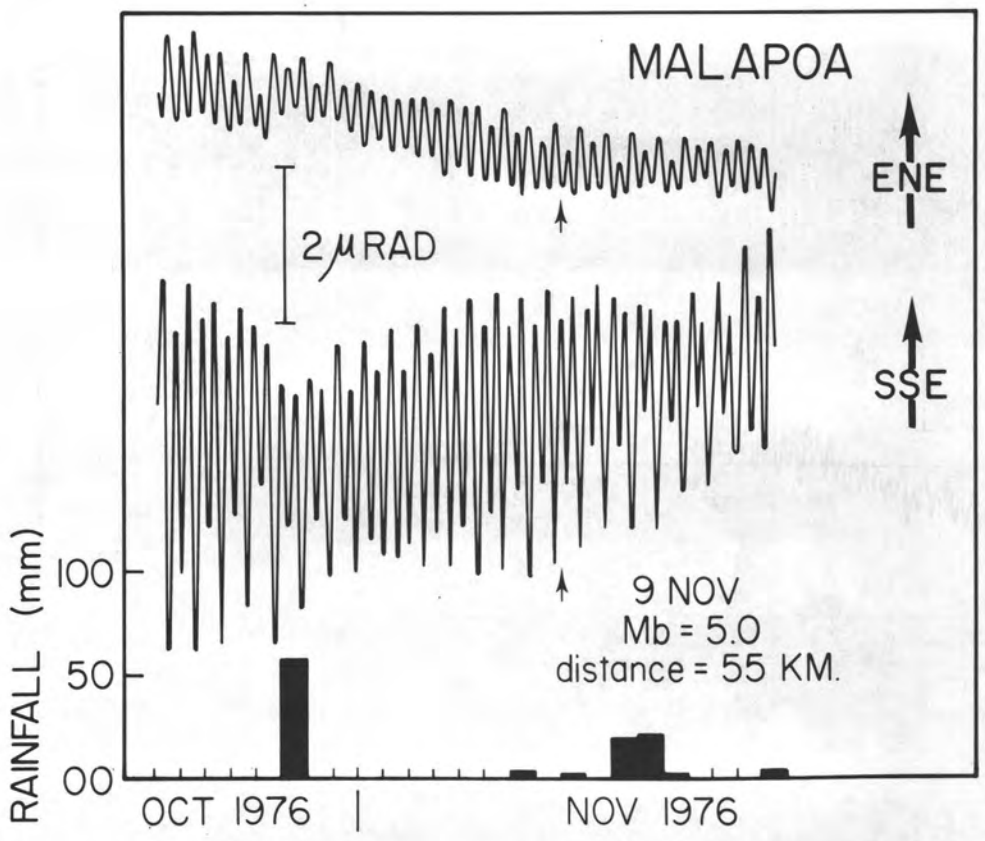
MALAPOA
ENE
2 μ RAD
SSE
9 NOV
Mb = 5.0
distance = 55 KM.
RAINFALL (mm)
100
50
00
OCT 1976
NOV 1976

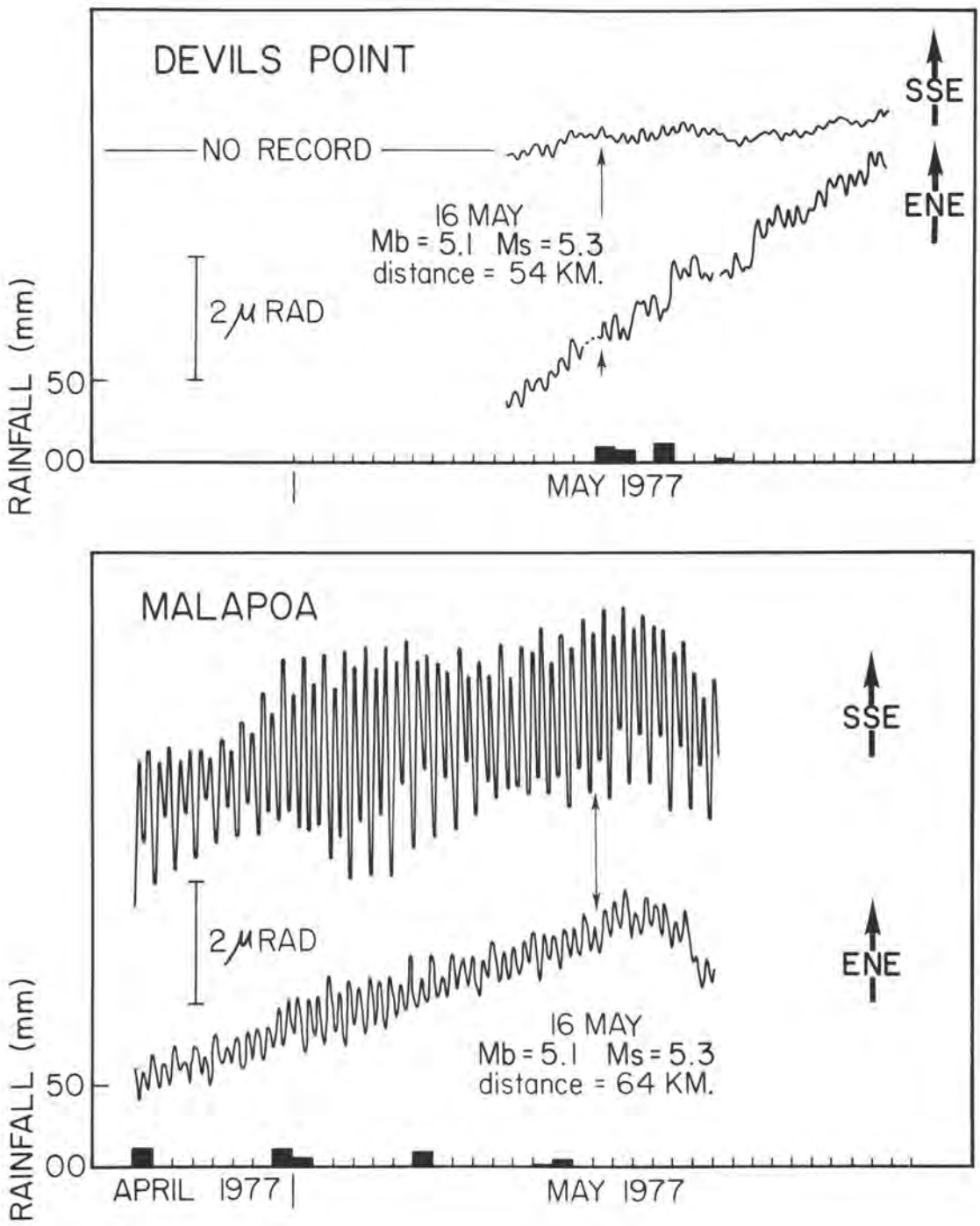
DEVILS POINT
SSE
NO RECORD
ENE
16 MAY
Mb = 5.1 Ms = 5.3
distance = 54 KM.
2μ RAD
RAINFALL (mm)
50
00
MAY 1977
MALAPOA
SSE
2μ RAD
ENE
16 MAY
Mb = 5.1 Ms = 5.3
distance = 64 KM.
RAINFALL (mm)
50
00
APRIL 1977
MAY 1977

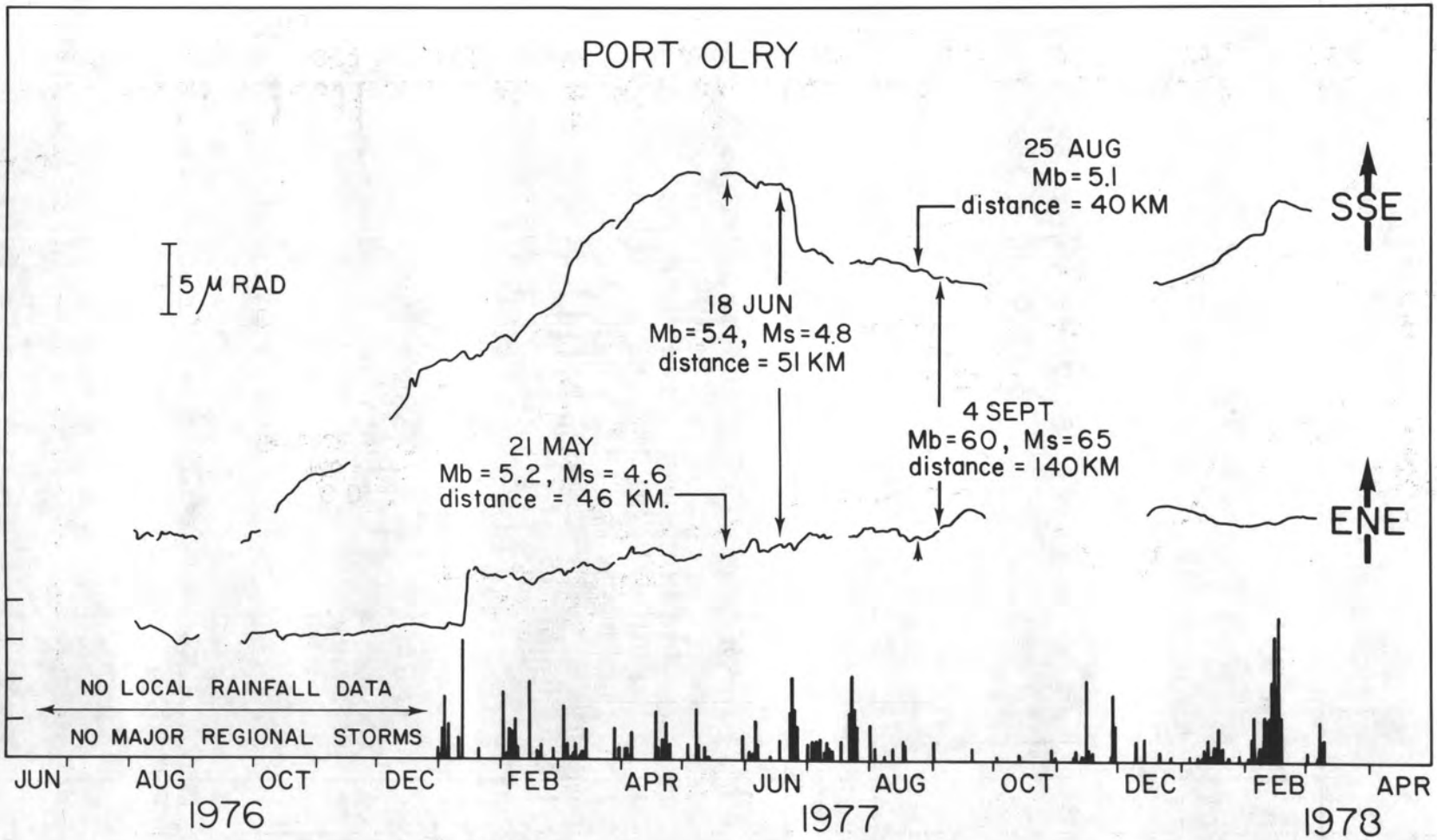
PORT OLRY
25 AUG
Mb = 5.1
distance = 40 KM
SSE
5 μ RAD
18 JUN
Mb = 5.4, Ms = 4.8
distance = 51 KM
4 SEPT
Mb = 60, Ms = 65
distance = 140 KM
21 MAY
Mb = 5.2, Ms = 4.6
distance = 46 KM.
ENE
200
100
00
NO LOCAL RAINFALL DATA
NO MAJOR REGIONAL STORMS
JUN
AUG
OCT
DEC
FEB
APR
JUN
AUG
OCT
DEC
FEB
APR
1976
1977
1978

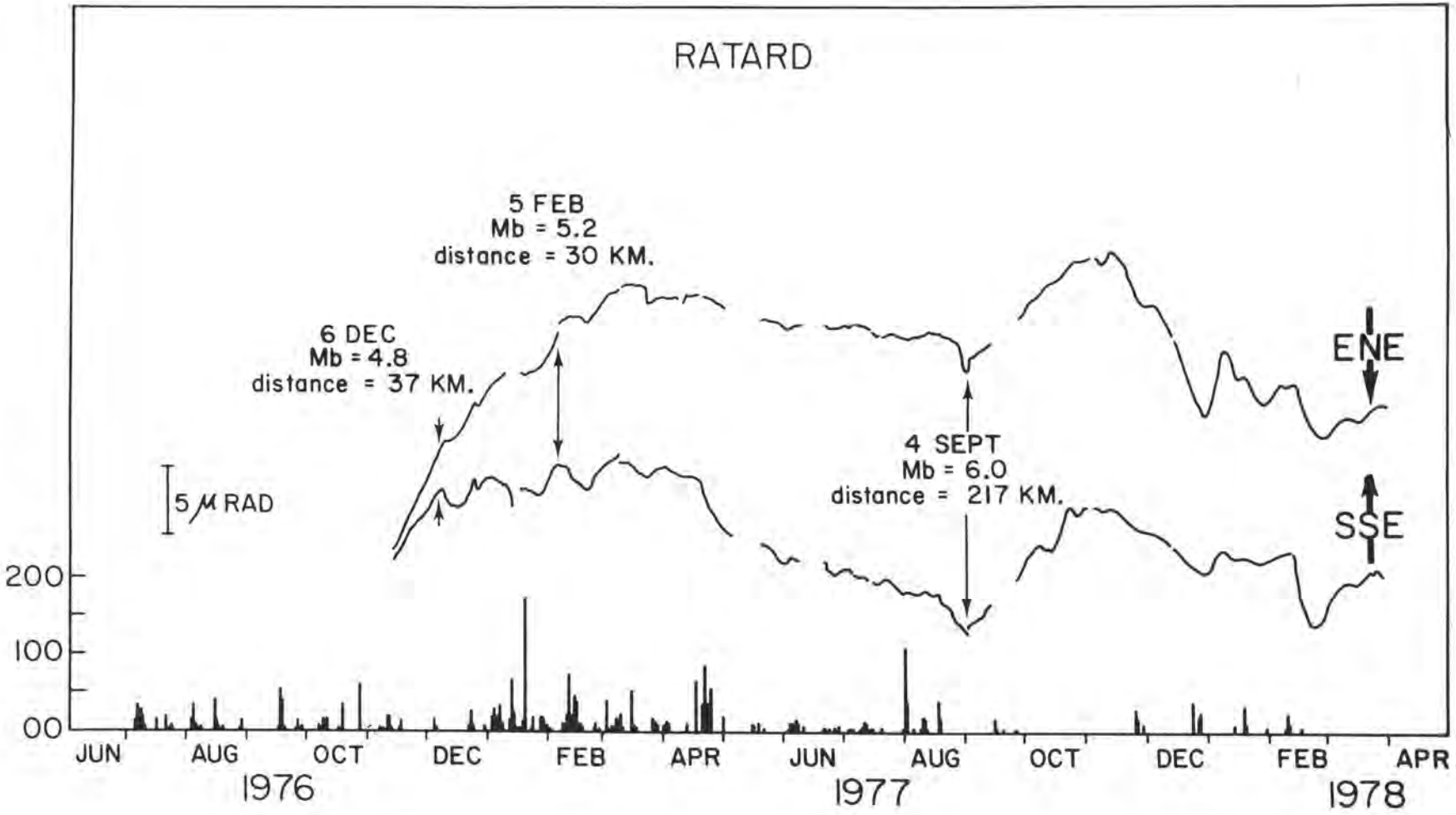
RATARD
5 FEB
Mb = 5.2
distance = 30 KM.
6 DEC
Mb = 4.8
distance = 37 KM.
4 SEPT
Mb = 6.0
distance = 217 KM.
ENE
SSE
5 μ RAD
200
100
00
JUN
AUG
OCT
DEC
FEB
APR
JUN
AUG
OCT
DEC
FEB
APR
1976
1977
1978

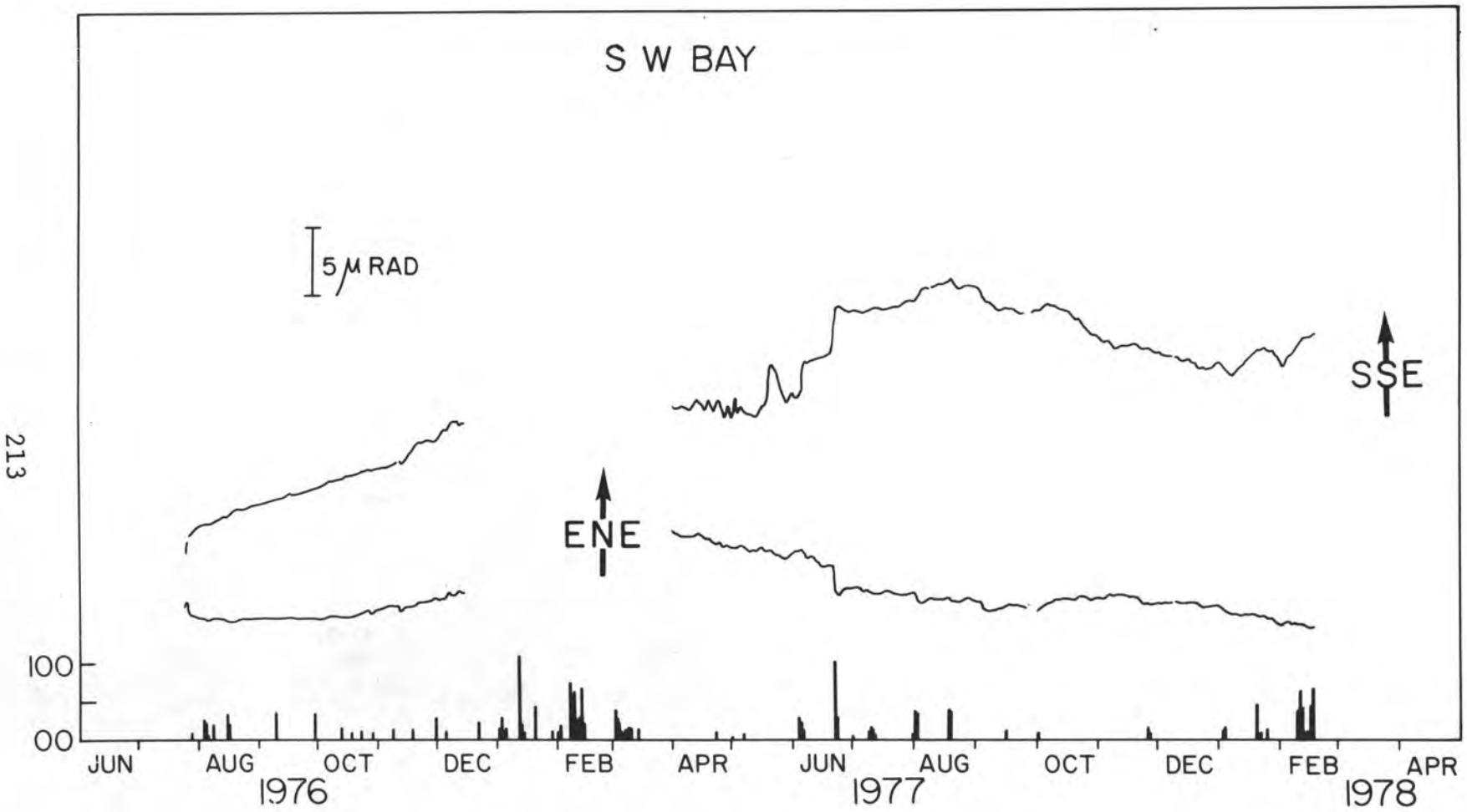
S W BAY
5 μ RAD
ENE
SSE
100
00
JUN
AUG
OCT
DEC
FEB
APR
JUN
AUG
OCT
DEC
FEB
APR
1976
1977
1978

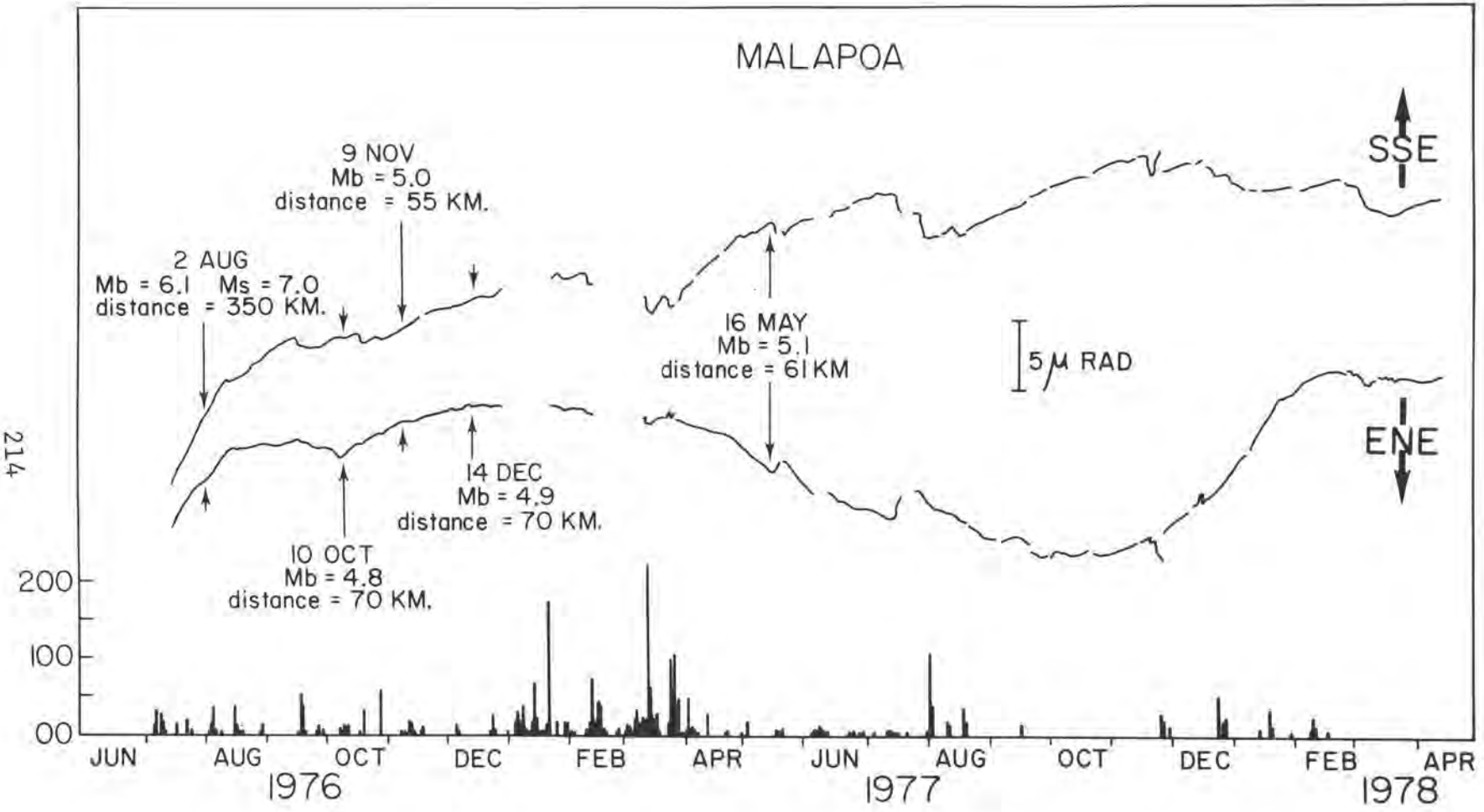
MALAPOA
SSE
ENE
9 NOV
Mb = 5.0
distance = 55 KM.
2 AUG
Mb = 6.1 Ms = 7.0
distance = 350 KM.
16 MAY
Mb = 5.1
distance = 61 KM
5 μ RAD
14 DEC
Mb = 4.9
distance = 70 KM.
10 OCT
Mb = 4.8
distance = 70 KM.
200
100
00
JUN
AUG
OCT
DEC
FEB
APR
JUN
AUG
OCT
DEC
FEB
APR
1976
1977
1978

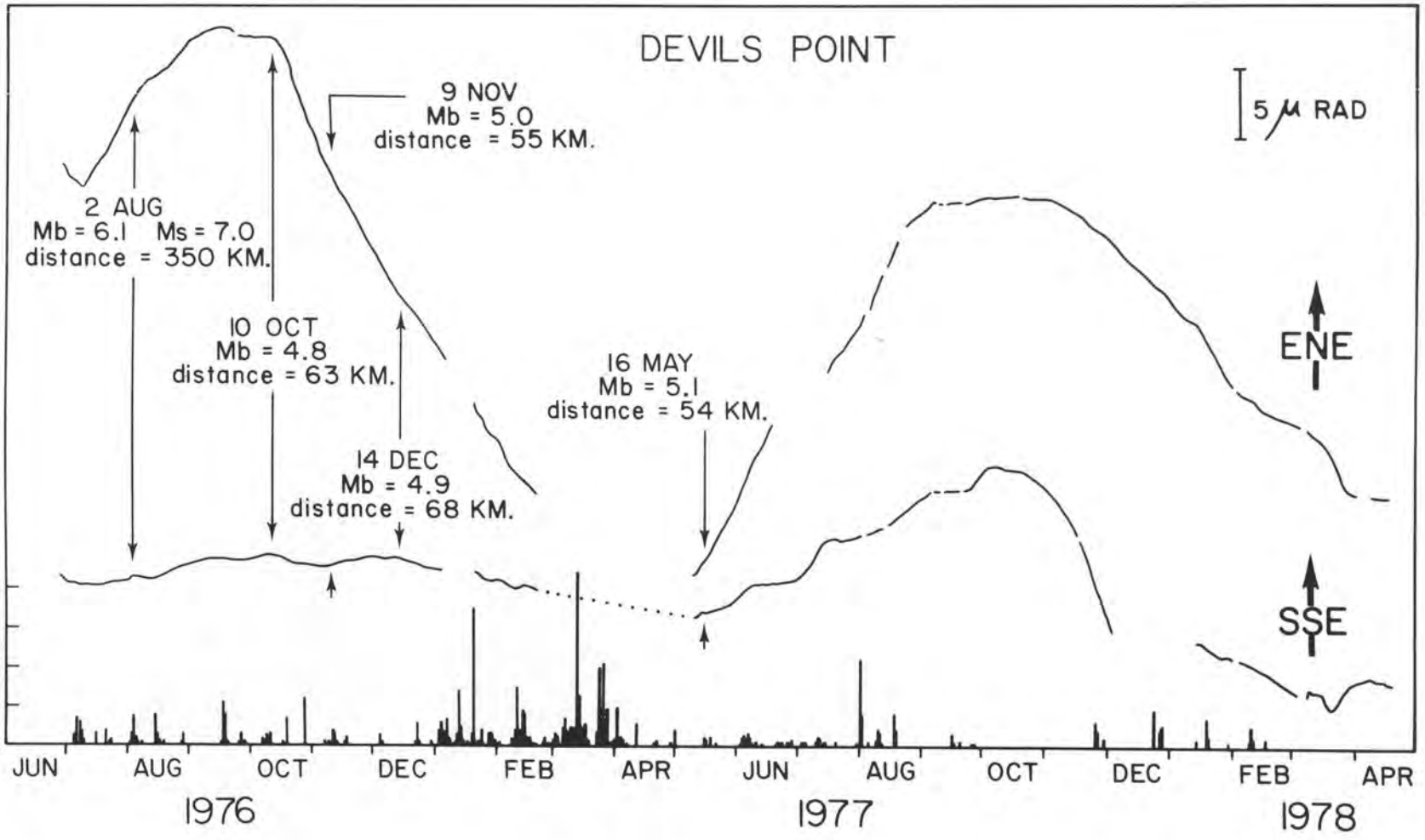
DEVILS POINT
5 μ RAD
9 NOV
Mb = 5.0
distance = 55 KM.
2 AUG
Mb = 6.1 Ms = 7.0
distance = 350 KM.
10 OCT
Mb = 4.8
distance = 63 KM.
14 DEC
Mb = 4.9
distance = 68 KM.
16 MAY
Mb = 5.1
distance = 54 KM.
ENE
SSE
215
200
100
00
JUN
AUG
OCT
DEC
FEB
APR
JUN
AUG
OCT
DEC
FEB
APR
1976
1977
1978

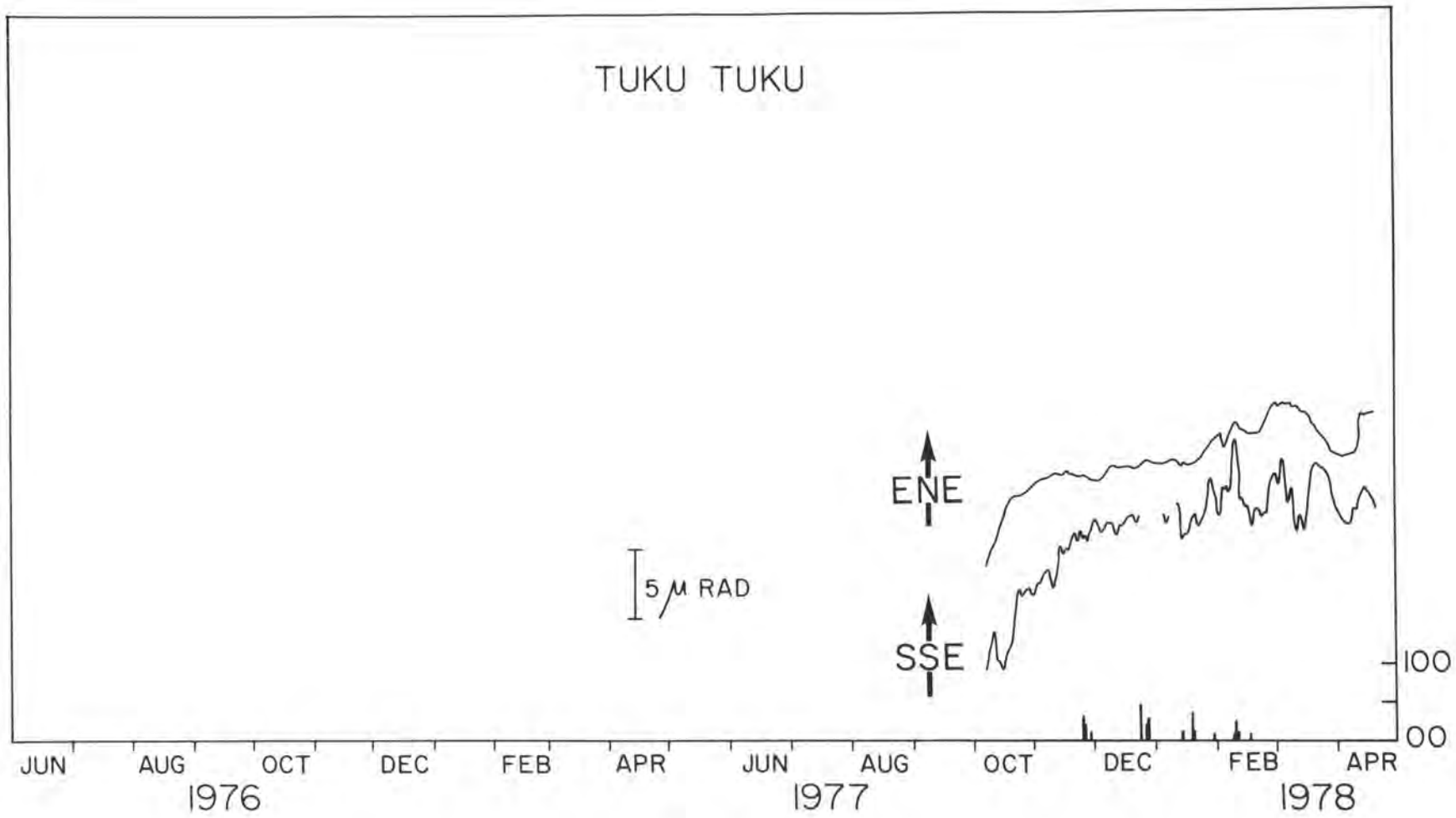
TUKU TUKU
ENE
SSE
5 μ RAD
100
00
JUN
AUG
OCT
DEC
FEB
APR
JUN
AUG
OCT
DEC
FEB
APR
1976
1977
1978

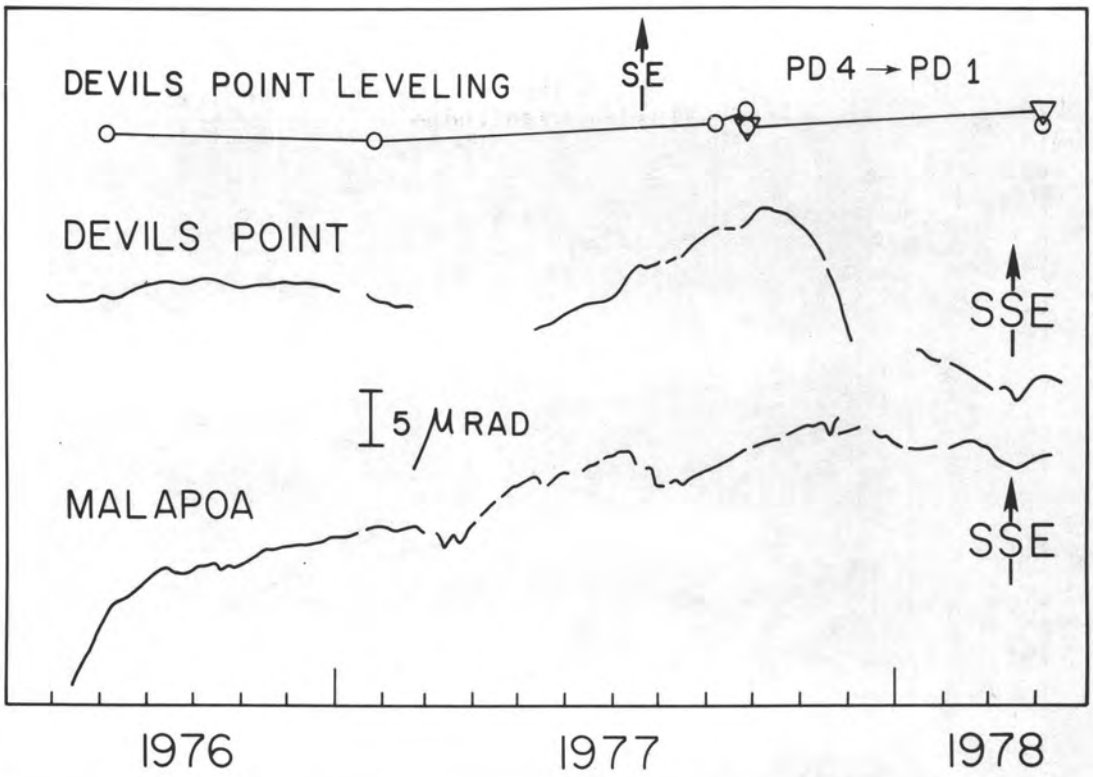
DEVILS POINT LEVELING
SE
PD 4 → PD 1
DEVILS POINT
SSE
5 μRAD
MALAPOA
SSE
1976
1977
1978

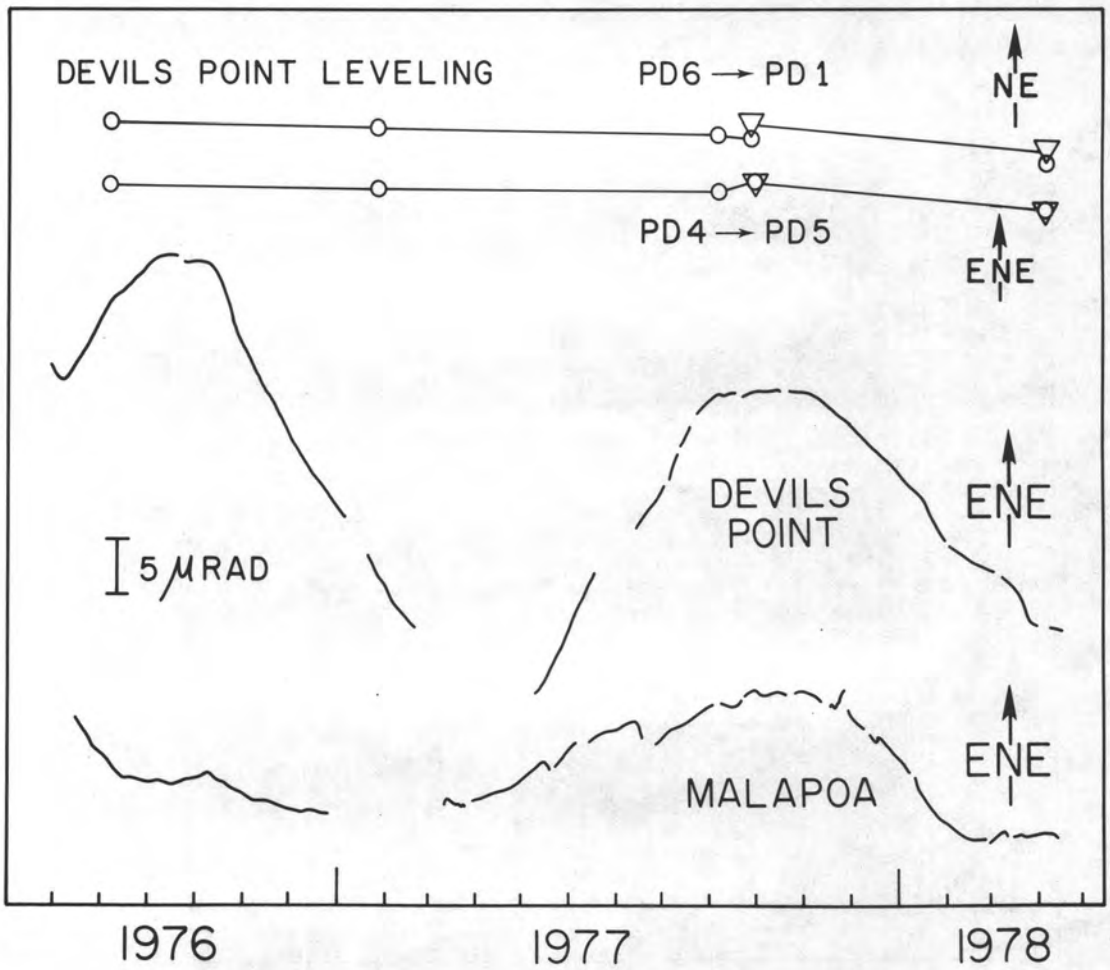
DEVILS POINT LEVELING
PD6 → PD1
NE
PD4 → PD5
ENE
DEVILS POINT
ENE
5 μRAD
MALAPOA
ENE
1976
1977
1978

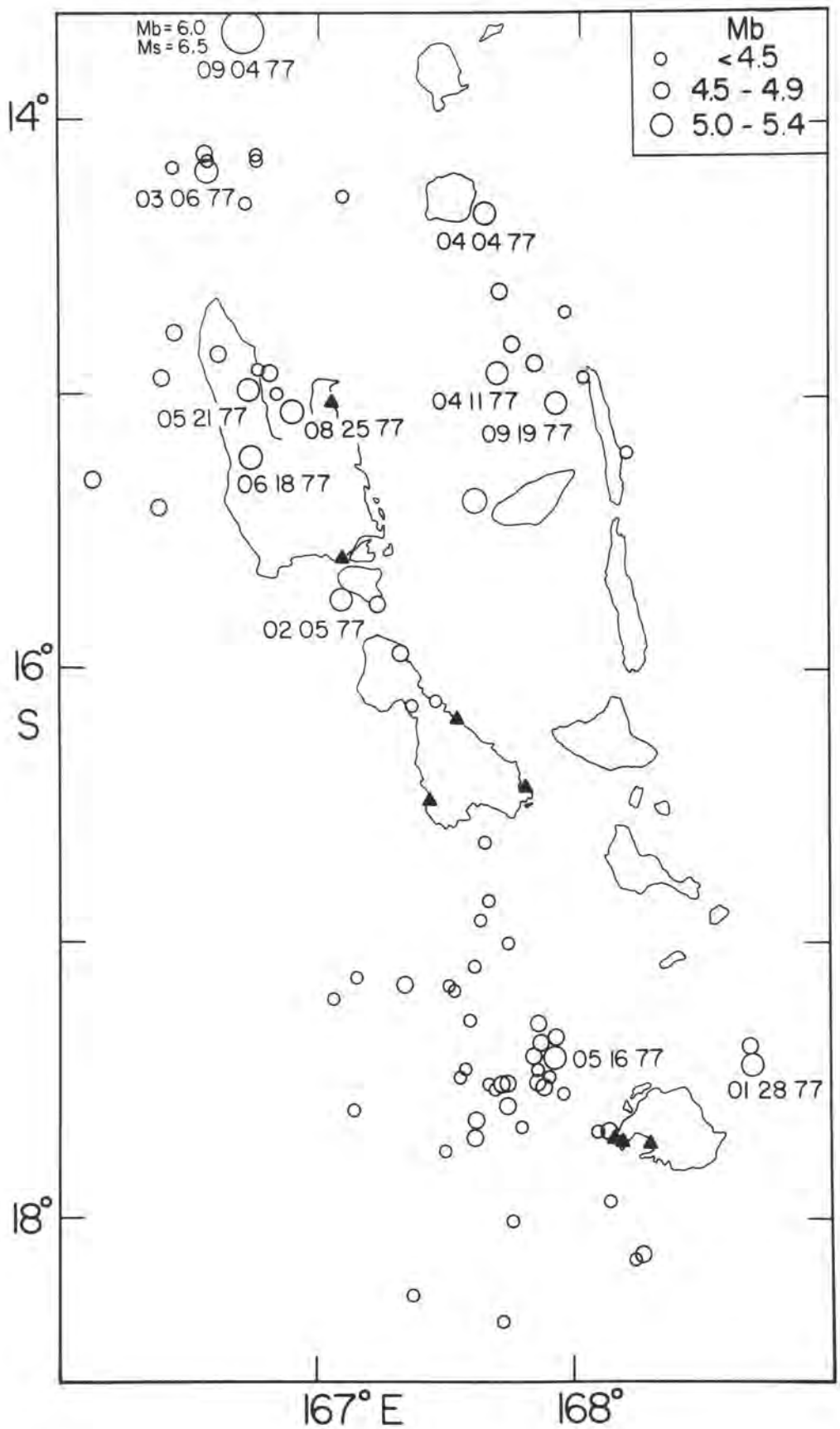
Mb
< 4.5
4.5 - 4.9
5.0 - 5.4
Mb = 6.0
Ms = 6.5
09 04 77
03 06 77
04 04 77
05 21 77
08 25 77
04 11 77
09 19 77
06 18 77
02 05 77
05 16 77
01 28 77
14°
16°
S
18°
167° E
168°

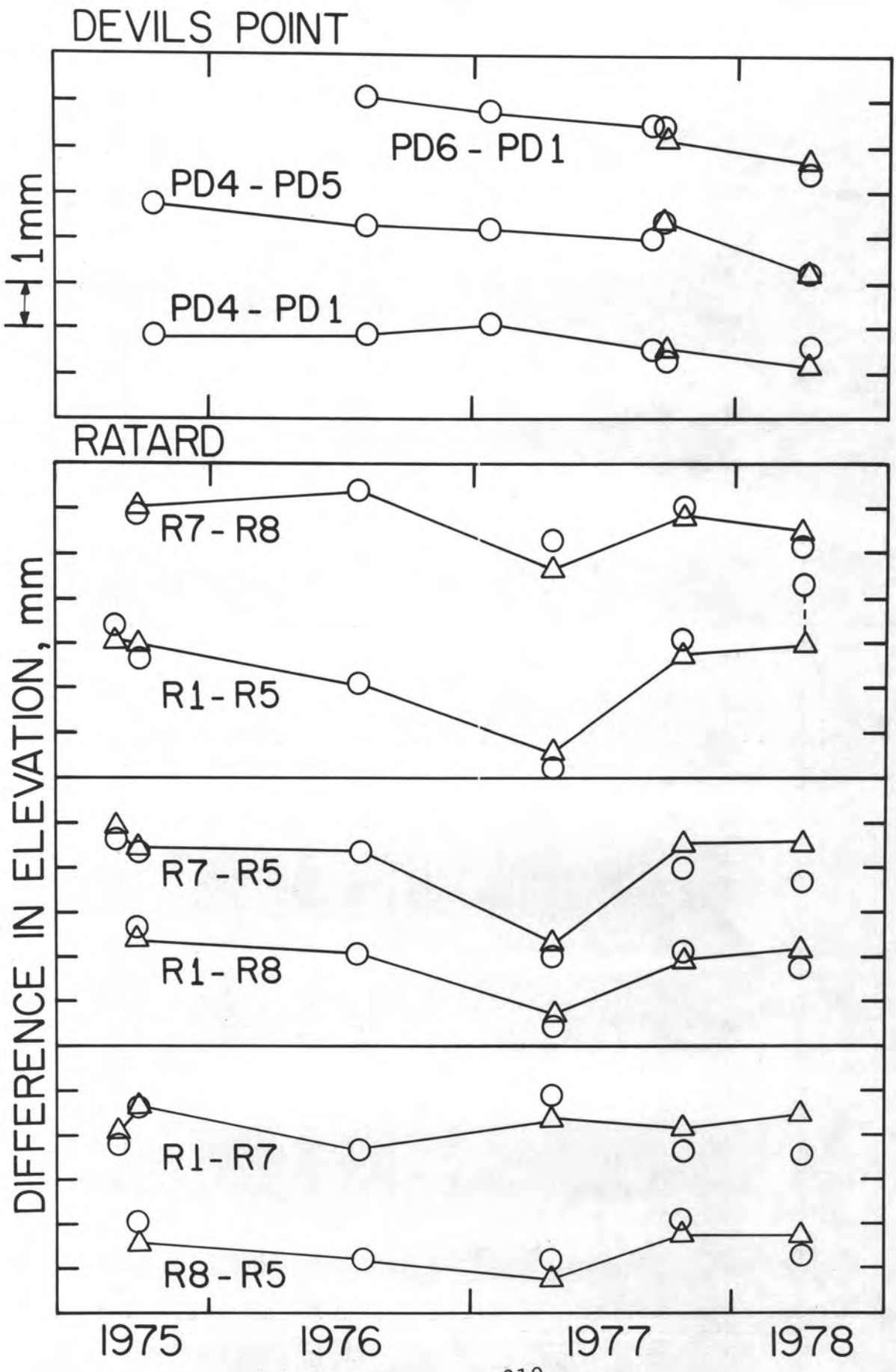
DEVILS POINT
PD6 - PD1
PD4 - PD5
PD4 - PD1
1mm
RATARD
R7 - R8
R1 - R5
R7 - R5
R1 - R8
R1 - R7
R8 - R5
DIFFERENCE IN ELEVATION, mm
1975
1976
1977
1978

UNADJUSTED
ADJUSTED
+5
0
-5
TILT DOWN IN DIRECTION OF AZIMUTH, MICRORADIANS
RATARD
JULY AUG 1976 - APRIL 1977
330
0
30
60
90
120
150
AZIMUTH, DEGREES

+5
0
-5
TILT DOWN IN DIRECTION OF AZIMUTH, MICRORADIANS
RATARD
APRIL 1977 - OCT 1977
330
0
30
60
90
120
150
AZIMUTH, DEGREES

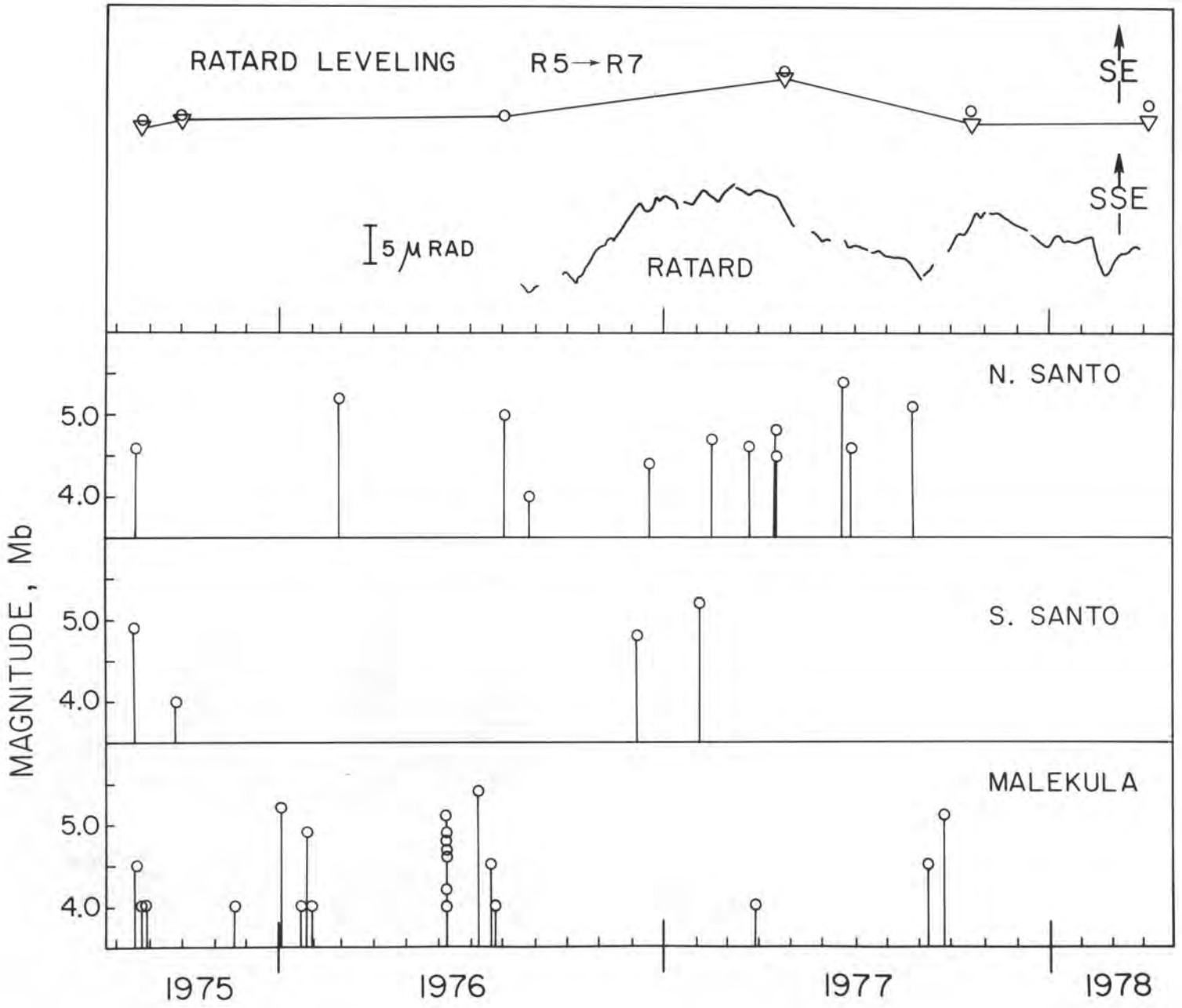
RATARD LEVELING R5→R7
SE
SSE
5 μ RAD
RATARD
N. SANTO
S. SANTO
MALEKULA
MAGNITUDE, Mb
5.0
4.0
1975
1976
1977
1978

Temporal Gravity Changes as Applied to Studies of Crustal Deformation

by

R. C. Jachens
U.S. Geological Survey
345 Middlefield Road
Menlo Park, Ca. 94025

Abstract

Temporal gravity variations accompany many types of crustal deformation. They arise from the combined effects of displacement of the observation site along the free-air gravity gradient and temporal variations of the subsurface density field. Measurements of temporal gravity variations can sometimes yield information about the spatial distribution of deformation and, when combined with independent temporal elevation data, can yield information about changes of the subsurface density field.

Compared with leveling and exterrestrial techniques, gravity techniques are relatively rapid and economical. They are well suited for studying rapidly occurring processes such as volcanic events or after-slip on normal or thrust faults. Networks having spatial dimensions of tens to a few hundreds of kilometers can be surveyed using automobile transport but drift exhibited by all relative gravimeters limits the size of networks that can be surveyed efficiently and economically with these instruments.

Modern gravimeters are capable of yielding measurements of gravity differences by a single meter having standard deviations of 5-15 μGal. Measurements can be made successfully under a wide variety of field conditions and the measurement process generally does not seem to be adversely affected by background noise, instrument vibration during automobile transport or large gravity ranges. Meter-dependent systematic errors including those arising from nonlinearities in gravimeter calibration functions contribute to overall uncertainties in measurements of gravity differences. The magnitudes of these uncertainties are being investigated.

Introduction

Observations of temporal variations of gravity can be used as an inexpensive and rapid means for detecting, monitoring, and studying crustal deformation associated with many active geologic processes. Such observations can yield qualitative or semiquantitative information on elevation changes and, when combined with independent elevation data, can yield information about temporal variations of the subsurface density field arising both from subsurface displacements and temporal variations of the density of materials in the subsurface. The effectiveness of gravity techniques as applied to specific cases of crustal deformation depends on the configuration of the local gravity field, the physical processes involved in the deformation, and the accuracy with which temporal gravity variations can be measured.

Assuming that the effects of earth tides, ocean tides, and variations in atmospheric pressure have been removed, gravity measured at a point fixed on the surface of the earth can vary with time as a result of two factors: 1) displacement of the observation point along the free-air gravity gradient and 2) time variation of the subsurface density field. Generally, both factors result in gravity variations of the same order of magnitude. The normal vertical gradient of gravity is approximately -3.09 μGal/cm whereas the actual free-air gradient typically may differ from this value by ±5% and in special situations may differ by more than 15% (Hammer, 1970). Gravity changes caused by variations in subsurface density field accompanying deformation may enhance, subdue, or dominate gravity changes resulting from vertical displacement and the relation between gravity change and elevation change $\Delta g/\Delta h$ may assume a wide range of values.

Relation between gravity change and elevation change

Some samples of possible relations of gravity change versus elevation change based on theoretical considerations are shown in figure 1. The values of $\Delta g/\Delta h$ shown in this figure were derived from simple crustal models and are presented primarily to illustrate the possible variability in $\Delta g/\Delta h$ for different geologic processes. The boundaries of the fields shown are approximate and do not represent strict limits. All values include both the effect of vertical displacement along a normal free-air gravity gradient and the effect of changes in the subsurface density field.

Based on a numerical model study of a dilating sphere buried in a homogeneous, elastic half-space, Rundle (1978) found Δg proportional to Δh and the ratio $\Delta g/\Delta h$ equal to -3.1 μGal/cm. For this model, the gravity change is equal to the free-air effect due to uplift. If the increased volume in this model were partially or completely filled with water, the magnitude of $\Delta g/\Delta h$ would be slightly smaller. In the same study Rundle found that Δg caused by thrust movement on an infinitely long dipping fault buried in a homogeneous, elastic half-space also was proportional to Δh. For a medium with density $\rho = 2.8$ gm/cm^3, $\Delta g/\Delta h$ was equal to -1.9 μGal/cm or equivalent to the free-air effect due to uplift plus the gravity effect due to mass added to the vertical section as was proposed by Barnes (1966).

For a simple model of a homogeneous, elastic plate having rectangular cross section and infinite length and subject to uniform horizontal compression or extension, Δg again is proportional to Δh. In this case, the gravity changes

due to changes of elevation and changes in subsurface density field are nearly equal in magnitude and tend to cancel. Thus the value of $\Delta g/\Delta h$ is approximately 0 μGal/cm. Numerical calculations of deformation and gravity change resulting from surface loads applied to radially symmetric, elastic earth models (Farrell, 1972) show a $\Delta g/\Delta h$ value near -2.3 μGal/cm.

When deformation is associated with processes dominated by fluid movement such as magma movement in volcanic areas or ground-water movement in areas subject to ground-water extraction, possible values of $\Delta g/\Delta h$ cover a wide range. The wide range is due in large measure to the range of subsurface volume changes possible in response to changes in pore pressure. For example, ground-water extraction in some areas is not accompanied by any appreciable subsidence of the surface whereas in other areas the removal of ground-water appears to be accompanied by almost a complete collapse of the resulting voids (Poland and Davis, 1969). Furthermore, in some cases, a certain amount of ground-water can be extracted before appreciable subsidence begins (Riley, 1970). In these situations, the relation between Δg and Δh probably would be nonlinear. Analogous behavior can be expected in volcanic areas.

$\Delta g/\Delta h$ relations measured in a limited number of cases are in general agreement with the results shown in figure 1 although exceptions do exist. Barnes (1966) and Oliver et al. (1975) remeasured gravity in regions that had undergone deformation associated with slip on subsurface faults. Barnes found that many observations of $\Delta g/\Delta h$ in southern Alaska fell close to a value of -1.97 μGal/cm (fig. 2) whereas $\Delta g/\Delta h$ values at stations along a profile extending NE from Valdez were closer to the normal free-air gradient. An anomalous value of $\Delta g/\Delta h$ was found near Anchorage, Alaska (point 1 in figure 2), an area in which a very small gravity change was associated with nearly 1 m of subsidence. Oliver and his coworkers determined a value of -2.15 ± 0.26 (s.d.) μGal/cm associated with deformation accompanying the 1971 San Fernando, California earthquake. Jachens et al. (1976) found a very good correlation between gravity changes and elevation changes that occurred during the November, 1975 deflation of Kilauea Volcano, Hawaii (fig. 3). In this case, $\Delta g/\Delta h$ equaled -1.71 ± 0.05 (s.e.) μGal/cm. Strange and Carroll (W. E. Strange, written comm. 1977) studied the relation between gravity change and elevation change resulting from ground-water extraction in the San Joaquin Valley of California. They found that a $\Delta g/\Delta h$ value near -3.0 μGal/cm existed in areas where water was withdrawn from confined aquifers but that a simple relation did not exist in areas where water was extracted from unconfined aquifers. Isherwood (1977) reported gravity changes and subsidence over a producing geothermal field at the Geysers, California. He found a $\Delta g/\Delta h$ relation of about 2.5 μGal/cm indicating that gravity changes due to loss of fluid from the subsurface were larger than those due to vertical displacement. $\Delta g/\Delta h$ values of -3.7 μGal/cm and near -10 μGal/cm reported by Kisslinger (1975) to have accompanied the Matsushiro, Japan earthquake swarm indicate that simple models such as those on which figure 1 is based are not sufficient to explain all observations.

On the basis of the preceding discussion, certain generalizations can be made concerning the study of temporal variations of gravity as related to crustal deformation. First, gravity changes accompany most types of deformation, and a knowledge of such changes can yield information about the spatial distribution of the deformation. Second, unambiguous estimates of elevation changes are not possible on the basis of gravity data alone. Third, in some

situations, e.g. San Fernando, California and Hawaii, the measurement of Δg and Δh at a few locations may permit the determination of $\Delta g/\Delta h$ that then can be used to infer elevation changes from measured gravity changes. Finally, the wide range of possible values of $\Delta g/\Delta h$ shows that, in some cases, observed values of this relation can effectively constrain the interpretation of the causes of the deformation.

Gravity Measurements

Several types of gravimeters have been satisfactorily used for temporal gravity studies, but recent measurements primarily have involved the use of LaCoste and Romberg model G and D meters with electronic readout. These instruments are thermostated for insensitivity to temperature fluctuations, are sufficiently rugged to survive most field accidents, and may alternately be used in a recording mode. They are capable of yielding measurements of relative gravity having single measurement standard deviations on the order of 5-15 μGal (H. W. Oliver, written commun. 1975; Lambert et al. 1977).

Recently, the U.S. Geological Survey conducted high-precision gravity surveys for the purpose of studying temporal gravity variations associated with geologic processes. Surveys were conducted on Kilauea and Mauna Loa volcanos, Hawaii in order to study crustal deformation and subsurface movement of magma that accompany volcanic processes. In southern California, a large network of high-precision gravity stations (fig. 4) was established to study time variations of the gravity field over the area of the southern California uplift (Castle et al. 1976; Castle et al. 1977). Gravity measurements were made primarily with LaCoste and Romberg model G gravimeters. Results from these surveys provide information about the characteristics and behavior of model G gravimeters under a wide variety of field conditions and indicate some of the capabilities and limitations imposed by their use in studies of temporal variations of gravity.

Survey Procedures

All gravity measurements were made along closed loops originating from a small number of secondary reference stations. Gravity at the secondary reference stations, in turn, was measured in a similar fashion directly with respect to a single primary reference station in each network. Each field station was occupied at least twice with sets of 2-4 gravimeters. Generally, reference stations were occupied at 4-5 hour intervals and 3-6 field stations were measured between reference station occupations.

Survey procedures were designed to reduce or eliminate possible sources of error due to imprecise tide corrections, site relocation problems, local terrain influences, magnetic field influences, clamp hysteresis effects and human blunders in reading and recording the data. To reduce or eliminate site relocation problems, local terrain influences and magnetic field influences, the reading sites were monumented, described and marked so that precise location and reading orientation could be recovered at any time. Clamp hysteresis effects were standardized by maintaining a fixed time of five minutes between unclamping and reading the gravimeters. The effects of imprecise tide corrections were reduced either by the use of a measured gravity tide or by frequent reference station reoccupations and the removal of a "drift"

having the form of a polynomial in time from each day's data. During the southern California surveys human blunders in reading and recording data were checked on-station by field reducing the data and comparing the gravity difference between two reading sites at each station as measured by the two gravimeters.

Data Reduction

Gravimeter readings were converted to gravity units by means of the calibration table provided by the manufacturer. Earth tide corrections were applied to the Hawaiian measurements on the basis of the record from a tidal gravimeter in operation on the summit of Kilauea volcano during the surveys. Tide corrections applied to the southern California measurements were calculated from the formulation of Longman (1959) with an assumed compliance factor of 1.16. The data then were examined for evidence of sudden changes of reading or "tares" and corrections were applied where necessary. Finally, the data from each day were analyzed by means of a least-squares procedure. The system unknowns for this procedure were the gravity differences between field stations and reference station and the coefficients of a time dependent "drift" polynomial. For the Hawaiian data, zero drift was assumed whereas for the southern California surveys, a "drift" having the form of a first- or second-order polynomial in time was assumed. A first-order polynomial was assumed if the reference station was occupied only twice and a second-order polynomial was assumed for days with three or more reference station occupations. The data from each gravimeter were analyzed independently and the standard deviations and standard errors discussed in the following sections are indicative of the repeatability attained with individual instruments. They do not relate to how well gravity differences measured by different instruments agree.

Repeatability

The reading accuracy of LaCoste and Romberg model G gravimeters with electronic readout is on the order of 2-3 μGal and laboratory tests indicate that the standard deviation of a single gravity difference measurement with a single instrument is on the order of 4-7 μGal. However, data from field surveys indicate that poorer results are to be expected when measurements are made under normal field conditions. Standard deviations calculated from data taken with four G meters in southern California averaged 11.5 μGal and similar results were found for the Hawaiian surveys. The increase in scatter of data taken under field conditions compared to those taken under laboratory conditions presumably reflects the influence of conditions not encountered in the laboratory such as magnetic effects, local terrain effects, site relocation problems, power fluctuations, the presence of background noise at the measuring sites, ambient temperature and pressure fluctuations, large gravity ranges, and amount of vibration experienced by the instruments. As mentioned in a previous section, survey procedures were designed to reduce or eliminate possible errors due to magnetic effects, local terrain effects and site relocation problems. The influence of power fluctuations on the gravimeter response has been investigated in the laboratory and results of tests indicate that power fluctuations are not the cause of the scatter.

Data from the southern California surveys suggest that, whatever the cause of the scatter, each meter responds differently. During this work, the gravity

meters were operated in pairs and presumably each member of a pair was subjected to the same environmental influences. However, a comparison between standard deviations of data taken with meters that were operated as a pair actually showed a negative correlation (correlation coefficient = -0.35). Also, during the three-month measurement period all meters probably experienced, on average, similar conditions yet average standard deviations for data from individual meters ranged from 9.8 μGal for G192 to 13.1 μGal for G425. These results indicate that real short-term fluctuations of the gravity field are not the primary cause of the scatter in the data because if they were, the standard deviations of data from paired meters should correlate.

The presence of high levels of background noise at the measuring sites makes reading gravimeters more difficult but generally does not adversely affect the measurement precision. Repeatabilities attained in Hawaii were microseism background noise typically reached ±30 μGal are not significantly different from those attained in southern California where the levels seldom reached ±10 μGal. Furthermore, one Hawaiian survey was conducted during the aftershock sequence following a magnitude 7.2 earthquake and no degradation of results was apparent.

Data from G192 were studied in an attempt to correlate the magnitude of standard deviations of data from a single meter with varying external factors including ambient temperature, gravity range, and amount of vibration experienced by the instrument. Standard deviations of data from surveys conducted under the uniform temperature conditions found in the desert during the fall were not significantly different from those for surveys where wide temperature ranges were encountered. A comparison between standard deviation and gravity range yielded a correlation coefficient of 0.09. The influence of ambient pressure fluctuations has not been investigated directly but tests by other workers (Kiviniemi, 1974) have shown that such influences are extremely small.

A somewhat surprising and welcome result of the southern California work is the discovery that the repeatibility attained during any given survey did not seem to depend on the amount of vibration experienced by the gravimeter during automobile transport. Figure 5 shows a comparison between standard deviation and road condition for gravimeter G192. Roads were divided into four categories with higher numbers corresponding to rougher roads. Category 1 includes smooth, paved roads whereas category 4 includes very rough trails where gravimeters commonly experienced large accelerations. The left side of figure 5 shows a comparison between average standard deviation of gravity differences corresponding to field stations and condition of the roads traversed immediately before reaching the stations. The right side of figure 5 shows a comparison between average standard deviations and average road condition over the entire loop containing the stations. In neither case is any correlation between standard deviation and road condition apparent. In particular, the standard deviations for category 4 surveys are no larger than those for paved road surveys. This result is in apparent conflict with the findings of Lambert et al. (1977) who report that surveys conducted over rough roads yielded higher standard deviations than surveys conducted over paved roads.

Gravimeter Drift

All gravimeters display drift and the scatter in the data may reflect a failure to understand or account for this process adequately. Figures 6 and 7

show examples of drift curves. In figure 6, drift curves for four meters covering a three-month period are shown. Gravimeters G8 and G161 were used together on one set of surveys and G192 and G425 were used to conduct another set of surveys. All meters display a long term, relatively smooth drift which seems to be unaffected by external influences. No apparent change in drift is seen when passing from field operations (shown by dots) where external conditions fluctuate over wide ranges to stable conditions (shown by gaps) where the meters were stored on heat, in a controlled environment. Gravimeters operated in the record mode show a similar steady long-term drift. This drift probably results from creep in the gravimeter suspension system and appears to be extremely linear over periods of days. Superimposed on the long-term drift is an irregular daily drift (fig. 7). Generally, the daily drift differs from the long-term drift in magnitude, linearity and even sign. On days when the meter has experienced a large drift during field work, the drift tends to change sign at night and at least partially recover. Vibration, ambient temperature fluctuations, battery power fluctuations and external time varying gravity fields caused by mass movements in the oceans and atmosphere all have been investigated as possible causes of this daily drift. Results to date indicate that none of these factors individually causes or controls the daily drift and efforts to predict it so far have been unsuccessful.

Gravimeter Calibration

The manufacturer provides a calibration based on bench measurements taken every 200 mGal over the entire range of the reading screw. This calibration is not detailed enough to reveal short wavelength periodic (circular error) and aperiodic fluctuations in the calibration function which arise from imperfections in the mechanical drive train of the reading system. Consideration of the gear ratios present in the LaCoste-Romberg model G gravimeter suggests that the most troublesome periodic nonlinearities should have wavelengths of 70.94, 35.47, 7.99, 3.94, and 1.0 counter units (Kiviniemi, 1974). An example of these nonlinearities is shown in figure 8. The upper panel shows the relative calibration function of G425 compared to G192 as a reference. The discrepancy between measured gravity differences (vertical scale) as determined by the two gravimeters is plotted as a function of the gravity difference. The curve was constructed from about 250 observations taken with each meter and averaged over 10 mGal intervals. The errors bars represent $\pm$ one standard error. The curve displays a distinct periodic variation superimposed on a linear trend. The fundamental wavelength of the periodicity is about 75 mGal (70.94 counter units). The bottom panel shows a fourier series spectrum of these data with amplitude plotted as a function of normalized wave number. The normalization factor is the wavenumber corresponding to a wavelength of 70.94 counter units. Two prominent peaks having amplitudes of 28 and 21 μGals occur at the expected wavelengths of 70.94 and 35.47 counter units respectively. Other comparisons suggest the presence of additional periodicities at shorter wavelengths. Additional calibration tests on a number of gravimeters including G192 and G425 have shown that the periodic nonlinearity in figure 8 is almost entirely in G425 and that roughly half the gravimeters tested show similar behavior. Aperiodic nonlinearities undoubtedly also exist in gravimeter calibration functions and these have been documented for some model D gravimeters (Lambert et al. 1977).

Discussion and Conclusions

Measurements of temporal gravity variations can be used to study crustal deformation associated with many types of active geologic processes. This has

been demonstrated in cases of coseismic deformation, volcanic activity and ground-water extraction. Other potential applications include studies of isostatic rebound, aseismic deformation in tectonic regions, and post-seismic after-slip on thrust or normal faults. Compared with leveling or exterrestrial methods, the gravity method is relatively rapid and inexpensive when applied to networks with dimensions of tens to a few hundreds of kilometers. For example, one person using two gravimeters was able each day to resurvey 7-10 stations of the 15-km network on Kilauea volcano, Hawaii. For large networks such as that established in southern California (figure 4), 3-5 adjacent stations can be measured during a day and, if desired, more widely spaced stations can be measured in little more than the time it takes to make two round-trips between them.

Gravimeters can be used successfully under a wide variety of external conditions. Rain, sleet, snow, strong winds and extreme heat were encountered during surveys discussed in this paper. Yet of these, only strong winds in forested areas and ambient temperatures that exceeded the thermostat setting of the gravimeters ($\sim$ 50°C) caused the surveys to be terminated. High levels of background noise at reading sites arising from microseisms or local earthquakes make reading gravimeters more difficult but do not seem to adversely affect the measurement precision. On the other hand, Rayleigh wave trains from large distant earthquakes can make measurement impossible.

Random errors associated with relative gravity measurements using gravimeters are large enough that, for most temporal gravity studies, multiple measurements are required to attain the necessary precision (Kiviniemi, 1974; Lambert and Beaumont, 1977). Evidence from model G gravimeter surveys in southern California and Hawaii indicates that the magnitudes of random errors are independent of a number of environmental influences and field conditions including temperature fluctuations, background noise level, gravity range and vibration level during automobile transport. This permits flexibility in the design of surveys and allows surveys to be conducted with a minimum of lost time.

Frequent reference station and field station reoccupations are required to successfully correct the measurements for daily drift. The need for multiple measurements and frequent reference station occupations limits the size of networks that can be surveyed efficiently and economically. Networks much larger than that shown in figure 4 probably would have to be surveyed using aircraft transport and erratic drift behavior probably would be a serious problem in such surveys (Hamilton and Brulé, 1967).

The presence of nonlinearities in the calibration function coupled with gravity meter drift during the period between successive reoccupations of a network of stations can result in apparent changes in gravity even when no real changes have occurred. For periodic nonlinearities these apparent changes in gravity easily can reach magnitudes of several tens of μGal and in the worst case (35 counter unit gravity difference between field station and reference station coupled with a 35-counter unit drift between successive surveys) can reach magnitudes in excess of 100 μGal.

Several possible ways exist for reducing errors from this source. If the same meters are to be used for each survey and only changes of gravity as seen

by individual meters are compared, then resetting the gravimeters to the same reading point at the beginning of each survey should substantially reduce the possibility of errors. Resetting model D gravimeters is a simple task but resetting model G gravimeters requires a factory adjustment. If gravity differences are to be compared between different gravimeters or if the gravimeters are not reset at the beginning of each survey, then detailed knowledge of the form of the calibration function is necessary.

Modifications of available gravimeters or successful development of new gravity measuring devices could greatly increase the usefulness of temporal gravity methods in studies of crustal deformation. Replacement of the nulling system of gears and levers currently used in many gravimeters, by some other system, e.g. electrostatic, could reduce or eliminate many of the present calibration problems. Also, modification of instruments or techniques to eliminate daily drift would permit more flexibility in survey design and allow networks of large spatial dimension to be surveyed. Development of a portable absolute gravimeter such as that proposed by Faller and Rinker (1977) also would eliminate constraints imposed by drift because such instruments are inherently drift-free. Furthermore, absolute gravimeters are capable of defining areas of stability and areas of change whereas relative gravimeters can only define areas of relative change.

References

Barnes, D. F., 1966, Gravity changes during the Alaska earthquake: Journal of Geophysical Research, v. 81, p. 451-456.

Castle, R. O., Church, J. F. and Elliot, M. R., 1976, Aseismic uplift in southern California: Science, v. 192, p. 251-253.

Castle, R. O., Elliot, M. R., and Wood, S. H., 1977, The southern California uplift (abs.): American Geophysical Union Transactions, v. 58, p. 495.

Faller, J. E., and Rinker, R. L., 1977, Plans for the development of a portable absolute gravimeter with a few parts in 10^9 accuracy (abs.): International Symposium on Recent Crustal Movements, Palo Alto, California, 1977, abstracts.

Farrell, W. E., 1972, Deformation of the earth by surface loads: Reviews of Geophysics and Space Physics, v. 10, p. 761-797.

Hamilton, A. C., and Brulé, B. G., 1967, Vibration-induced drift in LaCoste and Romberg geodetic gravimeters: Journal of Geophysical Research, v. 72, p. 2187-2197.

Hammer, S., 1970, The anomalous vertical gradient of gravity: Geophysics, v. 35, p. 153-157.

Isherwood, W. F., 1977, Geothermal reservoir interpretation from change in gravity: in Kruger, P. and Ramey, H. J., Jr. (Eds.), Proceedings third workshop on geothermal reservoir engineering, Stanford University, Palo Alto, California, Dec. 14-16, p. 18-23.

Jachens, R., Eaton, G., Lipman, P. and Okamura, R., 1976, Temporal gravity variations associated with the November 1975 deflation of Kilauea Volcano (abs.): American Geophysical Union Transactions, v. 57, p. 1015-1016.

Kisslinger, G., 1975, Processes during the Matsushiro, Japan, earthquake swarm as revealed by leveling, gravity, and spring-flow observations: Geology, v. 3, p. 57-62.

Kiviniemi, A., 1974, High precision measurements for studying the secular variation in gravity in Finland: Finnish Geodetic Institute Pub. no. 78, 68 p.

Lambert, A., and Beaumont, C., 1977, Nano variations in gravity due to seasonal groundwater movements: Implications for gravitational detection of tectonic movements: Journal of Geophysical Research, v. 82, p. 297-304.

Lambert, A., Liard, J., and Dragert, H., 1977, Canadian precise gravity networks for crustal movements studies (abs.): International Symposium on Recent Crustal Movements, Palo Alto, California, 1977, abstracts.

Longman, I. M., 1959, Formulas for computing the tidal accelerations due to the moon and sun: Journal of Geophysical Research, v. 64, p. 2351-2355.

Oliver, H. W., Robbins, S. L., Grannell, R. B., Alewine, R. W., and Biehler, Shawn, 1975, Surface and subsurface movements determined by remeasuring gravity, in Oakshott, G. B., (Ed.), San Fernando earthquake of February 9, 1971: California Division of Mines and Geology Bulletin 196, p. 195-211.

Poland, J. F., Davis, G. H., 1969, Land subsidence due to withdrawl of fluids: in Reviews of engineering geology iI, Geological Society of America, p. 187-269.

Riley, F. S., 1970, Analysis of borehole extensometer data from central California: International Association of Scientific Hydrology, UNESCO Pub. 89, p. 423-431.

Rundle, J. B., 1978, Gravity changes and the Palmdale uplift: Geophysical Research Letters, v. 5, p. 41-44.

Figure Captions

Figure 1. Examples of theoretical $\Delta g/\Delta h$ values associated with some geologic processes. The ranges of vertical displacements, Δh, shown are meant to be representative of the displacements that might occur during a single event. The fields shown in this graph include effects both from vertical displacement and variations in subsurface bulk density.

Figure 2. Plot of gravity changes versus elevation changes that occurred during the 1964 Alaskan earthquake (from Barnes, 1966).

Figure 3. Plot of gravity changes versus elevation changes that occurred during the November 1975 deflation of Kilauea volcano, Hawaii. Error bars equal $\pm$ one standard error. Also shown are $\Delta g/_{\Delta h}$ gradients that would have been followed had the gravity change and elevation change been related by a simple Bouguer relation. The gradient for $\rho = 0.0$ gm/cm^3 corresponds to the free-air gradient.

Figure 4. Map showing the locations of stations (dots) in a high-precision gravity network established to study deformation in southern California.

Figure 5. Comparison of standard deviation versus road condition for gravimeter G192. The left side shows average standard deviation of gravity differences corresponding to field stations versus condition of road leading to station. The right side shows average standard deviation versus average loop road condition. For road condition, higher numbers correspond to rougher roads.

Figure 6. Long-term drift curves of four gravimeters used in southern California surveys. Gaps in drift curves indicate times when gravimeters were stored on-heat in a controlled environment.

Figure 7. Examples of daily drift curves for G192. Solid lines indicate times of field surveys and dashed lines indicate overnight periods when the gravimeter was on-heat but not in use. Solid dots below some survey times indicate surveys conducted over rough or very rough roads.

Figure 8. Relative calibration function of G425 referred to G192. The upper panel shows the discrepancy between gravity differences as measured by the two gravimeters plotted against the gravity difference or range. The lower panel shows a fourier series spectrum of the data in the upper panel with amplitude plotted as a function of normalized wavenumber. The normalization factor is the wavenumber corresponding to a wavelength of 70.94 counter units.

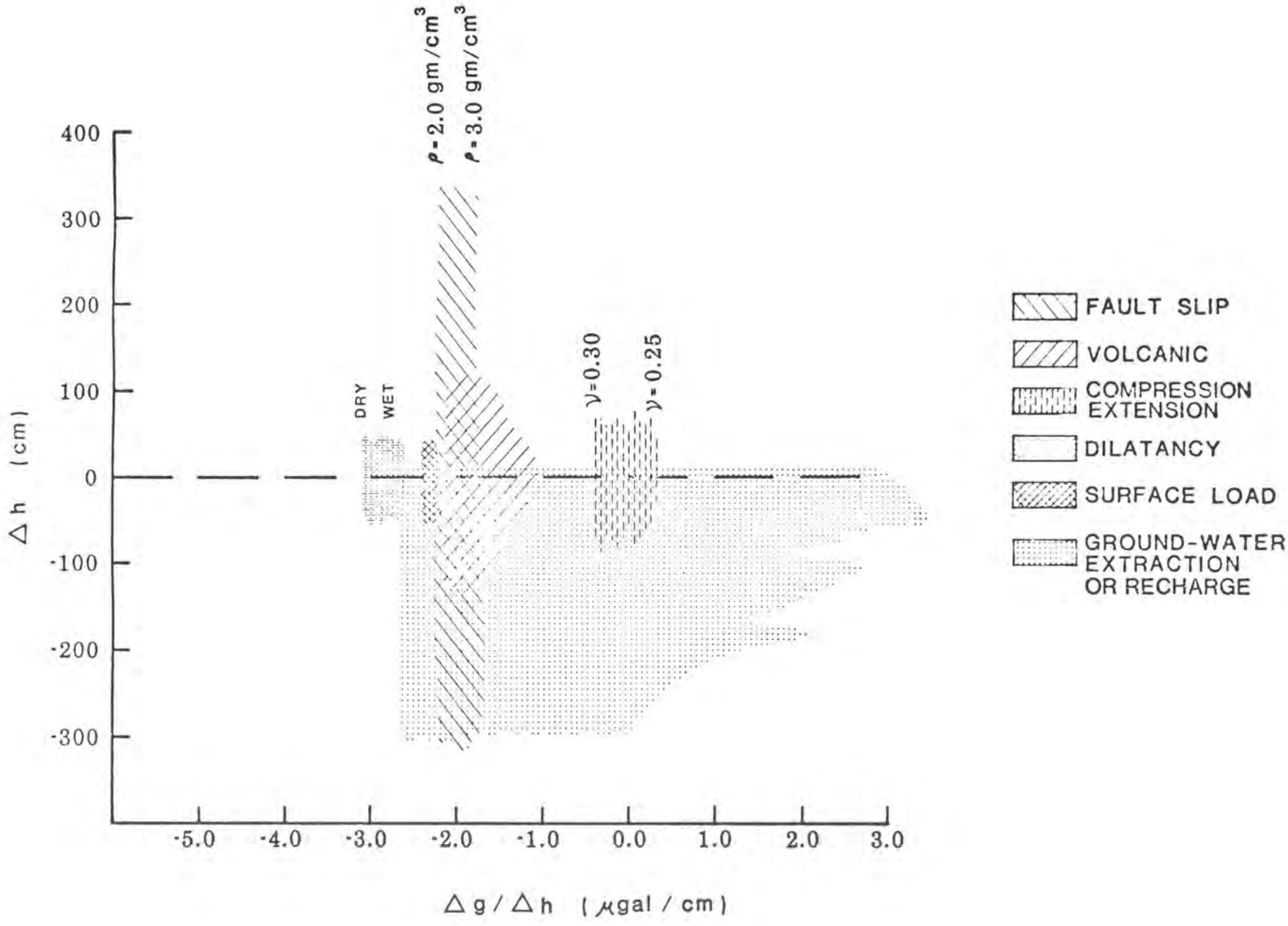
400
300
200
100
0
-100
-200
-300
Δ h (cm)
DRY
WET
ρ = 2.0 gm/cm³
ρ = 3.0 gm/cm³
ν=0.30
ν= 0.25
-5.0
-4.0
-3.0
-2.0
-1.0
0.0
1.0
2.0
3.0
Δ g / Δ h (μgal / cm)
FAULT SLIP
VOLCANIC
COMPRESSION
EXTENSION
DILATANCY
SURFACE LOAD
GROUND-WATER
EXTRACTION
OR RECHARGE

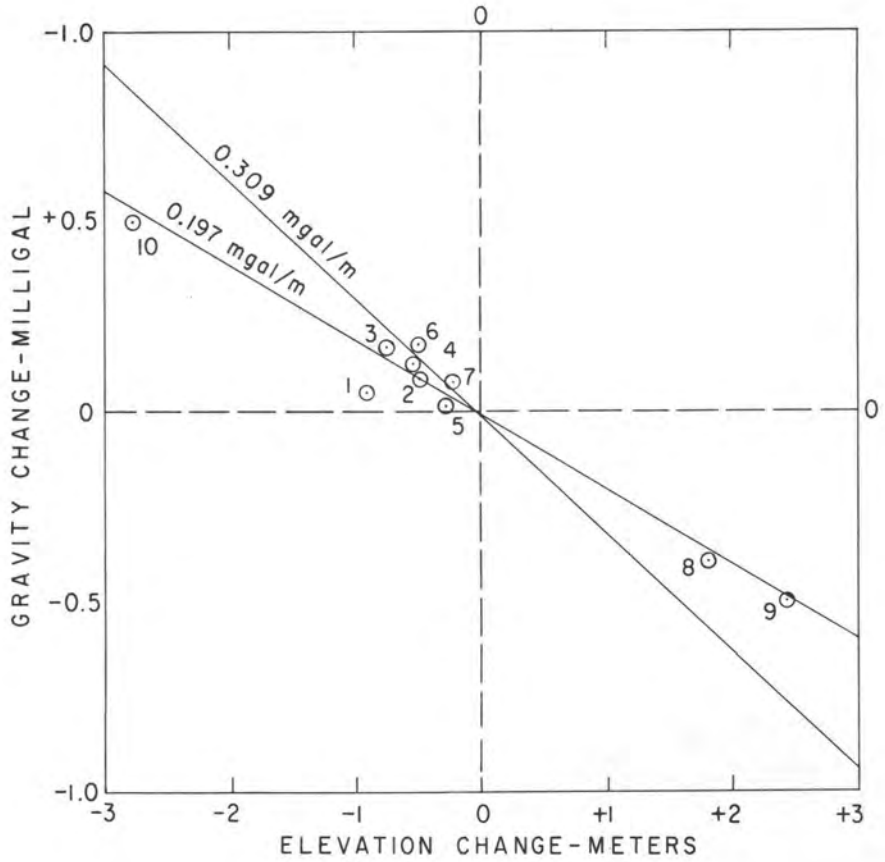
0
-1.0
+0.5
0
-0.5
-1.0
0.309 mgal/m
0.197 mgal/m
10
3
6
4
7
1
2
5
8
9
-3
-2
-1
0
+1
+2
+3
GRAVITY CHANGE-MILLIGAL
ELEVATION CHANGE-METERS

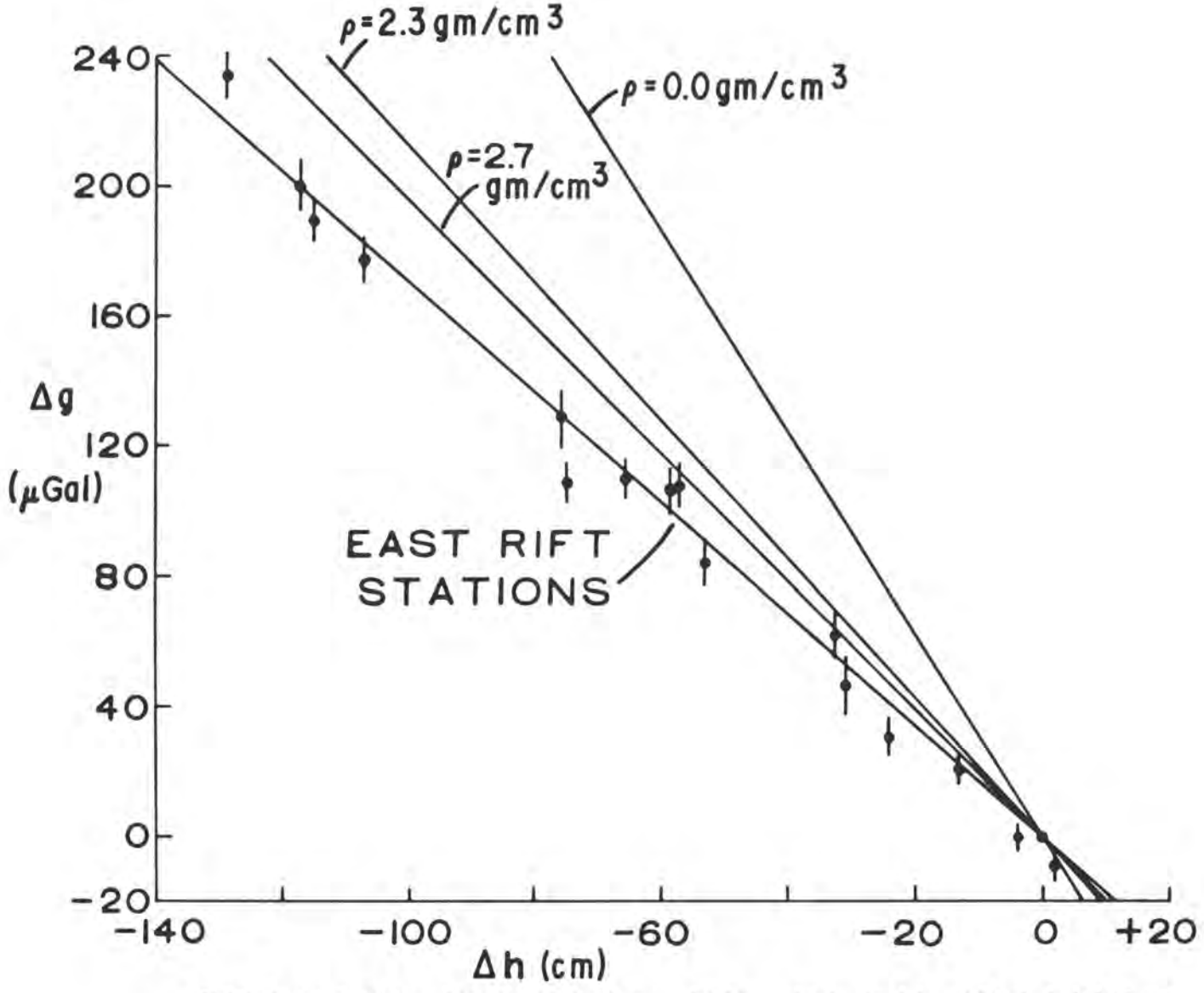

GRAVITY CHANGE VS ELEV. CHANGE

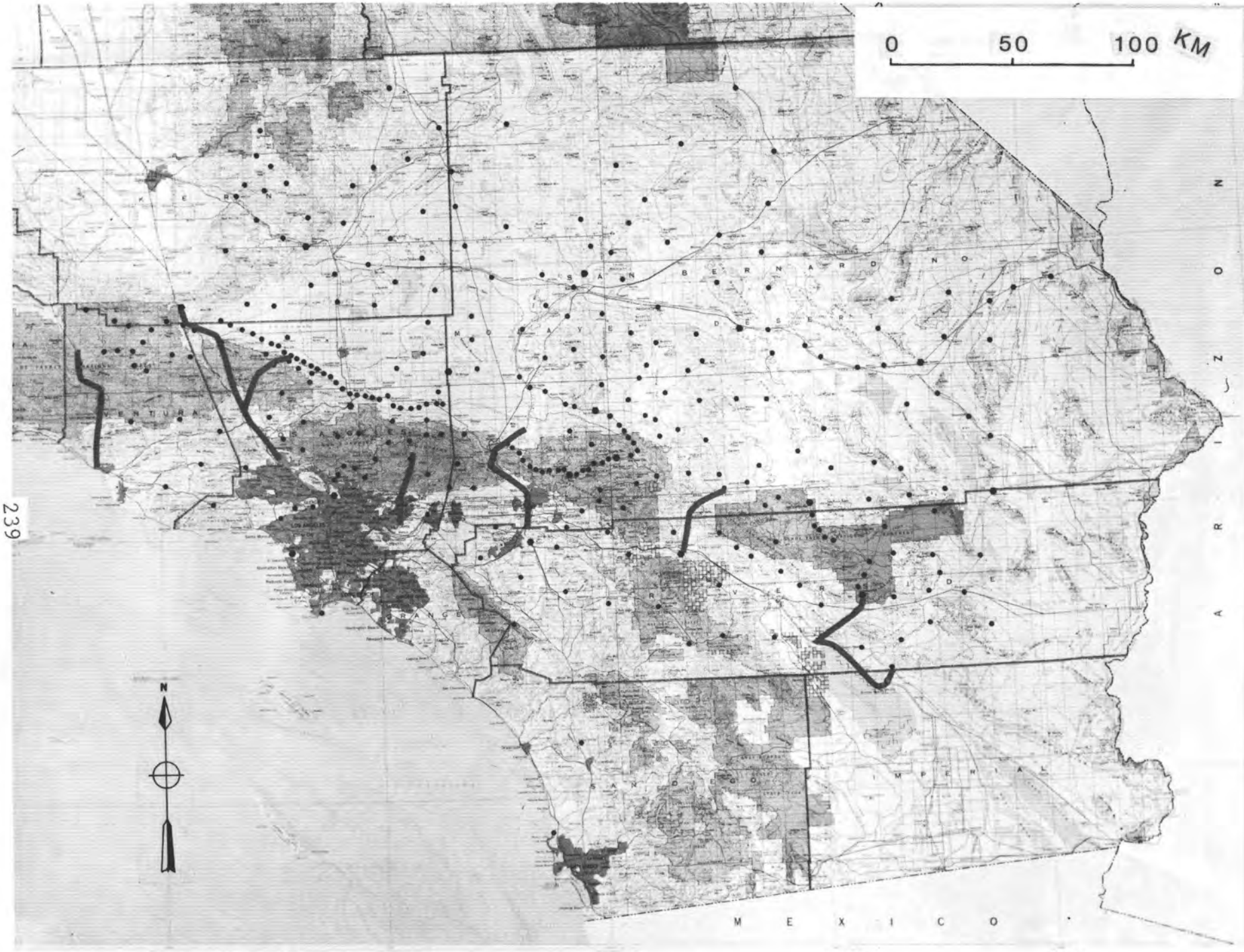
0 50 100 KM
35°
34°
33°
119°
118°
117°
116°
115°
N
239

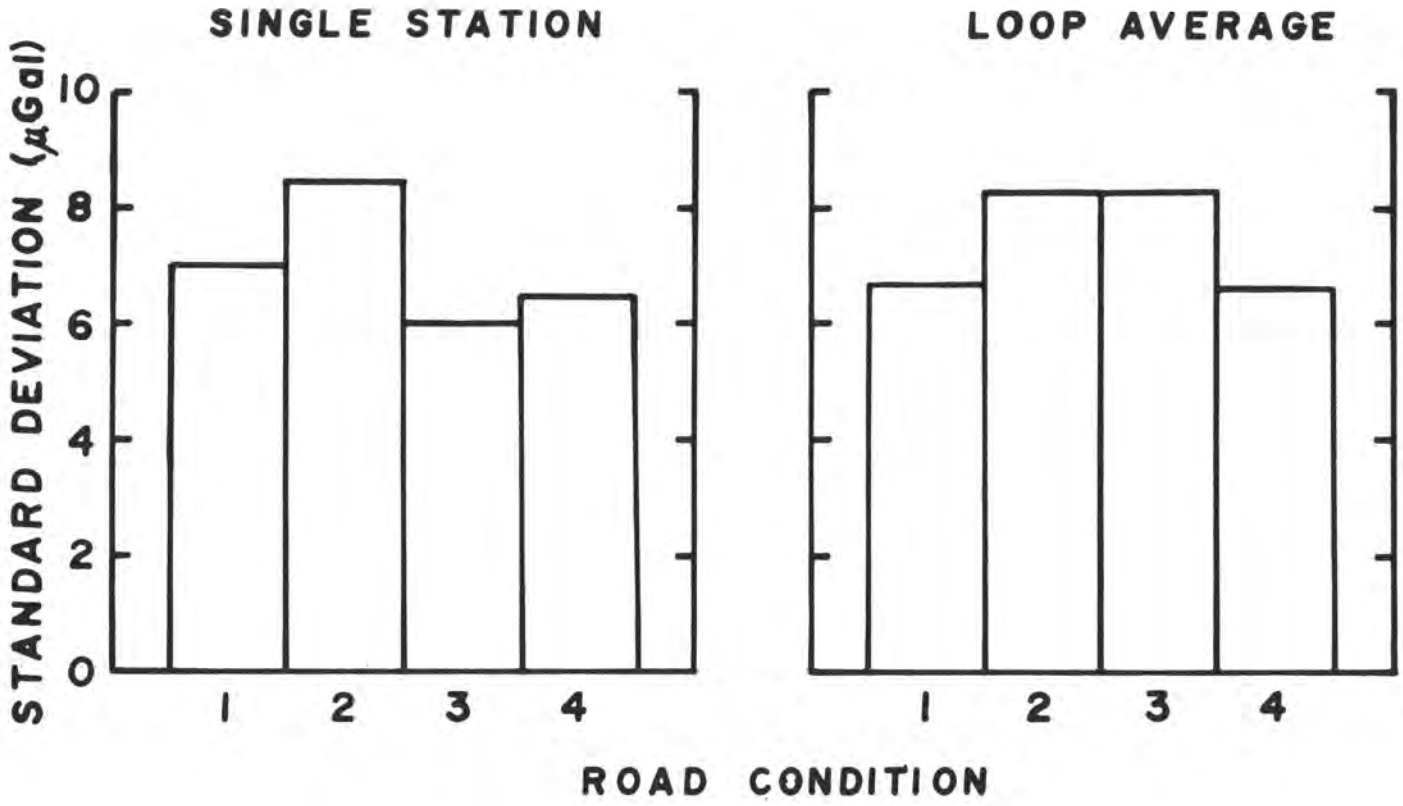
SINGLE STATION
LOOP AVERAGE
STANDARD DEVIATION (μGal)
0
2
4
6
8
10
1
2
3
4
1
2
3
4
ROAD CONDITION

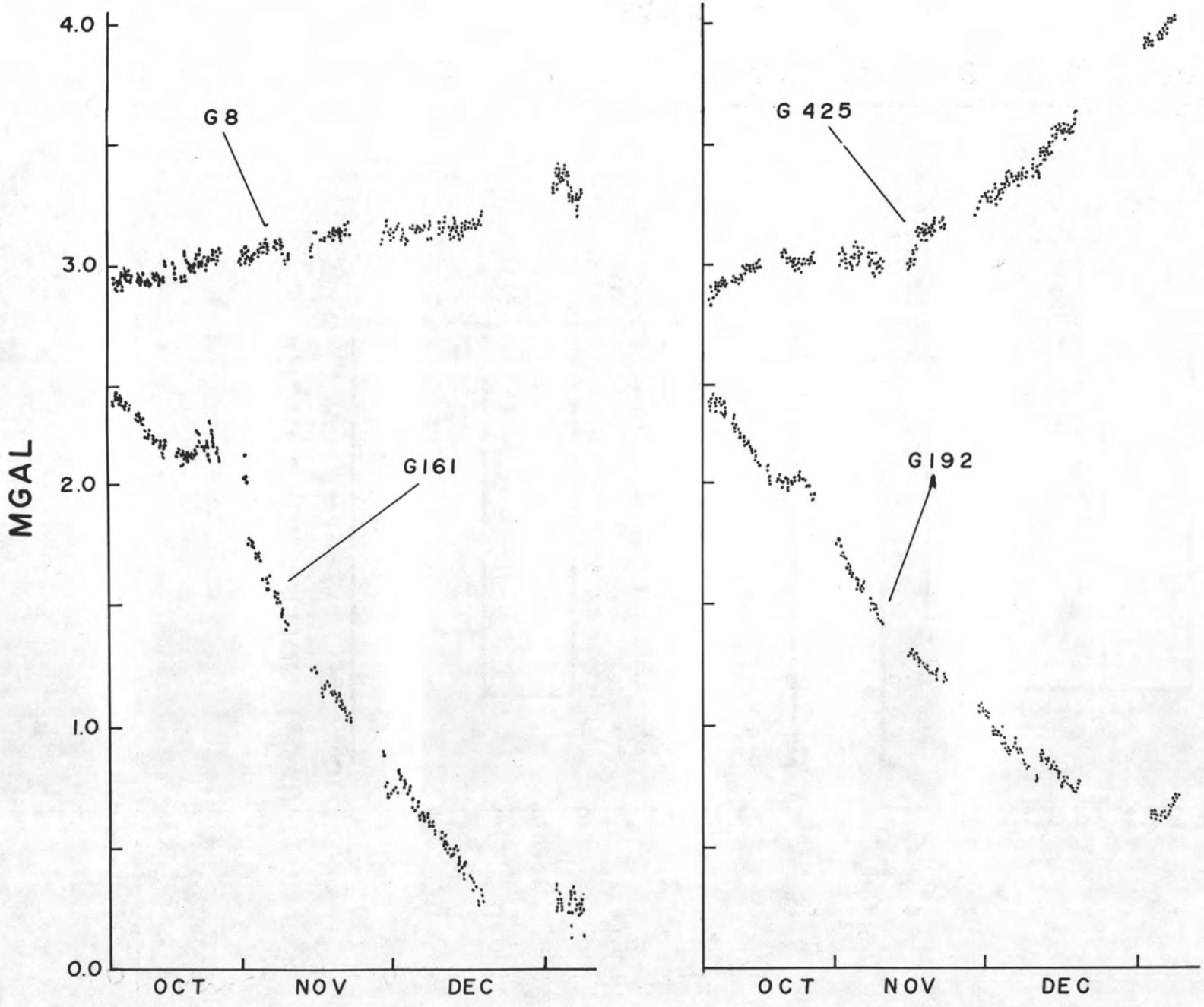
4.0
3.0
2.0
1.0
0.0
MGAL
G8
G161
G 425
G192
OCT
NOV
DEC
OCT
NOV
DEC

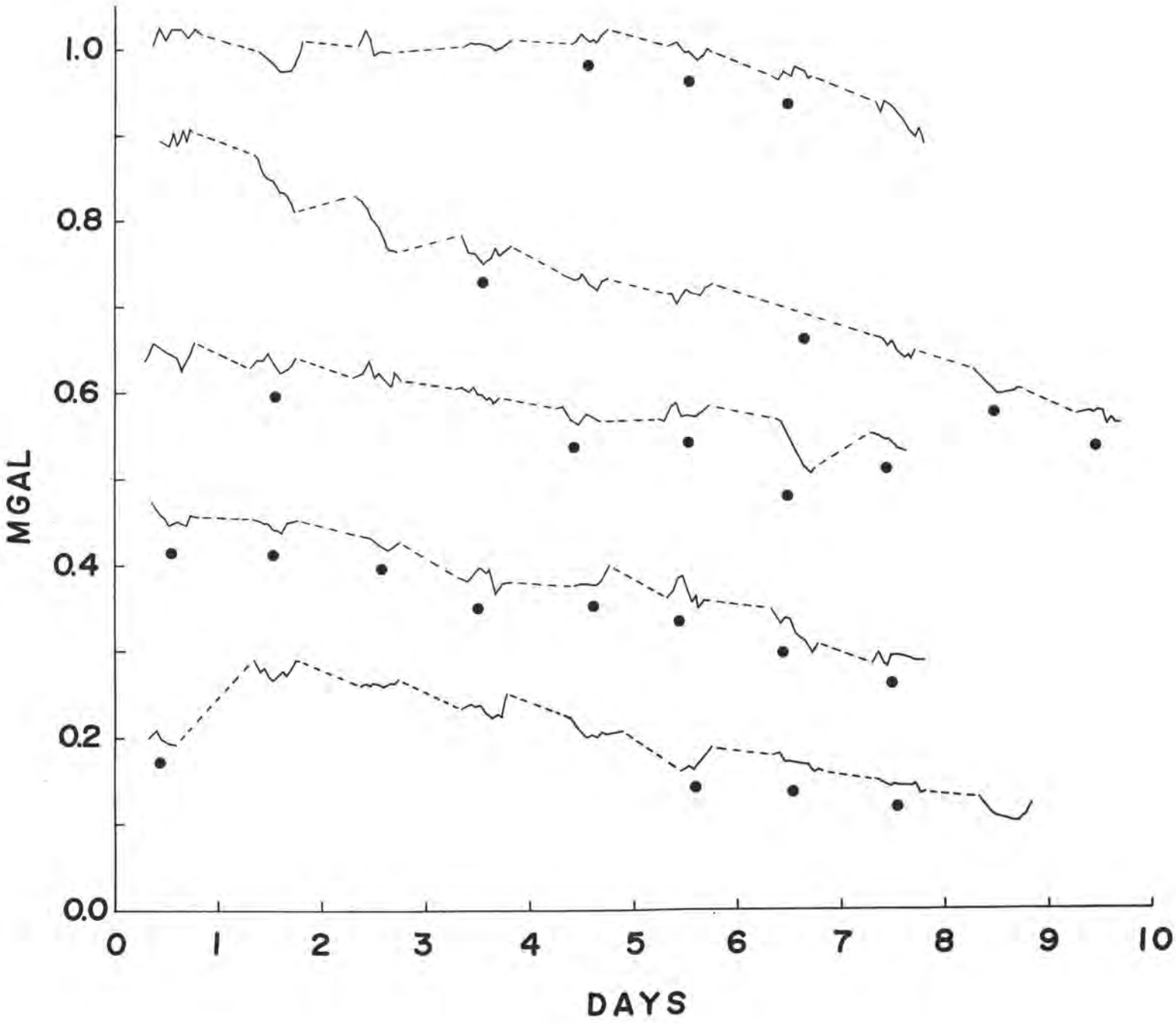
1.0
0.8
0.6
0.4
0.2
0.0
MGAL
0
1
2
3
4
5
6
7
8
9
10
DAYS

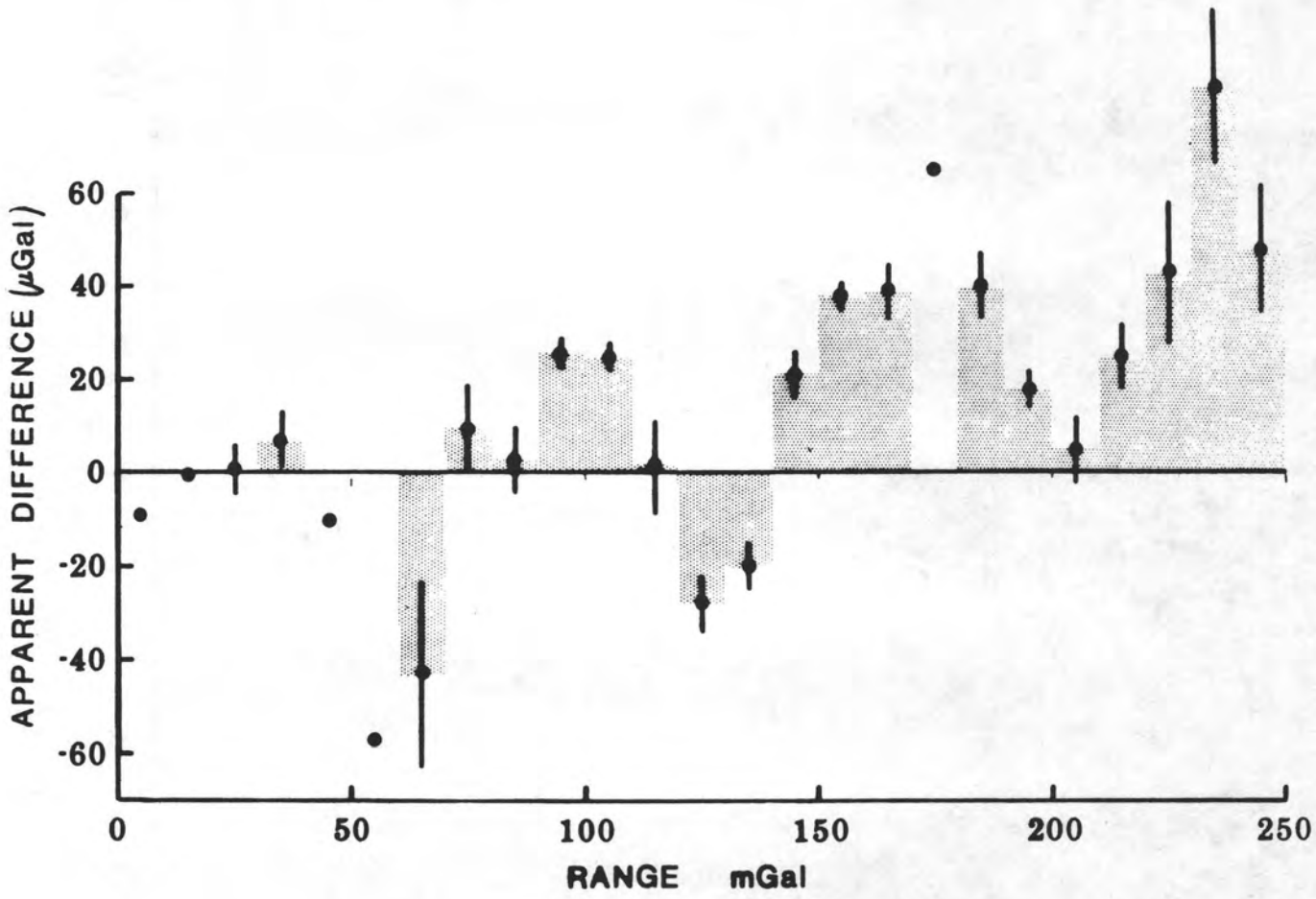
APPARENT DIFFERENCE (μGal)
60
40
20
0
-20
-40
-60
0
50
100
150
200
250
RANGE mGal

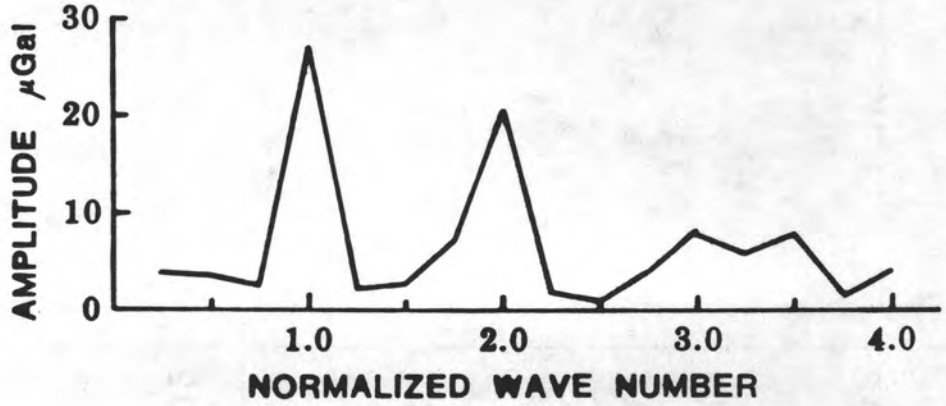
AMPLITUDE μGal
30
20
10
0
1.0
2.0
3.0
4.0
NORMALIZED WAVE NUMBER

DEPARTMENT OF THE INTERIOR
U. S. Geological Survey
345 Middlefield Road
Menlo Park, CA 94025

MEASUREMENTS OF LOCAL MAGNETIC FIELD, OBSERVATIONS OF FAULT CREEP, AND LOCAL EARTHQUAKES ON THE SAN ANDREAS FAULT, CALIFORNIA.

by

M. J. S. Johnston
B. E. Smith
R. M. Mueller

Open-File Report 78-809

ABSTRACT

Simultaneous records of local variations in magnetic field, fault creep and the occurrence times of local earthquakes have been obtained for the period early 1974 through mid-1977 along the San Andreas fault between the most southern extent of the 1906 earthquake fault break and the most northern extent of the 1857 break. The data utilized are primarily from stations located near the two ends of this section of the fault where strains accumulation is expected. The magnetic data show that local magnetic field variations up to 1.8 gammas with durations of a few minutes to several months have occurred. The creep data indicate both episodic events and changes in creep rate of up to 10 mm/yr lasting for six months or more. No clear magnetic transients or offsets are evident either simultaneous with or preceding the occurrence times of the episodic creep events by up to a day or so. Although some patterns of creep onset times at adjacent stations appear to correspond to some periods of longer term change in local magnetic field, these changes do not always occur and other groups of creep events have no corresponding changes in local magnetic field. Earthquakes with magnitudes less than 4.0 do not appear to correspond in time to local changes in magnetic field greater than 0.8 gamma or variations in the creep rate.

In order to explain the observations presented in this study, it appears necessary to allow for a substantial amount of deep aseismic slip without any obvious attendant changes in the time distribution or size of the local earthquakes. Changes in stress related to the surface expression of aseismic slip on the San Andreas fault can be estimated from dislocation models fit to these data and to observations of simultaneous strains and tilts at points near the fault. These stress values are on average less than one bar near the surface but are probably more than 10 bars in localized regions at depths of a kilometer or so.

INTRODUCTION

The history of high-quality magnetic measurements along active faults in California is extremely short. It is interesting but possibly coincidental that, even with this short history, the regions where significant local anomalies have been reported are at or near the ends of the recent major ruptures ($M > 8$) within the fault system. Details of most of the magnetic data can be found in Johnston et al. (1976), and Smith and Johnston (1976).

These data were obtained as part of a U. S. Geological Survey program for measuring total magnetic field along the fault systems with arrays of proton precession magnetometers (Figure 1a). The purpose of this programs is to identify local changes in the magnetic field that might be associated with active faults in the region. Theory and laboratory studies indicate that tectonomagnetic signals should occur as the result of stress induced changes in rock magnetization (piezomagnetic effects) and have been reviewed a number of times previously (e.g., Johnston et al., 1976a; Rikitake, 1976; Smith and Johnston, 1976; Stacey and Banerjee, 1974). The amplitudes and timescales of various other sources of local magnetic field changes are discussed by Johnston et. al (1976a).

Most of the magnetometer stations are located in two areas within the San Andreas fault system: (1) around the south end of the 1906 earthquake fault break, near station SN; and (2) around the north end of the 1857 break, believed to be between stations GD and AG (Figure 1a). The larger earthquakes in this region tend to occur near the ends of these fault breaks. Between these two areas the fault is presently creeping and the recorded earthquakes have magnitudes up to about 5.5. Near the center of the creeping section the rate of recorded creep is relatively high, about 30 mm/yr, but it decays to zero near the ends where strain accumulation is observed (Prescott and Savage 1978).

The continuous magnetometer measurements obtained from the various stations indicate that local changes in the magnetic field with amplitudes as high as 1.8 gammas have occurred (Johnston, et al., 1976a; Smith and Johnston, 1976). Although it appears likely that these changes are produced by piezomagnetic effects, and the largest change has preceded the largest earthquake, we have not yet searched for anomalies that occur simultaneously with local earthquakes less than 10 km distant for which $M < 4.0$ or with surface creep events. This will be attempted in this study.

Creepmeters along the San Andreas fault record short-term creep events which typically last from a few minutes to a few days and have measured displacements of up to 5 mm. It is not yet clear the degree to which these surface creep events reflect aseismic slip that extends down through the whole seismic zone (~15 km deep). Recent studies using arrays of tiltmeters and strainmeters that have recorded near-simultaneous strain events associated with creep events (Johnston, et al., 1976b; McHugh and Johnston, 1976; Mortensen, et al., 1977; Johnston et al. 1977) indicate that the creep seen at the surface probably occurs in the top 2 km of the crust. The short-term

creep events, therefore, probably do not play a significant role in the release of accumulated strain in the seismic zone (2 to 15 km deep). More likely they are just a surface response to deeper slip on the fault. Additional support for this possiblity comes from continuous geodetic strain measurements, obtained near Hollister, over baselines 3 to 9 km long. These data indicate that accelerated slip episodes, lasting for several weeks and extending to a depth of about 10 km, precede surface creep events by several weeks (Slater and Burford, 1978).

In this paper we will try to investigate the likely physical implications regarding changes in stress and other behavior of the fault at depth evident after comparing magnetic, creep and earthquake data from the section of the San Andreas fault between the south end of the 1906 fault break and the north end of the 1857 break.

DATA

The proton precession magnetometers used in this study have a sensitivity and precision of 0.25 gamma. All the magnetometer stations sample the total magnetic field simultaneously, once a minute, $\pm$ 0.2 seconds. The electronics are housed in an insulated fiberglass pit, 1.8 meters deep, buried in the ground so that only the top few centimeters is exposed. The sensor is housed on top of a wooden post about 2 meters above the ground. Each site is selected on the basis of: (1) low magnetic field gradient (~3 gammas/meter), (2) remoteness from any cultural objects that could significantly contaminate the magnetic field, and (3) proximity to known or suspected magnetic rocks adjacent to active faults. Each station automatically samples the total magnetic field, converts the data to a serial digital code, and telemeters the data to Menlo Park, California, via radio links and/or telephone lines. Each total field value is recorded on magnetic tape, and is later transferred to a computer where all data processing is done (Smith et al., 1978).

The diurnal variations of the total magnetic field, due to inospheric and magnetospheric effects, are typically 40 to 60 gammas. Since tectonomagnetic signals are probably not more than a few gammas (Stacey and Banerjee, 1976), it is necessary to reduce the diurnal variations by a factor of 50 or more. To accomplish this reduction, we first calculate the difference between two stations that are separated by less than a few tens of kilometers (usually adjacent stations). Simple differences reduce the diurnal variations generally more than a factor of 10. A five-day average further reduced the diurnal variations to an amplitude of about 0.50 to 0.25 gamma. The magnetic data presented in this paper are either individual samples or five-day running averages of differences between adjacent stations. The five-day running averages have typical standard deviations of about 0.40 gamma. We will discuss only those variations with amplitudes greater than two standard deviations. Two standard deviations for one-minute samples of the 0.80 gamma) magnetic field differences are typically less than two gammas. A summary of data obtained during the last 5 years is shown in Figure 1b.

The creep data used in this study are from the wire creepmeter network established by the U. S. Geological Survey (Yamashita and Burford, 1973, Nason et al., 1974; Schulz et al., 1976). More than 90 creep events have occurred since early 1974 at several creepmeter sites within an array of recording differential magnetometers. Figure 1 shows the location of recording magnetometers and creepmeters along the section of the fault where creep events occur. Table 1 lists the occurrence time, creep amplitude, and the distance to the nearest magnetometer for all the events considered at each creepmeter. Further details of creep events at these meters are listed in Schulz et al. (1976). The magnetizations of rocks in this area are typically in the range 10^{-4} to 10^{-3} e.m.u. In a few places they exceed 10^{-2} e.m.u.

For more than 60 of these creep events, concurrent magnetic field data have been obtained. Figure 2 shows three days of one-minute samples of magnetic difference-field and total-field data bracketing the times of the three largest creep events for which simultaneous data exist at the creepmeters XMR1, XFL1, XPR1, and CWC and at magnetometers around these creepmeters. The total-field record chosen in each case is the one closest to the creepmeter.

It is apparent that no clear magnetic transients greater than about 1 gamma have been observed simultaneous with or preceding these creep events by up to a day or so other than might be expected by pure chance. There are also no systematic offsets. For a number of the large creep events 10-minute and one-hour averages of the magnetic field differences have been calculated in order to reduce the noise. These data have the standard deviations less than 0.7 and 0.4 gammas respectively, for the periods around the times of the creep events. Transients or offsets of consistent form related to creep events are still not evident. With signal stacking and other filtering techniques it may be possible to reduce the noise in the data further. These techniques have not yet been applied comprehensively to the magnetic field data.

Of particular interest on Figure 2 are the data obtained at creepmeter XFL1 and the magnetometer LE, since the magnetometer is less than 300 meters from the creepmeter. It might be expected that correspondence between creep events and magnetic transients would be seen most clearly in these data. It is not apparent that this is the case for these data or in longer term averages where the resolution is greater. Figure 3 shows similar plots of data during the three largest creep events for which simultaneous data was obtained on the four creepmeters and magnetometers in the northern part of the array.

The broader questions, whether deeper slip on the fault might trigger earthquakes, episodes of local surface failure or change the long-term creep rate, are still open. Five creepmeters (XSJ2, XPR1, XFL1, XMR1 and XGH1) were chosen for this study on the basis of nearness to magnetometer stations and completeness of data (Figure 1). The creep data from these instruments show that right-lateral fault creep occurs at an approximately constant rate for the time frame of this study. In order to determine whether changes in creep rate correspond to changes in magnetic field, the average rate from these

records has been removed by determining the best linear fit to the data and subtracting this line from the original values; a technique similar to that employed in a previous investigation of the relationship between creep rate and moderate earthquakes (Burford, 1976). The detrended creep data show the small variations of creep rate much more clearly than do the untreated data.

The earthquake data used in this study are from the unpublished earthquake catalog compiled by the U. S. Geological Survey. A lower magnitude cutoff of 1.3 was chosen because it is the lowest magnitude that is likely to provide a complete data set in the regions studied. The earthquakes were then chosen to include only those that appeared to have occurred on the San Andreas fault and within 8 kilometers of a magnetometer station. Where adjacent magnetometers were located closer than 16 km apart, the set of earthquakes was further divided to include only the earthquakes closest to each magnetometer station. The earthquake sets are denoted by "earthquakes near (station code name)". The largest earthquake included in this study has a magnitude of 3.9, and the rate of occurrence of earthquakes below magnitude 3.0 is fairly steady. The earthquakes show little variation in magnitude with time. Therefore, in order to show more clearly what may be the more relevant earthquakes in terms of association with tectonomagnetic signals, we have chosen to plot earthquake moment.

The comparison of magnetic data, creep data, and earthquakes was made by plotting all three of these parameters on the same time scale. For the time period and regions included in this study, local changes in the magnetic field greater than 0.8 gamma occur only on the following difference records: SJ-HA, LE-HA, LE-BV, and LG-GD. All four of these difference records are shown in Figures 4, 5, 6 and 7, along with the most relevant plots of detrended creep data and earthquake moments. Gaps in the magnetic and creep data indicate periods where data were lost owing to a variety of reasons. In all cases we believe that the absolute reference has been maintained so that changes that span these gaps can be considered real.

A significant change in magnetic field on the SJ-HA record occurred during October 1974, lasted for the whole month, and had a maximum amplitude of 1.8 gamma (Figure 4). By comparison with other difference records, we know that this change was recorded at station SJ. Because the change was recorded only at station SJ, its source is probably within a few kilometers of this station. Unfortunately, the nearest creepmeter, XSJ2, was not operational until early November 1974. There are no obvious correlations between the XSJ2 creep data, the earthquakes near SJ, and the magnetic field record SJ-HA.

The local changes in magnetic field in October 1974 did occur one month prior to a magnitude 5.1 earthquakes (Smith and Johnston, 1976). This earthquake is not shown in the plotted earthquake data because it occurred to the east of the San Andreas fault and about 11 kilometers from station SJ. Because of the distance between the earthquake and the probable source of the magnetic field changes and the lack of a magnetic signal at the time of the earthquake, there is probably no direct relation between them. However, the magnetic field change could be explained by aseismic slip on the San Andreas

fault that may be related to the magnitude 5.1 earthquake by an interaction of the faults in the area, as discussed in detail by Smith and Johnston, (1976).

The difference record LE-HA (Figure 5) shows a magnetic signal with a maximum amplitude of 1.7 gammas occurring during the period June to August, 1975. Comparison with other difference records indicates that signals were recorded at both LE and HA, but in the opposite sense so that the difference LE-HA has the effect of adding the changes from these two stations. The character of the changes recorded at HA and LE can be seen to be dissimilar by comparing the SJ-HA (Figure 4) and LE-BV (Figure 6) records. The change at HA is positive and mostly smooth while the change at LE is negative, starts with a sudden event, and then is smoother. The correspondence in time of these magnetic field changes suggest that they may have the same or a related source.

The creep data plotted with the LE-HA record are from station XPR1. The creep events at this station occur fairly regularly. With a 120-day running average (heavy line), it is possible to smooth these events and emphasize the long-term character of the creep data (Figure 5). The average creep data show that only during the second half of 1975 was the creep rate significantly less than the average rate for the period of time included in this study. The start of the decrease in creep rate occurs during the change in magnetic field at stations LE and HA discussed above. The long-term trends of the averaged creep data from station XFL1 appear to be almost identical to XPR1, except that almost a year of data is missing starting from mid-1975. Both the XFL1 and the XPR1 data show that the creep rate at these stations was below average between mid-1975 and mid-1976, although the exact character of the change at XFL1 cannot be determined because of the missing data.

The plot of earthquakes near HA (Figure 5) does not show any apparent correspondence to the LE-HA record. It is interesting to note that the larger earthquakes occur during times of higher than average creep rate. The plot of earthquakes near LE shows a faily even rate of earthquakes up to magnitude 3.2 with no apparent correspondence to either the creep data or the LE-HA magnetic record.

There do appear to be some interesting correspondences between the LE-BV and XMR1 records. The difference record LE-BV (Figure 6) shows three significant magnetic field changes. One change of short duration and 1 gamma amplitude in September 1974 was recorded at station BV. The second change, occurring in mid 1975, was recorded at station LE and is the same signal discussed above in the section covering the LE-HA record. The third change, in late 1976 and early 1977, was one of complex character that appears to be recorded primarily at station LE. The detrended creep data from XMR1 have been smoothed with a 120-day running average, and both the original and smoothed data (heavy line) are plotted together in Figure 6. The average rate of creep decreased slightly at the end of 1974 and then sharply increased by 10 mm/yr during the first half of 1975. The long-term trends on both records are approximately mirror images of each other. The two short-term changes in October 1974 and June 1975 approximately bracket in time the high rate of

creep during the first half of 1975 and also occur within one day of creep events. (Because of telemetry failures, the exact time and duration of these changes in magnetic field cannot be determined.) However, all but the October 1974 signal on the LE-BV record were recorded at station LE, 11 kilometers northwest of creepmeter XMR1. There does not appear to be any significant correspondence between the earthquakes near BV and the LE-BV record or the XMR1 record.

The LG-GD record shows a 1.5 gammas change in magnetic field during the second half of 1976 (Figure 7). This change was recorded at station GD. The first data from stations LG and GD were obtained in June 1976, so that the time when this change began is not known. A creep event at XGH1 and a magnitude 3.9 earthquake, the largest to occur within 8 kilometers of station GD during the record period, occurred just after the end of the change in magnetic field (Figure 7).

DISCUSSION

The data presented in this study indicate that small-magnitude earthquakes do not correspond in time with the change in either the magnetic field or the creep rate. This fact is not too surprising since earthquakes in California or the size included in this study ($1.3 < M < 3.9$) appear to have slip dimensions of less than 1 kilometer (Bakun et al., 1976), stress drops of less than 20 bars, and depths of between 5 and 10 km (Thatcher and Hanks, 1973; Wesson, et al., 1973). Assuming a magnetic susceptibility of 10 e.m.u., tectonomagnetic models (Johnston, 1978) using the above parameters show that these earthquakes would not, by themselves, generate a surface anomaly greater than 0.1 gamma. Of course, if the earthquake is accompanied or triggered by larger scale readjustments of regional stress, then these could be reflected in the magnetic data. These stress changes could result, for example, from related aseismic slip on the fault (Stuart and Johnston, 1974) or be a consequence of the initial stress conditions near the fault. These conditions might be modified by earthquakes or other fault behavior such as pore pressure changes, comminution, and chemical changes. In either case, the changes in magnetic field would not necessarily be expected to occur at the same time as earthquakes.

Another general observation evident in these data is that the large majority of short-term creep events do not correspond to changes in magnetic field. This is consistent with expectations from tilt and strain measurements near active faults during creep events (Johnston et al, 1976b, McHugh and Johnston, 1976; Mortensen et al., 1977 Johnston et al., 1977) that the surface failure is of only limited extent, typically less than 1 km square. For this slip area and for typically slip amplitudes of a few mm, the maximum change in mean shear stress is about 0.2 bars and expected tectonomagnetic anomalies are less than 0.1 gammas (Johnston et al., 1978).

Large changes in magnetization have been reported in laboratory samples where deviatoric stress are in the kilobar range (Nagata and Carleton, 1968; Martin and Wyss, 1975) If these experiments model fault-zone behavior, then similar linear and nonlinear irreversible behavior might be expected in the

material near and on the fault face during failure (creep event). This should be easily detected on nearby sensitive magnetometers. These effects are not observed at sites as close as 270 meters from sections of the fault where creep events occur. The zone where failure is occurring, where grains of magnetic material are being reoriented and where the domain structure is changing, must therefore be quite narrow, typically less than a few tens of meters or the effects occurring in the laboratory experiments of Martin and Wyss (1975) do not occur in the natural situation.

Models of spatially varying aseismic slip over a larger area at depths between 2 and 10 km can be fit to the creep data and used to generate tectonmagnetic models that satisfy the magnetic data. However, it is obvious from these models that two main but opposing factors are in effect. On one hand to get observed changes in magnetic field for the observed magnetizations and stress sensitivities, it is necessary to have stress changes of more than a bar over quite a large volume. This can be most easily illustrated with the simplified model derived by Stacey (1969) in which the surface field anomaly ΔF in gammas is approximately given by

$$\Delta F \approx 80 I \sigma \qquad (1)$$

where σ is the change in mean stress and I is the total magnetization of the rocks in the region. For typical values of I and ΔF of 10^{-3} e.m.u. and 1 gamma respectively, the required change in mean stress is about one bar. On the other hand, this change in stress over a wide area implies large strains of at least 3 μstrain. The observation of geodetically determined shear and volume strain in this region on lines 10 to 20 km in long (Prescott and Savage, 1978) independently limits the allowed strain during the measurement period to less than one μstrain. Decreasing the size of the region in which stress perturbations are occurring (to perhaps a kilometer or so) in order to satisfy the geodetic data requires increased stress changes (in excess of 10 bars). Also, increasing the depth for fixed geometry requires rapidly escalating stress amplitudes to give the same surface anomaly. The important implication of these models are that, if the magnetic data are to be explained by stress perturbations, the source is probably quite localized (i.e. less than 5 km from AN), and the changes in stress are probably more than about 10-bars. We would argue, therefore, for a fault on which large heterogeneities in stress occur. The correspondence in time between the long-term creep rate at XMR1 and the changes in magnetic field recorded at LE, 11 kilometers to the northwest, is perhaps a good example of how these models might work. If a patch of the fault were slipping, stress concentration would be expected at the edges of this patch. If the patch is centered at XMR1 and extends northwest to a point near LE, then it would not be unreasonable to expect a change in creep rate at XMR1 to be related to a magnetic field change at LE. As more data become available, it will be possible to test and extend these models and their implications further. The occurrence of a moderate magnitude earthquake that breaks a substantial part of the seismic zone will also provide critical data on the amplitudes and interrelationship of the magnetic, creep, seismic and other data.

It is important to question whether any of the general fault models are precluded by these observations. Regardless of the details, the simplest general models of the fault in which the slip is assumed to be uniform or where slip occurs only during earthquakes, are certainly not consistent with these data. The intriguing patterns of behavior at, for example, GD, when a creep event and a magnitude 3.9 earthquake occurred shortly after the end of a change in magnetic field (Figure 7), and at LE and HA in 1975 during periods of retarded creep on nearby XPR1 and XFL1 creepmeters and of accelerated creep on XMR1 (Figure 5, and 6), argue for more complex and heterogeneous fault mechanics.

CONCLUSIONS

1. Local variations in magnetic field with amplitudes as high as 1.8 gammas occur within the seismically active segment of the San Andreas fault between the south end of the 1906 earthquake fault break and the north end of the 1857 break.

2. Long-term detrended creepmeter records along this section of the San Andreas fault show significant changes in creep rate (up to 10 mm/yr) lasting for several months.

3. Earthquakes with magnitude less than 4.0 do not appear to correspond in time to local changes in magnetic field greater tha 0.8 gamma or long-term variations in creep rate.

4. In contrast to the measurements reported by Breiner and Kovach (1968), magnetic field changes apparently do not occur clearly before episodic fault creep events at a measurement resolution of 0.5 gammas for hour averages and 3 gammas for 1-minute samples. This is consistent with expectations that stress-induced magnetic changes should not be observable for the small localized stress changes inferred from simultaneous observations of fault creep, and tilt, and strain around the creep occurrence point.

The long-term changes in creep rate show an approximate correspondence in time and space to some long-term changes in magnetic field. The data are too sparse to determine the significance of these apparent correspondences.

6. For fault models to explain the observations presented in this study, it appears necessary to allow for local heterogeneities in stress without any obvious attendant changes in the time distribution or size of the local earthquakes. These stress values are on average less than one bar near the surface but are probably more than 10 bars in localized regions at depths of a kilometer or so.

REFERENCES

Bakun, W. K., C. G. Bufe, and R. M. Stewart, 1976, Body wave spectra of central California earthquakes, Bull. Seis. Soc. Am., 66, 363-384.

Breiner, S. and Kovach, R. L., 1968, Local magnetic events associated with displacement along the San Andreas fault (California). Tectonophysics, v. 6,: 69-73.

Burford, R. O., 1976, Fluctuations in rates of fault creep associated with moderate earthquakes along the central San Andreas fault, EOS (Trans. Am. Geophys. Un.) 57, p. 1012.

Burford, R. O., S. S. Allen, R. J. Lamson, and D. D. Goodreau, 1973. Accelerated fault creep along the central San Andreas fault after moderate earthquake during 1971-1973, in Tectonic Problems of the San Andreas Fault System: Stanford Univ. Publ. Geol. Sci., 13: 268-274.

Johnston, M. J. S., 1978, Local magnetic field variations and stress changes near a slip discontinuity on the San Andreas fault, J. Geomag. Geoelec., (in press).

Johnston, M. J. S., A. C. Jones, and W. Daul, 1977. Continuous Strain measurements during and proceeding creek events, J. Geophys. Res., 82, 5683-5691.

Johnston, M. J. S., B. E. Smith and R. J. Mueller, 1976a, Tectonic experiments and observations in western U.S.A., J. Geomag. Geoelec., 28, 85, 95.

Johnston, M. J. S., S. McHugh, and R. O. Burford, 1976b, On simultaneous tilt and creep observations on the San Andreas Fault, Nature, 260, 691-693.

Johnston, M. J. S., B. E. Smith and R. O. Burford, 1978, Local magnetic field measurements and fault creep observations on the San Andreas fault, Tectonophysics, (in press).

Martin, R. J. and Wyss, M., 1975, Magnetism of rocks and volumetric strains in uniaxial failure tests: Pure and Appl. Geophysics, v. 113, p. 52-61.

McHugh, Stuart and Malcolm Johnston, 1976, Short period nonseismic tilt perturbations and their relation to episodic slip on the San Andreas fault, J. Geophys. Res., 81, 6341-6345.

Mortensen, C. E., R. C. Lee and R. O. Burford, 1977, Simultaneous tilt, strain, creep, and water level observations at the Cienega Winery south of Hollister, California, Bull., Seismol. Soc. Amer., 67, 641-560.

Nagata, T. and B. Carleton, 1968, Notes on piezoremanent magnetism of igneous rocks, J. Geomag. Geoelec. 20: 115-127.

Nason, R. D., Philippsborn, F. R. and Yamashita, P. A., 1974, Catalog of creepmeter measurements in central California from 1968 to 1972 - Open File Report #74-31, U. S. Geological Survey.

Prescott, W. H. and J. C. Savage, 1978, Strain accumulations rates in the western United States between 1970 and 1976: Journal of Geophysical Research (in press).

Rikitake, T., 'Earthquake Prediction', (Amsterdam, Elsevier, 1976).

Schulz, S. S., Burford, R. O. and Nason, R. D., 1976, Catalog of creepmeter measurements in central California from 1973 through 1950 Open File Report #77-31, U. S. Geological Survey.

Slater, L. E. and R. O. Burford, 1978, A comparison of long-baseline strain data and fault creep records obtained near Hollister, California, Tectonophysics (in press).

Smith, B. E. and M. J. S. Johnston, 1976, A tectonomagnetic effect observed before a magnitude 5.2 earthquake near Hollister, California, Journal Geophysical Research, 81, 3556-3560.

Smith, B. E., M. J. Johnston, R. O. Burford and R. J. Mueller, 1978, Magnetic field changes, earthquakes and creep events along the San Andreas fault, 1974-1977, J. Geomag. Geoelec. (in press).

Stacey, F. D., 1964, The seismomagnetic effect, Pure Applied Geophysics, 58, 5-22,

Stacey, F. D., and S. K. Banerjee, 'The physical principles of rock magnetization', (Amsterdam, Elsevier, 1974).

Stuart W. D., and M. J. S. Johnston, 1974. Tectonic implications of anomalous tilt before central California earthquakes, EOS (Trans. Am. Geophys. Un.) 56, 1196.

Talwani, P. and R. L. Kovach, 1972, Geomagnetic observations and fault creep in California, Tectonophysics, 6, 69-73.

Thatcher, W. and T. C. Hanks, 1973, Source parameters of southern California earthquakes, Journal Geophysical Research, 78, 8547-8576.

Wesson, R. L., R. O. Burford and W. L. Ellsworth, 1973, Relationship between seismicity, fault creep and crustal loading along the central San Andreas fault, in Prodeedings of the Conference on Tectonic Problems of the San Andreas Fault System, edited by R. L. Kovach and A. Nur. p. 303-321, School of Earth Sciences, Stanford University, Stanford, California.

Yamashita, P. A., and R. O. Burford, 1973, Catalog of preliminary results from an 18-station creepmeter network along the San Andreas fault system in central California for the time interval June 1969 to June 1973, U. S. Geological Survey Open File Report, 215 p.

FIGURE AND TABLE CAPTIONS

Figure 1a. Locations of recording proton precession magnetometers and creepmeters along the San Andreas fault.

Figure 1b Summary of data obtained during the last 5 years.

Figure 2. Plots of total field, differenced magnetic field, and fault creep for three days spanning the three largest events at XMR1, XFL1, XPR1, and CWC, for which simultaneous records exist.

Figure 3. Plots of total field, differenced magnetic field, and fault creep for three days spanning the three largest events at CWN, HRS, XSJ1 and SHN.

Figures 4-7 are plots of magnetometer differences (top), detrended creep (center) and earthquake moments (bottom). Labels on detrended creep data indicate station code name and average creep rate that was removed from original data. Gaps in both magnetic and creep data represent periods of no data, but absolute reference is believed to have been maintained so that changes that span these gaps can be considered real. The plots of creep data on Figure 3 and 4 also include 120-day running averages (heavy lines). The label for earthquake data indicates nearest magnetometer station (see text). Moments are in dyne-cm, and a magnitude scale is included.

Table 1 Creep meter identification codes, locations, and distances from the nearest recording magnetometer with occurrence times, dates and amplitudes of recorded creep events.

TABLE 1

Creepmeter and location	Creep event occurrence time (GMT)	Date	Amplitude (mm)	Nearest magneto-meter	Distance to nearest magnetometer (km)
XMR1					
(36°35.7'N,	1508	Jan 10, 1974	2.5	BV	1.54
121°11.2'W	0057	Jan 29, 1974	1.9		
	0015	Apr 14, 1974	2.9		
	1808	Jul 11, 1974	3.0		
	0837	Oct 03, 1974	2.3		
	1221	Feb 02, 1975	2.9		
	1617	Mar 07, 1975	1.1		
	0826	Apr 14, 1975	2.0		
	2134	Jun 29, 1975	2.5		
	1830	Oct 27, 1975	2.4		
	1256	Jan 25, 1975	1.7		
	1114	Apr 16, 1976	2.5		
	1902	Jul 29, 1976	2.3		
	0522	Nov 11, 1976	2.8		
XFL1					
(35°39.9'N,	1850	Jan 13, 1974	0.8	LE	0.27
121°16.3'W)	2323	Feb 01, 1974	1.7		
	1355	Jun 16, 1974	3.1		
	1828	Nov 24, 1974	1.5		
	2153	May 14, 1975	2.4		
	0354	Sep 29, 1975	1.9		
XPR1					
(36°43.4'N,	0058	Feb 25, 1974	2.0	LE	9.3
121°20.9'W)	1102	Mar 16, 1974	1.3		
	0119	Jun 07, 1974	0.7		
	0751	Jun 21, 1974	1.0		
	0243	Jul 27, 1974	1.3		
	0329	Aug 04, 1974	0.6		
	2200	Oct 21, 1974	0.7		
	1836	Oct 30, 1974	1.3		
	1611	Feb 15, 1974	2.4		
	0755	May 19, 1975	1.0		
	1137	May 21, 1974	1.3		
	0809	Jun 10, 1975	1.0		
	1815	Oct 04, 1975	2.3		
	2154	Nov 02, 1975	0.9		
	0745	Feb 09, 1975	0.2		
	1818	Mar 30, 1975	1.9		
	2048	Apr 20, 1975	2.2		
	1005	Aug 08, 1975	0.8		
	1925	Aug 30, 1975	1.6		
	1608	Sep 10, 1975	1.9		

Continue - Table 1

Creepmeter and location	Creep event occurrence time (GMT)	Date	Amplitude (mm)	Nearest magneto-meter	Distance to nearest magnetometer (km)
CWC					
(36°45.0'N,	1042	Apr 16, 1974	1.2	HA	5.9
121°23'W	0648	Jul 16, 1974	1.8		
	1902	Feb 16, 1975	2.9		
	0413	Feb 21, 1975	1.1		
	1458	Apr 10, 1975	4.1		
	1713	Sep 09, 1975	3.0		
	1519	Sep 28, 1975	1.9		
CWN					
(36°45.0'N,	0330	Apr 10, 1974	0.4	HA	5.9
121°23.1'W	0000	Aug 31, 1974	2.5		
	1902	Feb 16, 1975	2.9		
	0413	Feb 21, 1975	1.8		
	0413	Jun 20, 1975	3.1		
	2152	Sep 17, 1975	1.4		
	1940	Sep 28, 1975	2.5		
	1445	Apr 10, 1975	4.2		
	1521	Sep 28, 1975	2.0		
	1501	Dec 01, 1975	0.2		
HRS					
(35°45.3'N,	1315	Jan 07, 1975	2.2	HA	2.4
121°25.3'W)	0451	Mar 27, 1974	2.2		
	1200	Jul 22, 1974	2.3		
	0804	Aug 03, 1974	1.1		
	1922	Sep 14, 19741	0.9		
	1520	Sep 17, 1975	2.4		
	1339	May 10, 1976	2.4		
	0314	Sep 21, 1976	-0.6		
	1913	Sep 28, 1976	1.5		
	0413	Sep 29, 1976	1.0		
XSJ2					
(35°50,2'N,	2301	Nov 28, 1974	0.3	SJ	2.63
121°31.2'W)	0516	May 27, 1975	4.03		
	1034	Oct 01, 1975	2.6		
	0243	May 15, 1976	4.9		
SJN					
(36°51.3'N)	2339	Nov 28, 1975	0.9	AN	5.47
121°32.7'W)	1113	Feb 03, 1975	1.1		
	0813	Feb 15, 1975	0.1		
	1138	Mar 03, 1975	0.6		

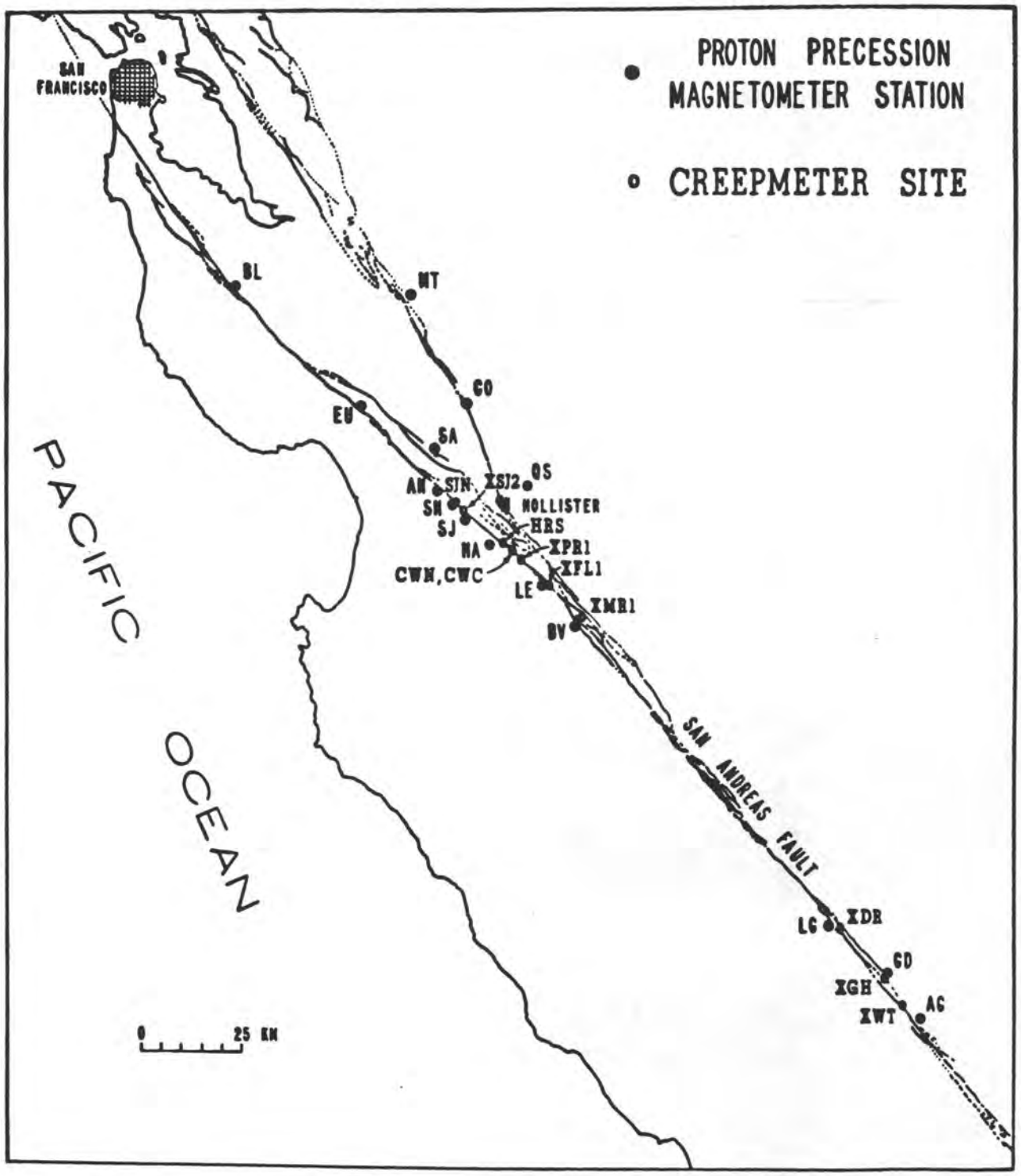
PROTON PRECESSION MAGNETOMETER STATION
CREEPMETER SITE
SAN FRANCISCO
BL
MT
CO
EU
SA
AN
SIN
XSJ2
OS
SN
HOLLISTER
SJ
HRS
HA
XPR1
CWN, CWC
XFL1
LE
XMR1
BV
SAN ANDREAS FAULT
LG
XDR
GD
XGH
AC
XWT
PACIFIC OCEAN
0
25 KM

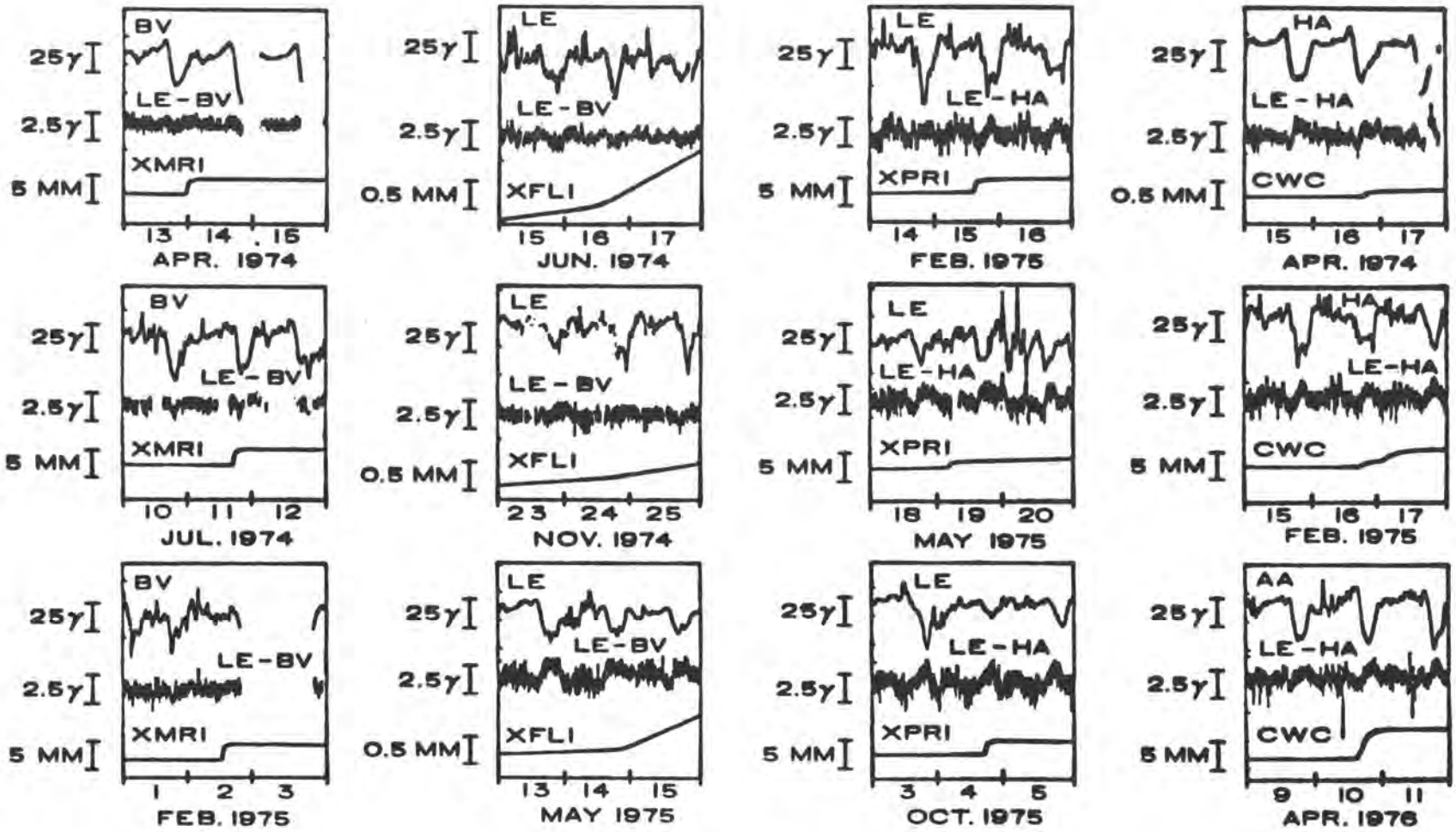
BV
25γ
LE-BV
2.5γ
XMRI
5 MM
13 14 15
APR. 1974
LE
25γ
LE-BV
2.5γ
XFLI
0.5 MM
15 16 17
JUN. 1974
LE
25γ
LE-HA
2.5γ
XPRI
5 MM
14 15 16
FEB. 1975
HA
25γ
LE-HA
2.5γ
CWC
0.5 MM
15 16 17
APR. 1974
BV
25γ
LE-BV
2.5γ
XMRI
5 MM
10 11 12
JUL. 1974
LE
25γ
LE-BV
2.5γ
XFLI
0.5 MM
23 24 25
NOV. 1974
LE
25γ
LE-HA
2.5γ
XPRI
5 MM
18 19 20
MAY 1975
HA
25γ
LE-HA
2.5γ
CWC
5 MM
15 16 17
FEB. 1975
BV
25γ
LE-BV
2.5γ
XMRI
5 MM
1 2 3
FEB. 1975
LE
25γ
LE-BV
2.5γ
XFLI
0.5 MM
13 14 15
MAY 1975
LE
25γ
LE-HA
2.5γ
XPRI
5 MM
3 4 5
OCT. 1975
AA
25γ
LE-HA
2.5γ
CWC
5 MM
9 10 11
APR. 1976

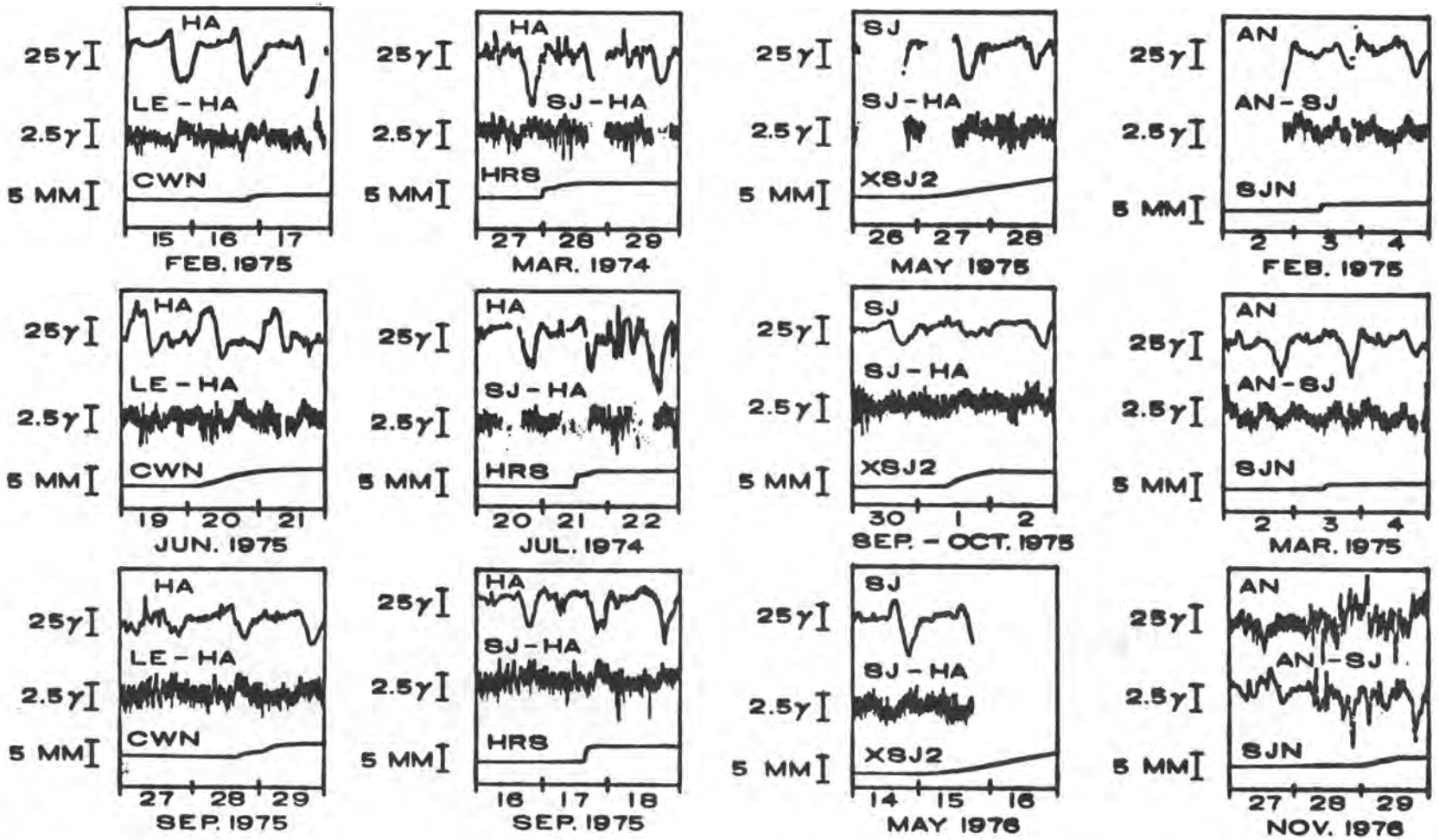
25γ
2.5γ
5 MM
HA
LE – HA
CWN
15 16 17
FEB. 1975
HA
SJ – HA
HRS
27 28 29
MAR. 1974
SJ
SJ – HA
XSJ2
26 27 28
MAY 1975
AN
AN – SJ
SJN
2 3 4
FEB. 1975
HA
LE – HA
CWN
19 20 21
JUN. 1975
HA
SJ – HA
HRS
20 21 22
JUL. 1974
SJ
SJ – HA
XSJ2
30 1 2
SEP. – OCT. 1975
AN
AN – SJ
SJN
2 3 4
MAR. 1975
HA
LE – HA
CWN
27 28 29
SEP. 1975
HA
SJ – HA
HRS
16 17 18
SEP. 1975
SJ
SJ – HA
XSJ2
14 15 16
MAY 1976
AN
AN – SJ
SJN
27 28 29
NOV. 1976

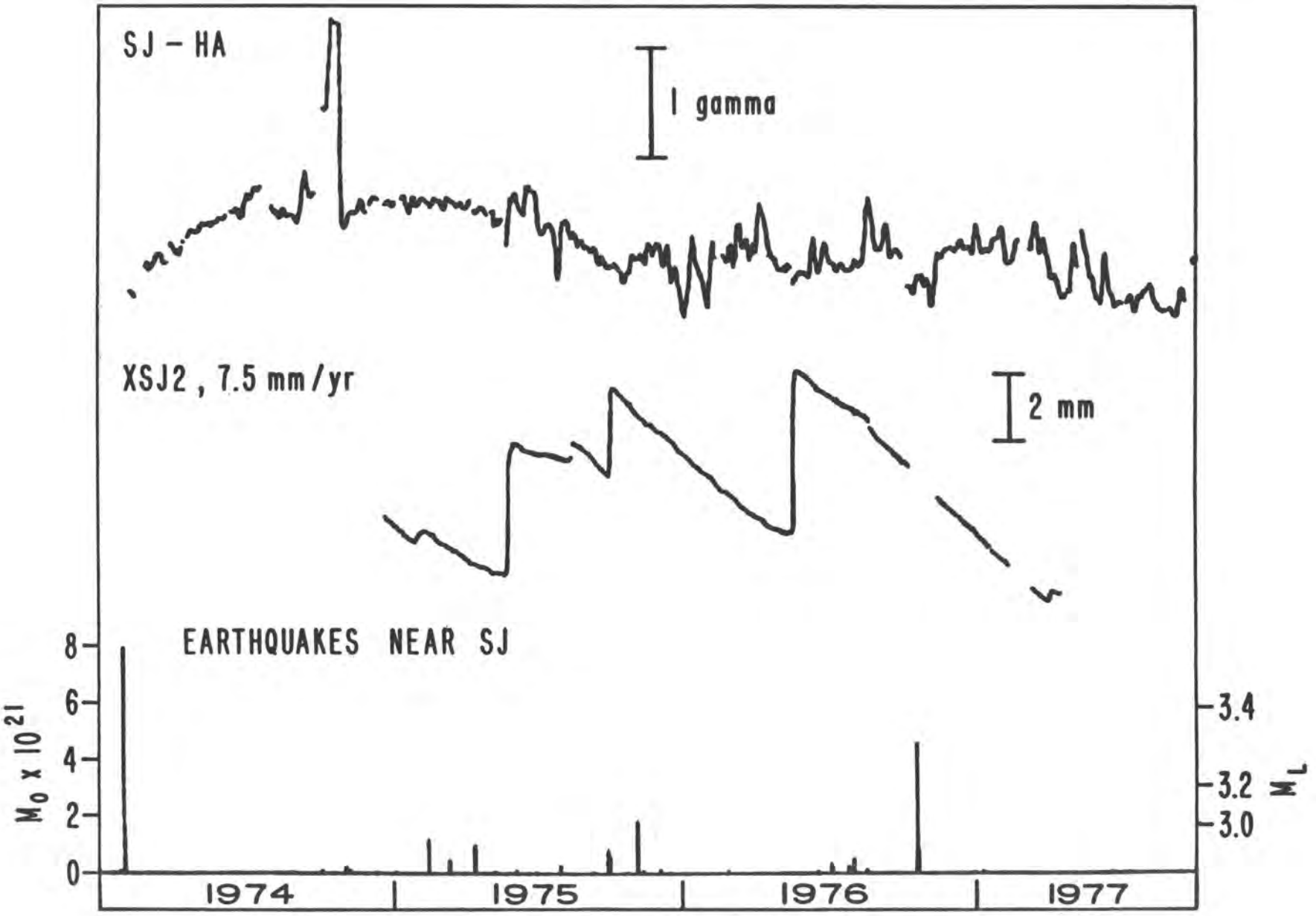
SJ - HA
1 gamma
XSJ2 , 7.5 mm/yr
2 mm
EARTHQUAKES NEAR SJ
$M_0 \times 10^{21}$
8
6
4
2
0
3.4
3.2
3.0
M_L
1974
1975
1976
1977

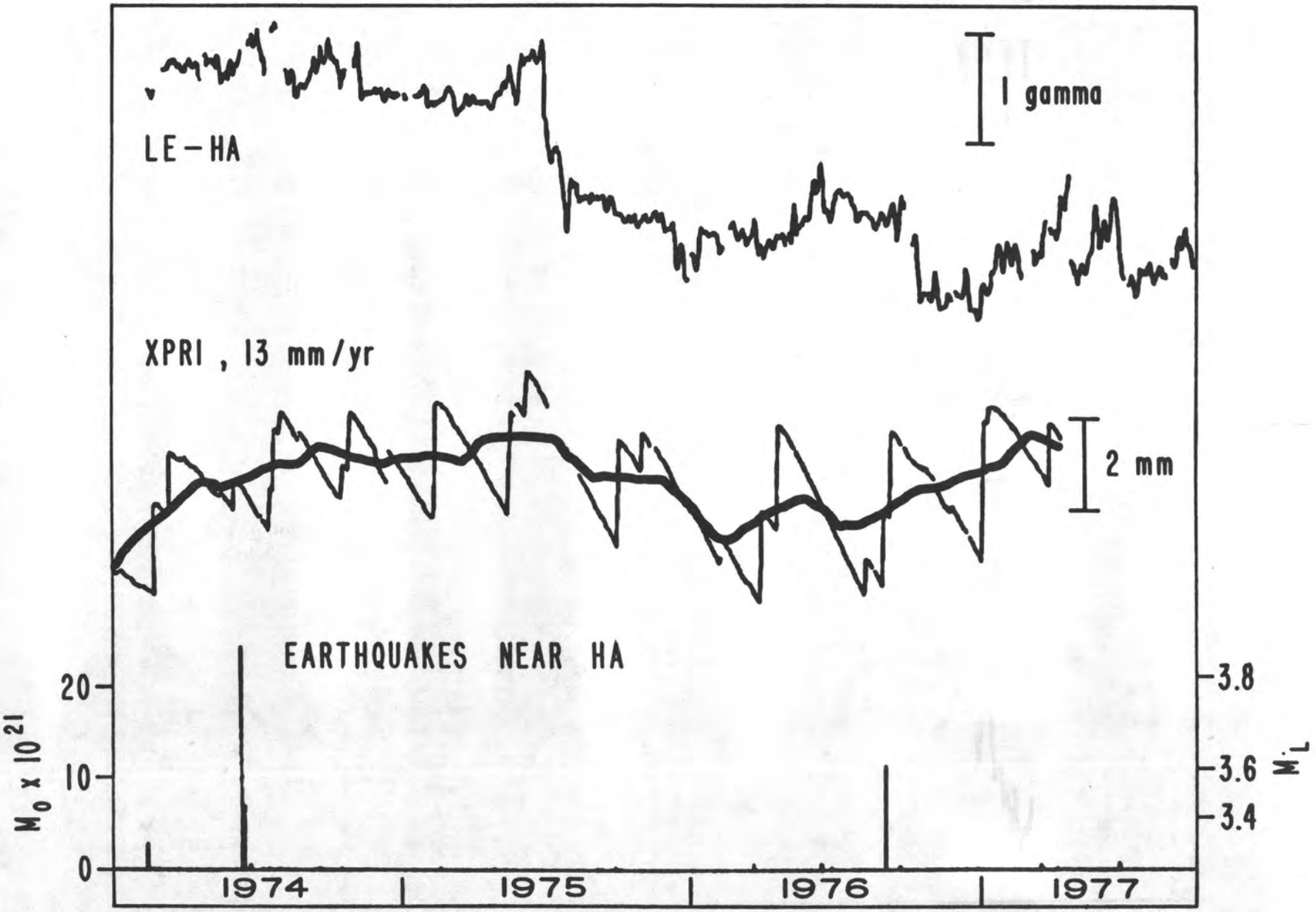
1 gamma
LE – HA
XPRI , 13 mm/yr
2 mm
EARTHQUAKES NEAR HA
$M_0 \times 10^{21}$
20
10
0
3.8
3.6
3.4
M_L
1974
1975
1976
1977

Figure

260E

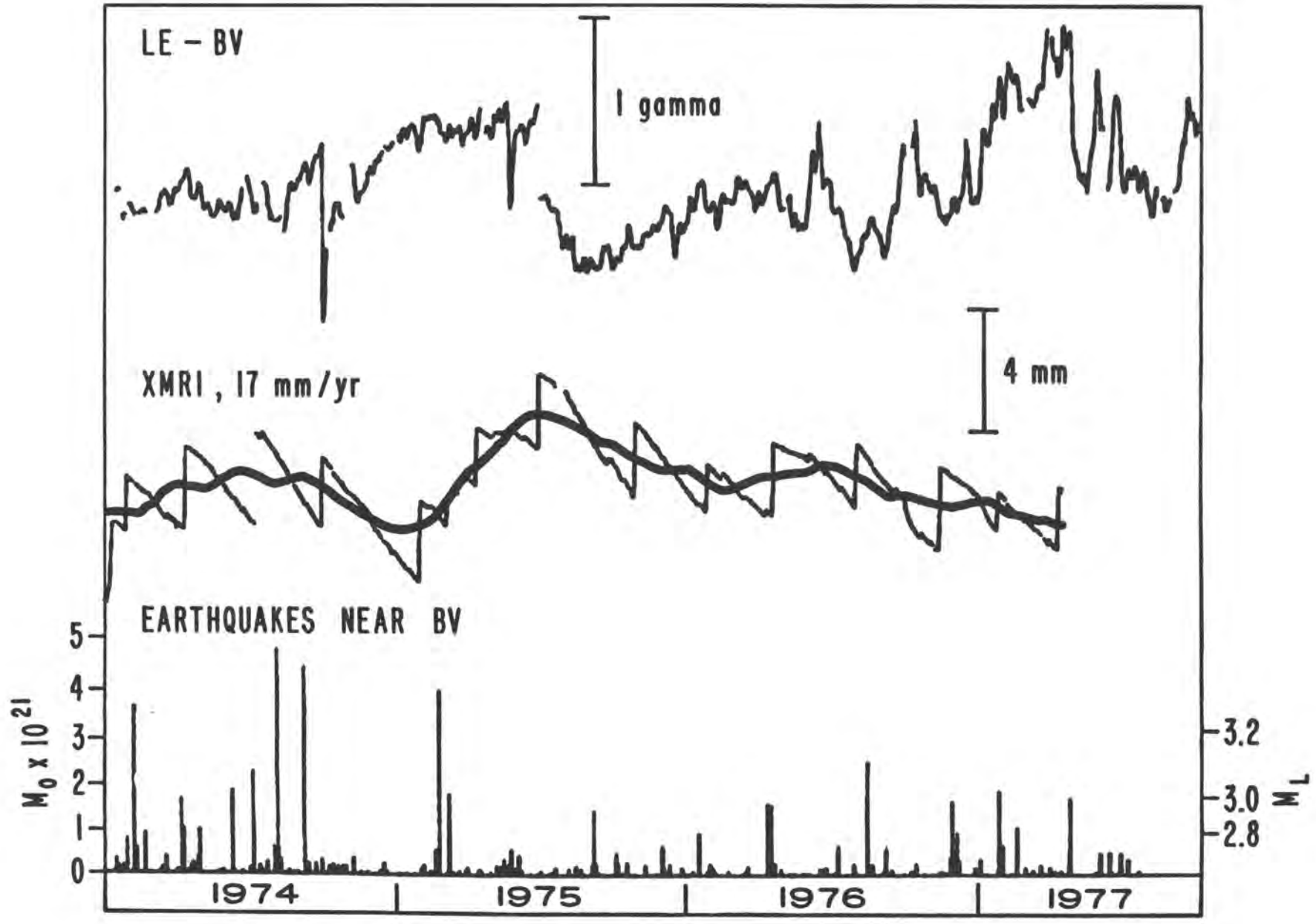
LE – BV
1 gamma
XMRI , 17 mm/yr
4 mm
EARTHQUAKES NEAR BV
$M_o \times 10^{21}$
5
4
3
2
1
0
3.2
3.0
2.8
M_L
1974
1975
1976
1977

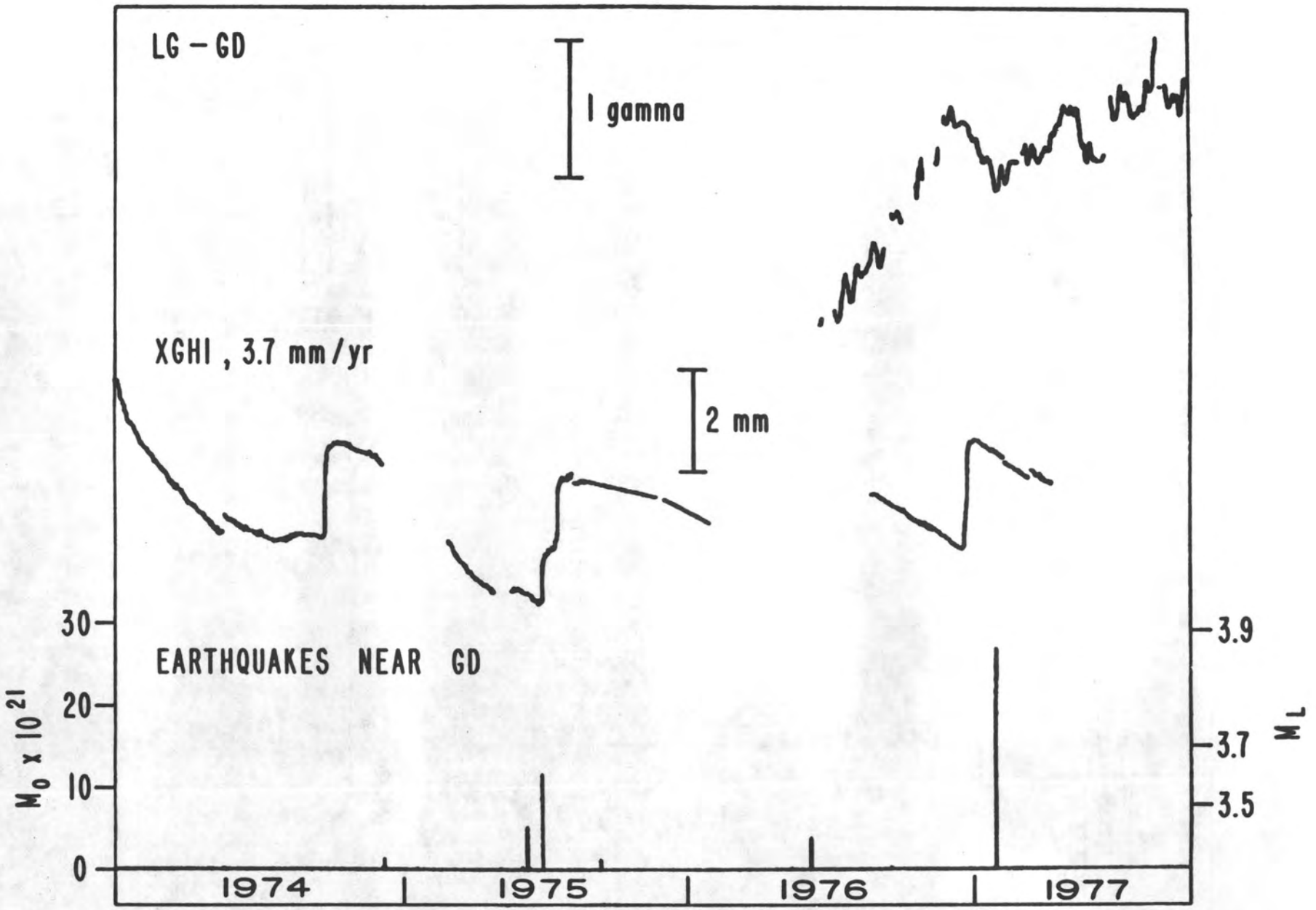
LG – GD
1 gamma
XGHI , 3.7 mm/yr
2 mm
EARTHQUAKES NEAR GD
30
20
10
0
$M_0 \times 10^{21}$
3.9
3.7
3.5
M_L
1974
1975
1976
1977

260G

USE OF ELECTROMAGNETIC METHODS FOR ASSESSMENT OF CRUSTAL STRESS CHANGES

A. F. Kuckes, A. Nekut and W. Phillips

School of Applied and Engineering Physics
Cornell University, Ithaca, NY 14853

August 1978

Introduction.

The large change of electrical conductivity which most rock exhibits in response to changes in mechanical stress makes insitu evaluation of crustal conductivity a particularly important aspect of earthquake prediction and of the experimental estimation of crustal stress change. Electromagnetic induction methods appear particularly promising for this purpose because of the possibility of designing a system capable of detecting very small changes in conductivity of rock in the 2-8 km depth range where earthquakes release much stress. In this report we will examine several design considerations of such a system and estimate several performance criteria.

The electrical conductivity of rock at modest temperature and pressure is dominated by the electrolytic conduction due to water trapped in pores and fractures. The conductivity of rock changes with stress principally because of changes in the electrical connections between rock pores, microfractures in the rock matrix, At 1 kbar of hydrostatic stress, a change of 100 bars stress leads to a conductivity change of about 2-5% for many rocks.[1]

Since the expected in situ change in conductivity is small, it is imperative to make these measurements with maximum immunity to changes in the conductivity at the surface due to changes of ground water, rainfall and other secular changes. The proposed system has this property in addition to the possibility of experimentally discerning whether changes observed are due to change in the deep crustal conductivity or to surface effects.

System to be evaluated.

In order to make realistic estimates, the specific system shown schematically in Fig. 1 will be evaluated. The source of excitation is a single turn, horizontal loop of wire about two kilometers in diameter carrying about 100 amperes of alternating current located about 6 kilometers on one side of the fault under study. At the observation point at 6 kilometers on the other side of the fault a magnetometer measures the horizontal field component, 90^{o} out of phase with the source current. The analysis below shows that this configuration is responsive to the crustal current flow which the source loop induces in the volume

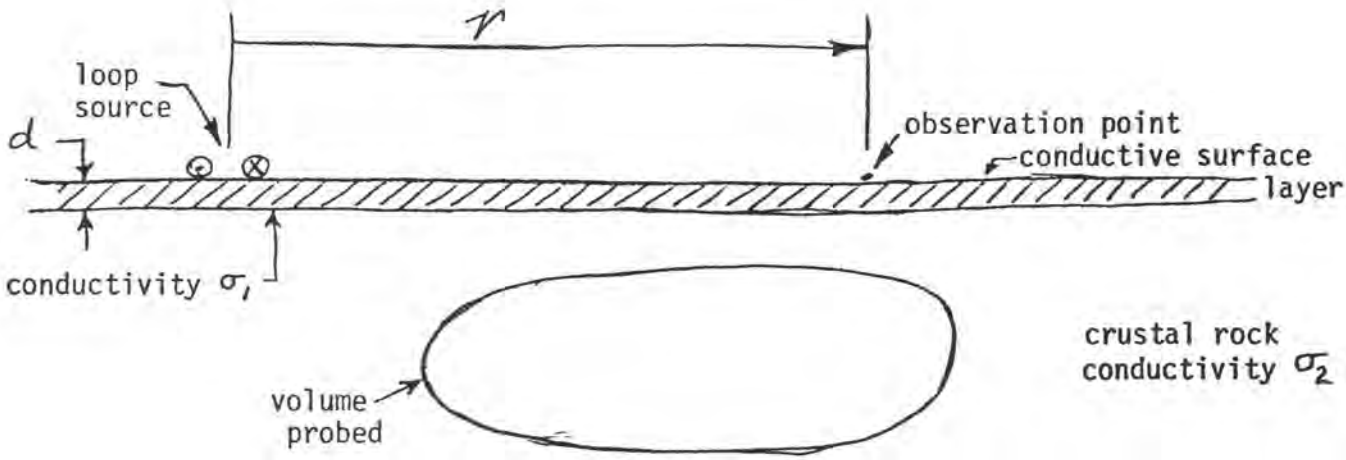

Fig. 1

denoted and that it is relatively insensitive to small changes surface current flow.

While the idealization chosen for evaluation no doubt overlooks many of the geologic complexities of a faulted region, it does permit estimation of the effects to be measured and of the effects which are likely to limit the performance of inductive methods in general for evaluation of temporal conductivity changes.

Basic considerations of analysis.

A basic principle of electromagnetism is that an temporally oscillating magnetic field penetrates only a limited depth into an electrically conductive material. The depth δ which a field oscillating at the radian frequency ω penetrates into a conductor of conductivity σ is given by

$$\delta = \sqrt{\frac{2}{\omega \mu_o \sigma}} \qquad \mu_o = 4\pi \times 10^{-7} \text{ MKS units} \tag{1}$$

A field oscillating at a frequency of 10^{-1} Hertz penetrates about 16 km into materials with $\sigma = 10^{-2}$ (ohm meters)$^{-1}$. In evaluating the idealization shown in Fig. 1 it is appropriate to normalize distance to δ, e.g. the important radial parameter is r/δ.

For a thin, conductive surface layer only the total conductance, i.e. the surface conductivity σ_1 times the thickness d is relevant, i.e. the important parameter characterizing a thin surface layer is its conductivity-thickness product $\sigma_1 d$. For the layer to be thin this product must be small compared to $\sigma_2 \delta$.

The magnitude of the electromagnetic field parameters are best described relative to the magnitude of the magnetic and electric fields B_o and E_o which the source loop would generate in free space. The free space magnetic field B_o of a source loop of magnetic moment m (m - electric current times the area enclosed by the source loop) at a point lying in the plane of the loop r meters away is

$$B_o = \frac{\mu_o m}{4\pi r^3} \tag{2}$$

The free space electric field generated at this point is

$$E_o = \frac{i\omega\mu_o m}{4\pi r^2} = i\omega r\, B_o \tag{3}$$

All electromagnetic variables vary in time as $e^{i\omega t}$.

Response of the system to crustal conductivity.

The horizontal magnetic field component B_r at the observation site for the configuration of Fig. 1 is identically zero in the absence of crustal current flow. Close to the loop, i.e. if $r/\delta \ll 1$, the dominant horizontal field component is 90^o out of phase with the primary field of the source. For $r/\delta \ll 1$ the important current flow in the earth is that generated directly by the inductive electric field of the source loop. For $r/\delta \gg 1$ it is necessary to compute the field patterns in an overall, self-consistent manner.

Before describing the results of detailed computations, it is useful to note a few basic properties of magnetic field generation by electric current. The free space magnetic field of a circular loop of current is shown in Fig. 2.

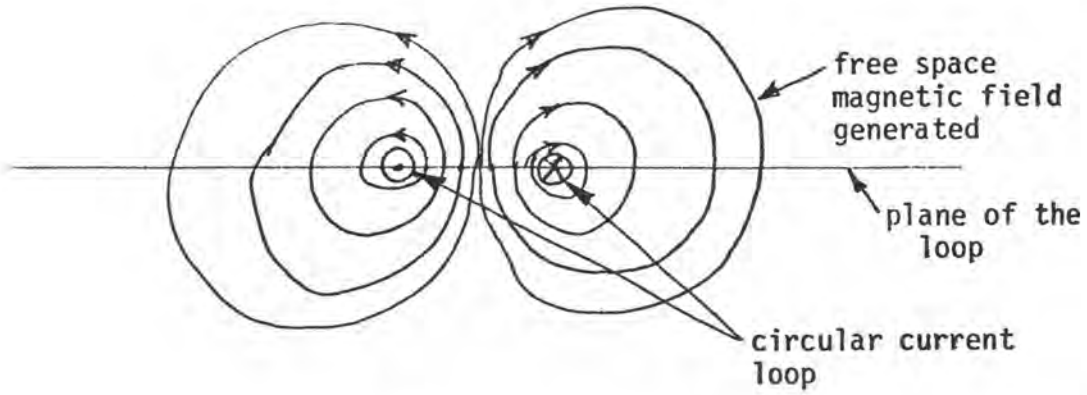

Fig. 2

The primary field at any point in the plane of the loop is entirely vertical and falls off with the cube of distance r from the loop as described in eq. (2).

Crustal current flows in response to the induced electromagnetic voltages, i.e. a voltage V around a closed path is given by $V = -\frac{d\phi}{dt}$ where ϕ is the total magnetic flux going through the path. Thus a current flow in the source $I_s = I_o \sin \omega t$ induces a 90^o out of phase secondary crustal current I_c i.e. $I_c \sim \cos\omega t$. The induced current produces a secondary magnetic field which at a remote location identifies this current flow and can be used to evaluate the crustal conductivity. Thus the induced current flow in the earth is concentric to the loop and is 90^o out of phase with that of the source. Fig. 3 shows loops of induced current flowing deep in the earth. Induced current flow which is not coplanar to the source and observation point produces a secondary horizontal field at the observation point. An induced surface current is coplanar to the source and if it does not pass directly beneath the observation point, it produces no horizontal field there. Due to the $1/r^2$ fall off of the fields generated by each current element, the induced surface current flow directly under the observation point gives horizontal field contribution there.

The exact, out of phase component of the horizontal magnetic field component B_r of the infinite half space configuration tabulated by

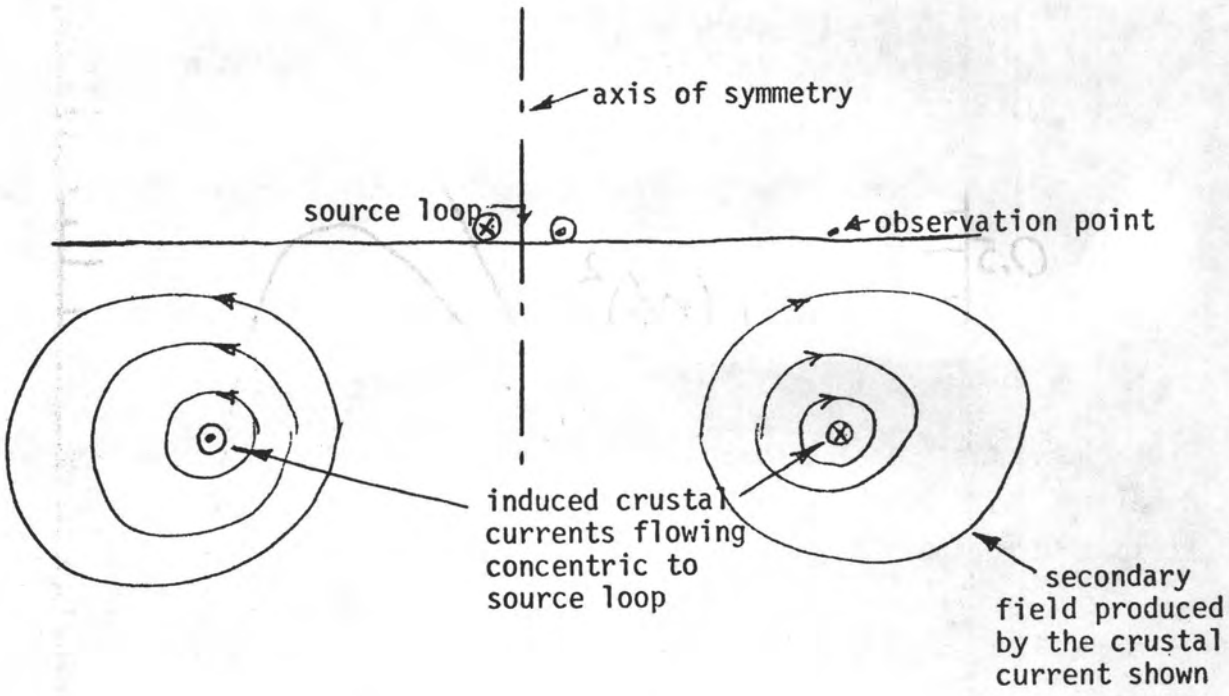

Fig. 3

Frischknecht [2] is shown in Fig. 4. For radii $r < \delta$ the response fields are effectively given by the simple interaction of the primary field with the crustal conductivity as described above, the result is that $B_r / B_o \sim \frac{1}{2}(r/\delta)^2$ for small values of r/δ . For larger radii the

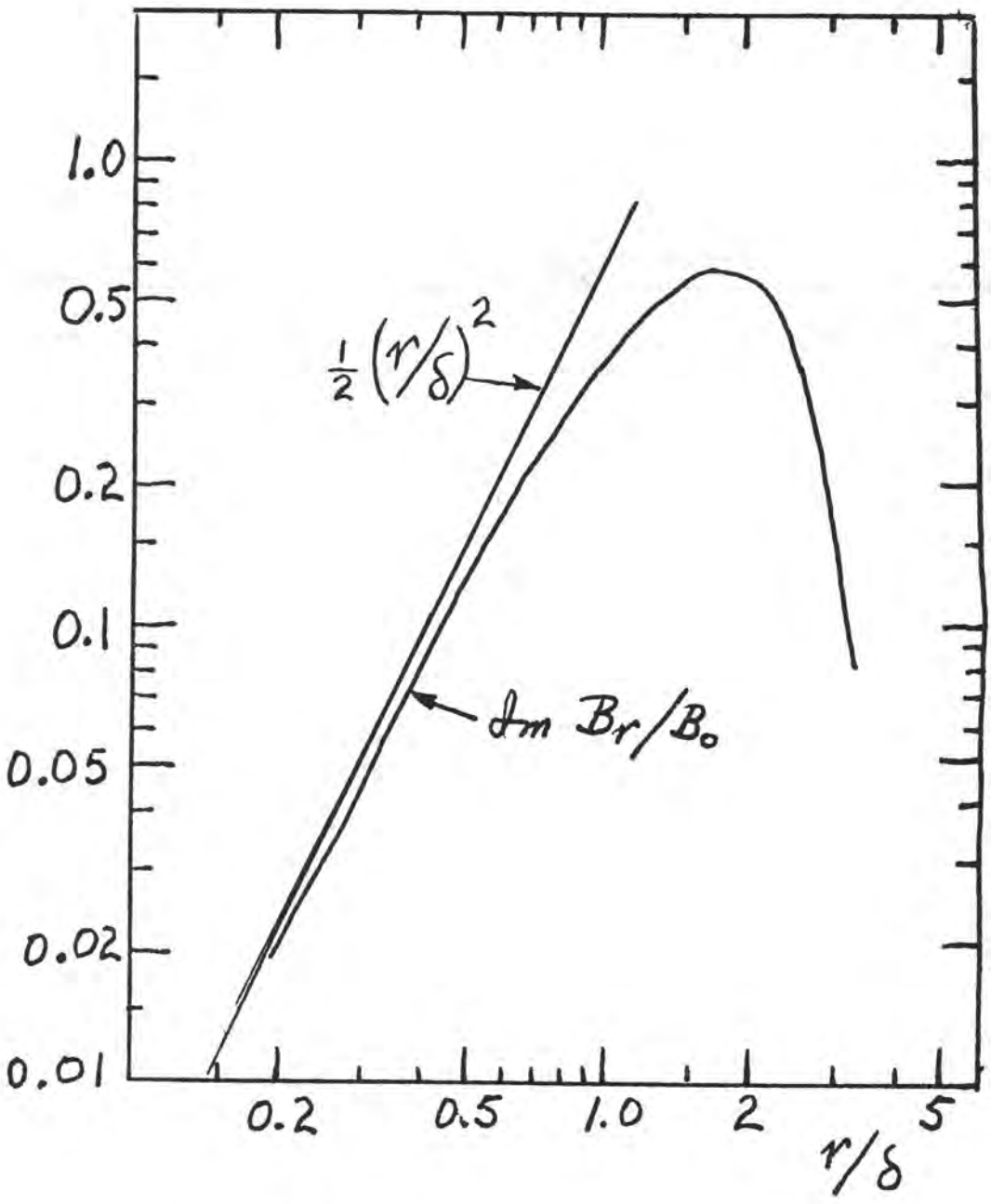

Figure 4. Radial response field B_r out of phase with the source field above an infinite half space of uniform conductivity as a function of radius r.

coupling of the primary and secondary magnetic fields cannot be neglected and the total self-consistent solutions as given by Frischknecht [2] are required.

Putting the observation point at about $r = 0.8\delta$ appears to be a good compromise between obtaining good signal and having good sensitivity to deep seated conductivity changes. At this distance, the fractional change in signal, i.e. δB_r, to change in conductivity $\delta\sigma$ of a uniform half space is given by

$$\frac{\delta B_r}{B_r} \approx \frac{\delta(r/\delta)}{r/\delta} = \frac{\delta\sigma}{2\sigma} \qquad (4)$$

Depth and volume probe by the system.

To estimate the depth effectively probed by the system we consider the configuration shown in Fig. 5 which consists of a thickness t of conductivity σ underlain by an insulator, i.e. $\sigma = 0$

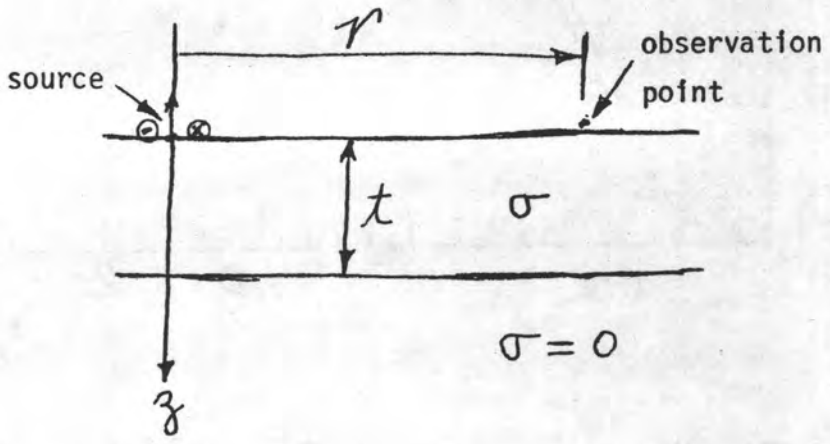

Fig. 5

The theoretical response B_r / B_0 is shown in Fig. 6 for several values of radius and conductor thickness t. For the small radii, i.e. $r/\delta \ll 1$,

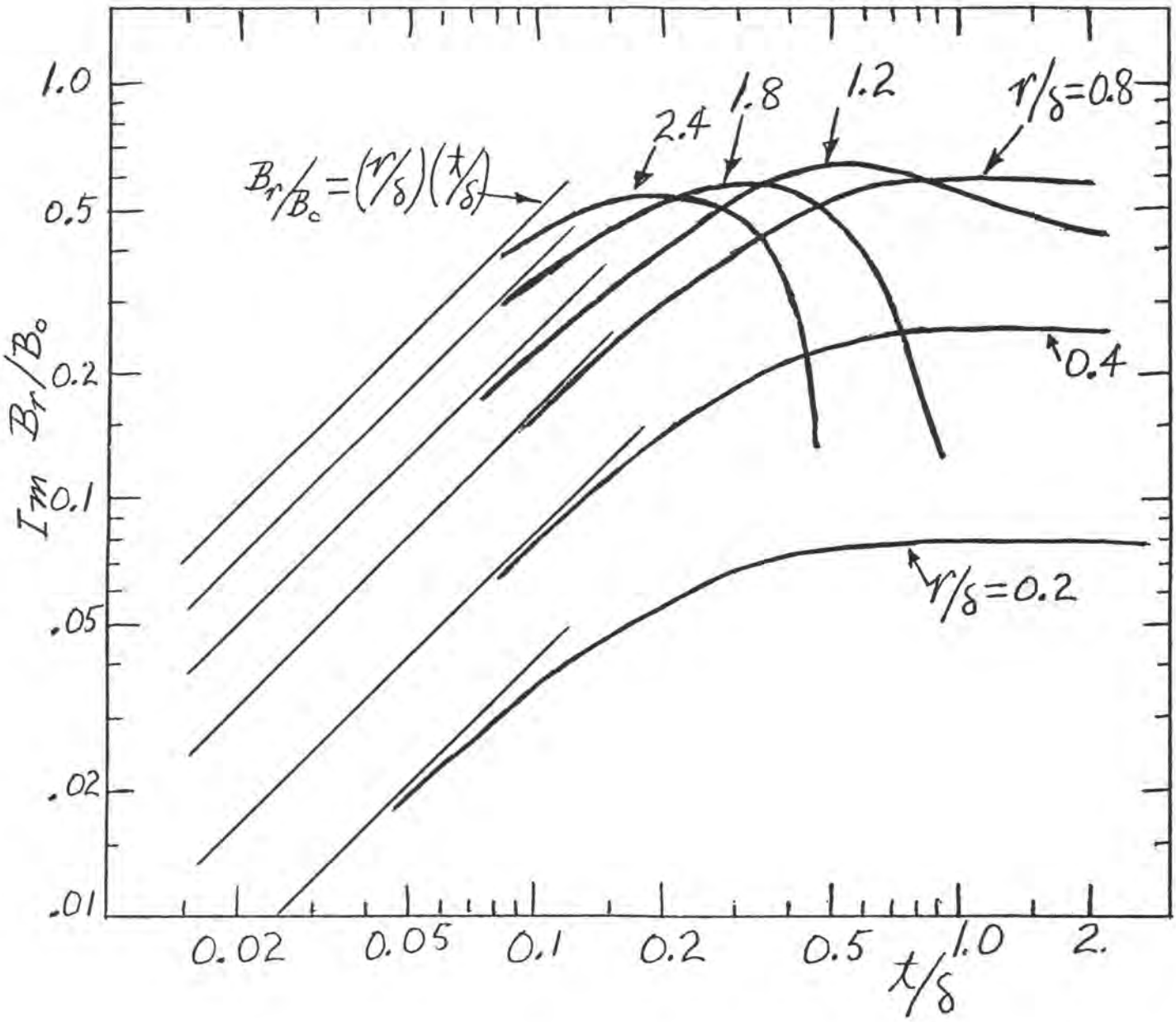

Figure 6. The quadrature response field B_r above a larger conducting material of thickness t underlain by an insulator.

the conductive material below about $z = \delta/2$ does not significantly change the response. Noting the rise and flattening of the graph for radius of interest $r = 0.8\delta$, we conclude that one half of the observed signal above a thick conductor, i.e. $t/\delta \gg 1$, apparently originates from the depth between 0.5δ and 0.18δ or alternatively said from the depth between $0.62r$ and $0.22r$. These considerations imply that to probe depths between 2.5-7.5 km, r should be about 12 km and $\delta = 15$ km.

The magnitude and functional variation of the response shown in Fig. 6 for the values of $t/\delta < 1/2$ shown can be understood on the basis of simple considerations. The field in the radial direction B_r generated by an azimuthal current density j flowing in a thin sheet of thickness t generates a radial magnetic field above it

$$B_r = \frac{\mu_o j t}{2} \tag{5}$$

The primary electric field E_o induced by the loop drives such an azimuthal current. At a radius r in the plane of the source, the azimuthal electric field E_o is given by (3). Noting that $j = \sigma E$ we obtain

$$\frac{B_r}{B_o} = \frac{i\,\omega\mu_o\sigma r t}{2} = i\,(\frac{r}{\delta})(\frac{t}{\delta}). \tag{6}$$

These approximate curves are shown in Fig. 6.

Another approximate way of estimating the probing depth into a uniform earth at a point for which $r/\delta < 1$ is to equate (6) and the approximate relation valid for small r/δ above a uniform conductor, i.e.

$$\frac{B_r}{B_o} \sim \frac{1}{2}\,(\frac{r}{\delta})^2. \tag{7}$$

The probing depth z_p obtained is

$$z_p \sim r/2. \tag{8}$$

This agrees approximately with that found using Fig. 6 above.

These considerations also give a criteria for estimating the contribution from a surface layer, and in particular the fractional change in the radial field $\frac{\delta B_r}{B_r}$ due to a change in the surface conductivity thickness product $\delta(\sigma d)_s$. Noting the simple superposition of fields valid for $r/\delta < 1$ we obtain using (6)

$$\frac{\delta B_r}{B_r} = \frac{2\delta(\sigma d)_s}{\sigma r} \tag{9}$$

Another important quantity to estimate is the effective volume probed by the system. To do this we can take note of the approximate current densities in the earth and horizontal field at the surface which they generate.

The magnetic field B a distance a above an infinite, uniform current sheet as shown in Fig. 7 is independent of the height a above the sheet, its magnitude is given by (5).

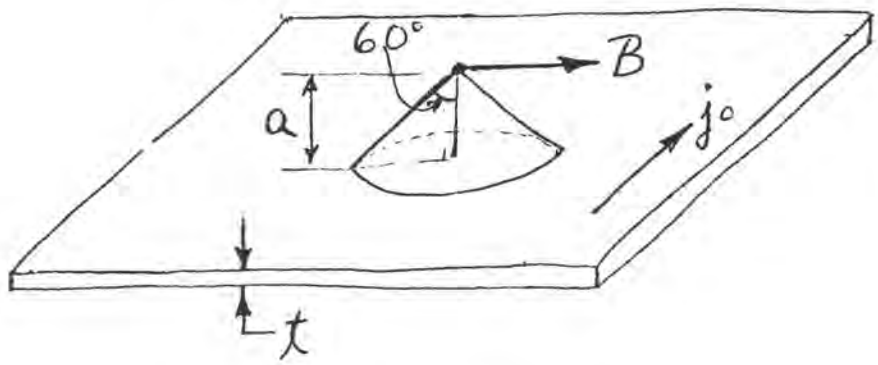

Fig. 7

The current elements which lie within a cone with about a 120^o apex angle under the observation point contribute 50% of the total field.

The distribution of important current flow induced within the earth is easily estimated for small values of r/δ. When $r/\delta << 1$, the

current density j is induced by the source loop acting alone; at the depth z radius R from the axis as shown in Fig. 8 the current density is given by

$$j = \frac{i\,\omega\mu_o\sigma m}{4\pi} \quad \frac{R}{(R^2 + z^2)^{3/2}} \tag{10}$$

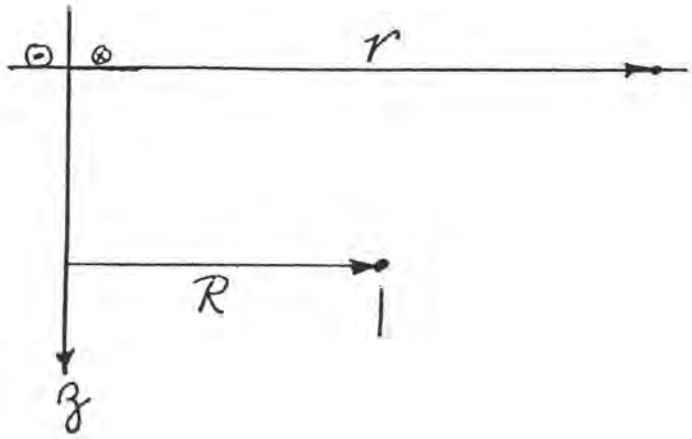

Fig. 8

Eq. (10) implies that to a depth of about $z \approx 0.5r$ each depth interval dz meters thick contributes uniformly to the response B_r at the surface. At a fixed depth z the maximum current density is at $R \approx 0.7z$. For depths greater than about $z \approx 0.5r$ the magnetic fields generated at the surface observation point is more akin to that generated by a current loop than a uniform current sheet and thus falls off rapidly as deeper currents are considered.

By combining these results we are able to outline the most important volume elements in which conductivity changes will have the greatest effect on the measurement of the quadrature part of the radial field B_r at the surface. For uniform conductivity σ each layer dz thick contributes about equally to a depth of about 1/2 the source to

receiver separation. Near the surface only those volume elements which lie in a cone with 1/2 apex angle of about 60^{o} are significant. At depths between 0.25r and 0.5r the most important volume elements will not be those directly under the observation point but will be at smaller radii since at any depth z the current density is maximum at $R = 0.7z$. Using these results, the most important volume elements probed are as shown in Figure 9.

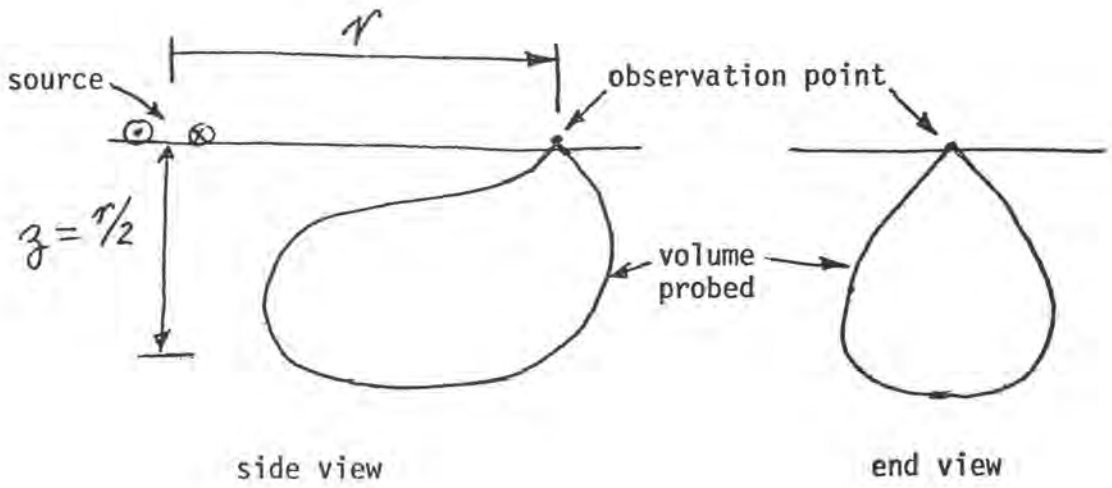

Fig. 9

Numerical Estimates.

For the San Andreas fault the principal release of stored stress energy during an earthquake occurs in the depth interval between 2-8 km. This leads to choosing the separation of the source and receiver to be about 15 km. The electrical conductivity of this region is by no means uniform laterally, our preliminary results lead us to choosing an average conductivity $\sigma \approx 10^{-2}$ (ohm meters)$^{-1}$ for purposes of estimation. To make $\delta \approx 15$ km leads to using an operating frequency of about 0.1 Hertz. To measure B_r / B_o to a precision of 0.1% requires signal averaging. Assuming that the overall noise is 5×10^{-12} voltsec/m^2/$\sqrt{\text{Hertz}}$ (geomagnetic

noise plus instrumental fluctuations), 100 amperes of current in a loop 2 km in diameter, a signal averaging time of a little less than a week is needed. If the loop is made from 350 MCM aluminum conductor (conductor diameter of 1.5 cm), the source will require 10 kilowatts of power. Thus a continuously operating, medium-sized system using a loop source is quite practical (a present galvanic system[3] operates at 150 kw).

To achieve a precision of 0.1% in the measurement of the pertinent electrical quantities should present no serious problem. Since only the local field ratio, i.e. B_r / B_o, is being measured, no absolute quantities need be recorded. A feedback method can be used to null the received magnetic signals to further reduce the need for particularly stable electrical components. Excessively precise phase synchronization between the source and receivers is also not a serious engineering concern.

The most serious limitation to doing temporally stable measurements of crustal conductivity has proven to be related to lateral variations of surface conductivity and to electrode stability.[3] The problems of electrodes is totally absent from the inductive method discussed. The analyses and experiments of Morrison et al[3] indicate that average change in the surface conductivity associated with rainfall, agricultural irrigation and seasonal changes is restricted to the upper 3-6 meters from the surface. Noting that the conductivity of tap water is about $10^{-2}(\text{ohm meters})^{-1}$, we estimate from (9) that $\delta B_r / B_o \approx 3 \times 10^{-4}$ from this effect.

Much more serious than uniform changes in the surface conductivity are the lateral variations which these changes exhibit. In the case of galvanic measurements, lateral non-uniformities are believed to be a dominant cause of the $\pm$ 3% fluctuations which the D.C. dipole-dipole studies show in the Hollister, California region.[3] Even though these lateral changes have rather limited current redistribution associated with them, they can lead to first order errors in the electric field[3] determination which seriously affects the stability of galvanic experiments. This effect is minimal with an inductive method. On the basis

of our present knowledge and experience with induction systems it would be surprising if lateral surface conductivity changes contributed spurious effects of greater than $\pm 1 \times 10^{-3}$.

Compensation for Near Surface Effects:

A simple and direct method of eliminating and estimating the small effects of near surface variations is to use two magnetometers at each observation station. One instrument is buried at a depth of about 50 meters or less and the other is kept at the surface. The sum of the signals from the two instruments will to first order have no contribution from the currents which flow in the layer between them. The difference signal between the two instruments will record the amount of surface current actually present and of the long term fluctuation of this current.

Conclusions:

These estimates show that a modest sized induction loop system is feasible for detecting small, long term changes of the electrical conductivity at the depths where the many sever earthquakes occur. The computations show that a system stability of about 0.1% should characterize an inductive system. Compensation for changes in the surface conductivity could reduce this even more. This level of sensitivity is sufficient to detect stress changes of the magnitude associated with earthquake phenomena in most rock types.

References:

1. Brace, W.F., and A.S. Orange, Electrical resistivity changes in saturated rocks during fracture and frictional sliding, J. Geophys. Res., 73 (4), 1433-1445, 1968.

2. Frischknecht, F.C., Fields about an oscillating magnetic dipole over a two layer earth and application to ground and electromagnetic surveys, Quarterly of the Colorado School of Mines, 62, p. 1-324, 1967.

3. Morrison, H.F., R.F. Corwin, and M. Chang, High accuracy determination of temporal variations of crustal resistivity, in The Earth's Crust, Geophysical Monograph 20, A.G.U., Washington, D.C., 1977.

Geodetic Leveling for Monitoring Crustal Deformations - A Critical Review

by

Muneendra Kumar
National Geodetic Survey
National Ocean Survey, NOAA
Rockville, MD 20852

Presented at the
Conference on Measurement of Ground Strain Phenomena
Related to Earthquake Prediction
Carmel, California
September 6-9, 1978

INTRODUCTION

With the increased public awareness to the changing environment, development of newer and better scientific techniques, the economic and inflationary impact caused by rapidly disappearing natural resources, and the humane concern for the loss of life and property in seismically active areas, the communities around the world have started showing awareness to phenomena as subtle as crustal deformation and its correlation to geodynamical, tectonic and seismological activities.

It is hoped that continuous efforts towards extremely accurate determination of the extent and the nature of crustal movements, ground strain and stress, and detailed analysis of such data may allow scientists to predict earthquakes successfully and reliably sometime in the future. However, the "timing" of such a prediction would be a key factor in deciding whether full advantage can be availed or not from such a capability.

Towards our goal of accurate determination and monitoring of vertical crustal motion, geodetic leveling as one of the most accurate measuring systems known to geodesists has already established its usefulness. This paper attempts to highlight some of the most sensitive and critical problems inherent in geodetic leveling which have significant impact on the quality of results and interpretations derived thereof from any leveling data. In addition, as a new approach "complete" testing of both Type I (α) and Type II (β) conventional errors for realistic statistical assessment of the vertical crustal motion investigations is recommended.

VERTICAL CRUSTAL MOTION PROBLEMS

To be able to study, investigate, and understand the complex crustal movement activity in an area, I foresee that such an effort can pose two distinctive types of problems depending upon the magnitude of the displacement rate involved.

(a) In the areas where this rate is of the order of a few mm per year, the accurate measurement of crustal motion with reliable and realistic statistics is extremely difficult. Keeping in view the present day accuracy limitation of our geodetic instruments, the job involved becomes challenging too. In such cases, the solution may only lie in designing our leveling surveys with extreme care and the most optimum layout with "adequate density and overlap" in line coverage. Such projects must also be performed under strictly controlled technical specifications. An excellent example of such a survey under controlled conditions is the recently completed 1978 Southern California Releveling Program (Figure 1). Unless the two time epochs between repeat levelings are "significantly" separated in time, where this limiting time separation can be statistically precomputed for a particular survey (Kumar, 1976), and the data assessed through complete statistical testing both for conventional α and β errors, the error budget inherent in the observations may possibly conceal meaningful results. Wassef (1976) has discussed a case wherein the predominant presence of height changes of

one sign (suggesting crustal motion) did not meet the prescribed α level of statistical significance. However, after relaxing initial value of α, the analyzer led his investigation to confirm some "predetermined result." This bias treatment could have been avoided if the β error was also tested to strengthen the statistical inference(s) from testing of the α error.

(b) Further, in areas like the San Joaquin Valley of California, the rate of movement to be measured through leveling may reach up to 25-30 cm per year (Holdahl, 1969; NOS, 1974; FGCC, 1976). In these situations it can be interpreted that the leveling surveys may have been performed on a constantly moving crust (Figure 2). In the absence of an "instantaneous" leveling in time, it is practically impossible to associate an epoch to various segments of a leveling network(s) in such an area.

USE OF GEODETIC LEVELING

Whatever may be the vertical movement type, subsidence or uplift, and whatever its rate, geodetic leveling has been in the past and is still being widely and frequently used to measure and monitor such motions.

Though geodetic leveling is a slow and expensive process, the data is generally available in abundance with quite extensive coverage both in time and area. Initially, the leveling was considered to provide elevations in a "stationary" mode and link bench marks in an area to a common vertical reference system. The practice to stamp elevations on to these bench marks was also followed. However, the improvement in instrumentation and theory, and the increased technical awareness and interest in crustal motion problems have changed our emphasis and brought in a new trend. Instead of treating a bench mark with its elevation as "stable", geodesists, geologists, geophysicists, and engineers now more frequently analyze the elevation change (other than due to local disturbances), and also draw inferences from repeat leveling surveys in geodynamical and tectonic terms.

A comparatively simple method of studying any crustal movement is through a profile (Figure 3), when observed elevation differences from repeated levelings (over the same route and with common bench marks) are available. In addition, several elaborate analytical techniques based on different mathematical modelings (Korhonen, 1961; Frost and Lilly, 1966; Holdahl, 1969; Gale, 1970; Vanicek and Hamilton, 1972; Vanicek and Christodulidis, 1974; Holdahl and Hardy, 1977; Holdahl, 1977; and Vanicek, et. al., 1977) have been suggested in recent times and used quite successfully in analyzing "scattered" geodetic levelings (Figures 4 and 5).

These theoretical studies have significant scientific contributions and have succeeded extremely well in "delineating a general trend" of vertical crustal movements for the area under investigation. However, if an effort is made to validate the associate movement rate(s) as obtained through these complicated mathematical modelings or surface

fittings, such an attempt is liable to face some problems. The most important and straightforward questions (which we can ask here) are:

(a) How much trust and reliability can we have in these "smoothened" crustal movement trends or rates?

(b) Are such trends or rates sufficiently accurate to provide a reliable contribution towards our ultimate goal of establishing an earthquake prediction capability?

In my opinion, the satisfactory answers to these questions are extremely difficult to find. The problems in this area can be attributed to the non-availability of reliable accuracy estimates, the limitations in the intrinsic quality, and the insufficient information of the relative accuracies of the level lines under analysis. The suitability and homogeneity of the data selected, the establishment of common reference point(s), and the possible presence of "discontinuities" due to major earthquakes between repeat levelings belonging to different time epochs will make any such study even more intricate.

RECOMMENDED PROCEDURE

In our handling of this difficult situation, the investigational approach can be improved upon by designing proper experiments under controlled conditions and complete statistical assessment of the results so obtained.

Some of the important factors, which have significant effect on the quality of results or inferences obtained from a crustal motion study based on repeat leveling surveys, are reviewed here in detail. An attempt has also been made to suggest remedial measures at the appropriate places.

Quality Control. - The basic quality and intrinsic accuracy of geodetic leveling are universally recognized. However, there are many sources of systematic errors which still baffle the geodetic community. Two striking examples in this respect (where suitable explanations still remain to be found) are:

(a) In the recently completed 1978 Southern California Releveling Program, one loop of 530 km first-order leveling has a misclosure of 201 mm where the permissible limit will amount to only 92 mm. It may be worthwhile to mention that this large loop misclosure has occurred in a program which was achieved in a short time-span of 15 weeks under special technical specifications (Loop A, Figure 1).

(b) A direct comparison between the first Trans-Canadian leveling from Halifax to Vancouver of 1910 and the same line of 1960 has revealed a difference of 2.2 meters where this discrepancy systematically builds up from one end to another.

Having situations like these to confront, I am convinced that not all level lines should be included routinely in crustal movement studies. If one has to select an "old" level line in his (or her) experiment, an extremely careful and detailed study of the related old field books is very important. In order to obtain a realistic estimate of the intrinsic quality of this old leveling data, the items to be investigated are the old field procedure, the type of checks used to minimize/control the systematic errors and to avoid blunders, and the types of instruments and rods used, their limitations, and calibration history. The pertinent remarks, if any, available in the field records may have direct/indirect impact on the accuracy of the old data and thus should be taken into account.

Epoch of Leveling Data. - In areas like the San Joaquin Valley, the correct time epochs to be associated with repeat levelings of different segments of a long level line are very important and extremely difficult to designate. The best solution to such a problem lies in the "instantaneous" leveling of the area. If this is not possible, an experiment should be specifically designed under a committed time span. The limitations of data and results should also be duly recognized, appropriately clarified, and stressed without any ambiguity.

Homogeneity of Data. - This factor can be treated as a direct extension of quality control (see section on Quality Control). The two sets of observations for two time epoch t_0 and t_1 used in crustal motion study should be free of systematic errors and "individualistic bias" i.e., ideally speaking the variance-covariance matrices for the two sets of observations are equal. In other words an experiment under controlled condition must not be time dependent.

Instances of crustal movement studies are available when a first-order, class I leveling from one agency has been compared with a third-order level line from a localized engineering project with a simple straightforward statement on the possible existence of their probable errors. An engineer, running a third-order level line for a local project, will be more interested in quick execution and completion of the job. In many cases, the engineer may be looking for immediate financial gain from the effort rather than long-term scientific involvement. The use of such data, as an "isolated" item for any crustal movement study, is just not correct. Moreover, as there will be too many limitations involved in this type of data, the effort required to establish its suitability for crustal motion investigation may not be worthwhile.

Common References. - Starting with a conglomerate of data from various projects, "scattered" or sparse coverage, and limited overlap in extent and time, an investigator faces a very important and extremely difficult task in the effort to correlate and homogenize such data to a common reference.

Often in this type of situation, some important bench mark(s) is selected in the study area and then an effort is made to tie the data to such a mark(s). If such a mark(s) is associated with an adjacent tide gage, the following assumptions regarding secular changes in sea level relative to the "reference" mark(s) become necessary to interpret the data:

(a) The "eustatic" (or worldwide) rise in sea level,
(b) the "apparent" change in sea level relative to the land.

If we are looking for small movement rates (see section on Vertical Crustal Motion Problems), the uncertainty associated with (a) above is at least two to three magnitudes greater than the rate involved (Gutenberg, 1941). A similar situation may arise with case (b) also. The periodic fluctuations in sea level from day to day, year to year, and one 19 year cycle to another vary over a very wide range (Figure 6). Some investigations are available where extremely low standard deviations of the order of 0.5 mm per year have been associated to the velocities in such changes. This type of standard deviations can be considered rather too optimistic, and the weighting scheme based on such numbers may be quite misleading. The results or inferences obtained may also show frequent inconsistencies and contradictions from one analysis to another.

Discontinuity in Data. - It is also quite likely that the data selected for any area may have "discontinuity", i.e. crustal deformation may have occurred, partly or otherwise, due to some episodic activity. This event can be artificial (or accidental) or natural due to some seismic upheaval.

The mathematical modeling or "correcting" for crustal deformations due to discontinuities has its own limitations. In any episodic activity it is necessary to have data both before and after the event to correctly delineate the associated displacements. Such information then avoids "contamination" of differential crustal movements in the area.

The total crustal deformations in many such cases have been "smoothened" as yearly linear rates between the two leveling epochs completely disregarding even major earthquakes in the area. The total picture presented does not mention about the discontinuity or what limitations are to be associated with the results obtained thereof. I feel alarmed to think what may happen if some analyst later goes one step further and extrapolates on the basis of such movement rates.

Extent of Releveling. - In studies involving geodetic leveling, the investigators, in general, have to deal with a conglomerate of data in time, extent, coverage, and/or overlap. A theoretical approach in such cases may be to fit a mathematical surface with scattered leveling segments. This may be the best solution possible to obtain a crustal deformation "trend" under the adverse conditions. In my opinion, it is imperative that the limitations be fully emphasized together with the involved hypotheses and assumptions and the statistical reliability of the results. Unless these points are fully clarified or mentioned, a strong possibility will always exist that the results may be misunderstood or misinterpreted by all concerned.

On the other hand, once a "trend" has been established and if the importance of the problem requires it, ideally speaking, a complete overlap in releveling is suggested. To determine reliable deformation rate(s) for the area under investigation, such relevelings should be at two or more time epochs. If the effect of a discontinuity is also to be correctly delineated and its contamination to be avoided, leveling surveys will be required before and after the discontinuity.

In the case of a seismic discontinuity, this, in turn, will mean an earthquake prediction capability to enable leveling before the episodic event.

However, a realistic approach may lie in a carefully designed experiment, executed under controlled conditions at least at three epochs, and complete statistical testing of results both for α and β errors.

STATISTICAL ASSESSMENT

The classical expressions of the probable errors of geodetic leveling are not completely rigorous and satisfactory as yet. The investigators are still searching reliable criteria for leveling accuracy (Thurm, 1971; Wassef, 1974; Remmer, 1975; Schadlich, 1976). Even in such a situation, inferences from repeat leveling surveys are amply justified and will be reasonably reliable so long established statistical tests are used with appropriate treatment.

Under the "necessary" half of any statistical analysis, a hypothesis is made and the same is then tested against a preassigned significance level or α error. After such a test has been made, a question can arise as to what happens if the hypothesis made is not true. As there is no information available to any investigator to predetermine whether the hypothesis being tested is true or not, under the "sufficient" half of the analysis, it is essential to complete the investigation by also testing β error (Dixon and Massey, 1957).

Alternatively, this additional testing can be reframed and stated differently i.e., controlling the chance of making an α error for an assumed hypothesis in any test, it would be most advantageous to have the chance of rejecting the hypothesis, if the same is not true, to

be as large as possible (or β error to be as small as possible). A very good example of such testing of both α and β errors has been established through simulated data for crustal motion investigations (Kumar, 1976).

The significance of testing the β error works in two ways:

(a) for a feasibility study to design an experiment,
(b) for obtaining reliable and more meaningful inferences from statistical testing of the results.

Thus, taking into consideration the importance of time and money available, if an experiment (even when it successfully meets a preassigned α significance level) has a chance of 85 percent β error of accepting (or only 15 percent chance of detecting) a failure or a substandard, it may be worthwhile to redesign the experiment. Further, this approach will also save us from obtaining contradictory results or inferences due to our faulty/incomplete data analysis.

SUMMARY

Fully recognizing the usefulness and importance of geodetic leveling in measurement and monitoring of crustal deformations and its evaluation for the possible prediction of earthquake in seismic zones, an attempt has been made here to describe some of the critical problems and limitations inherently involved in leveling data. Possible improvements in data handling, procedural treatment, and statistical analysis have also been suggested.

Once the use of available leveling data has established a "trend" in crustal movement investigations, it is essential that a specific experiment is designed and executed over statistically computed time intervals for accurate rate determination. The proper design of such an experiment depends basically on the reliable accuracy estimates for the repeat leveling surveys. Then, the time and effort spent in complete testing of α and β errors for the results obtained will always be rewarding in terms of analyzed inferences or deductions.

REFERENCES

Dixon, W. J., and P. J. Massey, Jr., 1957. Introduction to Statistical Analysis, pp. 244-261, Second Edition, McGraw-Hill Book Co., Inc., New York.

FGCC, 1976. Federal Geodetic Control Committee Report on Crustal Movement and Polar Motion Activities. National Oceanic and Atmospheric Administration, Rockville, Maryland.

Frost, N. and J. E. Lilly, 1966. Crustal Movement in the Lac St. Jean Area, Quebec. Canadian Surveyor, XX(4), pp. 292-299.

Gale, L. A., 1970. Geodetic Observations for the Detection of Vertical Crustal Movement. Canadian Journal of Earth Sciences, vol. 7, pp. 602-606.

Holdahl, S. R., 1969. Geodetic Evaluation of Land Subsidence in the Central San Joaquin Valley of California. Paper presented at the Fall Meeting of the American Geophysical Union, San Francisco, California.

Holdahl, S. R., 1970. Studies of Precise Leveling at California Fault Sites. Paper presented at the Fall Meeting of the American Geophysical Union, San Francisco, California.

Holdahl, S. R., 1977. Recent Elevation Changes in Southern California. NOAA Technical Memo. NOS NGS-7, Rockville, Maryland.

Holdahl, S. R., and R. L. Hardy, 1977. Solvability and Multiquadric Analysis as Applied to Investigations of Vertical Crustal Deformations. Paper presented at 1977 International Symposium on Recent Crustal Motion, Palo Alto, California.

Gutenberg, B., 1941. Changes in Sea Level, Postglacial Uplift, and Mobility of the Earth's Interior. Bulletin of the Geological Society of America, vol. 52.

Korhonen, J., 1961. Adjustment of Levelings in Region of Slow Vertical Movement. Annals of Academy of Science for Fennicee. Sec. A 111 61, pp. 127-142.

Kumar, M., 1976. Monitoring of Crustal Movements in the San Andreas Fault Zone by a Satellite-Borne Ranging System. Department of Geodetic Science Report No. 243, The Ohio State University, Columbus, Ohio.

NOS, 1974. National Ocean Survey Report on 1973 Releveling of the Houston-Galveston Area, Texas. National Oceanic and Atmospheric Administration, Rockville, Maryland.

Remmer, O., 1975. Leveling Errors in Statú Nascendi. Geodetic Institute of Denmark, No. 51, Copenhagen, Denmark.

Schadlich, M., 1976. Statistical Analysis in Precision Leveling. Vermessungstechnik, Vol. 24, No. 3, German Democratic Republic.

Thurm, H., 1971. Some Systematic Errors of Precision Leveling. Jena Review, 3, pp. 172-176.

Vanicek P., and A. C. Hamilton, 1972. Further Analysis of Vertical Crustal Movement Observations in the Lac St. Jean Area, Quebec. Canadian Journal of Earth Science, Vol. 9, pp. 1139-1147.

Vanicek, P., and D. Christodulidis, 1974. A Method for the Evaluation of Vertical Crustal Movement from Scattered Geodetic Relevelings. Canadian Journal of Earth Sciences, Vol. 11, pp. 605-610.

Vanicek, P., M. R. Elliott, and R. O. Castle, 1977. Four Dimensional Modeling of Recent Vertical Movements in the Area of the Southern California Uplift. Paper presented at 1977 International Symposium on Recent Crustal Movement, Palo Alto, California.

Wassef, A. M., 1974. On the Search for Reliable Criteria of the Accuracy of Precise Leveling Based on Statistical Considerations of the Discrepancies. Bulletin Geodesique, No. 112, pp. 149-163.

Wassef, A. M., 1976. Propagation of Error in Precise Leveling and Its Bearing at the Assessment of Recent Crustal Movements. Bulletin Geodesique, Vol. 50, No. 4, pp. 323-329.

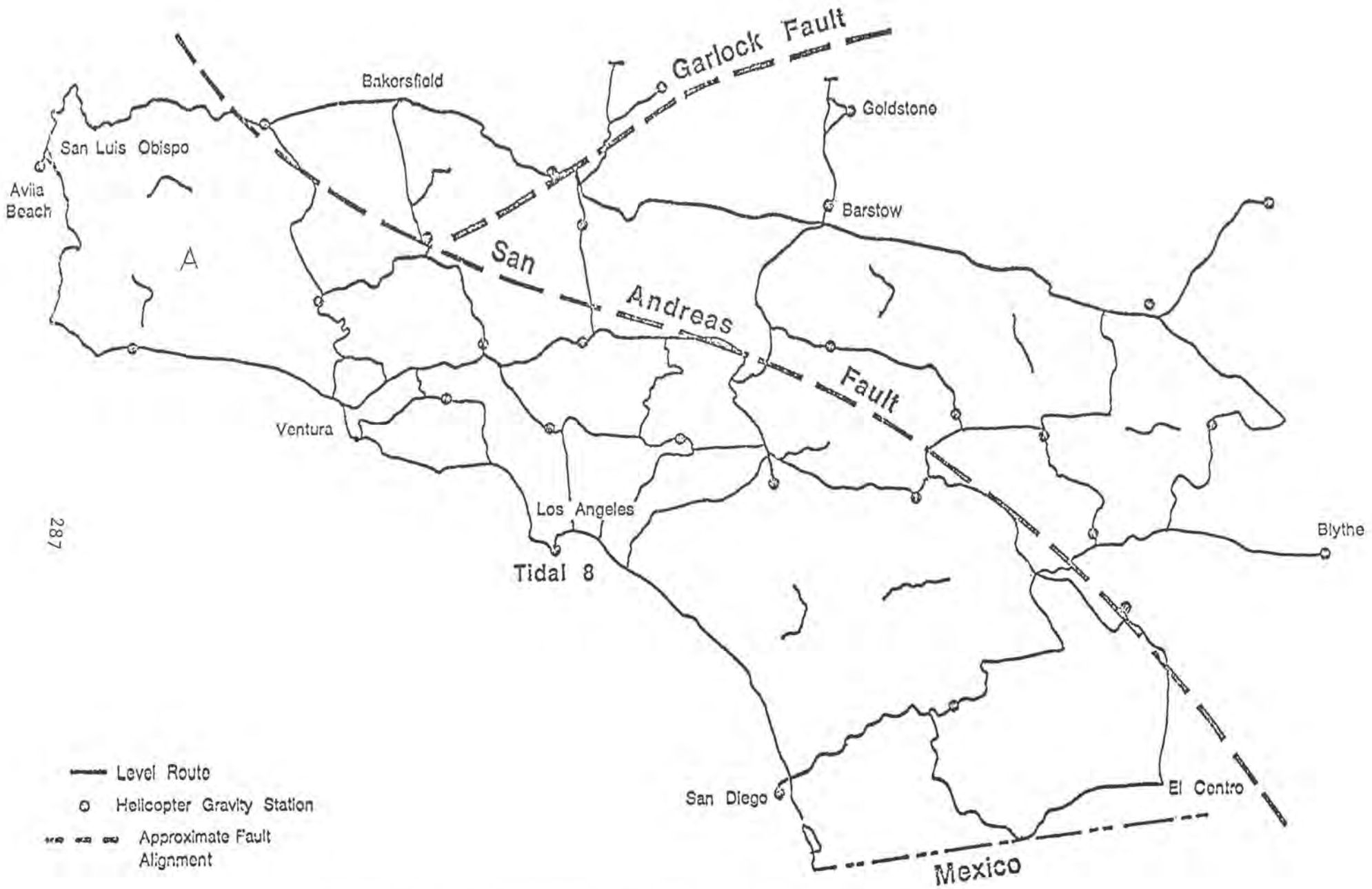

Figure 1: 1978 Southern California Releveling Program

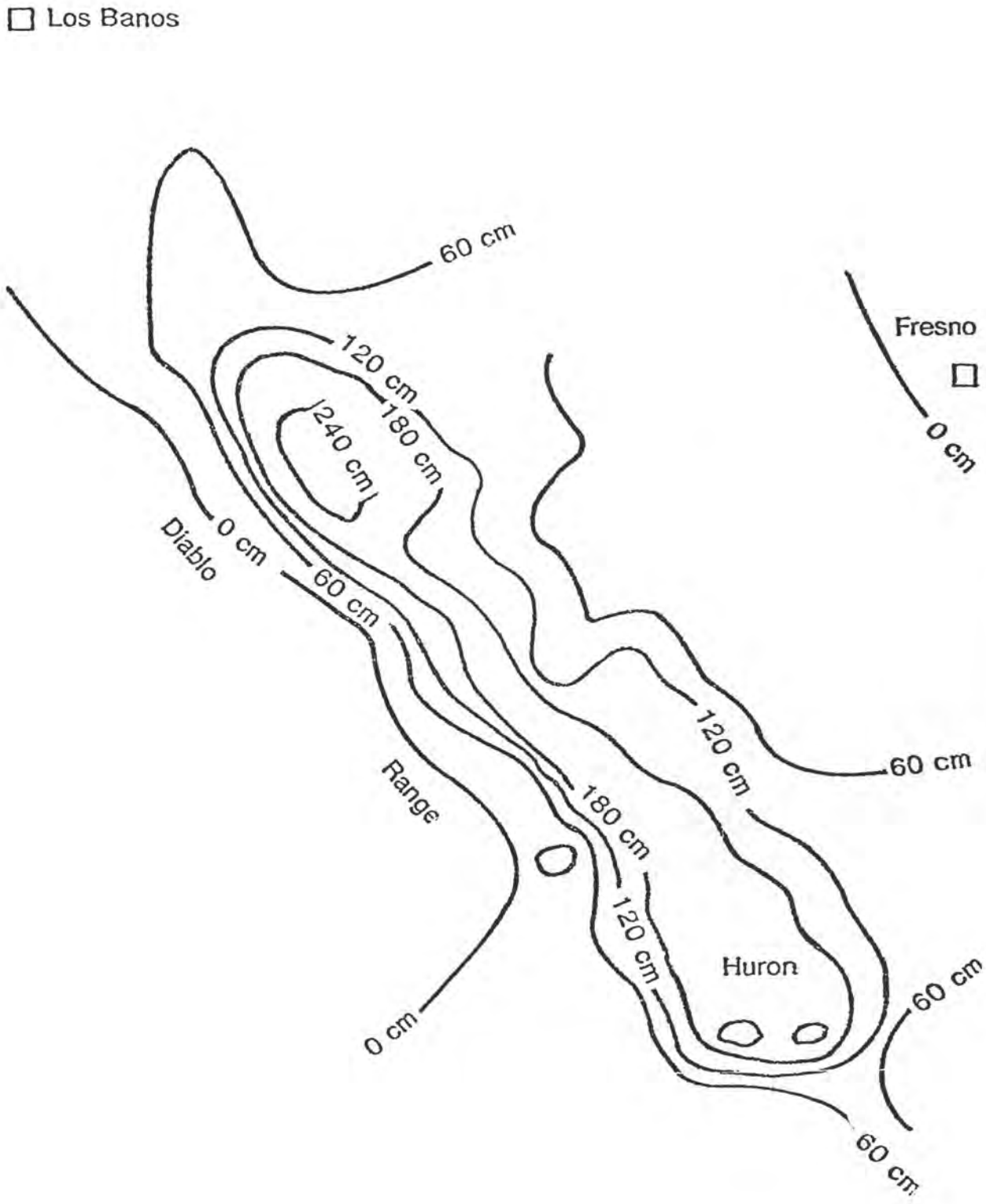

Figure 2. Relative Land Subsidence in San Joaquin Valley (1959 to 1969)

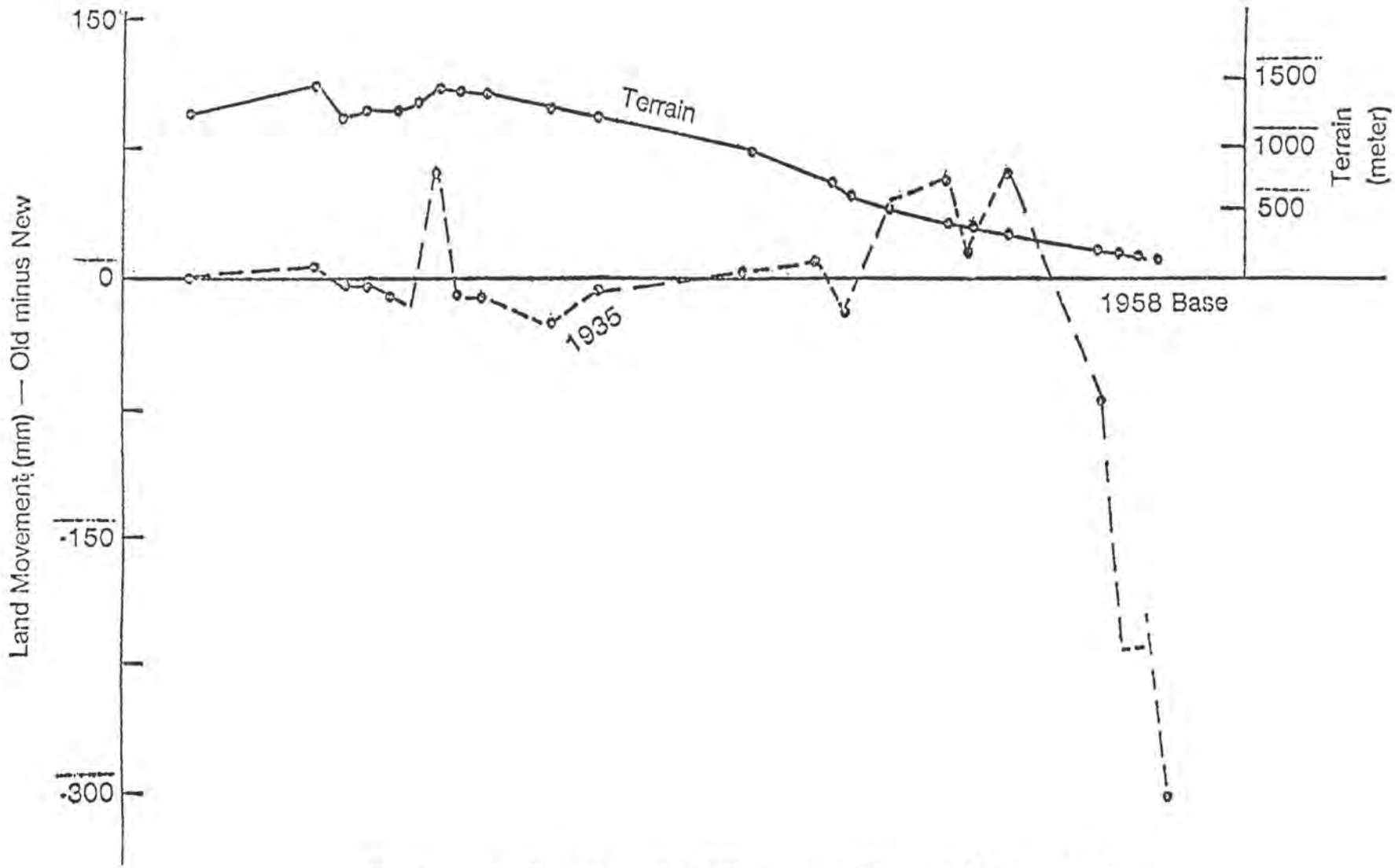

Figure 3. Profile of Elevation Differences in Texas (1935 to 1958)

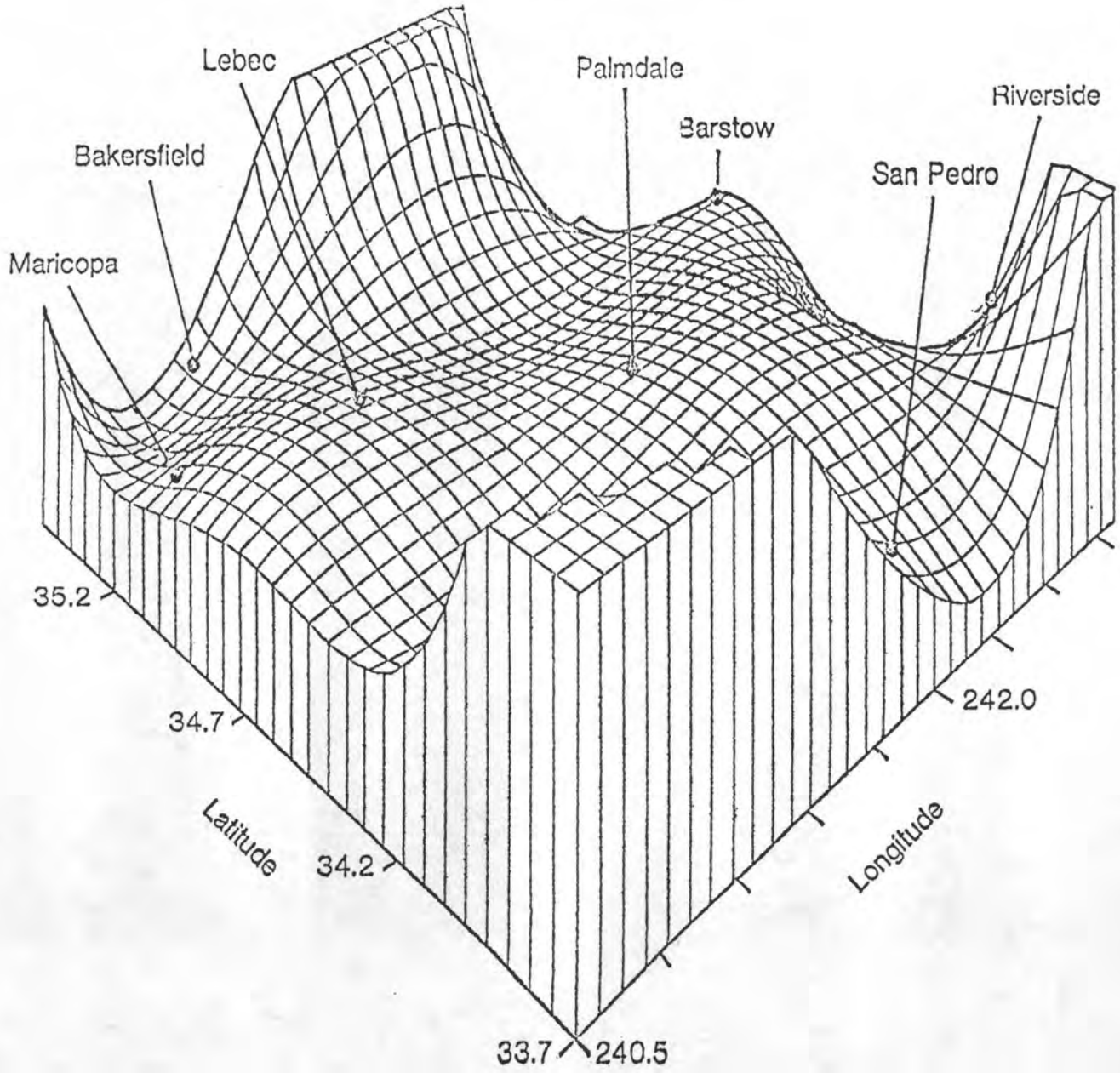

Figure 4. Velocity Surfaces in Palmdale Vicinity, 1906 to 1962 (Holdahl, 1977)

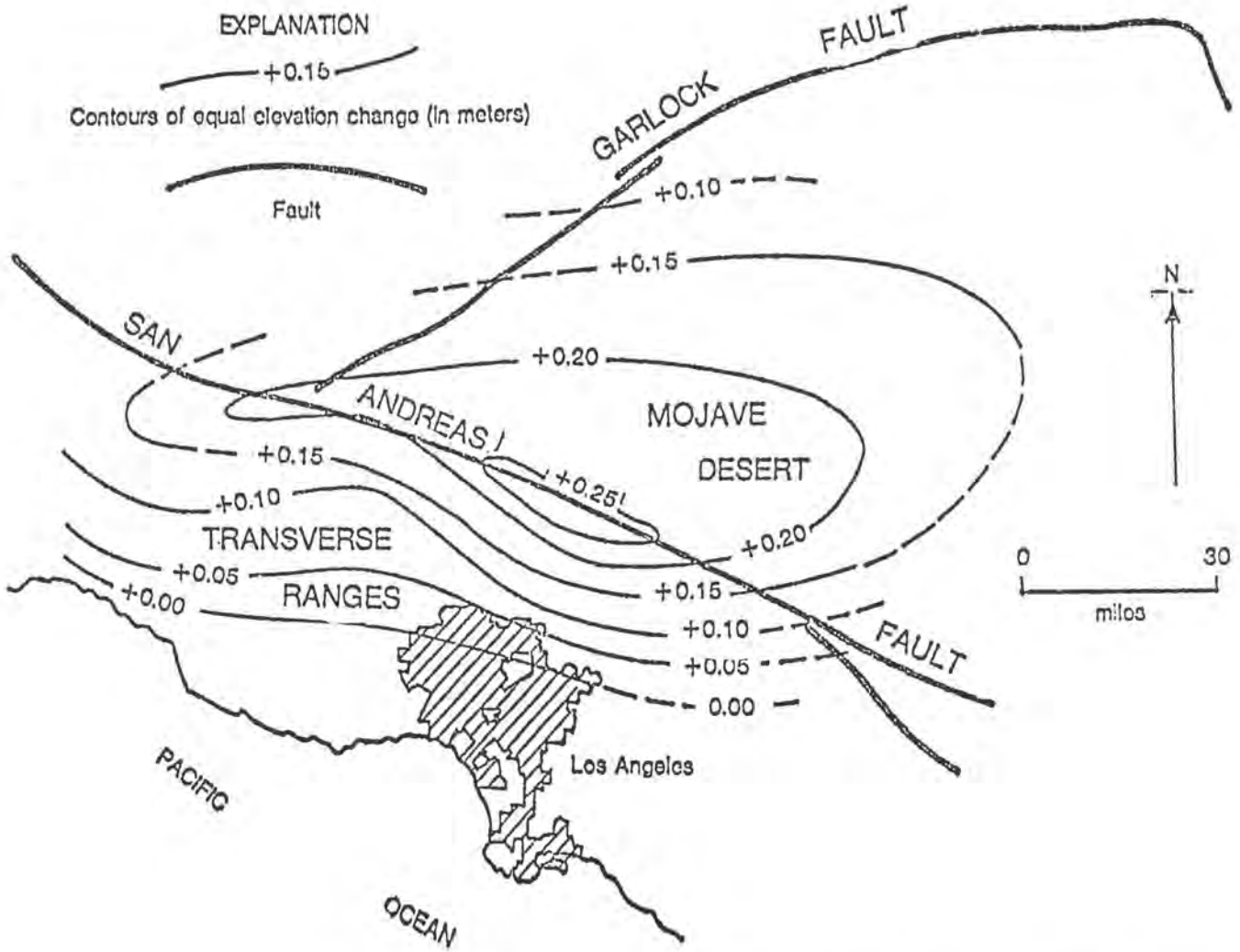

Figure 5. Relative Land Uplift in Palmdale Vicinity (By Courtesy of Dr. Robert O. Castle, USGS).

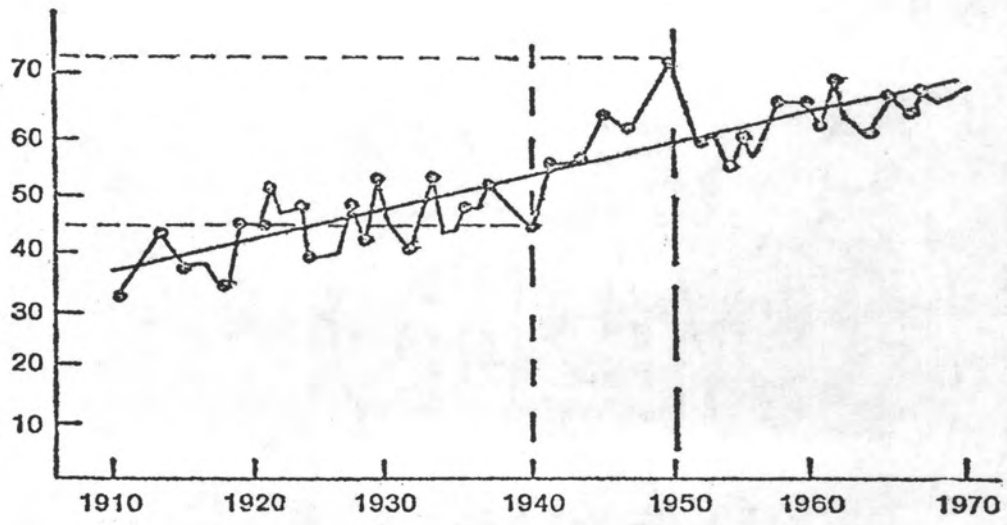

Figure 6. Variation of Mean Sea Level, Galeveston (Texas).

Published: 1978, 19th U.S. Rock Mechanics Symposium, University of Nevada--Reno.

J. M. Logan, Associate Professor, Department of Geology and Geophysics and Center for Tectonophysics, and L. W. Teufel, Graduate Assistant--Research, Department of Geology and Center for Tectonophysics, Texas A&M University, College Station, TX 77843.

The Prediction of Massive Hydraulic Fracturing from Analyses of Oriented Cores

ABSTRACT

An attempt has been made to predict the orientation of massive hydraulic fractures stimulated between depths of 2316 and 2464 m within the Muddy J Formation of the Wattenberg gas field, Colorado. Predictions were based upon a study of the properties of three oriented cores, one each from the west, central and eastern portion of the field and two unoriented cores from the central portion of the field.

A preferred orientation of fractures induced in point load tests is found for all five wells. The two oriented cores from the western and eastern well show a primary trend of about 335° (≠ 25°), while that from the central well showed a trend of about 110° (≠ 20°). The two unoriented cores also show a strong preferred orientation. This observed preferred orientation is corraborated by tensile strengths measured in Brazil tests. Additional support is obtained from triaxial compression tests done at confining pressure and temperatures simulating the hydrofracture depth. The strike of the induced shear fracture parallels (≠ 10°) the orientation of the fractures produced by point loading.

The second phase involves investigation of the composition, grain size, microfracture orientation, crystallographic orientation, grain dimensional orientation, and residual strain. Thin sections were cut parallel and perpendicular to the bedding plane and examined microscopically. In some cases sections were cut from two depths within the same well to determine vertical variability. The composition and grain size show no significant changes averaging about 65% quartz, 30% matrix, which is mostly clay, and 5% other minerals, and having a mean grain size of .11 mm. Essentially no microfractures are found in the undeformed material, and the crystallographic axes for the quartz grains are randomly distributed. The only two parameters that appear to possibly influence the fracture anisotropy are orientation of the dimensional axes of the quartz grains and the residual strain. In the wells on the east and west side of the field the long axes of the quartz are found to lie in the plane of the bedding and show a strong preferred orientation paralleling the direction of the fracture anisotropy. No preferred orientation is found in the other wells. The lack of outcrop precludes any in-situ strain measurements, but residual strain determinations were made from the cores by measuring the strain relief in the horizontal plane through the use of strain-gage rosettes and two over-cores of different sizes. All cores show the maximum elongation (or the direction of the maximum compressive stress) parallel to the fracture anisotropy. However, in the east and west wells the ratio of the magnitude of the maximum and minimum strain released through overcoring is 2 : 1 or less and is not considered to be sufficient to influence the fracture orientation. The wells from the center of the field, however, show ratios from 5 - 10 : 1, and are considered to be sufficient to influence the fracture orientation. Thus, it is concluded that the fractures oriented at 335° on the east and west side of the field are primarily controlled by the dimensional orientation of quartz grains, while those in the center of the field having an orientation of 110° are controlled primarily by the residual strain. Investigation of the subsurface geology shows a buried fault trending north east through the center of the field, which is postulated to have influenced the distribution of residual strain.

Following the prediction of the fracture orientation, and the hydrofracturing, Sandia Laboratories employed surface potential measurements to attempt to determine the orientation of the induced fractures. They were able to make determinations only in the eastern and central wells, but good agreement (≠ 10°) was found with the predictions from the core analysis.

INTRODUCTION

With the increased need for improved recovery techniques for hydrocarbons, tight reservoir rocks are receiving renewed attention. Massive hydraulic fracturing offers one technique for enhancing permeability and thus improving production. Despite it's widespread use, the processes involved in hydraulic fracturing are not well understood even today [1]. One of the needs is to be able to predict the orientation of the induced fracture and confirm this prediction by finding the newly formed feature. To this end a combined effort has been

undertaken by Amoco Production Co., Sandia Laboratories, and the U.S. Geological Survey [2-4]. This paper deals primarily with the efforts to recognize a fracture anistropy before the hydraulic fracturing effort and to try to relate this fracture anistropy to rock properties determined from analysis of well-core material. The predicted orientations are then compared with the results determined by electrical potential techniques developed by Sandia Laboratories. The approach to the prediction of the fractures is similar to that taken by Friedman and Logan [5] to assess the influences of residual elastic strain on the orientation of experimentally induced fractures in sandstones.

The five cores utilized in this study were taken from the Muddy "J" Formation in the Wattenberg gas field located in the Denver Basin. Three of the cores were oriented and two were unoriented (Figure 1). The latter, although not useable in predicting the true directional variations in properties, proved to be valuable in corraborating data from the oriented cores. The Muddy "J" sandstone occurs at a depth of about 2300 m and has a permeability ranging from 3 to 50 microdarcys. In two cases, cores were examined from two depths of the same well to determine vertical variability.

We will consider the procedures used in examining the cores first, and then present the results from the core analysis. Finally, we will attempt to integrate the results from the core analysis into the regional geology and compare the predicted fracture orientations with those determined by Sandia Laboratories.

PROCEDURE

The program utilized in the core analysis is shown in Table 1.

Fracture Anisotropy

Point-load tests were utilized as a quick and economical method of determining fracture anisotropy under room conditions. The load is applied through a central axis of an unconfined cylindrical specimen by means of a pair of opposed spherical indentors. Although an exact solution of the imposed elastic stress has not been found, the field is axially symmetric about the point load up to the onset of fractures and is such as to induce radial tensile fractures parallel to the cylinder axis [6, 7]. When several specimens from an isotropic rock are loaded to failure, and the orientations of the induced fractures are plotted with respect to a common external coordinate system, the trends (strikes) of the fractures on the plane normal to the cylinder axis (or in the plane of bedding) should be randomly distributed. If, on the other hand, the rock is anisotropic, the strikes should be relatable to the directional properties of the fabric. Fracture occures along a plane perpendicular to the direction of minimum tensile strength in the plane normal to the load axis.

Tests were made on discs taken from cores of all the wells investigated, and from two depths in two wells (II, V). Each disc was loaded between opposed 0.95-cm-diameter ball bearings mounted in an alignment device.

In that the fractures induced in the point-load tests are tensile fractures, the observed fractures anisotropy should be corraborated by Brazil tests. Such tests were made on all samples from the same intervals tested in the point load tests. Discs were oriented with respect to an external coordinate system, and the tensile strength measured. Strengths were determined at 15° increments of azmith directions. The variation of tensile strength normal to the bedding surface could then be determined.

It has been recognized that anisotropic effects are deminished with increasing confining pressure and temperature. In order to ascertain if the fracture anisotropy would persist at conditions simulating or exceeding the depth of burial, triaxial tests were conducted on specimens from each well, at a confining pressure of 70 MPa and 100°C. It has been noted [5] that the strike of the induced shear fracture will parallel the existing anisotropy if it exists at those conditions. Thus, if the fracture anistropy is significant, the strike of the induced fractures should show a preferred orientation and optimally should show the same orientation deduced from the point-load tests and the Brazil experiments.

Fabric Elements

If a fracture anisotropy is found to exist, this

information is sufficient to predict the orientation of the induced hydraulic fractures. It is, however, desirable to ascertain the fabric elements of the rock that might produce this fracture anisotropy. To this end, thin-section analyses were made of core material from all wells, and from separate depths in the two wells previously noted. Three mutually perpendicular thin sections were made at each depth and at least 300 data points were collected for each depth. Compositional and grain size analysis were determined from oridinary flat stage petrographic observations. Crystallographic and dimensional axis orientations were determined by universal stage techniques. In that the induced hydraulic fracture is assumed to be vertical, the fabric elements in the plane of the bedding were considered to be most significant. Fractures were mapped with respect to the known geographical directions in wells I, II, and III. Arbitrary coordinates were used for cores from wells IV and V, but all of the data from the same well are referred to by one coordinate system. Outcrop exposures are not sufficient to obtain measurements of the in-situ strain conditions, but residual strain measurements were made by overcoring techniques. The core recovered from the well is about 11 cm in diameter and a section about 30 cm long was used to place a strain-gage rosette on a surface perpendicular to the core axis. The rosette was allowed to stabilize for 48 hours, and was then overcored on a 5 cm diameter to a depth of 10 cm. Within two minutes of completing the overcoring the first measurements were made. These were continued until no further change was observed, a period of about 12 hours, and then allowed to stabalize for another 24 hours. A second over core, 2.5 cm in diamter, and 5 cm deep was then made and the measurements made.

General Geological Setting

After the fracture anistropy was determined and the fabric elements investigated, the geological setting and the presence of surface and subsurface faults in the vicinity of the wells was investigated to place the well information in a geological context. This information is particularly helpful in interpreting the residual strain information.

RESULTS

Fracture Anisotropy

The results of the point-load tests are presented in Figure 2. Data for five wells are presented and for two depths from well II. In all wells two types of fractures are induced. The majority of features are single fractures that trend completely across the specimens. Some fractures, however, have subsidary branches, invariably at about right angles to the main fracture, that extend from the main fracture to one edge of the specimen. The main trace of these bifurcating fractures is always within the cluster of single fractures. In wells I and II the fractures are clustered between 310° and 010°. In well III the main fractures range from 090° to 125°. The fractures in wells IV and V also show a strong preferred orientation with respect to the arbitrary coordinate systems.

Brazil tests of samples from the same depths show minimum tensile strengths in the same general direction as the preferred orientations determined from the point-load tests (Table 2). Additionally, the next-lowest value of the tensile strengths show a strong correlation with the orientation of the secondary fractures. No Brazil tests were conducted on the unoriented cores.

The results of the triaxial tests show that the fracture anisotropy exists at a confining pressure of 70 MPa and 100°C. The strike of shear fractures induced in such tests agrees in all cases with preferred orientations of fractures found in point-load tests.

Fabric Elements

Table 3 shows the composition and mean grain size for all wells investigated. The rocks are dominantly quartz, with little variation in content, except for the 2431 m depth in well V. The matrix material is dominately clay. The average grain size is about 10 mm for all wells except for the 2431 m depth in well V. Thus there is no variation in either composition or grain size within the wells investigated to suggest either an anisotropy, or that the behavior of the rocks in one well should differ from that in another.

Directional permeability measurements showed no directional variability. There were no significant numbers of microfractures present in the core material nor were there any concentrations of twin lamellae in the scattered grains of calcite. The c crystallographic axes were measured from all wells and are random.

The data for the dimensional orientation of the quartz grains is shown in Figure 3. The grains have a long to short axis ratio of about 1.8 - 2. In wells I and II there is a strong clustering of the directional orientation of the long axes between 330° and 010°. The agreement with the data on the fracture anistropy tests for the same wells is considered to be good. No strong secondary trends are present for the grain dimensional data for these wells. Well III does show some suggestion of more grains oriented between 080° and 090° than any other direction, but this concentration does not appear to be significantly more than other directions. Wells IV and V also do not show any preferred direction to the orientation of the long axes of the grains.

Data from thin sections perpendicular to the layering fro wells II and III clearly show that the long axes lie in the bedding plane and are almost horizontal (Figure 4).

The data for the residual strain measurements are summarized in Table 4 and Figure 5. All measurements during the strain relief indicated expansion in all directions and at all times. The amount of elongation deminished with time so the initial values are shown in Table 4. All wells showed a strong correlation of the direction of the maximum elongation with the fracture anisotropy deduced from the point-load tests. There are two distinct clusters of data as shown by the values of the microstrain (10^{-6} strain) measured during the strain relaxation. For wells I and II the ratio of the magnitude of the maximum 1 to miminum elongations is about 2 : 1. In wells III, IV, and V this ratio increases up to 10 : 1. It has been suggested [5] that ratios of the maximum to minimum strains should be of the order of four to one or larger to influence the direction of fracture propagation.

DISCUSSION

From the point-load data a clear fracture anisotropy appears to be present in the cores recovered from the Wattenberg Field. These preferred fracture directions are corraborated by data from the Brazil tests which show that the direction of the minimum tensile strength is closely aligned with the major fracture anisotropy. Even the secondary fractures found in the point-load tests are substantiated by secondary tensile strength minimums determined by the Brazil tests. The fracture anisotropy appears to persist to depths simulating 3,847 m (10,000 feet) as indicated by the results of triaxial tests. But despite the strong fracture anisotropy for each well, the directions are not uniform for all wells. The data for the wells on the western and eastern portions of the field (I and II) suggest that hydraulic fractures should form on a bearing of about 310° to 010° while the well from the central portion of the field (III) suggests a bearing of about 090° to 125°.

The fabric elements that appear to control the fracture anisotropy, also do not appear to be uniform throughout the field. Wells I and II have strong dimensional elongations of quartz grains that coincide with the fracture orientation, and we would interpret to control the fractures. There is also an orientation of the maximum elongation in the bedding plane, parallel to the fracture orientation, but we do not feel that the difference in the maximum and minimum strains are enough to control the fracture orientation if this were the only factor. The residual strain should enhance the influence exerted by the dimensional fabric, however. In wells III, IV and V the fabric elements look similar to each other, but different from the data presented for wells I and II. In wells III, IV, V there is not a strong direction of preferred orientation developed by the long axes of the grains. The dimensional axes are about random in their orientation and as such could not be interpreted as controlling the fracture anisotropy. The residual strain, however, shows a strong ratio between the maximum and minimum values of elongation in all three wells, and could be expected to

control the fracture orientation. In all three wells, the direction of maximum elongation (or the maximum principal stress in the bedding plane) coincides with the preferred orientation of the fractures. The consistancy of the data for these three wells, their general location in the middle of the field, and their differences from wells I and II, suggests that although the cores from wells IV and V are unoriented, that one might expect that the fracture orientation would take on a true orientation similar to that found in well III.

A review of the geology of the area suggests one reason for the dramatic difference in the magnitudes and orientations of the residual strains. A fault in the subsurface is known from seismic data [8] to trend northeast-southwest across the center of the field (Figure 6). This fault is believed to be high angle with the north side up. Theoretical solutions of a similar problem [9] suggest that such a tectonic situation would result in a reorientation of the stress field in the immediate vacinity of the fault, and particuarly on the downthrown side could result in the maximum principal stress taking a horizontal orientation.

Surface studies of lineations suggest trends in a general north-south and east-west direction [10], although the lack of surface exposure prevented measurement of the in-situ condition of stored strain.

Hydraulic fractures may be formed by the creation of new fractures or the opening of existing fractures. Additionally, fractures formed in one orientation at the well bore may curve once they leave the well bore. Thus it is interesting to look at a comparison of the predicted fracture orientation and the data obtained through use of electrical potential methods by Sandia Laboratories [4]. This comparison is shown in Figure 7. Unfortunately, data were only successfully obtained in two wells, where a prediction had been made; wells I and III. In both cases the agreement was within 10° which is considered to be exceptional. It is particularly significant that these two wells show the two different fracture orientations. Unfortunately no conclusive data was found from the tiltmeter studies [3].

CONCLUSIONS

A strong fracture anisotropy is found for the Muddy J sand of the Wattenberg Field, through the use of point-load tests, these results were supported by findings from Brazil and triaxial compression tests. Of the fabric elements investigated, only dimensional elongation of the quartz grains and residual strain appeared to contribute to the control of the fractures. Depending upon the well, both appear to have been significant. The variation of the condition of residual strain across the field may be explained by a change in the stress field produced by movement on a buried fault that transects the middle of the field. The agreement between the predicted fracture orientation and the fracture orientation detected by electrical potential methods was found to be very close. It appears that in some situations that the prediction of hydraulic fractures may be realized based upon direct, inexpensive measurements. Future work is planned to test this method in other areas.

ACKNOWLEDGEMENTS

Amoco Production Research Laboratory, Tulsa, Oklahoma, funded this research. Dr. M. Smith provided the data on the Brazil tests.

REFERENCES

1. Jaeger, J. C. and Cook, N. G. W. Fundamentals of Rock Mechanics, Methuen and Co., 513, 1969.
2. Smith, M. B., Holman, G. B., Fast, C. R., and Covlin, R. J. The azimuth of deep, penetrating fractures in the Wattenberg Field, 51st Annual Soc. Petrol. Eng. Fall Mtg. preprint 170 SPE 6092, 1976.
3. Wood, D. Preliminary Report, USERDA Contract No E (49-18)-2257, May, 1976.
4. Schuster, C. L., ed. Massive hydraulic fracture mapping and characterization program, Sandia Laboratories SAND-76-0095, February, 1976.
5. Friedman, M. and Logan, J. M. Influence of residual elastic strain on the orientation of experimental fractures in three quartzose

sandstones, Jour. Geophys. Res., 75, 387-405, 1970.

6. Reichmuth, D. R. Correlation of force-displacement data with physical properties of rock for percussive drilling systems, in Rock Mechanics, Proc. Symp. Rock Mechanics, 5th, edited by C. Fairhurst, 33-60, 1963.
7. McWilliams, J. R. The role of microstructure in the physical properties of rock, in Testing Techniques for Rock Mechanics, STP 402, 175-189, American Society for Testing and Materials, 1966.
8. Matusczak, R. A. Personal Communication, 1975.
9. Gangi, A. F., Min, K. D., and Logan, J. M. Experimental folding of rocks under confining pressures: Part IV--Theoretical analysis of faulted drape-folds, Tectonophysics, 42, 227-260, 1977.
10. Bradley, J. Personal Communication, 1975.

Table 1

CORE ANALYSIS PROGRAM

Fracture Anistropy

1. Point-Load Tests
2. Brazil Tests
3. Triaxial Compression Tests

Fabric Elements Studied

1. Composition
2. Grain Size
3. Directional Permeability
4. Orientation of Crystallographic Axes
5. Orientation of Microfractures
6. Orientation of Dimensional Axes of Quartz Grains
7. State of Residual Strain

General Geological Setting

Table 2

DATA-BRAZIL TESTS

Well	Azmuth Mimimum Tensile Strength	Azmuth Secondary Minimum Tensile Strength
I	335° - 010°	080° - 100°
II (2321 m)	310° - 335°	036° - 060°
III	095° - 125°	000° - 020°

Table 3

COMPOSITION AND GRAIN SIZE

Well	Quartz (%)	Matrix (%)	Other	Grain Size (m.m.) Mean	Range
I	59	36	5	.10	.02 - .21
II (2316 m)	61	31	8	.12	.05 - .30
II (2321 m)	62	30	8	.12	.04 - .25
III	69	28	3	.10	.06 - .20
IV	68	29	3	.10	.05 - .22
V (2368 m)	68	28	4	.11	.03 - .21
(2431 m)	81	17	2	.19	.08 - .29

Table 4

RESIDUAL STRAIN RESULTS

Well	Overcore	Maximum Elongation (μ strain)*	Bearing	Minimum Elongation (μ strain)	Bearing
I	1st (5 cm)	95	348°	77	258°
	2nd (2.5 cm)	38	338°	30	248°
II (2321 m)	1st (5 cm)	79	346°	41	256°
	2nd (2.5 cm)	25	336°	9	246°
II (2316 m)	1st (5 cm)	72	338°	38	248°
	2nd (2.5 cm)	25	333°	12	243°
III	1st (5 cm)	174	92°	82	2°
	2nd (2.5 cm)	50	117°	10	27°
IV**	1st (5 cm)	148	68°	27	158°
	2nd (2.5 cm)	47	65°	4	155°
V** (2368 m)	1st (5 cm)	151	342°	31	252°
	2nd (2.5 cm)	48	340°	4	250°

* Microstrain or 10^{-6} strain.

** Orientations with respect to an arbitrary reference system, but internally consistant for all data for these wells.

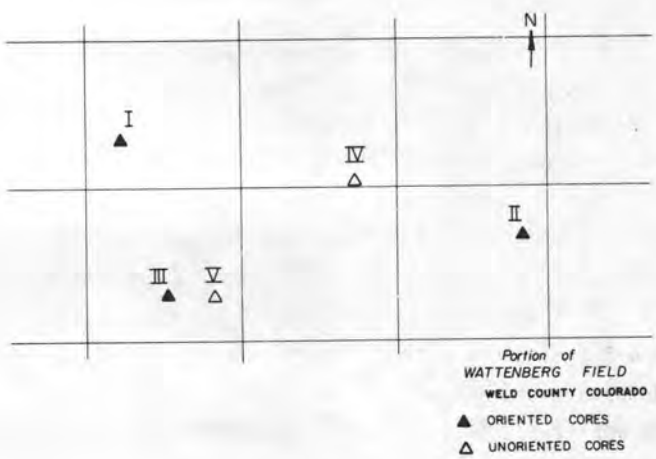

Figure 1. Map showing location of wells investigated in this core study.

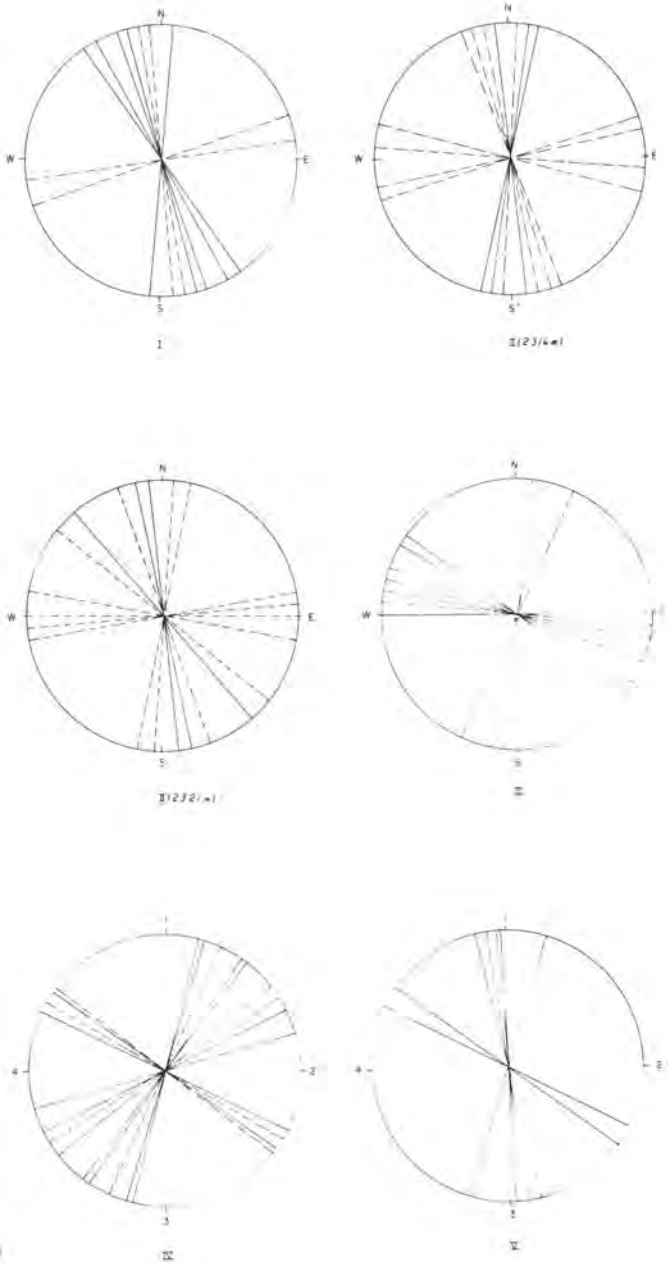

Figure 2. Fracture orientation diagrams for point-load tests from five wells. Well numbers and depths where applicable shown beneath each plot. Projections are looking down on the top of the bedding. Bifurcating fractures are shown by dashed lines. Wells IV and V are oriented with respect to an arbitrary coordinate system.

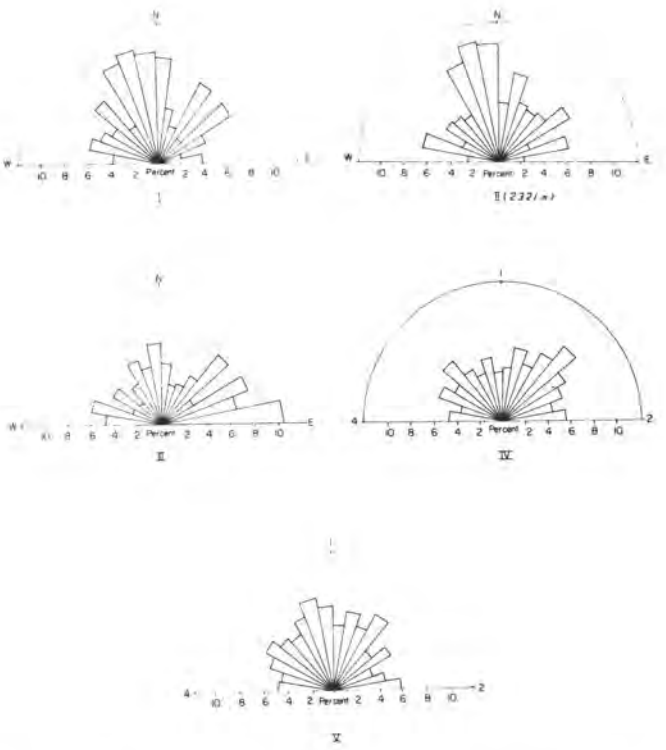

Figure 3. Rose diagrams showing orientation of long axis of quartz grains measured in the plane of the bedding. Well numbers shown beneath each diagram. Data are on at least 300 measurements.

Figure 4. Rose diagrams showing orientation of long axes of quartz grains in section perpendicular to bedding. Top and bottom of section are shown on left and right, respectively. Data are for at least 300 measurements. Note strong preferred orientation of axes in bedding plane.

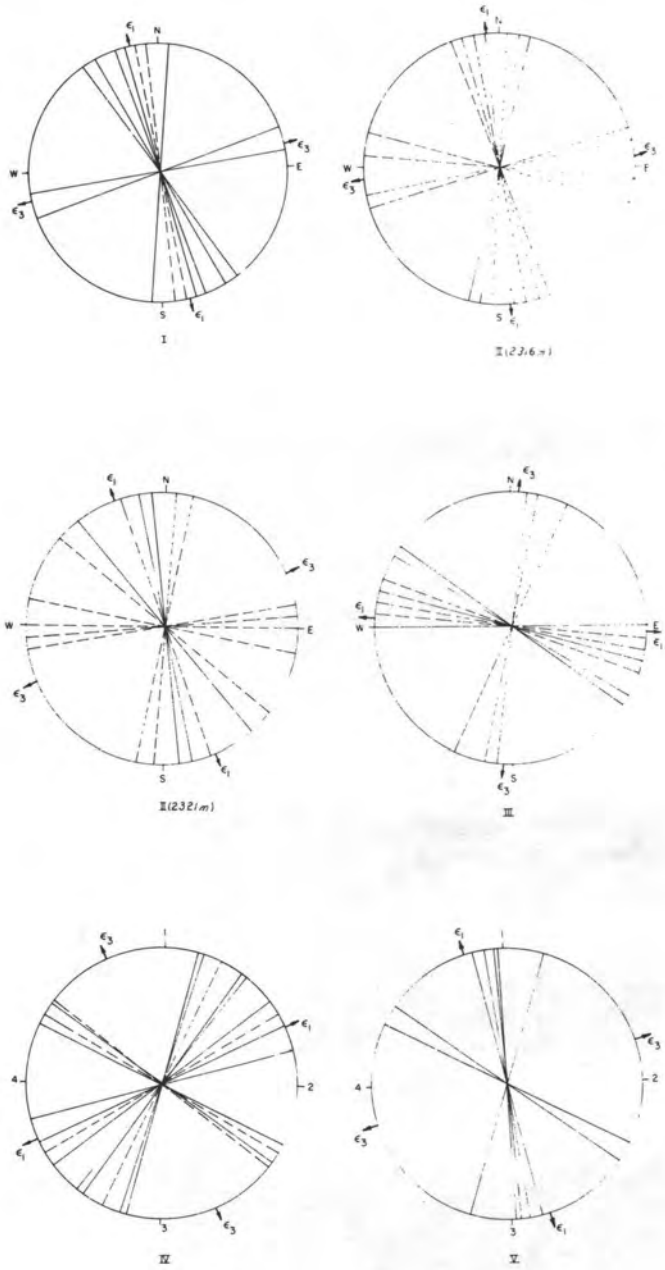

Figure 5. Fracture orientation data reproduced from Figure 2 with direction of maximum (ε_1) and minimum (ε_3) elongations in the bedding plane shown. Well numbers and depths where appropriate, are shown beneath each diagram.

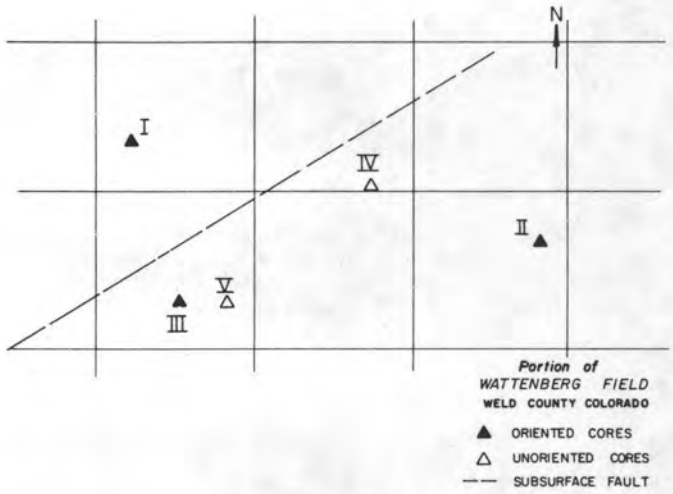

Figure 6. Map of wells investigated showing location of inferred subsurface fault.

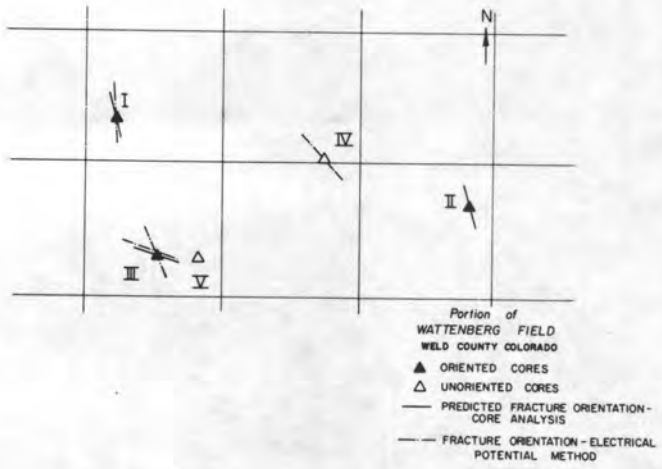

Figure 7. Map of wells investigated showing fracture predicted by this study (solid lines) and fracture orientation determined from electrical potential method (dashed lines).

Electrical Measurements as Stress-Strain Monitors

Theodore R. Madden

Department of Earth and Planetary Sciences
Massachusetts Institute of Technology
Cambridge, Massachusetts 02139

Acknowledgements

This work is supported by the United States Geological Survey under the Earthquake Hazards Reduction Program. A number of people have helped in these studies developing the instrumentation, installing the arrays, collecting and analyzing the data and thinking about what it all means. We wish to thank Dave Fitterman, George Keough, Gary Ruff, Tom Wilbur, James Wang, Jerry Lattoraca, Dave Smith, and Adolfo Figuera for their efforts. We also are indebted to Bill Brace, Joe Walsh, and Kate Hadley for teaching us many things about rock properties.

ELECTRICAL MEASUREMENTS AS STRESS-STRAIN MONITORS

Introduction

Many of the physical property measurements being made in connection with earthquake prediction studies are based on the concept that these properties are influenced by stresses or strains; especially so near the failure point. Electrical properties of rocks are controlled by the fluid in the pores and cracks of the rocks and, since this is the fraction of a rock most influenced by stresses, one should expect electrical measurements to be sensitive measures of changing stresses and strains. The strain changes that one is dealing with in these studies, however, are very small and even though the electrical responses can amplify the effect great sensitivity is needed in making the measurements.

Most of the literature on electrical measurements in earthquake prediction studies has ignored these quantitative aspects and has discussed very unrealistic variations. In this paper we wish to very briefly review our understanding of porous rock electrical properties and their strain relationships and to also examine the possibilities for electrical measurements to achieve useful sensitivities in these studies. In the first section we examine the factors that control the electrical conductivity of igneous and sedimentary rocks. These results are used in the second section to consider the quantitative aspects of conductivity, strain relationships, and also to review some of the existing experimental results. In the third section we examine some practical limitations on making sensitive field measurements and its effect on the usefulness of electrical conductivity measurements in earthquake studies. In the fourth section we review the streaming potential properties of rocks and possible surface electrical effects of changing pore pressures at depth. In the last section we examine some of the practical problems of making self potential variation measurements as indicators of pore pressure variations at depth.

I. Electrical Conductivity in Porous Rocks

In terms of their electrical and mechanical properties we can recognize three general types of rocks:

1. igneous and metamorphic rocks;
2. sedimentary rocks;
3. fault zone rocks.

Unfortunately, the most important class of rocks for this study, the fault zone rocks, are the least studied and we must proceed under the assumption that our insights about electrical and mechanical properties gained from studies on the first two

classes will not fail us in giving reasonable estimates of the behavior of rocks in the fault zone.

In the crustal environment the electrical conductivity of rocks is due to the presence of water in an interconnected system of pores and cracks within the rock. With the exception of certain plastic zones, such as salt beds and some marbles, no region of the crust seems devoid of such interstitial water and resistivities are 10^5 ohm-meters or less. In California, along the San Andreas, the observed resistivities are much less going from 10-20 ohm-meters in the Franciscan rocks to 300-500 ohm-meters in the granites.

The actual resistivity values depend on two factors, the conductivity of the pore fluid and the volume and geometry of the interconnected pore and crack spaces in the rock. The pore fluid conductivity at the temperature and pressure of the upper crust depends on the salinity of the fluid and on the temperature. The conductivity is approximately linearly dependent on the salinity which can vary by three orders of magnitude. The temperature effect is approximately exponential, but the activation energy is low so that the temperature effects are only about one order of magnitude from freezing to the critical point temperature. A dramatic change in the ability of dissolved salts to disassociate occurs near this temperature ($\sim 370^0$C) which causes a sharp decrease in conductivity with a further increase of temperature. This effect is offset by pressure, as seen in Figure 1, and also by high salt concentrations.

When the rock pores are extremely fine (less than .01μ) a further contribution, called the surface conduction, becomes important. This is an added conductivity due to an excess of ions electrostatically attracted to the mineral surface due to a net charge on the minerals. The potential caused by this net charge is called the zeta potential and is typically -50 to -70 mv for silicate minerals at room temperature. Clays have a very large surface conductivity and weathered rocks are usually much more conductive because of their clay content.

The effect of the rock pore geometry on conductivity is less well understood but extremely important in controlling strain effects on conductivity. Useful insights can be obtained by considering the interconnected crack and pores as a network and using certain properties of networks. Studies of the pore and crack sizes from SEM and capillarity measurements show that rock pores have a very wide range of widths, so that the network representing the rock conduction will have a very wide range of component values. If these are randomly distributed it is known that a subset of these components cannot form an interconnected system by themselves unless their number exceeds a certain fraction of all the elements, which fraction is called the critical probability. When the distribution function of

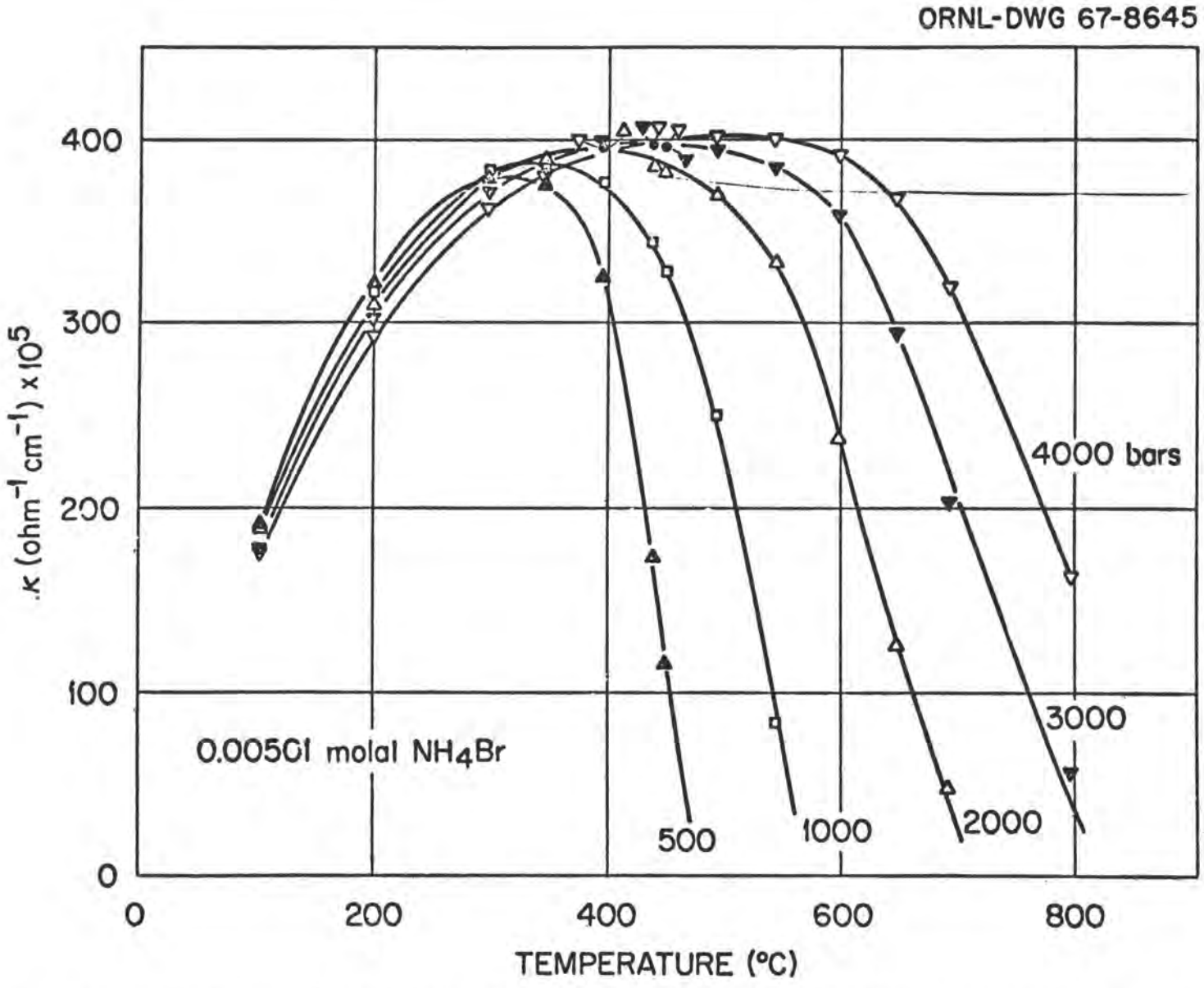

Figure 1 Isobaric Variation of Specific Conductances of 0.00501 *m* NH_4Br Solutions with Temperature at Pressures from 500 to 4000 bars. (Quist and Marshall)

network element values is very wide, the most conductive channels will be only a small fraction of all the channels and will not form an interconnected set. Thus current through these channels will also be forced to traverse much poorer conducting channels, which make porous rock conductivity inefficient. Numerical studies on the behavior of different types of networks have shown that when the distribution function is smooth, the resulting conductivity is well approximated by the geometric mean of the conductivity distribution. Thus very narrow cracks have an influence on the total conductivity far in excess of their contribution to the total pore volume. Since the narrow cracks are usually the most easily deformed ones, one can expect the rock conductivity to be sensitive to strain.

To use these results to predict electrical properties requires a good deal of information about crack and pore size distributions that is difficult to come by, but sedimentary rocks seem to have a very simple law that predicts their conductivities. This is known as Archie's law which states that the conductivity of the rock is the conductivity of the pore fluid times the porosity raised to some power.

$$\sigma_{rock} = \sigma_{fluid} \ (\text{porosity})^n$$

This power is generally just about 2. The law was originally based on a study of sandstones, but as seen in Figure 2, it is also very good for other types of sedimentary rocks. The power law behavior is typical of a construction of non-conducting particles of different sizes (sediment grains) immersed in a continuous conducting phase (pore fluid) but the exponent should depend on the grain shapes. Spherical grains should give the exponent 1.5, which is observed, and flatter shapes should raise this value. Why the exponent 2 is so common is not understood at present and thus Archie's law remains an empirical law. Figure 3 shows pore width distributions for some sedimentary rocks and their transport properties. Figure 4 shows a comparison of an Archie law prediction with predictions based on the more complex geometric mean calculation which needed capillarity measurements to estimate the pore width distribution.

Archie's law does not work as well with igneous rocks, however, and at low pressures igneous rocks are usually much more conductive than the law would predict. This is especially true for highly stressed rocks. Such rocks are found to have not only many more cracks, but also a much wider distribution of crack lengths. This complicates the geometric mean theory and leads to higher conductivities as the smaller scale cracks, if interconnected, will tend to act in parallel with larger cracks immersed among them and so on up the length scale

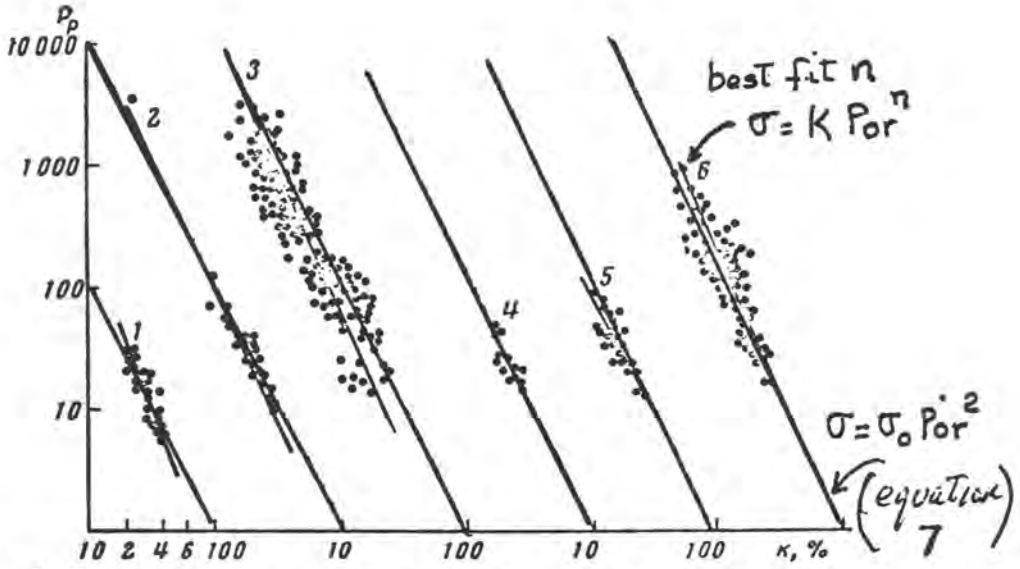

Fig 2 Relationship of the formation factor, P_p, to the coefficient of porosity, k, for carbonate (limestone) sedimentary rocks in the USSR and the USA: (1) limestones from Kazakhstan (from Sigal), (2) limestones from the Kuibyshev area, Bashkiria (from Kachurina) (3) carboniferous limestones from the Saratov Basin (from Eidman), (4) devonian limestone from Crosset, Texas, (5) oolitic limestone, Smackover formation, (6) Permian limestone, San Andreas Basin, Texas (from Archie).

(from Parkhomenko)

Pore Parameters and Flow Properties of some Sedimentary Rocks
Φ
FF
K in md
Pore widths in μ
Probability
0.1
0.3
1
3
10
30
100
23.2%
13.7
(8.7)
2.6
(3.2)
21.6%
17
(12)
18
(5.8)
15.7%
48
(16)
27
(56)
15.7%
38
(44)
9
(1.3)
14.8%
42
(33)
6
(7.3)
12.1%
83
(30)
4.4
(6.0)
6.2%
193
(112)
0.6
(0.4)

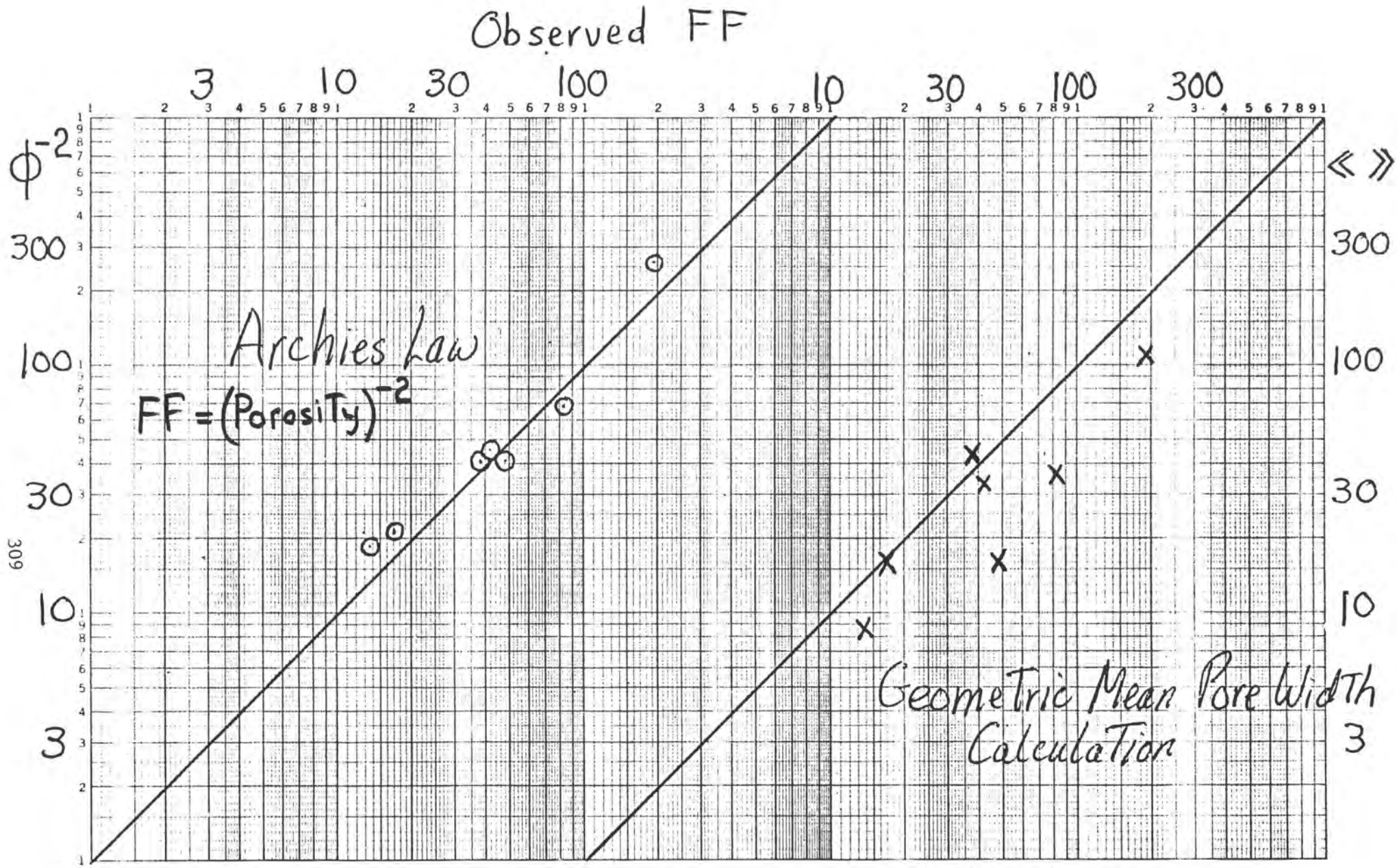

Fig 4 Comparison of Observed and Predicted FF

FF (Formation Factor) = $\sigma_{\text{Pore fluid}} / \sigma_{\text{rock}}$

(Madden, 1976). Figure 5 illustrates this sort of relationship.

We have attempted to study the effect of jointing on conductivity by making measurements around granite quaries. In New England these granites are heavily jointed near the surface but the electrical properties nevertheless were controlled by the microfractures (Madden, 1974). In fact, the resistivities were highest for shallow measurements away from the quarries, next highest for the measurements on the quarry floors, and the lowest were for the sample measurements (Madden, 1974). These results can be explained by the stress relief of quarrying and show the jointing to be unimportant. This is not unexpected as the joints contribute only a small fraction of the total crack density. (Westerly granite has about 400 M^2 of crack surface per cubic meter.)

II. Resistivity: Stress-Strain Relationships

Stress effects the electrical resistivity of rocks by opening or closing existing cracks and pores and also by creating new cracks. When the temperature is above the critical point temperature of water, pore pressure changes could also change the pore fluid conductivity. To understand the stress effects on the pore and crack parameters we rely heavily on laboratory studies. Most studies involve the effect of hydrostatic pressure, and much more data is needed on the effects of shear stresses, especially on sedimentary rocks. As we have mentioned above, virtually no laboratory studies exist on materials typical of the fault zone. Hydrostatic pressure increases the resistivity by closing down the conduction paths. Shear stress effects are more complicated. At low shear stresses, little change in resistivity occurs, until the onset of dilatancy, after which very large changes can occur.

Let us examine pressure effects first. It is usually assumed that the crack and pore closure follows the behavior of isolated cracks which depends on the crack or pore aspect ratio. Very narrow cracks (low aspect ratio) should close with modest pressures, while cylindrical pores should be little affected until the crushing strength of the rock is exceeded. Actually, of course, the real situation is more complex. Cracks probably never close completely because of surface misfits, but nevertheless rocks whose conductivity is dominated by their crack populations show very large resistivity changes at modest pressures. This is the typical behavior of low porosity igneous and metamorphic rocks. Since their porisities are low the volume changes accompanying these resistivity changes are small and the resistivity variation is a large amplification of the strain variation. Tables I and II give some typical results for such rocks.

$$\ll y^i \gg + \ll y^{i-1} \gg \leq \ll y^i + \ll y^{i-1} \gg \gg \leq \ll y^i + y^{i-1} \gg$$

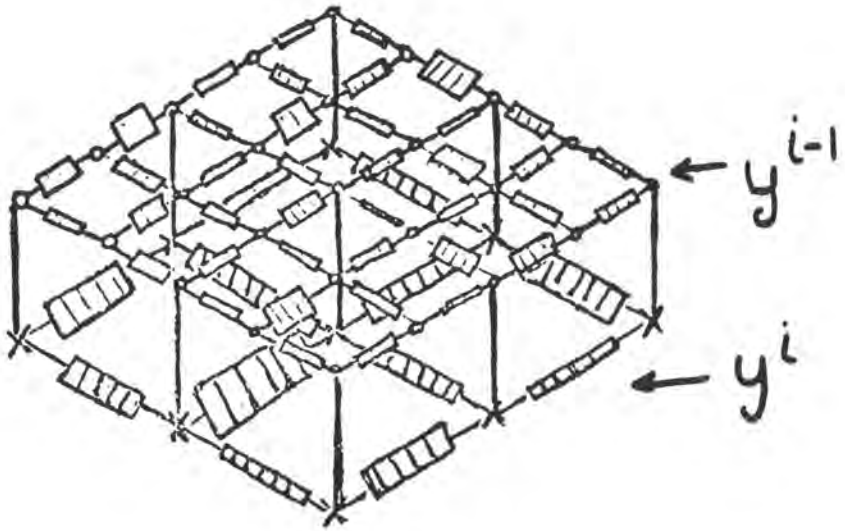

Interaction of Conduction Paths of Different Length Scales

Fig 5

$\ll \gg$ represents network averaging which is approximated by geometric mean

TABLE I.

Resistivity-Strain Amplification Factor $(\Delta\rho/\rho)/(\Delta\text{strain})$

Low Porosity Rocks Under Isotropic Stress (Brace et al., 1965)

Pressure, in bars	Westerly Granite	Stone Mtn. Granite	Casco Granite	Rutland Quartzite	Cape Cod Granodiorite
75	880	760	400	1350	1630
175	680	680	530	910	1500
375	460	590	640	600	570
750	300	560	530	400	360
1500	250	420	310	250	190
3000	160	350	210		110
Porosity	0.9%	0.6%	0.7%	0.5%	0.4%

TABLE II.

Resistivity:Stress Sensitivity $\%\Delta\rho/bar$

Low Porosity Rocks Under Isotropic Stress (Brace et al., 1965, 1968)

Pressure in bars	Westerly Granite	Stone Mtn. Granite	Casco Granite	Rutland Quartzite	Chittenden Dolomite	Blair Dolomite	Grenville Marble	Pottsville Sandstone	Black Slate ¶Bedding	Black Slate ⊥Bedding
75	.607	.702	.732	.777	.419	1.494	.811	.575	.211	.262
175	.291	.434	.462	.415	.225	.645	.425	.378	.154	.118
375	.143	.253	.264	.197	.152	.293	.156	.277	.175	.080
750	.082	.153	.142	.115	.071	.103	.114	.142	.105	.062
1500	.058	.097	.071	.063	.041	.049	.078	.076	.060	.035
3000	.034	.067	.042	.035	.030	.027	.048	.028	.038	.026
5000	.026	.052	.029	.026	.029	.018	.050	.031	.033	0.22
Porosity	0.9%	0.6%	0.7%	0.5%	1%	0.2%	0.4%	2.9%	1.2%	

For sedimentary rocks we can fall back on Archie's law to estimate the strain amplification factor. From Archie's law we obtain

$$[\Delta\rho/\rho]/\Delta\mu = 2/\text{porosity} \qquad (2)$$

Thus porous rocks have a much smaller amplification factor than the low porosity rocks listed in Table I.

Even though porous rocks are less stiff they show smaller resistivity stress effects. From dynamic measurements on dry rocks one can estimate the stress sensitivity with the use of equation 2. For sandstones in the 15-25% porosity range this gives a typical result of about .01% $\Delta\rho$/bar. Static measurements give higher values. Table III lists results of resistivity measurements under hydrostatic loading for samples which were allowed to drain during compression.

If longer time scales are involved chemical effects become important. These can enhance further crack growth and consolidation and also lower the porosity by cementation processes. This is observed in actual sediments under compression from the overlying sediments. Figure 6 shows a compilation of such data and this is transposed into a resistivity change using Archie's law in the scales shown at the right. These scales can be moved horizontally (not vertically) to fit the data and the ranges shown bracket almost all the data. These effects are irreversible and probably not directly applicable to the earthquake studies, but on the other hand, the laboratory time scale is probably too short and the real behavior lies somewhere in between.

Of greater importance in earthquake studies are the resistivity:stress relationships near the failure point of rocks. Rocks exhibit the phenomena of dilatancy before failure which is a volume increase produced by the shear stresses. This volume increase involves widening existing cracks and also creating new cracks. The two schools of thought about earthquake premonitory phenomena essentially differ in the emphasis they give these two effects. In any case, we should expect resistivity decreases to accompany increasing stresses in this regime, unless we are in the pore pressure and temperature range where the pore fluid conductivity would be strongly affected. In most situations this is unlikely so that laboratory data taken at low temperatures is still relevant. This data is hard to come by and we are indebted to Bill Brace and his coworkers for most of our knowledge about resistivity variations near failure. In order to map the resistivity stress relationships one needs several sets of measurements made with different confining pressures. Variations between different samples or different pore fluids are then adjusted by normalizing the data to a common stress situation which is usually taken as the isotropic stress

TABLE III.

Resistivity:Stress Sensitivity $\%\Delta\rho$/bar

High Porosity Sedimentary Rocks Under Isotropic Stress

(Brace et al., 1968 and Brace, 1974)

Pressure in bars	Bedford Limestone	Mixed Co. Sandstone
75	.040	
175	.022	
250		.030
375	.013	
750	.024	.005
1500	.011	.005
3000	.022	.009
5000	.006	.017
Porosity	12%	24%

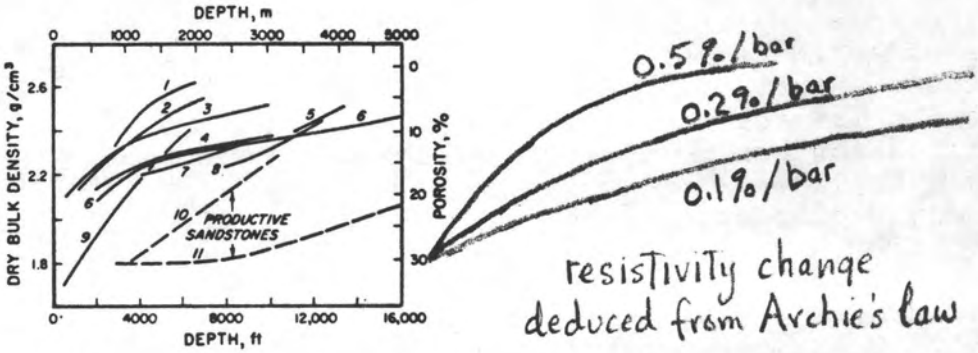

Fig. 6 Relationship between depth of burial and density (as well as poros... sediments from various localities. (After Dickey, 1972, fig. 5, p. 7; courtesy Int... Congr., Montreal.) *1* = Athy (1930), Pennsylvanian, Oklahoma; *2* = Dallmus ... Tertiary, Venezuela; *3* = Eaton (1969), Tertiary, California; *4* = Dickinson (1953) ... ry, Gulf Coast; *5* = Boatman, Louisiana; *6* = Griffin and Bazer (1969); *7* = Rochon ... Louisiana; *8* = Reynolds; *9* = Hedberg (1926, 1936), Tertiary, Venezuela; *10* = P... al. (1963), Germany; *11* = Atwater and Miller (1965), average sandstone, Louisiana

(from Wolf and Chilingarian, 1976)

results. This then allows plotting of all the data on one graph and from such a plot one can infer the results of different stress situations. Figure 7 shows such a plot based on four different experiments with Westerly granite. Besides the data trajectories, lines have also been drawn connecting points of equal shear stress. Unfortunately, the pressures are mostly too high to be directly relevant to earthquake phenomena, but the trend of the data seems to indicate even greater sensitivity at lower pressures. The maximum sensitivity shown is about .05%/bar which is considerably greater than the sensitivity to isotropic stresses at the same pressure, and I would expect this increased sensitivity to persist at lower confining pressures where the isotropic sensitivity is much larger. The strain amplification can no longer be described by a single number. Actually a large part of the data trajectories in the dilatant region involve very little net volume change as the mineral compression balances out the volume increase associated with the cracks (Brace, Paulding, and Scholz, 1966). The cracks themselves develop highly anisotropically so that there are very different strains in different directions. Combining the strain data on Westerly granite with the resistivity data give amplification factors of around 250-500. This result is quite remarkable considering that the net crack volume change for shear stressing is much less than that for isotropic stressing and the sensitivity must be explained by the increase in the number of cracks. Figure 8 shows how dramatically the crack population increases with stressing. The electrical effects are further enhanced because the crack length distribution is widened as explained in the first section. This is seen in the distributions shown in Figures 9, 10, and 11. This data was obtained by Kate Hadley from painstaking examinations of SEM pictures of granite samples stressed to various levels (Hadley, 1975). The division into stress-induced and virgin cracks was a conjecture of this author used to model resistivity effects (Madden, 1976). The crack density for the sample stressed to failure is actually close to the theoretical limit for the rock to remain whole if the cracks were isotropically distributed, but the theory needs to be developed further to treat the actual anisotropic distribution.

The data for sedimentary rocks is much thinner and less conclusive. Two sandstones measured by Bill Brace are shown in Figures 12 and 13. Only one run under non-isotropic stressing was given for the Pottsville sandstone, but its behavior is again so similar to that of the igneous rock samples one can infer what other conditions might give. The sensitivity of resistivity variations to stress in the dilatant region are again of the order of .05%/bar. The strain amplification factors are slightly less being about

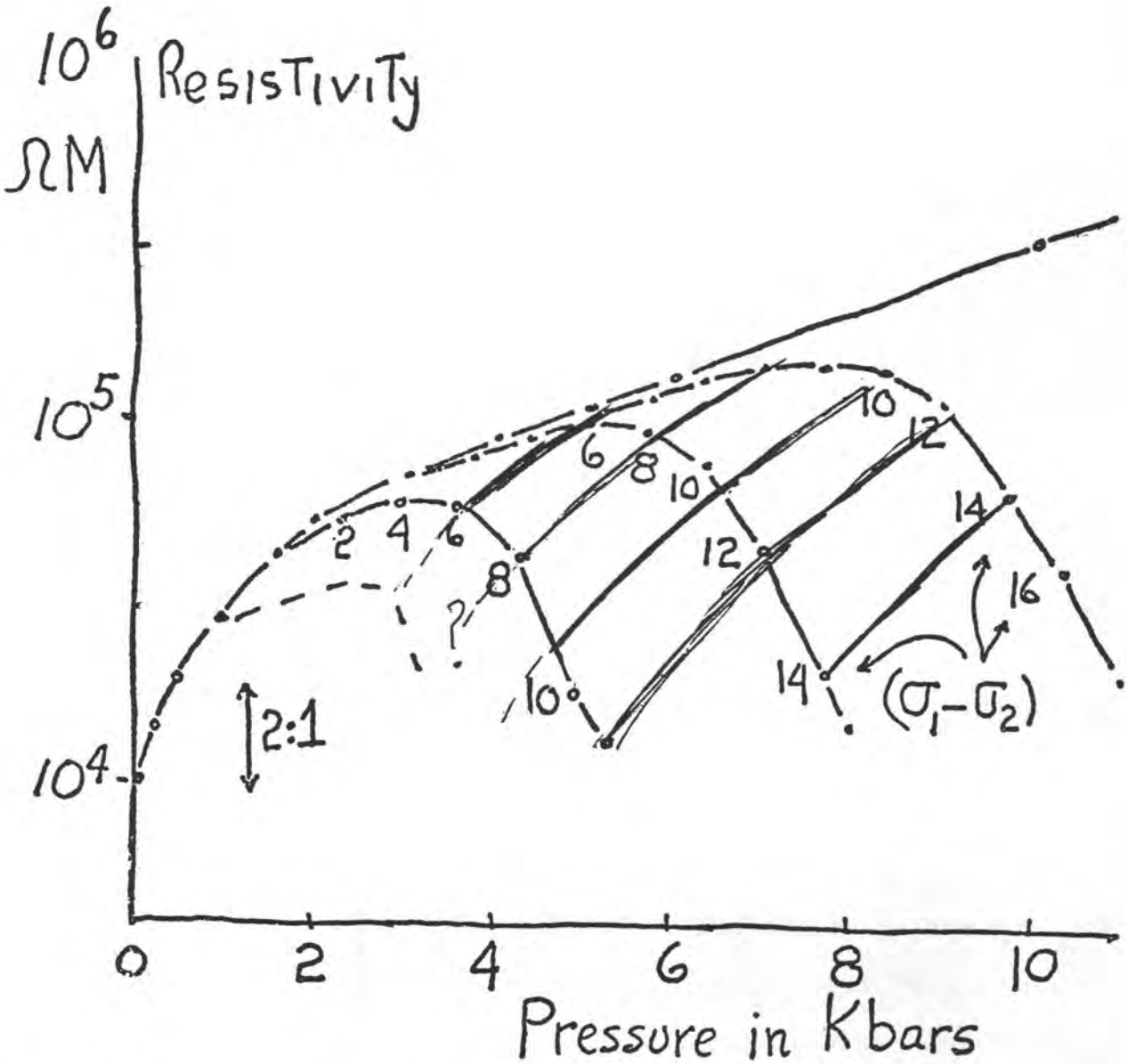

Fig 7 Resistivity of Westerly Granite for Isotropic and Triaxial Loading (from Brace et al 1965, 1968)

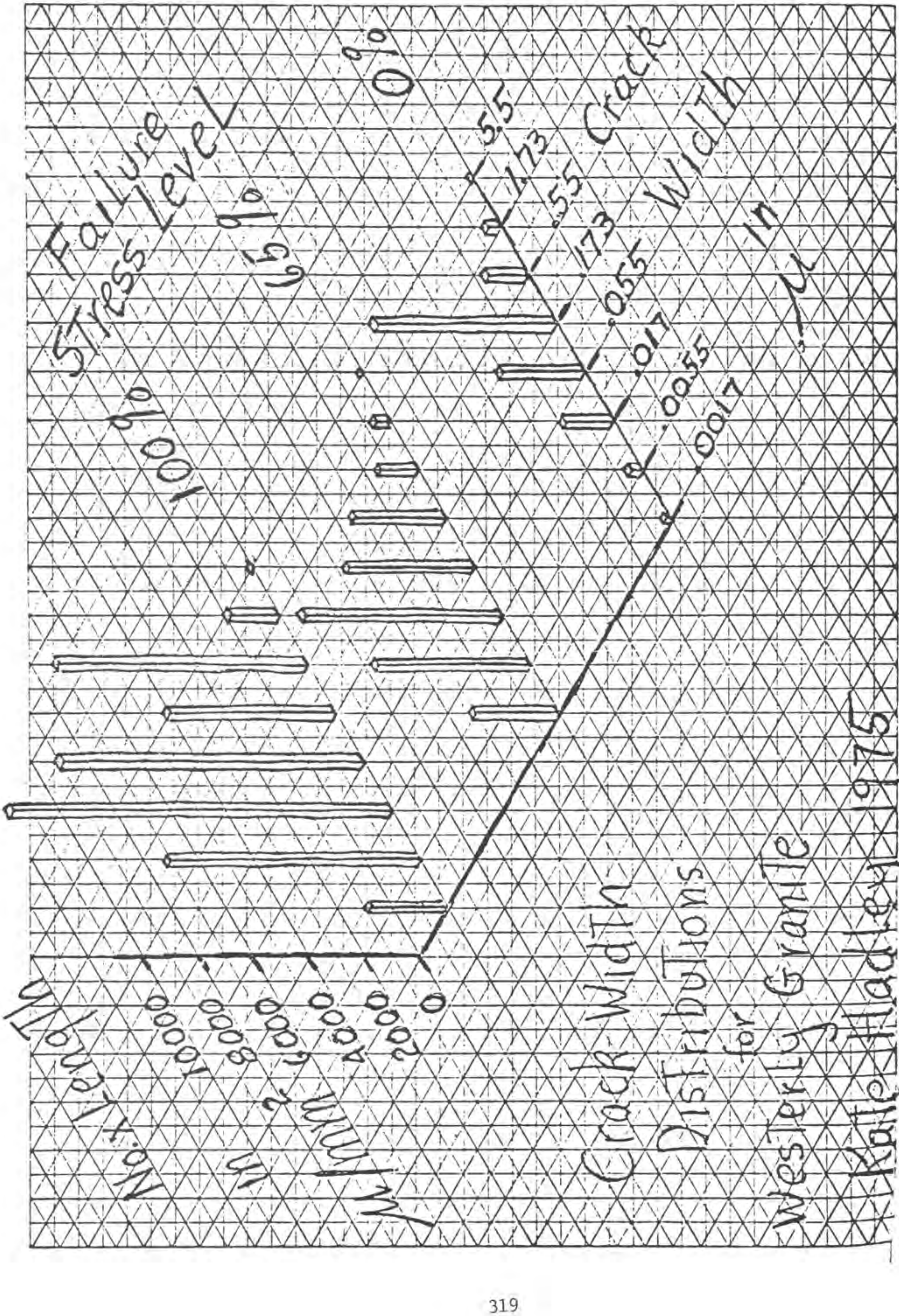
Failure Stress Level
100%
95%
0%
5.5
1.73
.55
.173
.055
.017
.0055
.0017
Crack Width
μ in
0
2000
4000
6000
8000
10000
Crack Width Distributions for Westerly Granite
Katie Hadley 1975

Fig 8

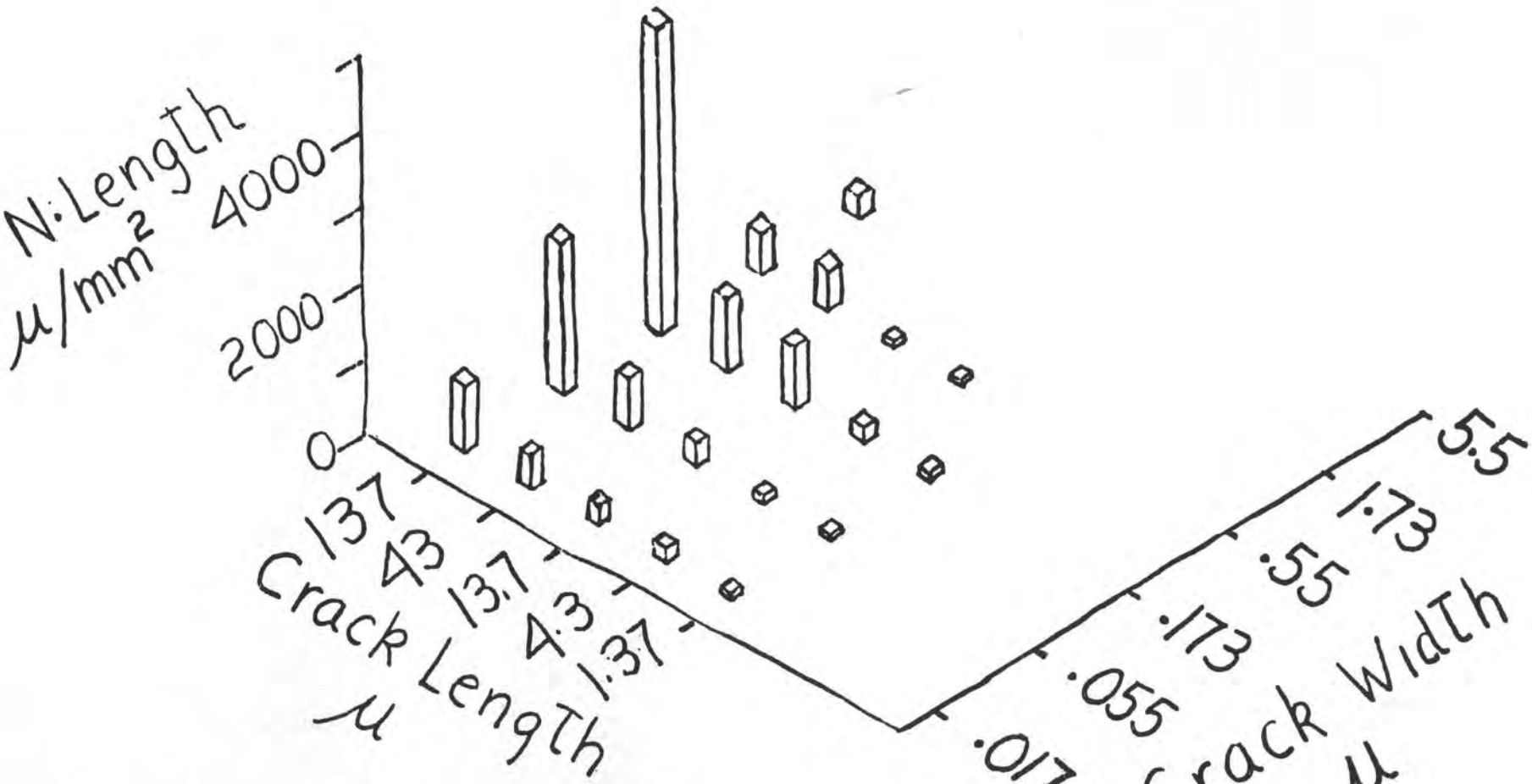

Crack Width and Length
Distributions
Westerly Granite unstressed

Fig 9 (K. Hadley 1975)

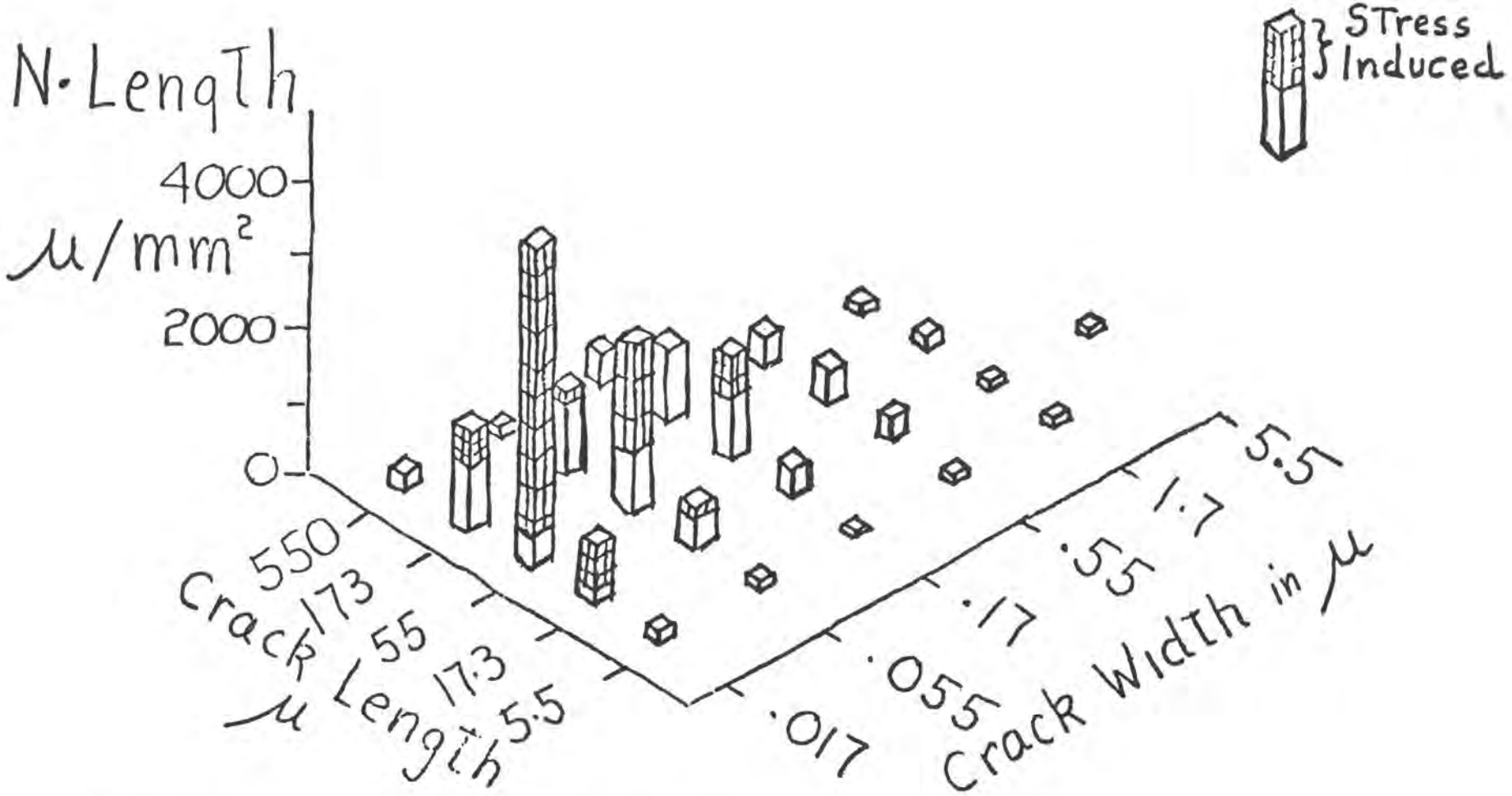

Crack Width and Length Distributions
Westerly Granite stressed to 65% of failure
(K. Hadley, 1975)

Fig 10

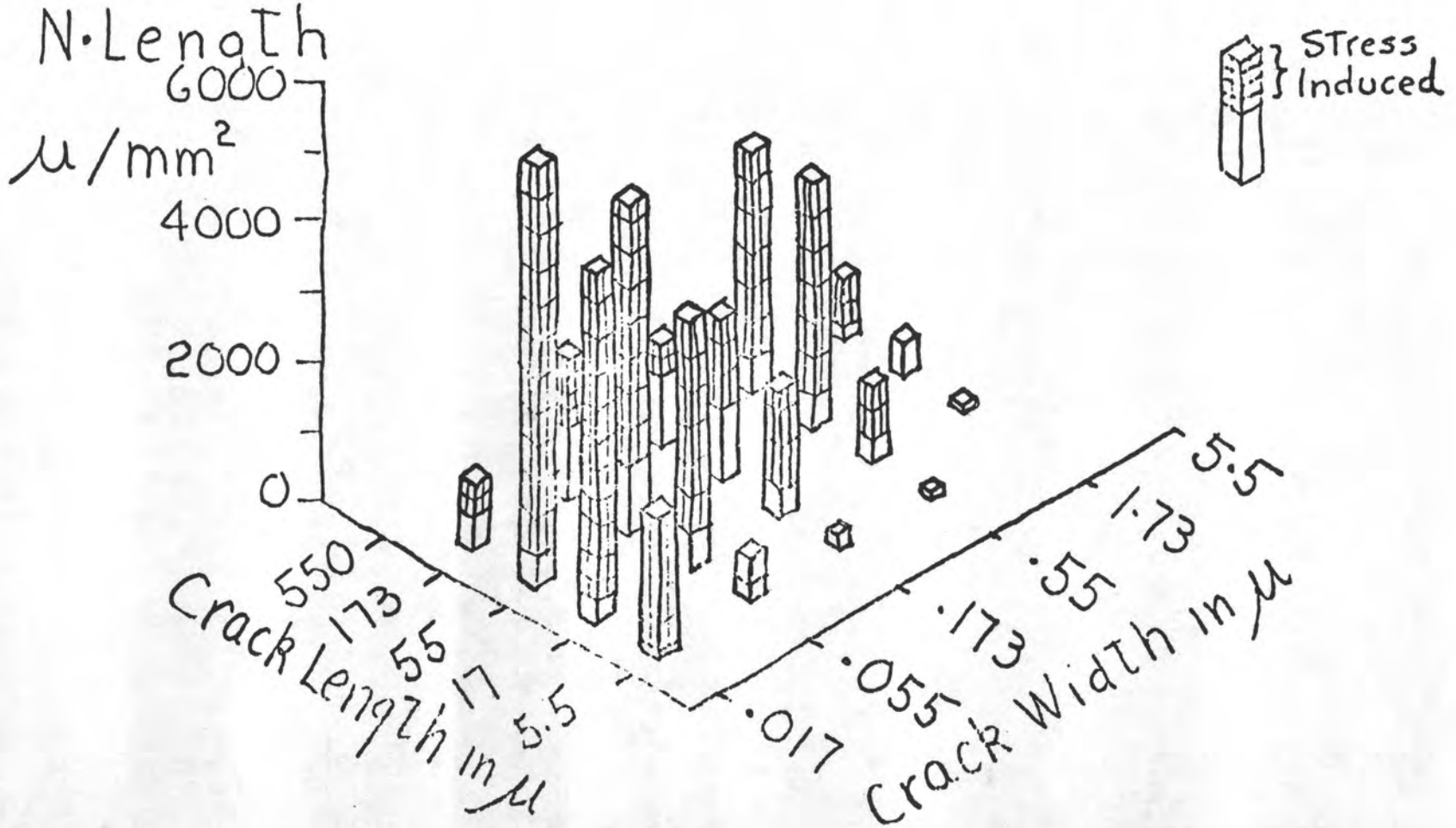

Crack Width and Length
Distributions
Westerly Granite stressed to 100% of failure
Fig 11 (K. Hadley, 1975)

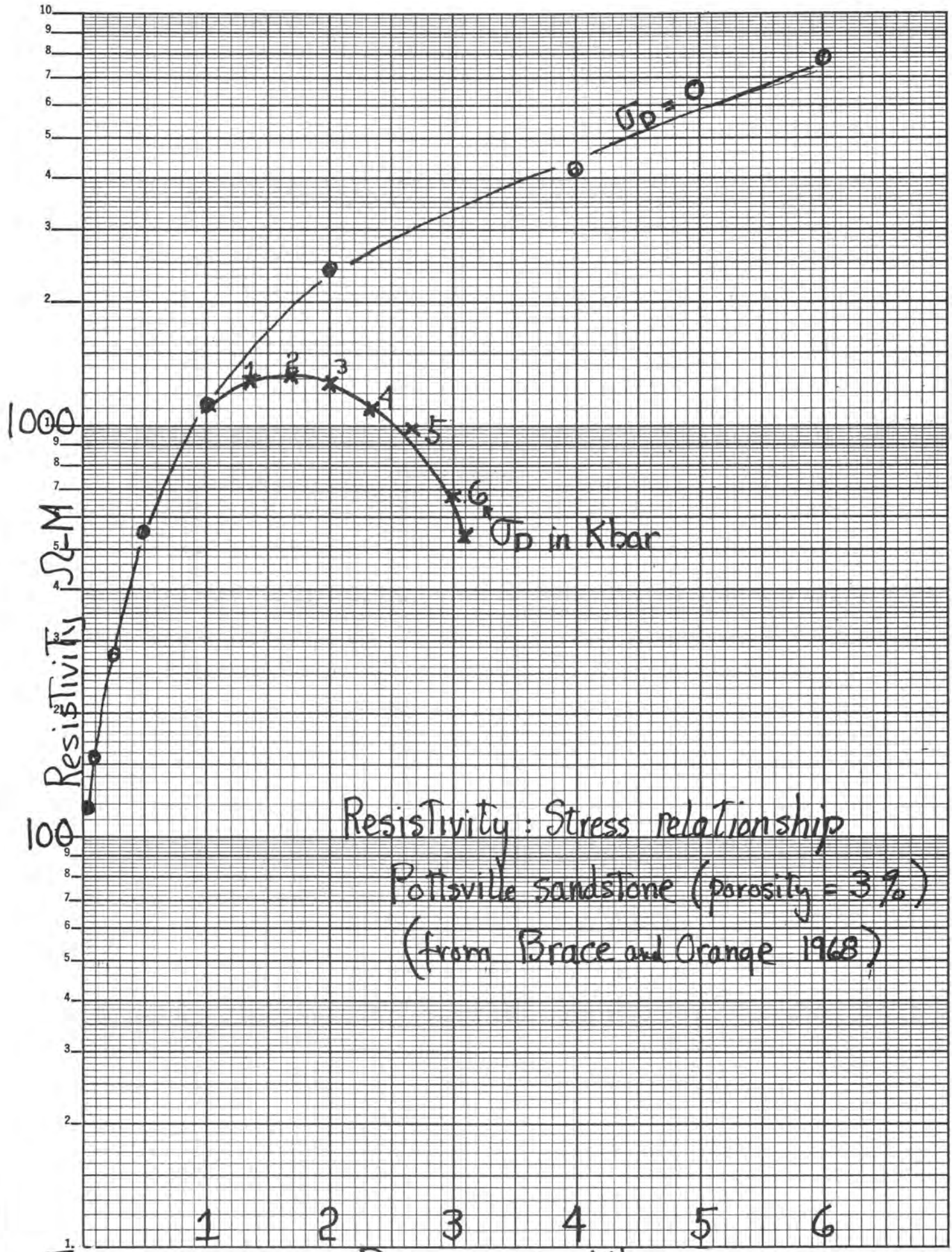
$\sigma_D = 0$
1
2
3
4
5
6
σ_D in Kbar
Resistivity Ω-M
1000
100
Resistivity : Stress relationship
Pottsville sandstone (porosity = 3%)
(from Brace and Orange 1968)
1
2
3
4
5
6
Pressure in Kbar

Fig 12

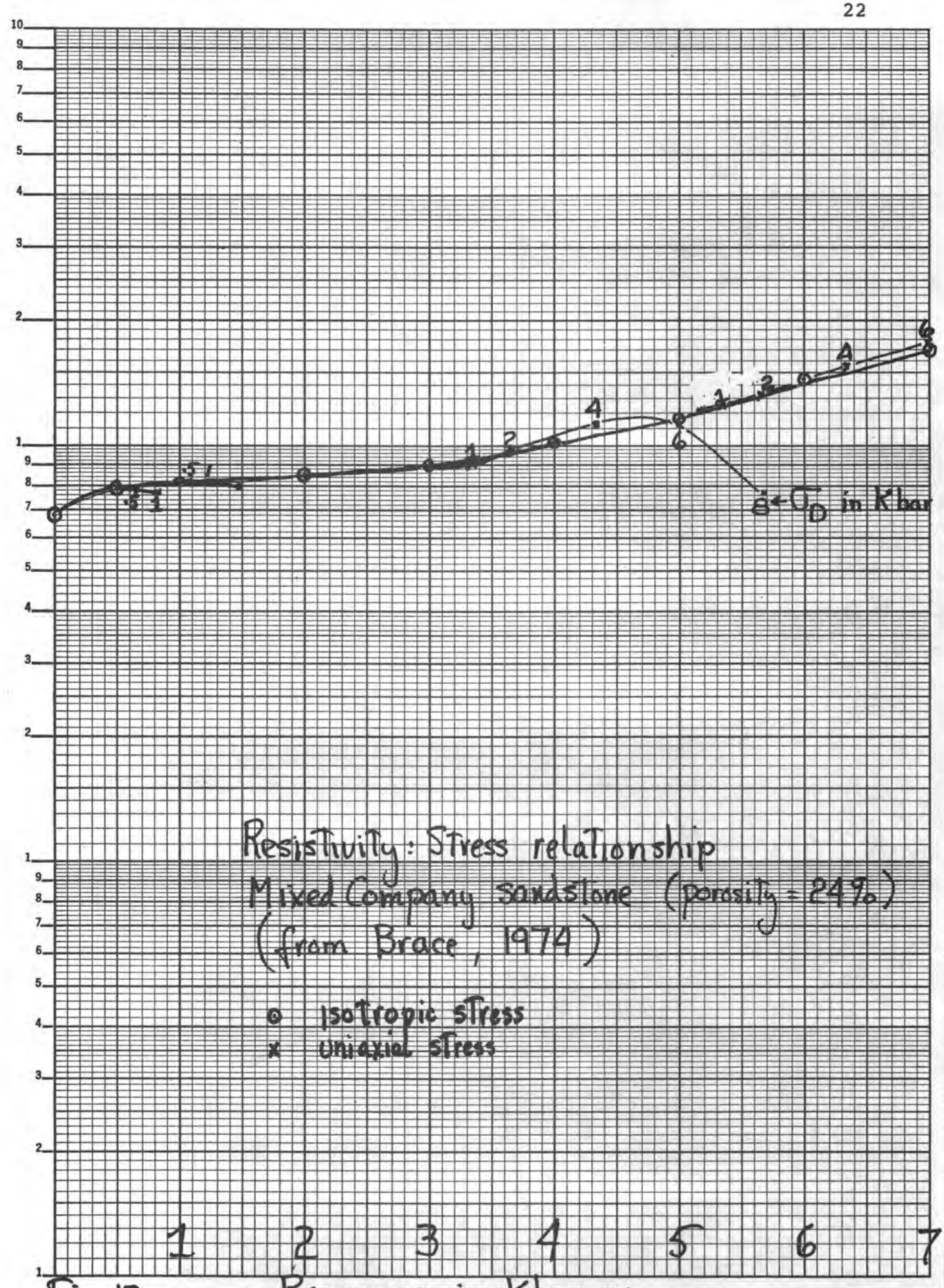
σ_D in Kbar
Resistivity : Stress relationship
Mixed Company sandstone (porosity = 24%)
(from Brace, 1974)
o isotropic stress
x uniaxial stress
Pressure in Kbar

Fig 13

100-200.

It appears from these results that cracks in the sandstone grains must be playing an important role in determing the electrical properties of the Pottsville sandstone. With more porous sedimentary rocks, the crack influence may be drowned out by the intergranular pore influence. Figure 13 shows resistivity data for a high porosity sandstone and the results are very different. Shear stresses have very little effect on the resistivity except perhaps just before failure. The effects of hydrostatic pressure loading were also unusual showing an inflection point at around 2 kbars. This behavior was seen in indepencent measurements. If these results are typical of fault zone properties one would be more pessimistic about the value of electrical measurements, but I believe this sandstone is not typical. The stress sensitivities are less than those inferred from dynamic measurements on other porous sandstones and dynamic measurements always underestimate the static effects. Nevertheless these results underscore the need to look at other rock types besides igneous rocks as fault zone rocks in some respects are more likely to resemble sedimentary rocks than igneous.

Some interest in partially saturated rocks has developed since reports by Yamazaki of observing an amplification factor of 2000 to 10,000 in a partially-saturated tuff (Yamazaki, 1967, 1974). The evidence for these amplifications is indirect and not completely convincing. The main evidence came from relating a diurnal resistivity change with the tidal strains. Unfortunately, data taken when the tidal phase would have shifted relative to any diurnal phenomena were not also shown so that one cannot truly distinguish tidal from diurnal effects. Laboratory studies on these same tuffs showed them to have large amplification factors when partially saturated but not exceeding 400, and then only at low pressures. Other sedimentary rocks tested did not give these effects (Yamazaki, 1966). In any case since these saturation conditions are not expected except at very shallow depths we have not stressed this aspect of porous rock electrical properties.

In summary, we find that the sensitivity of the electrical properties to stress and strain changes depends on the extent that cracks control the electrical conductivity. Igneous and metamorphic rocks are crack-dominated and give the highest sensitivities, while porous sedimentary rocks are least sensitive. Sensitivities tend to decrease with increasing pressure but a reversal of this trend occurs when dilatancy occurs. The behavior of fault zone rocks is still not known. One can presume that they have a high crack density in regions that sustain faulting, but whether or not such cracks control their electrical properties will depend on their porosities. With ordinary sedimentary rocks, the crack conduction across the grains becomes important at porosities of around 3-5%. Perhaps fault zone rocks would have higher crack densities and could tolerate slightly higher porosities while maintaining a crack control of their electrical properties.

In Table IV we have tried to summarize these results using depth and porosity as parameters. The coverage in the table is wider than the data base so that some of the numbers are interpolations and extrapolations and some are even conjectural, but we believe they are reasonable. We have somewhat increased the results for porous rocks under the assumption that the laboratory time scale underestimates the stress-induced changes. The largest unknown is still the question of where the fault zone rocks fit in the table. Until we have real data to work with, we tend to favor a guess that the behavior of 3% porous rocks is applicable. We also do not believe that larger scale fractures will have much of an effect on these properties.

At greater depths where the temperature exceeds 500°C large pore fluid conductivity changes can occur with pore pressure changes. These effects are very dependent on the actual pore pressure and pore fluid salinity, but for pore pressures which are hydrostatic rather than lithostatic and dilute solutions, changes of up to 0.2%/bar are possible.

III. Practical Aspects of Resistivity Strain Monitoring

The usefulness of resistivity measurements in earthquake studies depends on making measurements at a sensitivity high enough to detect the resistivity changes due to stress changes associated with the earthquake-related phenomena and also on nature providing us with a stable enough resistivity background so that the stress-induced changes are significant. Let us first examine the required sensitivity. The question of stress drops and ultimate strains are still matters of debate but earthquake stress drops of 1-100 bars and ultimate strains of 100 μ strain units are often quoted. Rikitake examined geodetic data from 26 earthquakes ranging in magnitude from 6.1 to 8.4 and found the median strain to be 50 μ strain units with only 2 cases over 100 and none over 170 (Rikitake, 1975). These results are not inconsistent with stress drops in the 10-100 bar range and give us some handles on the level of the expected resistivity changes. If the changes before failure are uniform in time and space one could conceivably be dealing with resistivity variations of the order of .005 to .01%/year (assuming strain rates of 0.5×10^{-6}/yr). Somewhat similar conclusions were reached by Dave Fitterman analysing expected resistivity variations along the San Andreas (Fitterman, 1976). Undoubtedly inhomogeneities must cause unequal stress distributions and it is conjectured that strain effects are accelerated prior to failure. This leads us to think that a 1% resistivity change is a sort of upper limit to what one might expect as a premonitory effect. Thus it seems to us

TABLE IV.

Estimated Resistivity: Stress-Strain Relationships

Amplification Factor $(\Delta\rho/\rho)/\Delta\mu$

Porosity in %		1	3	10	30	
Depth, km	0	500	100	20	7	
	1	400	100	20	7	non-dilatant strain region
	3	300	80	20	7	
	10	200	60	20		
	0	750	200	30	10	
	1	500	200	30	8	
	3	400	150	25	7	dilatant strain region
	10	300	100	20		

Stress Sensitivity $\%\Delta\rho$/bar

Porosity in %		1	3	10	30	
Depth, km	0	.4	.3	.04	.02	
	1	.2	.15	.04	.02	non-dilatant strain region
	3	.07	.10	.03	.02	
	10	.03	.03	.02		
	0	.5	.4	.1	.03	
	1	.3	.2	.1	.03	
	3	.1	.10	.05	.03	dilatant strain region
	10	.05	.05	.03		

that a 1% measurement accuracy is inadequate for earthquake studies, 0.1% marginal, and 0.01% desirable.

These conclusions raise real questions as to whether resistivity measurements can be useful in earthquake studies, for it might be possible that other effects could swamp the stress-induced resistivity variations. I do not believe this is the case, but rather the problems are technical ones that arise when trying to make the measurement at sufficient accuracy. The other factors that influence electrical conductivity are temperature, pore fluid salinity, and degree of saturation. Because of the high heat capacity and low thermal conductivity of rocks, it is difficult to rapidly change temperatures inside the earth. Diurnal temperature effects have a damping distance of a few centimeters and yearly temperature effects of about a meter. Long term climatic changes can penetrate deeper but must have correspondingly slower rates of change. Thus large scale measurements should be little effected by temperature effects. Figure 14 shows resistivity data from Melendy Ranch on the San Andreas obtained with an active resistivity system with 100 meter spacing. Any diurnal variation must be less than .01%. At this spacing some yearly variation should be observed. Figure 15 shows drift rates that might be attributed to temperature effects but, unfortunately, the equipment drift was also of this same order of magnitude. With spacings of a few kilometers the yearly temperature effect would also be insignificant.

We have less experience in hydrology to know much about salinity changes that might occur underground but, again, we doubt this will be a big noise factor. Changes in the water table could be the most important noise, especially in areas of intense irrigation, but to first order the total salt content of a region irrigating with underground water should not change. One should, however, keep an eye on well level changes in the measurement area to investigate possible correlations with resistivity variations.

Thus it seems that in principle resistivity variation monitoring is capable of resolving changing stress and strain effects at a low enough level to provide important information for earthquake prediction. Ideally these measurements should be made at a sensitivity of 0.01%, but certainly better than 0.1%. They should also be sensitive to variations occuring at several kilometers depth.

Making large scale resistivity measurements at this sensitivity is not a simple technical problem. Two different techniques are used, active and passive. The active measurements require large currents in order to obtain reasonable signal levels. The principal noise is the naturally occuring electromagnetic fluctuations and, for electrical measurements, the electrode potential fluctuations. The former can be reduced by using the long wavelength

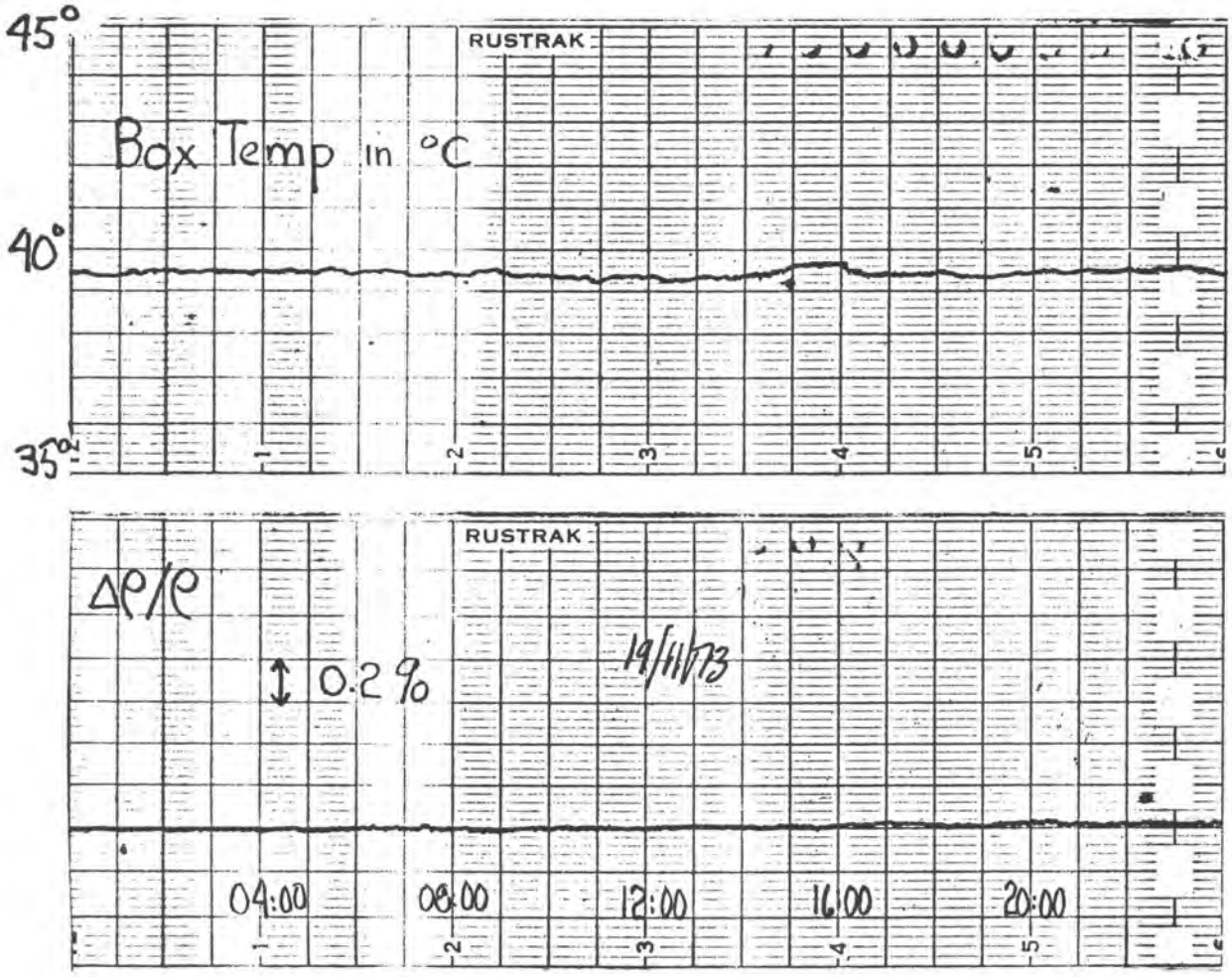

Fig 14 Resistivity Variation Recording from Melendy Ranch
100 meter Schlumberger array using fixed current at a fixed freq.

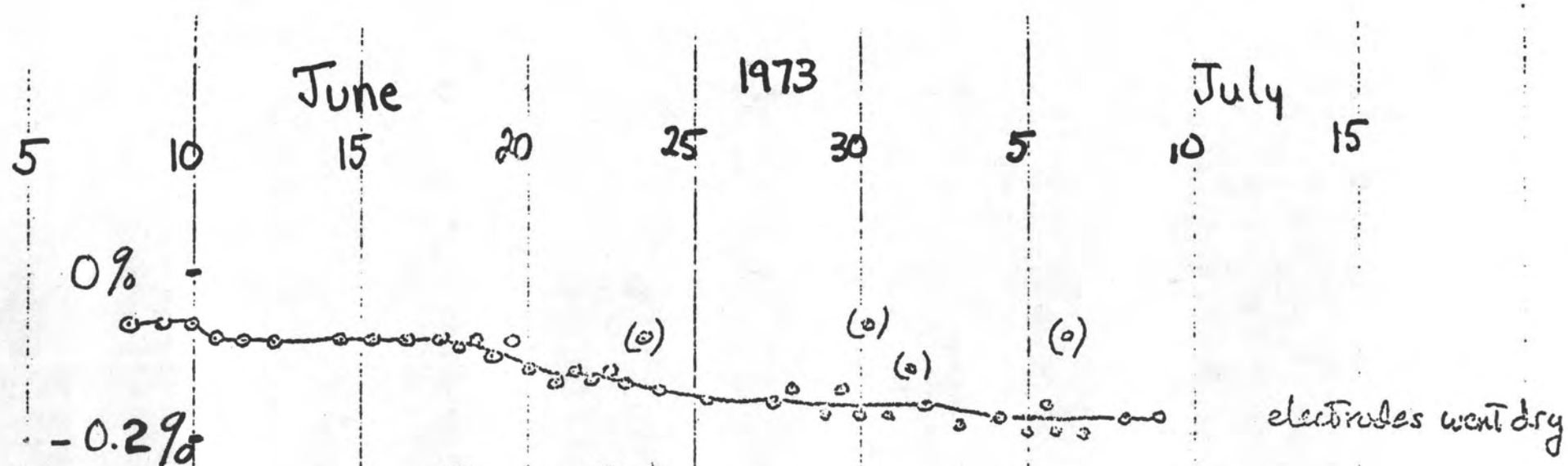

no Temp control
readings made at 40° crossovers
bad points all occurred with rapid Temp variations

Fig 15 Melendy Ranch Resistivity Variations June-July, 1973

character of the natural electromagnetic fluctuations, and both noise effects can be reduced by synchronous detection schemes. Although uniform near surface variations do not affect large scale measurements, non-uniform variations on the scale of the sending and receiving dipoles do affect the measurements. This is a more serious problem for electrically-coupled systems than for magnetically-coupled systems. Other sensitivity problems arise if the frequency content of the transmitted signal is not controlled well enough. This is a more serious problem for magnetically-coupled systems.

At the high sensitivity levels we are aiming for, every system must contend with the problems of the stability of the electronics and the insulation of the cabling.

Our own measurements are made passively using a telluric cancellation system. Telluric signals are the electric fields induced in the earth by magnetic field variations. The method has several inherent advantages, simplicity and depth of penetration, but it was not known what sensitivity levels could be achieved. In fact, we still do not know the limits of the method, but we have reached the 0.1% level. the method utilizes the fact that the telluric ratios at low frequencies depend on the integrated conductivity of the crust under the recording dipoles, and are very little affected by the frequencies as long as they are low, or the wavelengths of the signals as long as they are long. The frequency independence allows comparisons to be made by subtraction at wide bandwidths which simplifies the problem of obtaining high resolution. Because of the tensor nature of the surface electrical field, these subtractions must involve three signals which, for logistic reasons, are usually nearby dipoles. Thus one is detecting a gradient of resistivity variations, of, what is more likely, a change in the effective anisotropy of the resistivity. This last factor makes small scale telluric cancellation methods as equally applicable as the large scale measurements.

Figure 16 shows the arrays presently operating in two areas along the San Andreas. Telephone lines are used for the dipoles. Figure 17 shows data from the Palmdale array. S_A and S_B are used as the two independent signals into which any individual telluric signal can be decomposed. Changes in the magnitude of their contribution to the telluric signals are indicative of variations of resistivity. Tensor cancellations are recorded which allows high gains and thus greater sensitivity. The sensitivities shown in Figure 17 indicate the relative change in resistivity under a dipole needed to cause an unbalance at the output as large as the S_A signal. The adjusted data is the data after a small change in the cancellation settings has been simulated in the computer. Resistivity variations are detected by changes in the relative magnitude of the S_A and S_B components in these final outputs as determined by correlation analysis. These results are then inverted to

Fig 16 Palmdale Telluric Array

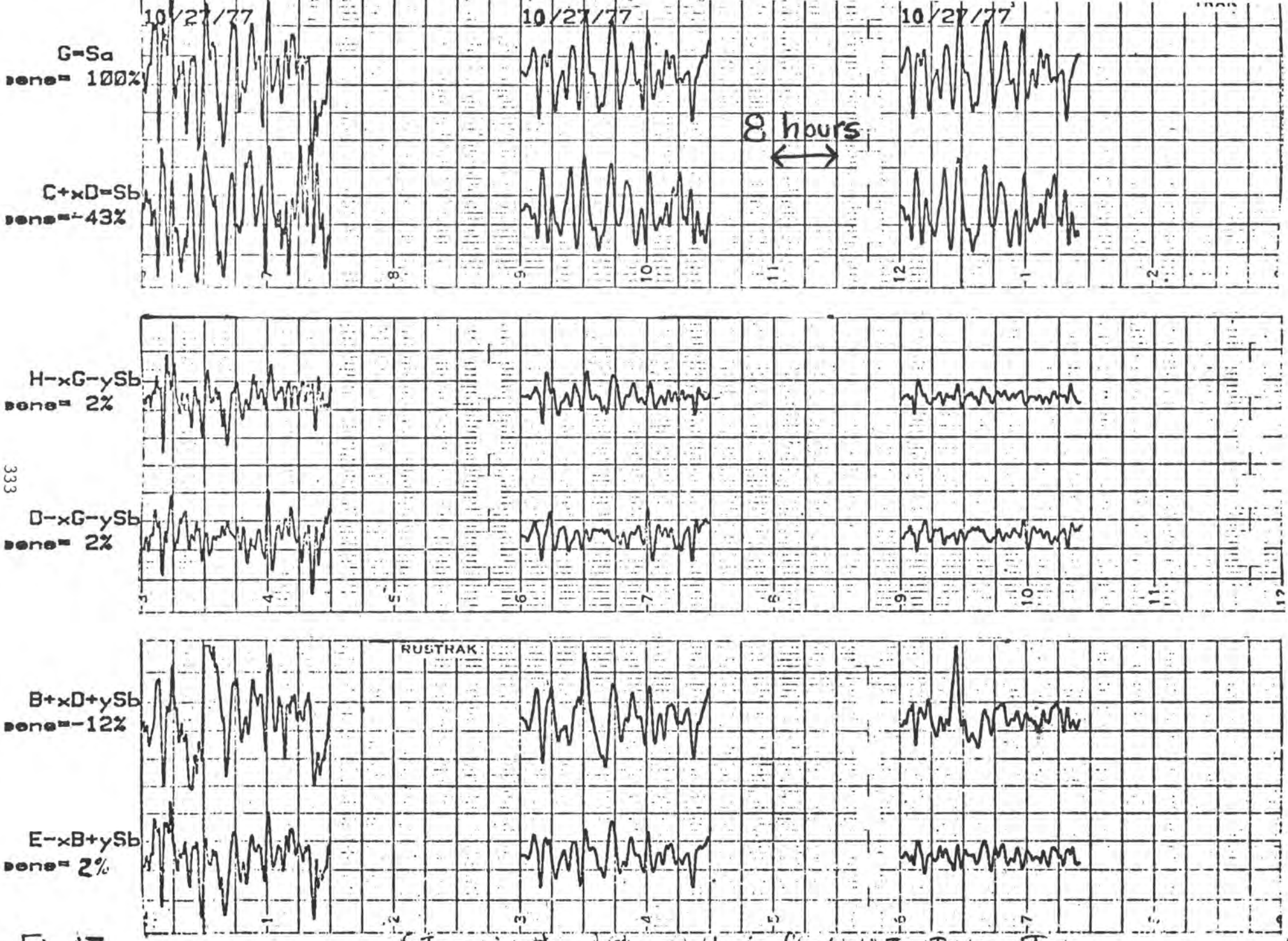

Fig 17 Steps in the data analysis for resistivity variations

assign variations to indivudal dipoles. In the data shown the array was still too limited to give unique inversion and a robust fit was used as noise (which has since been eliminated) was obviously present on dipole B. The results of this inversion are shown in Figure 18 along with the resolution matrix. All of this data was hand digitized off of Rustrack recordings which limits the resolution. The Palmdale data is now being digitized on-site by the Cal Tech Palmdale data gathering system and we will soon have more accurate data to analyze. The hand digitized results were at the 0.1% level, and we expect this to improve both because we will have a more accurate data base and also more data. (The recordings are continuous but the hand digitization limited the amount of data we could analyze.) There are noise problems, however, which will eventually set a limit to the sensitivity. Some of these have been recognized and cured or bypassed, but others still remain. On one line in the Hollister area, the 60 cycles picked up along the telephone line was being rectified by the electrode at Paicines, giving us low frequency noise. This was eliminated by bypassing the 60 cycles around the electrode. The results of this decoupling are shown in Figure 19. Tidal signals induced by offshore tidal currents were another noise source as they did not cancel in the same ratio as the rest of the telluric signals. At present we filter them out, but this is not the best solution as the diurnal signal, which is one of the most consistent telluric signals, is also filtered out. Other noise sources we have uncovered include a bad amplifier and a bad telephone line connection. Tracking down all these noise sources is a difficult and painstaking business, but we feel we can reach the .03% sensitivity level with our array. This level exceeds our present electronic stability and calibrations become important.

We have only recently begun to experiment with small scale measurements of the same type and do not yet know what sensitivity levels are possible.

IV. Streaming Potential Properties

Many theories of earthquake phenomena give the pore fluid pressure an important role. The experiences at Denver and the experiments at Rangley have even demonstrated pore pressure control of earthquakes. Porous rocks have the property of generating electrical signals when pore pressure gradients are imposed on them, and thus there is a possibility of directly determining by electric potential measurements, the buildup of unusual pore pressure conditions within the earth. This property is known as the streaming potential effect. It is a consequence of the rock minerals taking on a net electric charge in equilibrium with the pore fluids. For silicate minerals in neutral or basic solutions this charge isnegative due either to low valence cation substitution within the mineral or negative ion adsorption on the mineral. The potential created by this charge as seen from the solution side is called the zeta potential and is typically -50 to -70 mv at room temperature. This potential

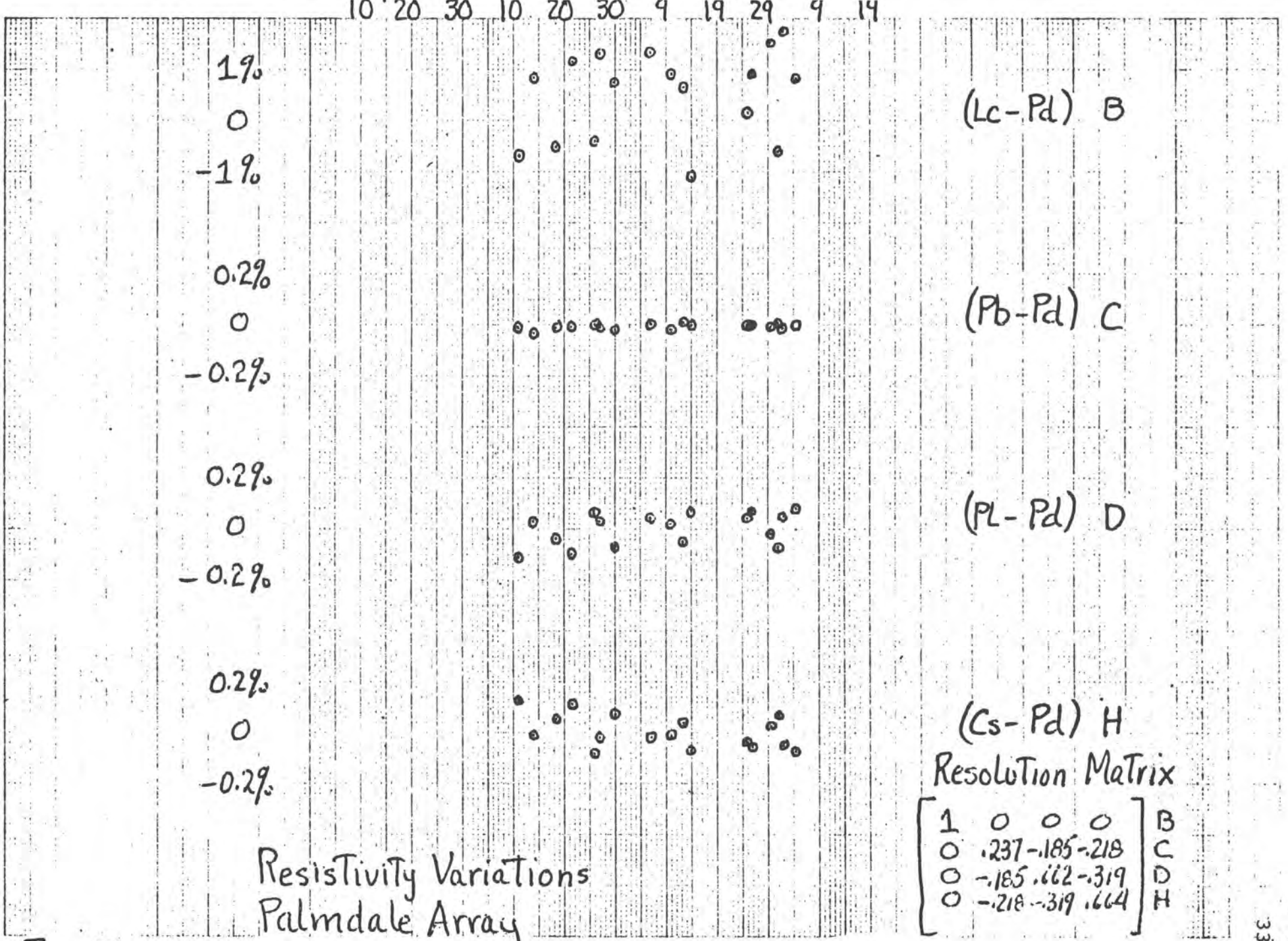

Resistivity Variations
Palmdale Array

Fig 18

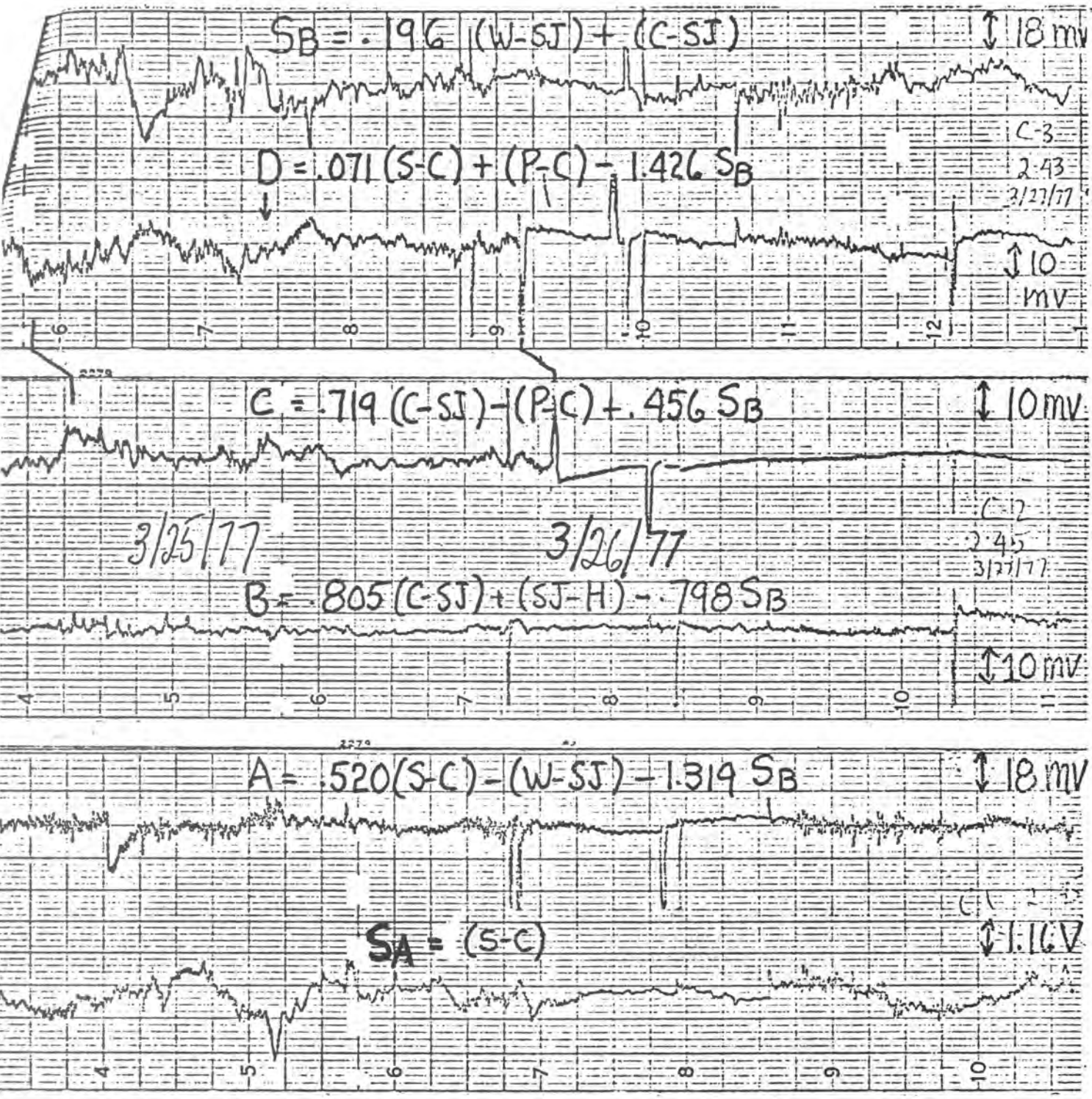

919 Effect of Noise Decoupling of Paicines Electrode
on 3/26/77

attracts an excess of positive ions which hover near the surface in a zone called the diffuse layer with a thickness of a Debye length. The debye length is inversely proportional to the square root of the ionic concentration and for 10^{-3}N solutions is .01μ. Negative ions are repelled, but the ionic concentration in the diffuse layer is still higher than in the solution and has a net charge equal and opposite to the mineral charge. Thus any fluid flow will drag this net charge along until a counterfield is set up that causes a conduction current which just balances the convected current. This counterfield is the source of the streaming potential. If the fluid flow is laminar a very general analysis can be made which shows that the streaming potential is virtually independent of the pore system geometry, and is linearly dependent on the zeta potential, the pore fluid resistivity, and the inverse of the fluid viscosity (Overbeek, 1952).

When the width of the pores or cracks of the rock are of the dimensions of the Debye lengths, the excess ions of the diffuse layer alter the effective conductivity of the pore fluid; which reduces the streaming potential. This can be allowed for by adding the excess conductance, called the surface conductance, to the pore fluid conductance. The resulting expression for the streaming potential is

$$\left(\frac{\nabla V}{\nabla P}\right)_{I=0} = \frac{\varepsilon\phi}{\eta(\sigma_s + 2\sigma/r)}$$

ε = fluid dielectric constant
ϕ = zeta potential
η = fluid viscosity
σ = fluid conductivity
σ_s = surface conductance
r = crack width or pore radius

For dilute solutions of resistivity, 50 Ω-M, the streaming potential is about 400 mv/bar, but this is reduced to a few millivolts for brine solutions. The highest streaming potentials are obtained in porous sedimentary rocks. Crack-dominated rocks have streaming potential values that in dilute solutions are some 30 to 60 times smaller.

This is probably due to the surface conductance effect and the fact that the narrowest cracks have the largest pressure drops. Some of the low values measured for igneous rocks may also be due to salt contamination which is difficult to eliminate. A reasonable estimate of the range of streaming potentials in situ near the surface would be 3 to 60 mv/bar. Unfortunately, however, we have at present almost no data on the temperature effect on the zeta potential. It seems likely that it should increase with temperature, but experimental data is badly needed.

It is often overlooked in discussing models of stream-

ing potential effects that there are no pore pressure gradients at the surface, where one is making the measurements, and thus one should not be able to measure any streaming potential effects at the surface. Indirect measurements of streaming potential effects at depth can be made, however, whenever the situation sets up an electric current flow. The streaming potential calculation was based on the balance between convected electric currents and conduction currents which is a no current situation. If inhomogeneities exist in the streaming potential properties, however, and a pressure gradient is impressed along the boundary, continuity of electric potential across the boundary cannot be maintained without setting up an electric current (Nourbehecht, 1963). Some of this current may pass under the surface and gives us a streaming potential signal even though the hydraulic pressure gradients are zero at the surface. Figure 20 shows a field example which was a good model for a small zone going dilatant. The slowly recovering negative potential was, we believe, caused by fluid flow back into the bomb cavity which has been outgassed by events which led to the short positive anomaly. In any case, the amplitude and the geometry of the negative anomaly was well predicted by fluid flow under gravity feed into a 25 meter radius zone assuming a 10 mv/bar difference in the properties of the tuff and the overlying alluvium and a 50 bar pressure drive. The source strength is given by the product of the low pressure zone radius and the pressure difference, so that a larger zone and a smaller pressure difference could give the same result. If dilatancy actually occurs on a large scale, the pressure differences could become huge so the water pressure would drop to the boiling point pressure which is less than 220 atmospheres when the temperature is below the critical temperature. Thus dilatancy gives a stress amplification for the pore fluid pressure, but compressive stresses do not. The amplification will not be as large as the resistivity amplification factor, and it will also be roughly inversely proportional to the porosity. We have not as yet examined this in the same detail as we have the resistivity amplification, but amplifications of from 2 to 10 seem reasonable.

V. Pore Pressure Variation Monitoring by Streaming Potential Measurement

Our knowledge of streaming potential properties at depth is far more limited than our knowledge of resistivity properties so that we must admit a large uncertainty in discussing the magnitude of possible anomalies. If we extrapolate the results of figure 20 to a zone about as large as its depth of burial one has a self potential anomaly of about 3 mv/bar and if the region was dilatant one perhaps

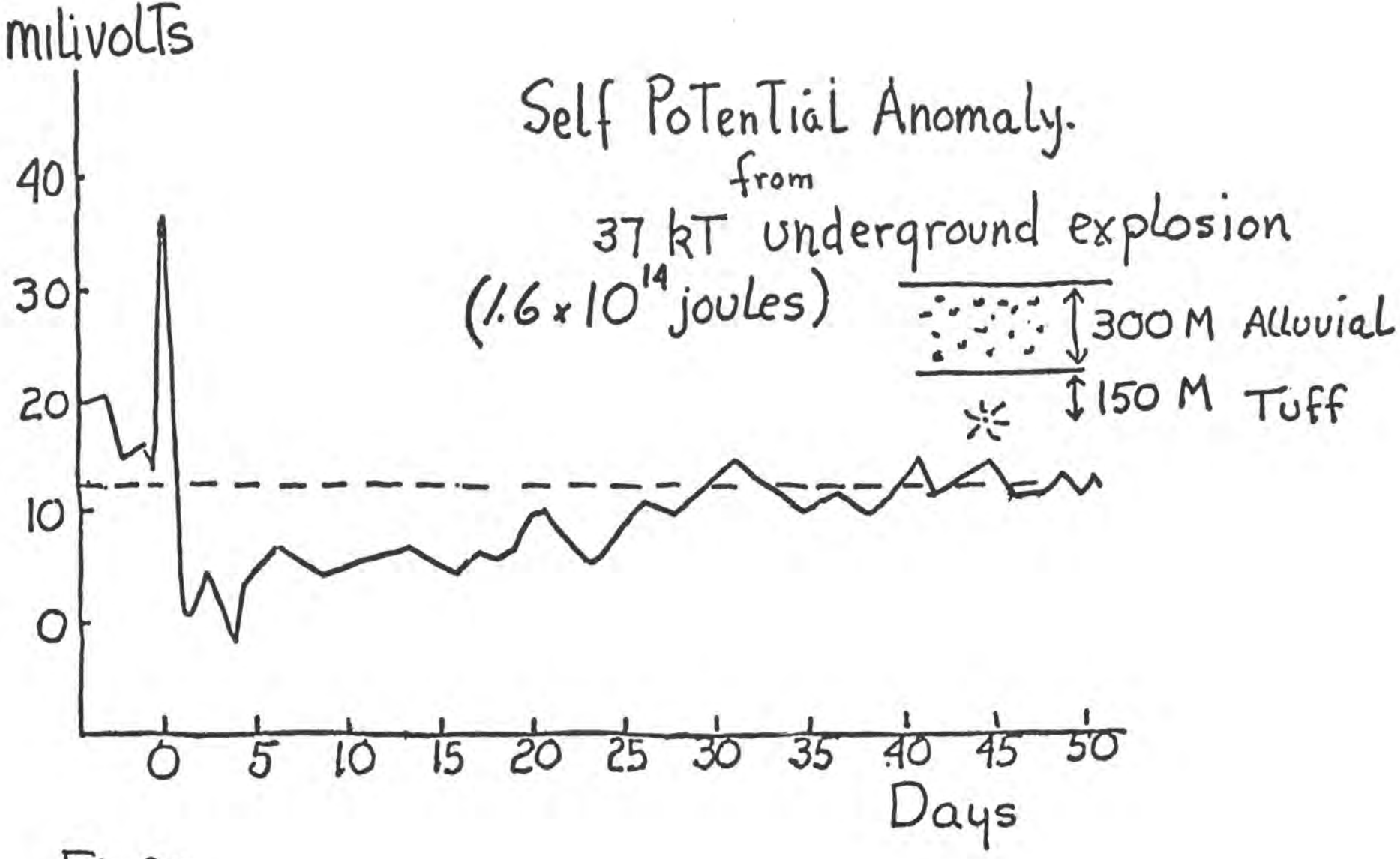
milivolts
Self PoTenTiaL Anomaly.
from
37 kT underground explosion
(1.6 x 10^14 joules)
300 M Alluvial
150 M Tuff
40
30
20
10
0
0
5
10
15
20
25
30
35
40
45
50
Days

Fig 20

could expect 6 - 30 mv/bar of tectonic stress. This however is probably a very optimistic estimate as we cannot always expect large differences in streaming potential properties at depth and more realistic numbers would be 0.5-3 mv/bar, In order to detect such anomalies we must be able to measure self potential variations of 0.1 to 0.6 mv/km. This is much less than the telluric signal amplitudes and detection is virtually impossible unless one cancels out the telluric signals. Thus the telluric cancellation arrays used to measure resistivity variations can also be used to monitor self potential variations. Figure 21 shows telluric signals with periods of a week and amplitudes of 5mv/km. which are largely eliminated by a scalar cancellation. Tensor cancellations are even better and in principle we can detect effects at the one bar level. We have uncancelled tidal signals that are up to 1 mv/km, but they are easily distinguished or filtered. Unfortunately, a different noise source becomes important at these levels which is electrode potential drifts and until improvements are made in the electrodes or in the monitoring of their drifts we cannot quite achieve these sensitivities. There are actually two problems, the drift of electrode potentials, and errors in determining the electrode potential. For convenience sake we have used solid Pb electrodes, but after several years of following their behavior we are dissatisfied with their performance and we are studying other alternative electrodes. The electrodes all show a strong drift during the first few months of burial going from -500 or 600 mv relative to an AgCL:KCL reference electrode to something like -300 or 400 mv. Since the sense of this change is opposite to that which one would expect from Eh and pH changes after burial, one must assume the nature of the electrode itself is changing. Figure 22 shows the long term behavior of the electrode potentials. A seasonal variation is apparent as well as the secular drift, but unfortunately a more erratic component also seems to be present. Some of this may be due to the measurement itself as a host of electrochemical signals such as diffusion potentials, thermoelectric potentials, and streaming potentials can be acting in the near surface between the electrode position and the point where the reference measurements are made. We have experimented with techniques to reduce this scatter such as having the reference electrode contact the soil at the bottom of capped holes about a meter deep, lined with plastic pipe. In some areas we seem to achieve a short term reproduceaability of one or two mv, but generally speaking we cannot define the electrode potential to better than 5 mv.

Figure 23 shows self potential variation results from the Hollister array relative to Salinas. This data consists of the low pass half of the tensor cancellation residuals which have been inverted to assign variations to individual electrode sites.

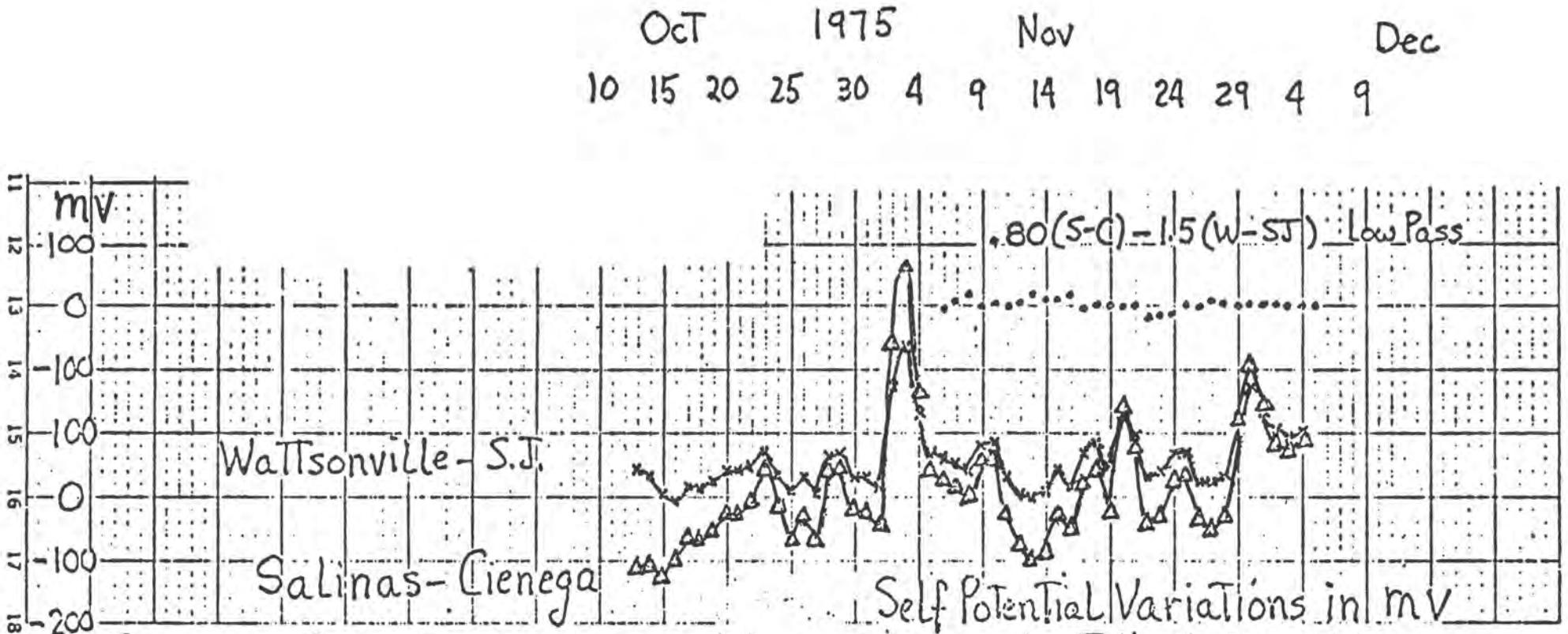

Fig 21 Reduction of Long Period Fluctuations by Telluric Cancellation

Fig 22 Electrode Potentials, Hollister Array
relative to Ag CL; KCL reference
⊙ surface measurement
× 1 meter depth

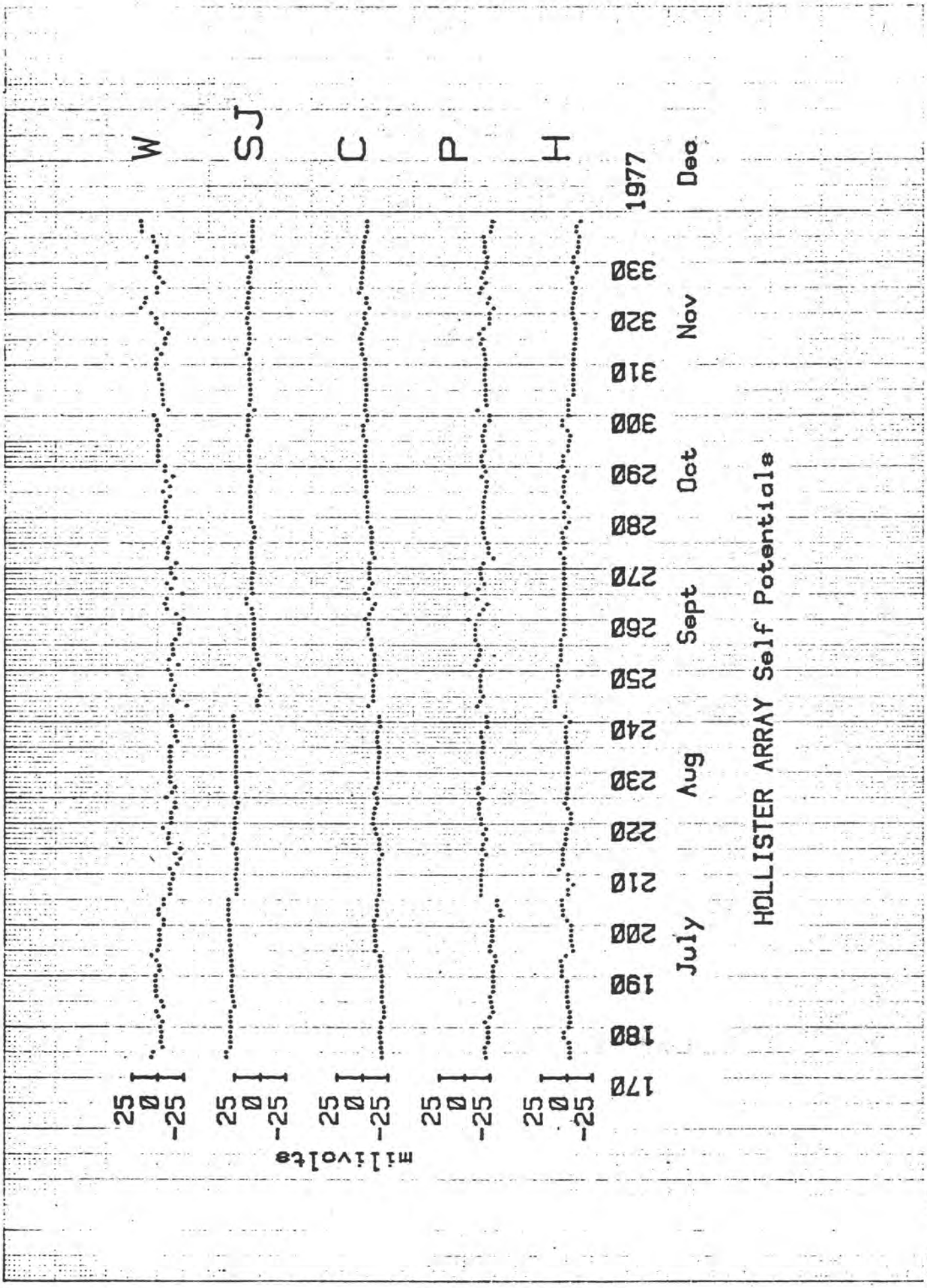
W
SJ
C
P
H
25
0
-25
millivolts
170
180
190
200
210
220
230
240
250
260
270
280
290
300
310
320
330
July
Aug
Sept
Oct
Nov
Dec
1977
HOLLISTER ARRAY Self Potentials

Fig 23

This inversion is inherently non-unique as any self potential variations that mimick the telluric fluctuation distribution are also cancelled out. This is a price that must be paid, however, if one hopes to detect self potential variations of a fraction of a millivolt per kilometer. The electrode potential trends have also been subtracted out. The low pass cutoff has been raised to eliminate tidal signals from the resistivity variation outputs so that some short period telluric variations are aliased into the data shown. This is especially apparent in the results for W. Jogs in the data appear at times when changes in the cancellation settings were made, and a large jog appeared in late August when new input circuits were installed, which seemed to indicate the SJ preamp had been faulty. Long term variations that represent about 1 mv/km are seen in this data, but we are not yet sure if they are not still due to the electrode potential measurement problem. Figure 24 shows a shorter stretch in which greater care was taken in reading the records, in order to search for possible effects of a local earthquake of magnitude 4.3, 18.5 kilometers SE of the Paicines electrode which occurred on November 4. The shorter period variations are more like 0.2mv/km and probably represent our present sensitivity limit. Some of this may be due to electrode potential variations which would be eliminated with better electrodes, but until we get data with improved electrodes we cannot distinguish the electrode potential variations from self potential variations. At this level we could still detect large dilatancy pore pressure drops, but variations at the 1 bar level will be unresolvable.

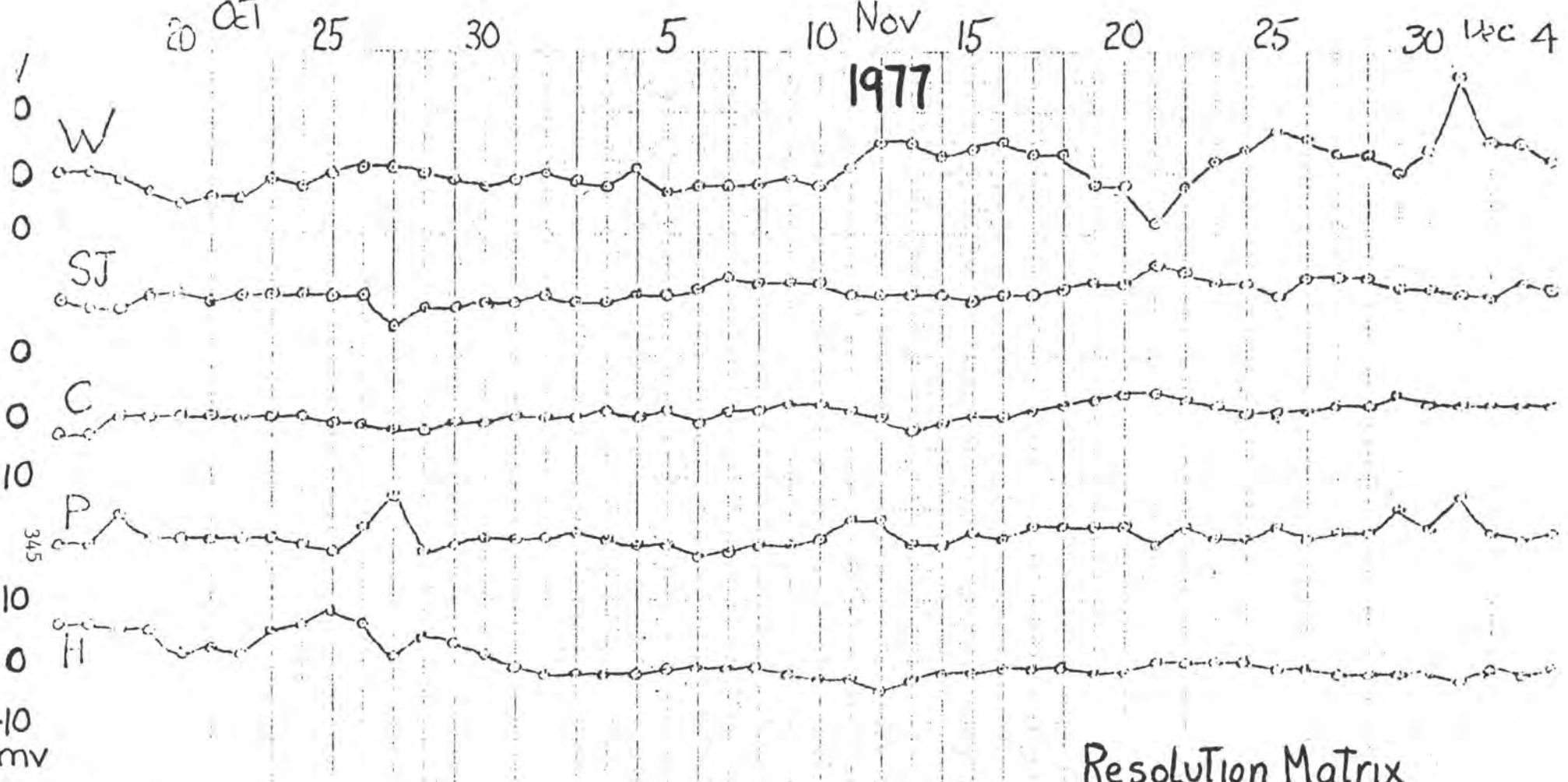

Fig 24 Station potential variations relative to Salinas
obtained by inversion of array variations
using strong damping and robust fit

Resolution Matrix

	W	SJ	C	P	H
	.46	-.22	-.02	.17	-.14
	-.22	.72	-.22	-.11	-.23
	-.02	-.22	.71	-.30	-.19
	.17	-.11	-.30	.43	-.12
	-.14	-.23	-.19	-.12	.58

References

Brace, W.F., A.S. Orange, and T.R. Madden, 1965, The effect of pressure on the electrical resistivity of water saturated crystalline rocks, Jour. Geophys. Res. 70, 5669-5678.

Brace, W.F., and A.S. Orange; 1968, Electrical resistivity changes in saturated rocks during fracture and frictional sliding, Jour. Geophys. Res., 73, 1433-1445.

Brace, W.F., and A.S. Orange; 1968, Further studies of the effect of pressure on the electrical resistivity of rocks, Jour. Geophys. Res., 73, 5407-5420.

Brace, W.F., B.W. Paulding, Jr., and C. Scholz, 1966, Dilatancy in the fracture of crystalline rocks, Jour. Geophys. Res., 71, 3939-3953.

Brace, W.F., 1974, Electrical resistivity of sandstone, Final report to Defense Nuclear Agency, contract no DNA-001-74-C-0057, 40 pages.

Elliott, S.E., and B.F. Wiley, 1965. Compressional velocities of partially saturated unconsolidated sands, Geophys., 40, 949-954.

Fitterman, D., 1976, Theoretical resistivity variations along stressed strike-slip faults, Jour. Geophys. Res., 81, 4909-4915.

Hadley, K. 1975, Dilatancy, further studies in crystalline rock, Ph.D. Thesis, M.I.T.

King, M.S., 1966, Wave velocities in rocks as a function of changes in overburden pressure and pore fluid saturants, Geophys., 31, 50-73.

Madden, T.R., 1974, Near surface electrical properties as a guide to mechanical properties, Final report to Air Force Research Lab, Contract no F-19628-72-C-0182.

Madden, T.R., 1976, Near surface electrical properties of rocks as a guide to mechanical properties, Final report to Air Force Research Lab, Contract no. F-19628-76-C-0070.

Madden, T.R., 1976, Random networks and mixing laws, Geophys., 41, 1104-1125.

Nourbehect, B., 1963, Irreversible Thermodynamic effects in inhomogeneous media and their application in certain geo-electric problems, Ph.D. Thesis, M.I.T.

Overbeek, J. ThG., 1952, Electrokinetic phenomena, Chapter V, in Colloid Science, Vol. I, Irreversible Systems , H.R. Kruyt, ed., Elsevier Publishing Co., Amsterdam.

Parkhomenko, E.I., 1967, Electrical Properties of Rocks, Plenum Press, N.Y., 308 pages.

Quist, A.S. and W.L. Marshall, 1968, Electrical conductance of aqueous sodium chloride solutions from 0 to 800° and at pressures to 4000 bars. J. Phys. Chem., 72, 684.

Rikitake, T., 1975, Statistics of ultimate strain of the earth's crust and probability of earthquake occurrence, Tectonophysics, 26, 1-21.

Simmons, G., and W.F. Brace, 1965, Comparison of static and dynamic measurements of compressibility of rocks. Journal Geophys. Res., 70, 5649-5656.

Wolf, H.K., and G.V. Chilingarian, 1976, Piagenesis of sandstones and compaction, Chapter 3 in Compaction of Coarse Grained Sediments II, Chilingarian and Wolf, editors, Elsevier Pub. Co.

Yamazaki, Y., 1966, Electrical conductivity of strained rocks. The second paper. Further experiments on sedimentary rocks. Bull. Earthquake Res. Inst., 44, 1553-1570.

Yamazaki, Y., 1967, Electrical conductivity of strained rocks, the third paper. A resistivity variometer, Bull. Earthquake Res. Inst., 45, 849-860.

Yamazaki, Y., 1974, Coseismic resistivity steps, Tectonophysics, 22, 159-171.

Tiltmeter Research at New Madrid and at Adak: The stability and reliability of shallow bore-hole tiltmeters

by: Sean-Thomas Morrissey and
William Stauder, S.J.

I. Introduction

One of the more challenging tasks that modern science and technology is attempting is the prediction of earthquakes. The U.S. Geological Survey, National Center for Earthquake Research, has been generally spearheading the effort to generate a realistic earthquake prediction capability, through its own in-house programs and a grants program to outside research groups. One of the areas of interest is the utilization of shallow borehole tiltmeters for premonitory tilt studies. After initial indications in Central California looked promising, sets of tiltmeters were provided to, among others, St. Louis University and CIRES at Colorado University for installation inthe New Madrid and Adak seismic research areas to operate in conjunction with seismic telemetry networks. In order to share technical staff and because of similar extremes in the environmental conditions at each research area, and for other practical considerations, a joint program between Saint Louis University and CIRES was arranged with technical support for both being supplied by St. Louis University. Hence the ensuing comments and observations apply to, or are the result of, tiltmeter installation and operation efforts in both areas.

After two years of effort in both New Madrid and Adak, we are now in a relatively good position to consider what we hope to achieve by the tiltmeter program, what obstacles we have encountered and our approaches to solutions to these problems, and what further developments and achievements we feel are necessary before the tiltmeter is either proven or dismissed as a useful tool for earthquake prediction.

II. What are we looking for?

The question of precursory tilts is complicated by a strange dichotomy between theory and observation: the theoretical estimates of what a tilt precursor might be disagree, at least in most published reports, by an order of magnitude or more from the observed "precursors" (McHugh and Johnston, 1977; Mortensen and Johnston, 1975, Johnston et al., 1978). As a useful first approximation to the amplitude of a tilt precursor, we might perhaps refer to the permanent displacements and tilts of the surface derived from dislocation models of the earthquake source. One can roughly assume that if the earthquake is an isolated event, with all its elastic strain energy accumulating during the "precursor interval," then at some little distance from the fault, the resultant precursory tilt would be of the same amplitude but opposite in direction from the co-, or post-seismic tilt. Modeling of this sort seems to indicate that an upper limit of our interest may be tilts within a distance several fault lengths of the order of 5 to 10 μ radians per year for precursors of large earthquakes (M=5 to 7) in areas of significant tectonic activity. (This latter figure is an

order of magnitude extrapolation based on a dislocation model of the great New Madrid earthquake sequence (Herrmann, et al., 1978) and assumes a return rate of every 100 years). Other direct measurements also support this figure as an upper limit to our expectations. For example, the Palmdale uplift resulted in an uplift of over 40 cm in about 40 Km over about a two-year period. This is readily measured by leveling surveys, but amounts to only 5 μ radians per year as the tiltmeter would measure it. For small earthquakes, of the magnitude 3 or 4 range, with a precursor interval of about a month, tilts as small as 0.1 μ radian may be significant. And, of course, there is the further problem that the spatial relation of the tiltmeter to the source mechanism greatly influences what one might see (Rosenman and Singh, 1973). By the model of these authors, at certain locations with reference to the fault, one could see nothing even in close proximity to a large earthquake. Conversely, as in the Palmdale situation, considerable tilt could be measured with no ensuing earthquake.

In keeping with the above considerations, for a tiltmeter to be useful for geodetic predictions, we are probably looking for tilt rates of the order of 5 μ radian per year or 0.1 μ radian per month. For any confidence in our measurements, then, we would expect an instrumental stability of 1 μ radian per year or 0.01 μ radian per month. These are difficult figures to measure with any confidence with the available technology. One could install an Ascania instrument (for about $100 K) in a deep hole, since this system currently has the best reputation for stability, but cost would prohibit effective deployment. To monitor precursory tilts effectively, studies indicate that we need tiltmeters in all quadrants and within a few fault lengths of the suspected fault zones of interest. It is this consideration that recommends the utilization of many inexpensive shallow borehole instruments. However, these instruments are difficult to evaluate, since the very method of installation is open to discussion, and tilt rates (or baseline drift) of several tens of microradians per year are common, and are "best regarded as normal drifts encountered in short base tiltmeters" (Allan, 1978). Hence the question of what is the rate of geodetic tilt, and also of the sense and amplitude of co-seismic tilting, has remained un-resolved because of the poor quality of data generally obtained thus far from shallow borehole tiltmeters.

It seemed to us, then, that the instrument system needed examination from an operational point of view, and also that studies were needed to establish the reliability of the tilt data. We determined to install tiltmeters in pairs, 10 meters apart. For reliability, signals from both instruments of the pair should agree within our expectations for any wavelength significantly greater than 10 meters. This, of course, assumes that the tiltmeters are identically installed in a homogeneous medium of topographic symmetry. Until such pairs of instruments agree, any interpretation of the data would be wishful speculation or extraordinary coincidence, at best.

III. Evaluation of the Instrument System.

Three aspects of the shallow borehole system were of critical importance to us: the innate stability of the instrument electronics system, the interfacing of this system with power, recording, and automatic re-zeroing equipment, and the installation of the borehole itself. The stability of the bubble itself has been favorably examined by others, (Johnston, 1975) and since the bubble would be at least 2m in the ground, it should not be subject to thermal extremes.

Our engineering efforts with the tiltmeter electronics have been detailed in technical reports as well as descriptions of our interfacing and automatic re-zeroing system (Morrissey, 1976, 1977; Stauder & Morrissey, 1978). It is sufficient to say that with appropriate modification of the thermally sensitive elements, the electronics system can be made stable to 10^{-8} radian/°C, with some units testing out to 2×10^{-9} radian/°C. This is well within the 1 μ radian/year expectation, since neither of our environments (New Madrid or Adak) have a 100°C range. Further a well-insulated environmental enclosure can minimize the daily thermal excursions to which the electronics are subject.

IV. The installation problem

The installation technique has presented a number of difficulties which affect instrument stability and/or confidence in the data recorded. The dry hole/aged iron pipe method of the USGS (Johnston and Mortensen, 1974) was clearly not suitable for New Madrid where the embayment floods, nor for Adak where the island environment is always wet, and where flooding occurs during the snow melt. We also felt that the introduction of the iron pipe added an additional interface problem and a possible source of very long term drift.

Our numerous installation experiments, beginning with experiments conducted at a farm in Creve Coeur, near St. Louis, in April of 1976, have been discussed in the technical reports (Morrissey, 1976, 1977; Stauder and Morrissey, 1978). The crux of the problem has always been an apparent problem with the sand pack. In the installation procedure the tiltmeter is mounted in the borehole by forcibly tamping a maximum density blend of silica sand around the instrument. As the installation proceeds, the compaction of the sand results in a reversed sense of tilt as the sand is added and tamped above a point about two-thirds of the length of the borehole. With further tamping above this point the instrument registers tilt towards, rather than away from the tamping pressure. Our hypothesis is that the sandpack becomes more rigid than the pipe and the pipe bends. This problem has been with us all along. Till recently we have always gingerly continued to pack the sand to the top of the tiltmeter, thinking that the more contact with the earth, the better, in agreement with others (Johnston, personal communication). However, in our experience this procedure makes the tiltmeter very susceptible to horizontal shear pressures induced by such things as surface loading by people, water, etc.

A fortuitous experiment indicates that the above procedure may not be the best. Last summer (1977), for reasons detailed elsewhere, a tiltmeter was installed at Adak at a 1 meter depth in glacial chert. Since the borehole was made by a throwing iron and excavated by hand, it was only 60 cm deep (an arm's length). The tiltmeter was otherwise installed as usual, but packed to only half its length in the F 140 sand. A surprising result was noticed: over the next six months the maximum drift of the EW component from the installation zero was 2 μ radians, and the net drift over 6 months was 0.3 μ radians. The NS component failed shortly after installation (attributed to damage to the tiltmeter in shipping) but became operable again through the months of January to April. During this period the NS component showed the same stability as the EW component. The net tilt for this instrument over one year was 12.8 μ radians down to the northeast, most this being accumulated in the spring months.

Unfortunately, we did not know of this result until December of 1977, since the tiltmeters are visited only twice a year. The other tiltmeters on Adak are installed the full length of the instrument at depths of 1 1/2 to 2 meter. Figure 1 is a comparison of data from the Adak South tiltmeter (to which reference is made above) to that from the Adak North unit. The 100 mph plus typhoon (a storm which wiped out half the seismic net) is evident, with considerable noise on the North data, but not much more than probably barometric loading on the South data. The magnitude 6.6 earthquake of November 4 is also evident. No significance can be attached to the magnitude of the apparent coseismic tilt since the auto-zeroing system in use at the time had only a 2 minute delay. Tilt steps which are off-scale are automatically returned on scale in this arrangement, thus masking the size of the tilt. We have installed a new digital system with a 4-hour delay so as not to obscure possible co-seismic tilt steps.

In the meantime, we had begun our installations at New Madrid, with less than encouraging results. The initial data had daily quasi-periodic excursions of more than 10 μ radians; even the 3 hz alluvial microseisms were greater than 1 μ radian. Because of disagreement between the units, the initial pair at NRM were re-installed several times in an effort to get the signals from the two instruments to agree, with no success. We felt it was pointless to install more instruments in an apparently useless fashion. Consequently, we began a search of the literature for further explanation of the source of the large diurnal amplitudes. An unpublished paper by JB Walsh (1975) on "Thermal strains and tilts" proposed that the diurnal wavelength tilts could be attenuated by an order of magnitude with every 40 cm increment in depth of burial of the instrument. Unfortunately, when we attempted to experiment with depth of burial at NRM in the fall of 1977 the instrument site was flooded, which obviously makes working in a hole difficult. In the meantime data were recorded continuously at NRM except for a break in mid-winter due to the unusually severe cold. The raw New Madrid data are presented in Figure 2.

22 Oct. to 19 November 1977.

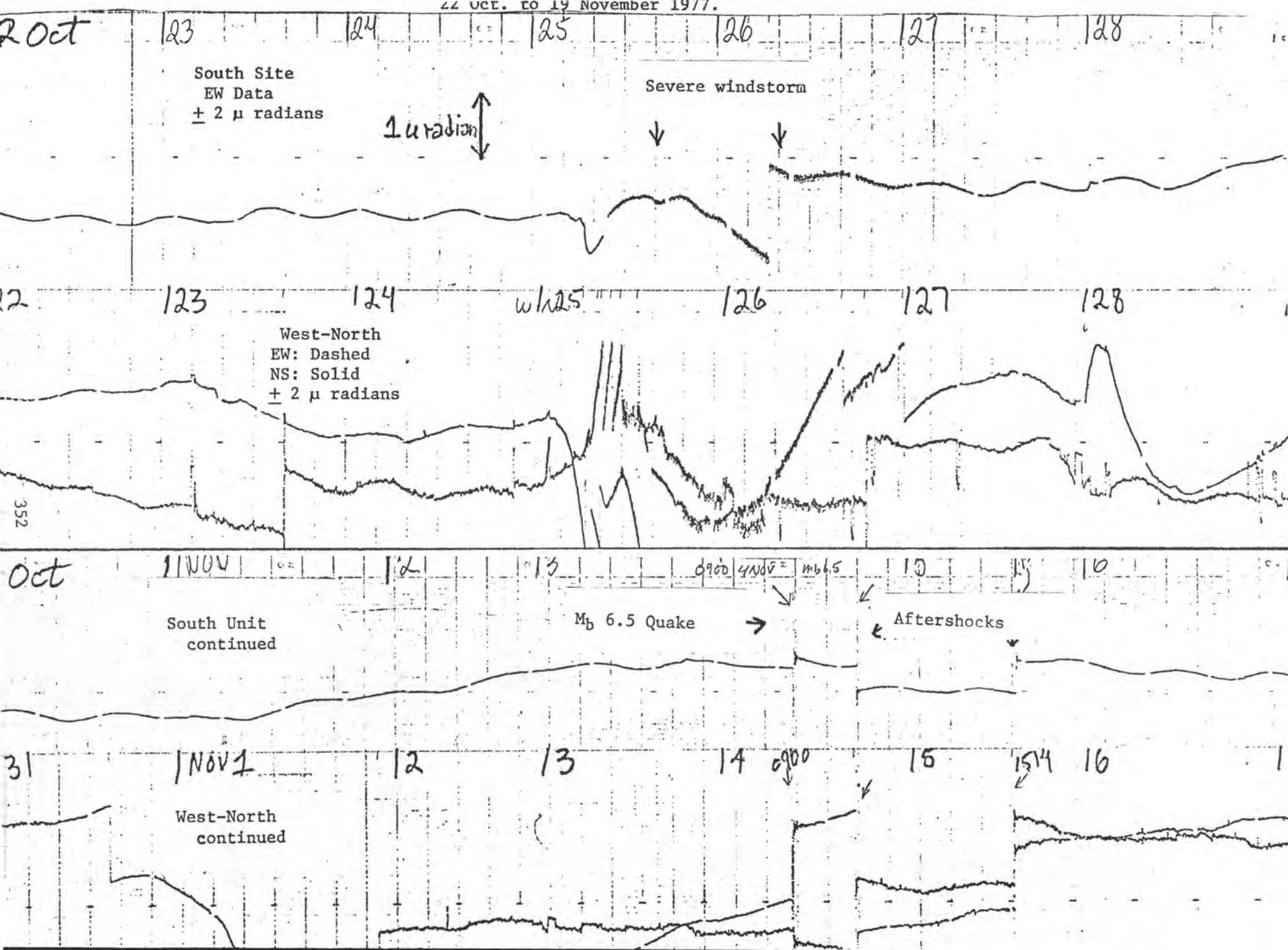

Fig. 2. New Madrid Data, June 1977 to February 1978: old installation method.
Solid line: no data: End point 27 April 1978. Units are 10 meters apart.

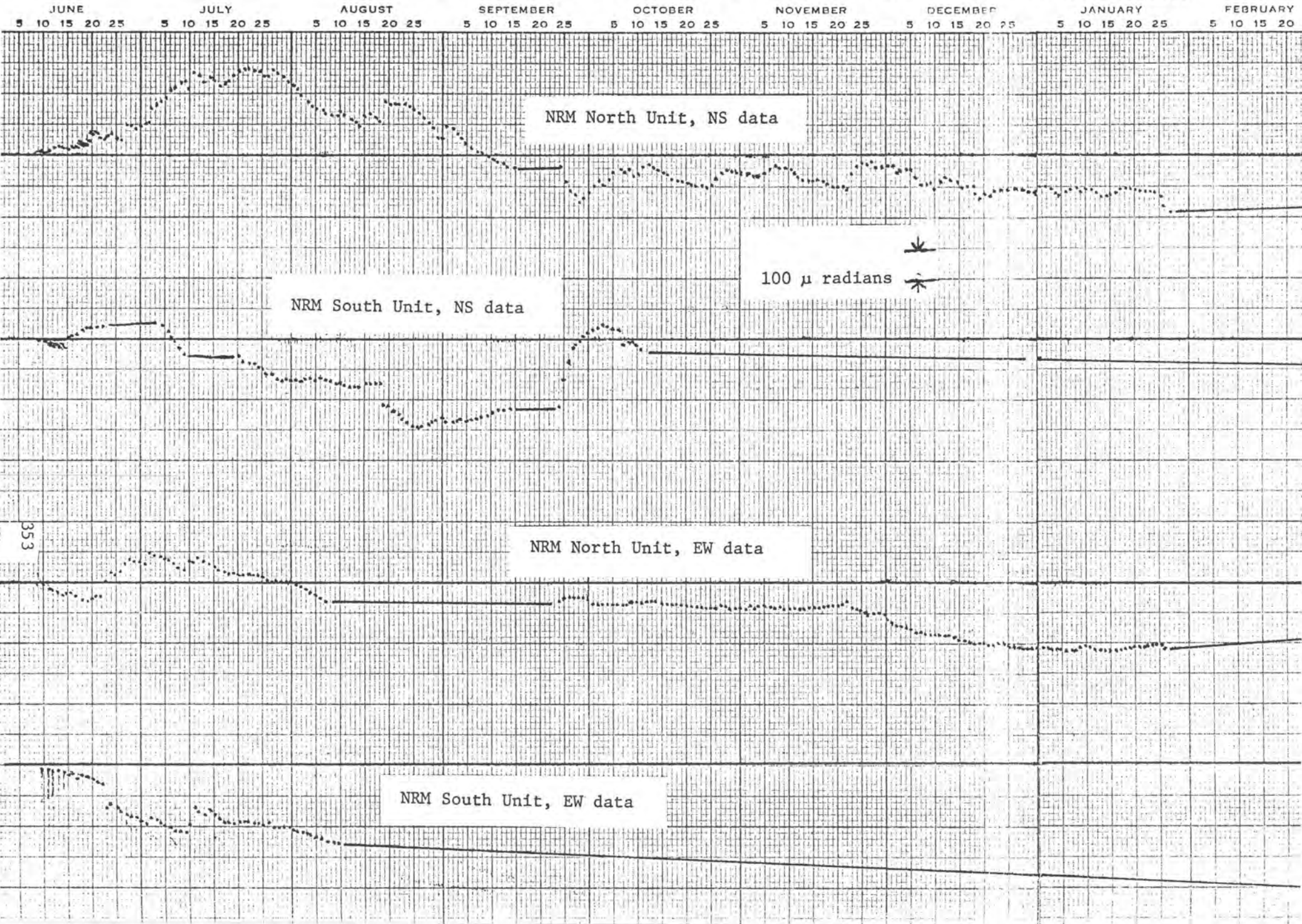

At this point, then, we had identified two possible avenues of improvement in the installation method which needed testing. Consequently, we re-developed the Creve Coeur test site in the spring of 1978. The first unit (west) was installed at a depth of 1 1/2 meters, but only half-packed in sand. Its initial stability was excellent, but with a yet notable susceptibility to diurnal surface thermal effects. The second unit (east) was installed at a depth of 2 meters. The diminished amplitude of the diurnal thermal tilts was almost as expected from the Walsh paper. A third unit (north) was installed at a depth of three meters. This unit stabilized very quickly, again showing a marked attenuation of the thermo-elastic diurnal tilts. Figure 3 is a sample of the data from all three instruments. The three units are in a triangle about 6 meters on a side. The amplitude of the North-South diurnal tilt is 15.8, 7.7, and 0.3 μ radians respectively, for each unit.

We are not concerned here about baseline stability, because a large annual tilt is probably present since the tiltmeters are not in topographically symmetric terrain (it slopes down to the North and West). Currently the shallow (West) unit is being deepened to three meters to try to track the north unit.

Also in the spring of 1978 experiments could resume at New Madrid. The diurnal noise had been varying from 2 to 10 μ radians in amplitude, generally diminishing over the winter. In June the north unit at NRM was removed and re-installed in the same hole, except that it was only half-packed in sand. Initial stability was excellent, even though the hole was filling with water. Figure 4 is a comparison of the data before and after this operation. The record is 10 μ radians full-scale. There is an obvious attenuation of the thermoelastic wave, and an increased baseline stability. Of course, half-packing the unit effectively increases its installation depth by 1/2 meter, so it is difficult to determine which change in method contributes more to the improved data, except in that the Creve Coeur experiment does not show such a tenfold decrease of the thermal wave due to the depth increment at this depth (2 meters). Both NRM units will soon be re-installed at a 3 meter or greater depth; and, hopefully, recorded with tidal sensitivity.

Further encouragement can be found in the initial results of the Adak '78 summer field trip, which has just been completed. We obviously wanted to re-install all the tiltmeters in a similar fashion to the South unit, since it behaved so well. We have also been less than content with the fact that the tiltmeters were installed in the surface soil layers that overly the more competent rock by about 2 meters. This soil consisted of alternate bands of dense clayey soil and loose volcanic ash. Rainfall usually resulted in large rotations of the tilt vector, probably because of saturation of the soils and resultant shear forces from the changing soil saturated load on inclined hillsides acting on the top of the tiltmeters, which, being fully packed in sand, were very sensitive to such disturbances. So a gasoline-powered rock drill/breaker was obtained so as to be able to penetrate the cherty morain at the south site, and also the rock at the west, north, and east sites. There are a total of seven tiltmeters in a triangular array about 2 Km on a side. The north and south sites were developed as dual tiltmeter sites, with the hopes that the units would track within 1 μ radian per year.

Figure 3: A comparison of three instruments installed at 1.5, 2, and 3 meters depth at Creve Coeur. Sensitivity is ± 2 μ radians. A weak teleseism is recorded on the right side.

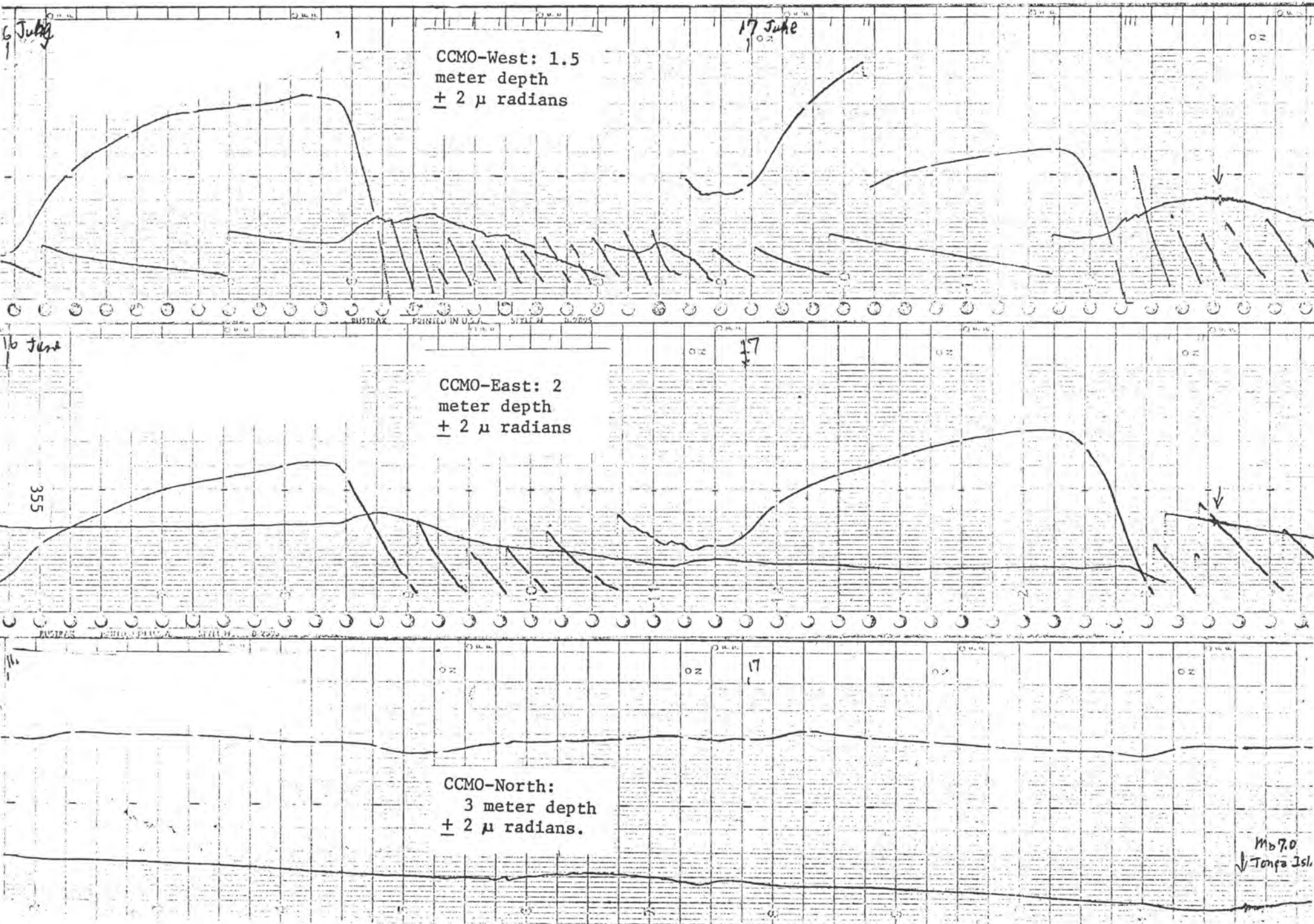

Figure 4: A comparison of NRM data before and after the borehole was re-installed only half-packed in sand. Bubble depth is 2 meters.
Chart sensitivity ± 5 μ radians: rate 1/4"/hour.

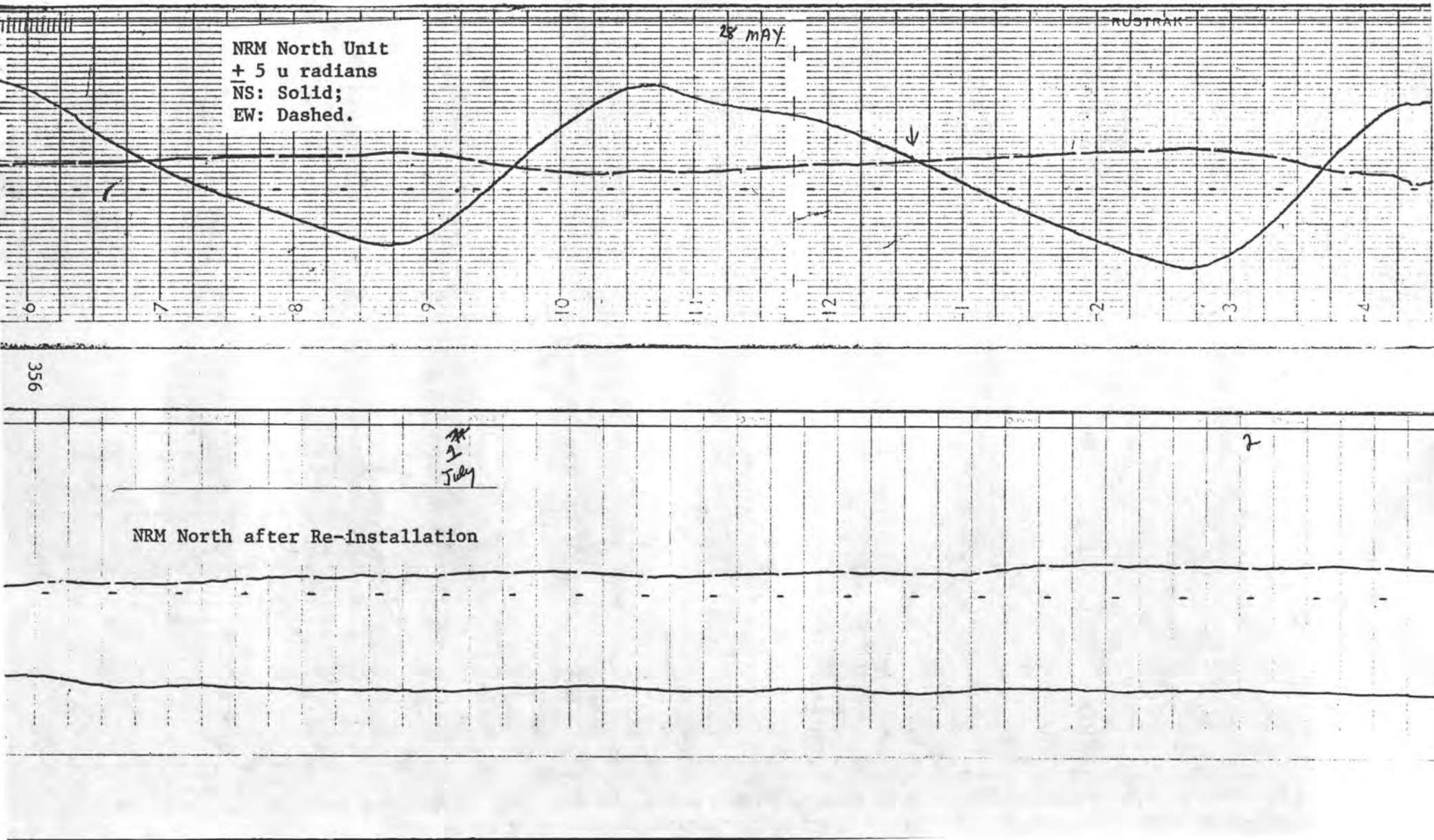

The initial results are quite promising. Most of the units stabilized within 12 hours. Figure 5 shows the first several days' data from three of the instruments. Two units did not stabilize quickly, and in both cases it is probably due to a rushed or inattentive effort in packing the sand. This leaves residual stresses that can take a week or more to settle out. We are hopeful that this improved installation technique will result in more coherent records of co-seismic tilts from local earthquakes, since there should be minimal settling of the installation. All the units were provided with the new digital auto-zeroing system with a 4-hour delay in order to avoid zeroing out co-seismic tilts. It is of note that, while teleseisms are regularly recorded at Adak and New Madrid on the tiltmeters, we have seen no co-seismic tilts at these times.

V. Data acquisition and interpretation.

Since tiltmeter data can generally only be meaningful if it is from several instruments and of considerable duration, large masses of data need to be assimilated and analyzed at once. Also, the dynamic range of tilts of interest (10^{-5} to 10^{-8} radian) is generally not realized with analogue recording systems. Hence automatic digital acquisition is essential and has been provided for most tiltmeter systems. Digital systems for both New Madrid and Adak are on order and will be insalled this fall and winter. The Adak data have been recorded for the last two years on a cassette data logger. Reduction and interpretation of these data will be discussed by J.C. Harrison of CIRES.

Aside from the problem of acquiring the data, there is a question of how to present tilt data. Since the events we are probably looking for are small changes of tilt rate or azimuth, they are difficult to discern against the baseline drift. Also, if we are trying to compare the data from two tiltmeters, we are interested in a presentation that will enhance any differences or agreements between two or more units, but still present the data along parallel time base lines. The usual presentation of tip-to-tail vectors wandering in circles, or the separates traces of orthogonal components plotted against time do not seem to satisfy our needs. To this end then, we have developed a presentation of tilt-rate vectors, in which the rate of change of tilt for a regular interval is plotted along a single time base. This scheme is naturally sensitive to first order changes, but should readily show if sets of tiltmeter data are coherent, or if there is any change in tilt rate or azimuth associated with earthquake activity. Figures 6 and 7 are examples of such tilt rate plots of New Madrid and Adak data. This is from raw data, sampled once a day, averaged over a 10 day running mean.

An effort is being made to "clean up" the Adak data, and perhaps with more samples a more coherent picture will emerge. In the current presentation, a tilt event (such as that from a heavy rain) that exceeds the running mean average can abruptly switch the azimuth of the tilt vectors. This method obviously needs considerable refinement before its usefulness is established.

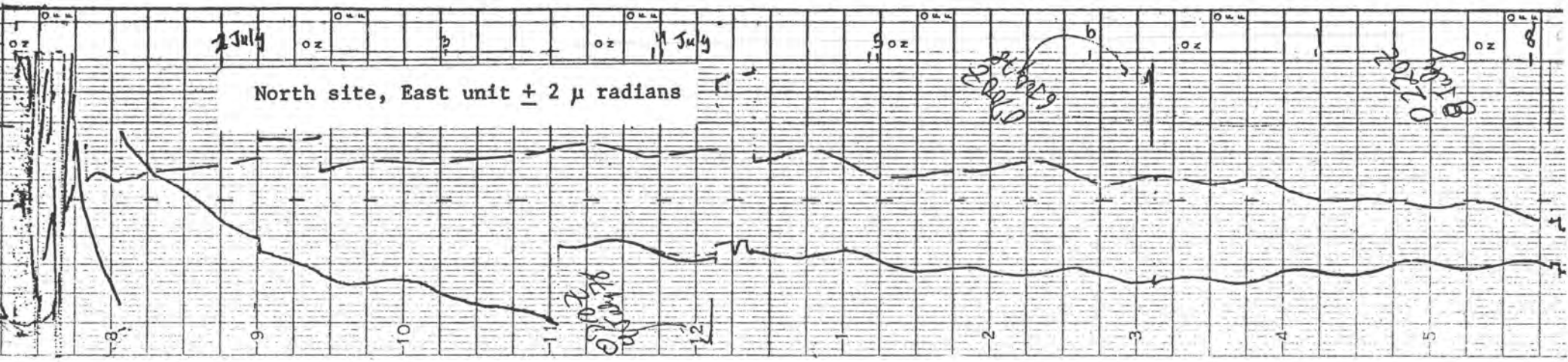
North site, East unit ± 2 μ radians
1 July
4 July

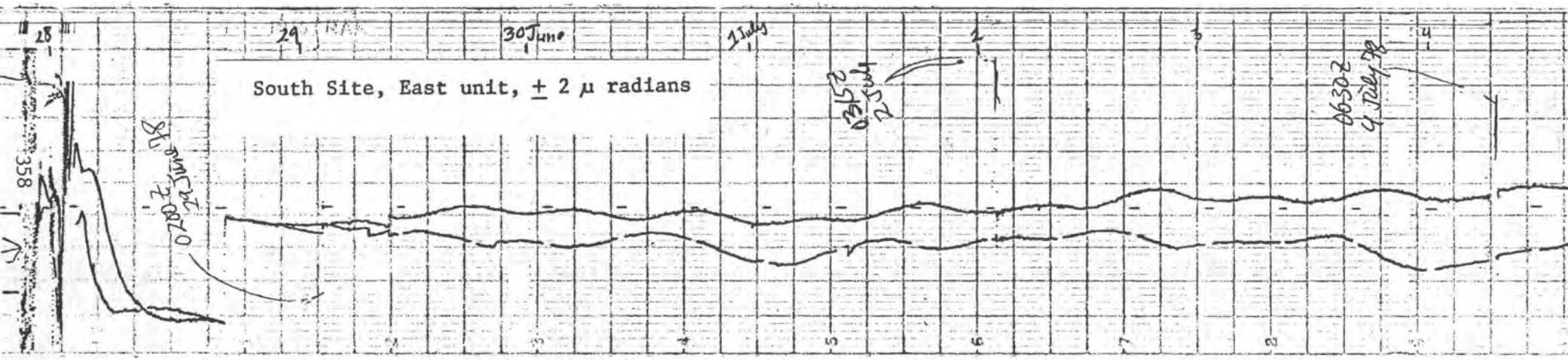
South Site, East unit, ± 2 μ radians
29
30 June
1 July

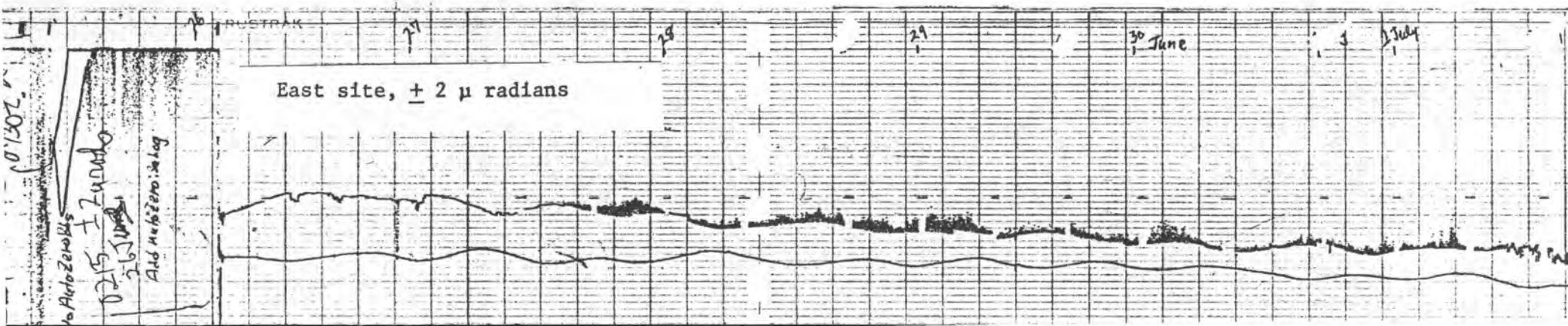
East site, ± 2 μ radians
29
30 June
1 July

Figure 6

New Madrid Tiltmeter Data
May - Sept. 1977

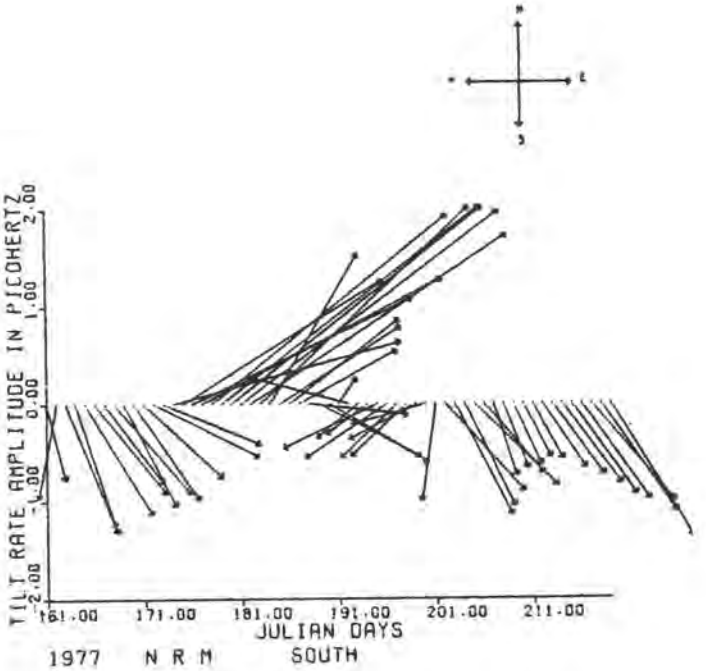

Tilt rate, NRM South unit

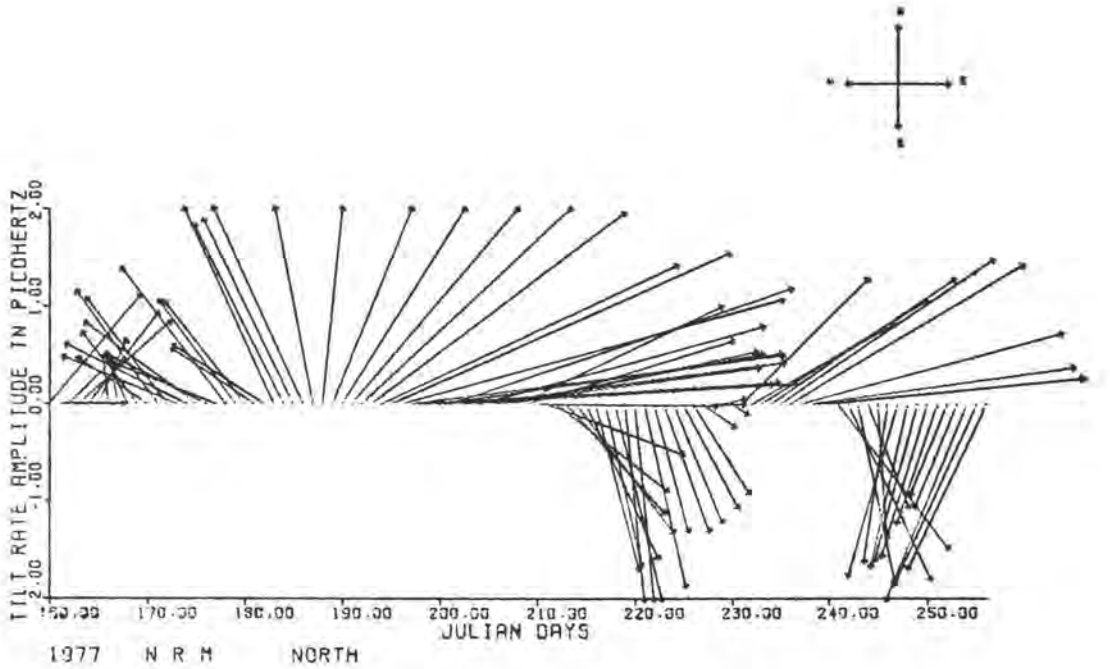

Tilt rate, NRM North unit

Adak Tiltmeter Data
July - December 1977

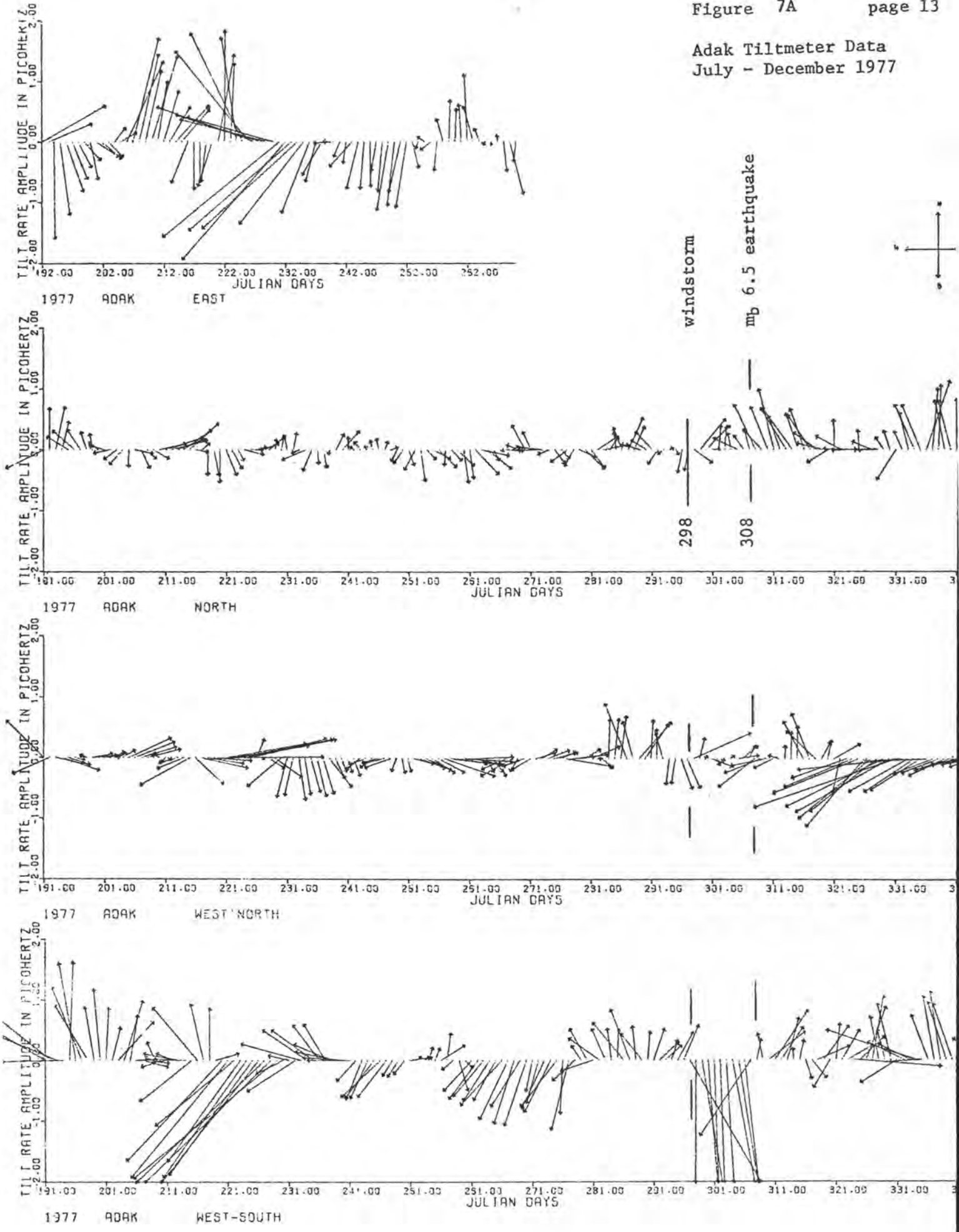

Adak Tiltmeter Data
July - December 1977
Log Amplitudes

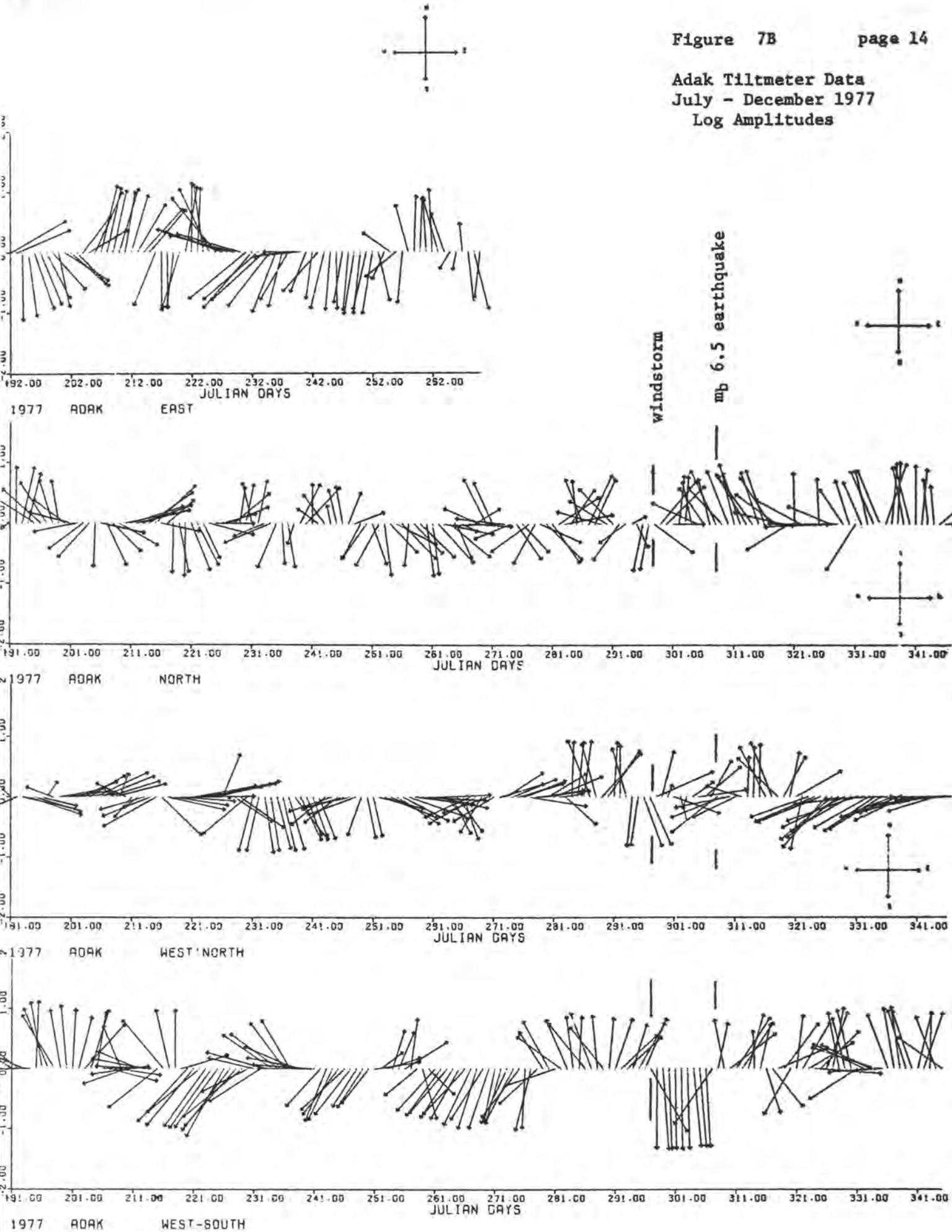

VI. Summary and Conclusions:

The usefulness of shallow borehole tiltmeter data to date for earthquake precursor studies has been generally shown to be marginal at best. The few papers on alleged tilt precursors are not that conclusive. Typically, the premonitory tilts reported have been single-instrument events, and so are quite open to doubt as to their true nature. We have serious doubts of the capability of many tiltmeter systems as presently installed to resolve precursory tilts of the order expected, that is, 1 μ radian per year or 10^{-8} radian per month. Until tiltmeters operated in pairs can be made to track with this accuracy, their usefulness will be in doubt.

We have found, however, that direct effects of environmental extremes on the instrument system itself can be minimized, and that new insights into the problem of interfacing the borehole with the environment are extremely encouraging. A problem with any geodetic measurement system is that it takes several months of watching the data before the results of any given experiment can be evaluated. Hence it seems that two years into the tiltmeter program has not been that long a time, and most certainly is not enough time to realize fully the potential of the shallow borehole tiltmeters. We find no practical or theoretical reasons why we should not be able to achieve the stability and resolution required. We have but to realize that the shallow borehole system is basically new and untried, and the techniques and assumptions that allow seismometers to agree ten meters apart can not as yet be applied to tiltmeters.

REFERENCES

Allen, R.V. Tiltmeter Observations near a Large Earthquake, Bull. Seism. Soc. Am., 68, 855-857.

Herrmann, R.B., S.H. Cheng, and O.W. Nuttli, Archeoseismology Applied to the New Madrid Earthquakes of 1811-1812, Bull. Seism. Soc. Am., In press (1978).

Johnston, M.J.S., and C.E. Mortensen, Tilt Precursors before Earthquakes on the San Andreas Fault, Science, 186, 1031-1034, 1974.

Johnston, M.J.S., Testing the Physical Parameters of Short Baseline Tiltmeters Intended for Earthquake Prediction Research; USGS open-file report, 1975.

Johnston, M.J.S., A.C. Jones, W. Daul, C.E. Mortensen, Tilt Near an Earthquake (m_L = 4.3), Briones Hills, California, Bull. Seism. Soc. Am., 68, 169-173.

McHugh, S. and M.J.S. Johnston, An Analysis of Coseismic Tilt Changes From an Array in Central California, J. Geophys. Res., 82, 5692-5698, 1977.

Morrissey, S.T., Special Study on the Adaptation of Commercial Tiltmeters for Monitoring Geophysical Phenomena in Harsh Environments, Unpublished, 1976.

Morrissey, S.T., A Study on the Adaptation of a commercial tiltmeter for monitoring earth tilts in unfavorable environments, Unpublished, 1977.

Mortensen, C.E., and M.J.S. Johnston, The Nature of Surface Tilt Along 85 Km of the San Andreas Fault - Preliminary Results from a 14-Instrument Array, Pure and Applied Geophysics, Proof copy, 1975.

Rosenman, M., and S.J. Singh, Quasi-static strains and tilts due to faulting in viscoelastic half-space, Bull. Seism. Soc. Am., 63, 1737-1752.

Stauder, W. and S.T. Morrissey, Semi-Annual technical report: Tiltmeter Array in New Madrid, Unpublished, 1978.

Walsh, J.B., Thermal Strains and Tilts, Unpublished, 1975.

THE ANALYSIS OF TILTMETER DATA

by

C. E. Mortensen

U.S. Geological Survey

345 Middlefield Road

Menlo Park, Ca. 94025

Abstract

Tilt data for periods as great as five years from 30 shallow borehole tiltmeter sites within the U. S. Geological Survey central and southern California tiltmeter networks have been characterized and examples of the data are presented. Long term secular tilt rates range from 0.5 to 50 or more μradians per year with typical values ranging between 5 and 20 μradians per year. Tests at the San Francisco Presidio vault and comparison of tilt measurements at the Presidio and Berkeley vaults with tilt measurements from shallow borehole tiltmeters along active sections of the San Andreas and other faults suggest that it should be possible to measure long term tilt with stability on the order of 1 μradian per year with the shallow borehole installations at sites with favorable local geologic and topographic conditions and with careful emplacement procedure.

Noise level and response to various sources of spurious signals vary widely for different period ranges and for different sites and appear to be critically dependent on local site conditions. The dominant sources of noise derive from meteorological effects acting at the earth's surface, at the instrument-earth interface, and upon local geology and topography. Mechanical and electrical stability of the instrument, stability of the instrument-earth interface, data processing errors and other problems can also contribute spurious signals. Clusters of instruments at varying distances and depths, comparison of instruments with different baselines and comparison with leveling results offer some possible techniques for isolating responses to various noise sources. Preliminary results of the application of some of these techniques suggest that some short period signals decrease in amplitude with depth.

Introduction

An experiment has been attempted in which a large array of tiltmeters have been installed along the San Andreas and other faults in California (Johnston and Mortensen, 1974; Mortensen and Johnston, 1975). A number of important questions are always at issue when a new set of measurements are made. These questions concern the quality of the data, the limitations of the measurements with respect to sensitivity and frequency response, and the relationship to tectonic activity and fault behavior.

When using crustal deformation measurements to study fault mechanics, the simplest expectation might be that the records of tilt and strain measuring instruments would show response only to anticipated signals such as earth tidal deformation, seismic waves, and perhaps during deformation associated with episodic aseismic fault failure related to surface creep events or earthquakes. Such records of episodic deformation might then be compared with other independent measurements and inverted to determine the mechanical behavior of the fault. An example of such a study may be found in Mortensen, et. al., 1977, where the authors were able to associate signals from a tiltmeter, a strainmeter, a water level recorder and two creepmeters with creep events on the San Andreas fault. While several assumptions were made in that study in deriving plausible models consistant with the data, there was no uncertainty introduced by having to extract a signal from a noisy record at the time scales of the creep event signals.

It is realistic to assume, however, that signals from unexpected sources may enter into the records, particularly in the case of shallow, high sensitivity measurements of ground deformation. Thus, it is especially important to determine the quality of the data by posing a number of questions and tests.

The initial and simplest questions posed include the following: Are earth tides observed and are they contaminated? Are long period seismic waves of appropriate amplitude observed? Are signals observed at the time of creep events and can reasonable models of fault behavior explain their character? What are the long term secular rates. Are secular rates or signal-to-noise ratio higher near active faults than at some distance from them? Is meteorological contamination observed in the data? What unexpected signals are observed and what expected signals are not observed? And the most important question for this experiment is, of course, what is the nature of observations related to earthquakes?

Some of the questions above may be answered by inspection of the data while others must be elucidated by various tests to determine, for example, the degree of coherence between adjacent instruments, the variation of signal-to-noise ratio with depth and baseline, the agreement of long term secular rates with independent measurements, the sources of signals for particular period ranges generated in the instrument, the installation or the earth.

Continuous monitoring of crustal deformation at high sensitivity with large arrays of shallow instruments is sufficiently recent that complete answers are not available even for some of the obvious questions enumerated above, while there are only afew preliminary results from some of the tests mentioned. The purpose of this paper is to focus on some of these questions, calling on the preliminary observations and test results.

Observations

In the U.S.G.S. tiltmeter networks in central and southern California, instruments have been installed relatively close to various active faults - typical between one and four kilometers and frequently closer. The disposition of instruments with respect to the fault were selected on the basis of dislocation solutions for sources at typical hypocentral depths. Long term secular tilt rates range from 1/2 μradians per year to 50 or more μradians per year with typical values ranging between 5 and 20 μradians per year. Table I summarizes cumulative tilt and estimates secular tilt rate at sites for which figures are available in central and southern California. Site locations are indicated in Figures 1 and 2.

While long term tilt can be determined for many sites within a few kilometers of the fault, and even as close as 300 meters (at the HAR site), only the record from the San Francisco Presidio vault (PDO) provides a measure of long term tilt at distances up to 10 kilometers from the fault (the vault is 9 kilometers from the assumed offshore trace of the San Andreas fault). The PDO instrument is fundamentally different from the type of installation employed as a standard throughout the central and southern California networks. However, a standard borehole type instrument installed beside the PDO instrument shows good agreement for a period of more than one year. Also the Berkeley instrument (BRK), which is similar in design and installation to PDO, but is within 1.5 km of an actively creeping section of the Hayward fault (Bolt, et. al., 1966), shows a long term tilt rate comparable to the typical rates observed with the shallow borehole installations close to active faults.

Figure 3 shows long term records from several sites in central California. The long term record from the Harris (HAR) tiltmeter site, near the Cienega winery, south of Hollister, provides an interesting look at tilt data observed within approximately 300 meters of the creeping section of the fault. Here the instrument is installed in the floor of an inactive mine reclaimed for geophysical monitoring use by the University of California, Berkeley Seismographic Station. The tiltmeter is installed approximately 100 meters into the tunnel and is covered by an estimated 16 to 18 meters of overburden. The tilt record produced at HAR, shown in Figure 3, has little energy in the period range of days to weeks, but shows a steady, high secular tilt rate which decreases gradually with time. Although temperature is not monitored inside the tunnel, the depth of overburden would imply a significantly smaller variation than is the case with the standard shallow borehole sites. Thus, instrumental and installation related thermal effects should be insignificant and thermoelastic effects should be greatly

attenuated. An estimate of the importance of each of these effects at the shallow borehole installations will be discussed later.

The vertical error bars subtending the HARN and HARE records in Figure 3 represent two standard deviations from successive measurements of a short aperature (127 m by 101 m) level array .8 km north of the HAR instrument. Unfortunately damage to the HAR recorder during heavy winter rainfall in 1978 prevents direct comparison of the level array results with instrumentally recorded tilt after November, 1977. Successive level array measurements represent the change in the attitude of a plane which provides the best fit in a least squares sense to elevation changes of many (5 to 10) individual bench marks. The error bars represent the precision of the measurement, while scatter of the fit of the plane to the measurements of the individual marks may imply a slightly less accurate result (Lisowski, personal communication), ie. the data may be non-linear over the dimensions of the array.

An important experiment both in establishing confidence in the ability of an instrument to detect the large wavelength deformations which are most interesting in the study of fault mechanics and in characterizing the waveforms (and thereby possibly inferring the behavior at the source) of the tilt changes with time is to operate more than one instrument spaced sufficiently closely that signals may be identified in the records and compare between instruments.

Many of the tilt records from instruments located within a few kilometers of the fault show considerable energy in the period range of days to several weeks. In this paper I shall refer to this as the intermediate period range. In Figure 3 the records from the Mt. Madonna (MTM) instrument and in Figure 4 the records from the Aromas (ARM) instrument provide typical examples of such variation. At the Aromas site, as at the Bear Valley (BVY and BV2) and San Juan Bautista - Avilla (SJB and AVA) sites, two instruments operated as redundant pairs provide some insight into the tilt variations in this period range.

Sources that may contribute to noise in the intermediate period range include meteorological effects, local surface instability, mechanical changes in the site or instrument, telemetry and data handling problems. Tilt changes in this period range are also potentially of interest tectonically, particularly with respect to earthquake prediction for local earthqukes of moderate size (M <5+), if current estimates of supposed precursor times are approximately valid (for example, Whitcomb, et. al., 1973).

Meteorological Effects

The two most important meteorological effects for intermediate period ranges are rainfall and temperature changes. Comparison of the ARM and AR2 parallel records in September 1976 (Figure 4) shows general agreement in response to rainfall on September 28th. At the Aromas site the instruments are spaced within 5 meters of one another. The rainfall responses for the San

Juan Bantista - Avilla instrument pair, however, do not generally agree, as is evident in the parallel records at the times of rainfall on February 23, and March 17, 1977. Here the instrument spacing is roughly 200 meters and the two instruments are sited in quite different geologic settings.

The San Juan Bautista site is located near the top of a relatively abrupt, well drained hill in fractured and weathered limestone, which outcrops near the instrument. The Avilla site is located approximately 200 meters north (closer to the fault) of the San Juan Bautista instrument in unconsolidated alluvium on a poorly drained, gentle topographic high. At the Avilla site long periods of rainfall frequently saturate the soil at the depth of instrument burial.

Apparently rainfall responses are highly dependent on very local surface conditions. The effects may result from differential soil expansion around the site and, if so, the response may be sensitive to the degree of saturation prior to rainfall. Another possible rainfall response mechanism may be differential loading due to inadequate and non-uniform drainage. Rainfall may also effect the instrument response by thermal conduction, saturating the soil and thereby lowering the absolute temperature or increasing thermal conductivity, or both. At a few sites all of these possible mechanisms may be operable. It may be valuable to monitor soil humidity at a few selected sites in order to test at least the first hypothesis.

The rainfall responses in the AVA record in February and March, 1977, shown in Figure 4, are typical for most tilt sites in form, though not in amplitude or duration (they are much larger than the typical responses at most sites). Rainfall responses seem to be relatively easy to identify and characterize by comparing tiltmeter records with rainfall records measured at a nearby location. Our current practice is to use rainfall (and temperature) data taken from the NOAA Climatological Data monthly summary, which lists daily recorded rainfall and temperature for stations spaced at roughly 20 to 40 kilometer intervals in the area of the tiltmeter networks. Rainfall is roughly coherent over those distances. Future plans call for the installation of several telemetered rain gauges to improve the density of coverage as well as the timeliness of the observations.

Temperature changes may contaminate the tiltmeter data by three possible mechanisms. These include thermoelastic effects in the ground surrounding the site, temperature changes acting on the interface between the ground and the instrument, and instrumental thermal sensitivity. At a given tiltmeter site it may be difficult to determine the relative importance of each of these effects.

The bubble sensor of the tiltmeter is highly sensitive to thermal gradients and therefore has been installed in a suitable metal case of high thermal conductivity and is buried at a depth of approximately 2.5 meters in order to minimize this effect. Kohlenberger, et. al. (1973), of Rockwell International have measured a significant thermal sensitivity in gain of the

instrument of .011 μradian per ^{0}C per μradian. Kinemetrics (1977) tested five tiltmeter electronics circuits for temperature response and found an average temperature sensitivity (a combination of zero shift and gain change) of .065 μradian per ^{o}C. Assuming a $22^{o}C$ temperature range, which is a high value for both diurnal and seasonal mean temperature variations in central California, and a typical tilt offset of 25 μradians, the gain sensitivity reported by Kohlenberger, et. al. (1973) implies a spurious tilt offset of 6.1 μradians. For this temperature range the Kinemetrics measurement implies a spurious tilt of 1.43 μradians.

Insulation of the tiltmeter electronics package reduces the range of daily temperature variation to approximately $.01^{o}C$ per day and reduces the annual variation of mean temperature by a factor of two. Thus tilt changes caused by gain sensitivity for daily temperature fluctuations are probably on the order of .003 μradian, while the annual response may be as large as 3 μradians. In the relatively benign California climate, therefore, the electronically induced thermal effect probably does not play the dominant role in thermal contaimination of the tilt data from instruments operating within the manufacturer's specification.

It is more difficult to test to determine the thermal effect of the tiltmeter installation (ground-tiltmeter interface). Details of the installation technique developed for U.S.G.S. tiltmeter networks are described by Mortensen, et. al. (1975). Whatever the details of the installation technique, if the site is radially symmetric and isotropic at the scale of the instrument baseline, it should respond only to temperature gradients. Thus, if the sensor is buried sufficiently deeply and is physically decoupled from the immediate surface, there should be a negligible effect on the instrument output due to the temperature response of the ground-tiltmeter interface. This will not generally be true for strainmeters where it is not generally possible to preserve symmetry in the installation (compensation may be necessary). The variability of thermal response between tiltmeter sites suggests that the installation eccentricity and material inhomogeneity immediately around the instrument may play an important roll in site response to temperature. It may be difficult to separate this response from thermoelastic effects and perhaps at best one can hope, with careful attention to detail at each site, to exactly duplicate the details of installations that show very low thermal response at some sites. For example, the section of record in Figure 5 shows that the Nutting (NUT) site has a low response to temperature changes. It is most likely then, that the Sage (SGS) site, with identical installation details, is responding strongly to a thermoelastic effect.

One test which may be of value in separating the contribution of the installation from that of the instrument may be to exchange instruments at one of the sites with redundant tiltmeters. Most sites do not have co-located instruments, however, and it may not be valid to extend the results of such a test at one site to all sites.

One approach to minimizing the thermal response of the installation may be to reduce the conductivity in the vicinity of the sensor by removing the steel tubing that lines the borehole, though this would increase the possible effect of thermal gradients. This approach is advocated by Morrissey (personal communication), and has been tested at one location (SGS) in central California. The thermal response at the SGS site showed no apparent change in character after the removal of the borehole tube. This appears to support the hypothesis, mentioned earlier, that the thermal response at this site is predominately a thermoelastic effect resulting from nearby steep, nonsymmetric topography. At other sites some of the other possible mechanisms mentioned for thermal response may be important, and removal of the borehole tube may have a more pronounced effect at some of these sites. Until we develop a more complete understanding of the interactions of all elements of the system to various thermal inputs we don't plan extensive modifications of the established tiltmeter network installations.

Mechanical Effects

The tiltmeter data are subject to spurious drift introduced mechanically by the instrument, the details of the installation, and local geologic conditions. Mechanical stability of the tiltmeter (representative units) used in U.S.G.S. tilt networks has been measured by various techniques, for example by Johnston (1976), and probably contributes less than 1 radian per year to long term drift in the data. This assertion is supported by the observation that a few of the sites listed in Table I show very low secular tilt rates. For example, the Libby (LIB) instrument shows a net tilt of .7 μradians during the first two years of operation.

The use of fine silica sand as a medium for coupling the tiltmeter and borehole tube to the surrounding soil has proven to be quite satisfactory. Again, the fact that a few of the sites in Table I show very low secular tilt rates tend to support this conclusion. At the Presidio Vault, a tiltmeter packed in sand in a steel cylinder similar to those used as casing in the boreholes has tracked the parallel component of an ajacent mercury tube tiltmeter within 0.5 μradian for more than a year.

A tiltmeter installation utilizing a reportedly highly stable expansive grout in place of the sand has been tested at one site in central California (MTH). No change in the character of the record from this site was observed after the change in installation technique. Although this does not constitute an appropriate test of the stability of the grout, it tends to support the conclusion that at this site, fluctuations in the record as large as 12 μradians per month are probably independent of installation technique and are most likely caused by local inhomogeneous and unstable geologic conditions.

It has been known since the first installations in 1973 that the tiltmeter displays a curious apparent reversal in sense of bubble displacement with respect to light pressure at the top of the casing during emplacement of the sensor when the sand has been packed to within 35 to 45 cm of the top of

the tiltmeter casing. This phenomenon, if not taken into consideration by the installer at the time of sensor emplacement, could cause significant stresses to be introduced into the instrument casing and surrounding sand pack. Installation procedures for U.S.G.S. tiltmeters establish a protocol that is intended to avoid this possibility (Mortensen, et. al., 1977). However, it is difficult to assess the degree of adherence to these procedures in practice. Morrissey (personal communication) reports encouraging results from tests of a technique that avoids the problem entirely by only partially packing the sensor in sand, leaving the top of the instrument free. We have planned a test that involves replacing the stainless steel casing of .635 cm thickness with a casing having 1.27 cm wall thickness, thus preserving the instrument baseline while maintaining rigidity over the full length. With this test it should be possible to determine whether the reversal phenomenon results from bending of the sensor casing or a redistribution of stresses within the sand pack.

Soil humidity, mentioned previously as having a possible relation to thermal site response, may have an effect on the mechanical stability of a site as well, particularly in clay rich soils where alternate swelling and desiccation may cause the sand pack to become lose. This may have been the reason that the Libby (LIB) tilt site became unstable after two years of very stable, reliable operation, although other sites, such as the Nutting site, with at least as bad clay soils, have operated dependably for nearly 5 years. Corrosion of the sensor casing at LIB discovered upon its replacement in February, 1976, indicates that water had intruded to the sensor.

Several sites have been abondoned due to local soil slumping or creeping. Site selection appears to be the most important factor in providing both mechanically and thermally stable, meaningful tiltmeter records. It is also the most difficult factor to assess in the analysis of the data.

Some of the effects caused by local or near-surface geologic inhomogeneities and instabilities may be attenuated significantly by extending the baseline of the shallow borehole tiltmeters. A prototype installation designed to test this approach is currently in operation at the Stone Canyon (STC) site, and results will be compared with the standard, short-baseline instrument nearby. Additional tests of this technique are planned for three other central California sites.

Other Effects

Perhaps it is worth mentioning here a few of the problems associated with routinely processing the tiltmeter data. Instrumental rezeros, adjustments, calibrations, telemetry glitches, and various malfunctions must be identified and removed from the records. Once the size of the network approaches 80 biaxial instruments, generating 160 records with sampling every 10 minutes, "cleaning" the data by hand on a regular basis becomes unfeasible. This necessitates the development of a comprehenisve automatic "cleaning" algorithm that functions dependably on data sets having a variety of characteristics

that vary between sites. This is a difficult and lengthly process involving continuous testing, monitoring and feedback to ensure the validity of the results. A prototype system for automatic cleaning has been developed within the Geolab Data Management system (Herriot, 1978) and is currently being tested.

Initial Attempts at Interpretation

Given the variety of possible influences to which the tiltmeter may be subjected, it is not surprising that the tiltmeter data are generally non-stationary (that is, ensemble means and autocorrelation vary with time). This non-stationarity presents a number of serious problems in attempting a definitive and rigorous analysis of the data. Since the various potential signal and noise sources may have effects which dominate particular period ranges it seems logical to examine the spectra of the data and to employ filtering in different frequency bands in studing particular effects. One may thus impose weak stationarity upon the data in a particular period range and compare the result with some phenomenon suspected of influencing the data strongly in that period range.

It may be, for example, that mechanical relaxation of the instrument casing and instrumental thermal response make significant contributions to a tiltmeter record only at periods greater than six months. These may be non-linear in character and the former effect is probably not cyclic, while the latter effect may be cyclic. On the other hand response due to eccentricity of the installation, rainfall response, and earthquake precursors for a certain class of earthquakes, may produce the dominant signals for periods between three weeks and three months. To establish the significance of the latter effects it may be helpful to eliminate the response due to the first effects. Typical power spectra of detrended tiltmeter data show energy peaks beyond the expected 12 hour and 24 hour peaks. However, a search for systematic patterns beyond the 24 hour peak has not been accomplished.

An initial crude attempt to determine the degree of coherence between instruments at various distances was conducted by comparing parallel records from the three sites with co-located instruments. Sections of these records are shown in Figure 4a, b, and c . Data from the parallel components were first reduced to daily averages and smoothed with a running mean with varying window lengths. A high-pass filtered output was generated by subtracting the smoothed data from the raw daily averaged data. The filtered outputs of the parallel components for each instrument pair were then cross-correlated. The filtered outputs for each pair of parallel records using the 30 day running mean window are plotted in Figure 6 and the respective cross-correlation coefficients are listed. Table II lists correlation coefficients for daily averaged data smoothed over varous running mean windows.

While parallel data from each of the instrument pairs showed significant correlation for the raw daily averages and for records smoothed with a 30-day running mean (Table II), comparison of the high-pass filtered parallel outputs may be more interesting. The filtered data from the instrument pair with the

attempting to analyse tiltmeter data. Some techniques have been suggested that may help in assessing the relative importance of these factors. As more information becomes available during this experiment, and from various tests, results may be fed back into the system in the form of improvements in instrumentation and installation technique. The use of tiltmeters has proved to be useful in the study of particular fault mechanics problems, and the variety of interesting questions that this technique promises to address suggests the potential fruitfulness of continued investigation.

Acknowledgments

The author wishes to acknowledge the assistance of Mr. Jim Herriot in adapting the Butterworth filter program, and the many useful discussions on digital filtering with Drs. Joe Fletcher, Alan Stepp, and Bill Bakun. The Butterworth filter program was written by Dr. Keith McCamy. Dr. Malcolm Johnston suggested many of the lines of inquiry and provided valuable critical review throughout the work. Several lines of inquiry were also suggested during consultations with Mr. Sean Morrissey.

REFERENCES

Almassy, W. T., Proposed new tiltmeter circuit test report, Engineering Report #18, Kinemetrics, Inc., 1977.

Beaumont, C. and J. Berger, Earthquake prediction: modification of the earth-tide tilts and strains by dilatancy, Geophys. J., 29, 203-226, 1974.

Bolt, B. A. and W. C. Marion, Instrumental measurement of slippage on the Hayward fault, Bull. Seism. Soc. Amer., 56, 305-316, 1966.

Herriot, J. W., Geolab, U. S. Geol. Survey Open File Rept. 78-700, 1978.

Johnston, M. J. S. and C. E. Mortensen, Tilt precursors before earthquakes on the San Andreas fault, California, Science, 186, 1031-1034, 1974.

Johnston, M. J. S., Testing the physical parameters of short baseline tiltmeters intended for earthqauke prediction, U. S. Geol. Survey Open File Rept. 76-556, 1976.

Johnston, M. J. S., Testing earthqauke precursor algorithms on tilt, strain, and magnetic field data from along the San Andreas fault, 12th International Symposium on Mathematical Geophysics, in preparation.

Kohlenberger, C. W., G. L. Cooper, W. T. Schmars, Dynamic properties of a new biaxial tiltmeter, presented at Seism. Soc. of Amer., Eastern Section, Golden, Colorado, 1973.

Mortensen, C. E. and M. J. S. Johnston, The nature of surface tilt along 85 km of the San Andreas fault-preliminary results from a 14-instrument array, Pure and Applied Geophysics, 113, 237-249, 1975.

Mortensen, C. E., R. C. Lee, and R. O. Burford, Observations of creep-related tilt, strain, and water-level changes on the central San Andreas fault, Bull. Seism. Soc. Amer., 67, 641-649, 1977.

Mortensen, C. E., E. Y. Iwatsubo, M. J. S. Johnston, G. D. Myren, V. G. Keller, and T. L. Murray, U.S.G.S. tiltmeter networks, operation and maintenance, U. S. Geol. Survey Open-File Rept. 77-655, 1976.

Stuart, W. D., M. J. S. Johnston, J. W. Herriot, Earthquake prediction with telemetered tilt data: rational (abstract), EOS, 57, 287, 1976.

Stuart, W. D. and J. W. Herriot, Tilt elbows before earthquakes, U. S. Geological Survey Open-File Rept., in this volume, 1978.

Whitcomb, J. H., J. D. Garmany and D. L. Anderson, Earthquake prediction: variation of seismic velocities before the San Fernando earthquake, Science, 180, 632-635, 1973.

Wood, M. D., N. E. King and C. W. Chang, Theory of a single-channel Wiener filter and applications to prediction of tilt data, U. S. Geol. Survey Open-File Rept., 77- , 1977.

FIGURE CAPTIONS

Figure 1. Central California tiltmeter locations.

Figure 2. Southern California tiltmeter locations.

Figure 3. Tiltmeter records (daily averages) from the Mount Madonna, San Juan Bautista, Nutting, Harris, Libby, Bear Valley, and Dry Lake tiltmeter sites in central California.

Figure 4a. Parallel records (daily averages) from the Aromas instrument pair.

4b. Parallel records (daily averages) from the San Juan Bautista-Avilla instrument pair.

4c. Parallel records (daily averages) from the Bear Valley instrument pair.

Figure 5. Parallel records (10 minute samples) from the Nutting and Sage tiltmeter sites. High and low daily temperatures are plotted below.

Figure 6. Data from parallel records at redundant tiltmeter sites filtered with a high-pass, 30-day running mean. The numbers to the right are the cross-correlation coefficients for each record pair.

Figure 7. Examples of filtered data from parallel records at redundant tiltmeter sites. Filter parameters and cross-correlation coefficients are listed in Table III. Only a short section of 10 min sampled data is shown.

TABLE I

Total net tilt (cumulative) and estimated secular tilt rates for California tiltmeter sites (where long term data are available). (units are radians; + implies down to the N or E tilt)

Sensor	Period	Tilt	Period	Tilt	Period	Tilt	Estimated Secular Tilt Rate μrad/yr
ARMN	11/74-4/77	-21.5	9/76-9/77	-10.0			-4
ARME		-21.0		-47.0	approx. 4-5 m spacing		0
AR2N			9/76-4/77	-2.3	good agreement between east		
AR2E				-8.0	components until last month of record		
BVYN	2/74-4/77	- 3.0	1/77-4/77	-6.0			+1
BVYE		+ 9.5		-5.0	approx. 4-5m spacing		0
BV2N			1/77-4/77	-4.0			
BV2E				-1.1			
BLMN	5/26-7/77	-13.3					-12
BLME		- 8.1					- 6
DRYN	9/74-7/77	- 2.1					+ 2
DRYE		0.0					- 2
LIBN	6/73-9/75	- 0.5	6/73-4/77	-97.0	site destabilized		
LIBE	6/73-9/75	- 0.5	6/73-4/77	+139.0			
MTHN	9/76-7/77	+ 1.9					-68
MTHE		-81.5					-42
MTMN	3/74-4/77	-5.0					- 2
MTME		-23.0					-10
NUTN	6/73-4/77	-69.0					-15
NUTE		-11.5					-14
GOHN	5/76-12/77	+ 5.3	some linear interpolation across gaps				
GONE		+39.0					
TUKN	2/77-12/77	+22.0					
TUKE		+ 0.9					
SARN	10/76-7/77	-51.1					-27
SARE		- 9.8					- 7
OSON	3/74-7/75	+17.8	some linear interpolation across gaps				+ 3
OSOE		-43.4					-39
TRHN	5/75-8/75	- 2.8	8/76-7/77	-27.0			-28
TRHE		+ 0.8		+33.1			+28
PTNN	12/76-9/77	+3.5					+10
PTNE		+11.6					+10
WHTN	12/76-9/77	+10.0					+ 9
WHTE		-33.0					- 6
MLCN	2/77-9/77	+2					+ 6
MLCE		+3					-13
PFTN	12/76-9/77	+20.0					-17
PFTE		+46.8					-54

Table I (continued)

Sensor	Period	Tilt	Period	Tilt	Period	Tilt	Estimated Secular Tilt Rate μrad/yr.
AVAN			8/76-4/77	-42.0			
AVAE				0.0	approx. 200 m spacing		
SJBN	3/73-4/77	+4.0	8/76-4/77	-21.0			- 2
SJBE		+5.0		+0.1			+ 1
STCN	1/74-11/75	+ 4.0	1/74-4/77	+82.0	site destabilized		+22
STCE		+22.0		+77.0			+24
WILN	4/75-8/75	+19.1	8/76-2/77	- 5.2			- 6
WILE		-17.5		+21.3			+20
TRCN	4/75-8/75	- 2.1	10/76-9/77	-13.4			+ 7
TRCE		+ 2.5		+15.1			+ 9
HARN	6/74-7/77	-42.5					- 7
HARE		-54.0	300 m from fault				- 6
GLNN	3/75-8/75	+19.3	3/75-8/76	+73.0	3/77-7/77	+2.2	+47
GLNE		+17.1		+55.4		+13.1	--
LRSN							+13
LRSE							- 4
GLHN	3/75-8/75	- 0.5	10/76/-7/77	+45.5			+35
GLHE		- 1.0	3/77-7/77	-40.5			-34
PDON							0.8
PDOE							0.5
BRKN							0.9
BRKE							9.0

TABLE II

CROSS-CORRELATION OF PARALLEL COMPONENTS AT REDUNDANT TILTMETER SITES

	ARMN-AR2N	ARME-AR2E	BVYN-BV2N	BVYE-BV2E	SJBN-AVAN	SJBE-AVAE
1 Day Averages	0.78	0.48	0.38	0.74	0.75	0.43
5 Day Running Mean Smoothing	0.79	0.46	0.43	0.78	0.76	0.43
10 Day Running Mean Smoothing	0.80	0.43	0.47	0.81	0.77	0.43
15 Day Running Mean Smoothing	0.81	0.42	0.48	0.84	0.78	0.45
20 Day Running Mean Smoothing	0.81	0.38	0.48	0.86	0.78	0.46
25 Day Running Mean Smoothing	0.81	0.37	0.47	0.88	0.78	0.49
30 Day Running Mean Smoothing	0.81	0.34	0.46	0.89	0.78	0.50

TABLE III

CROSS-CORRELATIONS OF FILTERED DATA FROM PARALLEL COMPONENTS AT REDUNDANT TILTMETER SITES

Filter*	Passband** (period)	Ratio of high-pass Cutoff to nyquist freq.	Ratio of low-pass Cutoff to nyquist freq.	ARMN-AR2N	ARME-AR2E	BVYN-BV2N	BVYE-BV2E	SJBN-AVAN	SJBE-AVAE
F1 high-pass	0-4 hr	.0952		0.08	0.03	0.10	0.05	0.02	0.01
F2 high-pass	0-14 hr	.0272		0.03	0.09	0.14	0.06	0.02	0.02
F3 high-pass	0-28 hr	.0136		0.54	0.18	0.21	0.08	0.04	0.05
F4 band-pass	6-14 hr	.0272	.0444	0.45	0.20	0.35	0.14	0.15	0.20
F5 band-pass	6-28 hr	.0136	.0444	0.50	0.26	0.33	0.12	0.10	0.12
F6 band-pass	14-28 hr	.0136	.0190	0.53	0.31	0.35	0.13	0.06	0.18
F7 band-pass	1-8 day	.0020	.0139	0.50	0.34	0.08	0.03	0.04	0.00
F8 high-pass	0-8 day	.0348		0.42	0.27	0.35	0.30	0.01	-0.02
F9 high-pass	0-16 day	.0143		0.38	0.20	0.24	0.36	0.27	-0.09
F10 band-pass	6-16 day	.0143	.0267	0.66	0.23	-0.14	0.39	0.50	-0.06
F11 band-pass	0-32 day	.0071		0.47	0.13	0.10	0.26	0.34	-0.06
F12 band-pass	14-32 day	.0071	.0114	0.47	-0.03	-0.42	-0.17	0.36	0.16
F13 band-pass	20-40 day	.0057	.0080	0.41	0.23	-0.53	-0.40	-0.61	0.29
F14 band-pass	30-60 day	.0038	.0053	0.68	0.88	0.37	0.25	0.82	-0.12
F15 low-pass	30 day-∞		.0053	0.41	-0.09	0.64	0.32	0.97	-0.81
F16 low-pass	60 day-∞		.0027	0.48	0.52	0.98	-0.45	0.98	-0.99

* Filters F1-F7 operate on 10 min data samples; filters F8-16 operate on daily averages

** band edges are attenuated 12 db from cutoff

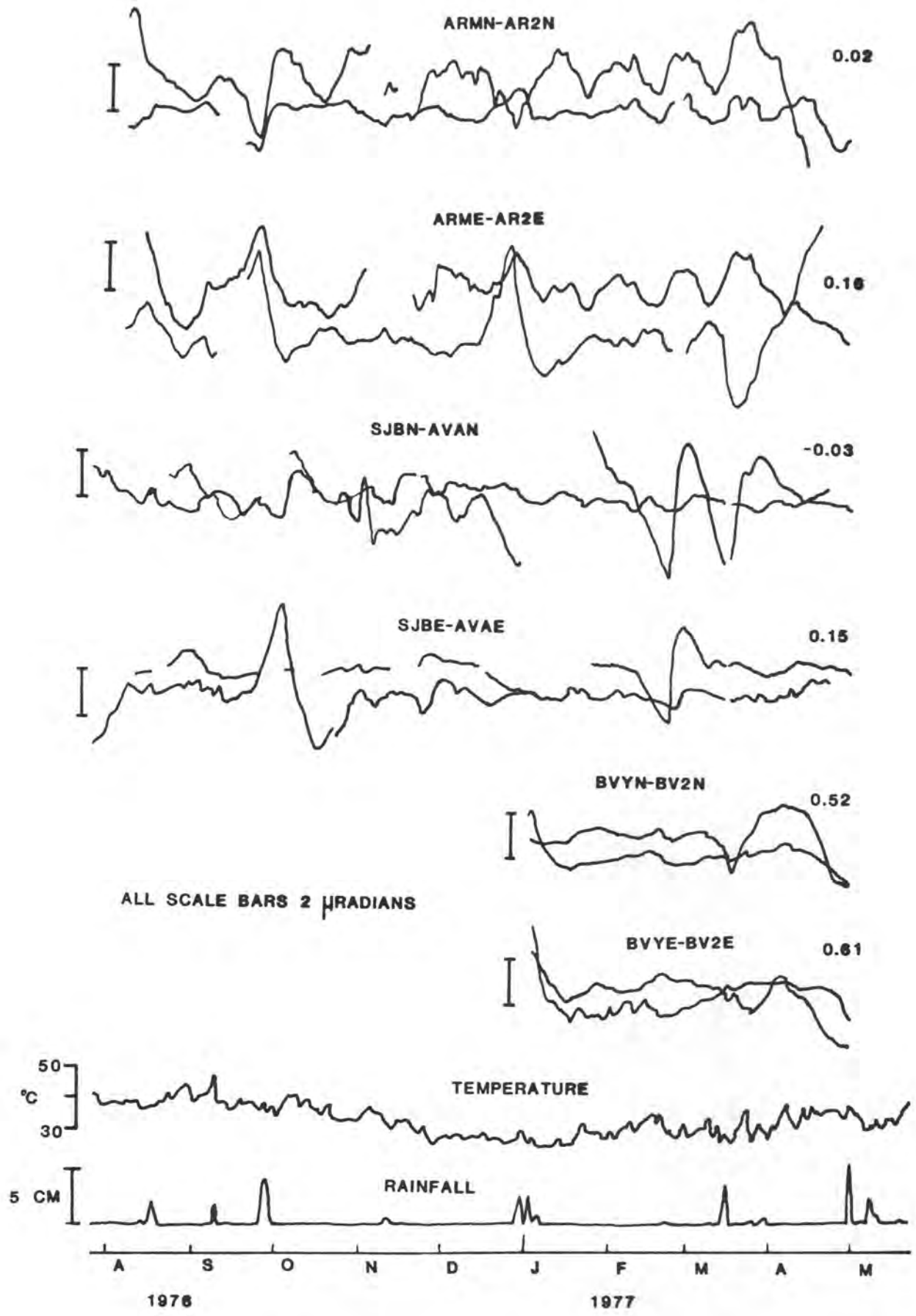
ARMN-AR2N
0.02
ARME-AR2E
0.16
SJBN-AVAN
-0.03
SJBE-AVAE
0.15
BVYN-BV2N
0.52
ALL SCALE BARS 2 μRADIANS
BVYE-BV2E
0.61
50
°C
30
TEMPERATURE
5 CM
RAINFALL
A
S
O
N
D
J
F
M
A
M
1976
1977

STM
CCK
CFT
ABM
JFP
TKT
CHM
FRM
GARLOCK FAULT
BIG PINE FAULT
WOR
PALMDALE
SAN GABRIEL FAULT
SAN ANDREAS FAULT
WIL
BUC
TRC
FALL
BFT
GLR
LRM
LRS
GLH
SNS
KWK
AZU
LAV
LOS ANGELES
SAN JACINTO FAULT
WEI
SAN BERNARDINO
PFT
PTN
RAN
LSB
MLC
WHT
FSC
FS2
WHITTIER – ELSINORE FAULT
TRP
HAM
TAB
FIG
CLK
TRH
OSO
BBD
0 10 20
KM
35°00'
34°00'
33°00'
120°00'
119°00'
118°00'
117°00'
116°00'

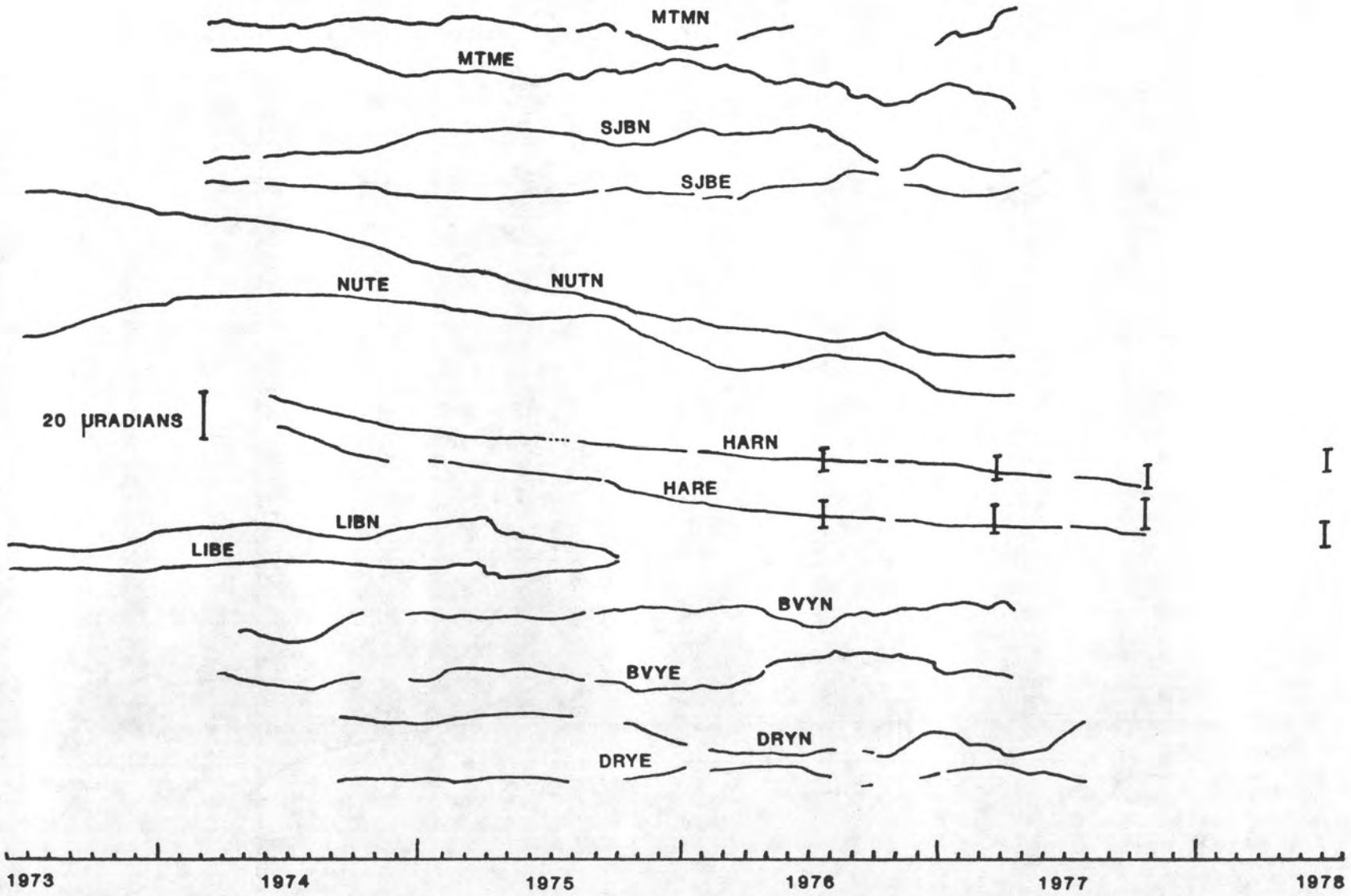
MTMN
MTME
SJBN
SJBE
NUTE
NUTN
20 μRADIANS
HARN
HARE
LIBN
LIBE
BVYN
BVYE
DRYN
DRYE
1973
1974
1975
1976
1977
1978

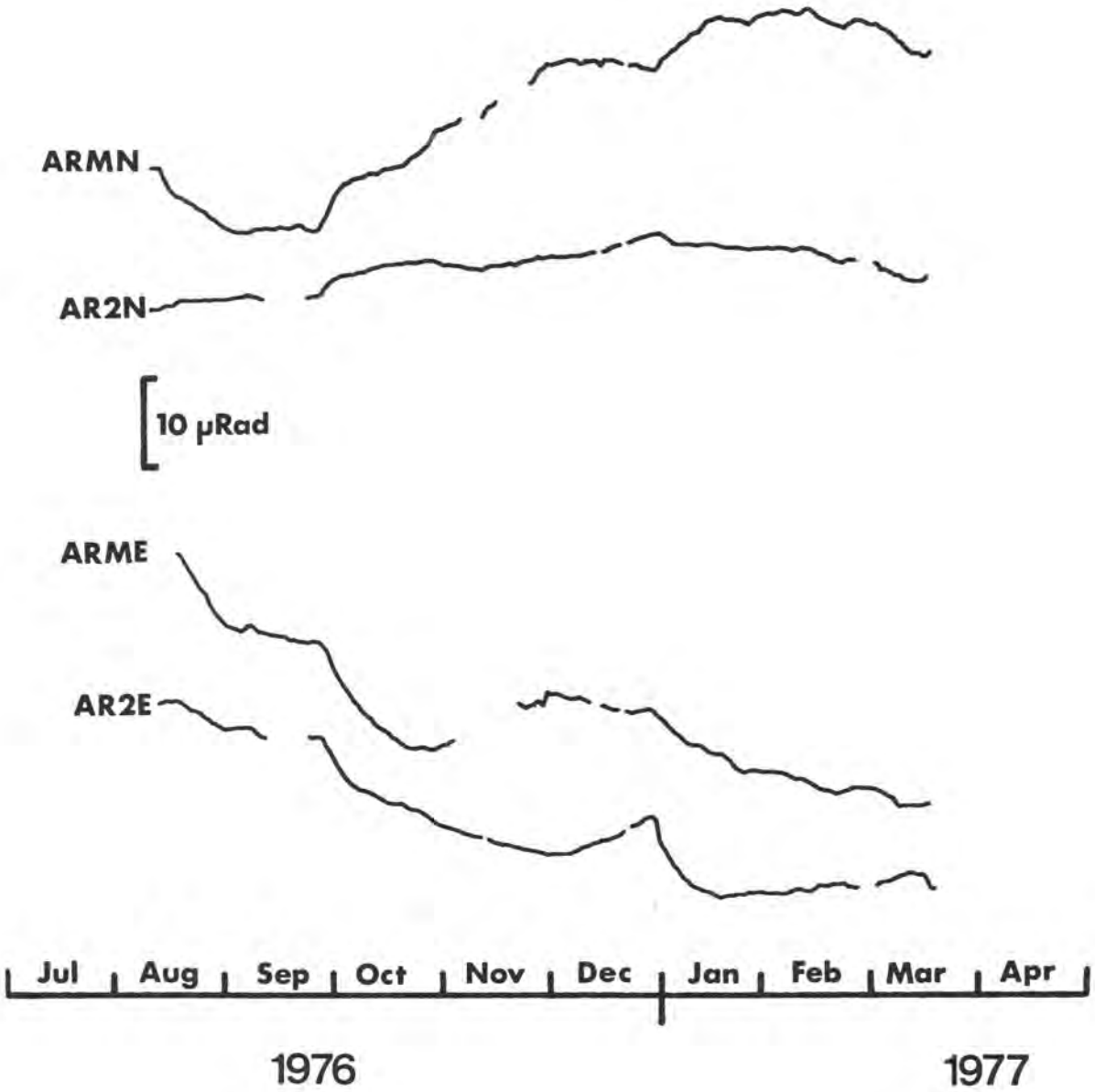
ARMN
AR2N
10 μRad
ARME
AR2E
Jul
Aug
Sep
Oct
Nov
Dec
Jan
Feb
Mar
Apr
1976
1977

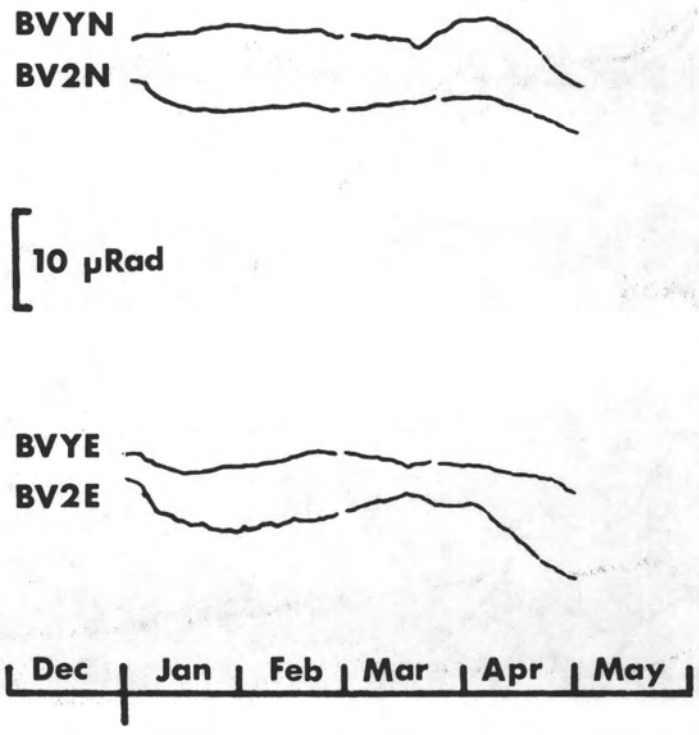
BVYN
BV2N
10 μRad
BVYE
BV2E
Dec
Jan
Feb
Mar
Apr
May
1977

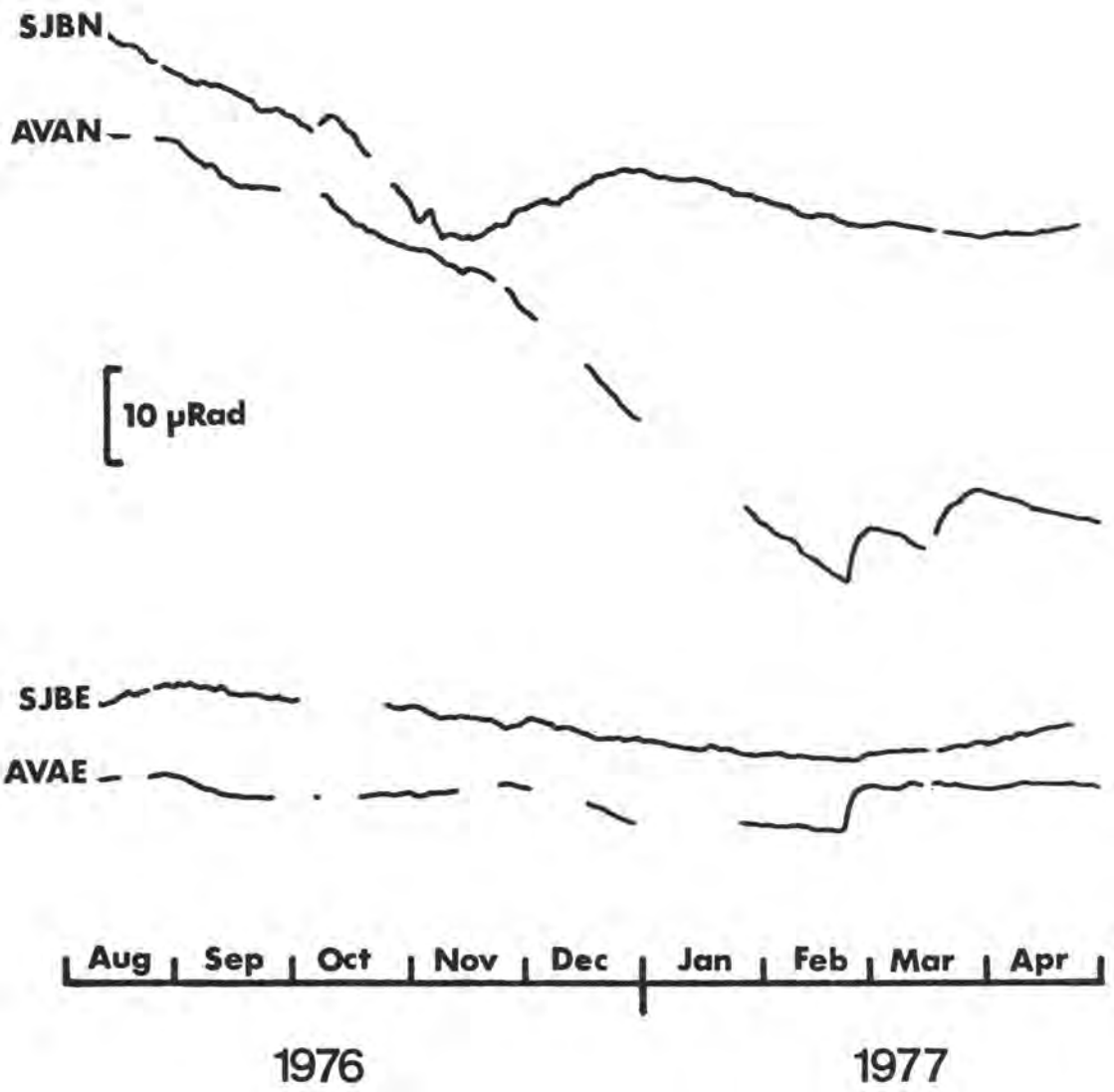
SJBN
AVAN
10 μRad
SJBE
AVAE
Aug
Sep
Oct
Nov
Dec
Jan
Feb
Mar
Apr
1976
1977

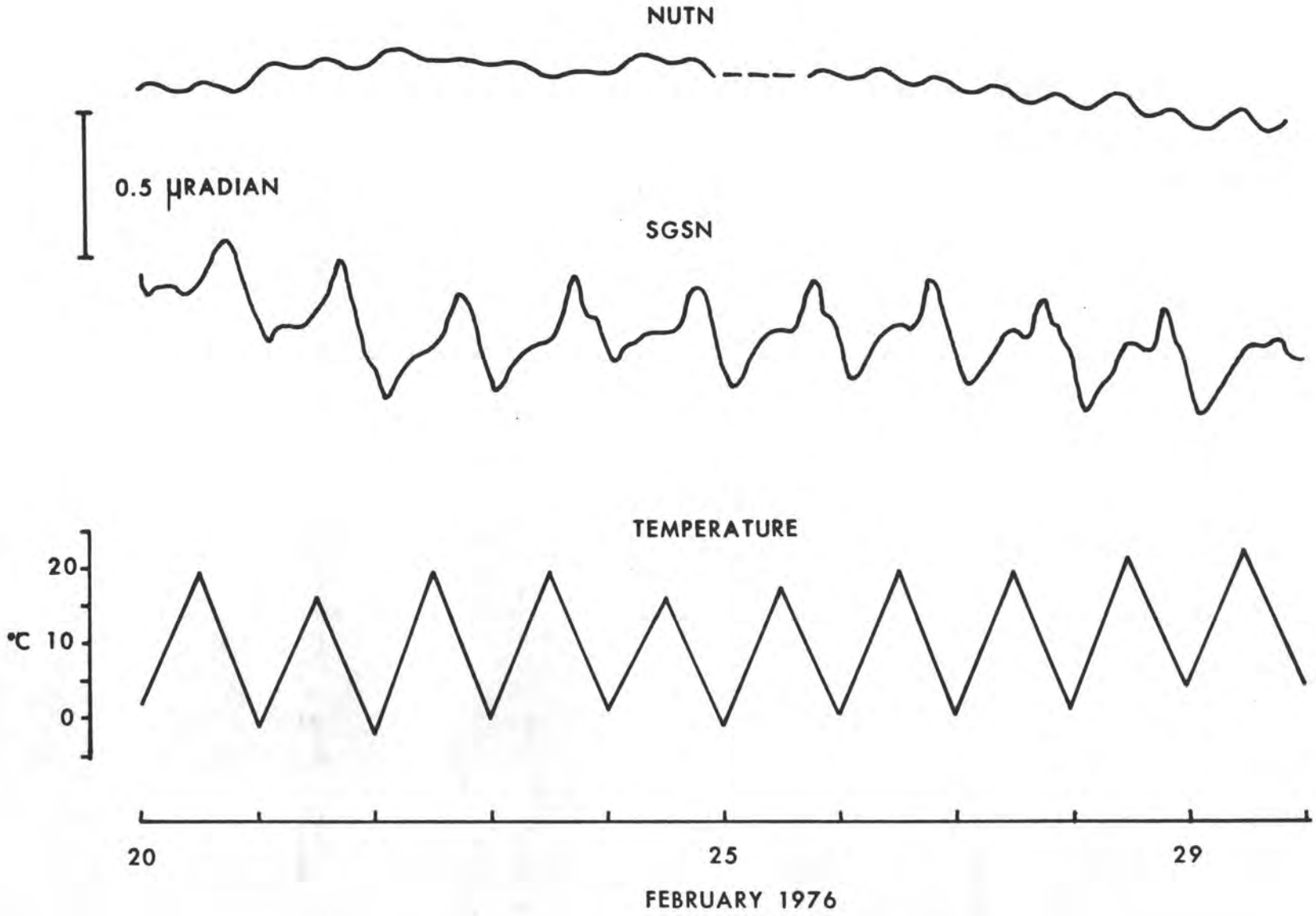
NUTN
0.5 μRADIAN
SGSN
TEMPERATURE
°C
20
10
0
20
25
29
FEBRUARY 1976

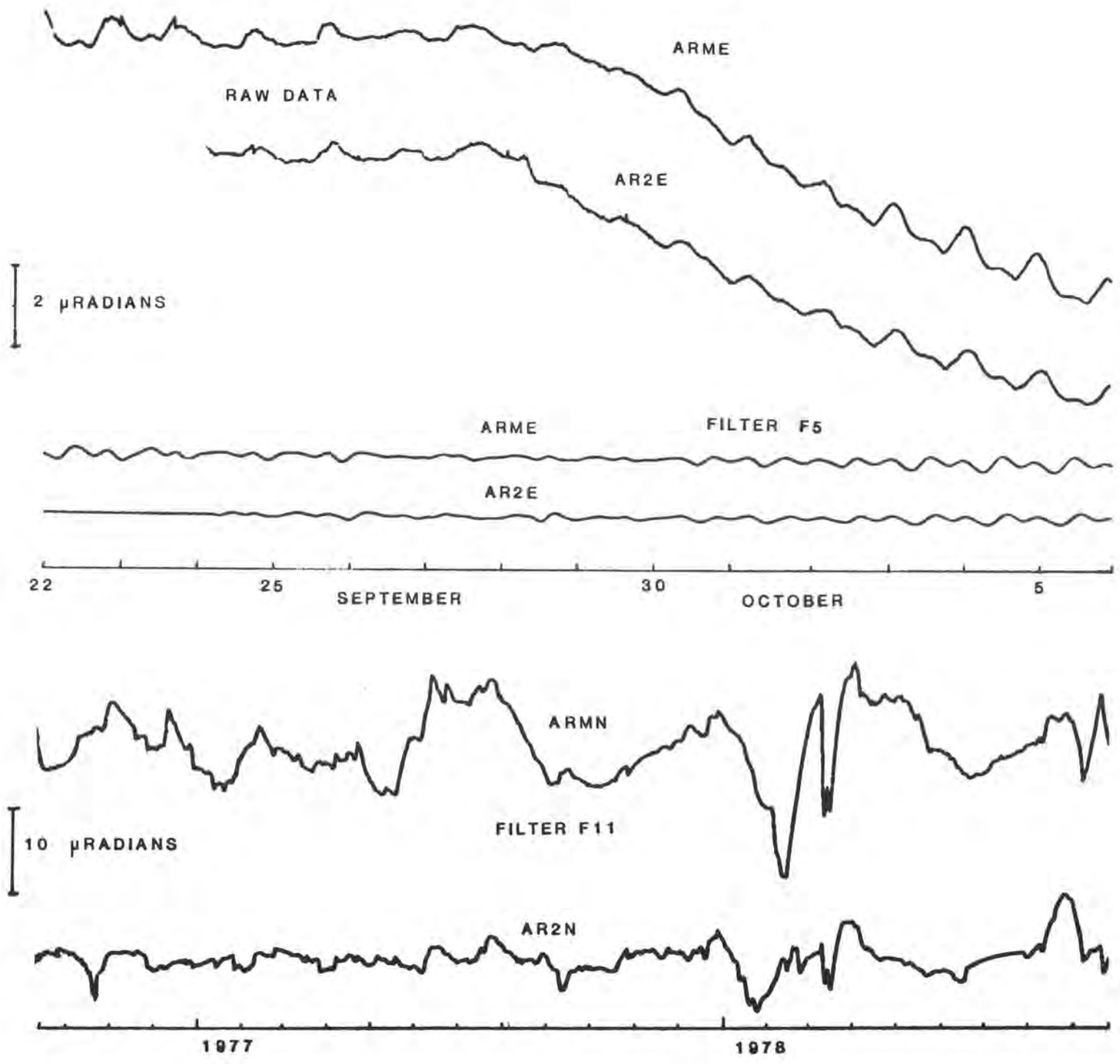
ARME
RAW DATA
AR2E
2 μRADIANS
ARME
FILTER F5
AR2E
22
25
SEPTEMBER
30
OCTOBER
5
ARMN
FILTER F11
10 μRADIANS
AR2N
1977
1978

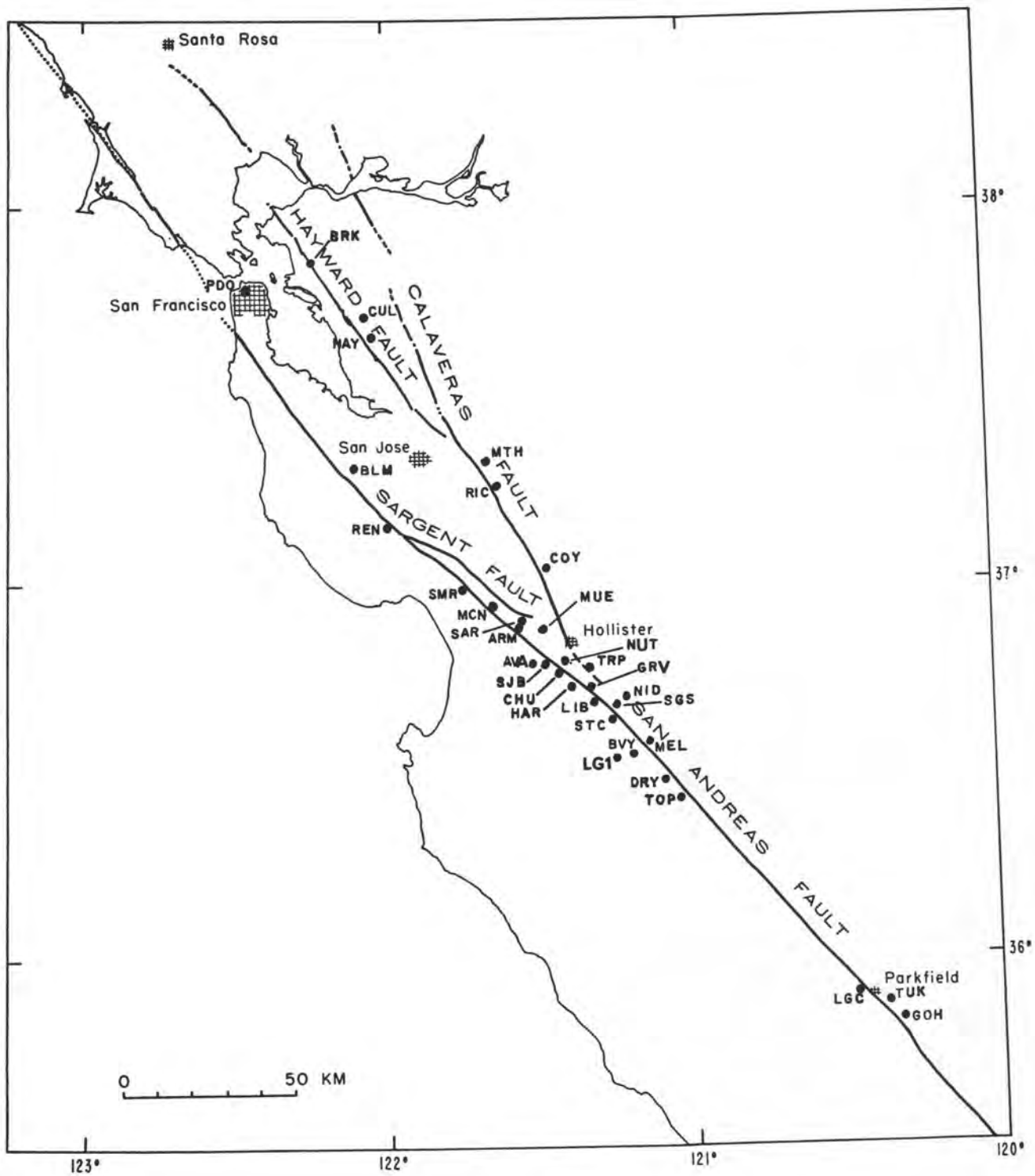
Santa Rosa
San Francisco
San Jose
Hollister
Parkfield
HAYWARD FAULT
CALAVERAS FAULT
SARGENT FAULT
SAN ANDREAS FAULT
BRK
PDO
CUL
HAY
MTH
RIC
BLM
REN
COY
MUE
SMR
MCN
SAR
ARM
NUT
TRP
GRV
AVA
SJB
CHU
HAR
LIB
NID
SGS
STC
MEL
BVY
LG1
DRY
TOP
LGC
TUK
GOH
0
50 KM
38°
37°
36°
123°
122°
121°
120°

THE TERRA TEK STRESS MONITORING SYSTEM: THEORY, CALIBRATION AND DATA FROM THE PALMDALE AREA, CALIFORNIA AND SALT LAKE CITY, UTAH

by:

H. R. Pratt
E. H. Hardin

Terra Tek, Inc.
Salt Lake City, Utah
December, 1978
TR78-75

ABSTRACT

The theory behind and calibration of a flatjack stress monitoring system developed at Terra Tek, Inc. is presented. The system is considered to be able to measure temporal change in stress in three flatjacks oriented at 120^{o} to each other, thus, enabling the horizontal stress field to be resolved.

Temporal stress data is presented from the Little Rock site near Palmdale, California and from the Little Cottonwood Canyon site, near Salt Lake City, Utah. Earthtides are easily recognizable as background data indicating the sensitivity of the system. The development of a borehole stressmeter using the same flatjack configuration is discussed and calibration data is presented. More development is required for the borehole stress monitoring system.

INTRODUCTION

One of the principal factors affecting seismicity and geodetic change in the earth's crust is the magnitude and direction of the stress field and its temporal variation. Two instrument types are presently employed to evaluate lithostatic (overburden) and tectonic (residual and applied-current) stresses in the earth's upper crust; those which measure absolute values of stress and those which measure relative changes in stress. The stress monitor is a flat-jack system developed to directly measure changes in stress.

Several techniques are currently used to measure changes in *in situ* stress; most involve surface gaging or a borehole drilled to the depth where stress is to be measured. Nearly all the instruments in use are actually strainmeters, since they measure strain or deformation and infer stress through the application of Hooke's Law. These methods have intrinsic uncertainties, since strain is not a linear function of stress in most cases, and since the stress-strain relation for loading may not concur with that for unloading (Walsh, 1978). These uncertainties require an approximation for the elastic modulus of the rock, since a linear rather than non-linear form is generally used to calculate stress. A rock sample removed from the formation of its origin may not yield a representative value for the elastic modulus, due to desication or microfracturing due to removal, handling or machining. Making reliable stress measurements by conventional means is then difficult in all but hard, competent rock. Stress relief methods require overcoring, which generally limits their effective depth; additionally, these methods have not been used to measure temporal variations in stress, with high data density and sensitivity. Terra Tek has developed a stress monitoring system to directly measure temporal change in stress.

THE STRESS MONITORING SYSTEM

The stress monitor developed by Terra Tek is apparently removed from many of the problems associated with other stress measurement techniques. During the past few years the development of this technique has steadily progressed. Most of the developmental work has centered on the refinement of theory of operation of the stress monitoring system and the design of an instrument with the required sensitivity and long-term stability.

Figure 1 shows the basic components of the stress monitor; a water-filled flatjack, pressure and temperature compensating reservoir and sensitive differential pressure transducer between them. To install the system, surfacial material is cleared away at the site and slots cut in the formation by drilling overlapping holes with a jackhammer. The flat-jack is grouted into the slot; three slots are radially oriented at 120^{o} angles about three meters from a common center. A vandal-proof instrument bunker is emplaced at the center of the array. Figure 2 shows such a bunker with all equipment installed.

The following illustrates an example of temporal stress change and correlates this change with strain change and seismicity. Figure 3 shows the actual recording of a precursory change in stress before a micro-earthquake that occurred on May 28, 1974, in a fractured quartz-monzonite stock near Salt Lake City (Swolfs and Barker, 1976). The magnitude of the stress precursor is about 10 millibars followed almost immediately by a stress drop of about 15 millibars. The time duration of the stress anomaly is about five hours. The recording shows that, in this particular case, a diagnostic variation in stress does take place in the vicinity of the rupture. There should be little doubt that measurements of stress, a

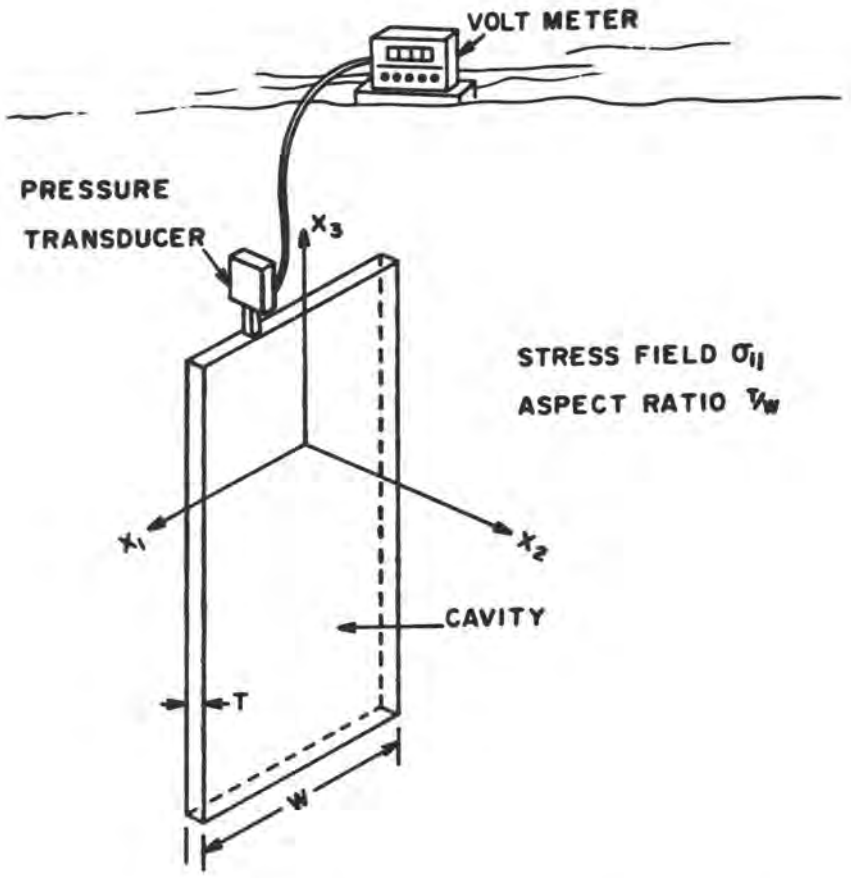

Figure 1. Schematic of the stress monitoring system illustrating the relationship of the stress to the flatjack orientation.

first-order parameter, will greatly aid the solution of problems associated with earthquake mechanisms and fracture processes. The data was also correlated with changes in the strain field and with increased local seismicity (Figure 3). The sensitivity of the stress monitoring is illustrated by typical diurnal and semidiurnal stress changes associated with earth tides, which have a strain magnitude of about 3×10^{-8} (Figure 4).

Figure 2. Photograph of instrument bunker at Little Rock Reservoir stress monitor site.

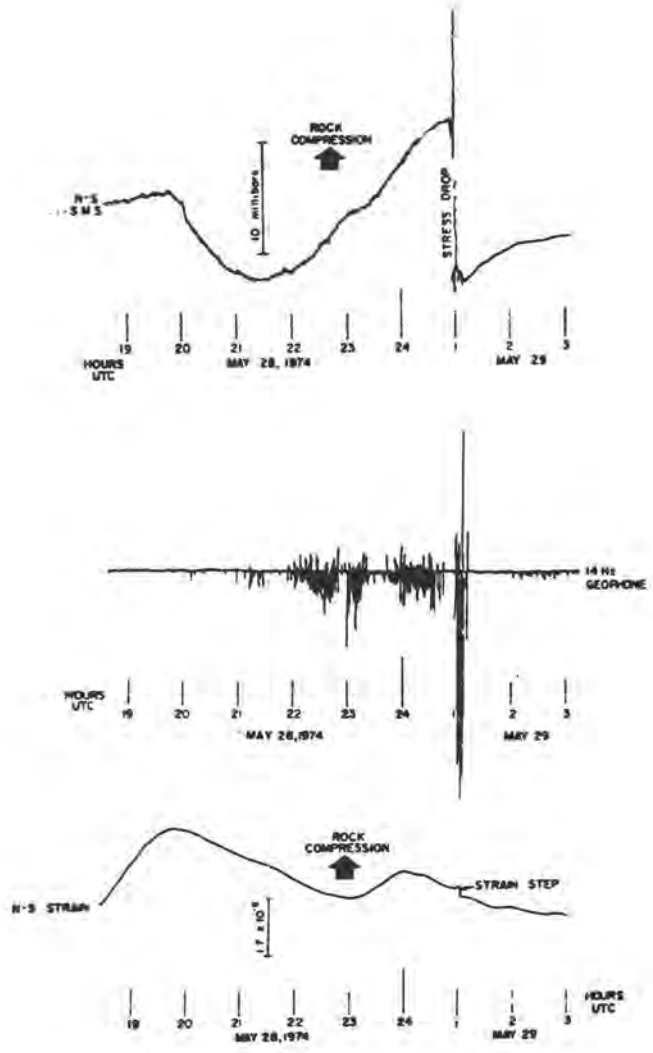

Figure 3. Stress, seismicity and strain as a function of time for a small event recorded by the Terra Tek stress monitoring system, a 14 H_Z geophone, and the University of Utah quartz rod stressmeter located near the event; May 28, 1974.

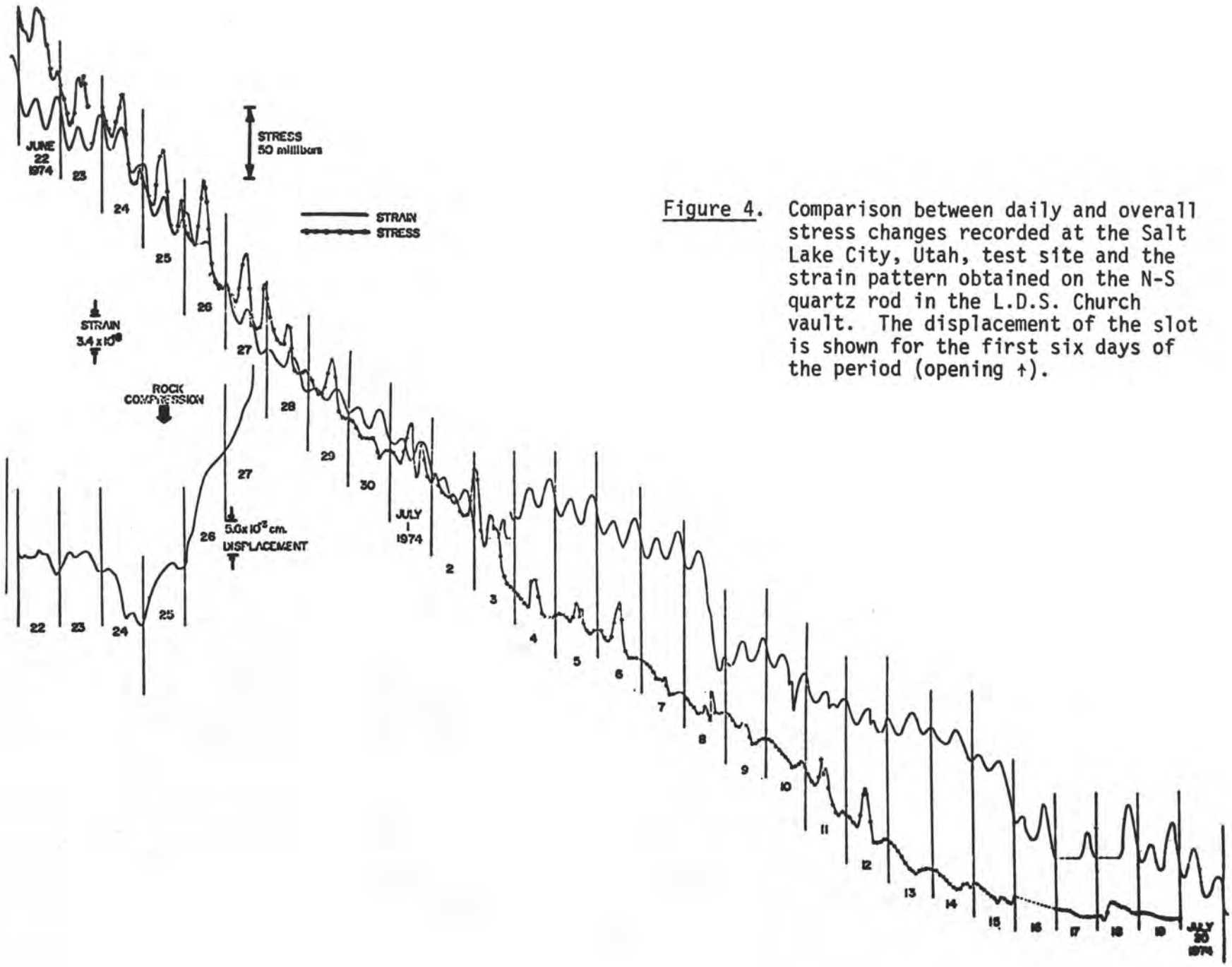

Figure 4. Comparison between daily and overall stress changes recorded at the Salt Lake City, Utah, test site and the strain pattern obtained on the N-S quartz rod in the L.D.S. Church vault. The displacement of the slot is shown for the first six days of the period (opening ↑).

THEORY

Stress Monitor System

Changes in the ambient stress deform the flatjack, causing pressure changes which are detected by the gage. A unique aspect of the stress monitor is that the flatjack can be designed to respond only to the compressive component of the stress field normal to the plane of the flatjack. The system is thus able to independently monitor the components of a delta stress rosette directly and without further measurements or calculations.

It is useful to consider a flatjack as an isotropic, liquid filled, "penny shaped" inclusion wholly contained in the rockmass. This model involves some assumptions: rock near the surface is usually anisotropic due to relaxation of residual strain and preferred orientation of joints or microfractures, and flatjack stiffness is usually not uniform in all directions. The field data and theoretical analysis suggest that these assumptions have no detrimental effect.

Because of the relative incompressibility of the contained liquid (water) compared to the compressibility of the empty cavity normal to its plane, any change in ambient stress will be compensated by a nearly equal change in pressure of the confined liquid (Walsh, 1972--Barker, 1975). The stress monitor system is, therefore, a highly compliant cavity in which incompressible liquid is confined. Because of the high slenderness ratio (diameter to thickness) of the cavity, a stress change parallel to its edge will cause a negligible deflection of the cavity walls and thus a negligible pressure change.

If we assume a constant temperature, the volume of the cavity, V_c, is a function of the internal pressure and the three components of stress:

$$V_c = V_c\,(P_c, \sigma_x, \sigma_y, \sigma_z) \tag{1}$$

and

$$dV_c = \frac{\partial V_c}{\partial P_c}\,dP_c + \frac{\partial V_c}{\partial \sigma_x}\,d\sigma_x + \frac{\partial V_c}{\partial \sigma_y}\,d\sigma_y + \frac{\partial V_c}{\partial \sigma_z}\,d\sigma_z \tag{2}$$

Assuming isotropicity of the matrix (earth) and a slenderness ratio much greater than unity, it can be shown to a good approximation:

$$\frac{\partial V_c}{\partial \sigma_x} = \frac{\partial V_c}{\partial \sigma_y} = -\frac{\partial V_c}{\partial K_r} \tag{3}$$

where K_r is the bulk modulus of the rock mass in which the cavity is made, σ_z is perpendicular to the plane of the cavity, and compressive stress is positive.

Let V_w be the volume of the cavity; since temperature is constant, V_w is a function only of pressure:

$$V_w = V_w\,(P_w) \tag{4}$$

and

$$dV_w = \frac{V_w}{P_w}\,dP_w = -\frac{V_w}{K_w}\,dP_w \tag{5}$$

where K_w is the bulk modulus of the fluid.

Since the fluid is pressurized in the cavity, $dV_c = dV_w$, also, $dP_c = dP_w$. Thus by substitution of (5) into (2), thus eliminating dV_c and omission of the subscript on dP:

$$dP\,\frac{1}{K_w} + \frac{1}{K_{cp}} = \frac{1}{K_{cz}}\,d\sigma_z + \frac{1}{3K_r}\,(d_x + d_y) \tag{6}$$

where

$$\frac{1}{K_{cp}} = \frac{1}{V_c}\,\frac{\partial V_c}{\partial P_c} \qquad \text{and} \qquad \frac{1}{K_{cz}} = -\frac{1}{V_c}\,\frac{\partial V_c}{\partial \sigma_z} \tag{7}$$

The compliance of the cavity to charge in internal pressure, $^1/K_{cp}$, is large due to the large slenderness ratio. The slenderness ratio is 60 for the flatjacks presently in the Palmdale area; the stiffness K_{cp} of these systems was determined *in situ* by injecting incremental volumes of working fluid into the cavity and measuring the pressure. It was found that K_{cp} is of the order of 10^{-2} kbar, whereas, K_w for the working fluid (water) is 28 kbar. We thereby neglect the $\frac{1}{K_w}$ term in (6). Simplified, the small pressure change in the cavity is related to change in the ambient stress by:

$$dP = \frac{K_{cp}}{K_{cz}} d\sigma_z + \frac{K_{cp}}{3K_r} (d\sigma_x + d\sigma_y) \tag{8}$$

Because of the large slenderness ratio, the ratio K_{cp}/K_{cz} is nearly 1:1. However, if K_r (matrix bulk modulus) = 300 kbar, then the ratio $K_{cp}/3K_r$ is of the order of 10^{-5} kbar. Thus, the system response to $(d\sigma_x + d\sigma_y)$ in the plane of the cavity is negligible.

A small mechanical inefficiency due to flatjack effects and the finite compressibility of water reduces the system response to $d\sigma_z$ to slightly less than unity.

The effects of temperature variation on pressure measurements from the stress monitor can be attributed to three sources:

(1) Temperature-induced drift of the differential pressure transducers.

(2) Thermoelastic stresses produced by non-uniform heating or cooling near the earth's surface.

(3) Pressure excursions produced by temperature related volumetric changes in components of the stress monitor system.

The transducers are internally compensated, so their drift is assumed negligible. Thermoelastic stresses are a real part of the stress record; there is no instrumental means of eliminating them from the data. However, temperature at depth is recorded at each site so that thermal system response may be evaluated and thermal trends may be removed from the data, if necessary.

Design of the Temperature Compensator

The flatjack and compensator are fluid reservoirs whose volumes are sensitive to ambient temperature and pressure. In order to relate changes in reservoir volume to pressure and temperature, we must consider the reservoir as two elements: container and fluid. Barker (1975) has shown that the reservoir response can be described as:

$$dV_c = \frac{\partial V_c}{\partial P_c} dP_c + \frac{\partial V_c}{\partial T_c} dT_c \qquad (9)$$

and

$$dV_w = \frac{\partial V_w}{\partial P_w} dP_w + \frac{\partial V_w}{\partial T_w} dT_w \qquad (10)$$

where V, P and T are volume, pressure and temperature, and the subscripts c and w denote container and fluid (water).

If all volume changes happen slowly and fluid volume equals container volume, then changes in the fluid volume equal changes in the container volume. Equating (9) and (10) thus gives:

$$\frac{\partial V_c}{\partial P_c} dP_c + \frac{\partial V_c}{\partial T_c} dT_c = \frac{\partial V_w}{\partial P_w} dP_w + \frac{\partial V_w}{\partial T_w} dT_w ,$$

or

$$\frac{dP}{dT} = \frac{\frac{\partial V_w}{\partial T_w} - \frac{\partial V_c}{\partial T_c}}{\frac{\partial V_c}{\partial P_c} - \frac{\partial V_w}{\partial P_w}}$$

The volume thermal expansion of the container will be much smaller than the expansion of the fluid, or

$$\frac{\partial V_w}{\partial T_w} >> \frac{\partial V_c}{\partial T_c} ,$$

so

$$\frac{dP}{dT} \cong \frac{\partial V_w}{\partial T_w} \Bigg/ \left(\frac{\partial V_c}{\partial P_c} - \frac{\partial V_w}{\partial P_w} \right) \tag{11}$$

Because the stress monitor measures a differential pressure between two reservoirs, the observed difference which can be attributed to thermal response should be:

$$\frac{dP}{dT} = \left(\frac{dP}{dT} \right)_{f_j} - \left(\frac{dP}{dT} \right)_{c_p} \tag{12}$$

where the subscripts f_j and c_p refer to flatjack and compensator, respectively. Substituting (11) into (12) twice gives the governing relation for thermal drift in the stress monitor:

$$\frac{dP}{dT} \cong \left[\frac{\partial V_w}{\partial T} \Bigg/ \left(\frac{\partial V_c}{\partial P} - \frac{\partial V_w}{\partial P} \right) \right]_{f_j} - \left[\frac{\partial V_w}{\partial T} \Bigg/ \left(\frac{\partial V_c}{\partial P} - \frac{\partial V_w}{\partial P} \right) \right]_{c_p} \tag{13}$$

Equation (13) indicates that temperature drift can be minimized by the design of a compensator with both volume and stiffness equal to the flatjack, or some other combination of these two parameters.

FIELD PROGRAM

Two complete delta rosette stress monitor systems were installed near Palmdale, California, in close proximity to the San Andreas Fault Zone and the Palmdale Uplift. One side is located 2 km from Elizabeth Lake, about 27 km West of Palmdale; the other about 500 m from Little Rock dam, 11 km East of Palmdale. The upper edge of each flatjack is buried at a depth of 1.5 m in the "granite" indigenous to the Northeastern flank of the San Gabriel Mountains. The sites were selected for competent rock near the surface, proximity to the San Andreas fault zone and Palmdale Uplift, and logistic feasibility.

The cells were pressurized to working pressure and allowed to equilibrate, then the volume of each cell and each compensator was measured. Because effectiveness of the stress monitor system demands the cells to be highly compliant relative to the host rock, field tests were done to determine this pressure-volume $(\frac{dV}{VdP})$ relation for each cell. This measurement was done by injecting small incremental volumes of working fluid into each pressurized cell and recording the attendant change in pressure. The cell compliance at Little Rock is about 0.005 bar^{-1}, and at Elizabeth Lake about 0.03 bar^{-1}, for an initial pressure of 3.2 bars.

The compliance of the host rock is estimated to be about 3×10^{-6} bar^{-1}. Thus, a highly compliant, pressure-competent inclusion is introduced in a non-compliant matrix and filled with water, whose compliance is about one order of magnitude greater than that estimated for the matrix. The compliance of the matrix and working fluid are assumed negligible; it is this which allows the flatjack concept for a stress monitor. Conversely, the stiffness of the inclusion is low, but not negligible, allowing the stress monitor to function at an acceptably high mechanical efficiency.

A softening bellows was affixed to each compensating cylinder, in an effort to approximate the compliance of the flatjacks and achieve temperature compensation. The compliance of each bellows and flatjack assembly was then determined in the manner described above. Site specific thermal drift coefficients were determined from these data. These factors represent the theoretical change in pressure due to an incremental step in rock temperature. Analysis of field data from the Little Cottonwood Canyon stress monitor in Utah indicates that unwanted pressure excursions can be minimized by selecting the proper compensator volume for each flatjack. For example, the thermal drift coefficients for one jack at the site initially fell in the range of 0.03 to 0.16 bar/^{o}C for working pressure between 0 and 3 bars. These coefficients were decreased to 0.0004 and 0.06 bar/^{o}C for the same working pressure range by reducing the compensator volume by half.

The temperature coefficients for the Little Rock and Elizabeth Lake sites can be decreased further by reducing the compensator volumes to increase their compliance. These modifications will be made as it becomes practical to make design changes to the apparatus. The calculated temperature coefficients for the Little Rock and Elizabeth Lake sites in their present configurations are presented with the compliance data in Table I .

TABLE I

PRESSURE AND TEMPERATURE COEFFICIENTS FOR LITTLE ROCK AND ELIZABETH LAKE SYSTEMS

(Based on observations made at 2 bar working system pressure)

ELEMENT	SENSING DIRECTION	VOLUME (ml)	$\frac{\partial V_l}{\partial T}$ (ml/°C)	$\frac{\partial V_l}{\partial P}$ (ml/bar)	$\frac{\partial V_c}{\partial T}$ * (ml/°C)	$\frac{\partial V_c}{\partial P}$ (ml/bar)	$\frac{dP}{dT}$ (bar/°C)
LITTLE ROCK RESERVOIR STRESS MONITOR							
Jack #1	N-S	1595	0.137	-0.077	0.016	19.88	-.068
Comp. #1		1626	0.140	-0.078	0.0081	1.781	
Jack #2	N60 E	1584	0.137	-0.076	0.016	6.783	-.062
Comp. #2		1626	0.140	-0.078	0.0081	1.628	
Jack #3	N60 W	1962	0.169	-0.094	0.020	7.627	-.047
Comp. #3		1627	0.140	-0.078	0.0081	1.958	
ELIZABETH LAKE STRESS MONITOR							
Jack #1	N60 E	2901	0.250	-0.139	0.029	53.78	-.061
Comp. #1		1627	0.140	-0.078	0.0081	2.048	
Jack #2	N60 W	2818	0.243	-0.135	0.028	32.43	-.078
Comp. #2		1626	0.140	-0.078	0.0081	1.568	
Jack #3	N-S	2233	0.193	-0.107	0.022	36.37	-.076
Comp. #3		1626	0.140	-0.078	0.0081	1.638	

* Assume a coefficient of volume thermal expansion of $10^{-5}/C^{o}$ for granite.

The California stress monitor systems were left pressurized at 2 bars for several months before final calibration to allow for long-term adjustment in the grout and rock adjacent to the jacks. Laboratory tests done at Terra Tek on this type of grout in similar application show this adjustment period to be sufficient. Several pressure cycles to zero system pressure and back to 2 bars were done to evaluate this stability. It was found upon repressurization, that stability was again achieved within one hour.

Data telemetry is provided for each site by a Terabit DA-76 microcomputer with an 8-channel, 12-bit A10 converter, and storage for over 8,000 data points. At each site, four of the eight ± 10.24 volt data inputs are not used. The software required for telemetry, data management and data reduction on Terra Tek's PDP 11/34 computer is complete. The Little Rock is on-line, and the Elizabeth Lake site requires only the installation of the telemeter.

BOREHOLE STRESSMETER

A miniaturized version of the stressmeter has been designed and built to fit a 7.5 centimeter diameter borehole (Figure 5a). The 15 cm tall device is self-compensating for pressure effects due to temperature and is capable of sensing stress changes in three horizontal directions 120^{o} apart. The active cells are coupled to the rock with grout and pressure in each cell is monitored by differential pressure transducers. The compensators are located directly above the three active cells, but remain decoupled from the rock.

The size, shape, volume and compliance of each active cell is nearly identical to its companion compensator to insure negligible temperature interference. The small size of the cells (4 cm x 6 cm), however, introduces a mechanical inefficiency to the device. In other words, the measured pressure change is smaller than the actual change in the ambient normal stress component perpendicular to the cell. Calibration tests are, therefore, necessary to determine the appropriate gage factor for the device. Preliminary laboratory tests indicate that the efficiency of the prototype device is about 25 percent or less.

Calibration of a non-compensated version borehole stressmeter for use at above ambient conditions was conducted in the Terra Tek laboratory using a granitic block (.66 x .66 x .46 m) in a large load frame. Stresses up to 4.14 MPa were attained. The block configuration and measured pressure/applied stress data are given in Figures 6 and 7 for loading in two directions 90^{o} apart. The results in Figure 6 show that jack 3, normal to the applied stress, measured 13% more pressure than the applied stress and that jacks 1 and 2 measured 78% more pressure than the

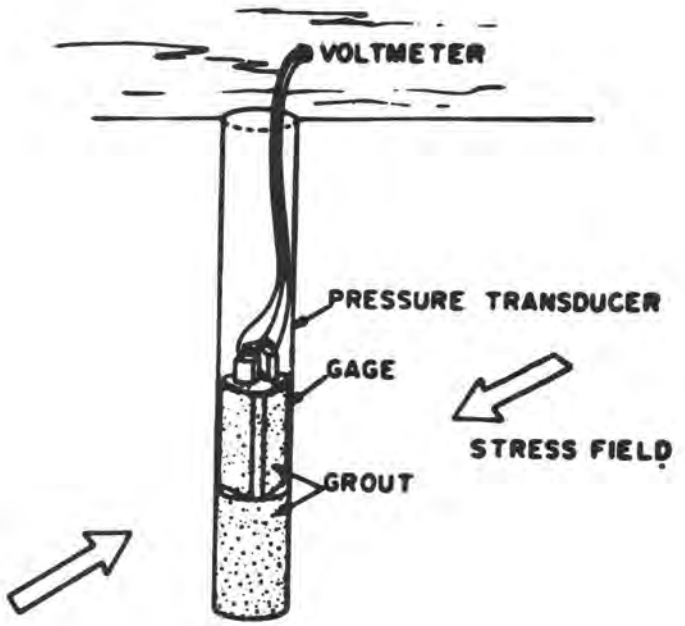

Figure 5a. A schematic of the borehole stressmeter.

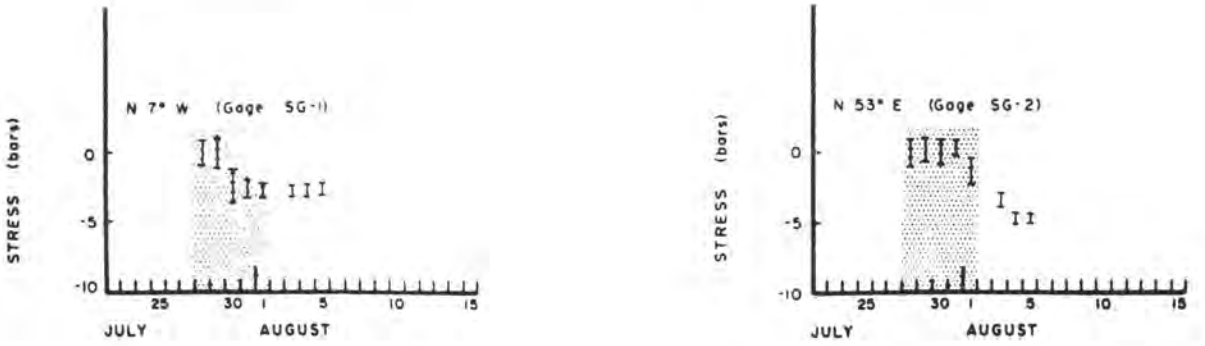

Figure 5b. Stress relief (compression monitored on two components of the stress gage during excavation of a sandstone block. Vertical bars indicate maximum daily variation--Swolfs and Brechtel, 1978).

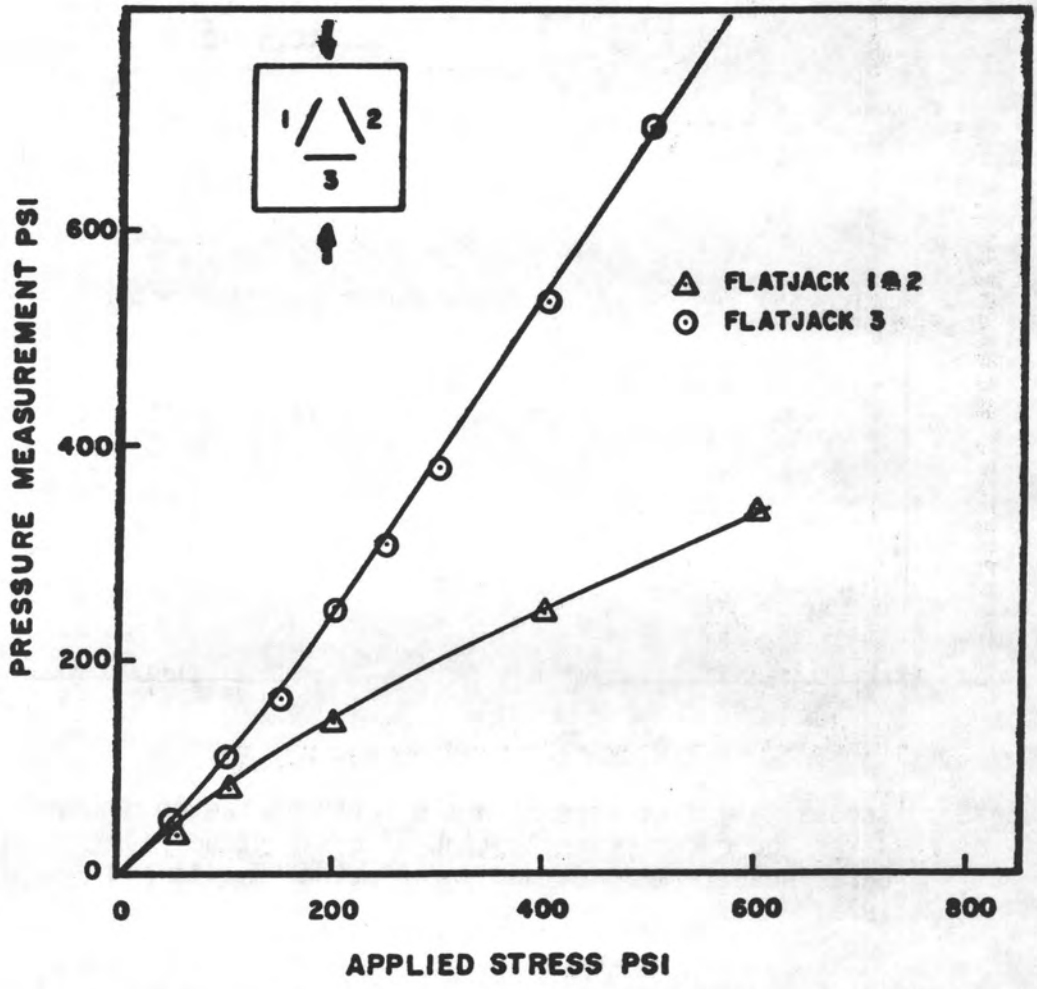

Figure 6. Pressure measured as a function of applied stress with jack 3 normal to the applied stress.

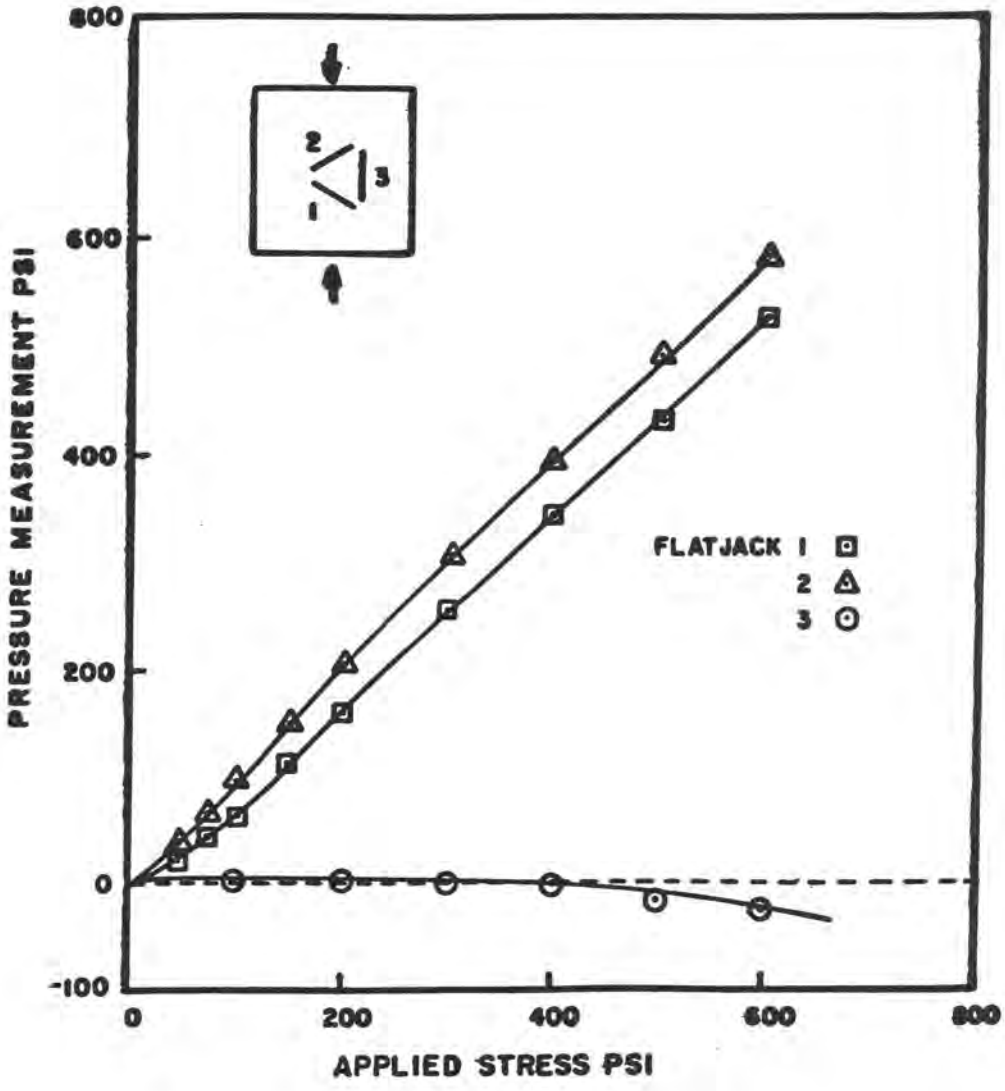

Figure 7. Pressure measured as a function of applied stress with jack 3 parallel to the applied stress.

calculated applied stress. Upon rotation of the block 90° and subsequent reloading (Figure 7), jack 1 measured zero stress as would be expected from theory, until a stress of 2.76 MPa was reached. Above this stress there is apparently a shear stress being generated, cross talk between the three jacks, or perhaps a reaction between the jack, grout and rock mass. Jacks 1 and 2 are measuring approximately the right stress values although they should be measuring equal stress levels. More evaluation of this data needs to be conducted. In addition, a sequence of finite element calculations have been conducted to estimate stresses that should be measured by the stress monitor during loading under a variety of boundary conditions (Yamada, 1979, in press).

We have also attempted to measure stress changes directly during excavation of a large block of sandstone using the borehole stressmeter, (Swolfs and Brechtel, 1978). The borehole stressmeter, when emplaced in a drill hole, gave the normal stress change along three different azimuths. Malfunction of one of the jack systems prevented a full stress determination during excavation. At 60 cm depth we observed a decompression of .55 MPa at N 7° W and of 1.08 MPa at N 53° E (Figure 5b). This data was compared to a U.S. Bureau of Mine gage, which registered strain changes in all three horizontal directions. The associated stress changes were calculated using 2.3 GPa for Young's modulus and 0.28 for Poisson's ratio; .55 MPa (N 7° W), 1.06 MPa (N 53° E), and 1.91 MPa (N 67° W). Thus, the stressmeter and USBM gage data gave comparable stress changes. It is interesting to note that previous stress measurements at various sites around the Rangely Anticline have yielded comparable results (de la Cruz and Raleigh, 1972). Using a variety of techniques, the surface stress

magnitudes averaged about 1.0 MPa. These data give some additional confidence that the borehole stress in functioning properly, at least to measure the magnitude to *in situ* stress.

DISCUSSION

The data analyzed from the stress monitors include six months of intermittent data from the Little Cottonwood Canyon, Utah site, and eleven days of data from the Little Rock Reservoir site near Palmdale, California. The data from Little Rock are presented in two sets--a short set representing about 48 hours, and a longer set representing about one week, during which time a malfunction occurred in the carrier demodulator for channel 3, which monitors the stress aligned N 60 W. The short set is presented as Figure 8 with the time-temperature series for this period as Figure 9. Note that the three channels have drifted apart by as much as 350 mbar in the interval between final calibration and this data set (about 45 days). The three flatjacks at this site were held at working pressure for several months before final calibration without appreciable drift. At the conclusion of final calibration, the pressure in the three flatjacks was allowed to equalibriate, then they were isolated from one another. It is probable that flatjack 3 was in compression relative to flatjacks 1 and 2 at this time. The delta rosette calculation for magnitude and orientation of the maximum compressive and shear stresses are presented as Figures 10 and 11 for the data of Figure 8. The shear stress is relatively constant whereas the compressive stress increases by nearly 50%. The orientation of these relative stresses is nominally N 65 W for compression and N 110 W for shear. It should be emphasized that these data reflect changes in the stress state of the near surface since the last time the three flatjacks were at equalibrium (October 26, 1978). The relative stress within a given time period can then be studied by constraining the three pressures to be equal at the beginning of the interval.

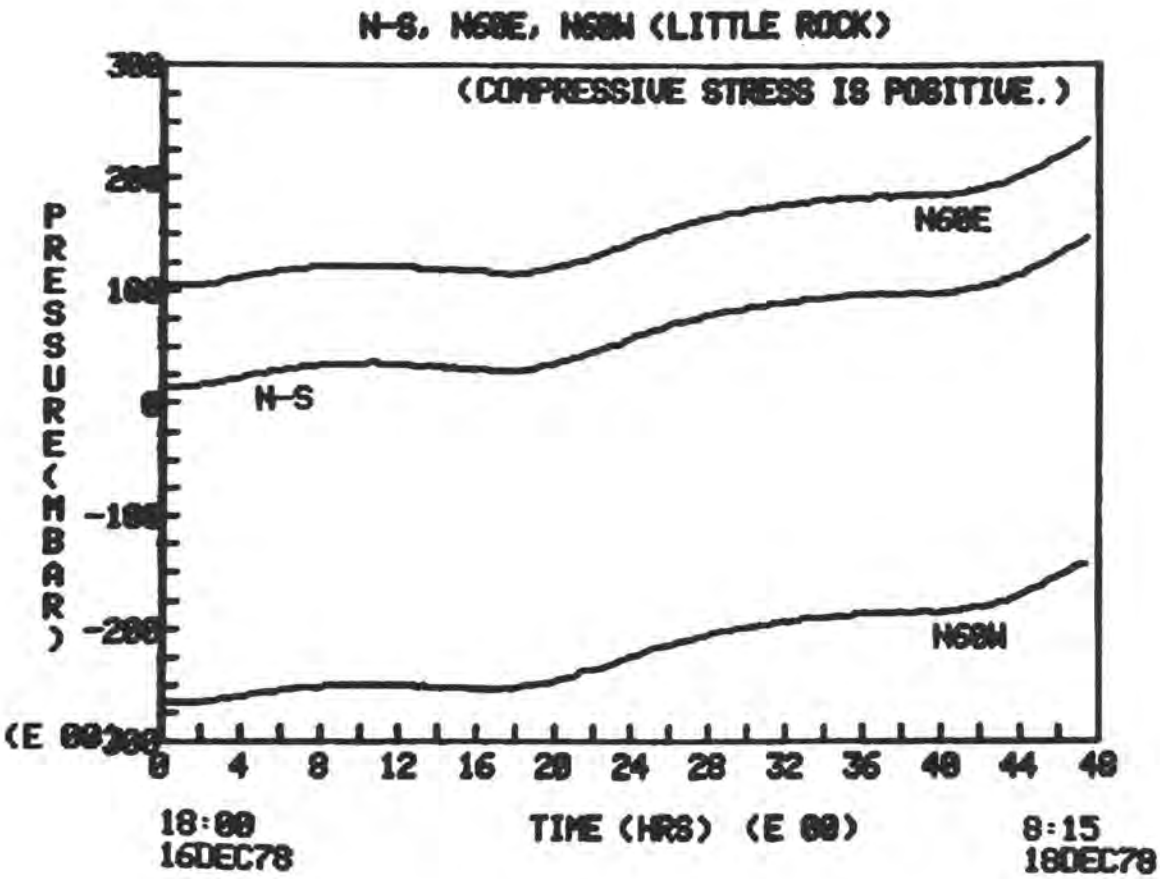

Figure 8. Telemetered data set from the Little Rock stress monitor taken prior to a malfunction in the electronics for the N60W channel. The compass bearings denote sensing direction.

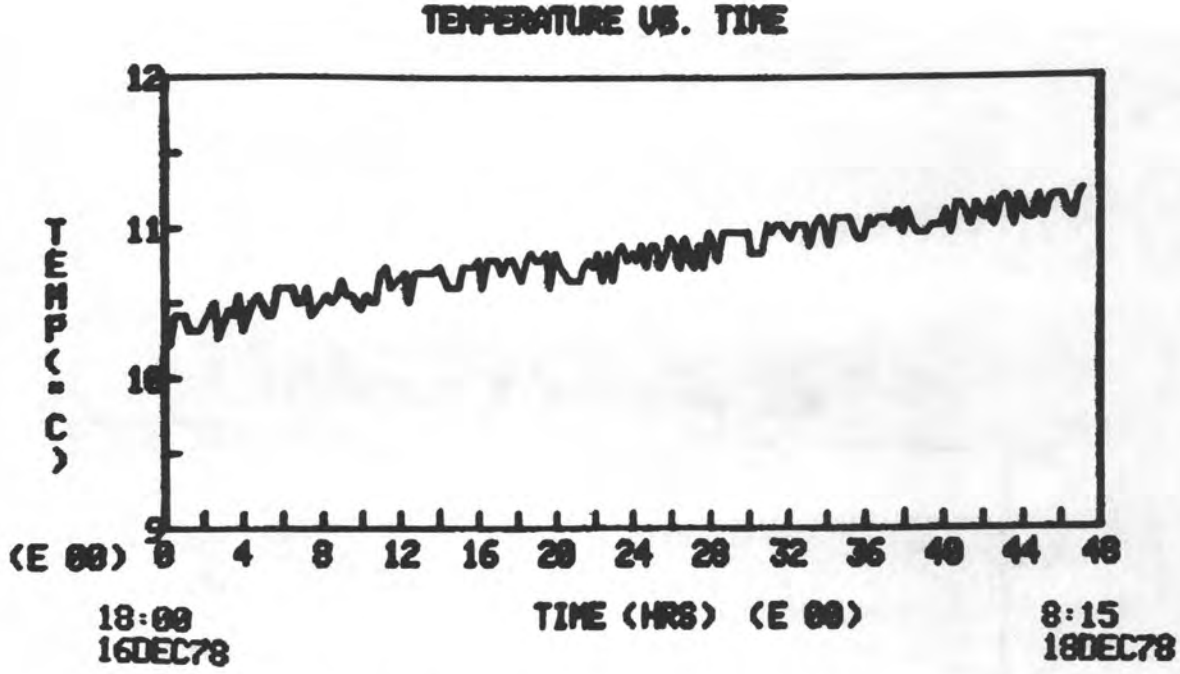

Figure 9. Temperature-time series recorded concurrently with the data of Figure 8. The sensing element is an RTD in a DC bridge, situated 1 meter below the surface in a small airspace adjacent to the compensators.

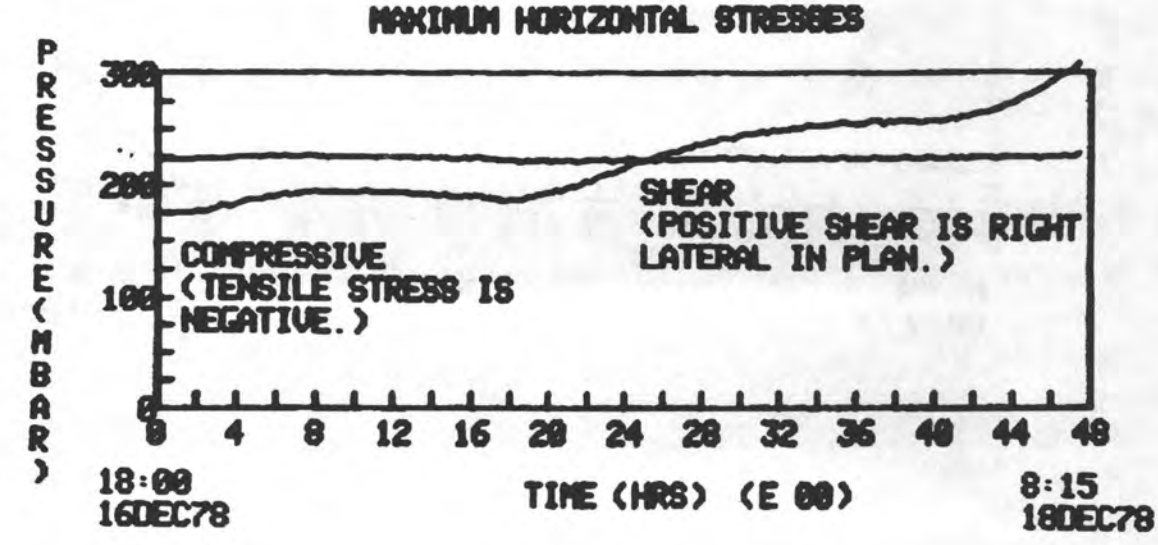

Figure 10. Results of the continuous delta stress rosette calculations for the stress data set of Figure 8. The maximum shear is relatively constant, though the maximum compression changes by more than 50%. These data reflect the change in the stress field since October 26, 1978.

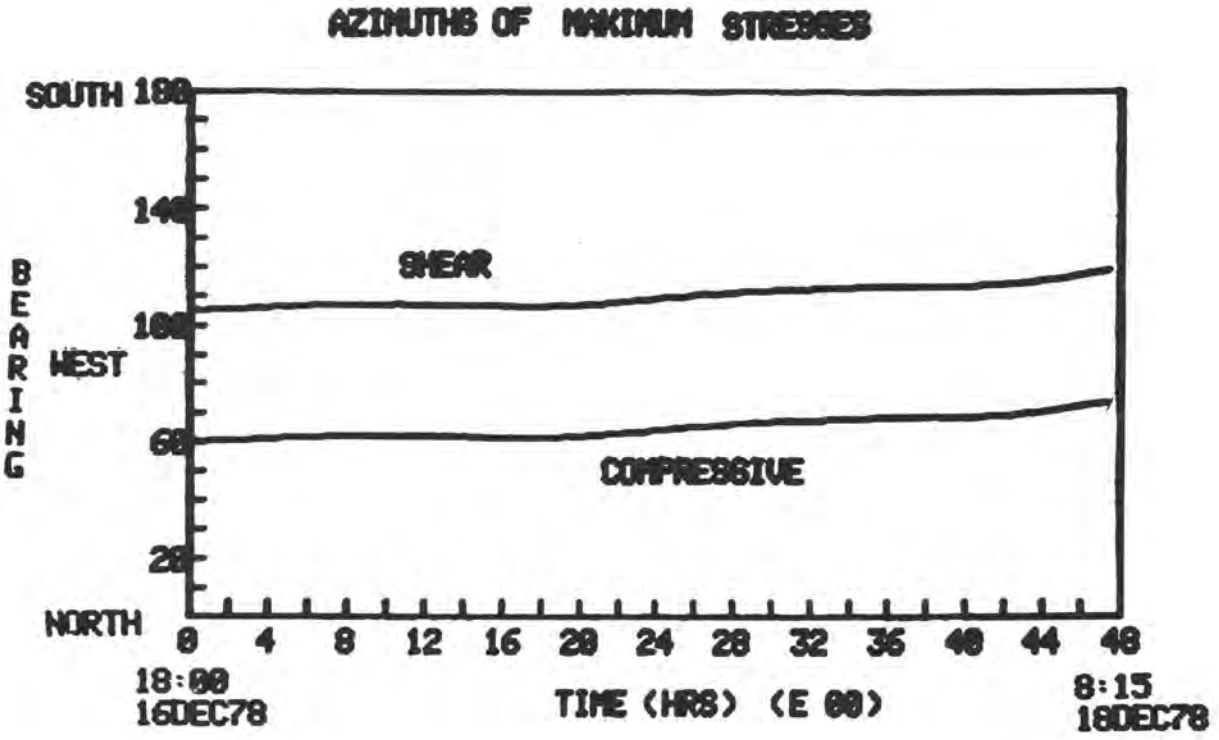

Figure 11. Calculated continuous azimuths of the maximum stresses of Figure 10. A plane stress solution was used, so the maximum shear and compressive stresses always differ by $\pi/4$.

Analysis of trends in the magnitude and direction of the principal relative stresses will form the basis of our data interpretation during the next year. Data for the N-S and N 60 E relative stresses for the one week period beginning shortly after the end of Figure 8 are presented as Figure 12, with the accompanying temperature data as Figure 13. The high in pressure and temperature evident in Figures 8, 9, 12, and 13 corresponds to an interval of heavy rainfall in the Palmdale area. Earth tides are evident as approximately 25 millibar pressure excursions every 24 hours. The temperature transducer at each California site is well coupled to the temperature of the compensators. It is possible that this high reflects a systemic thermal instrument response, in which case further adjustment to the compliance of the compensators should reduce the effect. The compensators are not as well insulated from changes in surface temperature as are the flatjacks, due primarily to burial depth. Thermal instrument response should then improve if the instruments are better coupled to the ground by filling and insulated from the air by burial.

The Little Cottonwood Canyon (Salt Lake City) Utah site was monitored for six months during early and middle 1978. Figure 14 represents this data; this 11-day data set from early September, 1978 shows especially good variability and high relative stress levels. A Cooley-Tukey fast fourier transform algorithm was applied to this 1024-point sample of data, yielding the frequency spectra of Figures 15 and 16 for the N-S and E-W aligned stresses, respectively. Here the amplitudes of the tidal components can be compared; the diurnal and semidiurnal components are strongest in the N-S alignment. Additional work is planned to determine the phase and tidal admittance of the stress data, and whether the stress data is coupled most strongly to theoretical tidal acceleration, tilt, or to local geology.

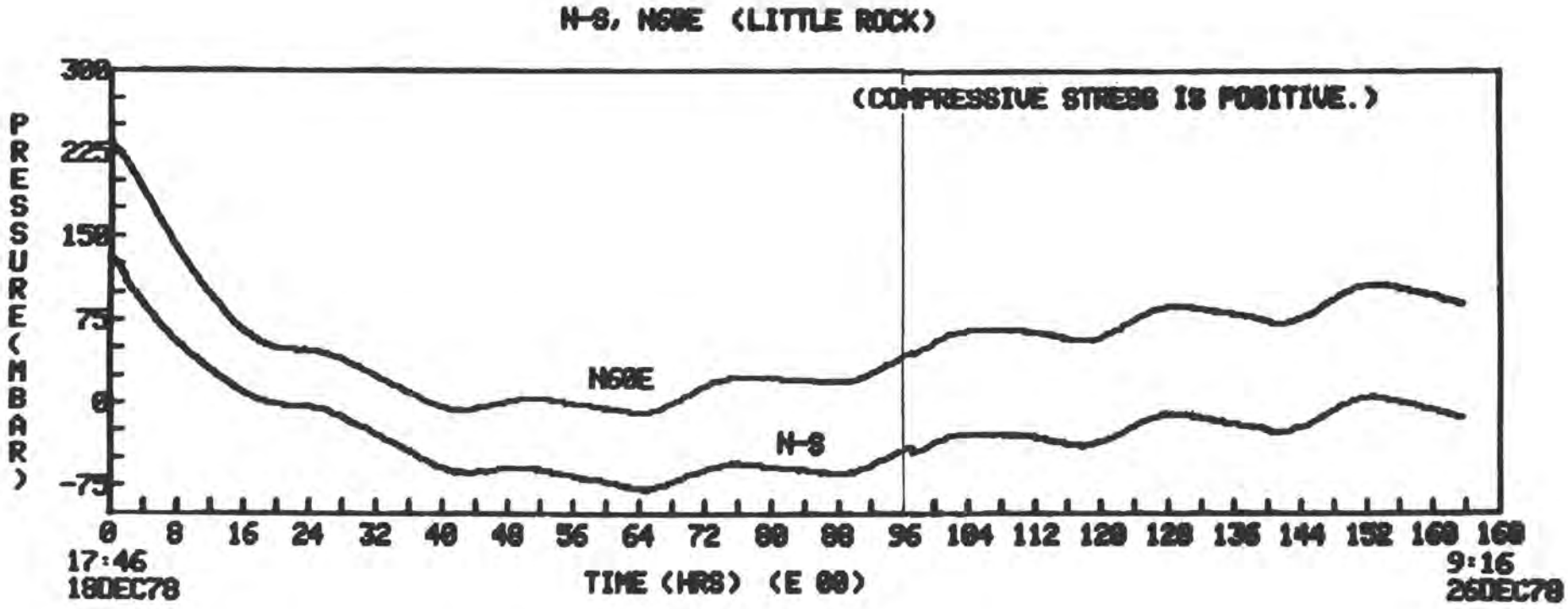

Figure 12. One week data set from Little Rock taken when channel 3 (N60W) malfunctioned. The location of the Little Rock stress monitor in a wash may make it susceptible to heavy precipitation. A period of heavy rainfall concluded about 12 hours before this data.

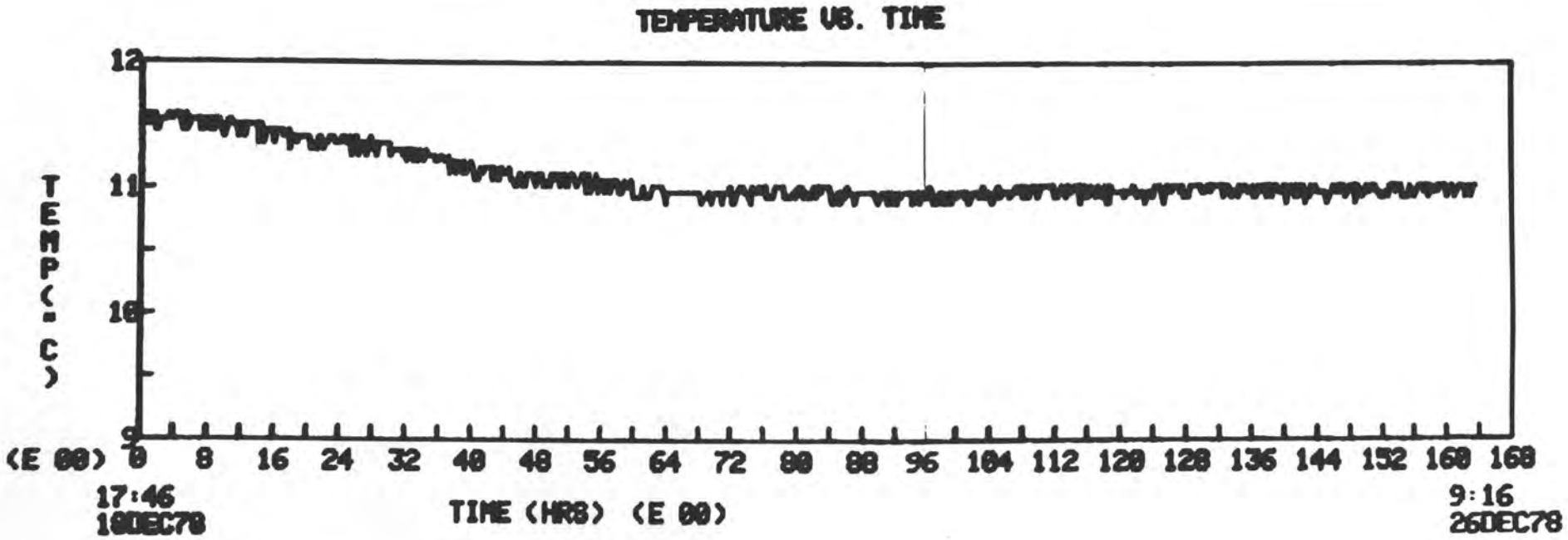

Figure 13. Temperature-time series recorded concurrently with the data of Figure 12, at the Little Rock site. The data originated from the same transducer as those of Figure 9.

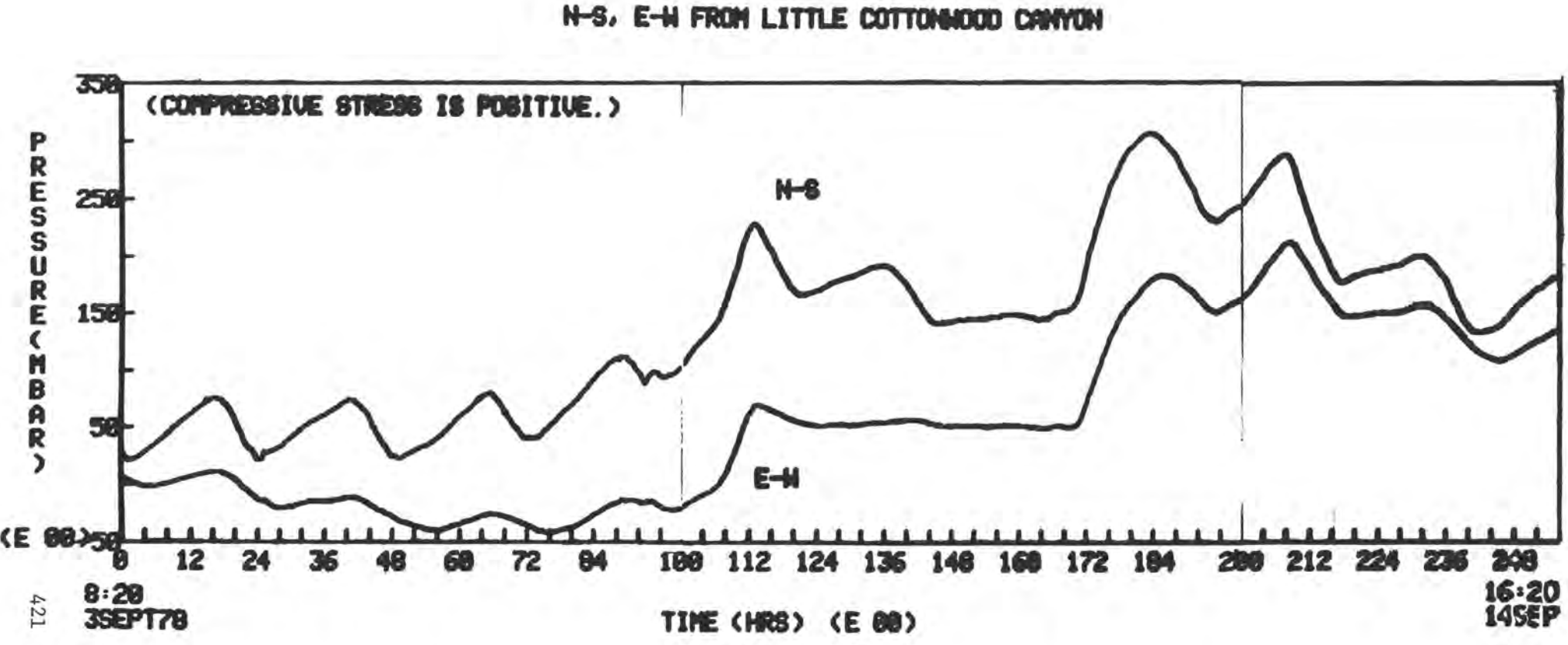

Figure 14. Pressure-time series from the Little Cottonwood Canyon, Utah stress monitor. Two flatjacks are emplaced in a shallow cave in a quartz monzonite stock near the Wasatch Fault.

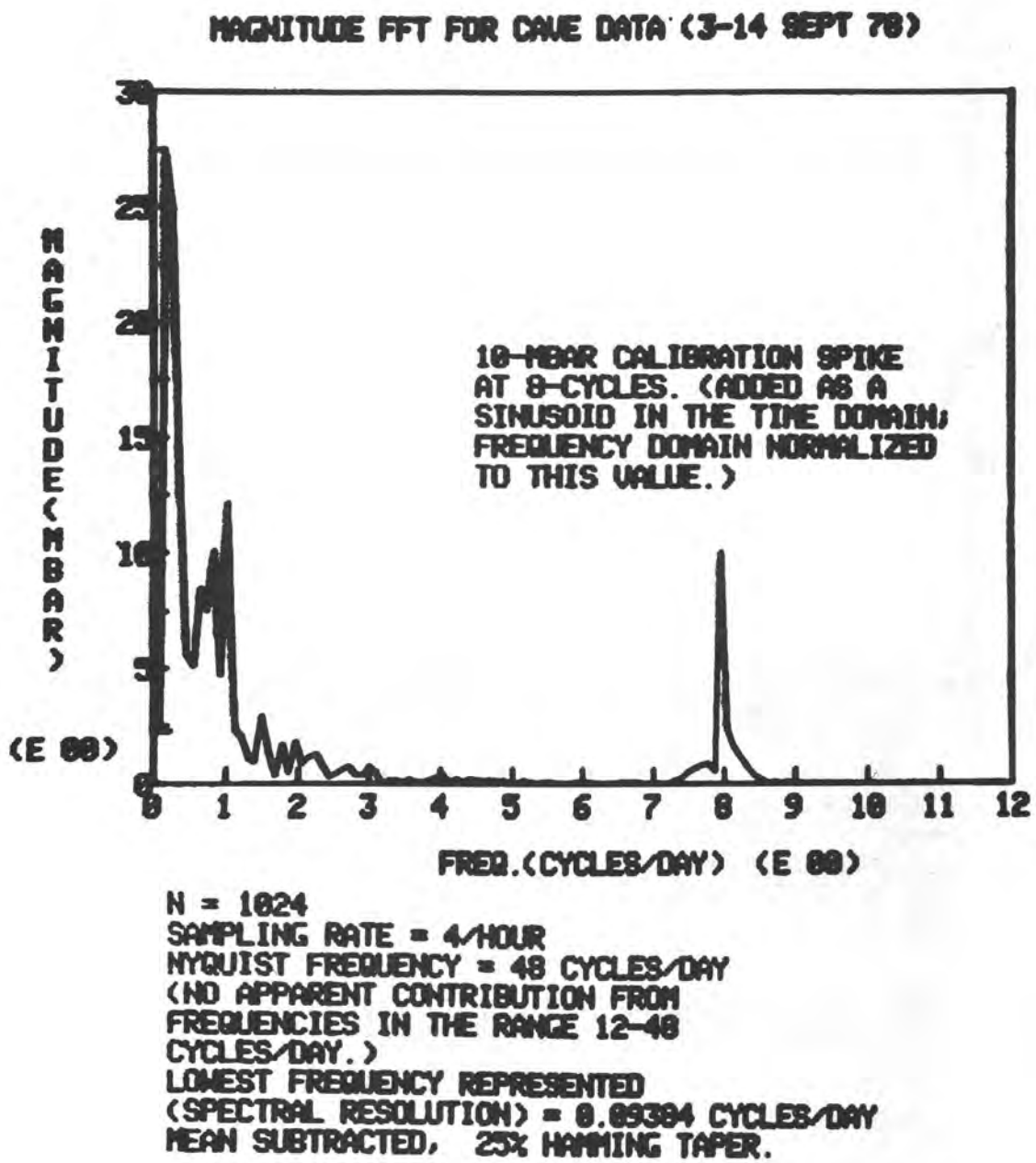

Figure 15. Frequency spectrum for the N-S stress data of Figure 14.

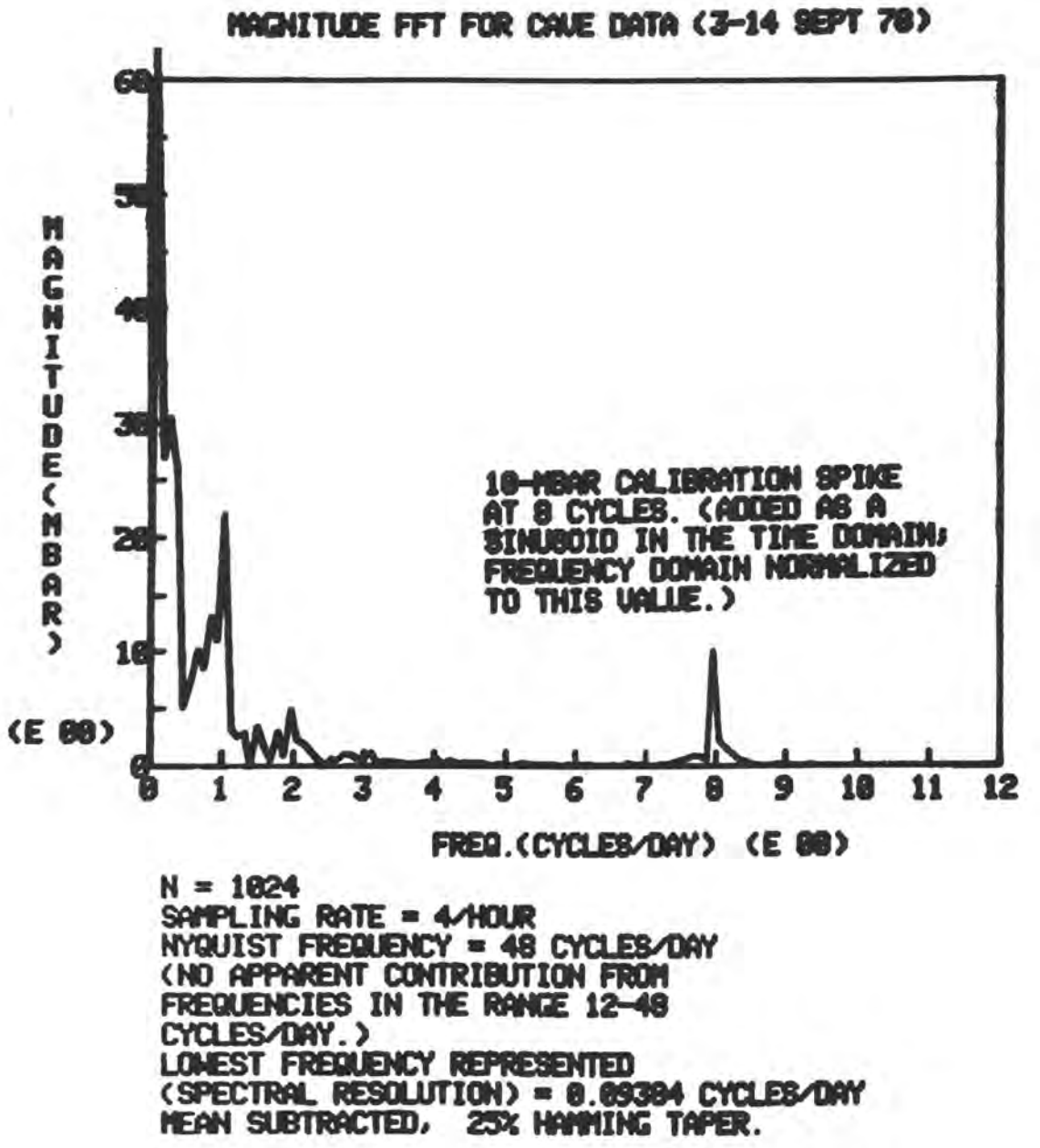

Figure 16. Frequency spectrum for the E-W stress data of Figure 14.

REFERENCES

1. Barker, L.M., 1975, unpublished work, Terra Tek, Inc.

2. Brechtel, C.E., 1978, unpublished work, Terra Tek, Inc.

3. de la Cruz, R. and Raleigh, C.B., 1972, Absolute Stress Measurements at the Rangely Anticline, Northwest Colorado, Int. Jour. Rock Mech. Min. Sci., vol. 9, p. 625-634.

4. Swolfs, H.S., Field Measurements of Tectonic Stress Variations in Southern California (Palmdale Uplift) Technical Proposal, Terra Tek, Inc., proposal P78-14, February, 1978.

5. Swolfs, H.S., Barker, L.M. and Pratt, H.R., 1976, Field Measurements of Tectonic Stress Variations in Central California and Utah, Technical Proposal, Terra Tek, Inc. Proposal P76-11, February, 1976.

6. Swolfs, H.S. and Brechtel, C.E., 1977, Mechanical Properties of an *In Situ* Jointed Sandstone, Terra Tek TR77-105, and submitted to the International J. Rock Mech. Min. Sci., 1979.

7. Walsh, J.B., 1972, unpublished work, M.I.T.

8. Walsh, J.B., 1978, unpublished work, M.I.T.

9. Yamada, S., 1978, Calibration and Analysis of the Terra Tek Borehole Stress Monitoring System, Terra Tek Report, in press.

BOREHOLE STRAINMETERS

I. Selwyn Sacks

Carnegie Institution of Washington
Department of Terrestrial Magnetism
5241 Broad Branch Road, N. W.
Washington, D. C., 20015

Table of Contents

Description of Instrument

In essence, the instrument consists of a liquid-filled resilient tube, which is buried in a borehole and held in intimate contact with the rock wall. Degassed silicon oil is employed as the liquid so that no gas bubbles would form in the reference volume after installation. It is, of course, imperative that the tube faithfully follow the minute distortions of the borehole down to 10^{-6} microns. This is ensured by prestressing the 3.2 mm thick steel tube with an expanding cement which bonds the strainmeter to the rock. After curing for about one more this cement expansion causes a prestress on the tube of about 0.5 kg/cm^2. The thickness of the tube wall can be chosen so that the apparent rigidity of the tube and its contents is nearly equal to that of the surrounding rock. Therefore, when the tube is buried and bonded to the rock, the strainmeter measures genuine strain in the rock and not an amplified strain on the surface of an empty hole.

A drawing of the instrument is shown in Fig. 1. As the strain in the surrounding rock changes, the tube is deformed, and the liquid is forced from reference volume A (diameter: 11 cm, length: 4 m) through constriction R into thin-walled bellows BL. The bellows extends or contracts displacing the liquid into or out of the gas space, the pressure of which remains substantially independent of the rock strain changes. The motion of this bellows is transmitted to arm L which rotates about flexural pivot P. The movement of the arm is measured by differential transformer DT as well as by bimorph-type Piezo-electric crystal B. The frequency response of the bimorph sensor and its associated F.E.T. amplifier is flat from 1 cps down to about a period of twenty minutes and at lower frequencies is strain rate sensitive. The output from the differential transformer is of course strain sensitive at all frequencies. At the present state of development, the internal noise from the bimorph is about 10^{-11} in terms of equivalent strain. The noise of the differential transformer sensor is at present about an order of magnitude larger, but this is almost entirely due to the noise of the reference oscillator and can be improved substantially by more refined electronic design. Valve V is used to mechanically center the system. The maximum volume strain which can be measured without opening the valve is 10^{-5}. A very wide range of internal calibration which meets the large dynamic range of the system is also provided

by means of the stiffer bellows C. This bellows is driven by a micrometer with differential screw threads controlled by a stepper motor. The minimum calibration step is 5×10^{-10} and the maximum 4×10^{-5}.

One of the original features of the system is the dual protection of the sensors against acceleration due to nearby earthquakes. (1) The high alternating pressures in the reference volume due to strong local earthquakes are filtered by a constriction between the reference volume and the sensing bellows. The diameter and length of the constriction tube are such that the effective acoustic resistance of the constriction together with the compliance of the liquid in the reference volume give a cut-off frequency of 1 cps. (2) The mechanical arm is further damped by the dash-pot which is made up of the fixed cylinder and moving piston of the differential transformer and is immersed in the liquid. Various improvements and simplifications have been made to the design since the 1971 model described, but the basic principals of operation are unchanged. Fig. 2 shows a schematic of the installation.

Theoretical Response to Body and Surface Waves

To arrive at the theoretical response of a perfectly matched buried volume strainmeter (dilatometer) to incident compressional and shear waves we follow the methods of Ewing, et al (1957) and Gupta (1966). The coordinate system used is shown in Fig. 3 . In a straight forward, but lengthy process, we arrive at an expression for volume strain for P waves with unit displacement amplitude and Poisson Ratio = .25. That is,

$$\theta_P = \frac{2\pi}{\lambda_P} \left[- \frac{2b^2 \sin M}{R} + i \frac{4a \cos M}{R} \right] \exp \left[i k (ct-x) \right]$$

where θ_P = volume strain from incident P waves,

λ_P = wavelength of incident P waves,

$a = 2 \tan e \tan f$, $b = 1 + 3\tan^2 e = \tan^2 f - 1$,

$R = 2a + b^2$, $M = kz \tan e$, $N = kz \tan f$,

$$k = \frac{2\pi \cos e}{\lambda_P} = \frac{2\pi \cos f}{\lambda_{SV}} ,$$

The volume strainmeter has no response to SH waves. Its response to SV energy at different angles of emergence is shown in Fig. 5. There are three angles at which there is zero output; grazing, 45° and normal incidence. There is no significant frequency dependence at any angle. In terms of shear waves at different epicentral distances, the 45° zero is equivalent to about $\Delta = 25°$ followed by a peak at about $\Delta = 40°$ for direct S. Except for core phases, seismograms written by the borehole instruments are similar to those from seismographs, with much enhanced low frequency resolution.

The response of the buried volume strainmeter to surface waves can be readily found by differentiating the expressions for displacements given in Ewing. Vertical and areal strains are added to give an expression for volume strain. The result is a simple exponential decay with depth

$$\left(\frac{\theta}{\theta_0}\right)_{\text{Rayleigh}} = \exp\left(-0.85\,\frac{2\pi z}{\lambda_R}\right.$$

where z = depth and λ_R = wavelength for Rayleigh waves. Volume strain reaches 0.5 of the surface value at $z = 0.13\,\lambda_R$.

Theoretical Response to Dilatancy

According to the dilatancy model (see Nur, 1972), preceding an earthquake there is a change in volume in the region in which an earthquake will occur. It is of interest to know how the borehole strainmeters (which act as dilatometers) will react to such slow volume changes at some distance from the source region. We will approximate the dilatancy by assuming a point source of expansion which is constant in time. (The strainmeter is assumed to be outside the source region.) The solutions for both an infinite space and a half-space can be obtained from Cagniard (1962, Ch. 8).

For an infinite space the displacement due to a point source of expansion at z = h and ρ = 0 (in cylindrical coordinates) is given by

$$\vec{u}^{\circ} = \frac{\delta V}{R^3}\,(\rho\,\hat{\rho} + (z-h)\hat{z}) \qquad (1)$$

c is the apparent velocity along the surface,

e = emergence and reflection angle for P waves,

and f = emergence and reflection angle for SV waves.

For SV waves, we get

$$\theta_{SV} = \frac{2\pi}{\lambda_{SV}} \; 2 \sin f \cos f \left[\frac{2b(1 + \tan^2 e) \sin M}{R} + i \frac{b(1 + \tan^2 e)(2\cos M)}{R}\right] \exp [i k (ct-x)]$$

The amplitude and phase behavior of volume strain due to P and SV waves with unit displacement amplitude as a function of emergence angle is given in Fig.4 and Fig. 5 .

Because of the low noise of the borehole strainmeters we have tested to date, it is of interest to consider their performance as high gain long period seismographs. Examination of Fig.4 shows that the response of a buried dilatometer to incident compressional waves as a function of angle of emergence is similar to that of a horizontal seismometer. The major difference is that its response near normal incidence is approximately proportional to frequency in the range zero frequency to frequency = rock volocity/ 10 x depth of burial. The curve denoted 0.01 wavelength in Fig.4 is equivalent to a wave period of 1.25 sec assuming a rock velocity of 4 km/ sec. The peak sensitivity occurs at emergence angle e = 20° which corresponds to an epicentral distance of Δ = 10° (surface focus) for direct P. At e = 60° (Δ = 55°), the sensitivity is down to 40% of the peak value. For e = 64° (Δ = 70°) the long period sensitivity is down to 27%, but the sensitivity at 1.25 second period is about 10% higher. At a depth of 50 M, long period is considered to be greater than 10 seconds. At greater angles of emergence, i.e. greater epicentral distances, this differentiating effect is progressively more pronounced, until at normal incidence the wavelength strain product is proportional to frequency. In our installations, the shortest period we are interested in recording is about one second, so that the differentiation need only be considered for the higher apparent velocity core waves.

where $\rho^2 = x^2 + y^2$, $R^2 = \rho^2 + (z - h)^2$ and δV is the total volume change of any volume including the source point $R = 0$ (see Fig. 6). The dilatation $\theta = \vec{\nabla} \cdot \vec{u}$ is zero for $R \neq 0$. Hence, strainmeters outside the source region would not be affected by a dilatation source.

The strainmeters, however, are not imbedded in an infinite space but, to a good approximation, are at the free surface of a half-space. Although Cagniard has solved this problem, his solution is obtained by taking the static limit of a dynamic problem. We will outline here a more direct derivation.

The displacement $\vec{u}$ can be written as $\vec{u} = \vec{u}^a + \vec{u}^b$ where $\vec{u}^a$ is given above by Equation 1 and $\vec{u}^b$ is the solution of the homogeneous Navier equation so that the normal stresses derived from $\vec{u}$ are zero at $z = 0$. That is,

$$(\lambda + 2\mu)\vec{\nabla}(\vec{\nabla} \cdot \vec{u}^b) - \mu\vec{\nabla} \times (\vec{\nabla} \times \vec{u}^b) = 0 \qquad z \geqq 0 \qquad (2)$$

and

$$\left.\begin{aligned} 0 = \sigma_{zz} &= \lambda\vec{\nabla} \cdot \vec{u} + 2\mu\, \partial u_z/\partial z \\ 0 = \sigma_{z\rho} &= \mu\,(\partial u_z/\partial_\rho + \partial \mu_\rho/\partial z \end{aligned}\right\} z = 0 \qquad (3)$$

where λ and μ are the Lamé coefficients. A general representation of $\vec{u}^b$ satisfying Equation 2 is the Papkovich-Neuber representation (see Sokolnikoff, 1956, Ch. 6)

$$\vec{u}^b = (\vec{\Phi} - \vec{\nabla}(\Phi_0 + \tfrac{1}{2}\alpha\vec{r} \cdot \vec{\Phi}))/\mu \qquad (4)$$

where $\alpha = (\lambda + \mu)/(\lambda + 2\mu)$ and

$$\Delta^2\Phi_\nu = 0 \qquad \nu = 0, 1, 2, 3. \qquad (5)$$

By symmetry the Φ_ν (and $\vec{u}^b$) can be thought of as resulting from a point of force at the image source point $\rho = 0$, $z = -h$ (see Fig. 6) Hence a useful representation for the Φ_ν satisfying Equation 5 is

$$\Phi = \sum_{l=0}^{\infty} B_{\nu l} P_l(\cos\chi)/R'^{l+1} \qquad (6)$$

where $R'^2 = \rho^2 + (z + h)^2$ and $\cos\chi = (z + h)/R'$. We have assumed that $\Phi_\nu \to 0$ as $R' \to \infty$. The solution is obtained by substituting Equation 6 into Equation 4 and applying the boundary conditions Equation 3. One finds,

then, that

$$\Phi_0 = \frac{3\mu + \lambda}{\lambda + \mu} \frac{\mu \delta V}{4\pi R'}, \vec{\Phi} = \frac{-\mu \delta V \cos \chi_2}{\pi \alpha R'^2} \tag{7}$$

which results in a dilatancy of

$$\begin{aligned} \theta &= \vec{\nabla} \cdot u \\ &= \vec{\nabla} \cdot u^b \\ &= \vec{\nabla} \cdot \vec{\Phi} / (\lambda + 2\mu) \\ &= -\frac{\mu \delta V}{\lambda + \mu} \frac{1 - 3\cos^2 \chi}{\pi R'^3} \end{aligned} \tag{8}$$

At the surface (z = 0) for $\lambda = \mu$ Equation 8 reduces to

$$\theta - \frac{\delta V}{2\pi [\rho^2 + h^2]^{3/2}} \{1 - 3h^2/(\rho^2 = h^2)\} \tag{9}$$

We assume that there is a spherical dilatant region enclosing the eventual fault such that the radius h is one-half the fault length, and that the dilatation is uniform, centered at R = 0 and of value 10^{-5}. This is equivalent to a point source dilatancy of strength $\delta V = 4/3\ \pi h^3 \times 10^{-5}$. Equation 9 becomes

$$\begin{aligned} \theta = &- \tfrac{2}{3} \times 10^{-5} \\ &\times [h/\sqrt{\rho^2 + h^2}]^3 \{1 - 3h^2/(\rho^2 + h^2)\}. \end{aligned} \tag{10}$$

Figure 7 gives the threshold strains (θ) based on Equation 10 as functions of epicentral distance (ρ) and fault length (2h) of the earthquake for which the dilatancy was a precursor. Also included are the magnitudes corresponding to fault lengths. For magnitudes below 5 the relationship is the appropriate one for the Matsushiro region ($m = 3.47 + 1.90 \log_{10} 2h$) and the relationships for magnitudes above 6 1/2 are due to Iida (1965). (That relationships applicable to small and large earthquakes do not extrapolate into each other was pointed out by Chinnery, 1969).

From Fig. 7 for a fault length of 20 km (nominally a magnitude 7 earthquake) a dilatancy of 10^{-5} can be detected at about 40 km from the center of dilatancy by a strainmeter array of the type described above for a detection threshold of 10^{-7}.

The precursory dilatation detection threshold is a function of the instrument noise level, the amount of dilatancy, and the size of the dilatant region.

Response in a High Acceleration Field

One of the main emphases in the design of the borehole strainmeter was that it should give reliable data when exposed to the high acceleration of a nearby earthquake. We suspected that many of the strain steps reported from quartz-bar extensometers were spurious. We compare some observations from the nearby 100 m quartz-bar extensometers with the borehole strainmeters in Table 1.

Table 1. Strain steps recorded by borehole strainmeters and quartz-bar extensometers.

Date	Time	Quartz-bar Extensometers ($\times 10^{-9}$)		Borehole Strainmeters (bimorph output) ($\times 10^{-9}$)		Epicentral Distance (km)		M	Intensity at MAT
	h m	N-S	E-W	MAT	NGN	To MAT	To NGN		
Feb. 26	03 32	0	−1.5	0	0	local		3.0	I
Mar. 20	10 13	−12	0	+4.8	+2.4	10	10	4.8	II
Mar. 22	19 40	0	+0.3	0	0	350	350	5.4	0
Mar. 22	20 10	0	+5.0	+0.1	0	5	12	3.4	I
Mar. 22	20 12	0	−3.5	0	0	4	11	3.6	I
Mar. 26	10 46	0	−3.5	+0.6	0	7	17	3.8	II

(+): extension or dilatation
(−): contraction or compression

Figure 8 shows local and regional earthquakes recorded on the strainmeters as well as on the 100 m quartz-bar extensometers. "B" is a record of an earthquake of M = 5.4 at a distance of 350 km. The upper two traces, from the Nagano (NGN) and Matsushiro (MAT) strainmeters respectively, show good agreement. The same event is also shown in "A", the small amplitude being due to low pass filtering applied to the extensometers. The third trace in "B" is a higher gain version of the second trace in which periods longer than 120 seconds are attenuated at 6 db/octave. "C" shows two similar local earthquakes from the same region that occurred less than two minutes apart. The strain steps on the strainmeters are of the order of 10^{-10}. The east-west extensometer, however, recorded a strain step of 5×10^{-9} for the first shock, but a step of opposite sign of 3.5×10^{-9} for the second shock. These discordant steps may be due to the extensometers' vulnerability to the strong vibration from a local earth quake. The north-south extensometer showed no step

above its noise which is somewhat less than 10^{-9}.

Explosion test. As previously stated, some doubt is thrown upon the authenticity of strain steps recorded by extensometers, particularly the 100 meter extensometers of Matsushiro, which the authors know best. When Y. Yamagishi struck the ground near one end of the extensometer with a heavy hammer, the trace did not resume the previous zero line and some apparent strain step was recorded. It was therefore decided to test the performance of the new strainmeters under fairly severe vibration conditions such as those likely to be encountered during local earthquakes.

A vibration best has been made on an extensometer of conventional type (S. Takemoto, 1970). The following test was, however, aimed at imposing high accelerations not only on the instrument but also on its surrounding rock in actual operational condition. A shot hole 5 meters in depth was drilled 9 meters away from the strainmeter borehole and dynamite of 25, 50, 100, 200, 400, 800 and 1,600 gms was fired at the bottom of the water-filled shot hole. To measure acceleration, a three component accelerograph of SMAC type (natural frequency: 20 cps, damping coefficient: $h = 0.65$, sensitivity: 100 gal/mm) was placed 7.3 meters away from the shot hole in the entrance of the main underground seismograph vault. Acceleration at a distance of 200 meters was also measured from the magnetic taype record of a three component seismograph in the main seismograph vault. Table 2 shows the accelerations, strain steps and weights of explosive.

Table 2. Explosion test.

Weight of explosive (gms)	Depth (m)	Observed strain step ($\times 10^{-9}$)	Acceleration (gal)					
			8.8 m away			200 m away		
			V	R	T	V	R	T
25	4.5	not perceptible	156	140	52			
50	4.5	0.24	246	185	61			
100	4.5	0.66	372	172	81			
200	4.0	0.72	510	153	120	0.13	1.0	1.1
400	4.0	1.80	1070	192	154	0.26	1.8	1.6
800	2.6	3.84	1560	352	285	0.85	2.4	2.2
1600	2.6	6.00	sat.	605	375	1.4	3.1	3.1

Although no definite scaling law between weight of explosive and trace amplitude has been established, the amplitude is proportional either to the weight itself or to its square root when the efficiency of explosions remains the same (J. Steinhart and R. Meyer, 1961). In Fig.9 acceleration measured at two points, 8.8 m (A) and 200 m (B) from the shot, is plotted against the square root of the weight of explosives. Since a fairly good proportionality is maintained between these two quantitities, the same efficiency seems to be maintained in all the explosions. Therefore, it is valid to assume that the volume of the fractured rock, V, is proportional to the weight of the explosive, W.

$$V \propto W \qquad (11)$$

According to half space theory, the strain step, S, will be proportional to the cube of the ratio of the radius, d, of the fractured rock and the distance to the strainmeter, r.

$$S \propto (d/r)^3 \qquad (12)$$

Since

$$V \propto d^3 \qquad (13)$$

and r is constant from (11), (12) and (13)

it follows

$$S \propto W$$

i.e the strain step is directly proportional to the weight of explosives. Fig.10 shows good agreement with the expected result.

It is rather difficult to estimate the absolute value of the strain step from small explosions, for the reported strain steps associated with large underground explosions vary according to the conditions of the explosion and its environment, although direct proportionality between strain steps and yields is common (P. R. Romig et al., 1969; S. W. Smith et al., 1969; D. D. Dickey, 1969; G. Boucher et al., 1971). Because the sense of all the observed strain steps is consistently compressional and the values accord with theory, no spurious behavior is suspected in the strainmeter.

The attenuation of the horizontal acceleration as measured at the two points for explosions of 800 gms and 1,600 gms is as follows:

Weight of explosive (gms)	Attenuation of acceleration	
	Radial	Transverse
800	1/147	1/130
1600	1/195	1/121

mean: 1/148

This value leads to the attenuation law of

$$\text{acceleration} \propto (\text{distance})^{-1.6}$$

The last two explosions were also felt in an office 230 m away, suggesting an acceleration of 1∿2 gal which further supports the above attenuation rate. If the acceleration at the strainmeter 46 m from the shot is interpolated, the following acceleration in gals obtained:

Weight of explosive, gms	Acceleration, gals	
	Vertical	Radial
800	110	25
1600	—	42

There is no doubt that the strainmeter was subjected to very high accelerations. These correspond to JMA intensity V or even VI, but yet caused no obvious spurious behavior. The strain step from the largest explosion was only 6×10^{-9}, whereas the strain step expected from an earthquake of magnitude 6 at a distance of 25 km, which would give the same intensity of vibration (V) at the instrument, would be approximately 10^{-6}∿10^{-7}.

Noise and Stability

The discussion on noise and stability is divided into three parts since different factors influence the noise in different frequency ranges.

a) Some seconds to about an hour periods. We found that the ultimate sensitivity of buried strainmeters was limited by atmospheric noise (rock strains induced by atmospheric pressure variations in space and time). The marked similarity between the noise on the strainmeter and a co-located microbarograph suggested the possibility of improving the signal-to-noise (S/N)

ratio by subtracting a suitably filtered signal from the microbarograph from the strainmeter output. Figure 11 shows the result of such a subtraction. The S/N improved by about 5, so the approach was deemed profitable. We digitized both outputs and computed the coherence (γ) (Foster and Guinzy, 1967; Haubrich, 1965) between the barograph and the volume strainmeter (see Fig. 12) The value of this statistic is that γ^2 at any given frequency is the proportion of the power in the strainmeter signal at that frequency which is coherent with the microbarograph signal. Since the coherent noise can be removed by linear filtering and subtraction, $1/\gamma^2$ is the easily obtainable improvement in the signal-to-noise ratio at that frequency. Thus, at frequencies where γ^2 is 0.8, we can obtain an improvement in S/N of a factor of 5 (7 dB), and where it is 0.95, an improvement of a factor of 20 (30 dB).

The coherence drops sharply for periods shorter than about 40 seconds. This drop is due in part to the increase in microseismic noise at these shorter periods and in part to the lack of spatial coherence at the higher frequencies.

When the spatial coherence of the atmospheric pressure fluctuations is high, a microbarograph sampling pressure at one or two points near the strainmeter is adequate for making the noise corrections. However, in order to make the best of all possible atmospheric noise corrections in an incoherent pressure field, we must use as a noise reference a barograph that averages the surface pressure with a weighting proportional to the sensitivity of the strainmeter. The barograph used in the coherence measurements samples the atmospheric pressure at two points separated by about 50 meters.

The fact that the "two-point" barograph works as well as it does tells us that the surface atmospheric pressure is quite coherent across the surface area sampled by the strainmeter. It is as though there were a pressure pattern "frozen"into the air and the air were moving over the surface at a uniform speed. This is in agreement with the findings of Priestley (1965) of high coherence for periods longer than 30 or 40 seconds. The only applicable work we have found in the open literature is that of Priestley, so we do not know how much or how rapidly the spatial coherence and the frequency-wave number of spectra of atmospheric noise vary.

Directional Strainmeters. The simplest borehole strainmeters respond to volume strain (omnidirectional). However, since atmospheric pressure is normal to the earth's surface, one might expect to reduce the sensitivity to atmospheric pressure by measuring only the horizontal strain components. Indeed, Ozawa (1957) had shown that the areal strain (the sum of the two horizontal strains) at the surface due to a normal load was identically zero when the loaded area did not include the strainmeter. We have computed (see Fig. 13) the vertical, areal, and volume strains which would be detected by a buried strainmeter as a result of a normal concentrated load on the surface as a function of distance from the borehole to the load. From these curves we can compute the strain at a depth due to any prescribed atmospheric stress distribution by taking a weighted average of the surface atmospheric pressure. By considering the problem in Fourier transform space, we can calculate the sensitivity of the earth-strainmeter system to the atmospheric pressure as a function of wave number. Figure 14 shows the response of a buried strainmeter to the atmospheric pressure field as a function of wave number. The wave number is the inverse of wavelength measured in units of the burial depth. The dominant component of atmospheric noise at ∿100-second period is due to turbulence in the boundary layer at the earth's surface. These disturbances travel at ∿5 meters/sec, giving a scaled wave number of 0.1, which, according to Fig. 14 is the value for which the areal strain component is least sensitive. Hence, the areal component is indeed the least sensitive to this principal source of noise. With this as motivation, the next strainmeter (2) was constructed with the same principal features as (1) except for the following points.

1. The response was shaped with high-cut hydraulic filters in order to reduce the possibility of ion depletion in the solion caused by large signals at moderate periods (∿20 seconds). Hydraulic filtering was chosen over electronic filtering because of the large dynamic range obtainable and because the filter had to be in the system ahead of the sensor.

2. In the second instrument, volume strain is resolved into the vertical and areal strains by connecting the sensors so that they measure the volume changes in two separate chambers that are effectively decoupled

from the walls or the bottom of the tube, respectively. The large chamber (see Fig. 15) responds only to areal strain, since the height of the volume is maintained by an unstressed column connecting the movable bottom piston with the fixed top of the chamber. The small chamber at the bottom of the instrument has a movable piston as a top and the fixed end of the tube as a bottom. Since the piston is connected to the top of the tube by a fixed length member, the length change due to vertical strain on the active length is reflected in a height change in the lower volume. Thus the volume change in the small chamber is the volume change due to vertical strain for the active length (∿1 meter) plus that due to areal strain in the relatively insignificant (∿1 centimeter) small chamber.

Results from this second meter have largely borne out the predictions. Figure 16 shows a sample of noise from both the vertical and areal components. The short-period (< 200 seconds) noise is indeed lower on the areal than on the vertical (or the omni). An unexpected finding is that the noise on the vertical component is small at periods longer than ∿500 seconds. We as yet have no explanation for this.

b) Medium Periods: 1/2 hour - 1 day. Noise has been found to be due to the local environment rather than the strainmeter itself.

The most serious source of noise is water movement in a local aquifer. Unlike the atmospheric effects, motion in the aquifer can result in local strains far in excess of the amount which results from a simple calculation based on change in water level applied to a uniform elastic medium; this amplification factor can be as much as many hundreds. Instruments such as extensometers, borehole strainmeters, or tiltmeters are affected by aquifer noise. Figure 17 shows the effect of rainfall on an extensometer in the Sanriku region of northeastern Honshu, Japan. It can be seen that enormous strain results from a few millimeters of rain.

An approximate amplification factor can be calculated as follows: Amp = measured strain/strain expected, assuming an elastic medium. Some assumptions are necessary in the calculation of expected strain because of uncertainties in the parameters controlling the runoff of the water and the mechanism by which the water gets into the aquifer. The time constant of the aquifer can

be determined from observations of the time lag between rainfall and resulting strain. The time constant for the example shown in Figure 17 is about one day. We assume that all the rain that occurs during one time constant is available to load the rock. During a 24-hour period starting on day 8 (Fig. 17), 10.7 cm of rain fell, equivalent to an applied pressure of 0.01 bars; for rock with a bulk modulus of 7×10^5 bars, calculated strain is 1.4×10^{-8}. The measured strain caused by this episode of rainfall was 8.8×10^{-7}. The amplification for this site is therefore 60.

Any disturbance of the aquifer may be expected to have a large effect on recorded strain if the strainmeter is near the aquifer. Because of the low-pass filter characteristics of the aquifer, local disturbances whose period is less than a few times the time constant do not propagate over large distances. An example of the low correlation of the noise on two borehole strainmeters just 300 m apart is shown in Fig. 18 . Bimorph 1 is fairly near (less than 100m) an automatic pumping station. The noise level at periods of 1/2 to 3 hours is about 3×10^{-8}. At the second borehole strainmeter site (bimorph 2), the noise level at these periods is about 5×10^{-11}, which is about that expected from atmospheric pressure fluctuations. However, the flow in aquifers is fairly complicated; distance from a well does not always guarantee low aquifer noise.

Lack of shorter period noise (period less than a few days) does not guarantee stability over much longer periods because an aquifer with a very long time constant at a large distance from an active well may have small short-period noise yet be very sensitive to the water level in the aquifer, which could change from year to year. Although aquifer noise is most apparent (on instruments, with sufficient sensitivity) at periods of less than a few days, presumably the same mechanism can affect the stability of the base line and, therefore, the secular strain measurement. This is of considerable importance in earthquake prediction.

c) Long-term Stability, weeks - years. A difficulty in assessing long term stability is that in general we do not know what secular strain might be appropriate at any particular site. Inter comparisons of closely spaced instruments which should be in the same tectonic environment allows such an assessment to be made. There are three strain-measuring instruments operating at the Matsushiro Seismological Observatory. Two borehole volume strainmeters, 300 m apart, are situated about 250 m from a pair of 100-m-long quartz bar horizontal

extensometers with N-S and E-W orientations. Figure 19 is a plan showing the locations of the various instruments.

The borehole strainmeters are dilatometers. Using the fact that the extensometers are installed at a free surface, the equivalent dilatant (volume) strain can be calculated from the data of the two horizontal extensometers. The result is $\theta_{extensometers} = [(1 - 2\sigma)/(1 - \sigma)](\varepsilon_{NS} + \varepsilon_{EW})$ where ε_{NS} and ε_{EW} are the strains measured by the two horizontal extensometers and σ is Poisson's ratio. Poisson's ratio for the Matsushiro region is not known, but must lie in the usual range of 0.25 and 0.3 $(1 - 2\sigma)/(1 - \sigma)$ is then in the range 0.66 and 0.57.

Figure 20 shows the secular strain results from the two borehole strainmeters, and the extensometers calculated for Poisson's ratio = 0.25. The three data sets agree moderately well and indicate a compressional volume strain rate of about 0.4×10^{-7}/year. The borehole instruments give values of about 0.36×10^{-7}/year and the extensometers give 0.48×10^{-7}/year ($\sigma = 0.25$) or 0.41×10^{-7}/year ($\sigma = 0.3$). Based on the extensometer data, the mean dilatant strain rate since April 1968 has been 0.66×10^{-6} per year. This strain rate is consistent with geodetic observations which show that the horizontal strain in the region of the Matsushiro earthquake swarm reached 3.7×10^{-4} (extension) at the swarm's peak in October 1966 and has been decreasing since then (Kasahara et al., 1967).

The intrinsic long-term noise of the strainmeters can be estimated from how well the instruments track. If one corrects for the differences in secular strain (Fig. 20) instrument 2 and the extensometers differ by less than 10^{-7} in the monthly readings with a mean difference of 0.5×10^{-7}. The mean difference between the monthly readings of borehole strainmeter 1 and the extensometers is 1.3×10^{-7}.

Since the early installations, all having stable baselines, in the Matsushiro-Nagano region, additional installations have given more insight into factors influencing long term stability. One source of noise is installation in an aquifer. Deposits such as limonite, in cracks and joints indicate passage of water. Sites with this characteristic (e.g. Mikkabi on the Pacific coast of Honshu, Japan) show enhanced sensitivity to rainfall and an unstable baseline, possibly with a large seasonal variation. Sites in

mudstone (e.g. Omaezaki) have shown strong compression since installation. While the reason for this (assumed spurious) compression is not really known at this time, the presence of certain clay minerals (e.g. montmorillonite) may be responsible. Figure 21 shows a possible mechanism. It was attempted to install the instruments below the aquifer, which is generally underlain by impermeable rock. Since all the early installations essentially leave the hole unplugged and full of water (because of the intersection of the aquifer), water penetrates to the previously dry rock in the vacinity of the instrument. If the rock contains a significant quantity of material (such as montmorillonite) which expands considerably if it gets wet, continuing and substantial compression will be registered by the strainmeter. Future installations should have plugged boreholes.

Observed Response to Body Waves and Surface Waves

The instruments were installed by mid January 1971 and became operational on a routine basis in mid March. Figure 22 shows a comparison of a distant earthquake (New Guinea) recorded by the strainmeter and those from a three component seismograph with 30 sec pendula. The earthquake occurred almost due south of the station so that the east-west component of the seismograph is almost transverse while the north-south component is radial to the source. It is clearly noted that P, S and Rayleigh waves are well recorded by the strainmeter but the Love waves, which are very large on the transverse component (east-west) 10 minutes after the commencement, do not show on the strainmeter. This is in accordance with theory because P waves are, of course, dilatational and SV waves are converted to P waves at the free surface, which therefore also produce a dilatational strain change, but Love waves of SH component alone cannot do so. From the sensitivity of the seismograph (1×10^{-4} cm/sec/mm), the maximum ground amplitude (peak to zero), A, and its period in the first P wave train are 3.3×10^{-3} cm and 6.0 sec respectively. Assuming that the P wave velocity is 4 km/sec near the surface, which has been ascertained to some extent by seismic prospecting, the wave length λ is 24 km. Then, the strain, $A/(\lambda/2\pi)$, is 8.6×10^{-9}. The sensitivity of the strainmeter is 3×10^{-10}/mm and the trace amplitude (peak to zero) corresponding to the maximum is 25 mm, which is 7.5×10^{-9} in strain. The two systems, i.e. pendulum and strainmeter systems, agree well with each other.

Extraseismic Redistribution of Stress

Earthquakes are generally assumed to result when the gradual stress buildup in a region eventually exceeds some critical local strength. The fracture which develops is thought to propagate at a velocity approaching that of shear waves; this is supported by laboratory experiments (T. Kitagawa and K. Yamamoto, 1975). There have, however, always been observations which cannot be explained by fracture in an otherwise perfectly elastic medium. The time periods between events in a foreshock-aftershock sequence, for example, far exceed the time necessary for elastic redistribution of stress. Clearly, one or more other mechanism must play a major role in the stress redistribution.

There have been various studies (H. Kanamori and J. J. Cipar, 1974; H. Kanamori, 1972; H. Kanamori and D. L. Anderson, 1975; H. Kanamori and G. S. Stewart, 1977) of particular earthquakes inferring coseismic processes with time scales longer than normally associated with earthquakes. However, the evidence for these so-called "slow" or "silent" earthquakes has generally been indirect (e.g., anomalous long-period spectral behavior [H. Kanamori and D. L. Anderson, 1975] or unusually long surface-wave coda [H. Kanamori and G. S. Stewart, 1977]), since the time scale of such processes lies outside the pass-band of conventional seismographs.

A network of Sacks-Evertson borehole strainmeters (I. S. Sacks et al., 1971) was installed along the seismically-active Pacific coast of Honshu south of Tokyo which enabled the investigation of the possibility of "infraseismic" mechanisms for redistribution of stress.

Here we report observations of stress redistribution which are interpreted in terms of events which we call "slow earthquakes". All our observations are consistent with the hypothesis that these slow earthquakes are similar to "normal" earthquakes in all respects except for slower rupture velocities and longer rise times. We describe slow earthquakes which occur separately from normal earthquakes and which were observed both on the recently-installed borehole strainmeters as well as on nearby extensometers.

In addition, we include other kinds of data which indicate that the stress buildup before an earthquake may be non-linear in time. In these cases the concentrations of stress appear to occur in a much shorter time preceding the earthquake than that calculated on the basis of magnitude-precursor-time formulae (Scholz, et al., 1973).

Strainmeter waveforms for normal earthquakes and slow earthquakes. In order to understand the characteristics of slow earthquakes, we first examine strain waveforms from normal earthquakes, particularly in the near field (less than 10 fault lengths) where observations of slow earthquakes are most convincing. Fig. 23 shows the radial strain field based on a modification of a dislocation model in the form presented by Harkrider (1976). The theory is oversimplified (e.g., a point source in an infinite space is assumed), but the results are expected to be qualitatively correct.

The waveforms shown in Fig. 23 can be treated as the superposition of two parts: a strain step which is proportional to the moment and which falls off as the cube of the epicentral distance, and a "radiated" pulse which is defined here to include both a term with zero total area which falls off with distance as well as a term whose area is proportional to the moment but which falls off with the square of the distance. Within a few fault lengths (e.g., Fig. 23a) the strain step dominates, while beyond about 20 fault lengths the step would not be detectable - except for an event with an extremely large fault offset.

Fig. 24a is a wide-frequency-range borehole strainmeter record from Matsushiro of a nearby small (m = 4) earthquake. The compressional wave is followed by a larger shear arrival, and the static offset "arrives" shortly after S. The basic low-frequency structure is emphasized and the higher-frequency oscillations suppressed in the (effectively) low-pass filtered version of the same record shown in Fig. 24b. This record and the one in Fig. 25a (a low-pass filtered record of the same earthquake from the Hokushin Observatory near Nagano) show good agreement with the theoretical strain record of Fig. 23c.

Fig. 25b shows a strain event recorded by a borehole strainmeter at Irako. Although the record shown is from a wide-frequency-range channel such as that used for Fig.24a, only low frequencies appear in the arrival. The wave-form is similar to that of the earthquake in Fig. 25a and to the theoretical waveform in Fig. 23a. Many such events have been observed on the recently-installed borehole strain-

meters as well as on some nearby extensometers. The radiated pulses and strain steps from such events appear similar to those from normal earthquakes except that the rise time and duration are about 100 times longer than those for earthquakes of similar moment. It is therefore possible to produce slow-earthquake waveforms which are in reasonable agreement with observation by using normal-earthquake theory with long rise times and low rupture velocities.

At closer distances, the theory then predicts records such as shown in Fig. 23a. Fig. 25c shows a slow earthquake with similar waveform. It should be kept in mind, however, that for observations on only a single instrument there is an unresolvable ambiguity between an event being near, slow and of a certain moment or further, slower and of a larger moment.

Events such as those in Figs. 25b and c differ from creep events in that in creep events there is no permanent change in the strain field (King, et al., 1975).

The expanded time scale for slow earthquakes means that almost no energy is radiated in the normal seismic frequency band, so that slow earthquakes can not be detected by seismometer networks used for earthquake location. Even with instruments of high mangification at low frequencies, only nearby events can be clearly identified, because theoretical considerations suggest (Sato, et al., 1973) that the low rupture velocities for these events result in low radiation efficiencies. Accordingly, such instruments are required in denser networks than presently exist in order to do multi-instrument correlations of individual slow earthquakes.

Foreshocks and aftershocks of slow earthquakes. Shallow earthquakes may have foreshocks and aftershocks which are considerably smaller than the main event. Slow earthquakes may exhibit similar behavior; Fig. 26 shows a slow earthquake accompanied by a foreshock-aftershock sequence. Relative to the step size, the foreshocks have larger radiated pulses than the aftershocks. If these are all at more-or-less the same distance and have similar rise times, one interpretation is that the foreshocks have higher stress drops. Such a phenomenon has been claimed for some instances for normal earthquake foreshocks and aftershocks (Archambeau, et al., 1977).

Slow earthquakes as precursors for a normal earthquake

Fig. 27 shows the relative locations of the borehole strainmeter at Shizuoka, the Fujigawa extensometers and the epicenter of an m = 5.5 earthquake which occurred on 15 June 1976. Also shown are the dates and (relative) amplitudes of strain steps associated with slow earthquakes observed at the two observatories. The Fujigawa extensometers have operated for several years, but slow earthquakes were recorded only during the period January-May 1976. The borehole strainmeter at Shizuoka commenced operation in early April 1976 and recorded slow earthquakes (of the opposite polarity from those at Fujigawa) from that time until early June. None of the events are recorded at both observatories. Based on the Fujigawa records, the slow earthquakes started about 150 days before the earthquake, which is an oft-quoted (Scholz, et al., 1973) precursor time for an earthquake of that magnitude.

A model consistent with these observations has been suggested by Y. Okada (personal communication, 1976). The observatories are on opposite sides and within a few kilometers of the Fossa Magna, a major geological discontinuity. (See Fig. 27). Okada notes that the relative amplitudes and polarities of the slow earthquakes at the two observatories could be explained if the slow earthquakes occurred on the Fossa Magna.

Other detections of preseismic stress redistribution

There are other data which indicate that the concentration of stress in an epicentral region may be very nonlinear in time. Four examples are given here.

Fig. 28 shows the tide-gauge record from Irozaki, on the tip of the Izu peninsula, Honshu, Japan for the day on which a nearby M = 6.9 earthquake occurred. In this region the return time for such an earthquake is many decades. As can be seen in Fig. 28, there is a deviation from the expected tide level apparent about 20 minutes before the earthquake. This deviation is in the opposite sense from the eventual level change due to the earthquake. An interpretation could be that, due to a nearby slow earthquake shortly before the normal earthquake, there was a buildup of strain of about 1/3 of that eventually released.

Rikitake (1976) describes a number of tilt changes that have been reported preceding large earthquakes. While the examples he gives do establish that large changes of ground level or tilt have occurred some days or hours before earthquakes, in most cases there are no instrumental observations which would allow quantitative estimates. One exception

is the Tonankai earthquake (M = 8) of 7 December 1944.

Leveling surveys in the region of Kakegawa (about 150 km northeast of the eventual epicenter) showed slight subsidence corresponding to a tilt of 3×10^{-6} rad. in the 10 years preceding the earthquake. On the morning of the earthquake (which occurred at 11:36 a.m. local time) a level-survey team was operating north of Kakegawa. Over a two-hour period (up to 12 noon) closure errors of 9 mm over 2 km were found; during this brief period the ground had tilted 4.5×10^{-6} rad. in the sense of uplift at Kakegawa. Comparison of a survey immediately after the earthquake with one completed a month before showed a tilt of about 10^{-5} rad. in the region north of Kakegawa. This total tilt was in the same sense as the rapid precursory tilt on the morning of the earthquake. Thus this precursory tilt and that due to the earthquake were approximately equal.

A possible interpretation is that the precursory tilt was due to a slow earthquake of moment comparable to the normal earthquake.

Stress buildup preceding an earthquake

The simplest model of events leading to an earthquake is that stress builds up gradually in the eventual earthquake region because of some process such as plate motion. Data from an earthquake which occurred off the Izu peninsula (Japan) does not seem to support this. On January 16, 1978, a shallow earthquake, M ≈ 7.0, occurred with its epicenter about 30 km from a S-E borehole strainmeter which was installed at Irozaki, at the tip of the Izu peninsula. The rupture from this earthquake propogated to within about 15 km of the instrument, i.e. the instrument was certainly in the near field.

The strainmeter came on line in April 1977, and by August the initial drift seemed to be less than the secular strain. In the 15 months up to mid-November 1978, the total strain accumulation was only 2.7×10^{-6}. Between then and early January there was a rapid compression of about 2×10^{-6}, which reversed four days before the earthquake. In this case too, there seems to have been stress redistribution directly preceding an earthquake.

If in some cases high stresses are not concentrated in the source region until possibly a few days (or less) before even large earthquakes, this would set the effective upper limit to the warning period that a specific prediction could provide for such events.

Propagating ground uplifts. Fig. 29 shows changes in ground level on the Izu peninsula detected by repeated level surveys. Between 1969 and 1975, a "bump" 6 cm high and about 16 km (to half amplitude) in diameter appeared near the east coast. In later surveys (January-March 1976) the deformation spread in a southwesterly direction, and by September 1976 the greatest uplift was some 18 km southwest of the original peak. This uplift (15 cm, over a diameter of 15 km or so) indicates a strain of order 10^{-5}. The velocity of propagation was about 2 km/month.

A similar velocity was found for some strain events propagating across Tohoku (Ishii, 1976). The extensometer observatories, Miyako and Sanriku near the east coast and Himekami in central Tohoku, recorded strain events of amplitude 10^{-5}, 2×10^{-6}, and 5×10^{-7} respectively.

Some instances of ground uplift such as that preceding the Niigata earthquake of 1964 are probably associated with dilatancy of the stressed rock in the earthquake region. It seems reasonable that bumps associated with dilatancy may grow but cannot move. However, bumps caused by stress heterogeneity and at a strain level of 10^{-5} or so are likely to propagate. These moving bumps may not be directly associated with an impending earthquake.

Acknowledgements

Many colleaques have collaborated in the various studies reported here: D. W. Evertson, S. Suyehiro, L. M. Dorman, J. A. Snoke and A. T. Linde.

References

Ewing, W. M., Jardetzky, W. S., and Press, F., Elastic Waves in Layered Media, McGraw Hill Book Co., Inc., New York, N.Y., 1957.

Gupta, I. N., Response of a vertical strain seismometer to body waves, Bulletin of the Seismological Society of America, Vol. 56, No. 4, 1966.

Nur, A., Dilatancy, pore fluids, and premonitory variations of t_s/t_p travel times, Bull. Seismol. Soc. Am., Vol. 62, 1217-1222, 1972.

Cagniard, L., Reflection and Refraction of Progressive Seismic Waves (translated and revised by E. A. Flinn and C. H. Hewitt Dix), McGraw-Hill, New York, N.Y., 1962.

Sokolnikoff, I. S., Mathematical Theory of Elasticity, 2nd ed., McGraw - Hill, 1956.

Iida, K., Earthquake magnitude, earthquake fault, and source dimensions, J. Earth Sci., Nagoya Univ., Vol. 13, 115-132, 1965.

Chinnery, M. A., Earthquake magnitude and source parameters, Bull. Seismol. Soc. Am., Vol. 59, No. 5, 1969-1982, 1969.

Steinhart, S. J. and R. Meyer, Explosion studies of continental structure, Carnegie Institution of Washington Publication, 622, 187-189, 1961.

Romig, P. R. et al., Residual strains associated with a nuclear explosion. Bull. Seism. Soc. Am., Vol. 59, 2167-2176, 1969.

Smith, S. W. et al., Transient and residual strains from large underground explosions, Bull. Seism. Soc. Am., Vol. 59, 2185-2196, 1969.

Dickey, D. D., Strain associated with the BENHAM underground nuclear explosion, Bull. Seism. Soc. Am., Vol. 59, 2221-2230, 1969.

Boucher, G. et al.,Strain effects of nuclear explosions in Nevada, Bull. Seism. Soc. Am., Vol. 61, 55-64, 1971.

Foster, M. R., and N. J. Guinzy, The coefficient of coherence: its estimation and use in geophysical prospecting, Geophysics, Vol. 32, No. 4, 1967.

Haubrich, R. A., Earth noise, 5 to 500 millicycles per second. 1. Spectral stationarity, normality and nonlinearity, J. Geophys. Res., Vol. 70, 1415-1427, 1965.

Priestley, Joseph, Taut correlation studies of pressure fluctuations on the ground beneath a turbulent boundary layer, M.S. thesis, Univ. of Maryland, 1965.

Ozawa, I., Study on elastic strain of the ground in earth tide, Bull. 15, Disaster Prevention Research Institute, Kyoto University, Japan, 1957.

Kasahara, A., A. Okada, M. Shibano, K. Sasaki, and S. Matsumoto, Electro-optical measurement of horizontal strains accumulating in the swarm earthquake area (3), Bull. Earthquake Res. Insti., Vol. 45, 159-288, 1967.

Kitagawa, T., and K. Yamamoto, Jishim: J. Seismol. Soc. Japan, Vol. 28, 207-216, 1975.

Kanamori, H. and J. J. Cipar, Phys. Earth Planet Interiors, Vol. 9, 128-136, 1974; Kanamori, H. Phys. Earth Planet Interiors, Vol. 6, 346-359, 1972.

Kanamori, H. and D. L. Anderson, Journ. Geophys. Res., Vol. 80, 1075-1078, 1975.

Kanamori, H. and G. S.Stewart, Trans. Am. Geophys. Union, Vol. 58, 1194, 1977.

Sacks, I. S., S. Suyehiro, D. W. Evertson, and Y. Yamagishi, Papers Meteorol. Geophys., Vol. 22, 195-208, 1971.

Scholz, C. H., L. R. Sykes, and Y. P. Aggarwal, Science, Vol. 181, 803-809, 1973.

Harkrider, D. G. Geophys. Journ. Roy. Astron. Soc., Vol. 49, 97-133, 1976.

King, G. C. P., R. G. Bilham, J. W. Campbell, D. P. McKenzie, and M. Niazi, Nature, Vol. 253, 420-423, 1975.

Sato, T. and T. Harasawa, Journ. Phys. Earth, Vol. 21, 415-431, 1973.

Archambeau, C. B. and C. Salvedo, Trans. Am. Geophys. Union, Vol. 58, 494, 1977.

Rikitake, T., Earthquake Prediction, Vol. 9, Developments in Solid Earth Geophysics, 112-119, (Elsevier Scientific Pub. Co., New York, N.Y., 1976.

Figure Captions

1. Schematic view of the strainmeter.

2. Schematic view of installation.

3. The coordinate system used in describing the response of an ideal buried volume strainmeter.

4. Volume strain resulting from P waves with unit displacement amplitude.

5. Volume strain resulting from S_V waves.

6. Geometry for a dilatation point source in a half-space bounded by a free surface. The source is at $z = h$ and $\rho = 0$.

7. The maximum distance at which a precursory dilatant strain of 10^{-5} would be detectable for noise thresholds of 10^{-6}, 10^{-7}, and 10^{-8} for various fault lengths and magnitudes.

8. Local and regional earthquakes recorded on the strainmeter as well as on the 100 m quartz-bar extensometers.

9. Relation between weight of explosive and acceleration. (A) 8.8 meters from the shot. (B) 200 meters from the shot. V: Vertical, R: Radial, T: Transverse.

10. Relation between observed strain steps and weight of explosive.

11. Example of analog subtraction of coherent noise from strainmeter signal.

12. Coherence squared between barograph and strainmeter.

13. The strain seen by a buried strainmeter due to a unit concentrated load at the surface as a function of distance from the load to the borehole. The strainmeter is buried at unit depth.

14. The sensitivity of a buried strainmeter to sinusoidal plane pressure waves in the atmosphere.

15. Schematic of combined vertical and areal strain-rate meter.

16. Rayleigh waves from two earthquakes (mb = 5.3, 5.4) in the Fiji region, recorded at DTM, Washington, D.C., on vertical and areal strain-rate meters. The earthquakes were about 10 minutes apart. Note that the signal-to-noise ratio for the areal meter is about twice that for the vertical meter.

17 Strain resulting from rainfall. The rain starting on day 8 eventually gets into the aquifer (just before day 9) causing a local strain buildup over the next day, even though the rainfall is diminished. The strain change is about 60 times greater than would be expected from water loading of a uniform elastic medium. These data were kindly provided by the staff of the Imaide-yama Observatory.

18. Comparison of the records from two borehole strainmeters 300 m apart. The upper and lower sets of recordings were made for the times indicated on the same day. The upper trace in each set is from bimorph 1; the lower two traces are from instrument 2, (bimorph 2) at different gains. The sensitivities to strain are marked on the upper traces. The earth tide periods are attenuated by about 25 times as much noise (at periods less than a few hours) on instrument 1 as on number 9.

19. Map of the Matsushiro Seismological Observatory area showing the location of the two borehole strainmeters and the 100-m quartz-bar extensometers.

20. Secular dilatant strain in the Matsushiro (swarm) region measured by three independent instruments located as shown in Fig. 19.

21. Sketch of strainmeter installation showing possible source of drift. The borehole penetrates impermeable strata allowing the water to reach the level at which the strainmeter is installed. If the rock in its vicinity contains some clay mineral such as Montmorillonite which expands when it gets wet, continuing compression will be registered by the strainmeter.

22. Comparison of a distant earthquake (New Guinea) recorded by the strainmeter and a three component seismograph of 30 sec pendulum.

23. Theoretical waveforms of radial strain vs. time of an event at different epicentral distances. (a) At close distances, there is a relatively slowly rising step. The duration is the time for which movement (rupture) occurs on the fault. (b) & (c) At greater distances the radiated pulse is observed because it decays with distance less rapidly than does the strain step. The rise time is the time needed for the strain to achieve 86% of its peak value.

24. Record from the borehole strainmeter at MAT of an m = 4.0 earthquake on 19 September 1973 at a distance of 15 km. (a) Broadband-response record. (b) Low-pass filtered record from a different sensor in the same instrument. This sensor has a higher noise level.

25. Low-pass filtered strainmeter record from the same earthquake as in Fig. 24 recorded at Hokushin, near Nagano (distance = 15 km, Hokushin -MAT distance = 13 km). This record can be compared with the theoretical waveform in Fig. 23c. (b) "Slow" earthquake record for 25 June 1976 from the broadband-response sensor of the borehole strainmeter installed at Irako, on the Pacific coast. Note the similarity between this record and that from a normal earthquake (above) as well as the theoretical waveform in Fig. 23c. (c) "Slow" earthquake record on 26 July 1976 also from Irako. This event is either of similar time scale yet at a closer distance compared to the one shown above or it is slower and at a similar distance.

26. Irako borehole strainmeter record for 25 August 1976. A slow earthquake, strain = 7×10^{-8}, is shown preceded by foreshocks and followed by aftershocks with strains less than 10^{-9}. Expanded-scale tracings of sample foreshocks and aftershocks are included. The strain record has been high-pass filtered at 25 min. period.

27. Time history of the slow earthquakes (recorded on the borehole strainmeter at Shizuoka and on the Fujigawa extensometers) preceding the m = 5.5 Yamanashi earthquake. The shizuoka observatory commenced operation in April 1976. The amplitude scales for the two instruments are not the same, but the relative polarity of the strain steps is as indicated. Also included is a map showing

the relative locations of the two observatories, the epicenter and the Fossa Magna.

28. Tidal-gauge record from the tip of the Izu peninsula for 9 May 1974. On this data an M = 6.9 earthquake occurred within a few kilometers of the tidal gauge. Note that preseismic motion is apparent about 20 minutes before the earthquake.

29. Propagating uplift on the Izu peninsula. Contours are marked in centimeters. The dates of the level surveys are marked.

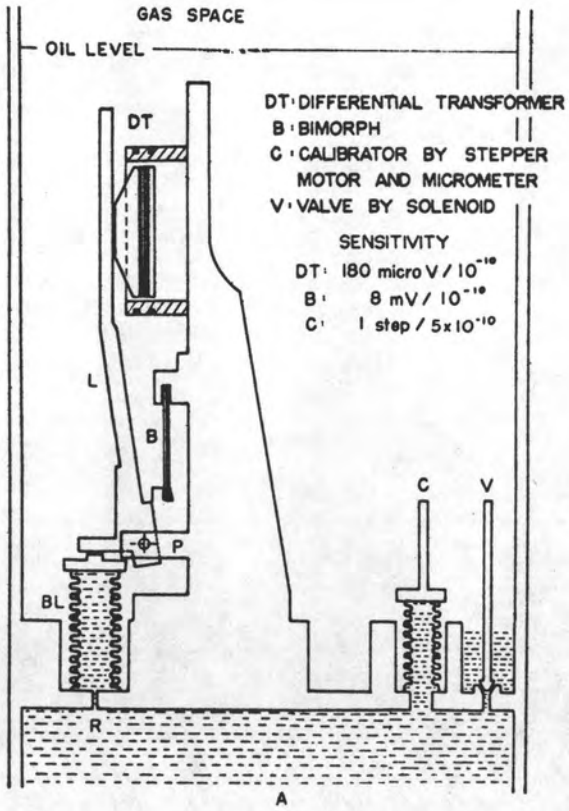
GAS SPACE
OIL LEVEL
DT: DIFFERENTIAL TRANSFORMER
B: BIMORPH
C: CALIBRATOR BY STEPPER MOTOR AND MICROMETER
V: VALVE BY SOLENOID
SENSITIVITY
DT: 180 micro V / 10^-10
B: 8 mV / 10^-10
C: 1 step / 5x10^-10
DT
L
B
C
V
P
BL
R
A

Fig. 1

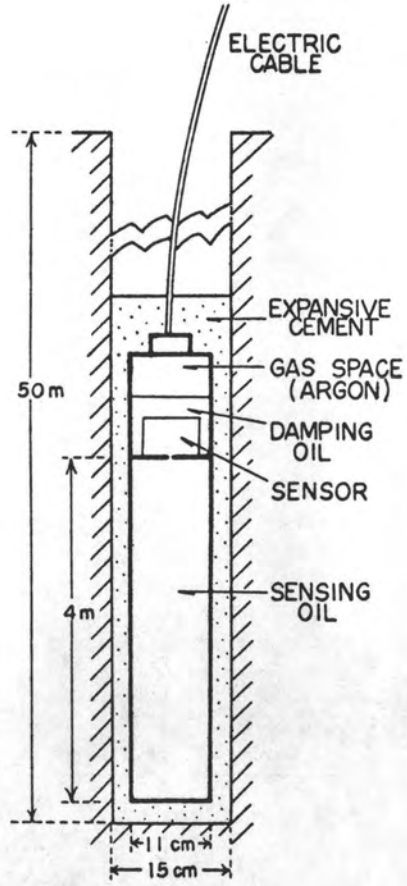
ELECTRIC CABLE
EXPANSIVE CEMENT
GAS SPACE (ARGON)
DAMPING OIL
SENSOR
SENSING OIL
50 m
4 m
11 cm
15 cm

Fig. 2

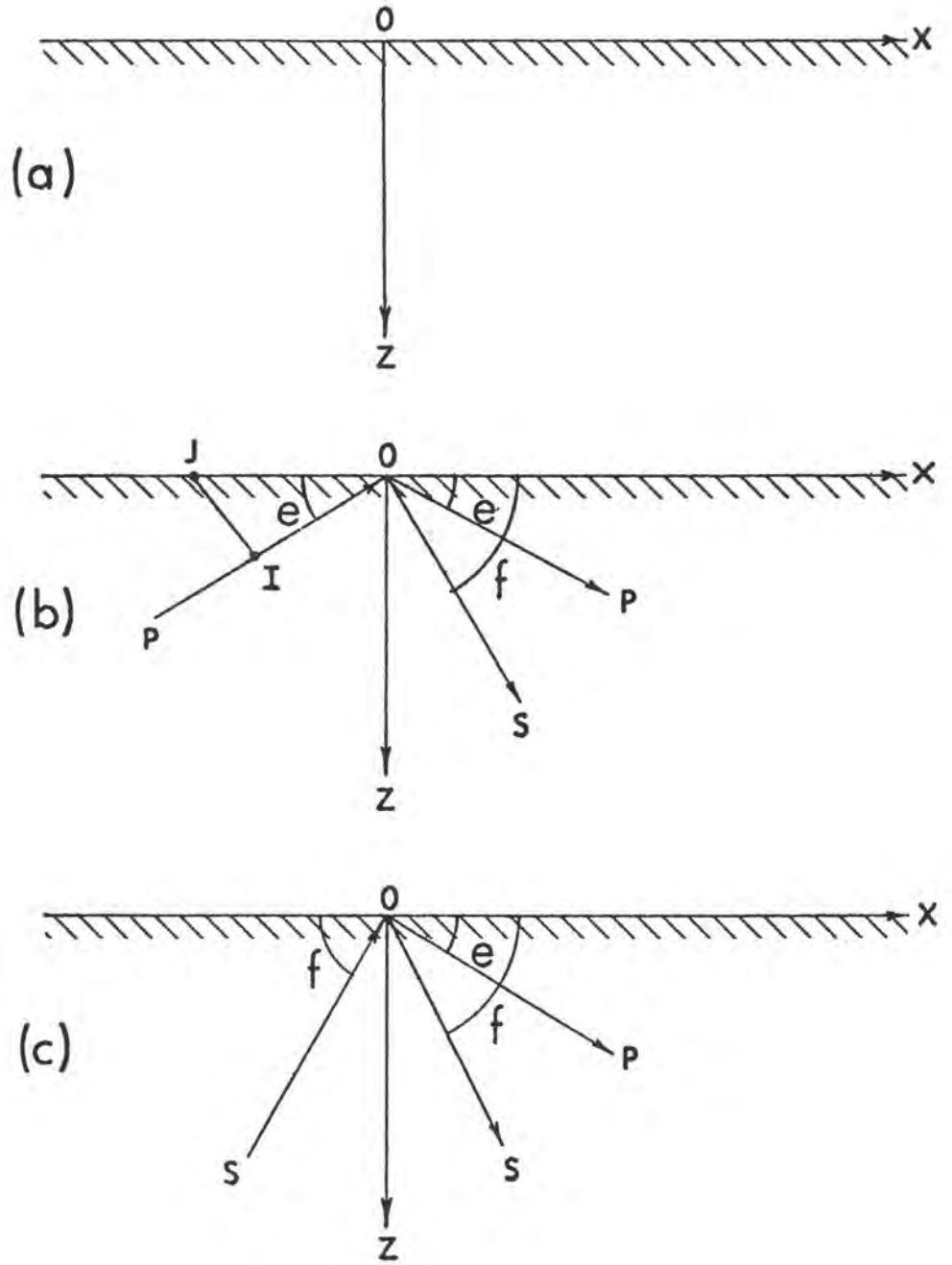

Fig. 3

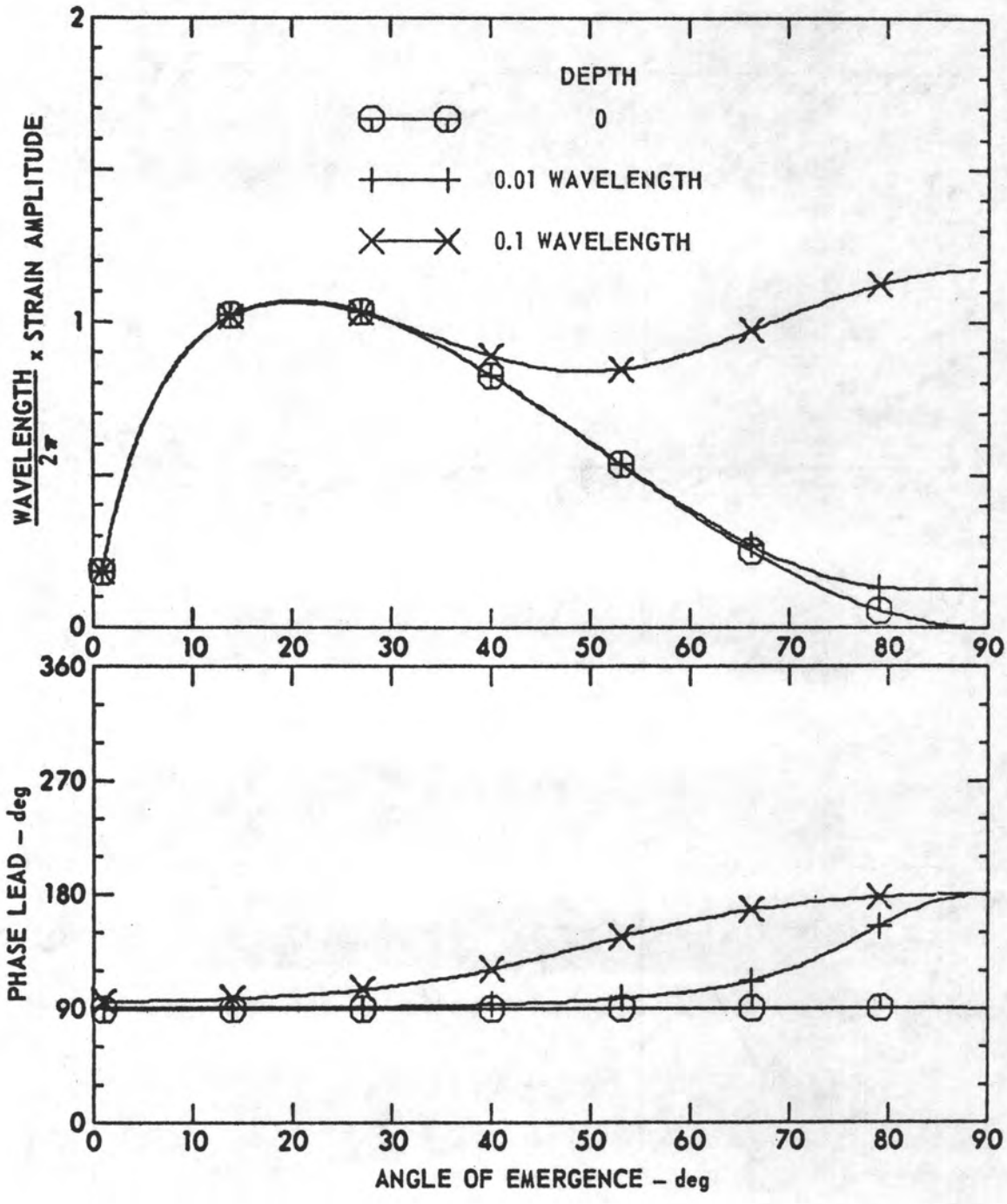
DEPTH
0
0.01 WAVELENGTH
0.1 WAVELENGTH
WAVELENGTH / 2π x STRAIN AMPLITUDE
PHASE LEAD – deg
ANGLE OF EMERGENCE – deg
0
1
2
90
180
270
360
10
20
30
40
50
60
70
80

Fig. 4

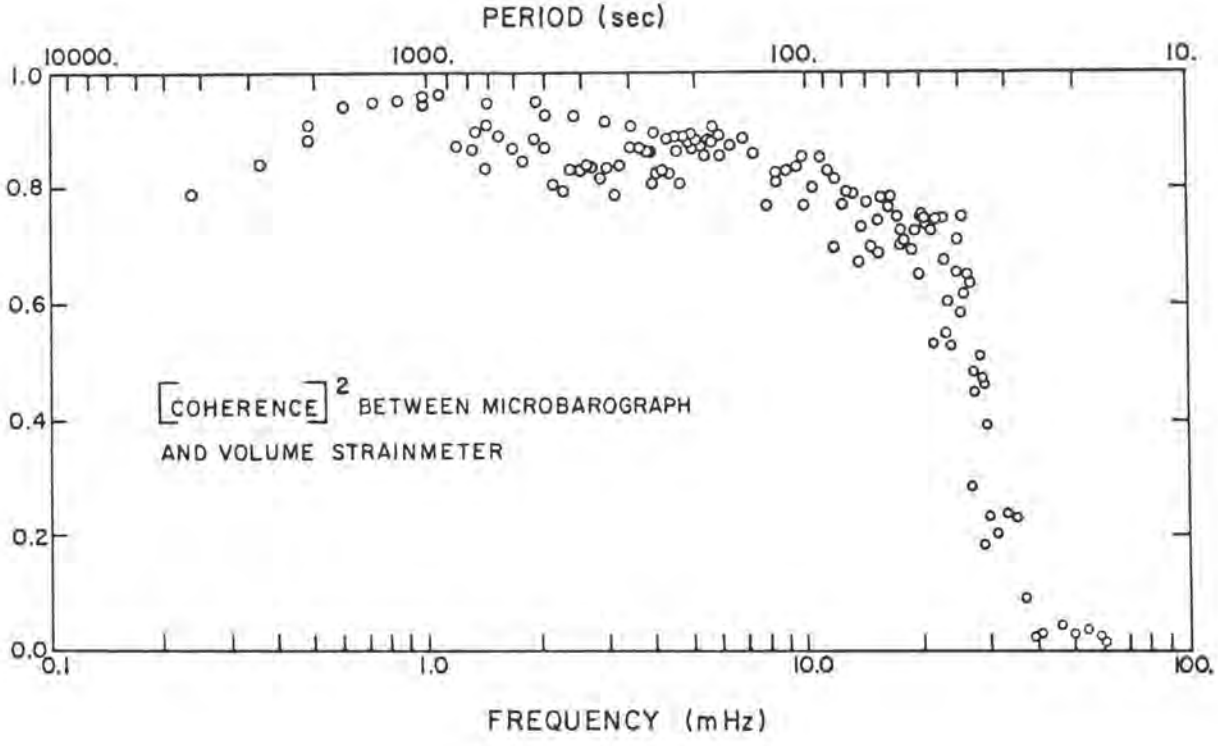
PERIOD (sec)
10000.
1000.
100.
10.
1.0
0.8
0.6
0.4
0.2
0.0
[COHERENCE]^2 BETWEEN MICROBAROGRAPH
AND VOLUME STRAINMETER
0.1
1.0
10.0
100.
FREQUENCY (mHz)

Fig. 12

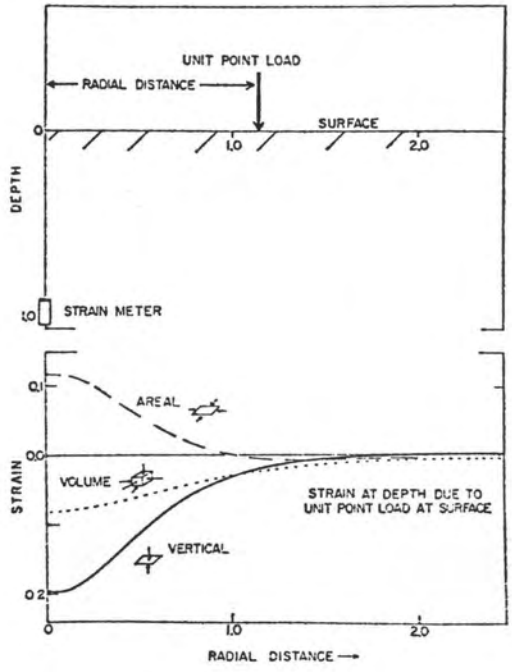
UNIT POINT LOAD
RADIAL DISTANCE
SURFACE
0
1.0
2.0
DEPTH
1.0
STRAIN METER
0.1
AREAL
0.0
VOLUME
STRAIN AT DEPTH DUE TO
UNIT POINT LOAD AT SURFACE
STRAIN
VERTICAL
0.2
0
1.0
2.0
RADIAL DISTANCE

Fig. 13

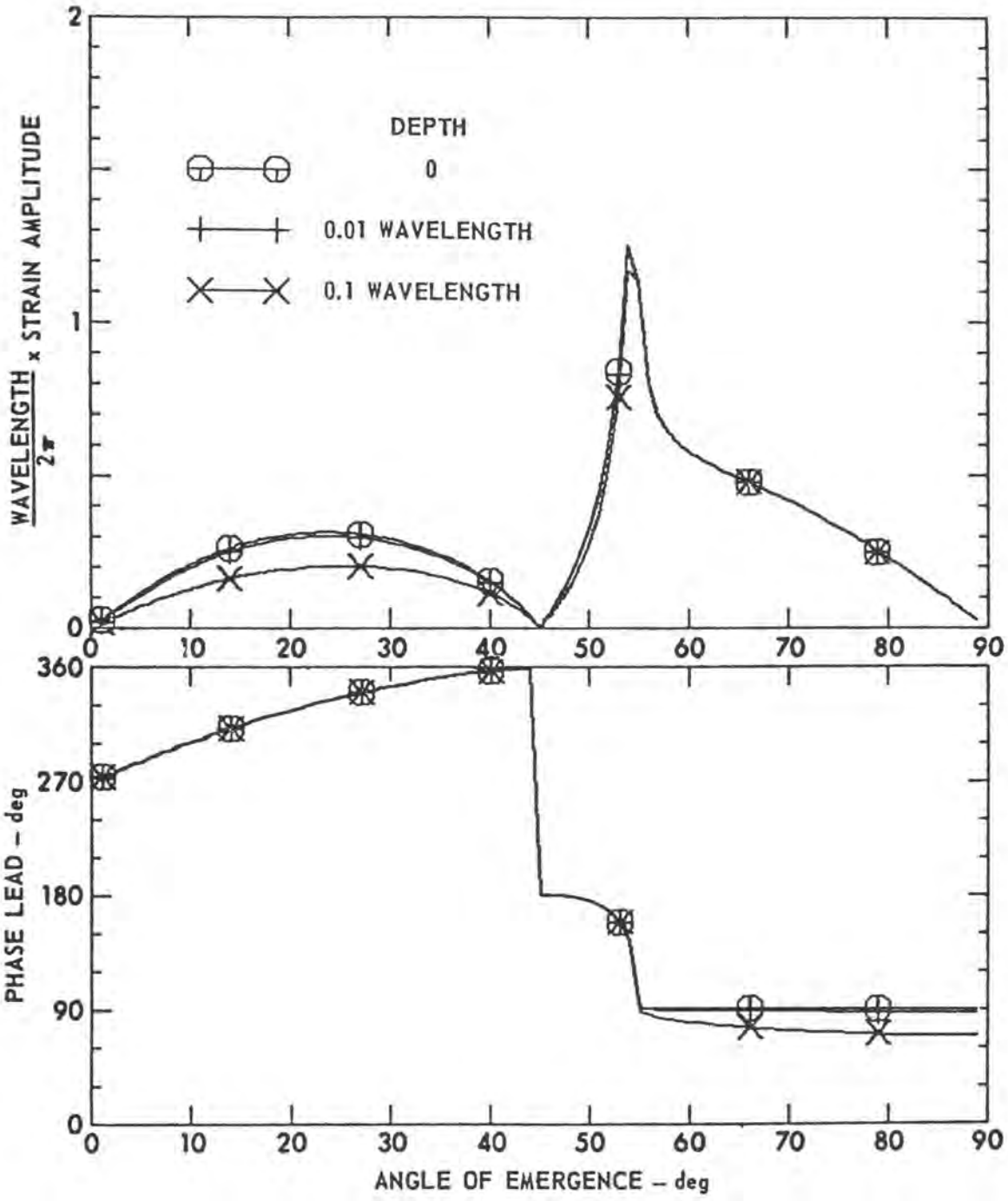
DEPTH
0
0.01 WAVELENGTH
0.1 WAVELENGTH
WAVELENGTH / 2π x STRAIN AMPLITUDE
PHASE LEAD – deg
ANGLE OF EMERGENCE – deg
0
1
2
90
180
270
360
10
20
30
40
50
60
70
80

Fig. 5

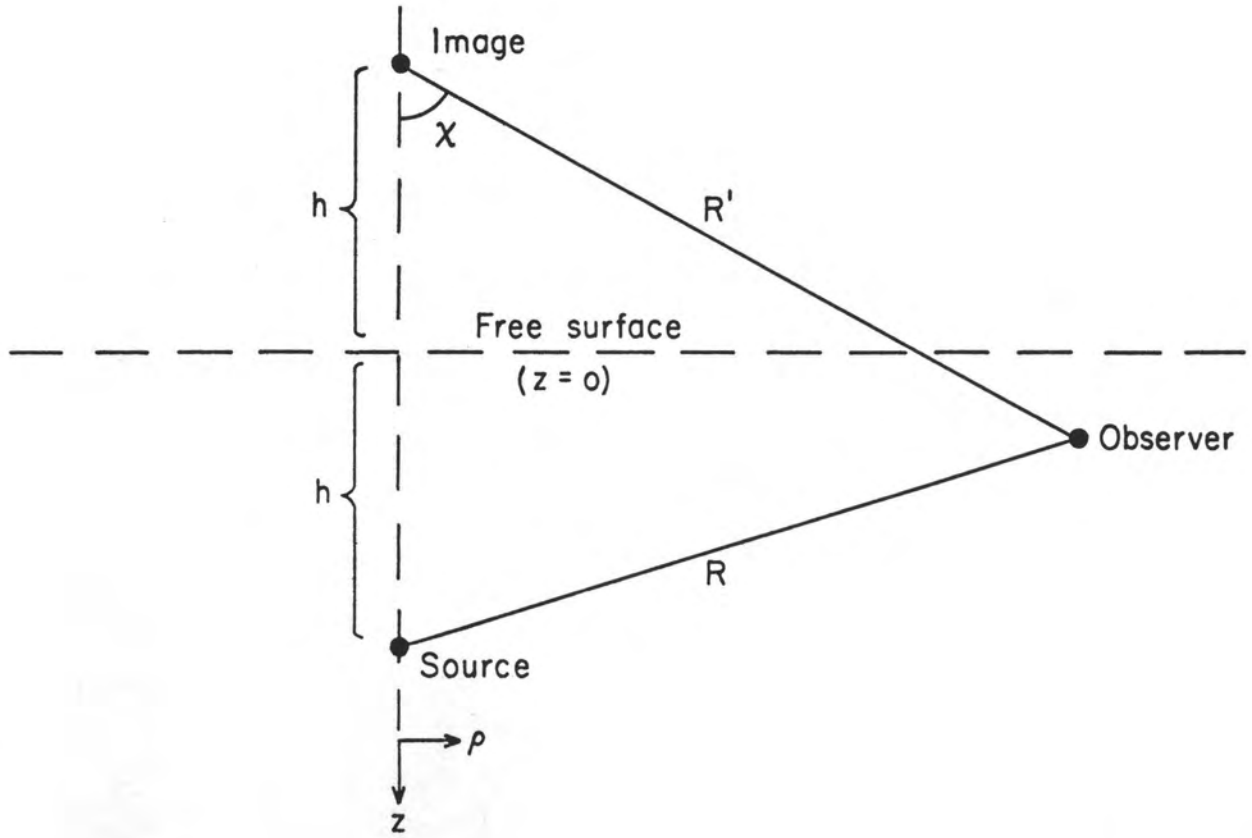

Fig. 6

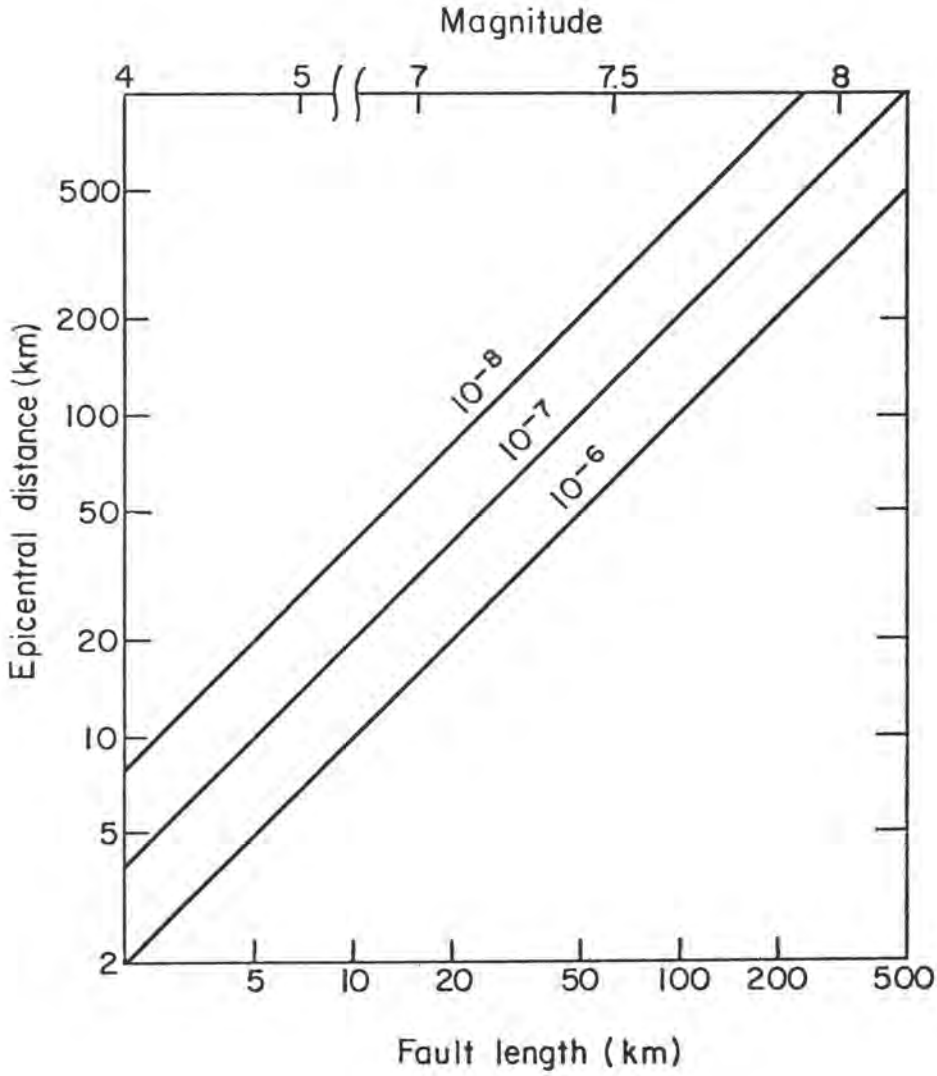
Magnitude
4
5
7
7.5
8
500
200
100
50
20
10
5
2
Epicentral distance (km)
10-8
10-7
10-6
5
10
20
50
100
200
500
Fault length (km)

Fig. 7

COMPARISON BETWEEN BOREHOLE STRAINMETER
AND QUARTZ BAR EXTENSOMETER

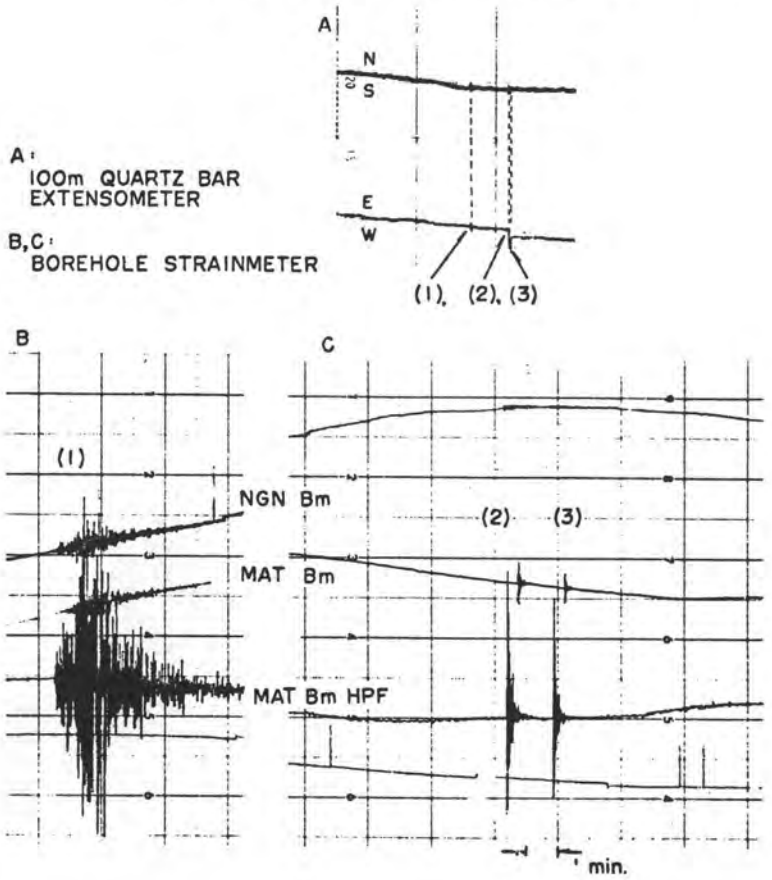

Fig. 8

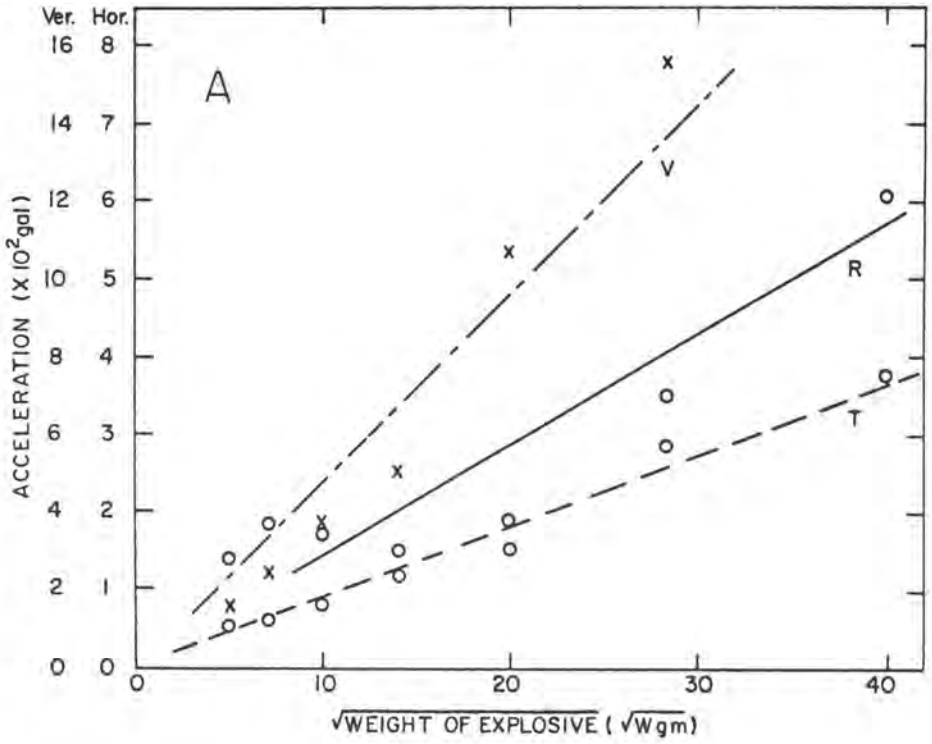
Ver.
Hor.
16
8
14
7
12
6
10
5
8
4
6
3
4
2
2
1
0
0
A
V
R
T
ACCELERATION (X 10² gal)
0
10
20
30
40
√WEIGHT OF EXPLOSIVE (√Wgm)

Fig. 9a

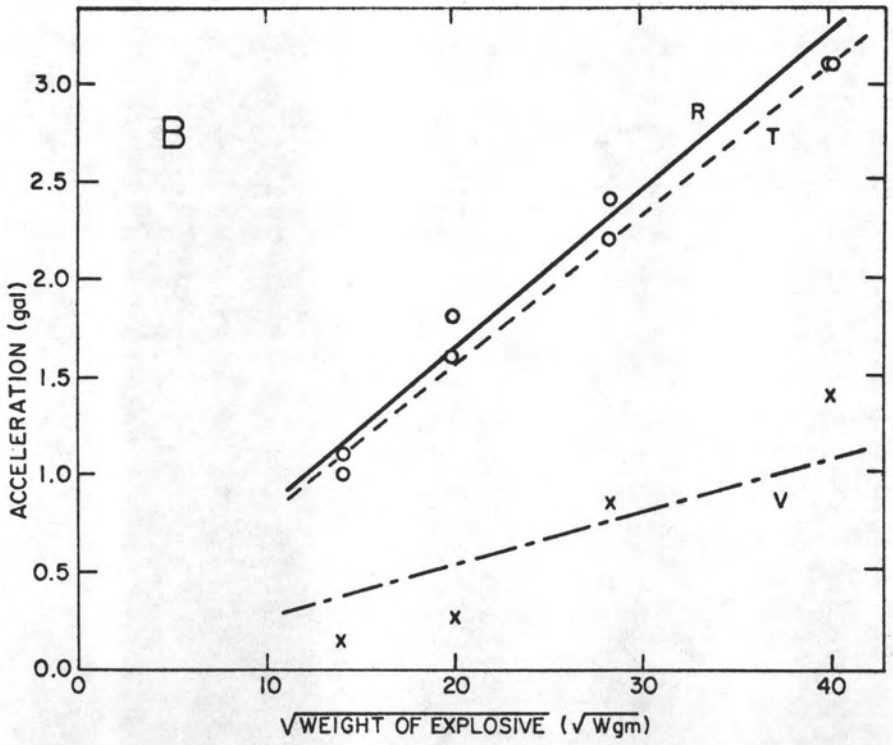
B
R
T
V
ACCELERATION (gal)
3.0
2.5
2.0
1.5
1.0
0.5
0.0
0
10
20
30
40
√WEIGHT OF EXPLOSIVE (√Wgm)

Fig. 9b

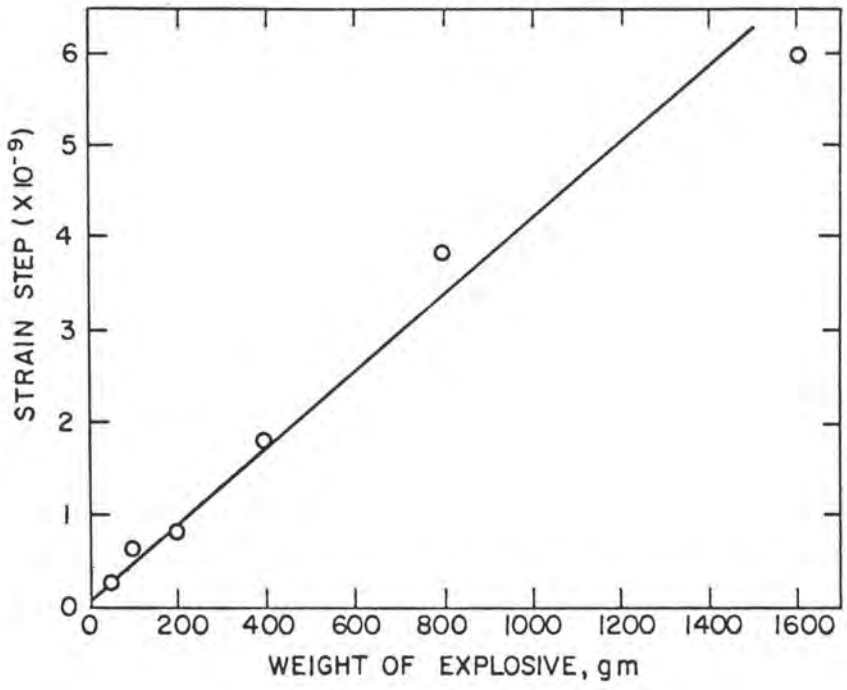
STRAIN STEP (X 10⁻⁹)
0
1
2
3
4
5
6
0
200
400
600
800
1000
1200
1400
1600
WEIGHT OF EXPLOSIVE, gm

Fig. 10

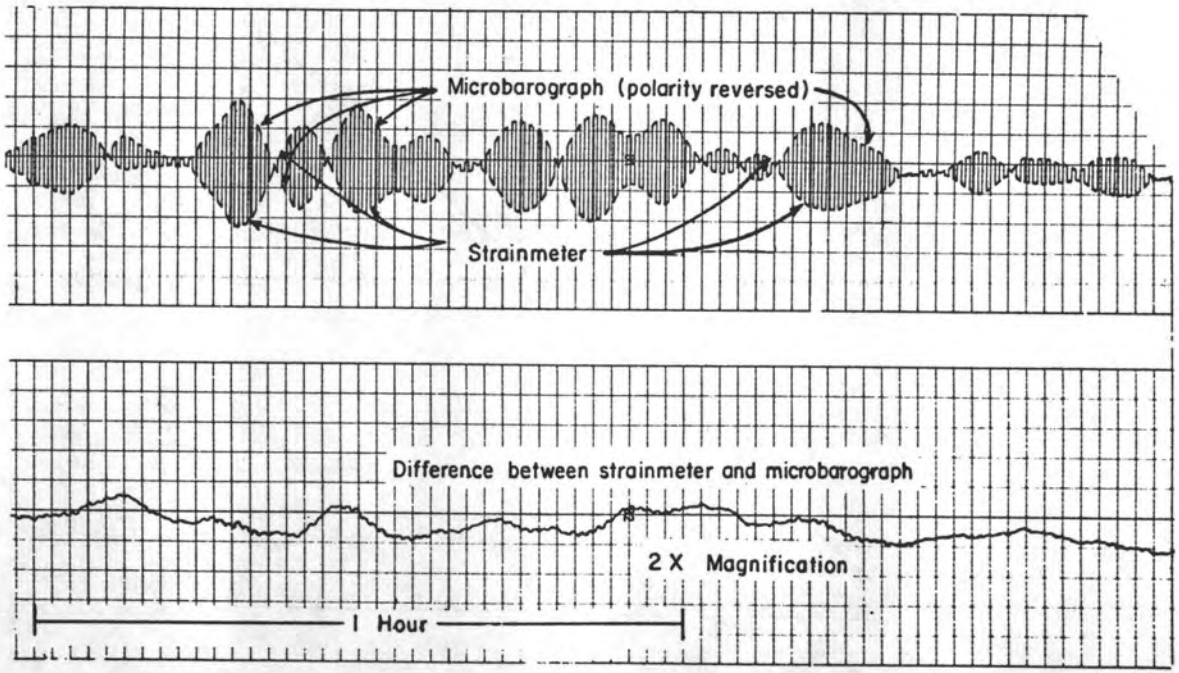
Microbarograph (polarity reversed)
Strainmeter
Difference between strainmeter and microbarograph
2 X Magnification
1 Hour

Fig. 11

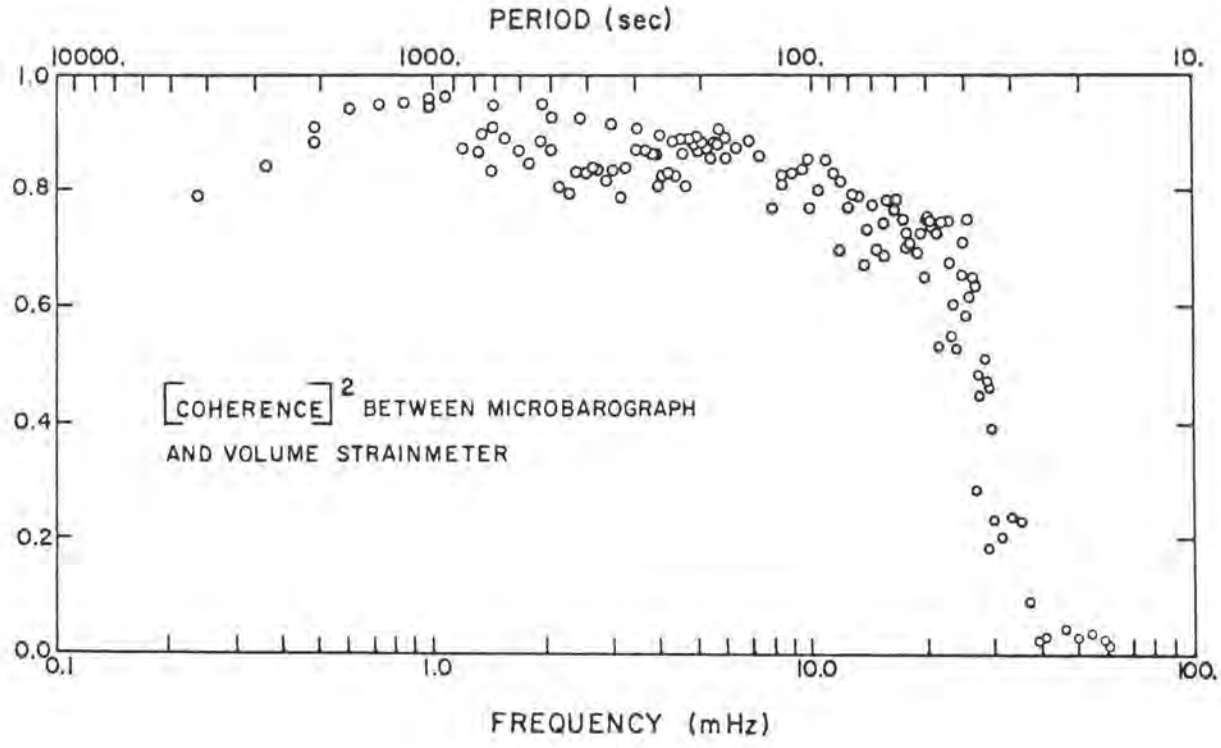
PERIOD (sec)
10000.
1000.
100.
10.
1.0
0.8
0.6
0.4
0.2
0.0
[COHERENCE]² BETWEEN MICROBAROGRAPH
AND VOLUME STRAINMETER
0.1
1.0
10.0
100.
FREQUENCY (mHz)

Fig. 12

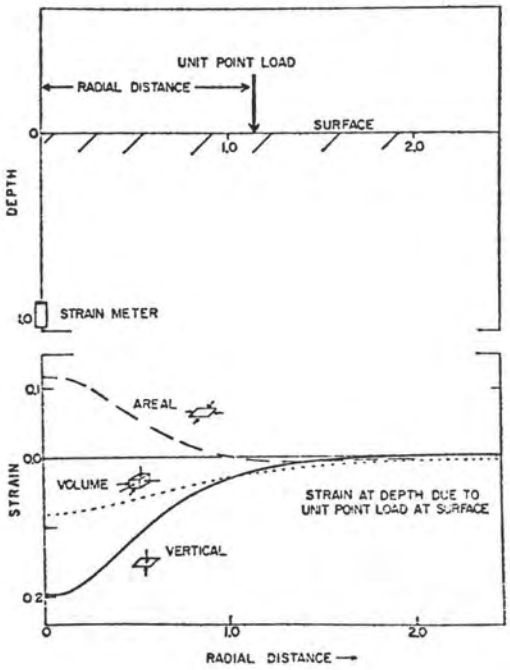
UNIT POINT LOAD
RADIAL DISTANCE
SURFACE
0
1.0
2.0
DEPTH
1.0
STRAIN METER
0.1
AREAL
0.0
VOLUME
STRAIN
STRAIN AT DEPTH DUE TO
UNIT POINT LOAD AT SURFACE
VERTICAL
0.2
0
1.0
2.0
RADIAL DISTANCE

Fig. 13

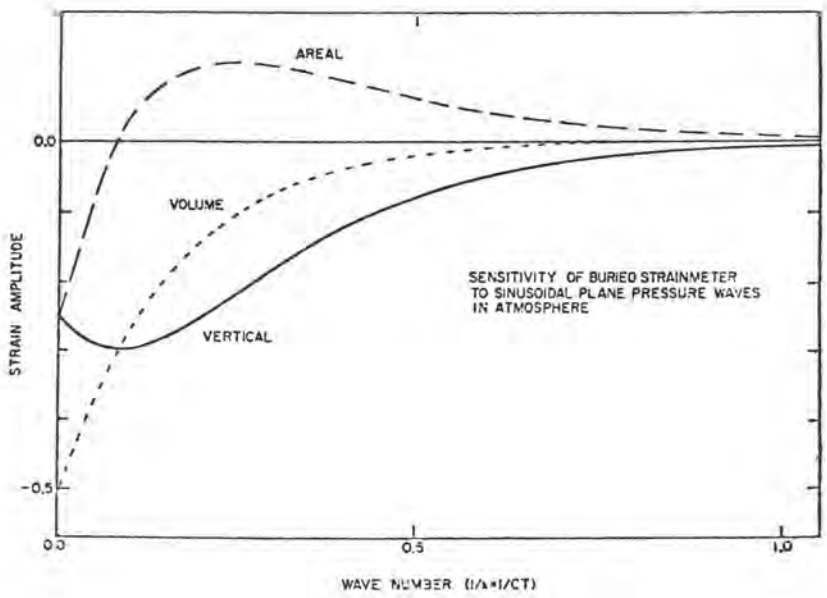
AREAL
VOLUME
VERTICAL
SENSITIVITY OF BURIED STRAINMETER
TO SINUSOIDAL PLANE PRESSURE WAVES
IN ATMOSPHERE
STRAIN AMPLITUDE
0.0
-0.5
0.0
0.5
1.0
WAVE NUMBER (1/λ=1/CT)

Fig. 14

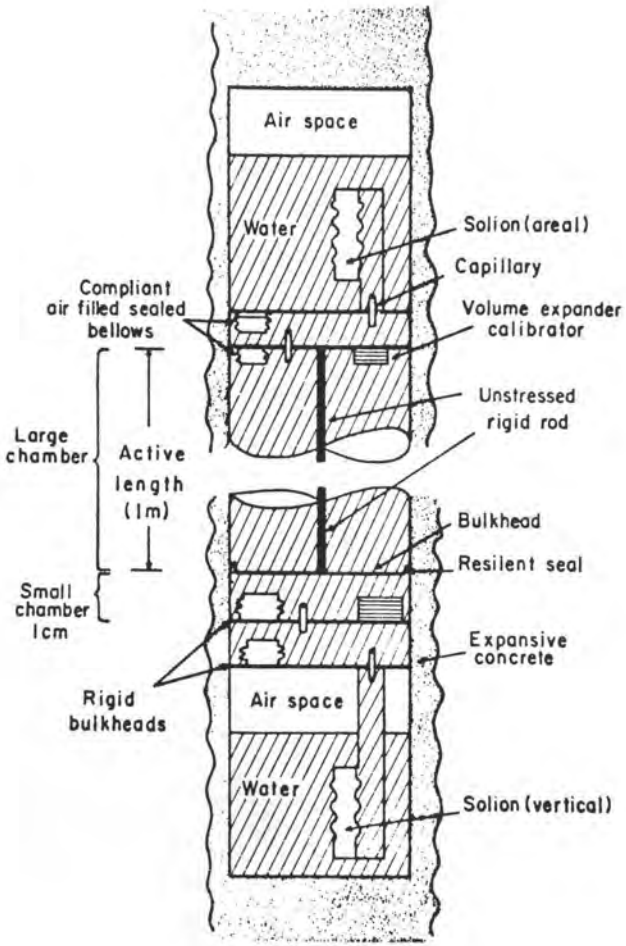
Air space
Water
Solion (areal)
Capillary
Compliant
air filled sealed
bellows
Volume expander
calibrator
Unstressed
rigid rod
Large
chamber
Active
length
(1m)
Bulkhead
Resilent seal
Small
chamber
1cm
Expansive
concrete
Rigid
bulkheads
Air space
Water
Solion (vertical)

Fig. 15

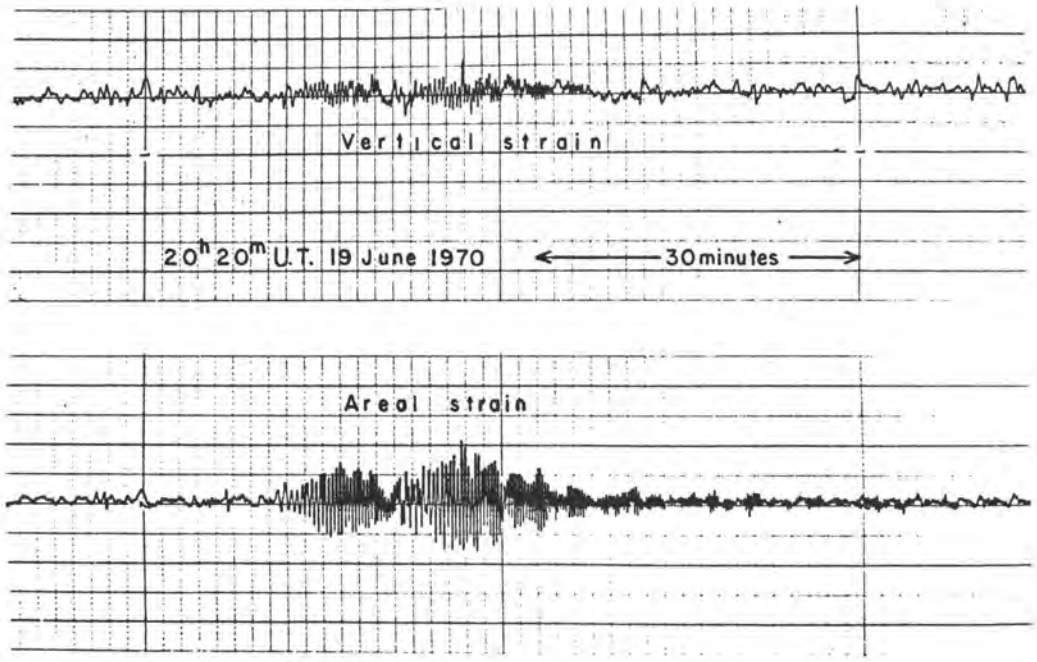
Vertical strain
20h 20m U.T. 19 June 1970
30 minutes
Areal strain

Fig. 16

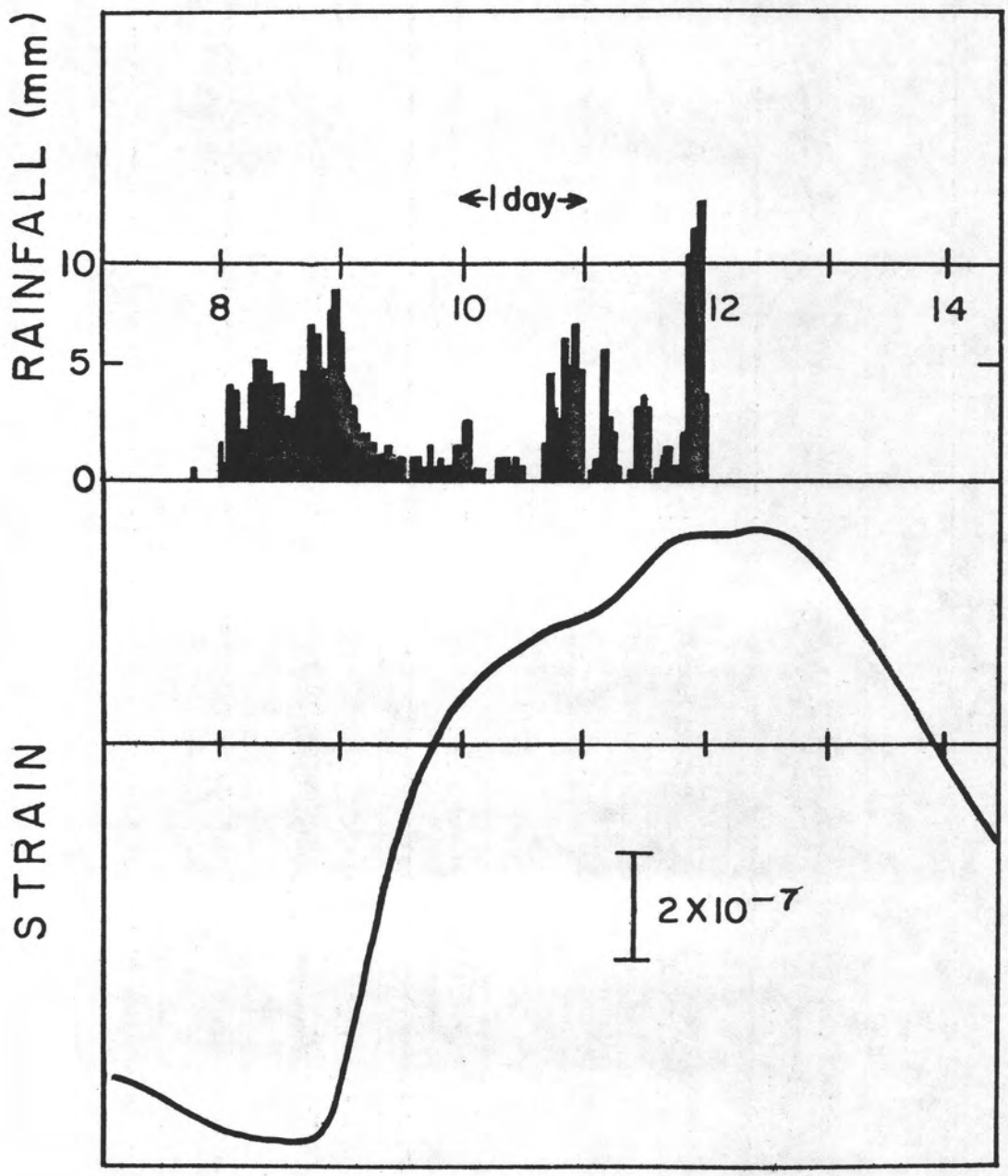

Fig. 17. Extensometer data.

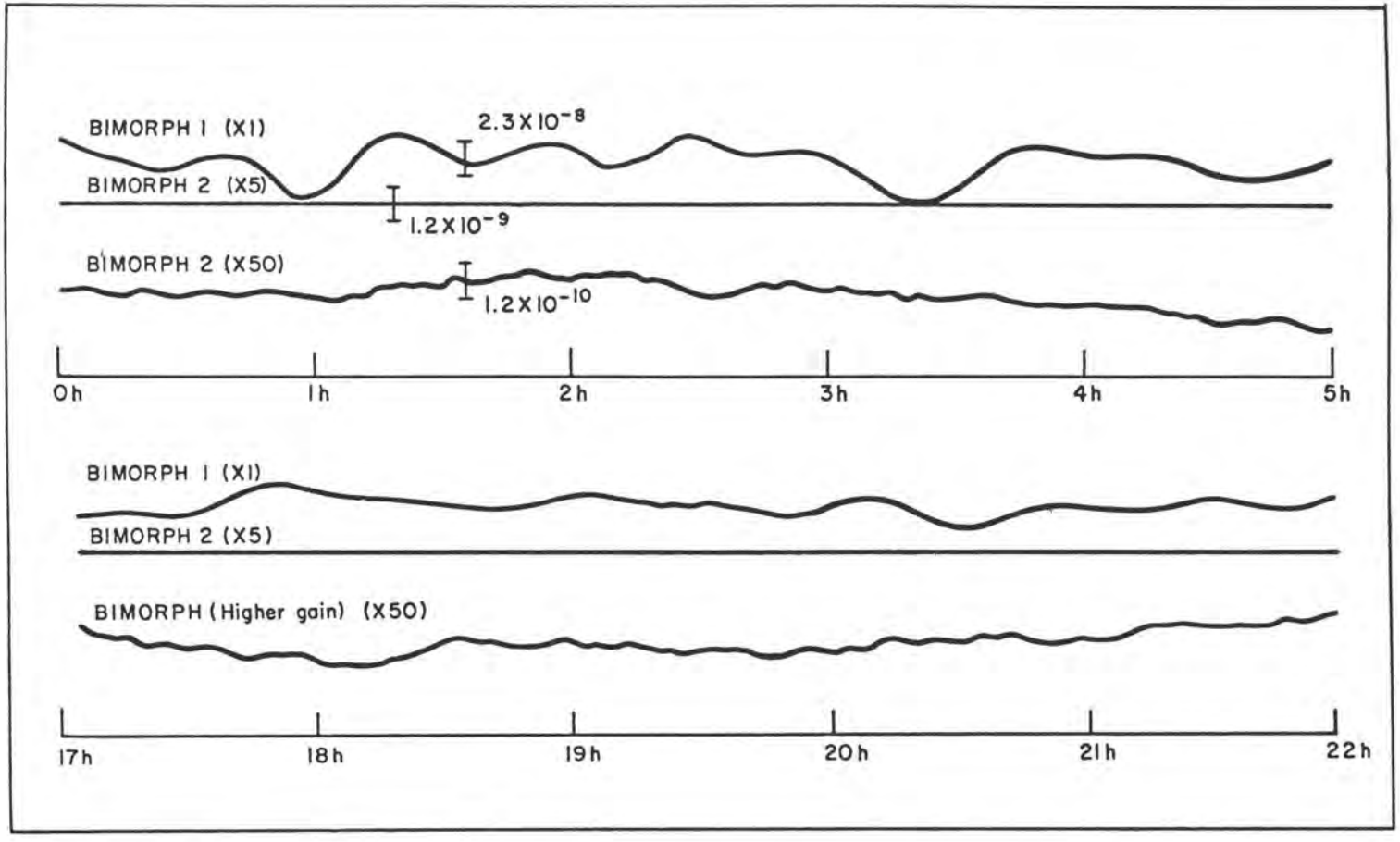
BIMORPH 1 (X1)
2.3X10⁻⁸
BIMORPH 2 (X5)
1.2X10⁻⁹
BIMORPH 2 (X50)
1.2X10⁻¹⁰
0h
1h
2h
3h
4h
5h
BIMORPH 1 (X1)
BIMORPH 2 (X5)
BIMORPH (Higher gain) (X50)
17h
18h
19h
20h
21h
22h

Fig. 18

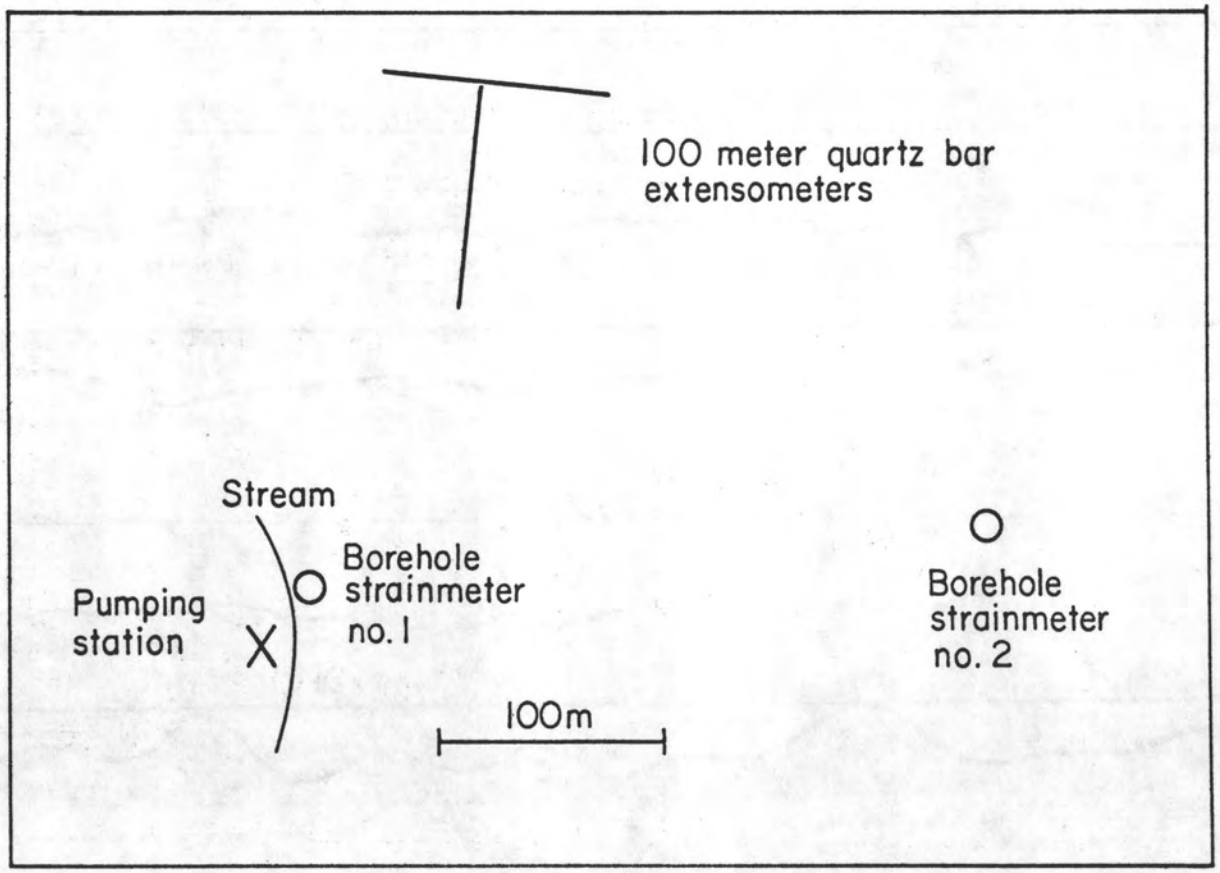
100 meter quartz bar
extensometers
Stream
Borehole
strainmeter
no. 1
Pumping
station
Borehole
strainmeter
no. 2
100m

Fig. 19

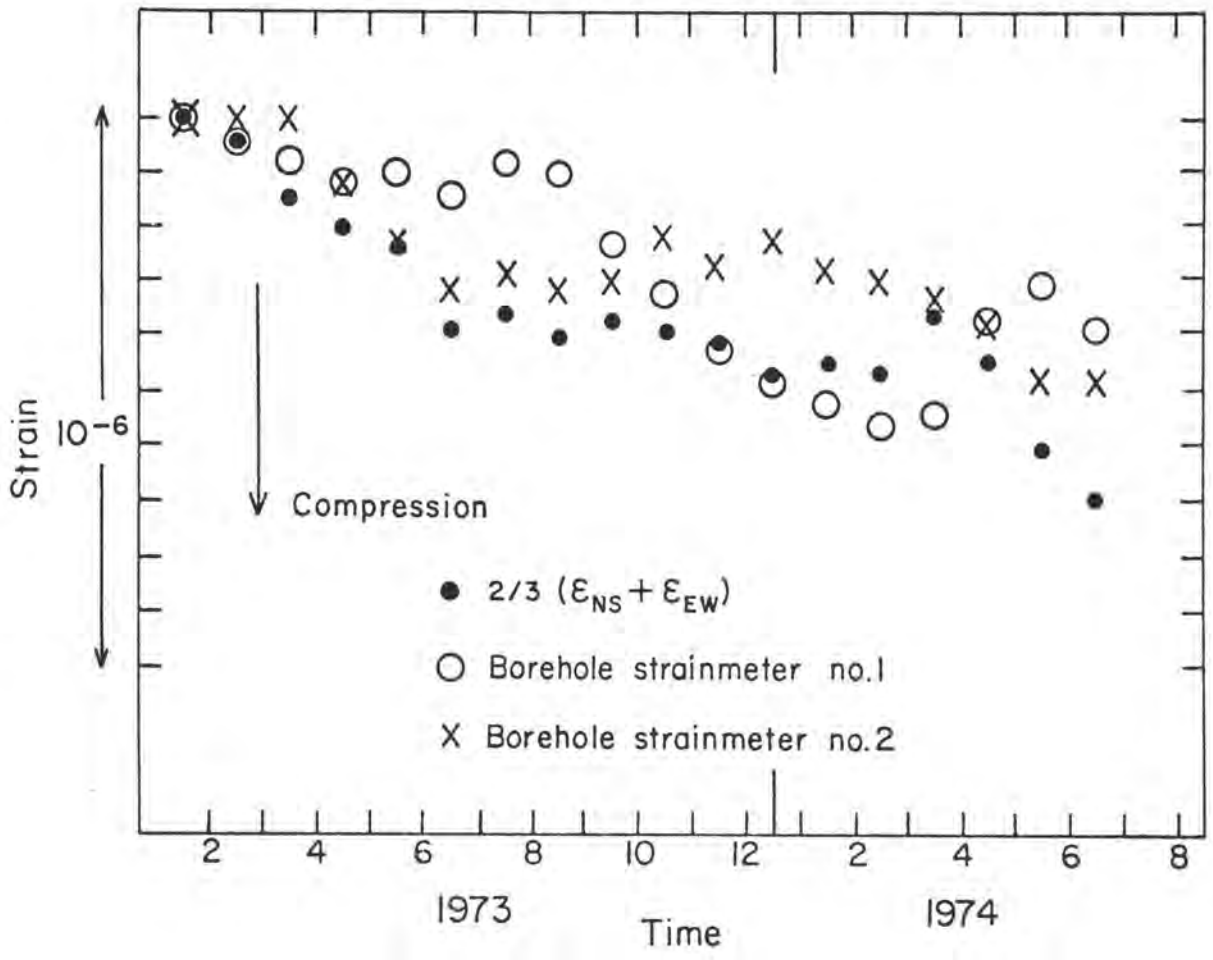
Strain
10^{-6}
Compression
● 2/3 ($\varepsilon_{NS}+\varepsilon_{EW}$)
○ Borehole strainmeter no.1
X Borehole strainmeter no.2
2
4
6
8
10
12
2
4
6
8
1973
Time
1974

Fig. 20

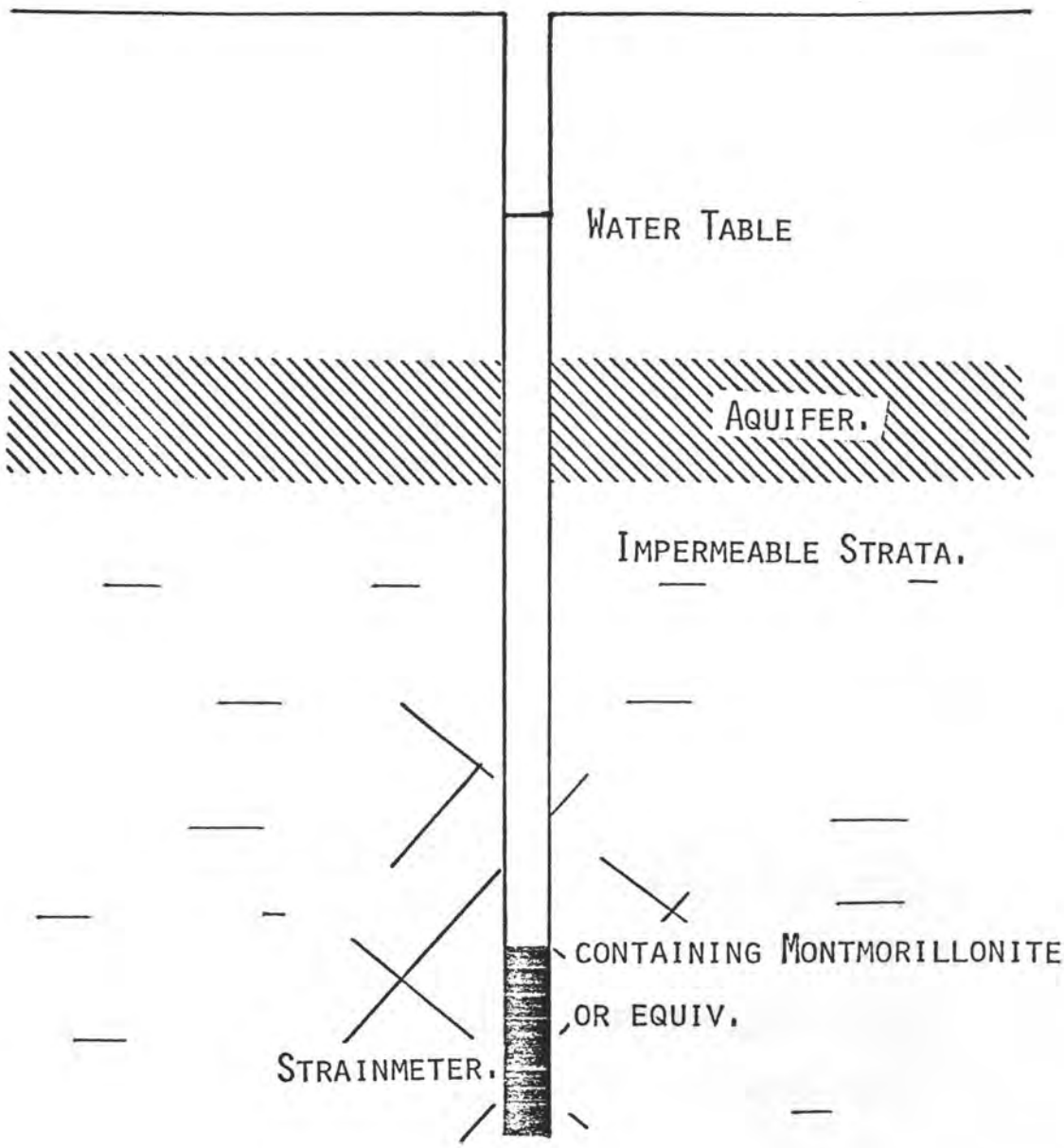
WATER TABLE
AQUIFER.
IMPERMEABLE STRATA.
CONTAINING MONTMORILLONITE
OR EQUIV.
STRAINMETER.

Fig. 21

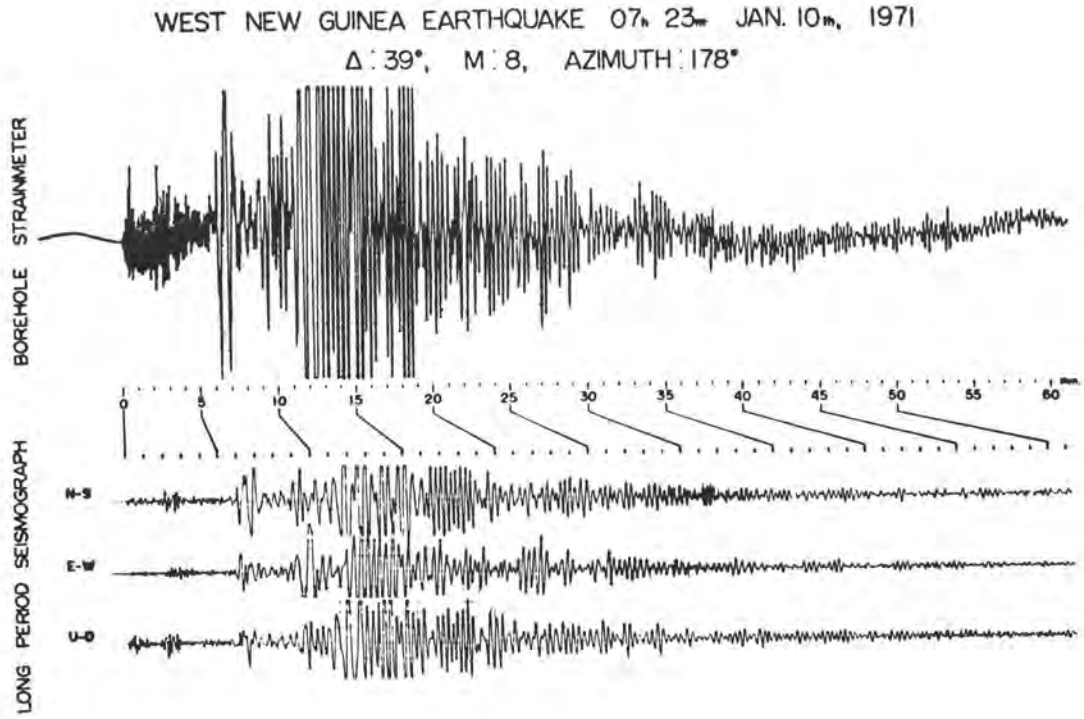
WEST NEW GUINEA EARTHQUAKE 07h 23m JAN. 10th, 1971
Δ : 39°, M : 8, AZIMUTH : 178°
BOREHOLE STRAINMETER
0
5
10
15
20
25
30
35
40
45
50
55
60
min.
LONG PERIOD SEISMOGRAPH
N-S
E-W
U-D

Fig. 22

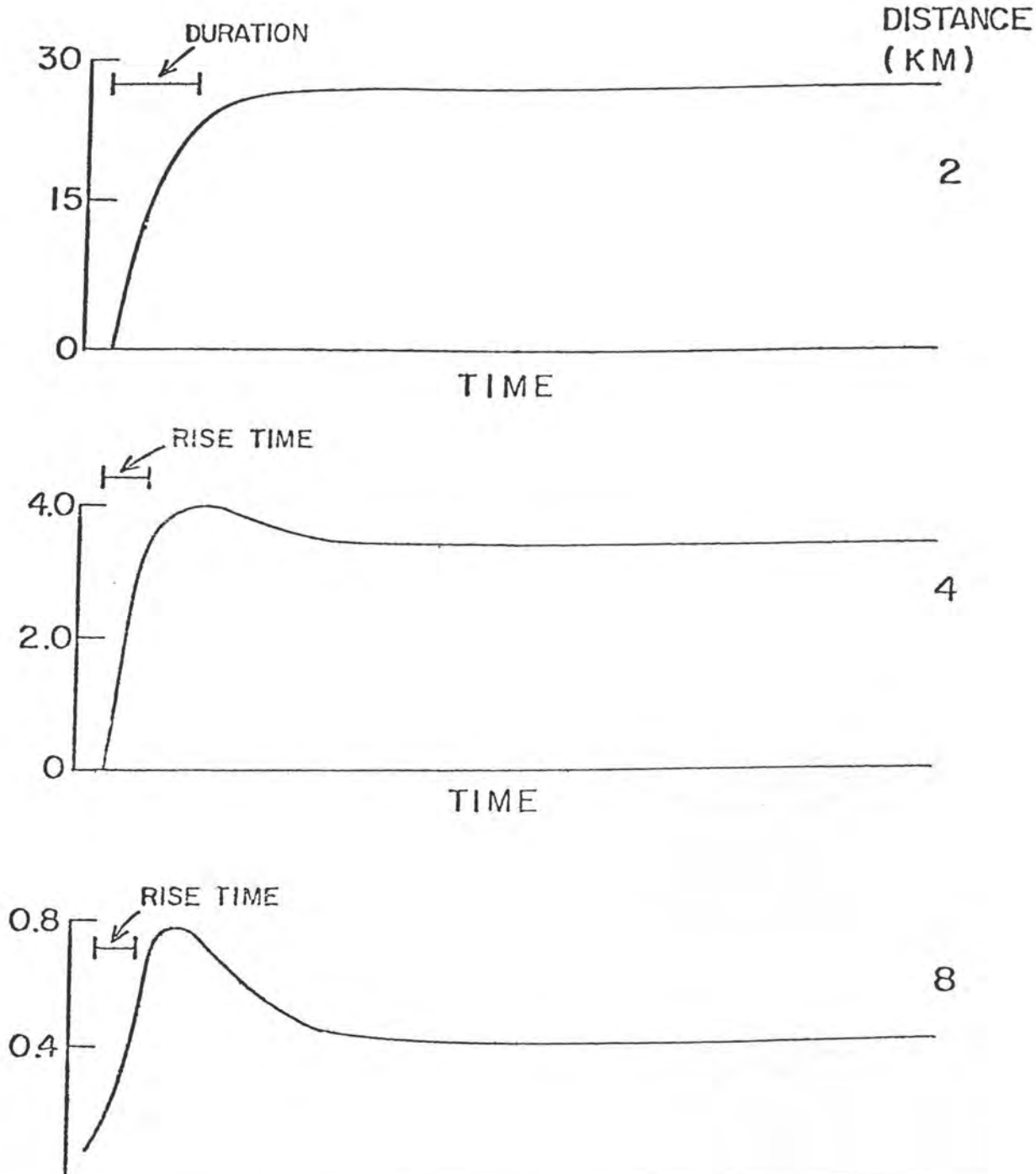
RADIAL STRAIN VS TIME
DISTANCE
(KM)
DURATION
30
15
0
TIME
2
RISE TIME
4.0
2.0
0
TIME
4
RISE TIME
0.8
0.4
TIME
8

Fig. 23

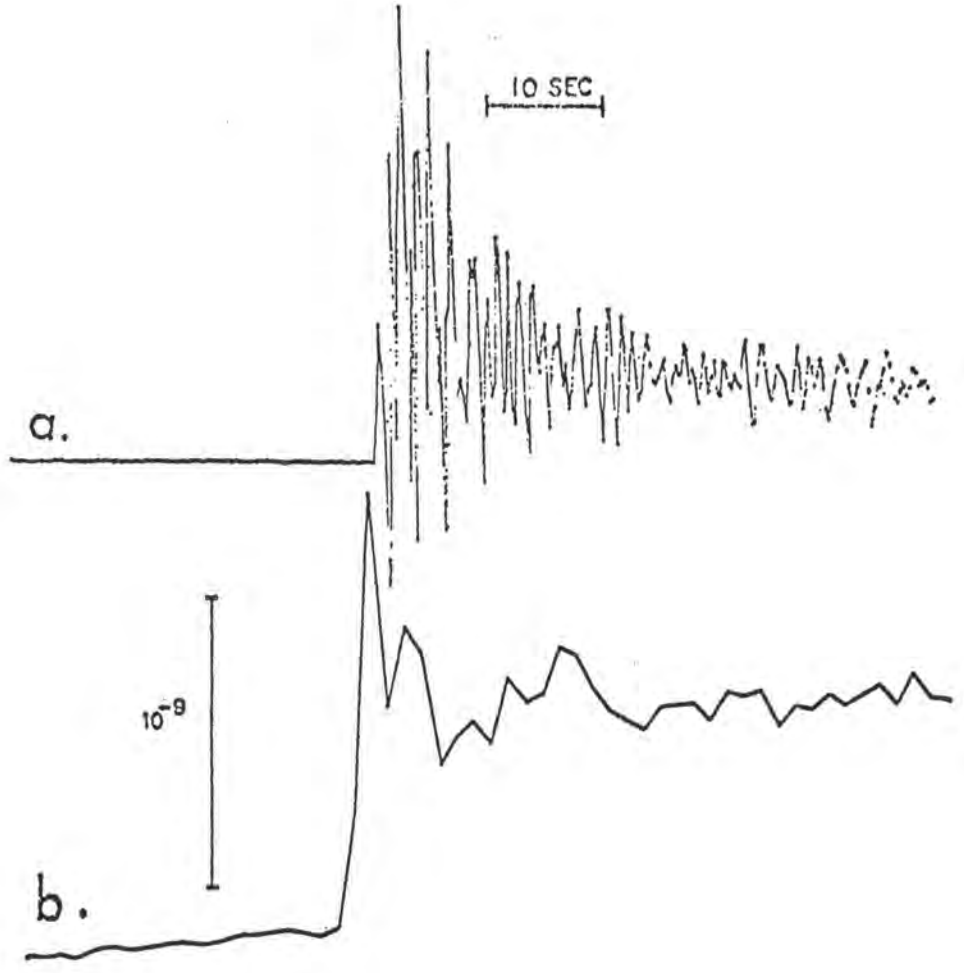

Fig. 24

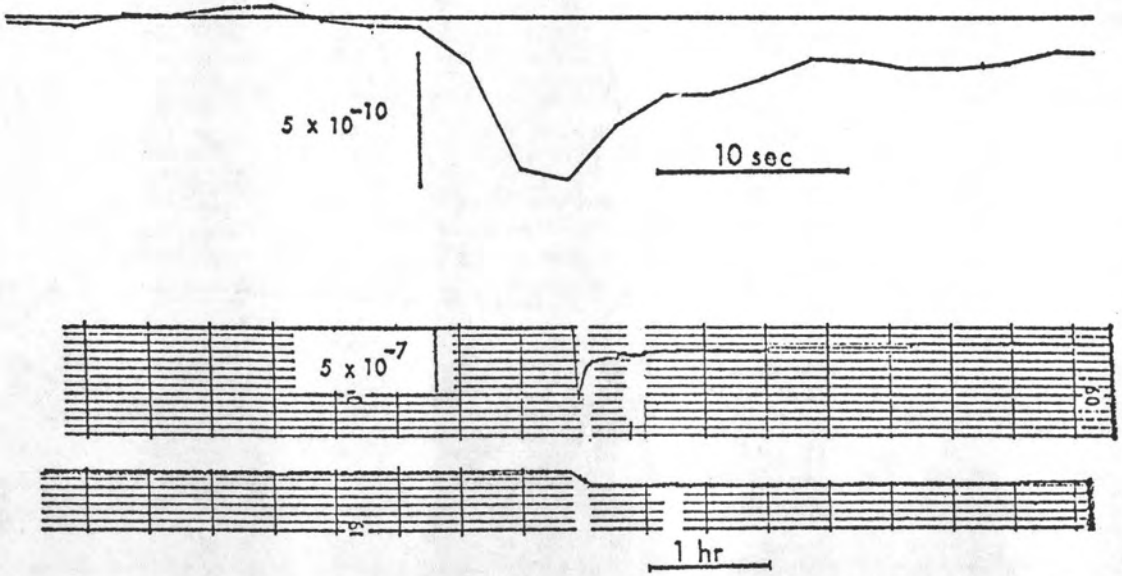

Fig. 25

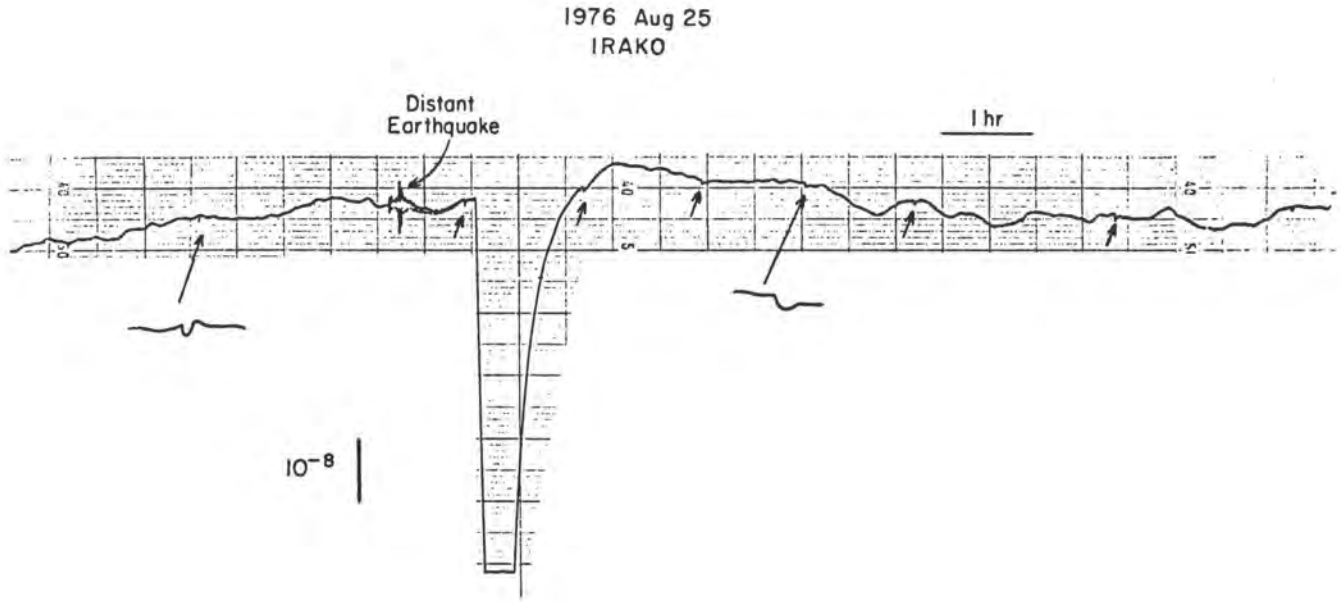

Fig. 26

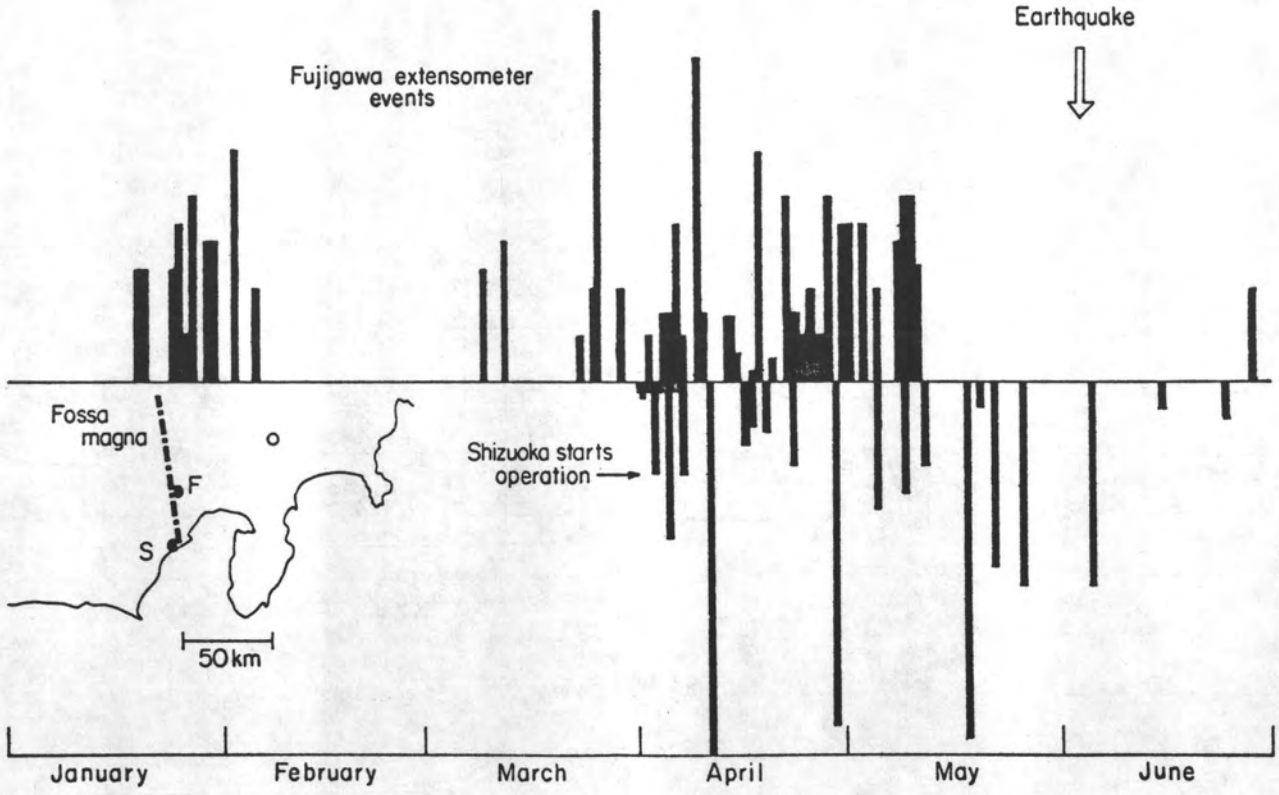
Earthquake
Fujigawa extensometer events
Fossa magna
F
S
o
Shizuoka starts operation
50km
January
February
March
April
May
June

Fig. 27

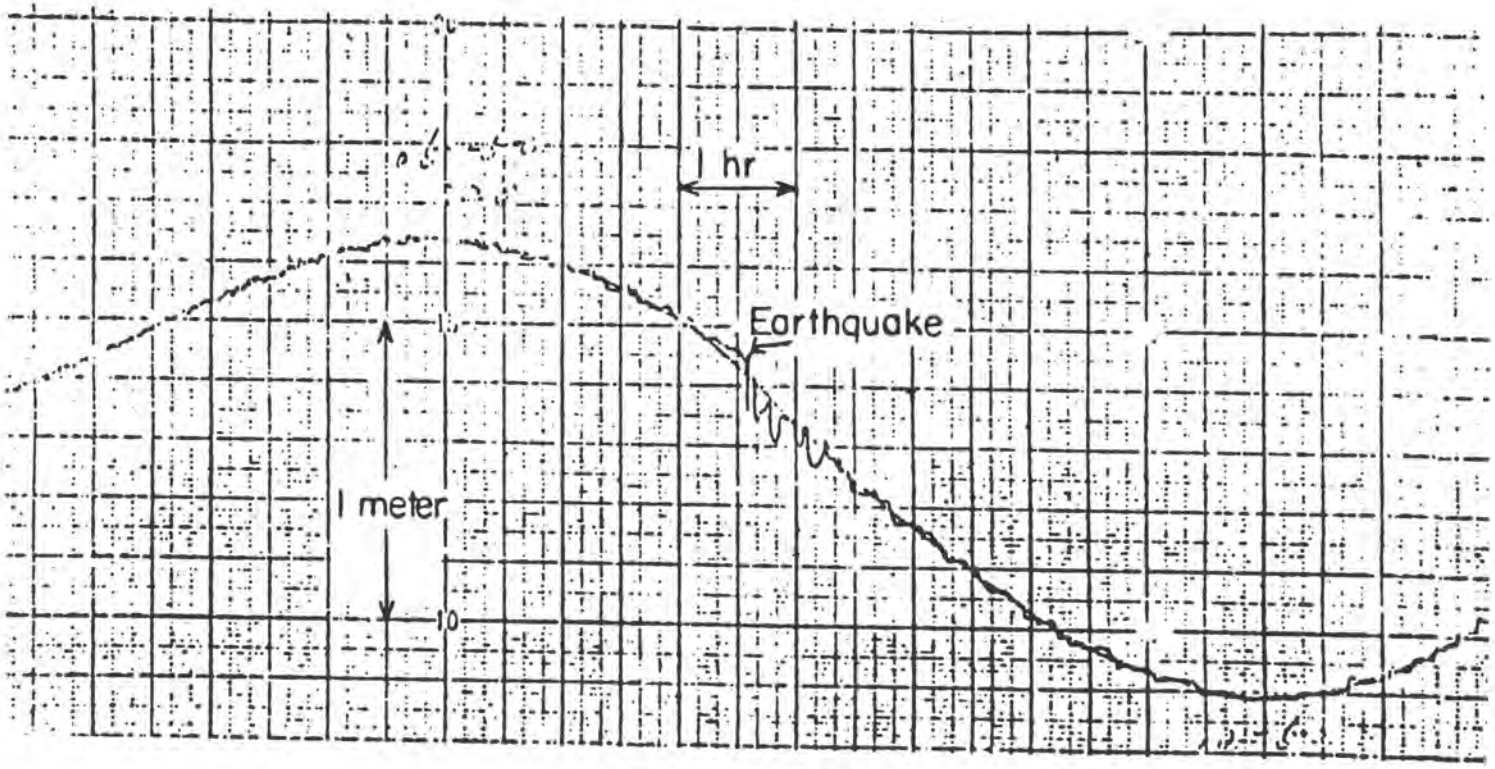

Fig. 28


AUGUST, 1976
+ 10
+ 15
0
0
0
FEBRUARY, 1976
+10
+6
+4
+5
+2
+3
0
1969—1975
+6
+5
+4
+3
+2
+1
0

Fig. 29

NEAR-SURFACE *IN SITU* STRESS MEASUREMENTS ALONG THE 1857 BREAK OF THE SAN ANDREAS FAULT

Marc L. Sbar
University of Arizona
Department of Geosciences
Tucson, Arizona 85721

Terry Engelder
Lamont-Doherty Geological Observatory
Palisades, New York 10964

Terry Tullis
Department of Geological Sciences
Brown University
Providence, Rhode Island 02912

ABSTRACT

Two teams, one using the "doorstopper" method and the other using the U.S. Bureau of Mines strain-relaxation technique, made in situ stress measurements at eighteen sites distributed about the San Andreas Fault near Palmdale. Twelve of those sites were along a 35 km transect running from the foothills of the San Gabriel Mountains into the western Mojave Desert southeast of Palmdale. The purpose of this experiment is to measure the tectonic stress field near a historically active fault where we expect it to be modified by the presence of the fault. Measurements of this type may be useful in evaluating the level of strain accumulation on active faults.

Principal stress orientations measured with the above two techniques were consistent at the same site and nearby sites, although the magnitude of stress determined with the Bureau of Mines technique was uniformly less than that determined with the doorstopper method. The maximum compressive stress (σ_1) at the northernmost sites is N-S to NNE similar to the regional stress field inferred from fault plane solutions of earthquakes in southern California. Nearer the San Andreas fault, the orientation of σ_1 is approximately E-W north of the fault and NW-SE to N-S south of the fault.

The favorable comparison of two in situ stress measuring techniques and the similarity to the regional stress orientations away from the fault suggests that we reliably determined the stress orientation present at a site. The stress pattern that was determined is consistent with a model in which the regional tectonic stress field is modified by the presence of a fault. It is not possible, however, using the available data, to distinguish the stress caused by residual or topographic effects from tectonically applied stress, or to account for modification of the stress field by decoupling across fractures. Thus without many more measurements we cannot be certain of the relative contributions of these factors or the correct explanation for the stress observed.

INTRODUCTION

In situ stress measurements have been used with some success to analyze stress fields on a continental scale. Studies on this scale demonstrated that the principal stresses are uniform in orientation over large regions in the interior of North America (Sbar and Sykes, 1973) and central Europe (Ahorner, 1975). Sbar and Sykes (1977) added more data to their earlier work and were able to define domains of different stress orientation in eastern North America. Greiner and Illies, (1977) using a strain-relaxation technique, found that the magnitude of the maximum compressive stress increased southward from central Europe to the Alps. The validity of these results is primarily founded on the favorable comparison of independent means of assessing the stress field and the consistency of the measurements in a given area. Encouraged by the success of the above studies we embarked on the present effort, a pilot study to measure the tectonic stress field near the locked section of the San Andreas fault in southern California.

Theoretical and photoelastic models of strike-slip faults (Rodgers and Chinnery, 1973; Barber and Sowers, 1974) predict that a reorientation of stress trajectories occurs near faults across which there has been strain accumulation. The degree of reorientation is directly although not simply related to the strain accumulation. Thus, measurement of stress pattern near faults may provide important information about the dimensions and long-range timing of the eventual rupture on the fault. To test this hypothesis we made 41 in situ strain relaxation measurements at twelve sites along a broad profile perpendicular to the San Andreas fault, southeast of Palmdale, and ten measurements at six sites at other locations near the profile (Figures 1 and 2 and Table 1). Both U.S. Bureau of Mines (Tullis) and doorstopper (Sbar and Engelder) measurements were made at the same site and at nearby sites as a check on the methods. Each group performed the field work and analysis separately, but with a large degree of cooperation.

EXPERIMENTAL TECHNIQUE

All strain-relaxation techniques involve measurement of strain as a rock is decoupled from the surrounding rock mass. The stress that had been exerted on the rock prior to decoupling may be calculated from the strain relaxation if data on the mechanical properties of the rock are also known.

The doorstopper technique involves the bonding of a 3 component, foil-resistance strain gauge rosette to the bottom of a flattened borehole. A 79 mm diameter hole was used in this study. Strain is measured as the rock is separated from the host rock by overcoring. The core with the gauge still attached is then inserted into a radial loading chamber to determine the elastic constants of the rock. Stress is calculated from the elastic moduli and strain recovered. The details of this technique are discussed by (Engelder et al. 1978 and Sbar et al, 1978).

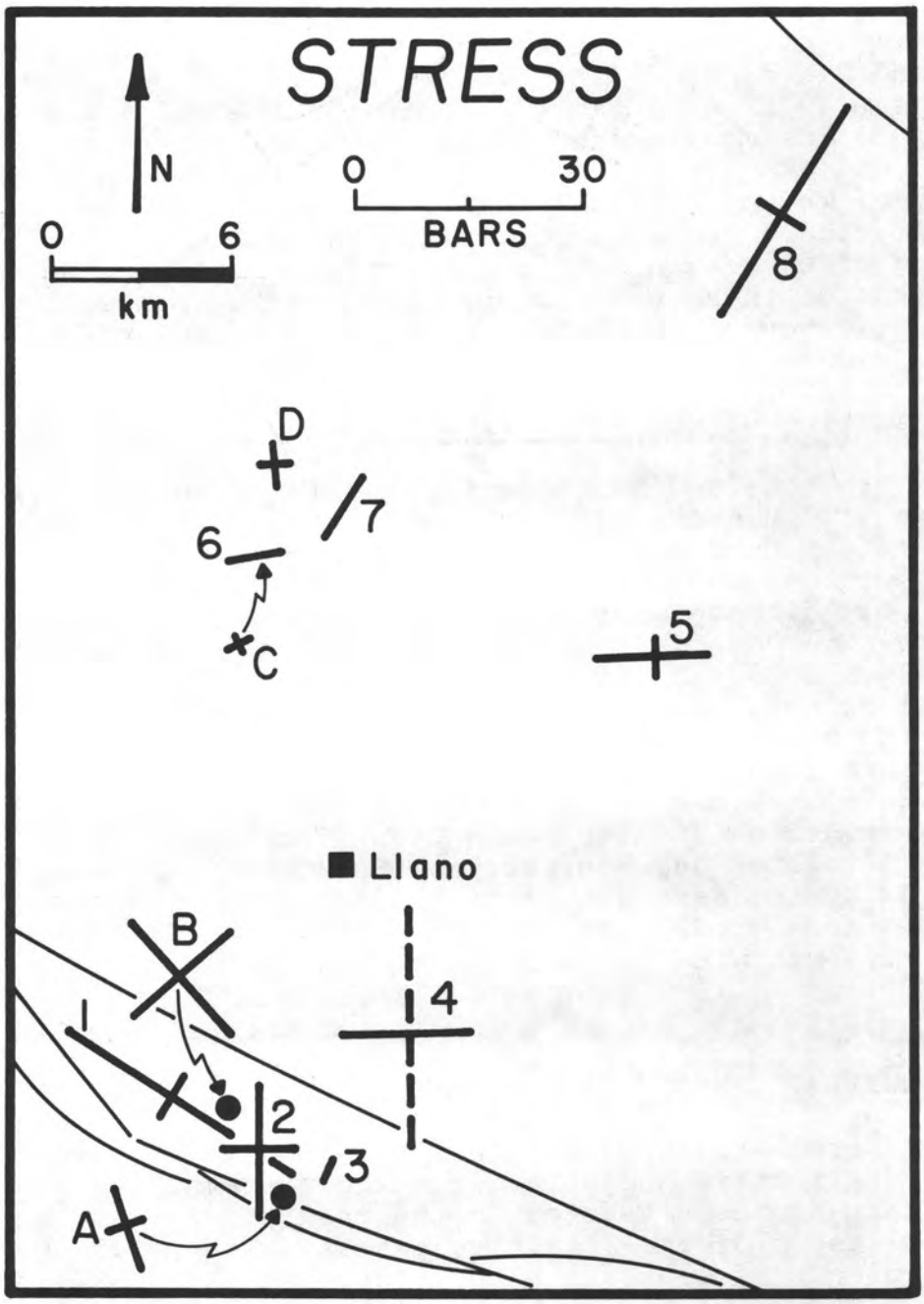

Figure 1 Tensor averages of the stress at each site. Letters refer to Bureau of Mines measurements and numbers refer to doorstopper measurements. Sites 6 and C are at the same location. Thin lines are faults.

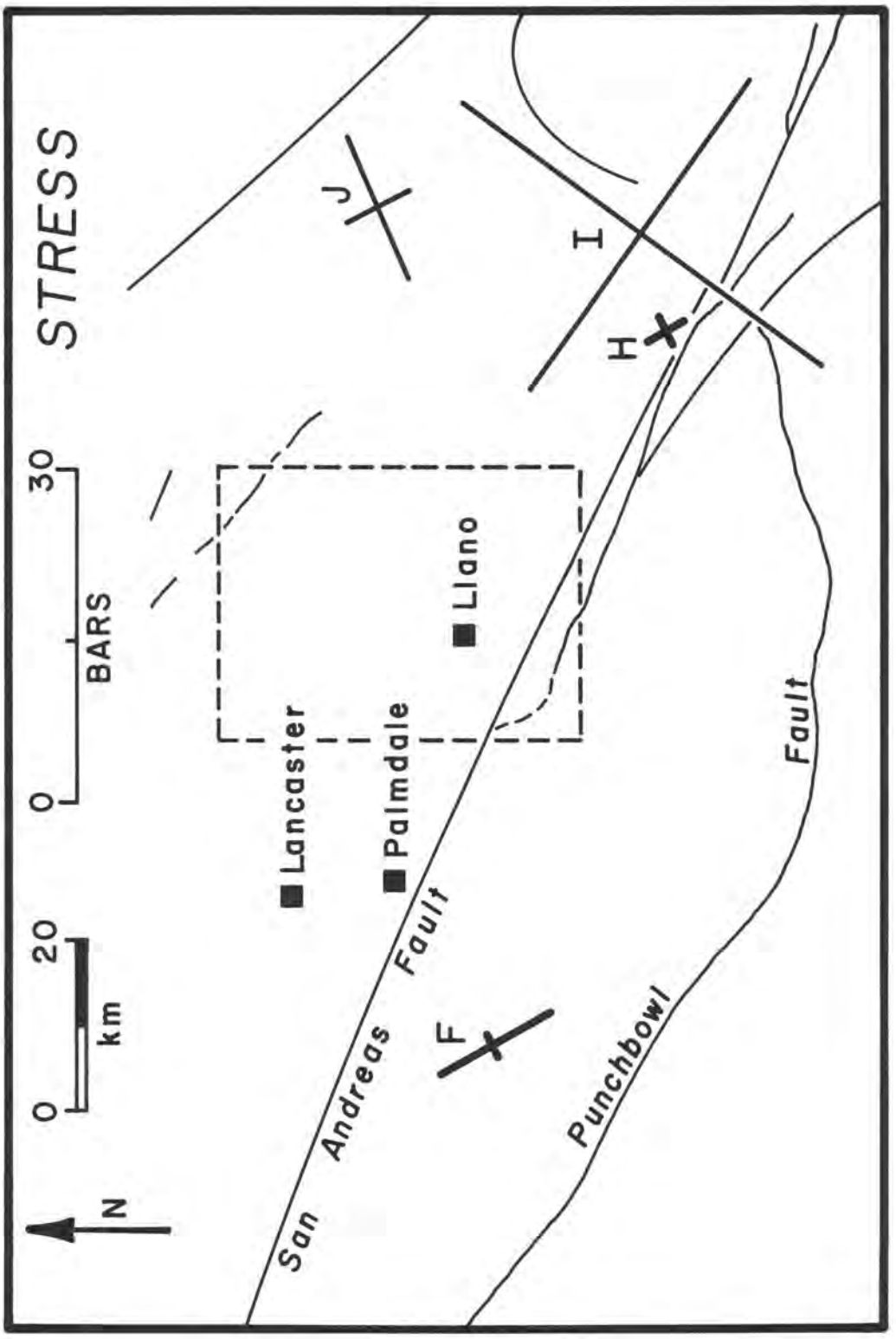

Figure 2 Bureau of Mines measurements outside of profile area. Box is area of Figure 1. Stress indicated by thick lines are more reliable than those denoted by thin lines.

TABLE 1 TENSOR AVERAGE STRESSES

SITE	σ_1 (bars)	σ_2 (bars)	Azimuth of σ_1	No. of Measurements
A	20.3	18.2	N42°W	3
B	12.9	6.6	N21°W	3
C	2.7	1.2	N61°E	3
D	5.9	4.4	N05°W	5 (only deepest 3 used in averag
E*	-1.81	-4.29	N20°E	2
F	11.3	2.0	N23°W	2
G*	3.89	1.87	N74°W	1
H	3.49	3.19	N30°W	3
I	41.7	34.0	N37°E	1
J	12.1	7.6	N64°E	1
1	35.4	5.5	N57°W	3
2	17.8	9.1	N - S	3
3	2.5	-1.4	N31°E	3
4	15.7	-31.7	N88°E	1
5	12.5	2.7	N87°E	1
6	6.6	0.7	N78°E	4
7	8.7	0.7	N32°E	2
8	32.9	8.2	N34°E	1

*Not plotted in Figures 1 or 2 because of questions about the competency of the rock or the measurements

TABLE 2 Effect of Topography

SITE	σ_1 (bars)	σ_2 (bars)	θ	ϕ	Relief (m)	Feature	Slope	Correction A	σ'_1	σ'_2	θ'	Correction B (bars)	σ''_1	σ''_2	θ''
2 a	22.1	10.8	N-S	N75°W	20	Valley	6°	1.2	18.9	10.5	N06°W	0.93	18.1	10.3	N08°W
b					10	Valley	24°	2	14.0	8.2	N34°W	0.93	13.6	7.7	N39°W
total								2.4	13.3	7.1	N43°W	0.93	13.1	6.4	N46°W
3	2.5	-1.4	N31°E	N05°W	135	Valley	30°	2.5	2.5	-1.4	N31°E	0.64	2.3	-1.8	N27°E
4	15.7	-31.7	N88°E	N-S	70	Valley	30°	2.5	6.3	-31.7	N88°E	0.52	5.8	-31.7	N87°E
5	12.5	2.7	N87°E	N40°E	180	Butte	17°	1.25	11.9	1.9	N89°W	0.28	11.8	1.7	N88°W

Notes: ϕ is the orientation of the topographic feature, correction A is a value by which the normal stress perpendicular to the feature (P_{11}) is divided, correction B is subtracted from P_{11}. σ' and θ' are values corrected for stress concentration. σ'' and θ'' are values corrected for both stress concentration and the Poisson effect.

The U.S. Bureau of Mines technique is similar but has some important differences. Instead of bonding a gauge directly to the rock a borehole deformation gauge is inserted into an EW (38 mm) hole. This gauge also measures 3 components of strain in a horizontal plane, perpendicular to the axis of borehole. The gauge is then overcored by a thin-walled 153 mm bit. The elastic moduli and stress are determined as above. See Hooker and Bickel (1974) for a more complete explanation. An important difference between the Bureau of Mines and the doorstopper method is that the former measures strain relaxation over a larger volume. As a result a larger fracture-free volume is necessary for the Bureau of Mines technique. Both types of measurements were made at depths from 1/2 to 3 meters. Since this is near the free surface we can assume that two of the principal stresses are horizontal and one is vertical. Thus true principal stresses in a horizontal plane and not secondary principal stresses are measured.

SITE SELECTION

The availability of competent outcrop was the primary control on the selection of sites. In addition we searched for places of low topographic relief and with wide fracture spacing. Thirteen of the sites described in this report were along a 35 km northeast trending transect which ran from the foothills of the San Gabrial Mountains near Valyermo to Adobe Mountain in the western Mojave desert. These sites were located in intrusive, metamorphic, and sedimentary rocks from Mesozoic to Tertiary (Upper Miocene) in age (Figure 3). The most fractured site attempted was site 4 where the joint spacing is 5 to 10 cm and the rock is foliated and has a cataclastic fabric. We selected this outcrop to determine the limit in fracture spacing that could be successfully sampled. We believe reliable measurements were obtained there although the failure rate was higher than at other sites. Joint spacing at other sites varied from 10 cm to more than 1 m.

Sites A, 2, 3, 4 were in valleys and site 5 was near the steep slopes of Black Butte (Table 2). The local relief is about 10 m at sites 6, 7, C, and negligible at 8. Site D was on a large flat area about half-way up Piute Butte. Five other sites were selected outside of the above transect using criteria similar to that above.

DATA

We made 29 doorstopper measurements at eight sites and 24 Bureau of Mines measurements at ten sites. The average stresses at each site are listed in Table 1. Only sixteen sites are plotted in Figures 1 and 2, since the results at two sites are considered marginal. For the doorstopper measurements the variation in orientation of the principal strains at the individual sites ranges from 15^{o} to 45^{o} for measurements where the ratio of maximum to minimum strain is greater than 1.5. At a site, the magnitudes of the principal strains were similar, but between sites, the

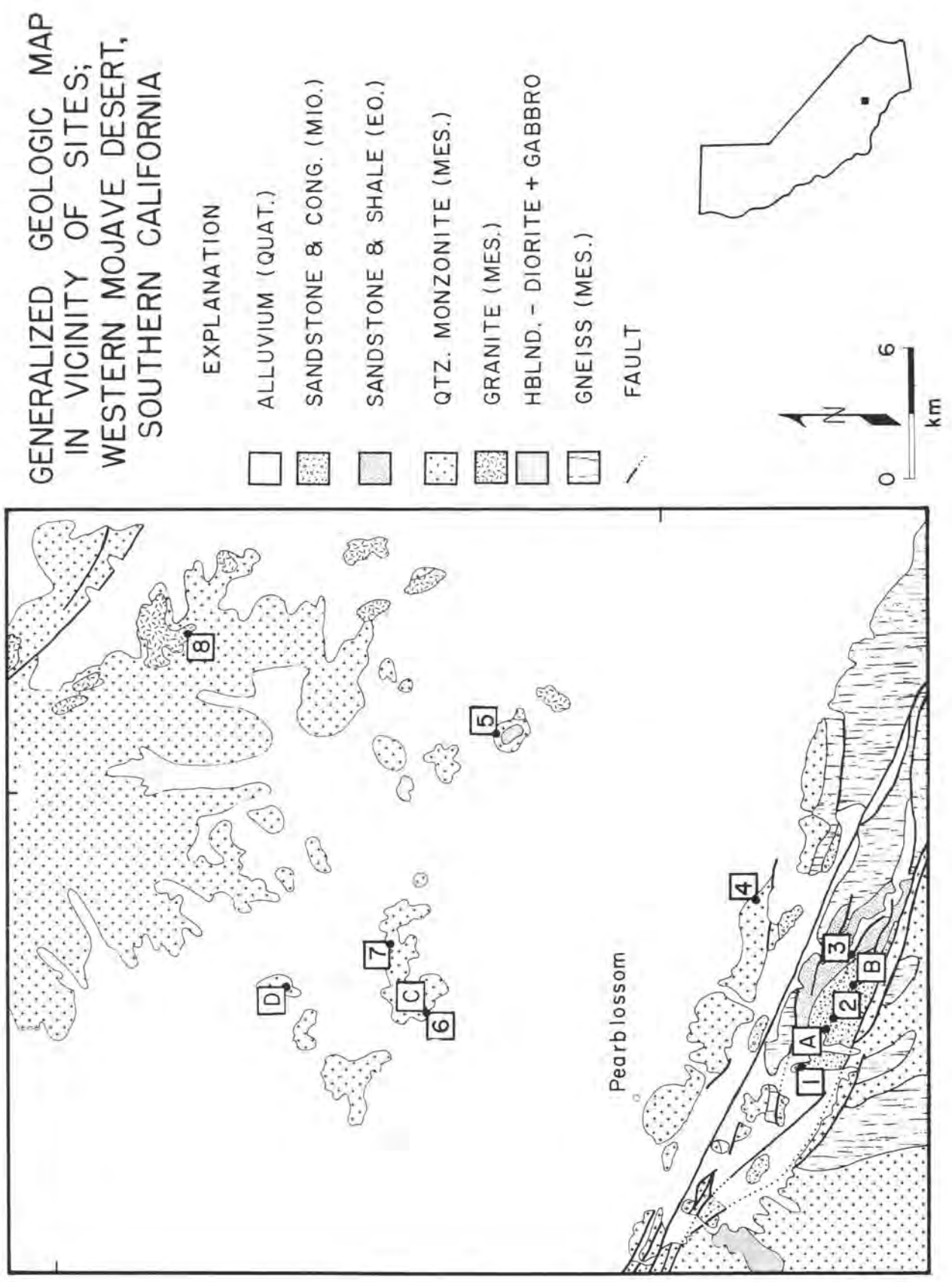

Figure 3 Map of generalized geology is vicinity of profile. Site designation as in Figure 1. The longest continuous fault in the southern part of the map is the San Andreas. The Punchbowl fault and various subsidiary faults are also shown. Geology simplified from Dibblee (1967).

variation in magnitude was more than a factor of ten. We determined elastic moduli and thus computed stress for eighteen of the doorstopper measurements. The scatter in these measurements varies from 8^{o} to 33^{o} at a site. The scatter in orientation of σ_1 for most sites using the Bureau of Mines technique is from 10^{o} to 17^{o}, less than for the doorstopper measurements. Most of the ratios were in the range 1.3 to 2.3. One site (H) with a ratio of 1.2 had a variation in trend of σ_1 of 60^{o}.

Tensor averages of stress are computed for each site and plotted in Figures 1 and 2. Sites 6 and C are on the same outcrop and show similar orientation for σ_1. Sites 4 and 5 also have east-west trending σ_1. South of the fault σ_1 trends from N 60^{o} W to north-south at four closely spaced sites in the Punchbowl formation. Site 3 farther to the east is in a different formation and has very low stresses. There σ_1 trends N31^{o}E.

The northernmost sites, 7, 8 and D, have trend for σ_1 of N30^{o}E to N5^{o}W.

INTERPRETATION

The strain relaxation observed at a site is influenced not only by regional tectonic stress, but also by topographic stress, residual stress, and the degree of outcrop coupling across fractures. One of the difficulties of near-surface strain relaxation measurements is the estimation of the relative contributions of regional tectonic stress and noise sources for each measurement.

Residual stress is locked into a rock during the course of its thermal, tectonic, and burial history. Equilibrium of residual stress can occur over a wide range of dimensions depending on the processes that have caused them. In certain situations the presence of residual stress can be detected by double overcoring. In this procedure, a second overcore is drilled within the first. Whether or not residual stress is detectable by this means depends on the relative dimensions of the two overcores and the equilibrium volume (Tullis, 1977). Time constraints allowed us to make double overcores only in the sedimentary rocks of site 1. No significant residual stress was observed at the scale of the overcore (Figure 4).

Both topographic and regional tectonic stress are external applied stresses. Topography may add a component of stress to the regional tectonic stress in two ways. First, lithostatic loading at the base of hillslopes can cause a Poisson expansion that is perpendicular to the mountain front or the axis of a valley (Jaeger and Cook, 1969, p. 356-358). Second, the slope of valleys causes a concentration of tectonic stress perpendicular to the valley axis (Harrison, 1976).

We have calculated the influence of these two effects using simplified two-dimensional models as described by Harrison to get an approximate measure of the influence of topography on our results. The corrected stresses are listed in Table 2. The stress concentration causes the normal stress perpendicular to the

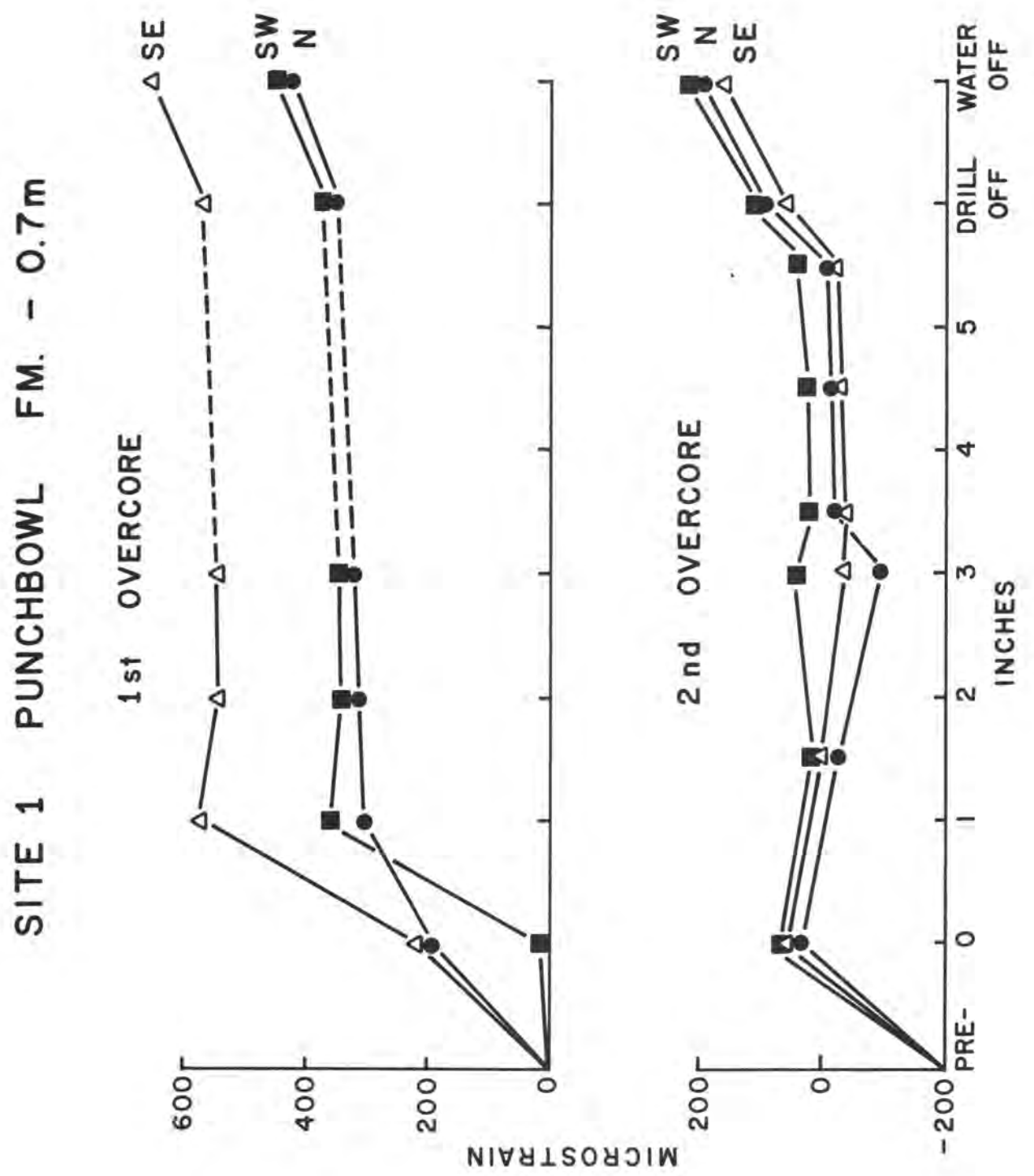

Figure 4 Example of strain relaxation during overcoring of a doorstopper guage. The value at PRE- on the abeissa was taken before the drilling water was turned on. The value at 0 is just prior to drill contact. The strain relaxation is the difference between the values at 0 and those at drill off. Other variations are due to the effect of water pressure on the rock prior to and after overcoring. These are not necessarily the same.

valley to be increased by the correction shown under A. Thus we divide by that factor. The correction listed under B is that due to lithostatic loading (Jaeger and Cook, 1969, p. 276 and 277). This is subtracted from the normal stress. The effect of a broad valley at Site 2 is listed as a and that of a smaller steeper valley as b. The combined effect is also shown. The topographic correction in this case brings the orientation of σ_1 for Site 2 closer to that of Sites 1, A and B. The effect of topography is essentially negligible when σ_2 is tensional. In more normal examples such as Sites 2 and 5, the effect can be significant. The closer σ_1 and σ_2 are in value the more impact topographic corrections will have.

Coupling of the outcrop on which the measurements are made to the earth is a problem which appears to affect the magnitude and possibly the direction of the stress observed. Engelder and Sbar (1977) found that the magnitude and reproductibility of surface strain relaxation measurements in northern New York appeared to be directly proportional to the horizontal dimensions of blocks bounded by vertical joints. If coupling across horizontal joints were a significant problem, we would expect a noticeable difference in measurements above and below sheet fractures. This was not observed in our data.

The mechanical properties of strata below the outcrop where a measurement is made may also weaken the coupling to the earth strain at depth. For example, the formation at site 3 is a sequence of interbedded sandstones and shales. Since we observed very low stress there (Figure 1 and Table 1), we suspect that coupling may have been poor across the shaly layers.

The magnitude of the stresses determined at nearby sites with the doorstopper technique is consistently higher than that with the Bureau of Mines technique. The relative magnitudes of the various sites, however, is the same. For example, the magnitude of sites A and 1 are higher than sites 6 and C.

It is possible that the variation in magnitude of the principal stresses from site to site as shown in Figure 1 may not represent a real variation in the stress at depth, but may be a function primarily of the coupling of the outcrop to the earth. The largest magnitude for σ_1 is about 35 bars. This may represent a lower limit for the near-surface stress in the survey area.

DISCUSSION

The P axes determined from fault plane solutions of major earthquakes in southern California (Sbar et al., 1978) are nearly horizontal and vary in trend from NNW to NE with most trending between N-S and NE. We infer from this that the regional σ_1 is approximately NNE trending throughout most of southern California. The results from sites D, 7 and 8 agree with this regional trend for σ_1. Closer to the San Andreas fault the orientations of σ_1 deviate from the regional trend. Those sites

to the north of the fault yield east-westerly trends and those to the south yield trends between N60°W and N-S. We have no ready interpretation for those results except that they are consistent with a model in which the regional stress field is modified by the presence of a fault on which strain is accumulating. More stress measurements are needed throughout this area to define the stress field in sufficient detail to compare with realistic models of strain accumulation on this portion of the San Andreas fault.

Temporal variations in the stress field may also exist in this area as indicated by the report of McNally and Kanamori (1977). They demonstrated that the P axes of fault plane solutions in the Juniper Hills area varied by as much as 90° in azimuth over a ten month period. These earthquakes were only a few km northwest of site 1.

CONCLUSIONS

In situ strain relaxation measurements south of Palmdale are repeatable at a site and the doorstopper and Bureau of Mines techniques compare favorably at nearby sites. This suggests that these techniques are capable of reliably measuring the stress field at a point. It is important, however, to realize that the stress measured may consist of components of tectonic, residual and topographic stress, and may also be influenced by variations in coupling of the outcrop to the earth.

The stress orientations obtained near the San Andreas fault are consistant with a model in which the tectonic stress field is modified by the presence of a fault, but there are insufficient measurements in the present study to eliminate other explanations for the pattern observed.

REFERENCES

Ahorner, L., 1975, Present-day stress field and seismotectonic block movements along major fault zones in Central Europe, Tectonophysics, v. 29, p. 233-249.

Barber, D.W., and Sowers, G.M., 1974, A photoelastic study of the effects of surface geometry on fault movements, in Advances in rock mechanics, Proc. 3rd Congress, Internat. Society for Rock Mech., p. 585-590.

Dibblee, T.W., Jr., 1967, Areal geology of the western Mojave Desert, California, U.S. Geol. Survey Prof. Paper 522, 152 p.

Engelder, T., and Sbar, M.L., 1977, The relationship between in situ strain relaxation and outcrop fractures in the Potsdam sandstone, Alexandria Bay, New York, Pure and Appl. Geophys. 115, 41-55.

Engelder, T., Sbar, M.L., Marshak, S., and Plumb, R., 1978, Near surface in situ stress pattern adjacent to the San Andreas fault, Palmdale, California, 19th U.S. Sympos. on Rock Mech., Stateline, Nev., 95-100.

Greiner, G., and Illies, J.H., 1977, Central Europe: Active or residual tectonic stresses, Pageoph v. 115, 11-26.

Harrison, J.C., 1976, Cavity and topographic effects in tilt and strain measurements, J. Geophys. Res. v. 81, p. 319-328.

Hooker, V.E., and Bickel, D.L., 1974, Overcoring equipment and techniques used in rock stress determination, U.S. Bur. Mines, Info. Circ. 8618, 32 p.

Jaeger, J.C. and Cook, N.G.W., 1969, Fundamentals of rock mechanics, Chapman and Hill Ltd., London, 515 p.

McNally, K., and Kanamori, H., 1977, Unusual seismic activity along the San Andreas fault near Palmdale, southern California, EOS, Trans. Am. Geophys. Union, v. 58, 1120 p.

Rodgers, D.A., and Chinnery, M.A., 1973, Stress accumulation in the Transverse Ranges, southern California, in Proceedings of Conference on the Tectonic Problems of the San Andreas Fault System, Publ. Geol. Sci., v. 13, Stanford Univ. Press, ed. R.L. Kovach and A. Nur, p 70-79.

Sbar, M. L., and Sykes, L.R., 1973, Contemporay compressive stress and seismicity in eastern North America: An example of intra-plate tectonics, Geol. Soc. Am. Bull., v. 84, p. 1861-1882.

Sbar, M.L., and Sykes, L.R., 1977, Seismicity and lithospheric stress in New York and adjacent areas, J. Geophys. Res., v. 82, p. 5771-5786.

Sbar, M.L., Engelder, T., Plumb, R., and Marshak, S., 1978, Stress pattern near the San Andreas fault, Palmdale, California from near to surface in situ measurements., J. Geophys. Res., in press.

Tullis, T.E., 1977, Reflections on measurement of residual stress in rock, Pageoph, Birkhauser Verlag, Basel, v. 115, p. 57-68.

Zoback, M., 1978, Preliminary stress measurements in the western Mojave Desert near Palmdale, EOS, Trans. Amer. Geophys. Un., v. 59, p. 328.

Sbar reported on in situ stress measurements in southern California using both the doorstopper and U.S. Bureau of Mines techniques. He proposed that these measurements are indicative of active tectonic stress and show the influence of the San Andreas fault on the regional stress field. Discussion immediately arose about whether the data were contaminated by residual stress. Engelder presented a comparison of the above strain relaxation techniques with stress direction inferred from fault plane solutions in western New York, where the residual and applied components are clearly separated. In this region the doorstopper method appeared to be more sensitive to residual stress than the Bureau of Mines technique, since the orientation of the principal stresses from doorstopper measurements are closer to that of the residual stress. The results from the Bureau of Mines technique are quite similar in orientation to the fault plane solution results. In southern California, however, the two strain relaxation techniques yielded similar orientations at the same site. A double overcore done at one southern California site showed no strain relaxation suggesting no locked in strain. The data presented by Sbar nonetheless are not sufficient to conclusively eliminate the possibility of contamination by residual stress.

Clark pointed out that doorstopper data he obtained in Michigan were similar to Sbar's in that they were reproducible on a local scale, but not over distances of 10km or more. This is not quite the same situation as in southern California. The latter data are reproducible at a site, and sites up to 10km away have similar orientations. There is, however, a spatial variation in the southern California data that is difficult to explain with a simple model.

Zoback's hydrofracture measurements were in the same area as the near-surface data of Sbar and others, but spanned the depth range from 80 to 250 m in three holes. He showed data that indicate a change in stress orientation below 200 m in two of the boreholes nearest the San Andreas fault. The deeper measurements had a NNW trending maximum principal stress (σ), while the shallower measurements

near the fault had east-west orientations. The shallower measurements have similar orientations to the near-surface strain relaxation data north of the San Andreas fault. Although the shallow hydrofracture data for two of the three measurements did not agree with nearby strain relaxation results. Zoback explained the variation in hydrofracture data by decoupling of the upper 200 m. The same might apply to the strain relaxation data. The only problem with the hydrofracture data is that J. Logan, when analyzing the hydrofracture data of oilfield, concluded that these measurements were related to residual rather than active stress. Clearly more work must still be done.

CRUSTAL DEFORMATION AND ASEISMIC FAULT SLIP NEAR HOLLISTER, CALIFORNIA

by

Larry E. Slater

Applied Physics Laboratory
University of Washington
1013 N. E. 40th Street
Seattle, WA 98195

CRUSTAL DEFORMATION AND ASEISMIC FAULT SLIP NEAR HOLLISTER, CALIFORNIA

by

Larry E. Slater

Applied Physics Laboratory
University of Washington
1013 N. E. 40th Street
Seattle, WA 98195

INTRODUCTION

The past decade has seen considerable effort expended to gain a better understanding of fault mechanics and crustal deformation. Central California has long been recognized as an active seismic region where many small, shallow earthquakes occur. Aseismic fault creep was first detected in 1958 along the San Andreas fault near the Cienega Winery (Tocher, 1960). The relationship between seismic and aseismic fault slip continues to be one of the major topics of discussion among solid earth scientists.

Savage and Burford (1970) found no appreciable strain accumulation in the region near Hollister, California, between 1930 and 1962. They suggested that "Movement of fault blocks appears to be accommodated by slip on the San Andreas and Calaveras faults." Wesson et al. (1973) suggest that "slip can be viewed as the migration of dislocations that move easily on most of the fault surface, but are pinned by the patches of difficult slip." These patches of difficult slip eventually fail, producing an earthquake. Savage and Burford (1973) found that "The average value for fault creep on the Calaveras in this sector is 15 mm/yr. Thus it would appear that all the relative movement detected by the geodimeter network can be accounted for by observed surface fault creep." The strain data of Johnston et al. (1977) suggest that the observed surface creep does not extend much deeper than 1 km. An examination of USGS Open-File Reports (Nason et al., 1974; Yamashita and Burford, 1973; and Schulz et al., 1976) provides several examples where surface creep events extend along the fault trace for distances approaching 10 km. Huggett et al. (1977) discussed the data collected during the first 210 days of the multiwavelength distance measuring (MWDM) experiment near Hollister, California. The most obvious characteristic of the MWDM data was probably the episodic behavior exhibited in the line length changes.

Assuming that all of the foregoing observations are correct, an appropriate model must provide 1) long-term rigid block behavior, 2) surface aseismic fault creep events that extend approximately 10 km along the surface trace but are limited in depth to the upper 1 km, 3) small earthquakes, and 4) episodic crustal deformation.

Since the introduction of high-precision EDM instruments, a growing concern has been the question of benchmark stability. Specifically, the response of benchmarks and/or local surface materials to heavy rainfall and desiccation requires further study.

DATA

The MWDM instrument developed at the Applied Physics Laboratory of the University of Washington (Slater, 1975; Slater and Huggett, 1976) was installed near Hollister, California, in September 1975. The MWDM instrument has made measurements over lines several kilometers long to a precision of 1 part in 10^7. The Hollister MWDM array consists of nine primary lines arranged in a radial pattern from the central instrument site. The lines vary in length from 3 to 9 km and are measured daily whenever possible. The lines terminate at permanently installed passive retro-reflectors that range from a distance of only 100 m to 7 km from the Calaveras fault (Figure 1).

The data taken with the MWDM instrument during the first 1006 days of the experiment are shown in Figures 2-4. Each data point represents the mean value of approximately 40 consecutive 10-second measurements taken daily on each line in the array. Data from lines that exceed 5 km in length have been arbitrarily omitted from the figures if the standard deviation from the mean of the 40 measurements exceeds 2 mm; data from lines less than 5 km in length have been omitted if the standard deviation is greater than 1 mm.

The length changes on the MWDM lines generally continue to exhibit the episodic behavior that was evident in the early portion of this work. The nature of these episodic changes and the MWDM data will be presented in more detail in the following sections.

LONG-TERM TRENDS

The long-term strain rates measured along the MWDM lines are approximated by the trend line slopes listed in Table I. The results of calculating the components of the strain tensor using a least-squares fit to the MWDM data, coupled with the suggestion of Savage and Burford in 1970, prompted the following interpretation. All detected line-length changes were assumed because of shear deformation parallel to the Calaveras fault. The assumed displacements are shown in Figure 5.

The relative displacement across the Calaveras fault is, from Figure 5, approximately 14 mm/yr north of Hollister and approximately 9 mm/yr south of Hollister. Station Pereira appears to be situated on a narrow sliver between the Calaveras and the Tres Pinos faults. The relative displacement across the Tres Pinos fault in this region appears to be approximately 4 mm/yr. The displacement across both

faults near Pereira is then 13 mm/yr, again in good agreement with the average surface creep rate reported by Savage and Burford (1973).

Table I.

Line	Number of Data Points	Slope (mm/yr)[a]	Assumed Displacement Parallel to Calaveras
Pereira	538	-4.60 ± 0.14	-4.69 mm/yr
Foothill	407	-0.11 ± 0.12	-0.18
Fairview	318	-3.31 ± 0.14	-4.85
Easy	563	-1.31 ± 0.15	-1.38
Gambetta	611	-1.81 ± 0.09	-1.81
Goat	502	11.35 ± 0.11	12.85
Knob	479	7.54 ± 0.06	11.49
Picket	656	-1.41 ± 0.11	-5.83
Poison	428	-9.56 ± 0.20	-13.52

[a]For first 1006 days of survey

Most of the MWDM lines show long-term trends that suggest rigid block motion when the displacements are resolved parallel to the Calaveras fault. The most notable exception is found in the data from Picket (only 5.8 mm/yr NNW relative to the central instrument site). This discord may be due, in part, to the line being nearly normal to the fault, thereby causing the resolved uncertainty in the measurement to be larger than for the other lines. A second, more likely, explanation is the large change in the line length during early 1978. This large extension, which may be due to heavy rainfall and subsequent desiccation, will be discussed further in a later section. If only pre-1978 MWDM data are considered along the line to Picket, the resolved displacement increases to 14 mm/yr. The line to Fairview shows a significantly higher strain rate than the lines to Gambetta or Easy. This may be due to the Ausaymas fault (Kilburn, 1972), although the location of this fault has been only suggested by hydrologic and seismic data in the past.

EPISODIC DEFORMATION

An examination of the data in more detail reveals episodic changes in the lengths of most of the MWDM lines (Figure 6). This episodic behavior typically consists of a fairly abrupt (a few days) change in strain rate. The periods of high strain rate often persist for several weeks and are evident on more than one of the lines in the array: for example, from day 0 to day 50 on Gambetta and Easy, from day 110

to day 130 on Goat and Knob, and from day 230 to day 270 on Gambetta, Easy, and Fairview. These episodic changes in line length were ascribed by Slater and Burford (1977) to episodic fault creep behavior corresponding to large-scale, essentially rigid block movements extending to considerable depth (~10 km) on the Calaveras fault near Hollister.

MWDM DISPLACEMENTS AND CREEP EVENTS

Aseismic surface fault creep along the Calaveras fault near Hollister, California, has been measured with several creepmeters since 1971 (Nason et al., 1974; Yamashita and Burford, 1973; Schulz et al., 1976). The measurements show that the magnitude of a typical fault creep event is a few millimeters, and the duration is several hours. Events are generally separated by several months during which little or no fault movement is recorded by the surface creepmeters. The depth to which this aseismic fault slip extends is important in determining its effectiveness in releasing strain energy along this portion of the plate boundary.

Displacements directly associated with surface creep events have only been observed when the affected MWDM line terminates within a few hundred meters of the creep zone (Slater and Burford, 1977). This observation is consistent with the findings of Johnston et al. (1977) and suggests that the very-short-term displacements (typically a few hours) observed across the fault trace extend to only a few hundred meters in depth. It is likely that this near-surface failure (the surface creep event) is the result of some form of deeper aseismic fault slip or strain accumulation. The geodolite and long-term MWDM data tend to rule out strain accumulation and favor a rigid block model. If the episodic behavior observed on the MWDM lines is due to deep aseismic slip on the major faults, it suggests that deep fault slip occurs in well-defined episodes typically of several weeks duration. It is also evident from Figure 6 that the periods (episodes) of high strain rate frequently do not coincide on adjacent baselines when there is an intervening fault zone (Goat and Gambetta are the best examples).

Figure 7 shows a simple screw dislocation model (Weertman and Weertman, 1964) that I believe may explain the observations discussed above. The model is infinitely long in the y direction and consists of a linear, homogeneous elastic material. The fault is assumed to be temporarily locked above a depth, D. The surface displacement predicted by the model is also shown in Figure 7. The surface displacement, V, is only in the y direction, and

$$V = \frac{b}{\pi} \tan^{-1}\left[\frac{x}{D}\right] .$$

At distances of more than 3D from the fault, the surface displacement closely resembles that expected from a rigid block model. I have assumed that the relative slip, b, is uniform with depth below D. I have

made no assumption, however, that the slip rate ($\dot{b}$) is constant, nor have I required that the relative slip be equally divided between, or simultaneous on, the blocks across the fault zone when the displacements are observed from a coordinate reference unaffected by the fault slip. I have assumed that D is approximately 0.5 km in the region north of Hollister (i.e., one-third the distance between the Calaveras fault and station Easy or Goat). Below a depth of D, the model exhibits episodic slip such as that suggested by the MWDM data from the lines to Goat, Easy and Fairview. It is not realistic to assume that a fault slip episode continues infinitely in the y direction. Since I have assumed that D is only 0.5 km, however, the two-dimensional model is adequate if I allow the slip to extend for several kilometers horizontally and avoid the end effects within a kilometer of the slip termination points.

The following is a hypothetical scenario using the foregoing model to produce displacements similar to those seen in the MWDM data. The process is shown in Figure 8 in four successive stages. The pre-slip stage is shown by the squares, which indicate the initial positions of three benchmarks at distances from the fault of -3D, 0.5D, and 3D. These locations are similar to the positions of Goat, Gambetta, and Easy when D is equal to 0.5 km. The first slip episode (stage 2) involves only the left "block." The circles in Figure 8 indicate the benchmark positions at the conclusion of the second stage. The benchmark at -3D is now located near the position that would be expected from symmetric, relative slip of amplitude b. The benchmark at 0.5D has also been displaced in the -y direction, opposite to that expected from symmetric slip on the fault. This behavior will be called the reverse drag effect. The movement of the benchmark at 3D is small. The slip of the left block has loaded the fault surface above D to a point still below failure (no surface creep has yet occurred). Stage 3 begins with the onset of episodic slip of the right "block" while the left block is stable relative to the frame of reference. The motion of the right block is in the +y direction. The displacements of the benchmarks at the conclusion of this slip episode, but before any surface creep occurs, are shown by the hexagons in Figure 8. Note that the benchmark at -3D has been displaced only slightly in the +y direction while the benchmarks at 0.5D and 3D have been displaced by considerable amounts in the +y direction. The final stage involves the surface aseismic creep event (relative slip, b, above a depth of D) and results in a considerable displacement of the benchmark at 0.5D. The final result of all four stages is an apparent rigid block movement of relative slip, b.

The data taken from the MWDM lines to Goat, Gambetta, and Easy between April 12, 1976, and June 30, 1976, are presented in Figure 9 along with the predictions of the model discussed in the preceding paragraph. Both the MWDM data and the model predictions were smoothed by a simple 5-day running-average filter. The slip rates of the model were derived from the MWDM data from the lines to Easy and Goat. A 9-day quiescent period was inserted between stage 2 and stage 3. The

data taken on the three lines show trends that are in good agreement with the predictions of this model. It is particularly interesting that the reverse drag effect is suggested in the MWDM data, and that surface creepmeters in the vicinity of station Gambetta recorded a 5 mm creep event on June 16, 1976. Two conclusions are suggested from this analysis. First, although creep events detected on the fault trace by creepmeters may only extend to depths of a few hundred meters, episodic, aseismic fault slip appears to extend to a depth of at least 10 km, thus providing possible means of accommodating plate motion that might otherwise contribute to a significant seismic release. Second, the region appears to be characterized by episodic, rigid block movement that is not necessarily symmetric or simultaneous across the fault surface.

It must be acknowledged that the above model does not fit all the MWDM data during that period. While the five lines extending to the north are all in reasonable agreement with the model predictions, the four lines extending to the south present a more complex problem. It may be that the area covered by the MWDM array consists of more than just two rigid blocks separated by the Calaveras fault. If the rigid block model is accepted with the condition that a particular slip episode does not extend indefinitely along a particular fault, we are forced to consider the area as being composed of a mosaic of rigid blocks separated by intersecting fault zones of finite width consisting of material exhibiting considerably lower rigidity than the nearby blocks.

SMALL EARTHQUAKES

If the mosaic, rigid block model is correct it may explain the considerable discrepancy between the long-term geodetic displacements and the displacements deduced from seismic moment calculations. The low number of small earthquakes compared with aseismic creep activity along the Calaveras fault near Hollister in the past 3 years may be the result of the low rigidity fault zone. This discrepancy is consistent with the work of Wesson et al. (1973) who suggested that, "slip can be viewed as the migration of dislocations that move easily on most of the fault surface, but are pinned by the patches of difficult slip."

BENCHMARK AND SOIL STABILITY

The MWDM data also show large changes in several of the line lengths that appear to be related to locally heavy rainfall. Line-length changes that are thought to be definitely caused by rainfall are indicated in Figures 2-4 by the letter R; those by rainfall and/or subsequent desiccation by RD; and those changes whose causes are less certain, but suspect, are indicated by R?.

By way of comparison, one of the largest creep events yet recorded occurred near the central instrument site on the Calaveras fault in 1977. This creep event (nearly 9 mm relative slip) is indicated by C in Figures 2-4.

Rainfall effects have also been noted in creepmeter and shallow borehole tiltmeter data (R. O. Burford and M. J. S. Johnston, private communication). These data generally show a trend to reset to pre-rain levels within a week or two. The MWDM data also exhibit this resetting trend generally. Unlike the creepmeter and tiltmeter data, however, the MWDM data indicate a reset time of at least a month. Whether this longer reset time is due to a more pervasive or deeper effect is unclear at this time. What is clear is that rainfall may have a large and long-lasting effect on certain lines. The resetting toward pre-rain levels is generally apparent after each period of rainfall, but it is not obvious that the resetting is complete even after a few months. If the reset is not complete, there will obviously be a long-term change in line length that may or may not be related to tectonic phenomena. It should be pointed out that the benchmark most susceptible to rainfall, Easy, is on a very flat valley floor; therefore, the common problem of downhill creep is not expected.

Benchmarks in high-precision EDM arrays that are subject to rainfall effects must be identified. Once certain lines are suspect, either they should be monitored daily to detect this resetting trend or, if they are measured infrequently, care must be taken to avoid times following locally heavy rainfall. If neither of these precautions is taken, the resulting data must be viewed with a critical eye.

The related problem of desiccation also deserves mention. Desiccation cracks near station Picket have been observed to exceed 5 cm in width and 1 m in depth. The crack configuration is approximated by closely packed hexagons. If the benchmark in question is near the perimeter of the hexagon, the displacement may be very large compared to the precision of the measurement.

The stability of benchmarks and the response of the near-surface material to atmospheric perturbations, particularly rainfall, appear to be a significant problem in high-precision geodetic measurements. There is a need for further study of this problem, perhaps including the redesign of benchmarks and installation procedures, depending on whether vertical or horizontal deformation data are desired.

ACKNOWLEDGMENTS

I thank Jim Savage, Bob Burford, and Malcolm Johnston, at the National Center for Earthquake Research, U. S. Geological Survey, for their many suggestions and stimulating discussions over the past three years. The availability of recent data from them has been much appreciated. I would also like to thank the people and the City of Hollister

who have kindly allowed continued access to their property. This work was supported by the U. S. Department of Interior, Geological Survey, under Contract 14-08-0001-15877.

REFERENCES

Huggett, G.R., L.E. Slater, and J. Langbein, 1977, Fault slip episodes near Hollister, California: initial results using a multiwavelength distance-measuring instrument, J. Geophys. Res., 82, 3361-3368.

Johnston, M.J.S., A.C. Jones, and W. Daul, 1977, Continuous strain measurements during and preceding episodic creep on the San Andreas fault, J. Geophys. Res., 82, 5683-5691.

Kilburn, C., 1972, Ground-water hydrology of the Hollister and San Juan valleys, San Benito County, California, 1913-68, U.S. Geol. Survey, Water Resources Division, Open-File Report, 44 pp.

Nason, R.D., F.R. Phillippsborn, and P.A. Yamashita, 1974, Catalog of creepmeter measurements in central California from 1968 to 1972, U.S. Geol. Survey, Open-File Report No. 74-31, 287 pp.

Savage, J.C., and R.O. Burford, 1970, Accumulation of tectonic strain in California, Bull. Seismol. Soc. Amer., 60, 1877-1896.

Savage, J.C., and R.O. Burford, 1973, Geodetic determination of relative plate motion in central California, J. Geophys. Res., 78, 832-845.

Schulz, S.S., R.O. Burford, and R.D. Nason, 1976, Catalog of creepmeter measurements in central California from 1973 through 1975, U.S. Geol. Survey, Open-File Report No. 77-31, 480 pp.

Slater, L.E., 1975, A multi-wavelength distance-measuring instrument for geophysical experiments, Ph.D. thesis, Univ. of Wash., Seattle.

Slater, L.E., and G.R. Huggett, 1976, A multiwavelength distance-measuring instrument for geophysical experiments, J. Geophys. Res., 81, 6299-6306.

Slater, L.E., and R.O. Burford, 1977, A comparison of long-baseline strain data and fault creep records obtained near Hollister, California, 1977 International Symposium on Recent Crustal Movements, July 25-30, 1977, Stanford, California (to be published in Tectonophysics).

Tocher, D., 1960, Creep on the San Andreas fault--creep rate and related measurements at Vineyard, California, Bull. Seismol. Soc. Amer., 50, 396-404.

Weertman, J. and J.R. Weertman, 1964, Elementary Dislocation Theory, Macmillan, New York, 213 pp.

Wesson, R.L., R.O. Burford, and W.L. Ellsworth, 1973, Relationship between seismicity, fault creep and crustal loading along the central San Andreas fault, Proceedings of the Conf. on Tectonic Problems of the San Andreas Fault System, 13, Stanford, 303-321.

Yamashita, P.A., and R.O. Burford, 1973, Catalog of preliminary results from an 18-station creepmeter network along the San Andreas fault system in central California for the time interval June 1969 to June 1973, U.S. Geol. Survey, Open-File Report, 215 pp.

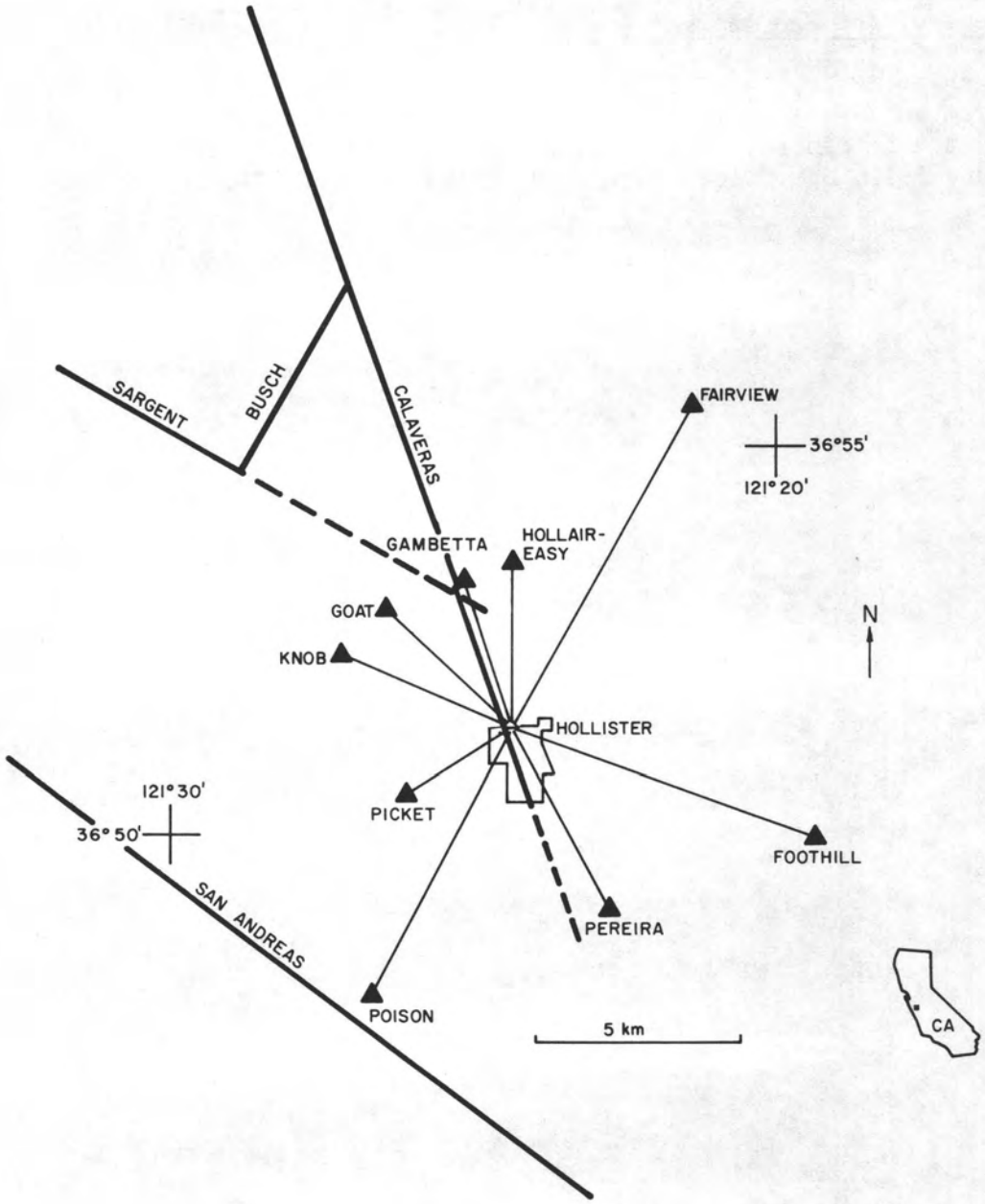
SARGENT
BUSCH
CALAVERAS
FAIRVIEW
36°55'
121°20'
GAMBETTA
HOLLAIR-
EASY
GOAT
KNOB
N
HOLLISTER
121°30'
36°50'
PICKET
FOOTHILL
PEREIRA
SAN ANDREAS
POISON
5 km
CA

Figure 1.

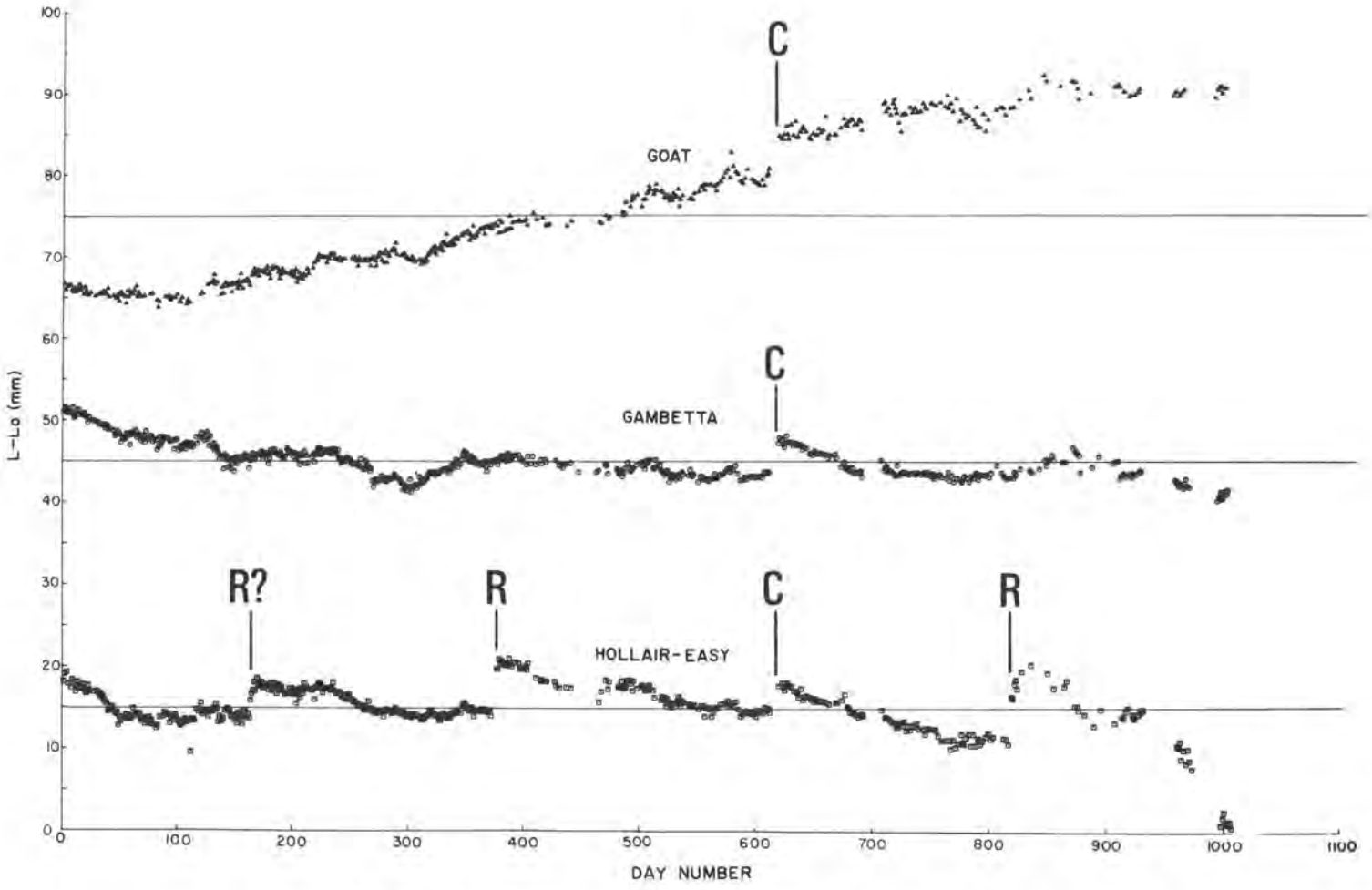

Figure 2. MWDM data for the first 1006 days.

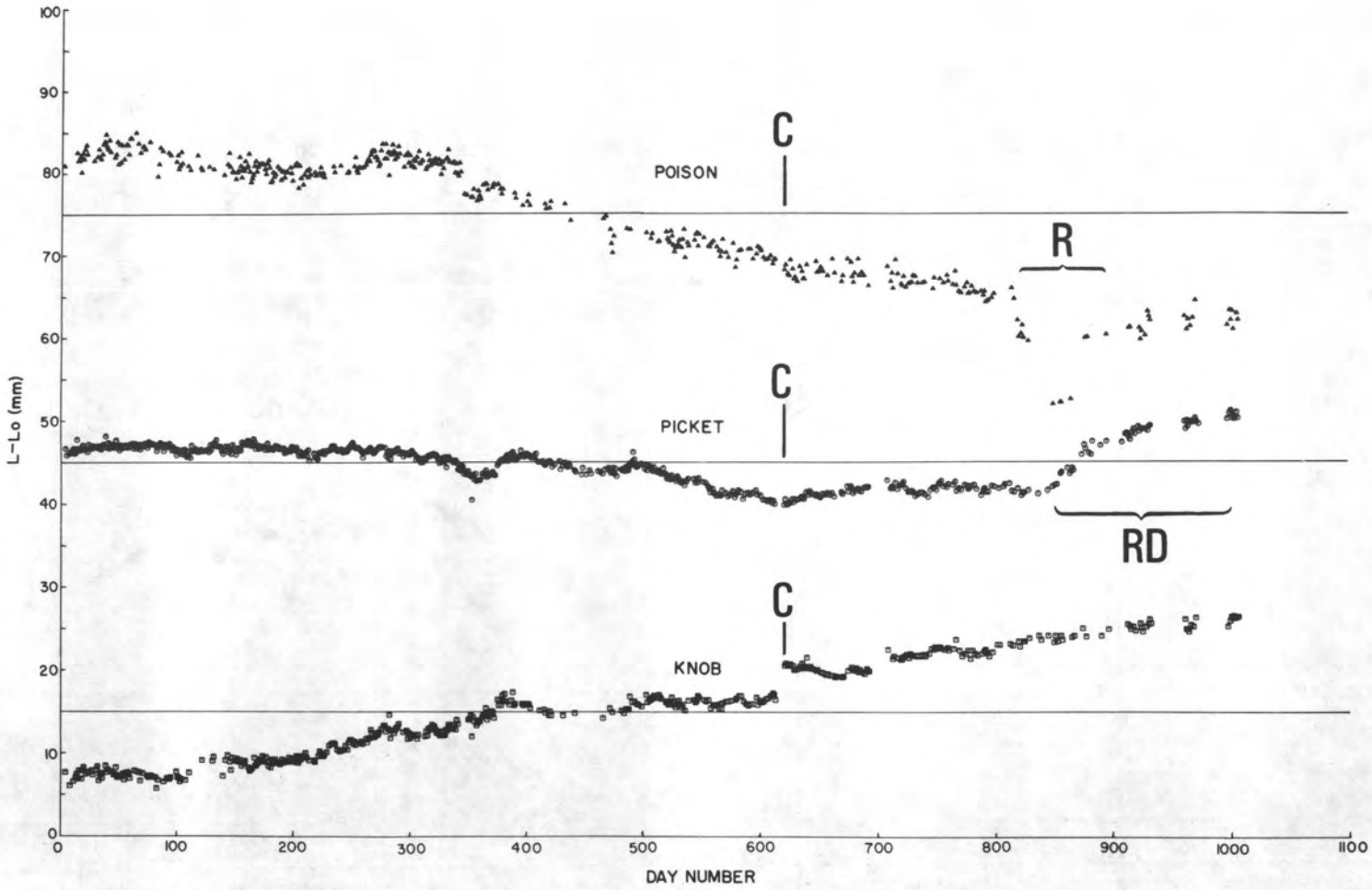

Figure 3. MWDM data for the first 1006 days.

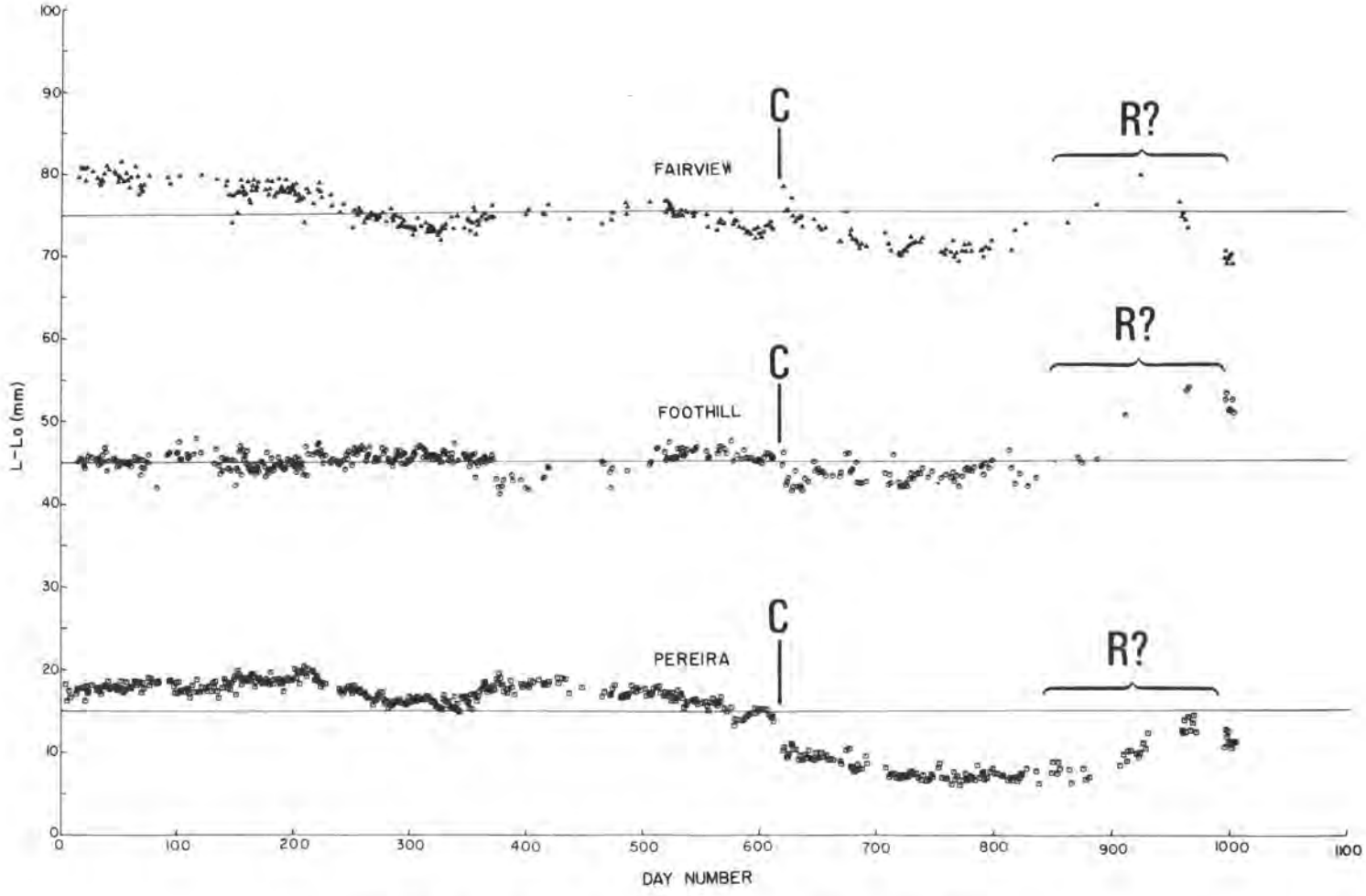

Figure 4. MWDM data for the first 1006 days.

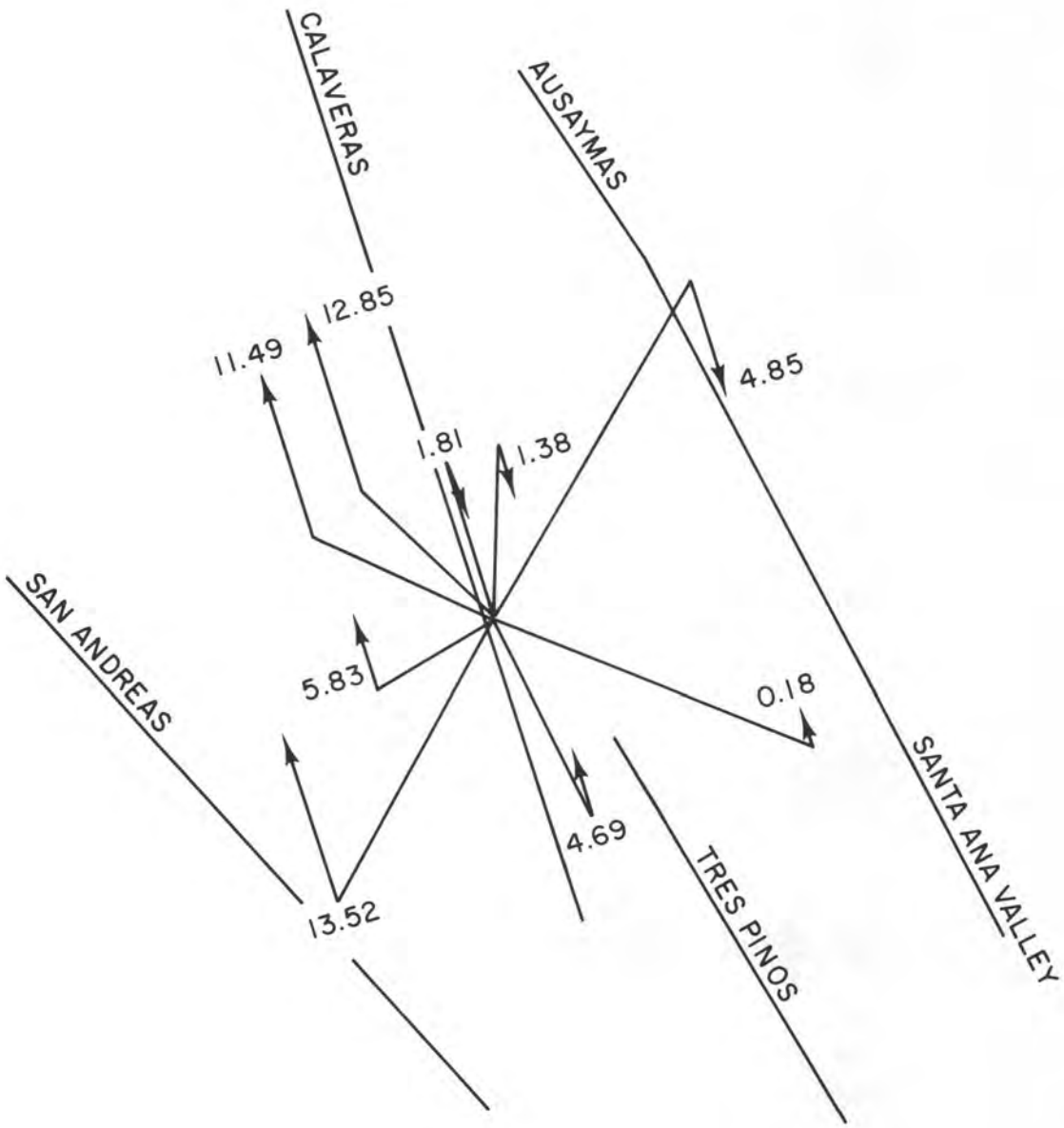

Figure 5. Long-term data resolved parallel to the Calaveras fault. Displacements are in millimeters per year.

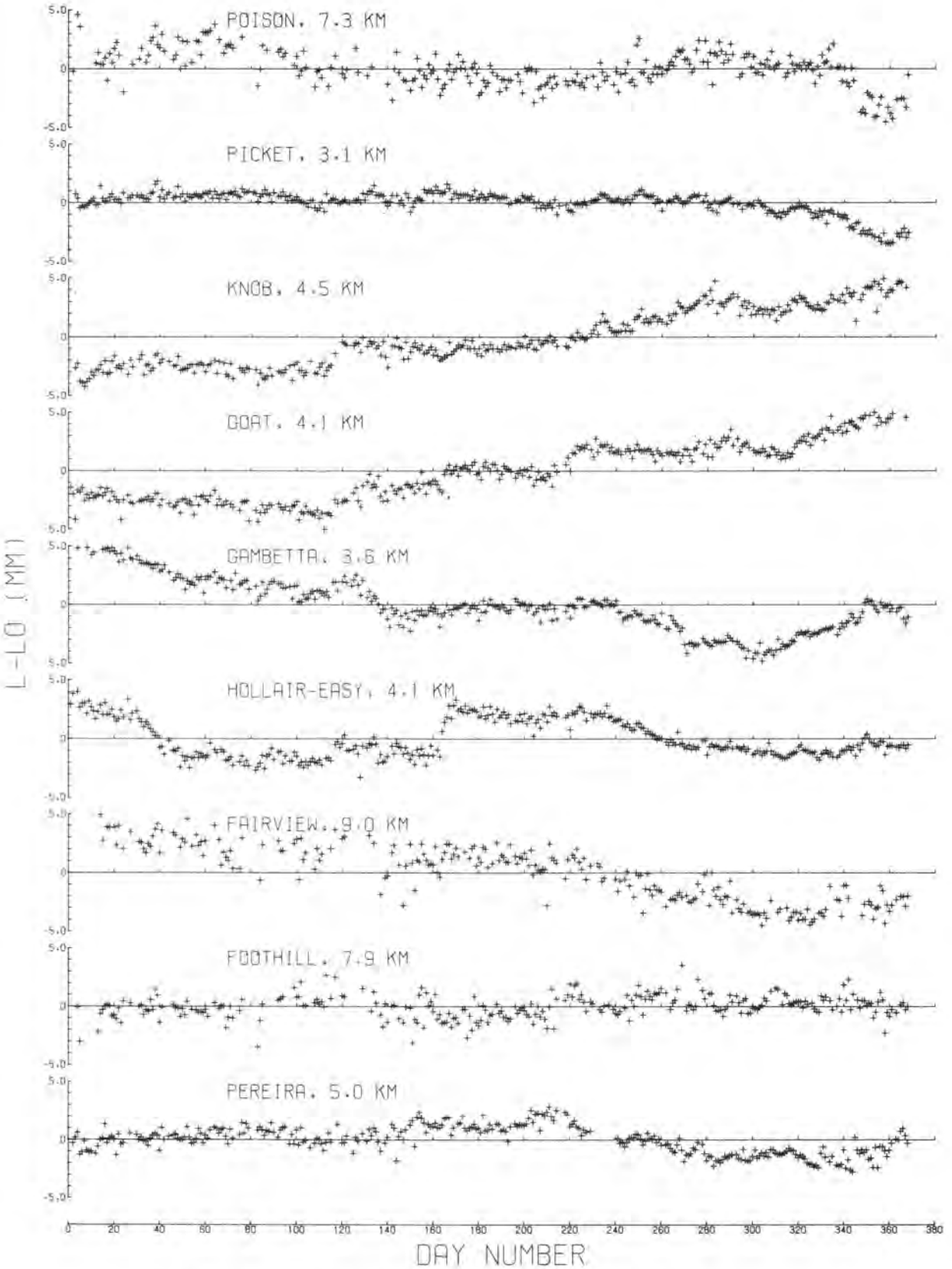

Figure 6. Detailed MWDM data through day 380.

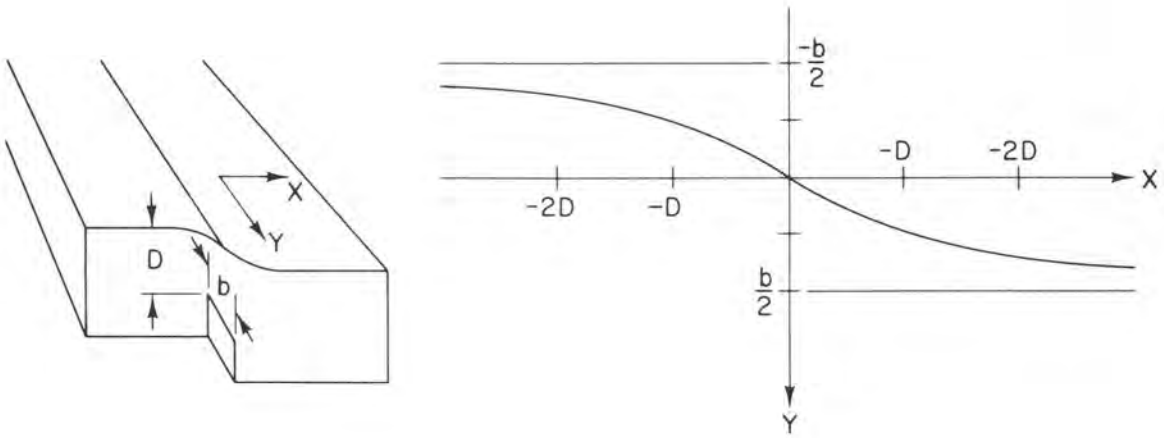

Figure 7. A simple screw dislocation model and the resulting displacement at the free surface. Slip has been assumed to be uniform with depth below a depth D. No slip occurs above D. The model is two dimensional and thus displacement is only in the y direction. The straight lines at ± b/2 illustrate the same slip, b, if it extends to the surface (rigid block motion).

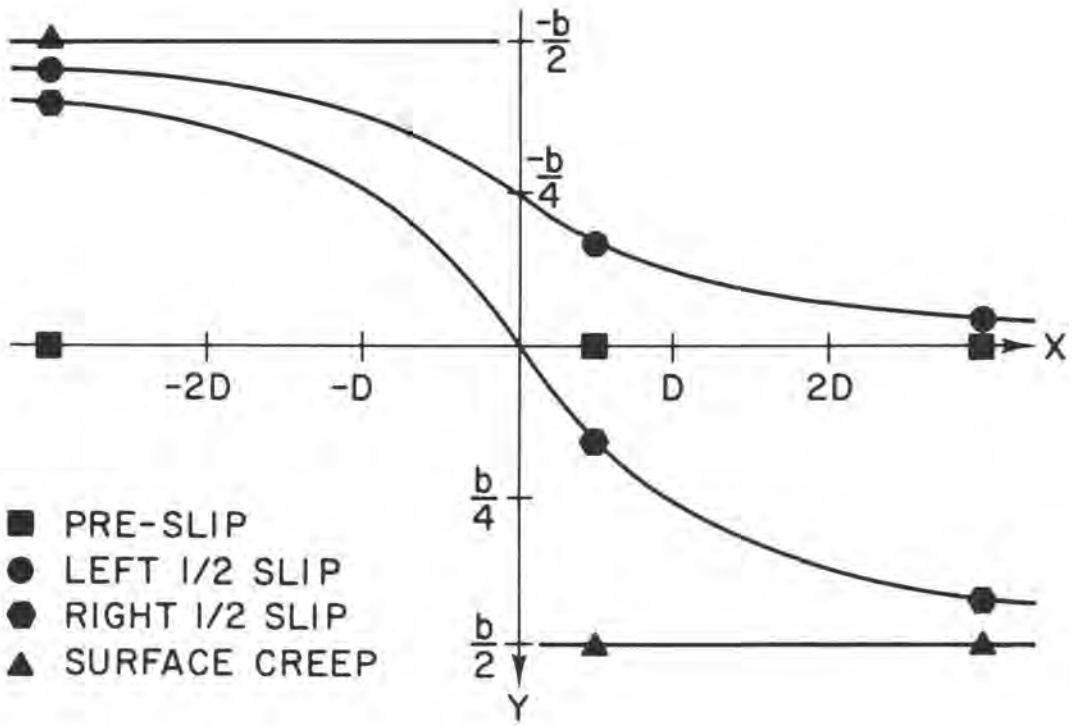

Figure 8. Free surface displacements as detected from an unaffected reference frame when motion of the left side and right side of the model do not exhibit simultaneous slip. The left block slips first in this example, then the right block, and finally the near surface failure occurs (the surface aseismic creep event).

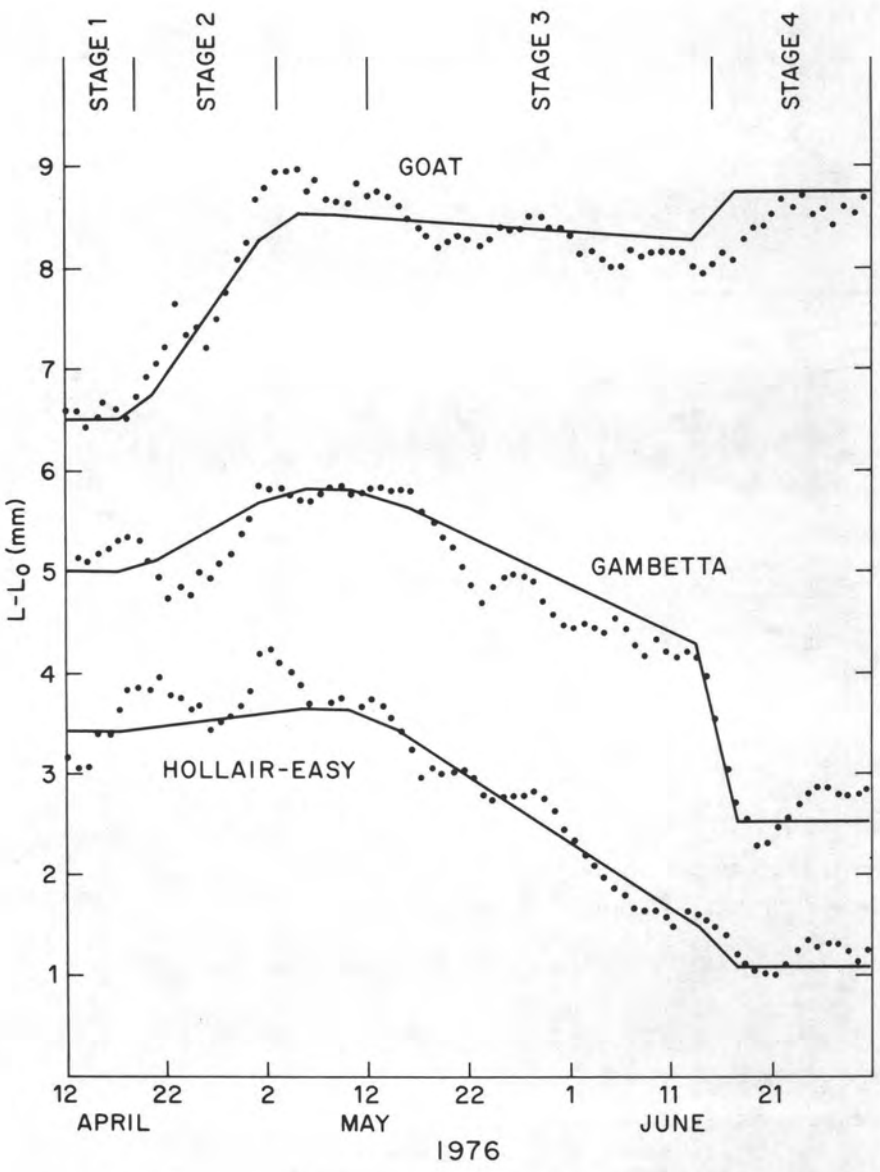

Figure 9. Smoothed data from Goat, Gambetta, and Hollair-Easy taken between April 12, 1976 and June 30, 1976. The solid lines are the line-length predictions from the model illustrated in Figure 7. Both the MWDM data and the model predictions have been smoothed by a simple 5-day running average filter.

Tilt Elbows before Earthquakes

by

W. D. Stuart and J. W. Herriot

U.S. Geological Survey

Menlo Park, CA

ABSTRACT

A rigorous procedure for detecting anomalies in shallow borehole tiltmeter data prior to small and moderate earthquakes is described. The procedure rests on a precise anomaly definition, a statistical method for detecting significant anomalies, and a semi-empirical model relating anomaly and earthquake parameters. Application of the procedure to two components of one tiltmeter shows that most suitably close earthquakes for which data was available were preceded by anomalies, but about three fourths of all anomalies were false alarms.

INTRODUCTION

In this paper we describe a procedure for detecting anomalous ground tilting precursory to small and moderate (magnitude M 3 to 6) earthquakes near the central San Andreas fault. The three basic elements of the procedure are (1) the definition of a precursory tilt change to be a sudden and persistent change of tilt rate from one constant value to another, i.e. an elbow in the tilt record, (2) a statistical algorithm designed to detect significant anomalies and measure their magnitude, and (3) a semi-empirical model relating anomaly parameters (magnitude, location, time) to earthquake parameters (magnitude, location, time). The procedure is tested by searching three years of data measured by one tiltmeter and shorter segments by three other tiltmeters for anomalies prior to earthquakes whose parameters are known ab initio. As will be seen, such a test is equivalent to estimating model parameters.

Anticipating earthquakes with tilt or other deformation data amounts to reversing the above procedure. To forecast earthquakes, an established or tentative model would be used to transform observed anomaly parameters into expected earthquake parameters. Although several informal attempts at anticipating earthquakes have been made with earlier versions of the model to be discussed, rigorous forecast procedures are not considered in this paper.

In the remainder of this paper we discuss the logic of correlating precursors with earthquakes, the proposed method for detecting precursory tilt anomalies, and the results obtained from applying the method to data measured by four shallow borehole tiltmeters.

LOGIC OF CORRELATING PRECURSORY ANOMALIES AND EARTHQUAKES

The logic of detecting precursory anomalies and assigning them to earthquakes is discussed in this section. The next section describes in detail the procedures specifically applicable to tiltmeter data and earthquakes observed near the central San Andreas fault.

In general, all studies of earthquake precursors require (1) the definition of an anomaly, (2) a method for measuring anomaly and earthquake parameters, and (3) a model relating anomaly and earthquake parameters. Qualitatively, an anomaly is usually thought to be a departure from a pre-existing or secular trend. The difference between the new and old trends

is called a residual and is one of several possible measures of anomaly magnitude. Physically, the anomaly may be due to the addition of a new earthquake-related mechanical process to the cause (perhaps multiple) of the secular trend. Such a partition of physical causes, of course, may be artificial in that a single physical theory might account for secular, anomaly, and the earthquake instability. Some examples of qualitatively defined precursory anomalies are U-shaped t_S/t_P changes (e.g. Scholz et al., 1973; Whitcomb et al., 1973; Aggarwal et al., 1975), loss of tidal coherence between tiltmeters (Wood, 1973), and tilt azimuth changes (Johnston and Mortensen, 1974).

Most geophysical data containing anomalies contain also signals called "noise" of extraneous and perhaps unknown origin. Thus, not only must an ideal anomaly be defined precisely, but a statistical method must be designed to recognize the anomaly and measure its magnitude and significance with respect to the noise. In other words, a large anomaly masked by large noise and a small anomaly masked by small noise are equally useless. Below, we define an anomaly to be a change in tilt rate and measure the significance of the rate change by an analysis of variance method. Another rigorous method for detecting anomalous tilt using predictive error filtering techniques is described by Wood and King (1977).

Earthquake parameters are usually well determined. The relevant earthquake parameters are magnitude (or moment), origin time, depth, and epicenter location.

The final ingredient of a precursor study is the model relating precursor and earthquake parameters. A model may also be considered to be a transform or mapping. Although models are often only implicitly assumed, their use is always manifest whenever one assigns a particular precursor to a particular earthquake. The common practice is to connect a large anomaly with the biggest earthquake closest in space and time in some sense. Thus the assumed model is that precursor magnitude should decrease with increasing epicentral distance and decreasing earthquake magnitude. A model may be an empirical function such as a low order polynomial, or be derived from physical theory.

A model also plays a circular role in matching anomalies with earthquakes. The model form is assumed, initial values of model constants are estimated, and then anomaly-earthquake pairs or groups consistent with the model are selected. An example is the reported linear increase of the logarithm of precursor time with earthquake magnitude (e.g. Scholz et al., 1973). In this example, not only is the form of magnitude-time relation assumed, but also an anomaly magnitude decrease with increasing epicentral distance and decreasing earthquake magnitude. If the second assumption were not made, an earthquake of some magnitude somewhere in the earth could always be found to satisfy an arbitrarily chosen precursor time. This method, also used in the present study, is justified by physical plausibility, the confidence of estimates of model constants, and the fact that in general one model will be more successful than all other models in explaining the observations.

Another common assumption is that tilt anomalies at a location form a 1 to 1 mapping with earthquakes, i.e. one and only one anomaly is related to a single earthquake. Although plausible, there is yet no physical reason to suppose that this mapping is true. Two other possibilities are that (1) one

anomaly at an instrument is related to several earthquakes grouped in space and time (an earthquake swarm or cluster), and (2) several anomalies precede a single earthquake (an anomaly swarm). A special case of (1) may be an earthquake and its foreshocks or aftershocks. Furthermore, there is the possibility of ambiguity when nearby anomalies and earthquakes obey a 1 to 1 mapping, but have overlapping precursor time intervals.

Even if a 1 to 1 anomaly-earthquake mapping physically exists but precursors are not reliably detected, two types of mismatches are possible: (1) false alarms - a detected anomaly is not followed by an earthquake, and (2) surprises - an earthquake is not preceded by an anomaly. Hereafter, an anomaly that is matched to an earthquake is called a precursory anomaly or simply a precursor. In the results described below, the ratios of the number of earthquakes having a precursory anomaly to the number of false alarms and to the number of surprises are used to measure success.

Both false alarms and surprises are expected to exist for theoretical reasons. False alarms are likely when faulting is barely inertially stable, as at the onset of rapid aseismic slip episodes. Surprises are expected because the free surface tilt field produced by precursory deformation near an earthquake focus is likely to have zeros. One example is the theoretical tilt field produced by a double-couple source buried in an elastic half-space.

METHOD FOR DETECTING ANOMALIES

We now describe a specific anomaly definition, detection algorithm, and model for application to shallow borehole tiltmeter data. Data for the north and east components of each tiltmeter are analyzed separately. The instrument names are ARM, LIB, NUT, and SJB, and an appended letter identifies the component, e.g. ARMN is the north component of ARM. These abreviations stand for Aromas, Libby, Nutting, and San Jaun Bautista, respectively. Locations of the tiltmeters and details of instrumentation and installation are given in Mortensen and Johnston (1975) and Mortensen (1978). Although data from other instruments is available, only SJB data is completely analyzed because it contains the largest apparent anomaly prior to a large nearby earthquake (M=5.1) and it is one of the most reliable instruments. Daily average tilt has been computed from hand digitized strip chart records prior to September 1, 1975 and from telemetered data after. Data segments of obviously non-tectonic origin such as instrument failure have been removed, but possible rainfall effects are ignored. Tilt fluctuations with rainfall occur occasionally, but they could be either of local site or tectonic origin and are retained. Data for each instrument contains a few one-day gaps which have been replaced by interpolation, but otherwise gaps have not been filled with synthetic data.

The ideal precursory tilt anomaly is postulated to have the form of a sudden slope change between two straight line segments of a single tiltmeter component. This form is motivated partly by inspection of tilt and earthquake data, and partly by results from theoretical models for deformation preceding earthquake instability. The right side of Figure 1 shows an ideal anomaly in hypothetical data. The two line segments L_1 and L_2 have respective lengths in time of $d_1=t_2-t_1+1$ and $d_2=t_4-t_3+1$, and slopes b_1 and b_2.

The anomaly time $t_3=t_2+1$ occurs at the slope change which resembles an elbow. The slope difference $b=b_2-b_1$ is the residual tilt rate, and estimated anomaly magnitude A_O in observed data is defined to be

$$A_O = |b| \Delta t_O$$

where $t_5 \geq t_4$ is the earthquake origin time and the time interval of a precursory anomaly is $\Delta t_O=t_5-t_3+1$. Units for b and (t_5-t_3) are microradians/day and days. Anomaly magnitude is presumably a quantity that can be related to physical theory.

Because of "noise" in measured tilt data, no ideal tilt elbows exist, and so an algorithm is needed to detect forms which more or less resemble ideal elbows. Slope changes are detected in the following way. At each time t (e.g. t_3) dividing data segments L_1 and L_2 on the left side of Figure 1, the $F_2(t)$ statistic is computed by the analysis of variance method due to Draper and Smith (1966) based on an idea of Ergun (1956). Repeating the calculation at successive points in time gives an $F_2(t)$ time series as shown in Figure 2 where pulses coincide with the most significant slope changes in the adjacent tilt data. F_2 is related through an integral to the probability that the hypothesis of slope equality is false. Thus the likelihood of slope difference increases with increasing F_2. Here, however, we do not compute probabilities, but use F_2 merely as a relative indication of slope change significance. A_O is computed using the time at the F_2 peak for the value of t_3 and the corresponding least squares estimates of the two line slopes for b.

Values of Δt_O in actual tilt data appear to increase from about 10 to 35 days as earthquake magnitude increases from 3.0 to 5.1. By trial, the most successful ratio of d_1/d_2 is about 2 with little dependence on earthquake magnitude over the above range. In all cases described here, d_1 = 20 days, and d_2 = 10 days. This value of d_2 is used because tilt data was lost (e.g. instrument off scale) soon after onset of several anomalies and 10 days is the minimum observed precursor time interval for the earthquakes used here. In addition, the number of anomalies and earthquakes in this study is too small to determine precisely the consequences of varying d_1 and d_2. It appears that actual tilt data during time intervals corresponding to L_1 and L_2 is smoother than during preceding time. Thus L_1 may be regarded either as a secular trend or as a precursor to L_2.

Figure 2 shows $F_2(t)$ and tilt data for the two best examples of precursory anomalies. The first example is for SJBN and SJBE in late October, 1974, about 35 days before the M=5.1 Hollister earthquake. Mortensen and Johnston (1976) previously reported anomalous precursory tilting at SJB and other sites for this earthquake. The second example is for LIBE in June, 1975, 10 days prior to a nearby M=3.2 earthquake. Tables 2-5 give additional data.

Although $F_2(t)$ provides a vivid graphical representation of anomalous slope changes, it alone is potentially inadequate because noisy data with large slope changes gives large F_2 whereas the ideal elbow requires zero noise. The F_2 method, however, does have the virtue that very small slope changes in nearly noise-free data give large F_2; such small changes are likely to be missed by a visual search for anomalies. Note also that large

F_2 does not necessarily imply large A_o. This is born out by the weak positive correlation of the two variables. The magnitude of anomalous F_2 peaks also seems to be independent of $|b|$.

Recent work on quasi-static models for earthquake instability and preceding deformation provides a tentative theoretical basis for defining an anomaly to be a sudden slope change (Stuart, 1979; Stuart and Mavko, 1979; Archuleta and Stuart, 1978). Reconciling anomalous tilt with physical theory is not attempted here, but the theory suggests that the anomalies may be due to accelerating, sub-inertial fault slip near the pending focus. In the context of a physical theory, of course, the search for precursory signals would be replaced by a systematic inversion of time-dependent ground deformation to estimate the likelihood of dynamic instability. No theoretical explanation for low precursory tilt noise exists, however.

Since the number of anomalies and the earthquake magnitude range are small, we assume a simple empirical form for the model which relates anomaly and earthquake parameters. In particular, we assume that (1) earthquake magnitude M is a linear function of theoretical precursor time Δt_t, and (2) theoretical anomaly magnitude A_t equals M/r where r is the tiltmeter-epicentral distance in km. The equations are

$$\begin{aligned} M &= a_1 + a_2 \Delta t_t \\ A_t &= M/r \\ A_t &= a_3 A_o \end{aligned} \qquad (1)$$

where a_1, a_2, and a_3 are constants to be estimated. The assumption that all r and Δt_t are independent in equations (1) implies the unlikely situation that all earthquakes have mechanically similar precursory tilt. Therefore, actual departures from a heterogeneous crustal structure and nonstationary faulting (e.g. seasonal or rainfall triggered) are potential sources of model failure. One might also reasonably expect that tilt precursors associated with deep earthquakes would be smaller than precursors associated with shallow earthquakes because of the greater distance. A successful physical theory could replace equations (1) with deterministic equations involving remote boundary conditions and constitutive and geometric properties of the fault zone and elastic surroundings. In fact, merely replacing M with moment in (1) would give equations having a closer correspondence with quasi-static mechanical theory and allow a better fit to data over a broader range. Equations (1), for example, are not viable for $M \leq 0$.

There are several equivalent ways to estimate constants a in equations (1). The one chosen here is to make initial rough estimates of a using the anomalies for the M=5.1 and 3.2 earthquakes in Figure 2. These two earthquakes involve the least ambiguity of association with their preceding, well-defined elbows. The estimates of a are next used to match up lists of candidate earthquakes and anomalies. The tentative matchup is then used to refine values of a and the process is repeated.

The next section discusses the results of the matching attempt for both components of SJB and the effects of varying model parameters. Analysis of other tiltmeter data is incomplete, but unpublished work indicates similar results.

RESULTS

The analysis of all SJBN and SJBE data is discussed first; then for the M=5.1 Hollister earthquake, additional data from NUT and ARM are considered. Table 1 summarizes the amount of SJB tilt data available for calculating F_2. Numerous gaps in the data and the requirement of 30 continuous days of data for the F_2 calculation result in about half as many F_2 points as the tilt data duration. The tilt gaps are evident in Figure 2. F_2 gaps in Figure 2 are indicated by $F_2 = 0.$ segments. Tilt data prior to September 1, 1975 was obtained from hand digitized strip chart records. Later data was obtained from telemetered measurements which had spurious data removed manually and by a computerized procedure (Herriot, 1978).

Tables 2 and 3 list all $F_2 > 50.$ anomalies computed from SJBN and SJBE data. Also shown are values for b, the best fit slope difference between L_1 and L_2, and s_1 and s_2, the standard deviations of the residuals. In the Note column, precursor anomalies are numbered for comparison with earthquake data in Table 4. Table 4 contains data for all events whose theoretical anomaly A_t is greater than the threshold value of 0.20. Earthquake source parameters are from routine hypocenter locations using data from the U.S. Geological Survey seismometer network.

Figure 3 shows the line through points corresponding to the final earthquake-anomaly matchups including LIB data on Table 5. Model coefficient values of this line are $a_1=2.0$, $a_2=0.125$. For each earthquake of magnitude M, an anomaly is assigned to an earthquake only when its occurrence time falls within the time range given by the line ± 5 days. Unmatchable $F_2 > 50.$ peaks are classified as false alarms, and earthquakes giving $A_t > 0.20$ for which no $F_2 > 50.$ exists are classified as surprises. Essentially the same model obtains if one selects the first anomaly preceding earthquakes with large A_t by (1) or similar equations (Herriot et al., 1976). Of all the 29 F_2 anomalies detected, 8 are precursory and 21 are false alarms.

The large number of false alarms is a deficiency of the method although, as discussed below, the number may be reduced by raising the F_2 threshold. The cause of false alarms is unknown, but several possibilities may be tentatively ruled out. The first possibility is that false alarms could be associated with rainfall. However, no correlation between dates of false alarms and heaviest rainfall seems to exist. Another possibility is that false alarms have large standard deviations of residuals, s_1 and s_2, regardless of the value of the F_2 peak. However, there is not a strong correlation between false alarms and s_1 or s_2 in Tables 2 and 3. The same is true for subsets defined by F_2 thresholds greater than 50. Thus the surplus of false alarms in this analysis and the similar earlier work by Herriot et al. (1976) and Stuart et al. (1976) cannot be reduced using the noise criterion alone.

After 9-1-75 when the tilt data is from telemetry rather than strip charts, s_1 and s_2 appear to be generally larger, the fraction of false alarms is higher, and the tilt data has a more rugged appearance as though its scale factor were larger. The reason for the differences between the two types of data is unknown.

For 13 (marked N, E) of the 24 earthquakes in Table 4, gaps in the tilt data prevent calculation of F_2 on both components during the entire time

window when an anomaly is expected from the model in Figure 3. Of the 11 remaining earthquakes, 3 earthquake clusters defined by similar epicenters and overlapping model precursor times Δt_t plus 5 days occur. The number of clusters plus solitary earthquakes is 8, and of these, 6 have a precursory anomaly on at least one component. The remaining two earthquakes without anomalies are classified as surprises and are marked by S. If no earthquake clusters are allowed and only a one to one anomaly-earthquake assignment is made, the number of surprises is 5.

Tables 6 and 7 summarize the anomaly-earthquake matchups. The symbol N_A is the number of earthquakes having a precursory anomaly on at least one tiltmeter component, N_F is the number of F_2 false alarms, and N_S is the number of earthquakes or earthquake clusters without any precursory F_2 anomaly (surprises). The context indicates whether N_F applies to an individual component or to the total for both components. For the F_2=50. threshold, N_A/N_F=6/21=0.29, and N_A/N_S=6/2=3.00. The results show that most earthquakes are preceded by precursors, but a relatively large number of anomalies are false alarms.

Figure 4 compares observed and theoretical anomaly magnitudes, A_o and A_t, for the earthquakes in Table 4 having precursory anomalies in Tables 2 and 3 and Figure 3. The theoretical line is a visual fit to the data (ignoring the isolated point, right side) which show more scatter here than they do in Figure 3. The model coefficient a_3 is 0.15. One reason for the greater scatter may be an inherent spacial complexity of tilt fields. A magnitude-precursor time relation may be faithfully followed, but the tilt amplitude of the ground surface may vary rapidly with position.

In the analysis so far, threshold values of F_2, A_t, and Δt_t have been fixed. We now examine the effect of varying these thresholds on the number of earthquakes with at least one precursory anomaly N_A, false alarms N_F, surprises N_S, and their ratios N_A/N_F and N_A/N_S. Table 7 shows that raising F_2 threshold values from 50. to 200. decreases the number of precursory anomalies and false alarms, but increases the number of surprises. The ratio of anomalies to false alarms increases while the ratio of anomalies to surprises decreases. Thus raising the F_2 threshold alleviates the problem of excessive false alarms at the expense of additional surprises. Preliminary analyses of data from other tiltmeters agree with this tradeoff between false alarms and surprises. At thresholds of 200. and higher, the number of N_A and N_F data points is too small for meaningful analysis. In addition, further improvement of N_A/N_F is prevented by the two obdurate false alarms SJBN, 3-27-76, and SJBE, 10-26-74.

A similar variational analysis by raising the A_t threshold is not so rewarding since most of the earthquakes have precursory anomalies (surprises are few). Lowering the A_t threshold increases the number of earthquakes to consider, but many of them have precursor time intervals overlapping with intervals of the earthquakes in Table 4. The qualitative effect of lowering the A_t threshold is to increase N_A and N_S and decrease N_F; thus a tradeoff of N_S and N_F similar to the one with the F_2 threshold occurs here. Changes of F_2 and A_t thresholds (independently) in the same sense have the same effect on N_A but opposite effects on N_F and N_S.

Increasing the precursor time window from ±5 days to ±7 days with respect to the model line in Figure 3 has a small impact on N_A, N_F, and N_S.

In Table 4 the two additional earthquakes occurring on 1-18-77 and 3-16-77 can be matched to the same anomalies assigned to earthquakes on 1-19-77 and 3-12-77. If only one earthquake corresponds to one anomaly, the number of precursory anomalies, false alarms, and surprises is unchanged from the situation for ±5 days. Decreasing the time window to ±3 days removes two precursory anomalies and adds two false alarms. The earthquakes occur on 7-23-75 and 1-19-77; the first earthquake retains a precursory anomaly on the SJBE component, but the second earthquake becomes a surprise.

We now examine more closely the M=5.1 Hollister earthquake which had precursory anomalies on three nearby tiltmeters, SJB, NUT, and ARM. Table 8 and Figure 3 show that the observed precursor times ranged from 33 to 37 days. ARM is the most distant tiltmeter, 20 km from the epicenter, and seems to show a stronger anomaly than NUT which is only 12 km away. ARMN and ARME also have anomalies about 20 days prior to the earthquake, but the anomalies lie outside the 10 day acceptance window for precursors.

In summary, the analysis of this paper indicates that sudden changes of tilt rate have occurred before several small and moderate earthquakes near the San Andreas fault. Anomaly and earthquake matchups appear not to violate assumptions that (1) anomaly magnitude decreases with decreasing earthquake magnitude and increasing distance, and (2) precursor time interval is proportional to earthquake magnitude.

The anomaly detection method seems to successfully find tilt rate anomalies prior to most sufficiently close and large earthquakes. On the other hand the method has several shortcomings. The most obvious defect is the excessive number of false alarms. Another limitation is the lack of precise statistical techniques for judging the significance of model parameter estimates and ratios of anomalies to false alarms and surprises. Formulation of such techniques does not appear to be straightforward because of the large number of empirical constants, the lack of a one to one anomaly and earthquake correspondence, and overlapping precursor intervals. Finally, the large number of gaps in the tilt data suggests caution in accepting the results presented above until analyses of continuous data are available.

ACKNOWLEDGMENTS

We thank A. Steppe for suggesting the analysis of variance method. Numerous discussions with M. J. S. Johnston and C. E. Mortensen have been very helpful.

REFERENCES

Aggarwal, T. P., L. R. Sykes, D. W. Simpson, and P. G. Richards (1975). Spatial and temporal variations in t_S/t_P and in P wave residuals at Blue Mountain Lake, New York: Application to earthquake prediction, Jour. Geophys. Res. 80, 718-732.

Archuleta, R. J., and W. D. Stuart (1978). Instability model for 3-dimensional strike-slip earthquakes (abs.), EOS 59, 1205.

Ergun, S. (1956). Application of the principle of least squares to families of straight lines, Industrial and Engineering Chemistry 48, 2063-2068.

Draper, N. R., and H. Smith (1966). Applied Regression Analysis, John Wiley and Sons, New York, 39-40.

Herriot, J. W. (1978). Geolab, U.S. Geol. Survey Open-File Report 78-700, Menlo Park, Calif.

Herriot, J. W. W. D. Stuart, and M. J. S. Johnston (1976). Earthquake prediction with telemetered tilt data: Procedure (abs.), EOS, 47, 287.

Johnston, M. J. S., and C. E. Mortensen (1974). Tilt precursors before earthquakes on the San Andreas fault, California, Science 186, 1031-1034.

Mortensen, C. E. (1979). The analysis of tilt meter data, in Proceedings of Conference VI, Measurement of Ground Strain Phenomena Related to Earthquake Prediction, edited by J. F. Evernden, U.S. Geol. Surv. Open File Report (this volume), Menlo Park, Calif.

Mortensen, C. E., and M. J. S. Johnston (1975). The nature of surface tilting along 85 km of the San Andreas fault - preliminary results from a 14-instrument array, Pure and Applied Geophysics 113, 237-249.

Mortensen, C. E., and M. J. S. Johnston (1976). Anomalous tilt preceding the Hollister earthquake of November 28, 1974, Jour. Geophys. Res. 81, 3561-3566.

Scholz, C. H. L. R. Sykes, and Y. P. Aggarwal (1973). Earthquake prediction: A physical basis, Science 181, 803-810.

Stuart W. D. (1979), Strain softening prior to two-dimensional, strike-slip earthquakes, Jour. Geophys. Res., in press.

Stuart, W. D., M. J. S. Johnston, and J. W. Herriot (1976). Earthquake prediction with telemetered tilt data: Rationale (abs.), EOS 57, 287.

Stuart W. D., and G. M. Mavko (1979). Earthquake instability on a stike-slip fault, Jour. Geophys. Res., in press.

Whitcomb, J. H., J. D. Garmany, and D. L. Anderson (1973). Earthquake prediction: Variation of seismic velocities before the San Fernando earthquake, Science 180, 632-635.

Wood, M. D., and N. E. King (1977). Relation between earthquakes, weather, and soil tilt, Science 197, 154-156.

Wood, M. D. (1973). Methods for prediction and evaluation of tidal tilt data from borehole and observatory sites near active faults, Phil. Trans. Roy. Soc. Lond., A274, 245-252.

TABLE 1

SUMMARY OF SJB TILT AND F_2 DATA

	SJBN	SJBE
Start date	3-8-74	3-8-74
End date	4-22-77	4-22-77
Days time span	1142	1142
Days of tilt data plus one-day gaps	983	951
Days of nonzero F_2 data	592	542
Ratio of nonzero F_2 to time span	0.52	0.47

TABLE 2

ANOMALY DATA FOR SJBN, $F_2 > 50.$

Date		F_2	b 10^{-3} μrad/day	s_1 10^{-3} μrad	s_2 10^{-3} μrad	A_o μrad	Note
1974	8-9	191	33	15	30	--	F
	9-21	75	19	21	13	--	F
	10-22	187	81	26	83	3.00	1
1975	2-7	193	-99	23	104	2.38	2
	5-2	86	-21	22	13	--	F
	7-13	59	33	39	22	0.33	3
	10-10	130	168	147	55	--	F
	10-31	72	-127	135	112	--	F
	11-15	93	140	141	74	1.40	4
1976	1-8	165	168	109	117	--	F
	3-27	778	158	33	72	--	F
	4-15	94	-127	106	125	--	F
	5-31	88	-193	193	131	--	F
	7-13	87	-165	177	64	--	F
	9-2	55	157	200	126	--	F
	12-26	103	-315	304	145	7.56	5
1977	2-9	74	109	82	154	--	F
	3-26	171	124	67	107	--	F

Notes: 1, 2 ... Number of earthquake having at least one precursory anomaly.

F - False alarm no earthquake.

5 precursory anomalies, 13 false alarms.

Telemetered data starting 9-1-75.

TABLE 3

ANOMALY DATA FOR SJBE, $F_2 > 50$.

Date		F_2	b 10^{-3} μrad/day	s_1 10^{-3} μrad	s_2 10^{-3} μrad	A_o μrad	Note
1974	8-7	97	40	39	20	--	F
	10-26	901	-72	19	25	2.38	1
1975	4-30	61	12	16	6	--	F
	7-6	258	-42	25	15	0.71	3
	8-11	219	54	29	37	--	F
	11-28	55	71	91	58	--	F
1976	4-25	164	-162	128	38	--	F
	7-30	160	263	201	107	--	F
	9-2	95	-169	159	118	--	F
	12-22	62	114	140	74	--	F
1977	2-23	109	144	92	162	2.45	6

Notes: 1, 3, ... Number of earthquake having at least one precursory anomaly.

F - False alarm, no earthquake.

3 precursory anomalies, 8 false alarms.

Telemetered data starting 9-1-75.

TABLE 4

EARTHQUAKE DATA FOR SJB $A_t > 0.20$

Date		M	Depth km	r km	A_t	Δt_o	Note
1974	3-31	3.4	5.1	14.6	.23	--	(1 1) N E
	4-17	3.3	4.8	14.6	.23	--	S (1 1)
	6-14	3.1	5.3	14.7	.21	--	N E
	11-28	5.1	5.8	13.2	.39	37-, 33	1 (2 2)
	11-28	3.1	6.6	16.1	.21	--	(2 2) N E
	11-29	3.3	4.5	13.9	.24	--	(2 2) N E
	12-31	3.8	8.7	15.2	.25	--	(2 N E
1975	1-23	3.0	9.1	12.1	.25	--	(2 3) N E
	1-29	3.2	1.4	2.8	1.14	--	3) N E
	2-7	3.1	8.8	11.8	.26	--	(2 3) 4) N E
	3-3	3.8	8.0	14.9	.26	24, —	2 (3 4) 5) E*
	3-3	4.3	8.0	14.9	.29	24, —	S (3 4) 5) E*
	3-15	3.6	7.1	14.8	.24	--	(3 5) N E
	7-23	3.2	2.1	14.4	.22	10, 17	3
	11-3	3.0	4.1	1.5	2.00	--	S
	11-25	3.1	5.4	12.6	.25	10, —	4
1976	5-20	3.3	10.1	11.3	.29	--	N E
	10-18	3.3	6.1	0.6	5.50	--	N E
	10-23	3.4	8.9	11.4	.30	--	6) N E
	10-24	3.4	6.9	6.2	.55	--	6) N E
1977	1-18	3.3	5.6	14.7	.22	--	S (4 7)
	1-19	3.6	9.1	15.1	.24	24, —	5 (4 7)
	3-12	3.5	9.6	11.1	.32	—, 17	6 8)
	3-16	3.2	6.6	14.3	.22	--	S 8)

Notes:
- 1,2, ... Number of earthquake having at least one precursory anomaly.
- S Surprise, no precursory anomaly on either component.
- (1, ... Earthquake epicenters are less than 3.5 km apart (including aftershocks).
- 1), ... Earthquake model Δt + 5 days overlaps with that for other earthquakes.
- N,E Insufficient tilt data available for north, east component.
- * Anomaly matches two earthquakes; first one chosen.

Notes for t column:
- 37- Precursor time could be less than 37 days because F_2 peak is not an interior maximum.
- — Dash indicates insufficient tilt data or no precursory anomaly for this component.

TABLE 5

ANOMALY AND EARTHQUAKE DATA FOR LIB

Anomaly LIBE (Insufficient data LIBN)

Date	F_2	$b \times 10^{-3}$ 10^{-3} μrad/day	s_1 10^{-3} μrad	s_2 10^{-3} μrad	A_o μrad
1975 6-4	452	89	32	43	0.89

Earthquake

Date	M	Depth km	r km	A_t	Precursor time Δt_o days
1975 6-14	3.2	5.6	3.6	.89	10

TABLE 6

SUMMARY OF ANOMALY-EARTHQUAKE MATCHUP

ANOMALIES		EARTHQUAKES	
Total SJB $F_2 > 50$ anomalies	29	Earthquakes $A_t > 0.20$	24
Precursory anomaly F_2	8	Earthquakes with sufficient tilt data on at least one component	11
False alarms - N_F	21	Earthquakes with at least one precursor (1 to 1 matchup) - N_A	6
		Earthquakes with precursors both components	2
		Surprises (1 to 1 matchup)	5
		Surprises (earthquakes with overlapping precursor times counted as one earthquake) - N_S	2

Ratios

N_A/N_F	6/21=0.29
N_A/N_S	6/2 =3.00

TABLE 7

EFFECT OF INCREASING F_2 THRESHOLD ON

N_A, N_F, AND N_S

F_2 Threshold	SJBN N_F	SJBE N_F	SJB Totals				
			N_A	N_F	N_S	N_A/N_F	N_A/N_S
50	13	8	6	21	2	0.29	3.00
100	5	3	5	8	3	0.63	1.67
150	4	3	3	7	5	0.43	0.60
200	1	1	2	2	6	1.00	0.33

TABLE 8

SJB, NUT, ARM TILT DATA FOR THE M=5.1,

11-28-74 HOLLISTER EARTHQUAKE

	Tilt Component						
	SJBN	SJBE	NUTN	NUTE	ARMN	ARME	ARME
Anomaly Date 1974	10-22+	10-26		10-25+	11-8	10-25	11-7
F_2 (>40)	187	901		67	477	155	41
b 10^{-3} μrad/day	81	-72		16	-70	-83	78
10^{-3} s_1 μrad	26	19		16	27	30	122
10^{-3} s_2 μrad	83	25		18	28	93	28
A_t	.35	.35	.43	.43	.26	.26	26
r (km)	14.6	14.6	12.0	12.0	19.7	19.7	19.7
Precursor Time Δt_o (days)	37-*	33		34+*	20	34	21
A_o μrad	3.00	2.38		0.54	1.40	2.82	1.64

* See Notes for Δt_o, Table 3

FIGURE CAPTIONS

Figure 1. Anomaly definition and parameters.

Figure 2. Tilt and F_2 data for SJBN, SJBE, and part of LIBE components.

Figure 3. Earthquake magnitude M vs. observed and theoretical precursor times, Δt_o and Δt_t, for anomaly-earthquake matchups. Number beside point identifies earthquake on Table 4.

Figure 4. Theoretical vs. observed anomaly magnitudes, A_t and A_o. Slope of line is $a_3 = 0.15$.

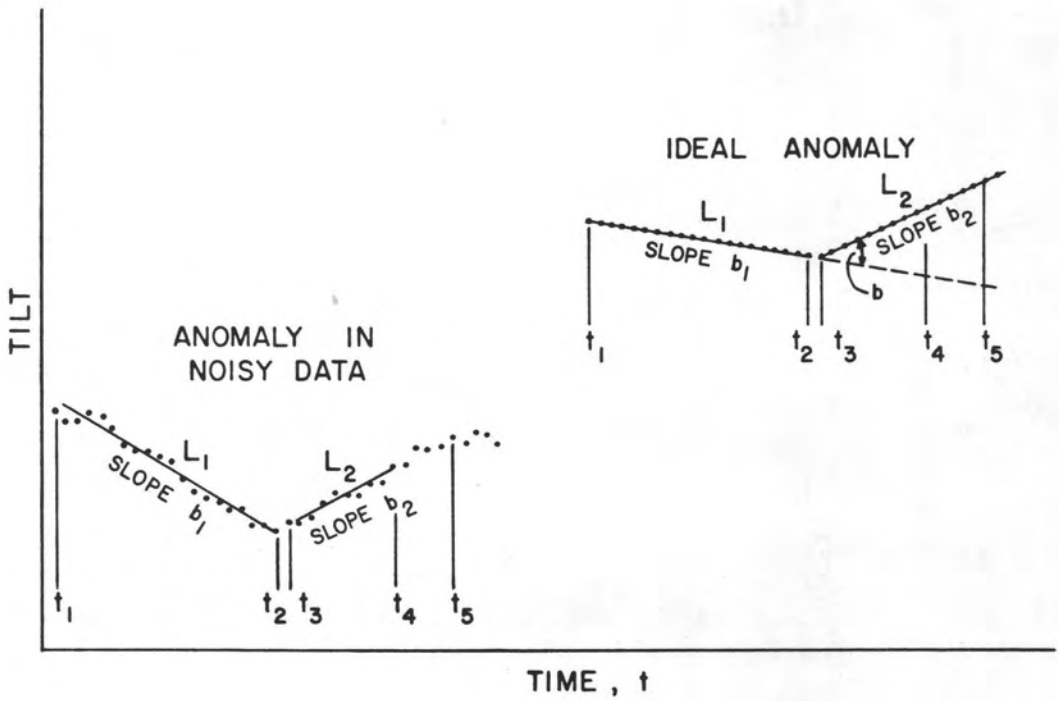
TILT
IDEAL ANOMALY
L1
L2
SLOPE b1
SLOPE b2
b
t1
t2
t3
t4
t5
ANOMALY IN
NOISY DATA
L1
L2
SLOPE b1
SLOPE b2
t1
t2
t3
t4
t5
TIME , t

fig. 1

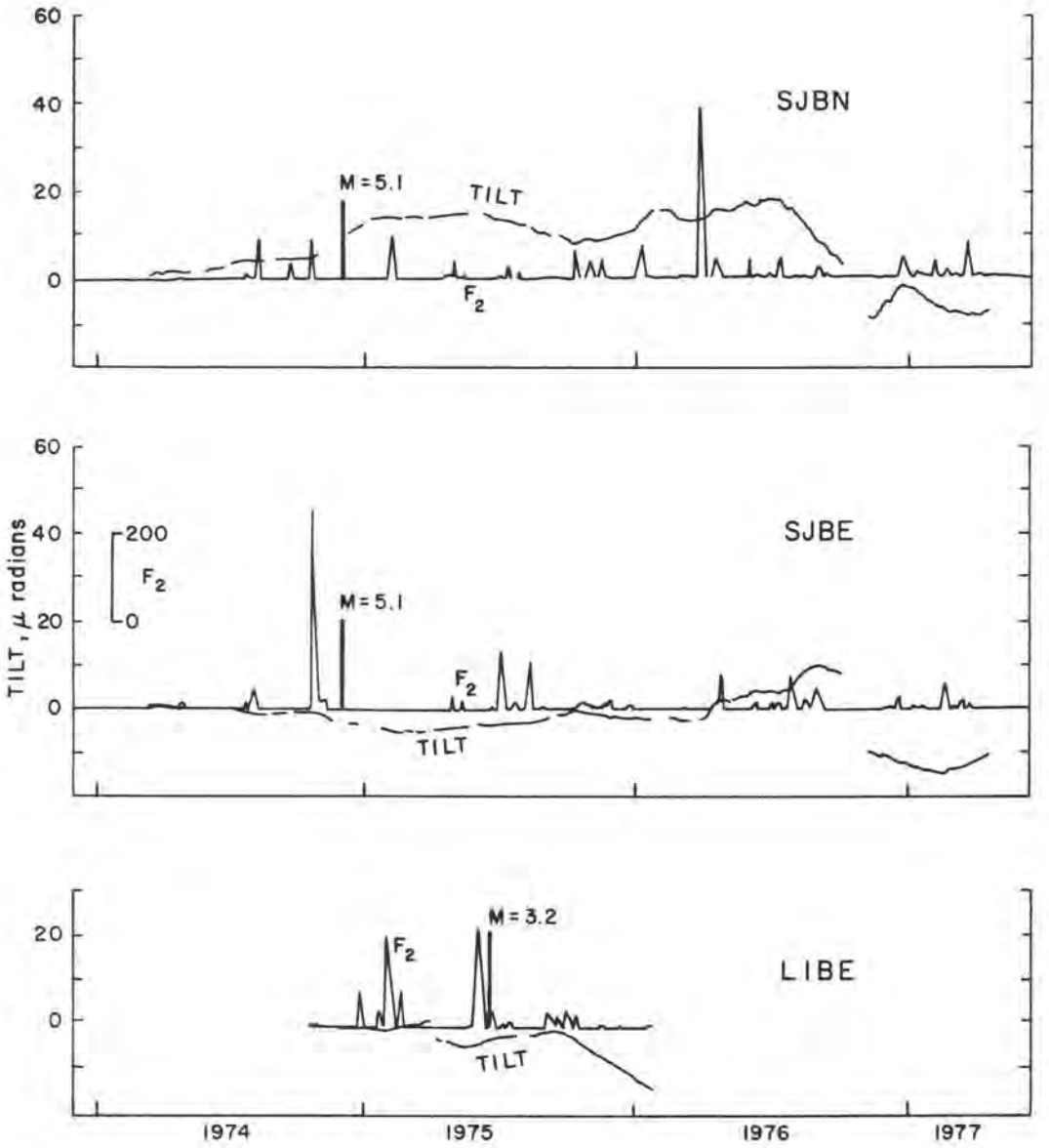
60
40
20
0
SJBN
M=5.1
TILT
F2
60
40
20
0
TILT, μ radians
200
F2
0
SJBE
M=5.1
F2
TILT
20
0
M=3.2
F2
LIBE
TILT
1974
1975
1976
1977

fig. 2

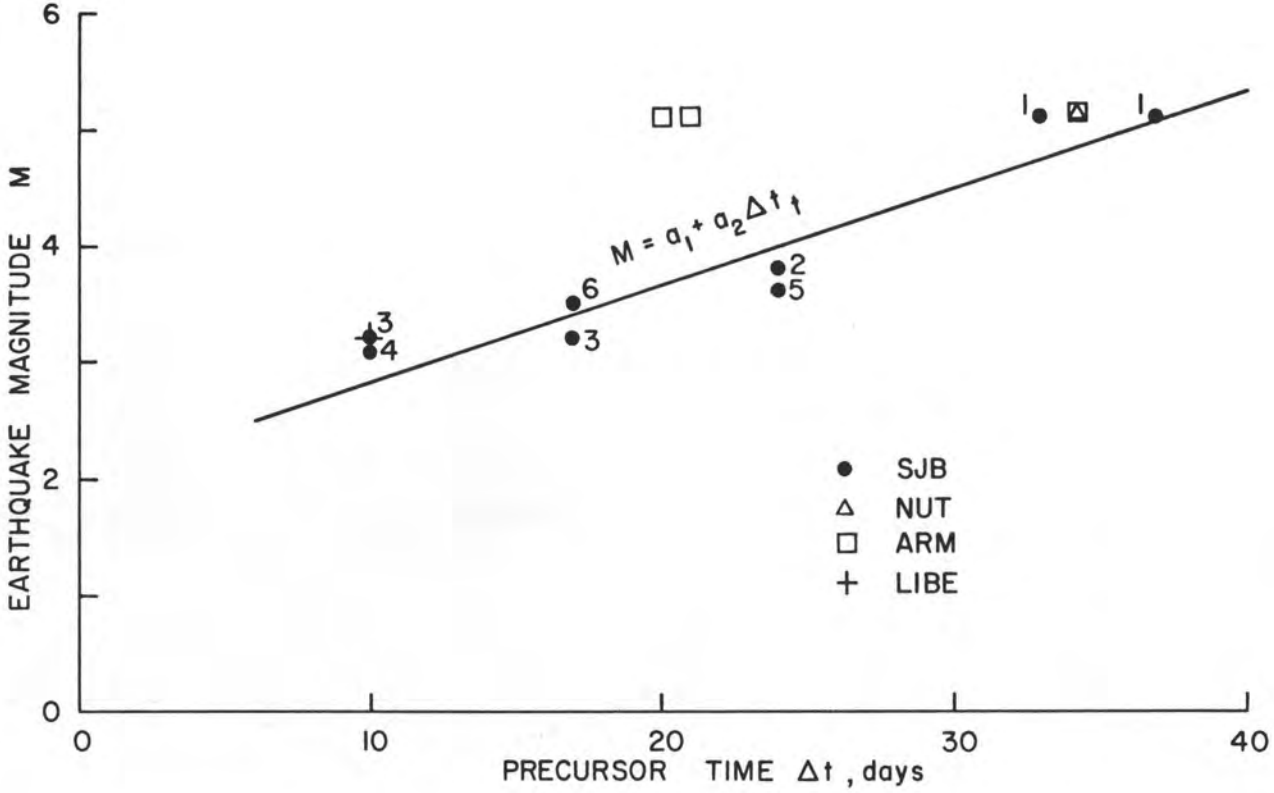
EARTHQUAKE MAGNITUDE M
PRECURSOR TIME Δt , days
M = a1 + a2 Δt
SJB
NUT
ARM
LIBE
0
2
4
6
0
10
20
30
40
1
1
1
2
5
6
3
3
4

fig. 3

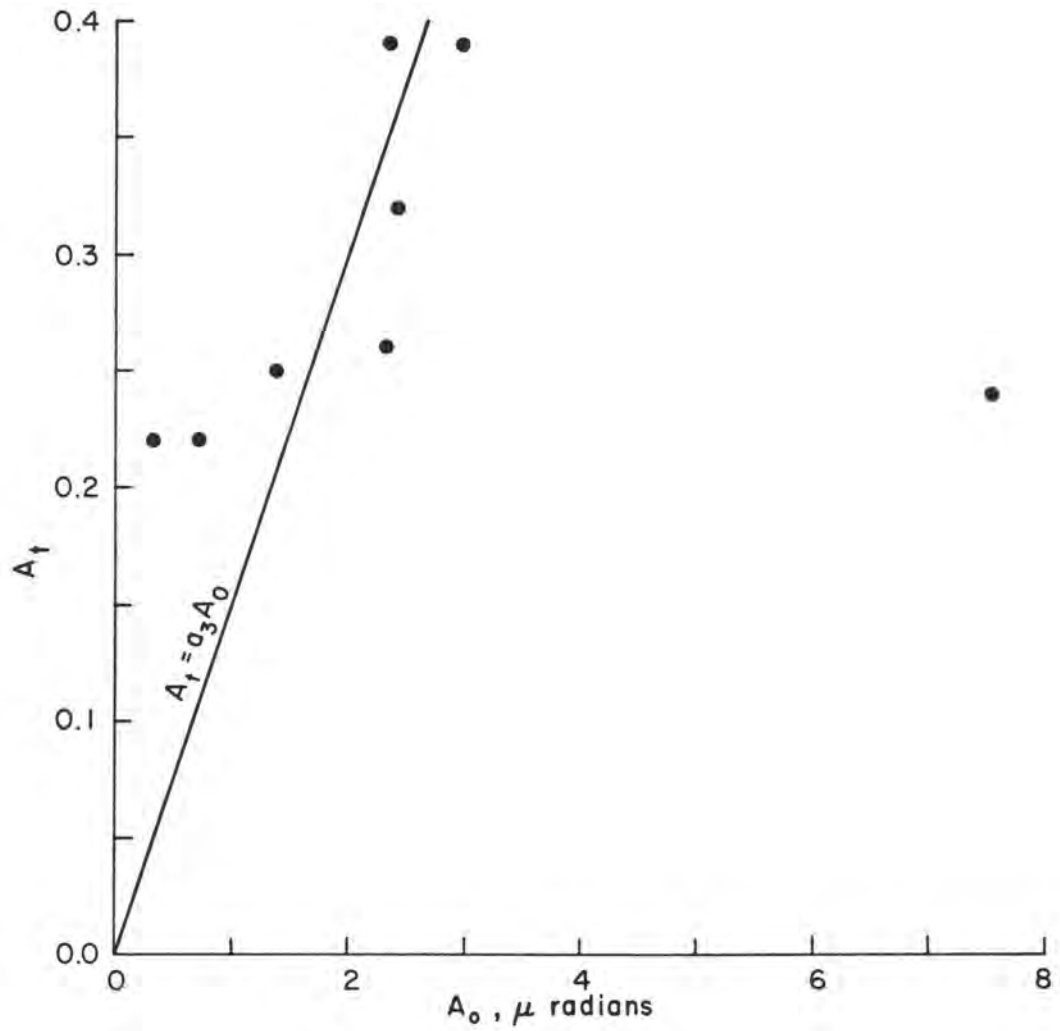

fig. 4

THE DRY TILT METHOD OF MEASURING CRUSTAL TILT

by

Arthur G. Sylvester
Department of Geological Sciences
and Marine Science Institute
University of California
Santa Barbara, California 93106

for

Conference on Measurement of Ground Strain
Phenomena Related to Earthquake Prediction,
September 7-9, 1978

Sponsored by the U.S. Geological Survey
Earthquake Hazards Reduction Program

THE DRY TILT METHOD OF MEASURING CRUSTAL TILT

by

Arthur G. Sylvester
Department of Geological Sciences
and Marine Science Institute
University of California
Santa Barbara, California 93106

ABSTRACT

The dry tilt method of measuring crustal tilt employs a precision optical level in the center of an array of three precision leveling rods set on each of three permanent benchmarks arranged at the apices of a triangle having side lengths of from 30 to 40 m. Tilt vectors are determined from elevation changes of the benchmarks, and the method is so simple and quick that the tilt vectors can be computed in the field with a pocket calculator. When measurement procedures are followed rigorously, a sensitivity of 3×10^{-6} radians (three microradians) may be obtained.

INTRODUCTION

The dry tilt method of measuring crustal tilt was developed by Kinoshita, Swanson and Jackson (1974) to document inflation of Kilauea Volcano, Hawaii, during its eruptive cycle. More formally termed spirit level tilting, it is an optical method of measurement in contrast to tiltmeters employing water, mercury or some other fluid. In Hawaii the dry tilt measurements complement those of borehole tiltmeters as well as short-base (3 m) and long-base (50 m) water-tube tiltmeters.

More recently the dry tilt method has been used on La Soufriere Volcano, Guadaloupe (Fiske, 1976) and in the southern California uplift (Sylvester, 1977; Sylvester, Riggs and Blackmur, 1977).

The purpose of this report is to describe and discuss the methodological procedures as we have learned them, particularly from Gary Puniwai (Hawaiian Volcano Observatory), and have practiced them in California. The objective is to make the details of the method known so that others may understand and appreciate it, and better still, use it themselves.

PRINCIPLES

Three points are required to determine the orientation of a plane in space. The change in orientation (tilt vector) of the plane after a rotation (tilt) can be determined from the change of elevation of each point in the time interval T_1-T_2 by the following equations, assuming the geometry shown in Figure 1:

$$\tau N = -K_1\delta(Y-X) - K_2\delta(X-Z) \quad (1)$$

$$\tau E = K_3\delta(Y-X) + K_4\delta(X-Z) \quad (2)$$

where $K_1 = \frac{l0 \cos \phi}{ly \sin (\phi-\theta)}$; $K_2 = \frac{l0 \cos \theta}{lz \sin (\phi-\theta)}$;

$K_3 = \frac{l0 \sin \phi}{ly \sin (\phi-\theta)}$; $K_4 = \frac{l0 \sin \theta}{lz \sin (\phi-\theta)}$;

then tilt azimuth $\theta = \arctan (\tau E/\tau N)$ (3)

and tilt plunge $\tau = \sqrt{(\tau N)^2 + (\tau E)^2}$ (4)

The equations are the corrected versions of those originally given by Eaton (1959). The equations are valid only when the line XY trends northeast (Fig. 1).

ARRAY CONFIGURATION

The optimal configuration of three points for the dry tilt method describes an equilateral triangle having side lengths of from 30 to 40 m (Fig. 2). This geometry yields a shot distance of from 20 to 23.1 m which is less than the 25 m maximum length permitted for precision first-order leveling, but which still defines a relatively long-base tilt array. Smaller arrays are established when constrained by topography, such as narrow canyons.

We establish an array by setting a benchmark from 20 to 23.1 m from the center point. Using a T2 theodolite at the center point, 120° angles are turned from the first benchmark to establish rays along which the other two benchmarks are set. Ideally the shot lengths from the center point to each benchmark should be equal so that the level need not be refocused during the dry tilt measurements. Thus, shot lengths are taped to the nearest decimeter, and angles are turned to the nearest 0.5° when the array is initially established.

Care must be taken to select reasonably level sites, about 100 m square or more. Ideally, the absolute elevation difference between benchmarks ought not exceed one meter in order to assure that the level sights fall in the center half of each leveling rod when it is placed on the benchmark.

We take care to choose sites having radial symmetry. We deliberately avoid sites near oil and water wells, landslides, recently imposed loads such as bridges and large fills, sites likely to be developed or plowed for agricultural purposes, and sites likely to be subject to vandalism. In our experience, the noisiest data are obtained from tilt sites on ridge crests, forested areas and on bedrock, whereas data showing least noise are obtained from sites on wide open flats underlain by relatively thick deposits of alluvium.

BENCHMARKS

Each of the three benchmarks is permanent and consists of 1/2 inch (1 cm) thick steel rod which is driven to refusal and then capped by a rounded stainless steel tip (Fig. 3). We use 4 foot (1.3 m) long steel rods, threaded at each end so that they can be coupled together with ground rod couplings to reach a firm footing. The tip is threaded to screw on top of the rod and is fastened with thread lock compound to discourage removal by vandals.

The uppermost 0.5 m of the benchmark is decoupled from the ground by a PVC or transite pipe jacket, but the rod is supported in an upright position by filling the pipe with coarse, untamped gravel to the level of the tip. A cap on the pipe keeps out water and dirt. A rod, stone cairn or large boulder is all that is needed to mark the center point.

Materials for a single benchmark range in cost from $5 to $25, exclusive of machining. An array requires from two to four hours to establish, depending upon the number of rods to be driven for each benchmark, the density of the brush to be cleared, etc.

INSTRUMENTATION

The instrumentation we use, together with the 1978 catalog prices, is as follows:

Wild N3 precision level	$ 3208
3 Wild GPL-3 precision invar rods and support stays	5384
Surveyor's umbrella	35

The Wild N3 is one of only four precision levels approved for first order precision leveling. It is always shaded with an umbrella or tent from direct sunlight; a tent is useful in wind; however, good data are generally not obtained in strong wind.

Three precision leveling rods make surveying the array simple and quick, but two rods are sufficient and are merely leap-frogged during the measurement procedure.

PROCEDURE

The leveling rods are always attached to the same support stays, and they are labelled "X," "Y," and "Z," to match their respective benchmarks in every survey. The rods and benchmarks are also color coded to facilitate matching rod and benchmark from survey to survey.

After the level is set up in the center of the array, we generally wait about 10 or 15 minutes to allow the tripod to adjust to having been jammed in the ground. It has been our experience that the first set of the data shows strange variations and does not contribute to closure if we start measurements immediately after the level is set up.

After the instrument is carefully leveled, the rods are read in pairs beginning with Y-X, and each pair is read three times or as many times as required until the variation among three consecutive differences is less than 0.010 cm. This is shown in Figure 4, which is a typical layout of the notes. Note how the last reading of the first set, an X reading, is used as the first X reading in the second, or X-Z set, and so also for the second and third set.

The calculated closure is the algebraic sum of the Y-X difference and the X-Z difference, and it should equal the observed Z-Y difference within ±0.006 cm. The calculated and observed closures are adjusted in the field, usually by adjusting the observed differences having the greatest variation (Fig. 4). Should the observed and calculated closures differ by more than 0.006 cm, measurements should be repeated between rod pairs having the greatest variations in their differences until an acceptable closure is obtained. This may necessitate resurveying the entire array.

The elevation changes between any two surveys are obtained by subtracting the earlier data from the most recent, and these values are then inserted into the equation having constants previously determined for the geometry of that particular array. The results are the tilt components: positive values for north and east components, negative for south and west components. Thus a positive north component and a negative east component indicates a north-west tilt azimuth.

The tilt in microradians is calculated by plugging the north and east tilt components into the general equations for tilt azimuth, Ø, and plunge, τ.

All calculations can be done in the field with a pocket calculator.

REPRODUCIBILITY, PRECISION, ACCURACY

With superior equipment in good adjustment, with careful attention to detail, and with rigorous, systematic measurement procedure, a sensitivity of from 2 to 3 x 10^{-6} radians (2-3 microradians) can be achieved by the dry tilt method (Kinoshita, Swanson, and Jackson, 1974, p. 92). This is the same order of magnitude as the short-base water-tube tiltmeter that has been so fundamental in tilt measurements in Hawaii for the past 20 years, but it is two orders of magnitude less sensitive than the present state-of-the-art borehole tiltmeters. The latter tiltmeters, however, yield point measurements, whereas the dry tilt method has a relatively long baseline.

This sensitivity is sufficient to document relatively large crustal tilts which are observed on flanks of active volcanoes and which are thought to precede large earthquakes (Selwyn Sacks, oral communication, this conference, 1978), but it may not be sensitive to long term strain accumulation or to tilt prior to small and moderate earthquakes.

We have done a number of tests to determine the sensitivity and reproducibility of the dry tilt method for measuring crustal tilt in southern California.

The first test checked observational variations among six different instrumentmen at a single site during a five hour period of daylight. After each instrumentman completed his readings, the instrument and the leveling rods were picked up and reset. The results are shown diagrammatically in Figure 5. The mean of the six determinations is plotted at the center of the concentric circles, and each circle represents one standard deviation from the mean. Most of the observations are within one microradian of the mean; those showing greater deviation reflect degree of previous experience. Thus, Mowles, Rockwell and AGS have had much experience, Fisher and Riggs had no prior experience before this test, and Minor had had minimal experience. The test shows that reproducibility among different instrumentmen is very good.

The second test checked the reproducibility of measurements at two sites, 48 km apart, over a 12 hour period at night. The equipment was dismantled after each site was surveyed and transported to the other site where the measurement procedure was repeated. For this test we chose a site that has been relatively "quiet" over a one-year period (90th St. E) and one that has been relatively "noisy" over a period of one and one-half years (Upper Cajon Creek). The data for this test are tabulated in Table I.

Each of the surveys on 4-5 July is compared with a survey done one month earlier on 3-4 June. The variation from survey to survey can be judged from the observed elevation differences (Y-X, X-Z, Z-Y) which, themselves, are the averages of three consecutive sets of readings that must agree with one another within 0.010 cm. The results of this test show very good agreement among each site survey with small standard deviations of tilt azimuth from 1° to 2.5°, and of tilt plunge of one microradian.

The third test checked the reproducibility of surveys of six sites within a 28 km^2 area over a five day period (Table II) during which most of the surveying was done at night. The data in Table II are presented similarly to those in Table I. Good reproducibility was achieved for determinations of tilt plunge with standard deviations ranging from 1 to 3 microradians, but the standard deviations of the tilt azimuths are large, unacceptably large, until it is realized that a small change in tilt plunge from horizontal can yield a major change in tilt azimuth. Thus the dry tilt method is relatively insensitive to changes of tilt azimuth when the tilt is very small, that is within the standard deviation of the tilt plunge.

Inasmuch as three points are the minimum required to define the orientation of a plane in space, additional benchmarks provide redundancy and confidence in the primary measurements. We prefer to set three more benchmarks adjacent to, but a few meters away from, the first three, thus establishing a separate dry tilt array which we measure and calculate separately. We have established redundancy arrays at those sites which we considered to be unusually noisy, that is, where we suspected one of more benchmarks were unstable. In each case, the new redundancy arrays show much less apparent tilt, and for this reason, any given array and its redundancy array do not track each other well. The older, apparently unstable arrays are now abandoned in favor of the new, apparently more stable redundancy arrays. We are gradually establishing redundancy arrays at all dry tilt sites to quantify the accuracy of our measurements. We have also established several dry tilt arrays adjacent to borehole tiltmeters in southern California for temporal and quantitative cross-checks between the two tilt-measuring methods. Comparative data between the two methods are given by Kinoshita, Swanson and Jackson (1974, p. 92).

PROBLEMS

Dry tilt measurements simply are not done conveniently or well enough in rainy and windy weather. The leveling rods should not be exposed in prolonged rain, and the wind creates problems too numerous to relate. Foggy or overcast weather is ideal dry tilt weather, because the temperature is cool and constant, and an umbrella is not needed.

Temperatures in excess of 20° over flat open ground often cause heat waves during the daytime, leading to poor measurement results. Measurements

during rapid temperature fluctuations, such as occur at sunset, yield poor results. These difficulties force us to do much of our surveys at night when the air is generally still, free of heat shimmer, and the temperature fluctuations are minor. We illuminate each rod with a fixed 6-volt flashlight beamed at the reading elevation.

We have experienced some difficulties with destruction or loss of benchmarks due to unusually severe winter floods and vandalism. Areas prone to floods can be anticipated, whereas vandalism can be alleviated by establishing arrays on private property with the owner's knowledge and permission.

RESULTS

One of the conventional ways to plot tilt data is by means of a vector diagram as shown in Figure 6. In addition, we plot the τN and τE tilt components separately in xy graphs; changes in the tilt vectors themselves can also be plotted in polar plots.

During the past one and one-half years of observing more than 40 dry tilt arrays in the initially recognized area of the Palmdale uplift (Castle, Church and Elliott, 1976), we have observed no consistency in regional patterns of tilt that we can sensibly attribute to tectonic tilt. We suspect secular and seasonal variations may be quite large. We are unable to evaluate rigorously the effect of the unusually heavy winter 1978 rainfall on measureable tilt in the uplift area; however, preliminary analyses yield the surprising conclusion that the effects are minimal with some glaring local exceptions.

An interesting pattern of tilt is shown in the central part of the uplift (Figure 6). There a radial-outward tilt was observed in the period March-April, 1978. The tilt area coincides spatially with the epicentral area of an unusual cluster of minor earthquakes that commenced in November, 1976, and continued sporadically through February, 1978 (McNally and others, 1978). Unfortunately the dry tilt arrays in that area were established only in February, 1978, so it is not possible to relate the tilt pattern with tectonic activity, but it is a tantalizing result and bears watching.

ACKNOWLEDGMENTS

Dr. R. I. Tilling, Scientist-in-charge of the Hawaiian Volcano Observatory, provided the opportunity to visit the Observatory in 1976 to learn methods of measuring crustal tilt. Gary Puniwai coached me in the method, procedures and calculations of dry tilt. Experience in California has been gained with University of California, Santa Barbara, students Robert Blackmur, Nancy Riggs, Thomas Rockwell, and Larry Voors.

The research has been supported by the U. S. Geological Survey, Department of the Interior, under USGS Grants No. 14-08-0001-G-390 and No. 14-08-0001-G-475.

REFERENCES CITED

Castle, R. O., J. P. Church, and M. R. Elliott, 1976. Aseismic uplift in southern California. Science 192, 251-253.

Eaton, J. P., 1959. A portable water-tube tiltmeter. Seism. Soc. Americal Bull. 49 (4), 301-316.

Fiske, R. S., 1977. Threat of eruption at La Soufriere. Earthquake Information Bull. 8 (6), 27-29.

Kinoshita, W. T., D. A. Swanson, and D. B. Jackson, 1974. The measurement of crustal deformation related to volcanic activity at Kilauea Volcano, Hawaii. pp. 87-115 in Civetta et al., eds., Physical Volcanology, Elsevier Pub. Co.

McNally, K. C., H. Kanamori, J. Peckmann, and G. Fuis, 1978. Seismicity increase along the San Andreas fault, southern California. Science, in press.

Sylvester, A. G., 1977. Dry tilt and leveled alignment arrays, Palmdale uplift, California. EOS, 58 (6), 496.

Sylvester, A. G., Nancy Riggs, and R. W. Blackmur, 1977. Results of dry tilt measurements for 1977, Palmdale uplift, California. 1978 Fall Meeting Program, American Geophysical Union, San Francisco, p. 29.

TABLE I

UPPER CAJON CREEK (26)

	0235 hrs. 4 June	2030 4 July	0005 5 July	0655 5 July	0845 5 July	Mean	SD
Y-X	-172.302	-172.278	-172.300	-172.291	-172.296	-172.291	0.010
X-Z	170.392	170.578	170.590	170.586	170.595	170.587	0.007
Z-Y	1.910	1.700	1.710	1.705	1.701	1.704	0.004
θ		N82E	N88E	N85E	N86E	N85E	2.5°
τ (in μradians)		57.4	57.4	57.6	59.4	58.0	1.0

90TH ST. E. (19)

	1855 hrs. 3 June	1935 4 July	0255 5 July	0515 5 July	Mean	SD
Y-X	36.199	36.247	36.243	36.239	36.243	0.004
X-Z	-45.550	-45.577	-45.573	-45.572	-45.574	0.003
Z-Y	9.351	9.330	9.330	9.333	9.331	0.002
θ		N35E	N37E	N36E	N36E	1°
τ (in μradians)		12	11	10	11	1.0

TABLE II

LLANO (4)

	0855 hrs. 30 June	2210 9 July	1850 10 July	0430 12 July	0255 13 July	1830 13 July	Mean	SD
Y-X	81.328	81.331	81.333	81.311	81.334	81.318	81.325	0.010
X-Z	-103.115	-103.112	-103.110	-103.093	-103.105	-103.100	-103.104	0.008
Z-Y	21.787	21.781	21.777	21.782	21.771	21.782	21.779	0.004
θ		N90E	N90E	S13E	S82E	S19E	S59W	39°
τ (in μradians)		1.7	2.9	6.7	4.7	4.4	4.0	1.9

CIMA MESA (34)

	0230 hrs. 30 June	0720 10 July	0120 11 July	2335 11 July	2335 12 July	0015 14 July	Mean	SD
Y-X	140.177	140.170	140.172	140.169	140.154	140.177	140.168	0.009
X-Z	-109.613	-109.616	-109.616	-109.599	-109.600	-109.613	-109.609	0.008
Z-Y	- 30.564	- 30.554	- 30.556	- 30.570	- 30.554	- 30.564	- 30.560	0.007
θ		262	267	160	211	245	229	44°
τ (in μradians)		2.9	2.3	4.0	6.6	3.3	3.8	1.7

TABLE II (Cont'd.)

VABM WARD (38)

	2325 hrs. 29 June	0920 10 July	0235 11 July	2145 12 July	0055 13 July	0145 14 July	Mean	SD
Y-X	-181.621	-181.617	-181.622	-181.632	-181.624	-181.649	-181.629	0.012
X-Z	38.010	38.010	38.008	38.022	38.028	38.019	38.017	0.008
Z-Y	143.611	143.607	143.614	143.610	143.596	143.630	143.611	0.012
θ		N80E	N59W	S16W	S31E	S62W	S19W	84°
τ (in μradians)		1.3	0.9	3.8	5.5	8.2	3.9	3

PUNCHBOWL PARK (37)

	0555 hrs. 30 June	0100 10 July	2105 10 July	0135 12 July	2125 12 July	2150 13 July	Mean	SD
Y-X	- 9.056	- 9.050	- 9.050	- 9.055	- 9.055	- 9.052	- 9.052	0.002
X-Z	-145.568	-145.577	-145.576	-145.561	-145.559	-145.551	-145.565	0.011
Z-Y	154.624	154.627	154.626	154.616	154.614	154.603	154.617	0.010
θ		N22E	N28E	S26E	S24E	S29E	S88E	70°
τ (in μradians)		2.6	2.4	2.5	3.2	6.4	3.4	1.7

TABLE II (Cont'd.)

LANDING STRIP (33)

	0055 hrs. 30 June	0830 10 July	1050 11 July	2230 11 July	0020 13 July	0055 14 July	Mean	SD
Y-X	16.569	16.596	16.578	16.579	16.578	16.582	16.583	0.008
X-Z	-158.179	-158.173	-158.166	-158.168	-158.172	-158.175	-158.171	0.004
Z-Y	141.610	141.604	141.588	141.589	141.594	141.593	141.594	0.006
θ		S24E	S48E	S52E	S58E	S71E	S50E	17°
τ (in μradians)		2.0	6.3	6.0	4.6	5.1	4.8	1.7

MURPHY LANE (36)

	0340 hrs. 30 June	0235 10 July	2210 10 July	0030 12 July	2255 12 July	2235 13 July	Mean	SD
Y-X	296.300	296.301	296.299	296.298	296.291	296.302	296.298	0.004
X-Z	-109.532	-109.523	-109.523	-109.532	-109.530	-109.529	-109.527	0.005
Z-Y	-186.768	-186.778	-186.776	-186.766	-186.761	-186.773	-186.771	0.007
θ		S59E	S48E	S60W	S54W	S77E	S13E	67°
τ (in μradians)		3.0	2.8	0.6	2.7	1.4	2.1	1.0

Fig. 1. Geometry of dry tilt array. Station X is always the southernmost point, Y and Z are designated counterclockwise, the line XY must be northeast of east to compute tilt according to the equations given in this paper. The triangle sides, ly and lz, can vary in length from 30 to 40 m. Angles are measured to the nearest 1/2 degree, lengths are taped to ±0.1 m.

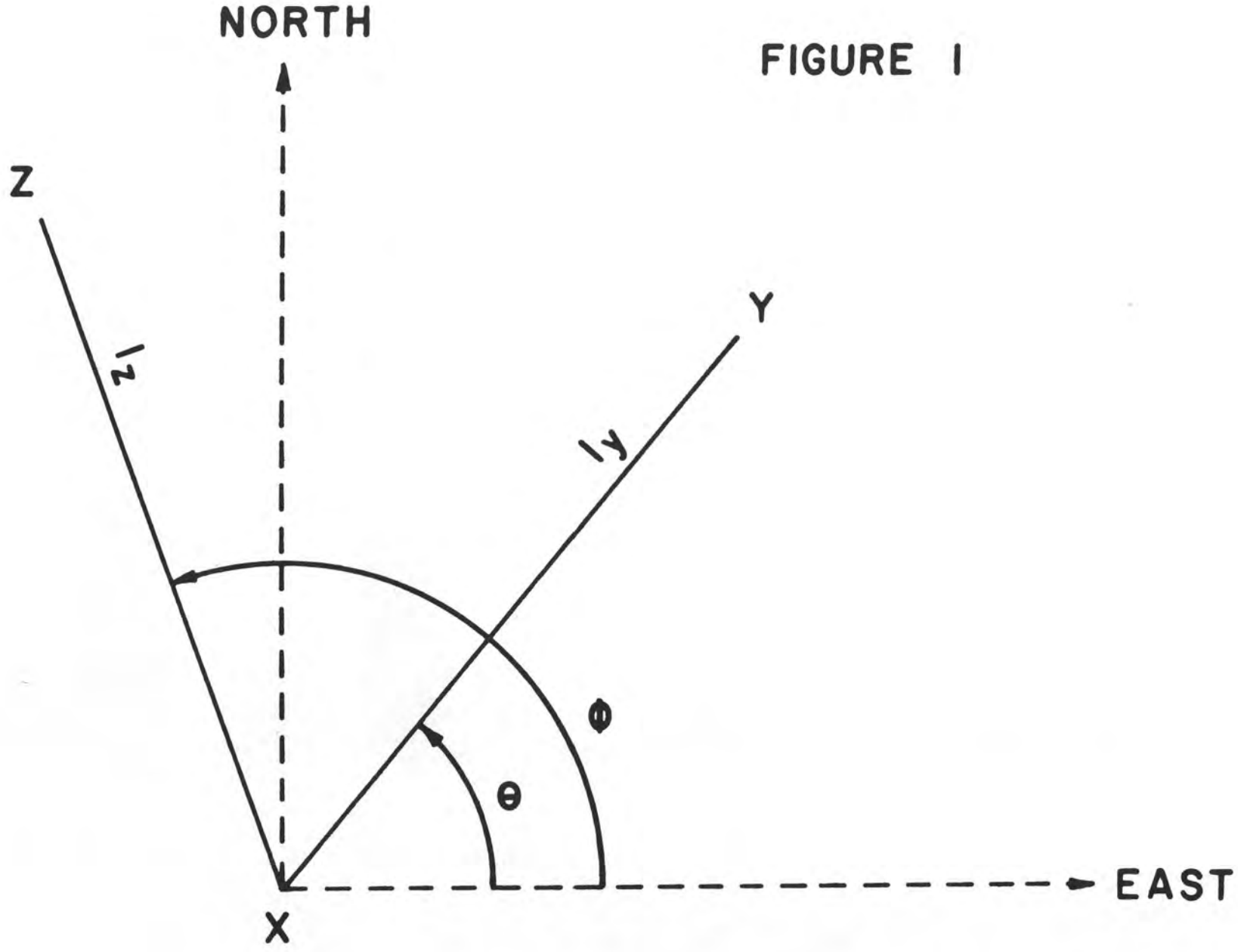

FIGURE 1

Fig. 2. Schematic layout of a dry tilt array with level rods erected upon benchmarks at the apices of the array. The level is set up over a monument in the center of the array.

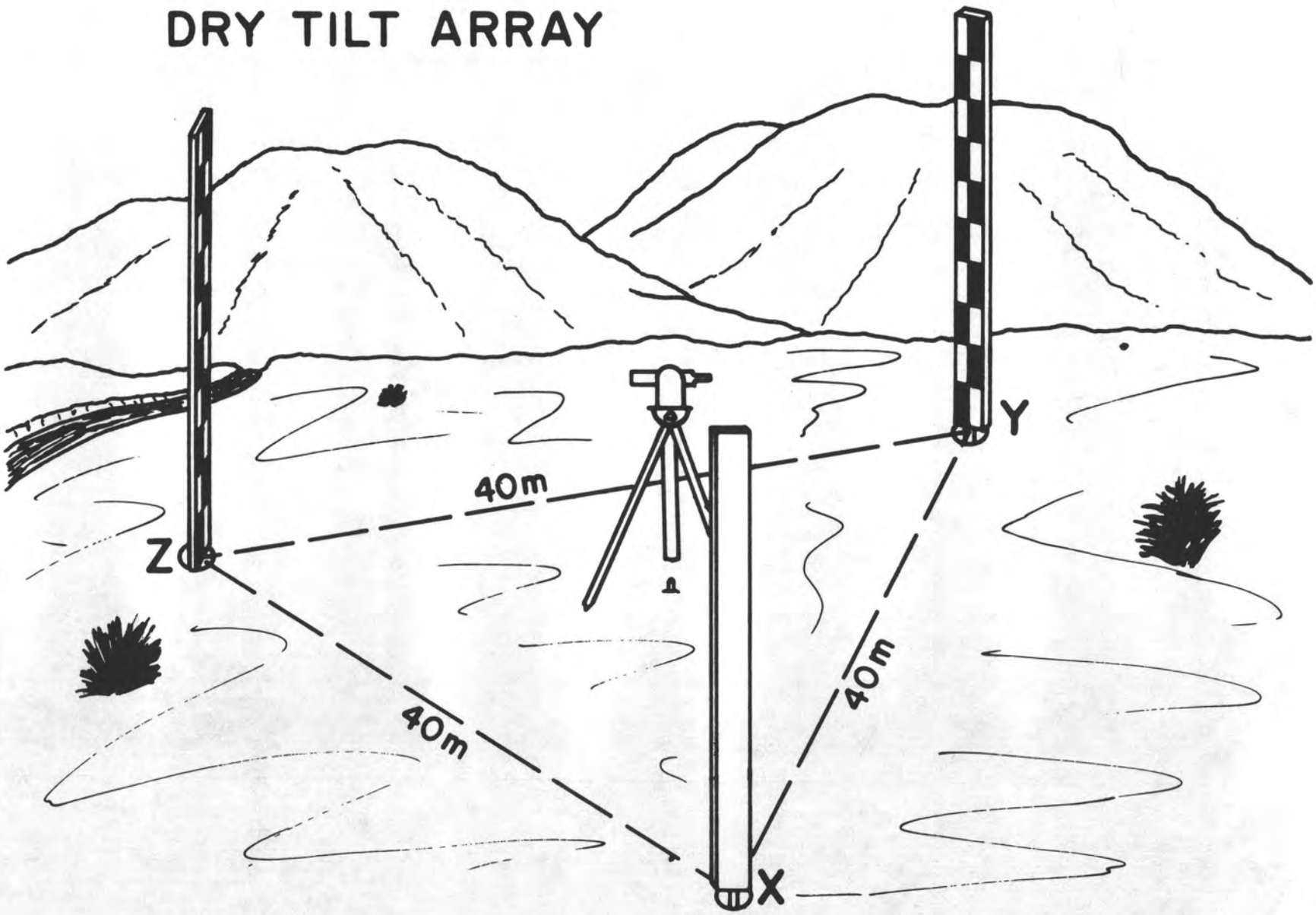

Fig. 2

Fig. 3. Schematic representation of a dry tilt benchmark.

DRY TILT BENCHMARK

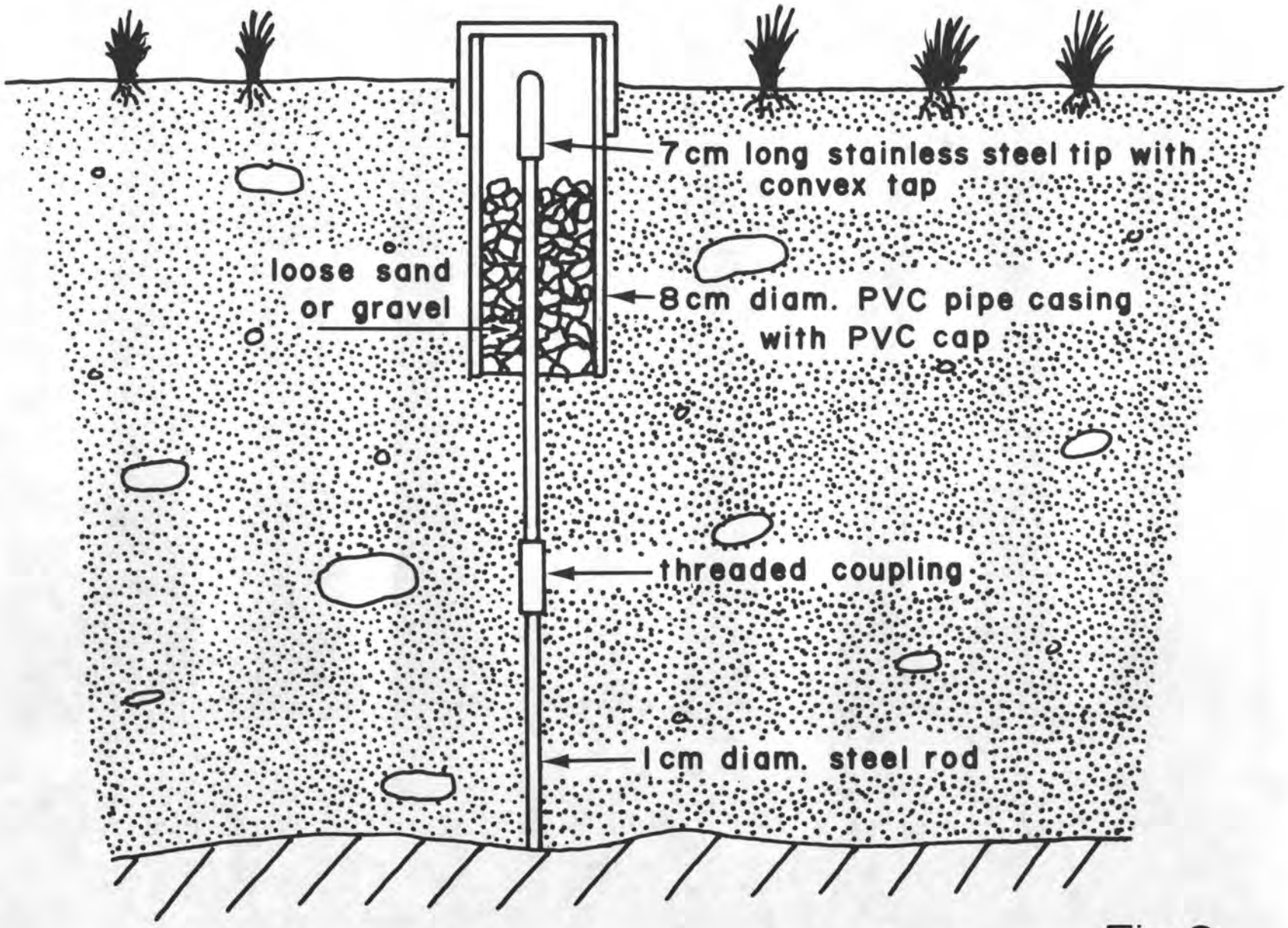

Fig. 3

Fig. 4. Typical layout of notes for dry tilt array.

32) TVOORS, AGS

27 APRIL 1978 Ave. 25 E

		Δ			
sunlit Y	197.153	53.396	143.757	shaded X	28°C
	.163	.401	.762		28°C
	.189	.408	.781		
	.161	.383	.778		29°C
	.161	.388	.773		29°C
	.159	.389	.770		
	.160	.388	.772		
		.388			
X	143.772	-66.667	210.439	shaded Z	29°C
	.767	.672	.439		29°C
	.765	.668	.433		
		.669			
Z	210.433	13.278	197.155	Y	29°C
	.432	.277	.155		29°C
	.435	.279	.156		

33) Clear, light gusty NW breeze, meadowlarks
slight heat shimmer

Start 1235 hrs, T = 28°C Stop 1310 hrs T = 29°C

		ADJUST
Y-X	53.388	53.390
X-Z	-66.669	-66.668
Z-Y calc	+13.281	+13.278
Z-Y obs	13.278	+13.278

	27 APRIL	13 APRIL	δ
Y-X	+53.390	+53.427	-37
X-Z	-66.668	-66.734	+66
Z-Y	+13.278	+13.307	-29

TN = 0.144 (-37) - 0.144 (+66) = - 14.832

TE = 0.258 (- 37) + 0.258 (+66) = 7.482

θ = S27E

τ = 16.6 μrads

FIGURE 4

564

Fig. 5. Mean and standard deviation in microradians of surveys by six instrumentmen of single dry tilt array during five-hour period of daylight. The instrument and leveling rods were reset after each survey. Mowles, Rockwell and AGS are instrumentmen with much experience. Riggs and Fisher had no prior experience with the instrument prior to the test, and Minor had minimal previous experience.

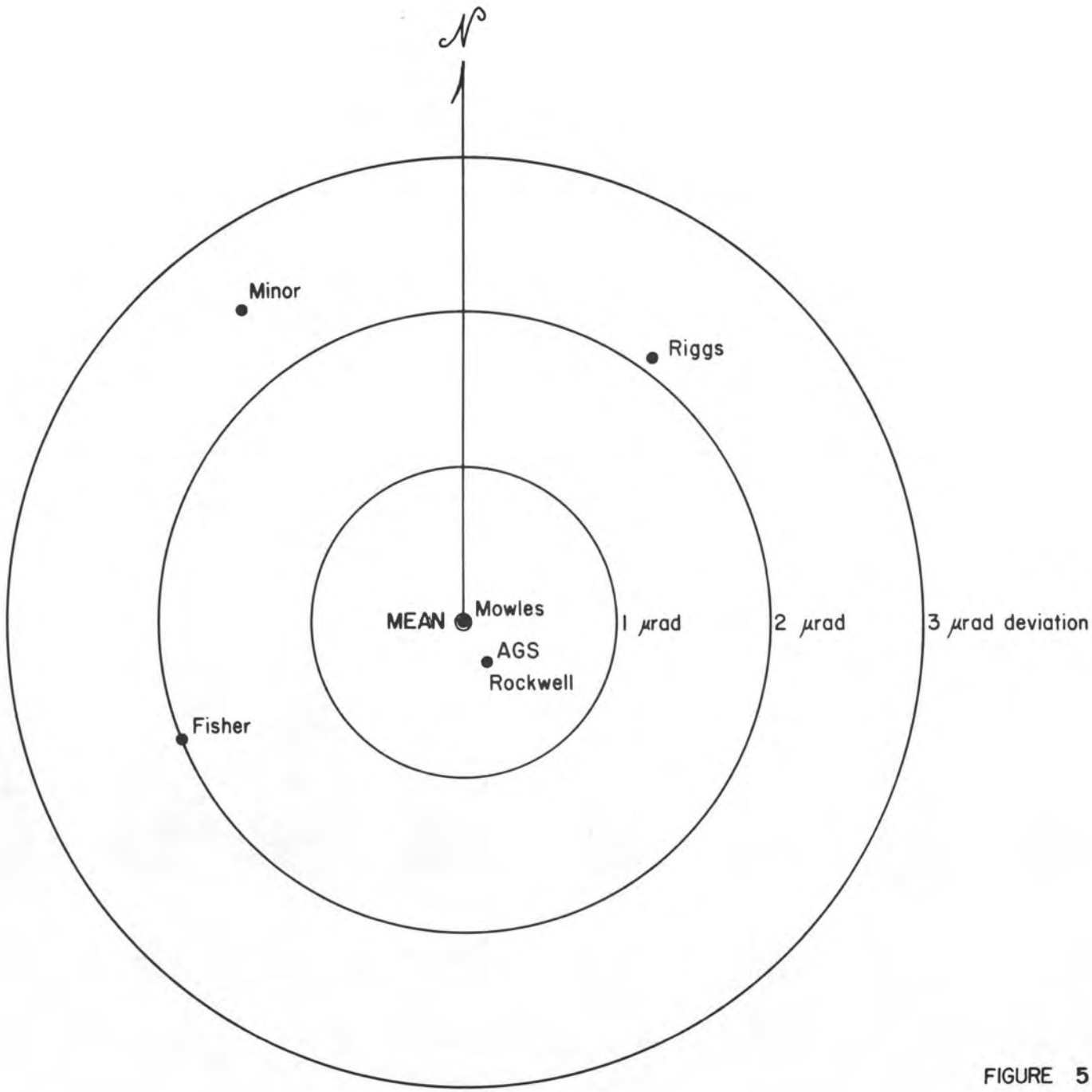
N
Minor
Riggs
MEAN
Mowles
AGS
Rockwell
Fisher
1 μrad
2 μrad
3 μrad deviation

FIGURE 5

Fig. 6. Tilt vectors for March-April, 1978, Palmdale uplift region. The black dots are locations of all dry tilt arrays. Vectors for a cluster of arrays in the Juniper Hills area, southeast Palmdale, show a pattern of radial-outward tilt ranging from 5 to 40 microradians.

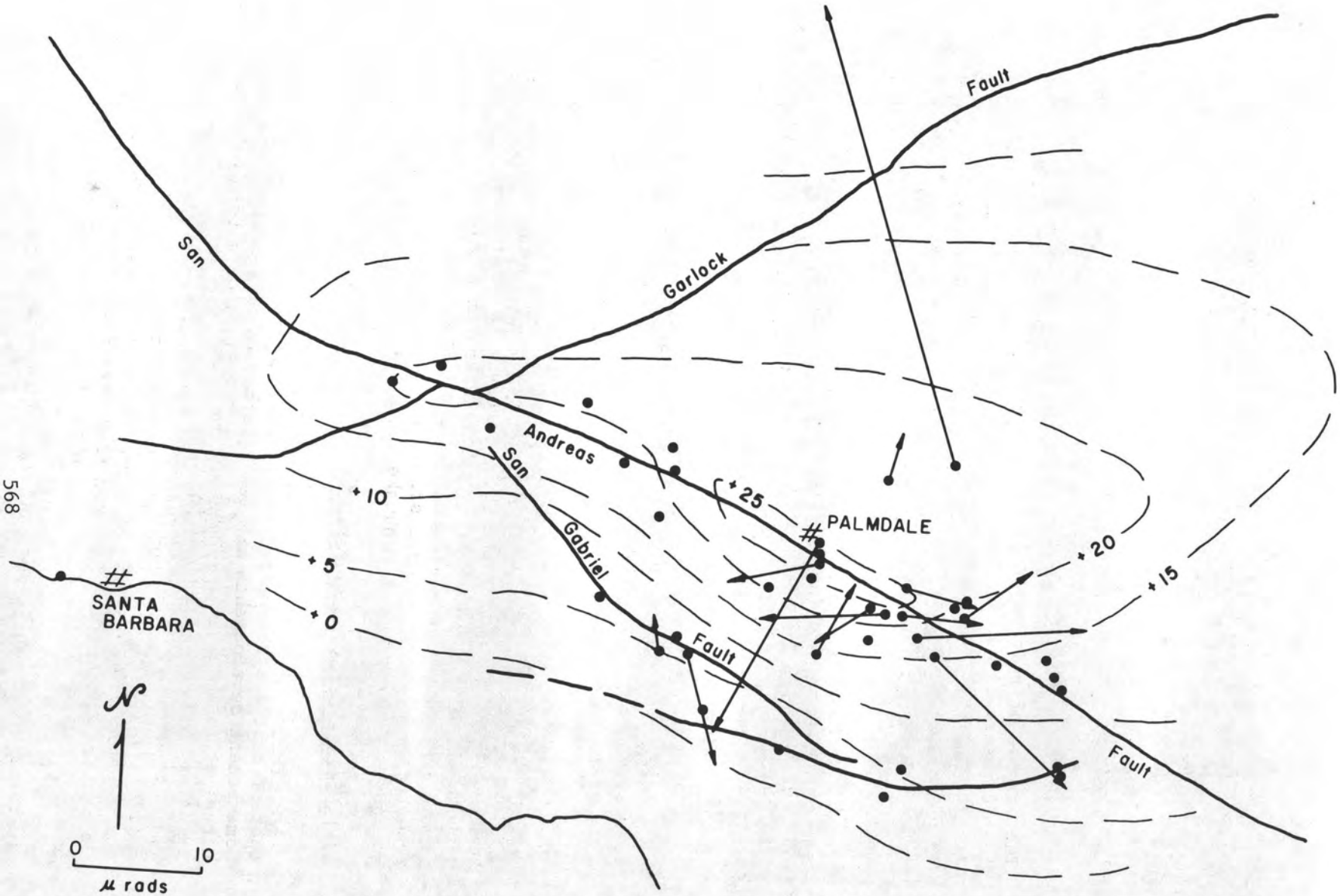
San
Andreas
Fault
Garlock
Fault
San
Gabriel
Fault
Fault
+25
+20
+15
+10
+5
+0
PALMDALE
SANTA
BARBARA
N
0
10
μ rads

FIGURE 6

REPORTS ON OBSERVATIONS OF CRUSTAL STRESS AND CRUSTAL DEFORMATION, AND THEIR ANOMALOUS CHANGES RELATED TO EARTHQUAKES IN CHINA

Yutaka Tanaka

Geophysical Institute, Faculty of Science, Kyoto University,
Kyoto, Japan

Introduction

The purpose of this paper is to introduce the current situation in China of observations of crustal stress and crustal deformation, and some recent results of these observations. In particular, the anomalous changes preceding the great earthquakes which occurred in 1976 (Tangshan in Hopei Province, Yenyunan-Ninglang on the border of Yunnan and Szechwan Provinces, and Lungling in Yunnan Province) are explained as basic data for medium-term, short-term, and imminent predictions of earthquakes.

Descriptions in this report are based on unpublished results presented by Chinese scientists in Peking and Kunming, and on some experiences in visiting observatories and amateur stations, etc. Some Chinese papers and textbooks are also used as references.

I. Crustal Stress

A distinctive feature in the field of crustal stress in China is the observation of stress changes related to earthquake occurrence. Automatic recording systems have not yet been introduced, but almost continuous observation has been made by taking readings several times a day, and numerous examples of anomalous changes preceding earthquakes have been observed.

Regarding earthquake prediction and studies of tectonic stress state, it is assumed that the predominant stresses in the upper part of the Earth's crust are in general horizontal, and therefore only stresses in the horizontal plane are measured. This assumption is based on the results of three-dimensional stress measurements carried out at mines and on the analysis of earthquake mechanism.

1. Absolute Stress Measurements

i) Method. The method of absolute stress measurements is the same as that of Hast's stressmeter[1] employing the principle of magnetostriction. Some recent developments are the reformation of a cell in the form of a nickel alloy spool, the method of cell setting in a bore-hole, and stress relief techniques by overcoring.

In advance of in situ measurements calibration of the stressmeter is usually performed by inserting the cells in a hole drilled in a large rock specimen ($45 \times 48 \times 80$ cm), loading them with about 60 kg/cm^2 in a laboratory testing machine, and then overcoring them by a stress release channel 150 mm in diameter. Results of laboratory experiments show that the amount of scatter in measured stress values is only ±10% and that in the direction of major principal stress is ±3°.

ii) Experimental measurements at the Ershihli-changshan mountain range[2]. At two sites 10 km apart at the foot of the Ershihli-changshan mountain range stresses were experimentally measured. Three cells were fixed in three directions horizontally in a vertical bore-hole of 36 mm diameter at intervals of 10 cm, and then stresses around the three measuring points were released in turn by overcoring with a stress release channel of 150 mm diameter. Measurements were continuously taken at a depth of between 7 m and 17 m with four sets at Wuhsiungsze, and at a depth of between 3 m and 55 m with 18 sets at Pangshan.

As a result of a series of stress measurements, major principal stress (σ_1), minor principal stress (σ_2), direction of σ_1(φ) and maximum shear stress (τ) were calculated by the least squares method.

The results are as follows:

	σ_1	σ_2	φ	τ
Wuhsiungsze	26 ± 2 kg/cm^2	4 ± 2 kg/cm^2	N73° ± 3°W	11 kg/cm^2
Pangshan	4 kg/cm^2	1 kg/cm^2	N60°W	---

The measurements at Wuhsiungsze were more accurate than those made at Rangely in Colorado[3] by the USBM method. To explain the low value at Pangshan, the existence of a tensile fault trending NNE-SSW is emphasized. There is also an active fault striking N10° ~ 20°W at a distance 3 km away from Wuhsiungsze, and the direction of major principal stress measured at the site is perpendicular to the fault. Through the series of measurements, it was realized that directions and magnitudes of maximum stress were greatly influenced by regional geologic structures.

iii) In situ stress measurements at magnesium mines and photoelastic experiments in the laboratory. In situ measurements were carried out at magnesium mines in the southern part of Liaoning Province. Then, in the laboratory some disturbances of stress trajectories caused by fissures were simulated in a photoelastic model test by cutting into an epoxy resin plate in the same pattern as that of the fissures in situ, and compressing the plate from various directions.

Figure 1 shows the line of major principal stress obtained by a photoelastic experiment (compressed from the direction of the large arrows) and the direction of major principal stress obtained by in situ stress measurements. The test site is marked by an open circle. Thus, the results of the photoelastic model test are used in correcting the direction of major principal stress determined by in situ measurements.

iv) Absolute stress measurements in North China (Huapei region). Crustal stress measurements were taken at six sites in the Peking area, two sites in the Tangshan area, two sites in the Haicheng area and one site near Xingtai City. Figure 2 shows the directions of the major principal stress at each site. The direction is ESE-WNW or E-W and the magnitude is 25 to 36 kg/cm^2 at the Peking and Tangshan areas, and ENE-WSW or E-W and 90 to 160 kg/cm^2 at the Haicheng area. The depth of the measuring point was less than 100 m, mostly 30 to 40 m, so the stress value in the Haicheng area must be much higher than the average

value compared to the measuring depth.

These directions of horizontal principal stress by in situ measurements coincide remarkably well with the orientation of the principal stresses deduced from the fault plane solution for the 1975 Haicheng earthquake (N75°E) and for the 1976 Tangshan earthquake (N86.5°E).

By reproducing the systems of main faults in the Peking area in an epoxy resin plate, a photoelastic experiment was carried out. In Figure 3 the thick lines represent the fault system, the thin lines represent the lines of minor principal stress and the arrows show the directions of major principal stress determined by in situ measurements. This figure is an example of an experimental case under compression from the N60°W - S60°E direction.

2. Observation of Changes in Crustal Stress

i) Observation by means of a magnetostrictive cell. This method is used at professional observatories. The same type of instrument as is employed for absolute stress measurements is fixed in a bore-hole at a depth of 30 to 100 m. The bore-hole must be drilled at least 40 to 50 cm into bedrock, and the cells settled in three directions horizontally in the bedrock. A dummy cell is put in the cell hole in a stress-free state for correcting such disturbances as temperature. At a calibration test before observation, the coefficient between the instrument reading and applied load is estimated by applying a pressure change of about 10 bar to a fixed cell in a rock piece set on an uniaxial compressive machine.

At the Kunming Standard Seismograph Station the daily mean of stress change is calculated as the average of readings taken every two hours 12 times per day. An automatic recording system is under development at present.

This method has been adopted at stations in 9 out of 21 professional observatories in Yunnan Province and at scores of other stations all over China.

ii) Simple stressmeter using changes of contact electric resistance. Carbon corpuscles for telephone transmitters and rubber corpuscles are stuffed into rubber tubes in the ratio of 1:1 or of 4:3, and these sensors are put in three radial directions in a flexible thin metal pipe. It has been devised in various ways such as putting springs on both ends of a rubber tube. The principle of measurement is very simple: when stress changes, contact electric resistance between carbon corpuscles changes. A Wheatstone bridge is used to measure contact resistance change; however, various ways have been devised for electric circuits to make measurement more convenient by amateur groups. Scale in figures is usually shown in μA, rarely in Ω, and is not converted to the unit of stress.

The metal pipe setting sensors are made waterproof by using a plastic pipe and cap, and then laid underground. For this purpose a large hole 1 to 2 m in depth is made and then a small hole around 1 m in depth is drilled in the bottom of the large hole. The pipe containing the sensors is buried as the rubber tube is held in a horizontal position, and then the hole is filled with soil.

Instructions for observation with the simple stressmeter appear in textbooks;[4,5] for example, when it is set near a fault, one of the components should be set at a right angle to the fault, or for half a month after setting up, the instruments will not be stable, so measuring values are useless in the beginning, etc. Many pages are devoted to giving such practical advice.

At a middle school in Chienshui, Yunnan Province, a simple stressmeter is set 1 m under the observation tunnel's floor which is 5 m under the ground surface. Readings on the meter are carried out in a building at the entrance to the tunnel.

This instrument is not suitable for observing secular changes of stress, but is effective to detect short term anomalous changes on a large scale. It is said that about 40 amateur stations in Yunnan Province have a simple stressmeter of this type and hundreds are in use in all of China.

iii) Examples of stress changes before and after earthquakes. The Haicheng earthquake on February 4, 1975, M=7.3. At a station 50 km from the epicenter, crustal stress began to increase seven months before the occurrence of the earthquake and the change in stress reached a maximum of 4.31 kg/cm^2. Figure 4 shows the changes of major and minor principal stresses (σ_1,σ_2) and the direction of σ_1 (φ_1) . The direction of the major principal stress changed suddenly just before the earthquake occurrence. At another station 300 km from the epicenter stress changes of 1.05 kg/cm^2 were observed.

It is stated in "Earthquakes and their Prediction"[4] that anomalous changes of crustal stress appeared from 7 to 10 months before the occurrence of the earthquake at several stations in Hopei and Liaoning Provinces. The name of the station, epicentral distance, value of maximum change of compressive stress and its date are as follows:

Examples: Shenyang, 100 km, 5.43 kg/cm^2, August 3, 1974
Chinchow, 100 km, 3.94 kg/cm^2, August 14, 1974
Dairen, 200 km, 2.65 kg/cm^2, August 15, 1974

Especially at Chinchow located on the westward extension line of the seismic fault of the Haicheng earthquake (one node of the fault plane solution), the maximum shear stress was 1.60 kg/cm^2 and the strike of the maximum shear plane was nearly in E-W. This direction and left lateral characteristics coincide with those of the lateral motion of the seismic fault.

The Tangshan earthquake on July 28, 1976, M=7.8. Figure 5 shows the stress changes observed at a point 100 km from the epicenter, using σ_1 , σ_2 and Φ . Because σ_1 and σ_2 are almost equal, apparently the direction of the major principal stress Φ changed suddenly to nearly 90°.

Annual variations of stress are also noticed. However, in the curves of σ_1 , σ_2 and Φ sudden changes appear twice preceding earthquakes. The first is the Horinger earthquake of magnitude 6.3 on April 6, 1976 which occurred in Inner Mongolia, 390 km west of Peking and the second is the Tangshan earthquake. Precursor-like changes before the Tangshan earthquake are extremely notable.

Figure 6 shows stress changes observed by the simple stressmeter at amateur stations just before the occurrence of the Tangshan earthquake. Before the earthquake, from 3.5 months at Luanhsien (epicentral distance of 50 km) 3 months at Paoti (60 km) and Changli (80 km), and 2 months at Chiaoho (230 km) stresses began to increase or decrease and immediately before the occurrence remarkable changes were observed in succession at each station.

The Lungling earthquakes on May 29, 1976, M=7.5 and 7.6. The curves in Figure 7 show changes in each observed component of stress. The observed results have not yet been converted into the change of principal stress. It is probably an observation at Hsiakuan, 180 km from the epicenter. In N30°E-S30°W and E-W components anomalous changes appeared one year before the occurrence of events. Crustal compressive stresses increased firstly, became calm again, and then descended. A given explanation was that there are three epochs of stress concentration, strengthening and release of stresses.

It is also said that a stress change of 3 to 4 kg/cm^2 was observed at the Kunming station, as much as 400 km away from the epicenter.

The Yenyuan-Ninglang earthquakes on November 7, M=6.9 and December 13, M=6.8, 1976. Stress changes at Kunming (epicentral distance of 300 km), Yungsheng (75 km) and Sungming (300 km) are shown in Figure 8. The tendency of stress change in the several months before the earthquake was below average for the most part. This was the only explanation given in a presentation at Kunming City. At Sungming station anomalous changes occurred 20 days before and began to recover 10 days before respective occurrences of both earthquakes (M=6.9 and 6.8). A similar tendency can be seen in the changes at Kunming and Yungsheng.

The Yungshan (Chaotung) earthquake on May 11, 1974, M=7.1. According to a report[6] of the Seismological Brigade of Chengtu different modes of stress change appeared respectively at two stations, Tsoushihshan, located on the azimuth of the tension axis in the focal mechanism, and Luting near the nodal line of the earthquake 260 km northwest of the epicenter. A short term precursor in stress change was also observed by the simple stressmeter at Huitse amateur station.[4]

Miscellaneous. The simple stressmeter at Yuhsi amateur station, Yunnan Province, had a sudden change four days before an earthquake, and as the change returned to normal the earthquake (M=4.6) occurred.[4]

As mentioned above, stress measurements have been carried out at exceedingly numerous stations, and seem to produce valuable data for earthquake prediction. Most of the observation stations have their own empirical formula; for example, the magnitude is estimated from the duration time of anomalous change or from the duration time and amplitude of the precursor.

II. Crustal Deformation

The distinctive features of geodetic survey and continuous observation of crustal deformation in China are the use of numerous short level and base line nets and tiltmeters of the horizontal pendulum type. Because precise short leveling, precise base line measurements and continuous observation by a tiltmeter are usually carried out on the ground surface or in a shallow tunnel, the obtained results are affected greatly by

annual and daily variations and by rainfall. Therefore, except for a few special observation stations such as where the earth tide is observed, it seems to be impossible to detect microchanges of the order of μrad and μstrain.

However, there are some merits. The observations are so stable, accurate (low sensitivity but exact), and continuous that unusual changes larger than daily or seasonal changes can be easily found. Furthermore, the distribution of observation stations including amateur stations is sufficiently dense. This situation makes it possible to observe precursory phenomena before large earthquakes occur under the Chinese continent.

There are not many extensometers, creepmeters or water tube tiltmeters, but nets of short base line, measurements of stress change and nets of short level line compensate for them.

It has been important for China to observe unusual phenomena, investigate a law of nature through experience and then predict earthquake-occurrence based on this law. Automation in high sensitivity and centralizing data by telemetering seem to be the next step in the field of crustal deformation.

1. Observations at Tahuich'ang Crustal Deformation Observatory

Papaoshan fault is one of the main active faults in North China. It strikes in the NE-SW direction and extends over 200 km through the western suburbs of Peking City. Tahuich'ang Crustal Deformation Observatory 20 km southwest of Peking was established on the fault in 1969 for the purpose of studying the causal relation between fault movements and seismic activities.

Along the northeast part of the fault, numerous earthquakes occurred in the several years before the Tangshan earthquake. Paichiat'an seismological station is located near the fault, 20 km northeast of Tahuich'ang.

At Tahuich'ang observatory a short level line of 26 m crosses the fault at a right angle and a Zeiss Ni004 level is set on the center pillar in the middle of the level line. In an underground room parallel to the level line a 24 m quartz extensometer with a magnifier of optical interferometer and a 24 m water tube tiltmeter also cross the fault.

Niuk'ouyü observatory was constructed on the same fault at the same time 25 km from Tahuich'ang, and has the same arrangement. Every four hours observations are carried out by a reading and leveling. The observational results of short leveling at Tahuich'ang and Niuk'ouyü since 1969 and of the water tube tiltmeter at Tahuich'ang since 1971 and of the extensometer at Tahuich'ang since 1973 are shown in Figure 10. The curves show results in which the mean annual variation from observed monthly means has been eliminated. However, large disturbances due to remarkable rainfalls in 1973 and 1974 yet remain. On the curve of the extensometer annual variation has not been completely eliminated because of the short observation period. The results of the water tube tiltmeter and short leveling show a good coincidence, and it is enough to prove their accuracy. The results of short leveling at Niuk'ouyü show a similar curve.

2. Anomalous Crustal Deformation Before the Tangshan Earthquake on July 28, 1976, M=7.8.

i) Precursory changes observed at the Tahuich'ang and Niuk'ouyü stations. In May of 1975, that is, 14 months before the occurrence of the Tangshan earthquake, the eastern hanging-wall of the Papaoshan thrust fault began to uplift against the west side, and in five months relative vertical displacements reached 1.2 mm. Similar phenomena were observed at Niuk'ouyü, and the relative uplift continued until September or October of 1975.

The results of the extensometer shown in Figure 10 retain some annual variations, besides this, lateral displacements of the fault affect the expected pure extension due to instrumental structure. Although it is not clearly shown, a change of compression can be noticed since May, 1975 coincident with the relative vertical displacements.

This is the first stage of unusual crustal movements, namely, crustal stresses began to concentrate rapidly in this area. The Papaoshan fault was compressed in an E-W direction and the hanging-wall of the fault uplifted relative to the foot-wall.

It seems that tectonic stress in the E-W direction had begun to increase already from 1971 in this area. The push-pull in the initial motion of seismic waves observed at the Paichat'an seismological observatory during the period from 1956 to 1971 was not systematic and not dependent upon epicentral direction. However, in the period between 1971 and 1976, the initial motions of the earthquakes which occurred in the east and west quadrants centering in Paichat'an station were pull and those in the north and south quadrants were push. In this period, the directions of initial motions were systematized (regulated). That is the compressive stress increased in an E-W direction and every earthquake in this area began to hold its maximum compressive axis in an E-W direction.

The second stage was a stable period which extended to April, 1976. The third stage occurred in May and June as an abnormal accelerative period. Relative uplifting of 0.6 mm was observed during these two months at Tahuich'ang. During the period from the beginning of the anomalous changes to July of 1976, just before the earthquake, the amount of relative uplift totaled 1.7 mm which is equivalent to almost six times that of the previous six-year average.

Observed results of the extensometer showed 0.1 mm extension in the two days immediately before the occurrence of the earthquake. This may be the fourth stage for reversed changes occurred in many cases.

The four stages of anomalous changes mentioned above are the same as each stage of relative elevation change which appeared on the short leveling at Jinxian 190 km from the epicenter in the case of Haicheng earthquake (reference Figure 10).

ii) N-type changes in crustal deformation before earthquakes[7]. The pattern in time changes of the anomalous deformation which appeared at Tahuich'ang and Jinxian before the earthquakes is the same as that of the characteristic curves before the principal fracture observed by strain gauges buried in a compressive part between two planes of principal

shearing stress in the uniaxial compression test of pieces of plaster or of compound pine resin and paraffin. This characteristic deformation is called the N-type change after its shape of curve.

As similar examples, the results of short leveling at Ningho station before the Fengnan earthquake on May 25, 1970, M=5.2, and at Yahoying before the Hoshun earthquake on June 5, 1971, M=5.2, are mentioned. These two short level lines are located within the pull quadrant of the shocks. On the other hand, the results at Hsiangho before the Wenan earthquake on September 21, 1973, M=4.5, show that the anomalous changes before the earthquake were of the arc-type, and around the time when they became normal again the event occurred. Hsiangho is located in the push quadrant. Even in the compression test case the strain gauges in the tensional parts showed this same type of change and the strains did not change rapidly just before the fracture of the test pieces.

iii) Anomalous changes observed at some short level lines in Hopei Province. In the results observed at Hsiangho 100 km west of the epicenter of the Tangshan earthquake, where the 26 m short level line crosses the Hohsilu fault in an E-W direction, a relative elevation change began to occur in May, 1975, in the same period as at Tahuich'ang and it reached 2 mm by August, in only three months.

Anomalous elevation changes began also along both short level lines from about July of 1975. One of the level lines is across the Tsangtung fault at Tsangchou, 180 km southwest of the epicenter. The other, at Hongshan 400 km southwest of the epicenter, is in a N-S direction but not across any fault. The changes are shown in Figure 11.

3. A Net of Short Level Lines at Chuhsiung, Yunnan Province and the Directional Characteristics of the Anomalous Ground Tilt Immediately Before the Earthquakes.

Chuhsiung County is located 120 km west of Kunming City and the short level line net crosses a small fault striking in a N30°W-S30°E direction at a distance of 4 km west of there. However, the following observed results have no relation to this fault.

A Zeiss level is set on a pillar in a shed and four concrete bases 1 m high on which targets are mounted are found 25 m from the center pillar in four directions forming a square. The bases were built in April, 1975 and stabilized in the beginning of 1976. Readings of this level are carried out once between 9 and 10 a.m. every morning.

To summarize the observed results in 1976, firstly, the observational error was ±0.077 mm except in the case of a large amount of precipitation. When an elevation change of at least one base is more than three times the error (0.077 × 3 mm), it is recognized as an abnormal change. Secondly, regarding the occurrence of earthquakes larger than M=5 which occurred within 300 km of Chuhsiung, anomalous tilting occurred without exception. The conclusion was reached that anomalous changes appear at epicentral distances even greater than 300 km in the case of great earthquakes.

When observed values in three among six level lines connecting two bases show more than 0.12 mm of change in a day (0.7"/day in maximum tilt-rate), it is decided that there is a possibility of earthquake

occurrence. Actually, moderate earthquakes of M=5 to 6 occurred within three days of the appearance of a sudden change in ground tilt. Moreover, it was noticed that the direction of maximum tilt indicates either the epicenter direction or its opposite direction without exception (Figure 12).

Regularity in daily tilting direction does not exist. However, secular tilt change shows a regular trajectory in a long term. In the case of earthquakes under M=5, its long term change keeps the same trajectory. In the Lungling earthquakes on May 29, 1976, M=7.5 and 7.6 (epicentral distance of 300 km), however, from about 25 days before the occurrence the tilt direction suddenly changed and the maximum elevation change reached 0.53 mm. The observed tilt direction was N104°W and the direction of the epicenter was N100°W.

As for the Sungpan earthquakes on August 16 and 23, 1976, both M=7.2, even though it occurred at a distance of 900 km, its maximum change was 0.22 mm and the tilt direction was N21°E. The direction of the epicenter was N17°E, so the difference was less than 5°. Regarding small earthquakes the error is relatively large due to the small amount of change. For example, in the earthquakes of September 19 and February 16, the shifting of the vectors of anomalous tilt before each earthquake can be seen in Figure 12. Before the major aftershock of the Lungling earthquake the tilting direction was irregular and no sudden changes appeared.

Precursory tilt before the Yenyuan-Ninglang earthquake. The sudden change observed on November 5, 1976 was 0.21 mm in the N14°W direction (right side in Figure 12). Earthquakes had occurred in this direction on October 21 (M=4.3) and November 4 (M=4.0), so these two earthquakes must be considered as the foreshock of the coming large event, the Yenyuan-Ninglang earthquake. The magnitude was estimated to be around seven because of the foreshock occurred nearer than the epicenter of the Sungpang earthquake and the amount of tilt change was on the same order as that, but there was uncertainty in the prediction of magnitude.

The Yenyuan-Ninglang earthquake occurred on November 7 with a magnitude of 6.9. The epicenter was located at a distance of 270 km from the Chuhsiung level line net in the N9°W direction. This was only 5° different from the predicted direction.

A similar change was observed also before the earthquake which occurred December 13 (M=6.8, epicentral distance of 260 km). As these changes recovered after the shocks, they are considered to be elastic deformation of the crust.

In Yunnan Province, 14 short level line nets are presently set and each one crosses a fault. Except for Chuhsiung, observations are made every day only at the net crossing the Hongho fault, but these observations are not precise. At the other nets observations are carried out only once a month. At Chuhsiung, when unusual changes had continued for more than 24 hours, the changes were observed almost without fail. The conclusion in Kunming was that if short level nets like Chuhsiung existed in at least three different places, more exact positions of epicenters could be predicted.

4. Some Other Examples of Anomalous Tiltings and Results of Geodetic Surveys

i) Anomalous tilting before the Yenyuan-Ninglang earthquakes observed at Ninglang by tiltmeters. The N-S component of the tiltmeter at Ninglang station within 20 ~30 km of the epicenters began to change unusually from the end of September, 1976 and reversed suddenly on November 5 at the same day as at Chuhsiung. An earthquake of M=6.9 occurred two days later. This sudden change reversed again after the shock and anomalous changes continued, but once again it turned on December 2 and an earthquake of M=6.8 occurred on December 13 (Figure 13). This change shows the coincidence with an occurrence period of anomalous changes in geomagnetic declination at the station.

ii) Results of resurvey of trilateration after the Lungling earthquake on May 29, 1976. Information regarding the precursory crustal deformation before the Lungling earthquake is contained in Suzuki's report in this text.

After the Lungling earthquake resurveys of trilateration were carried out at four triangles with a side length of 14 to 26 km and running approximately in a N-S direction, in which the epicenter is located. The obtained results were that the maximum compressive strain was 33 μstrain and the direction of the compressive axis was N20°E-S20°W. This direction coincided with that of the tectonic stress in a wide area. However, the pressure axis obtained from an analysis of the occurrence mechanism of the main shock was in the NW-SE direction, and this does not coincide with the results of geodetic surveys.

The facts that the earthquake occurred at a secondary fault and that the seismic activity had a tendency to be of swarm type were cited as reasons for this. This was because of the complicated fault system in this area.

iii) Strain changes along the Chuchiang fault before and after the Tunghai earthquake in Yunnan Province on January 5, 1970, M=7.7. The relative horizontal and vertical movements of the Chuchiang fault observed at a short base and level line net on the fault after the occurrence, and the results of the resurvey of trilateration around the fault have already been reported in "Acta Geophysica Sinica".[8]

In Figure 14, the principal strains obtained by the resurveys of trilateration and short base line measurements at three nets, maximum pressures obtained by fault plane solution of earthquakes and maximum stresses inferred from Quarternary tectonics based on geological and geomorphological research are summarized. The directions of compressive stresses or strains show very good coincidence and express the state of crustal stress in the area. An interesting fact is as follows: among three parallel faults, the two at each side show right lateral motions and the middle one shows left lateral motion.

Concluding Remarks

As mentioned above, in China anomalous changes of crustal stress and crustal deformation as well as gravity changes are very remarkable even

at a distance from the epicenters. One of the reasons for this seems to be that an increase of tectonic stress in a wide area causes stress concentration at many weak points or planes in the crust, and when an earthquake occurs at one of these, crustal stress is redistributed in the wide area. The large amount of anomalous changes at places far from the epicenter are probably due to this. Even if the anomalous changes are not caused directly by the processes in the source mechanism of the predicted earthquakes, if they are used to predict earthquakes as a part of the tectonic process, they are nonetheless valuable.

In any case, the success in predicting earthquakes in China is based on their accurate, incessant and systematic observations, and the dense distribution of professional and amateur stations.

References

[1]Hast, N., The measurements of rock pressure in mine, Seriges Geol. Undersökun. Årsbok, Ser. C, Avhandl. Uppsat., 52(3), 1-183, 1958.

[2]Seismogeological Brigade, Nat. Seis. Bureau and Inst. Geological-dynamics, Geol. Sci. Bureau, Stress measurements at the Ershihli-changshan mountain range, (in Chinese), Coll. Geol. Treatises, Inst. Geologicaldynamics, 204-210, 1975.

[3]De La Cruz, R. V., and C. B. Raleigh, Absolute stress measurements at the Rangely Anticline, Northwestern Colorado, Int. J. Rock Mech. Min. Sci., 9, 625-634, 1972.

[4]Earthquake Office, Revolutionary Com. Kwantung Prov. and Canton Seis. Brigade, Earthquakes and their Prediction (in Chinese), revised 2nd edition, Kwantung People's Publishing Co., 1976.

[5]Editorial Group of Questions and Answers on Earthquakes, Questions and Answers on Earthquakes, (in Chinese), revised edition, Geological Publishing Co., 1977.

[6]Earthquake Office, Revolutionary Com. Szechwan and Chengtu Seis. Brigade (ed.), On the characteristics of precursory anomalies related to the Chaotung earthquake, (in Japanese, tr. Y. Zushi), Recent Studies for Earthquake Prediction in the People's Republic of China, Review Res. Disas. Prev., No. 18, 1975.

[7]Group of Experimental Seis., Inst. Geol., Academia Sinica, The precursory phenomena and spacial distribution of fractures and earthquake prediction, (in Chinese), Sci. Geol. Sinica, No. 3, 213-221, 1976.

[8]Geod. Surv. Brigade for Earthq. Res., Nat. Seis. Bureau, The characteristics of the crustal deformation associated with the Tunghai earthquake, Yunnan, in January, 1970, (in Chinese), Acta Geophys. Sinica 18(4), 240-245, 1975.

Figure Captions

Fig. 1. Distributions of stress trajectories (thin lines) caused by fissures (thick lines) displayed by the photoelastic experiment. The arrows with the open circles show the direction of the major principal stress according to in situ stress measurements at a magnesium mine in south Liaoning Province. The stress trajectories have been disturbed by the fissures. The large arrows forming two lines show the direction of compression in the laboratory test.

Fig. 2. The directions of horizontal compressive stress in North China (the Huapei region) as determined by in situ measurements. Hsingtai is also known as Xingtai.

Fig. 3. Stress trajectories in the Peking-Tientsin region displayed by photoelastic model simulation.
Thick line — fault system; Thin line — line of minor principal stress; Arrow — direction of major principal stress as determined by in situ stress measurements.

Fig. 4. Changes in crustal stress before the occurrence of the Haicheng earthquake observed at a station 50 km from the epicenter.

σ_1 : major principal stress
σ_2 : minor principal stress
} unit: bar

φ_1 : direction of major principal stress (σ_1).

Fig. 5. Change in crustal stress before the occurrence of the Tangshan earthquake in Hopei Province observed at a station 100 km from the epicenter. An earthquake of M=6.3 occurred in Horinger, Inner Mongolia, 390 km west of Peking on April 6, 1976.

Fig. 6. Anomalous changes of ground stress before the Tangshan earthquake observed by the simple stressmeter at amateur stations (unit: μA).

Fig. 7. Changes in crustal stress before the occurrence of the Lungling earthquake in Southwest Yunnan Province (unit: μh).

Fig. 8. Sudden changes in crustal stress immediately before the occurrence of the Yenyunan-Ninglang earthquake on the border of Yunnan and Szechwan Provinces (unit: μh). Epicentral distances at Kunming, Yungsheng and Sungming are 300 km, 75 km, and 300 km, respectively.

Fig. 9. Location of the Papaoshan fault, and the Tahuich'ang Niuk'ouyü and Paichiat'an observatories.

Fig. 10. Crustal deformations observed by the extensometer, water tube tiltmeter and short leveling at Tahuich'ang, and by short leveling at Niuk'ouyü. I, II,...IV show the stages of anomalous change before the earthquakes. The lowermost curve shows crustal deformation before the Haicheng earthquake in Liaoning Province which was observed by short leveling across the Jinzhou fault at Jinxian 190 km from the epicenter.

Fig. 11. Changes in relative vertical displacement before the Tangshan earthquake obtained by short leveling (5 day averages).

Fig. 12. Left: Directions of imminent precursory tilts observed at the Chuhsiung net of short level lines just before the occurrence of some earthquakes and their epicenters. The open circles show the positions and magnitudes of the earthquakes. The numerals indicate the dates of occurrence in 1976.
Right: Vector diagram before and after the occurrence of the Yenyuan-Ninglang earthquake on November 7.

Fig. 13. Anomalous changes of ground tilt recorded by the horizontal pendulum tiltmeter at Ningland 20 ~ 30 km from the epicenters of the Yenyuan-Ninglang earthquakes. The unit is the reading value in mm on the scale. Earthquakes of M=6.9 and 6.8 occurred on November 7 and December 13, respectively in the Yenyuan-Ninglang area (reference Fig. 12).

Fig. 14. Tectonic stress field and three parallel faults in the Tunghai-Shihping area.

Solid arrow: axis of principal strain by trilateration;
Broken arrow: axis of principal strain by short base line measurements;
Double arrow: direction of principal compressive stress inferred from Quaternary tectonics.

The solid and open parts in the mechanism solutions (upper hemisphere projection) of earthquakes are dilatation (pull) and compression (push), respectively.

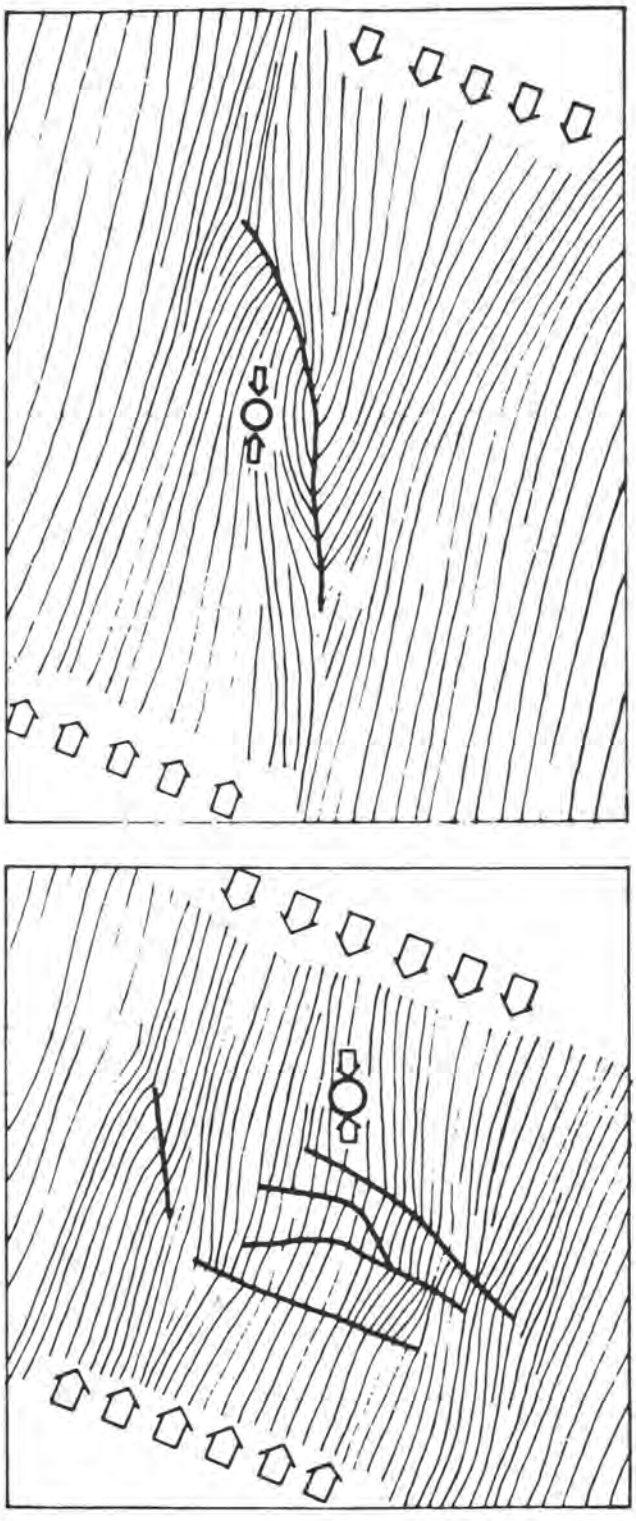

TANAKA Fig. 1

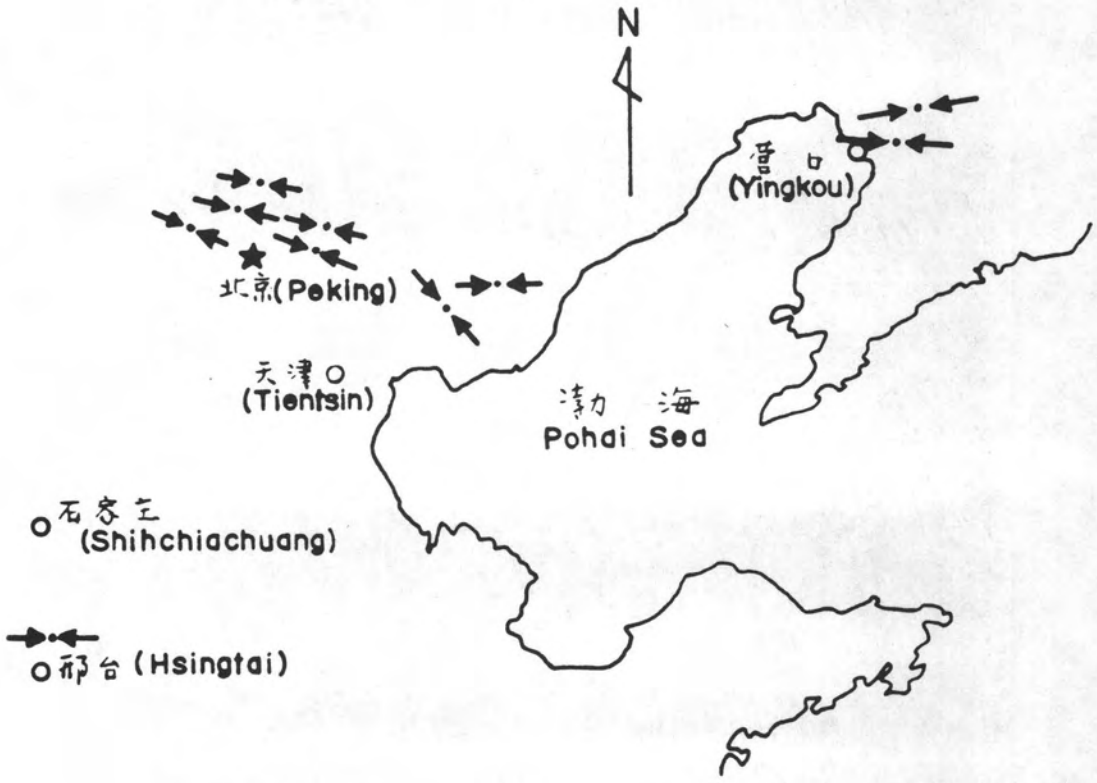
N
營口
(Yingkou)
北京(Peking)
天津
(Tientsin)
渤 海
Pohai Sea
石家莊
(Shihchiachuang)
邢台 (Hsingtai)

TANAKA Fig. 2

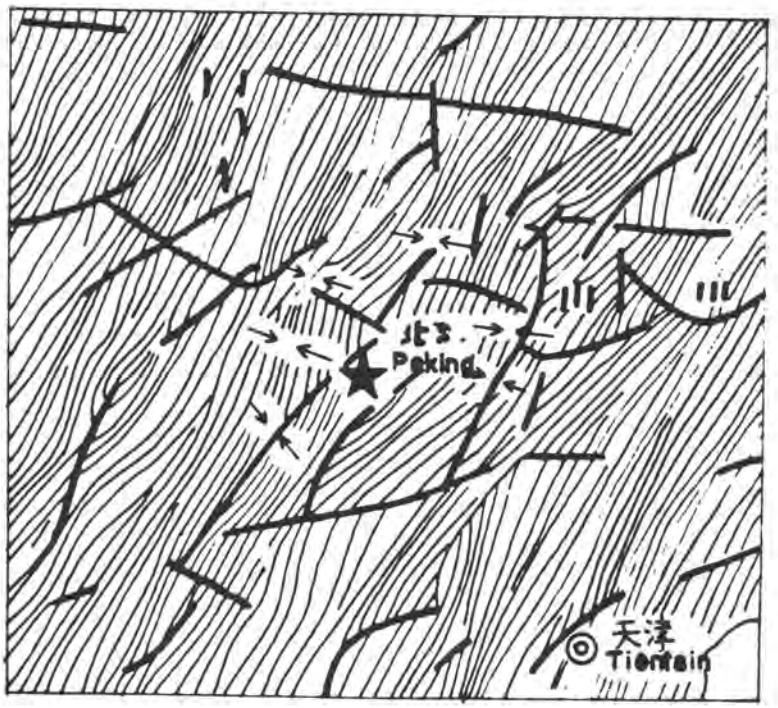

TANAKA Fig. 3

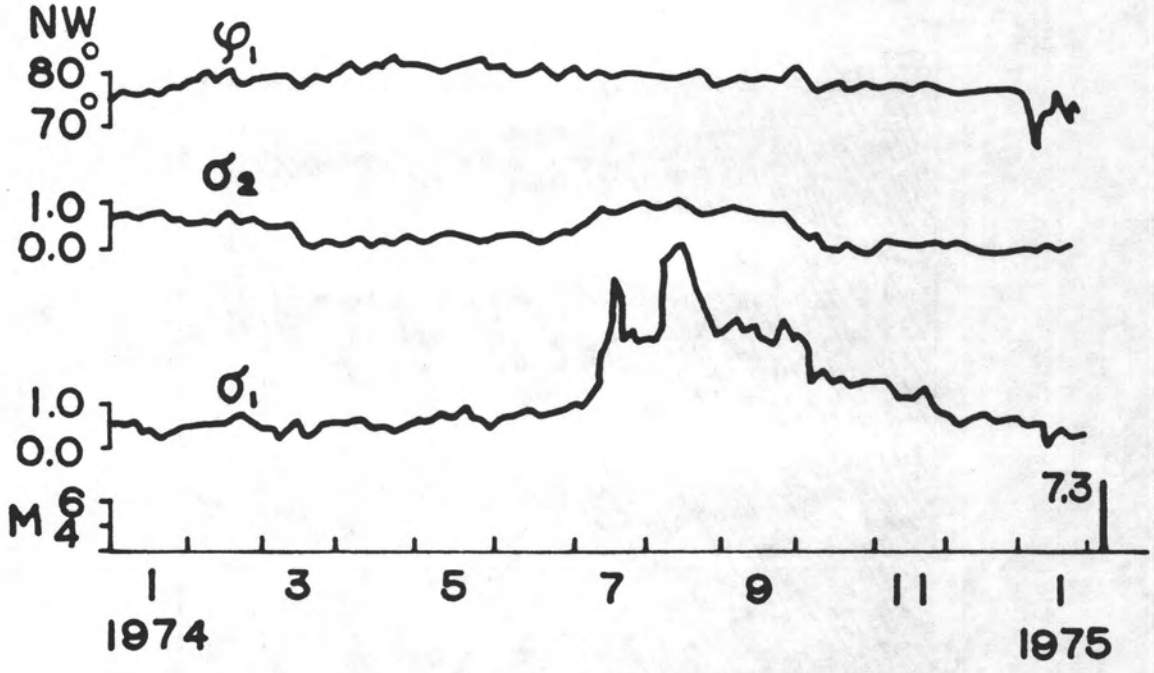

TANAKA Fig. 4

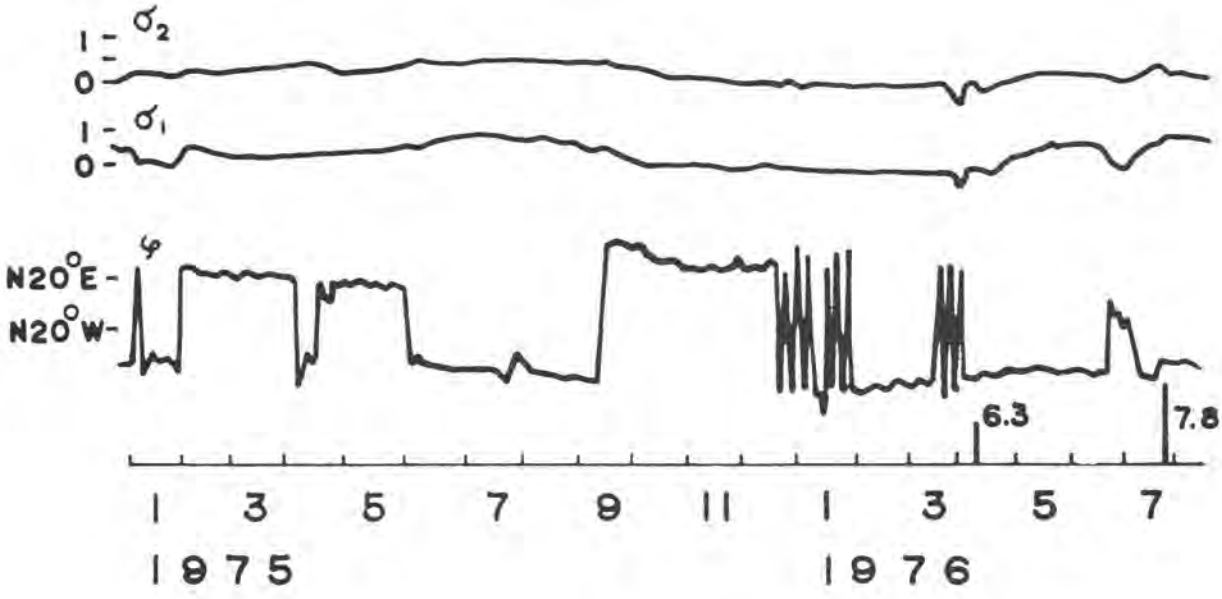

TANAKA Fig. 5

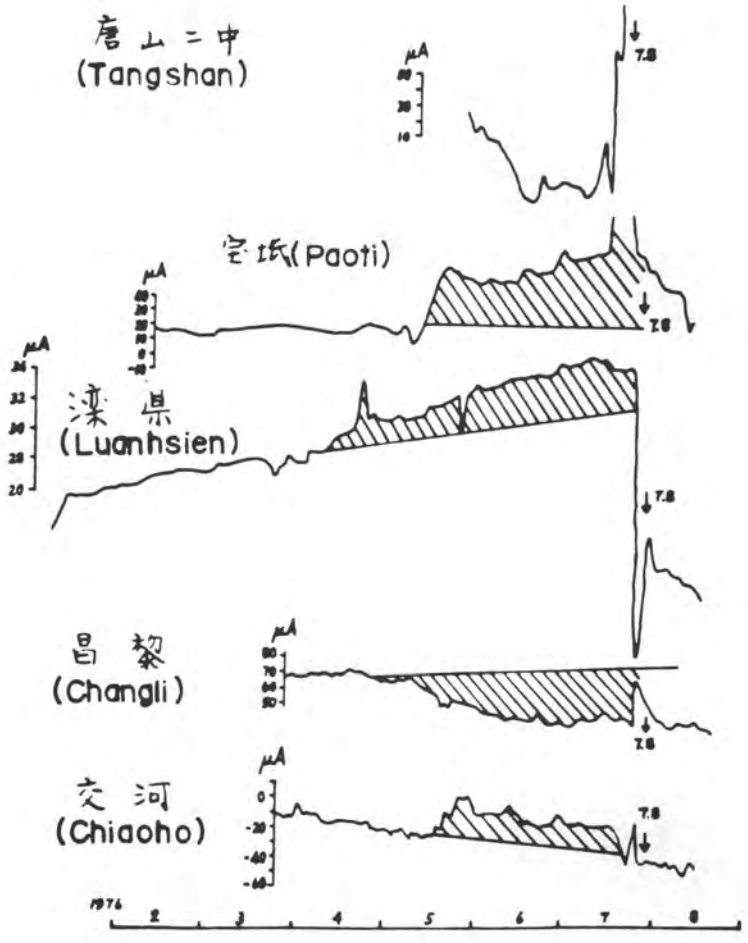
唐山二中
(Tangshan)
寶坻(Paoti)
滦県
(Luanhsien)
昌黎
(Changli)
交河
(Chiaoho)
μA
7.8
1976

TANAKA Fig. 6

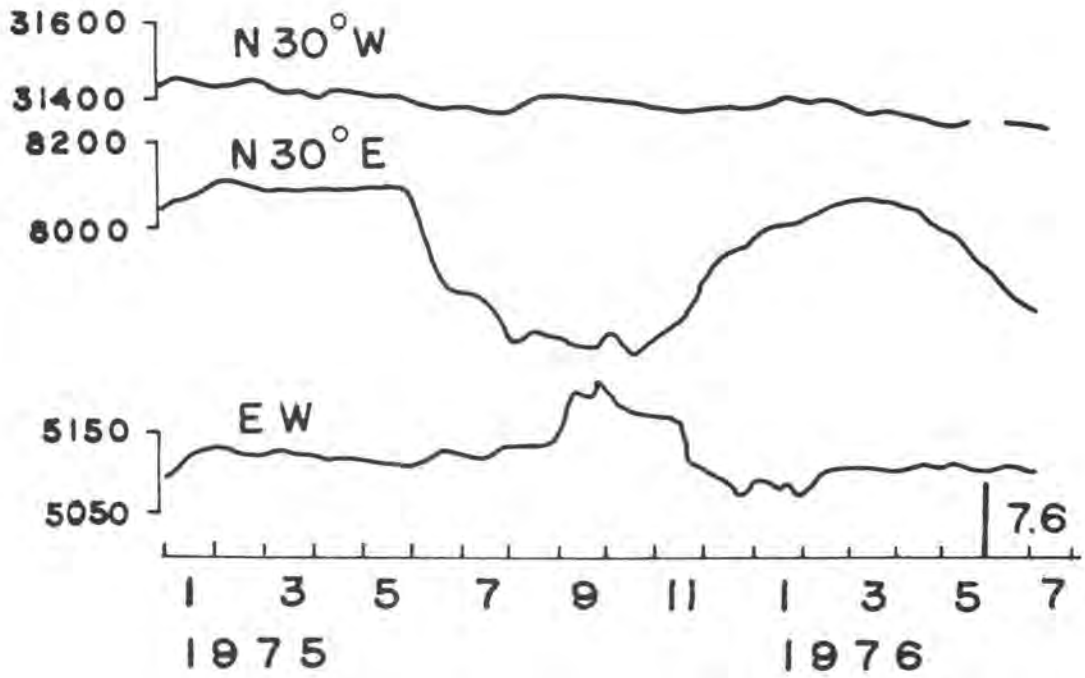
31600
31400
N 30° W
8200
8000
N 30° E
5150
5050
E W
7.6
1 3 5 7 9 11 1 3 5 7
1975
1976

TANAKA Fig. 7

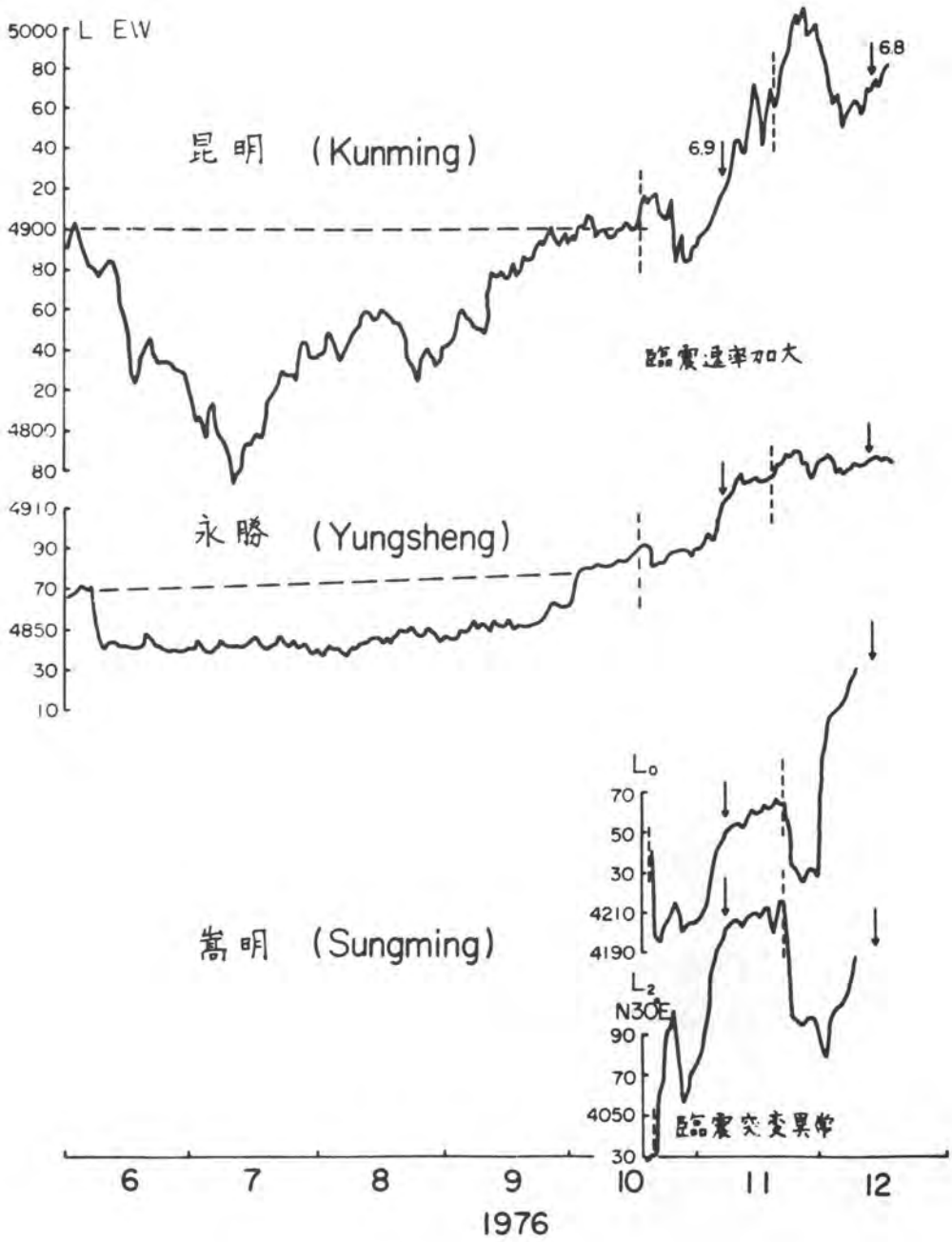
5000
L EW
80
60
40
20
4900
80
60
40
20
4800
80
昆明 (Kunming)
6.9
6.8
臨震速率加大
4910
90
70
4850
30
10
永勝 (Yungsheng)
L_0
70
50
30
4210
4190
L_2
N30E
90
70
4050
30
嵩明 (Sungming)
臨震突変異常
6
7
8
9
10
11
12
1976

TANAKA Fig. 8

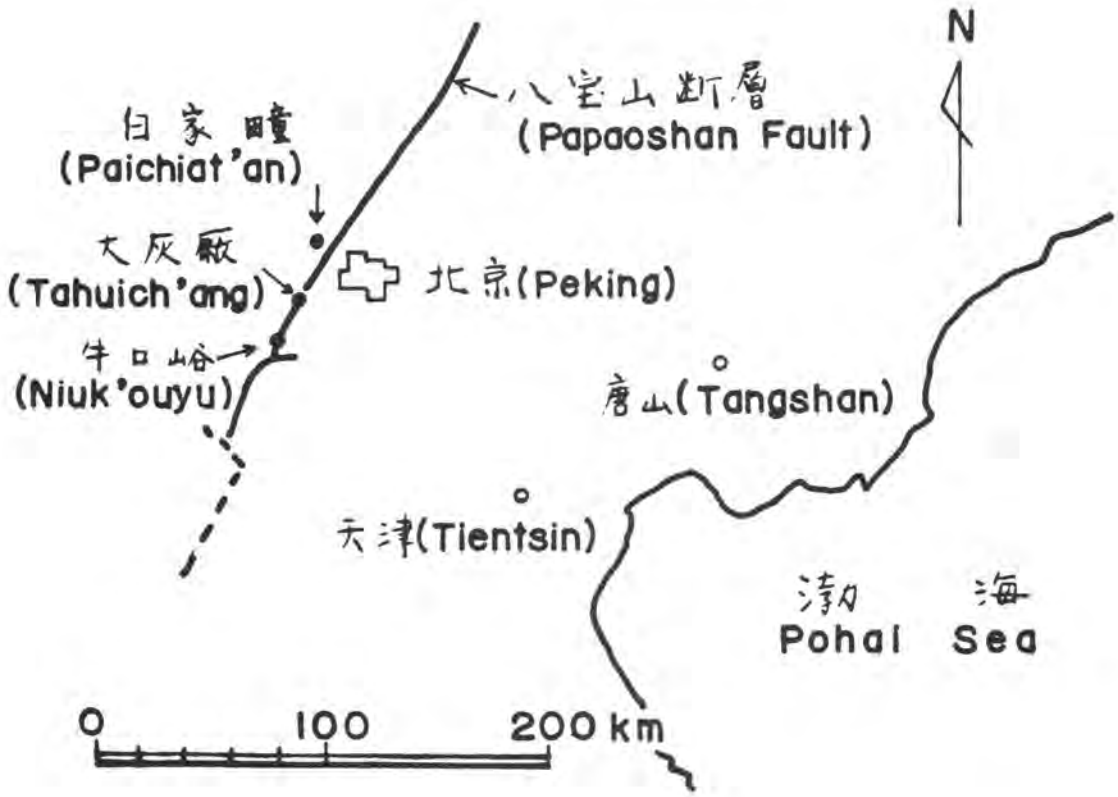
N
八宝山断層
(Papaoshan Fault)
白家疃
(Paichiat'an)
大灰厰
(Tahuich'ang)
北京(Peking)
牛口峪
(Niuk'ouyu)
唐山(Tangshan)
天津(Tientsin)
渤海
Pohai Sea
0
100
200 km

TANAKA Fig. 9

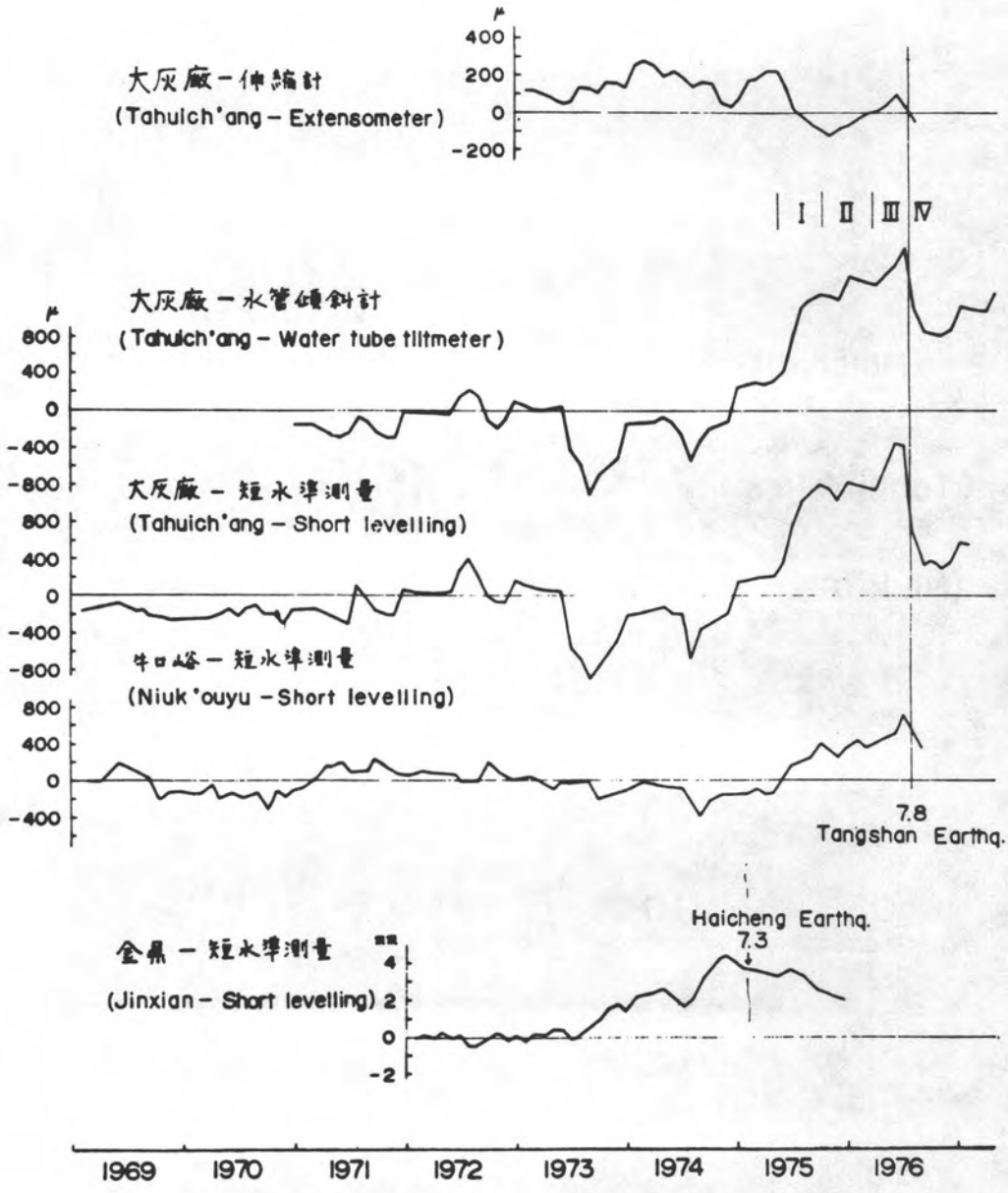

TANAKA Fig. 10

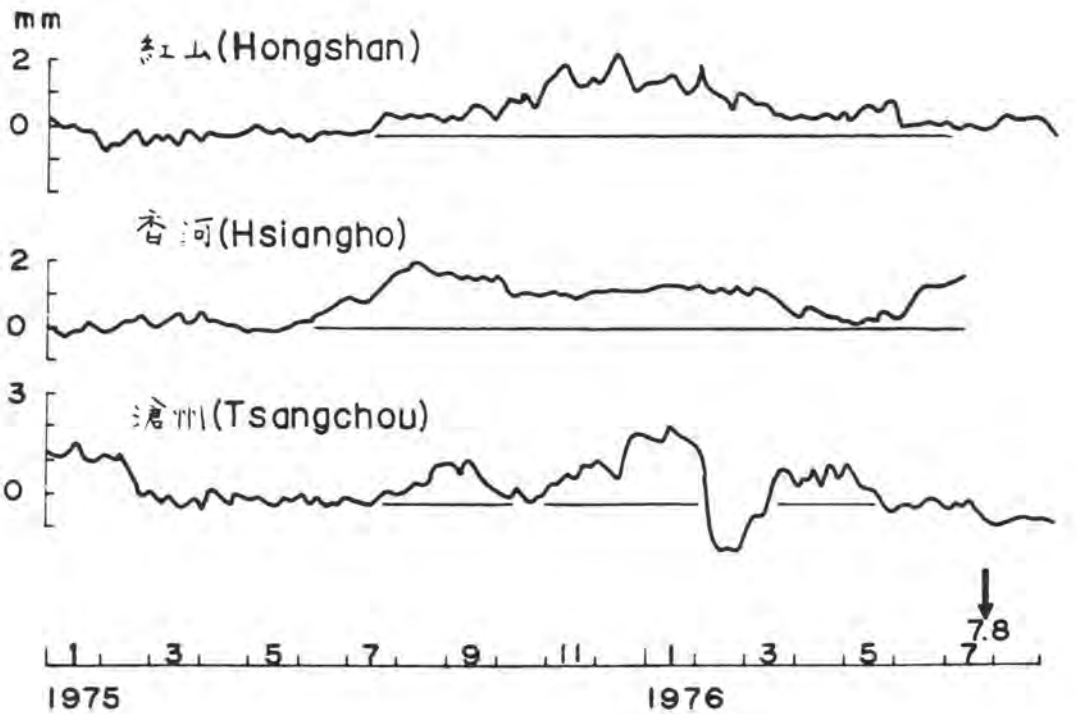

TANAKA Fig. 11

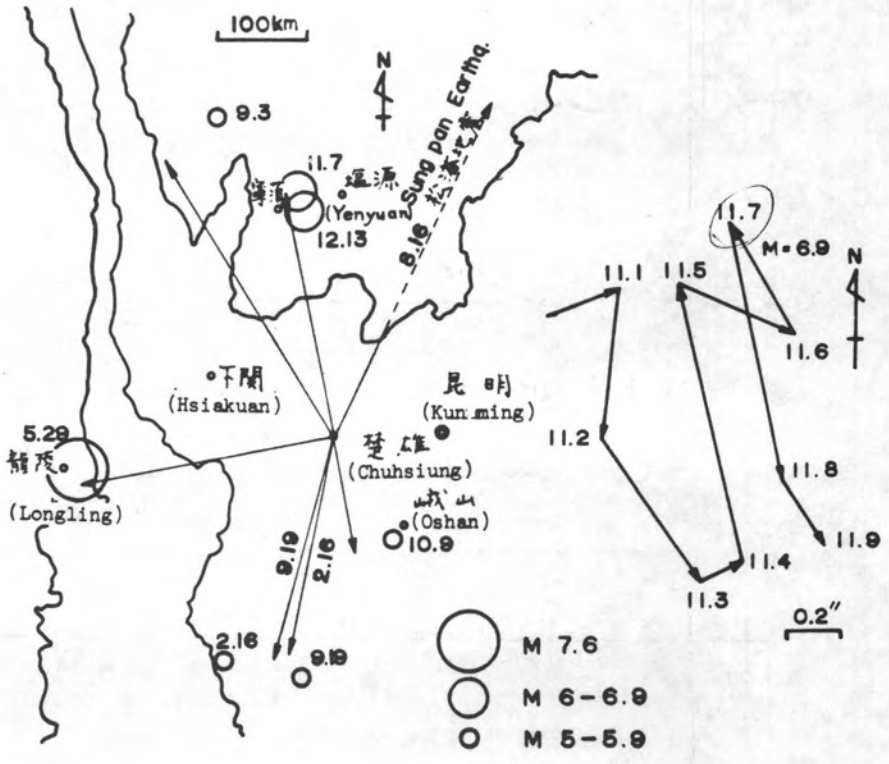

TANAKA Fig. 12

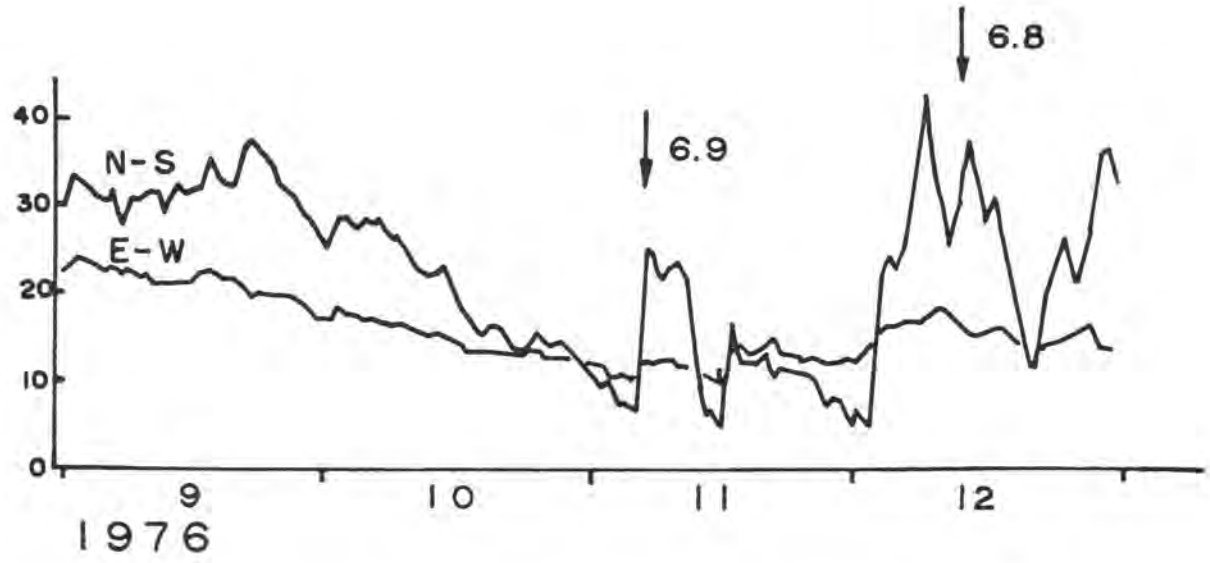

TANAKA Fig. 13

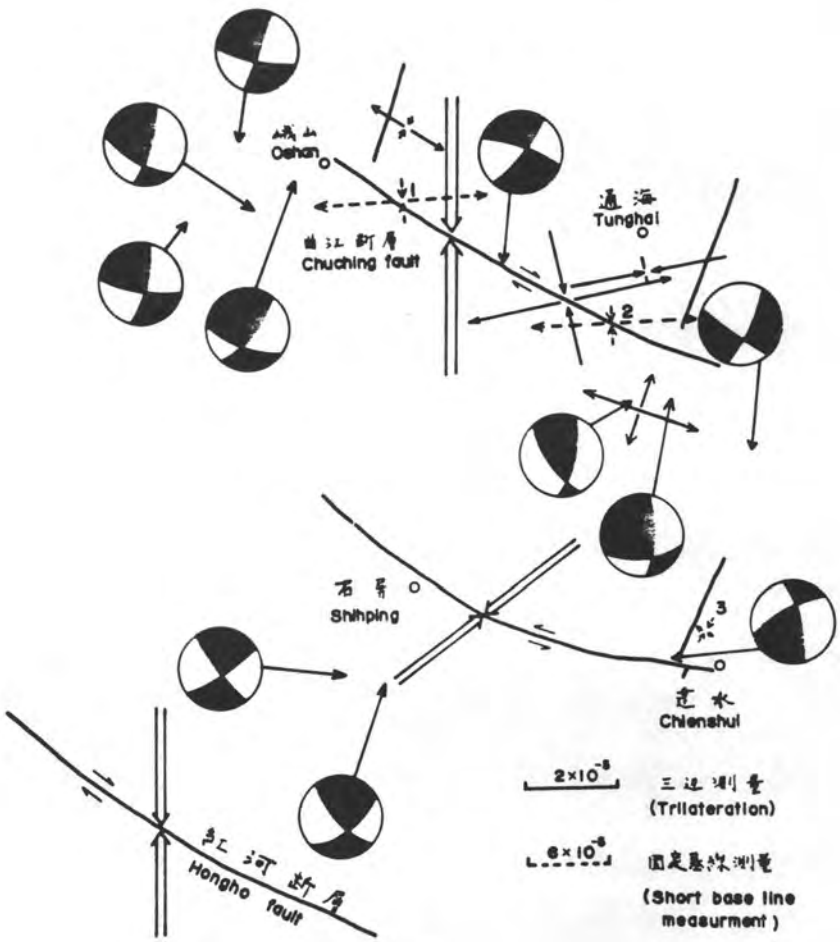

TANAKA Fig. 14

Measurement of In Situ Stress, Natural Fracture Distribution, and Fracture Permeability in a Well Near Palmdale, California

Mark D. Zoback

U.S. Geological Survey
345 Middlefield Road
Menlo Park, CA

Submitted to: Workshop on Measurement of Ground Strain Phenomena Related to Earthquake Prediction

INTRODUCTION

In situ determination of the mechanical state of crustal materials can add greatly to our knowledge of earthquake processes. This paper describes measurements of in situ stress, natural fracture distribution, and fracture permeability currently being carried out by the U.S. Geological Survey in wells drilled in tectonically active areas. Sets of such measurements have been carried out in a profile of wells drilled at various distances from the San Andreas fault near Palmdale, Calif.; measurements from one of these wells are presented, discussed in detail, and compared with surface-stress measurements.

In Situ Stress Determination

Determination of the magnitude and orientation of the principal components of stress in the vicinity of crustal earthquakes sets limits on physical models of earthquake processes. Current estimates of the magnitudes of in situ stress vary within a range of nearly one order of magnitude (Lachenbruch and Sass, 1973; Hanks, 1977).

We have developed a system for measuring insitu stress based on the hydraulic fracturing technique. Using inflatable straddle-packers a portion of a well or borehole is isolated, then pressurized until a tensile fracture is induced at the wellbore. As shown by Hubbert and Willis (1957), a fracture should form once the borehole pressure reaches the breakdown pressure, P_b, given by

$$P_b = T + 3S_h - S_H - P_o, \qquad (1)$$

where S_H and S_h are the maximum and minimum principle horizontal compressive stresses, respectively (compression is positive), and T is the tensile strength of the rock. The fracture should form at the azimuth of S_H. Once the fracture has been extended, pumping is stopped, the well is sealed off (or shut in), and a shut-in pressure is measured. This pressure is equal to the minimum principal compressive stress, S_h, because the fracture should propagate in a plane perpendicular to the direction of S_h, (assuming one principal stress is due only to the weight of the overburden, S_v). When $S_h < S_v$, (1) the fracture both initiates and propagates in a vertical plane, (2) S_h is taken to be equal to the shut-in pressure, and (3) repeatable and reliable estimates of S_h can easily be made (see Haimson, 1973; Bredehoeft and others, 1976; Zoback and others, 1978). When $S_n > S_v$, a vertical fracture initiates at the wellbore but rotates into a horizontal plane as it propagates. In this case S_h must be determined from a shut-in pressure measured immediately after fracture initiation and from pumping pressures measured at low flow rates (Zoback and Pollard, 1978).

Recovery of the core for determination of tensile strength can be expensive and difficult, but an alternative to eq. (1) for computing S_H can

be used. By repeatedly pressurizing the well, the pressure at which the fracture opens abruptly (at zero strength) can be determined and S_H calculated by substituting T=0 into eq. (1) (Zoback and Pollard, 1978).

Natural Fracture Distribution

Fractures greatly influence the mechanical properties of crustal materials, and their effects on seismic velocity, attenuation, electrical resistivity, and permeability are well known. Almost all earthquake prediction hypotheses emphasize the role of fractures, and the ability to determine the crustal distribution of fractures is important. The understanding of natural fracture patterns may supply a new form of data relevant to earthquake studies, and detailed knowledge of the fracture distribution within an area may aid monitoring of various earthquake precursors. For example, proper use of oriented fractures can be used to amplify the effects of tectonic stress on strain signals and variations in seismic velocity.

In order to determine the state of stress in a well, a knowledge of the fractures present is also required. These fractures alter the stress concentration around a borehole but more importantly, pre-existing fractures may open instead of the theoretically anticipated hydraulic fracture. The presence of mud in the borehole before pressurization can prevent some fractures from opening (Zoback and others, 1976) but it is clearly necessary to avoid existing fractures whenever possible. To accomplish this we surveyed the wells with an ultrasonic televiewer*, which is essentially a rotating acoustic transducer that reflects a sonic pulse off the borehole wall. The amplitude of the reflected pulse is displayed as brightness on a three-axis oscilloscope (and camera) as a function of depth and azimuth; a continuous record is obtained by raising the tool slowly in the hole. A flux gate magnetometer is mounted in the tool to trigger azimuthal sweep so that the strike, dip, and apparent width of natural fractures can be obtained.

Fracture Permeability

Fluid flow through fractures has been invoked to explain time-dependent earthquake processes, such as the decay and migration of aftershocks and reservoir-induced earthquakes, as well as various time-dependent earthquake precursors. Using the same inflatable packers used for the hydraulic fracturing experiments, natural fracture systems can be isolated and their permeability determined. A particularly convenient method, described in detail by Cooper and others (1967), is to apply a pulse of pressure (above the normal hydrostatic head) and then observe its decay.

*Manufactured by Simplec Manufacturing Co. under license from Mobile Oil Co. Use of trade names is for descriptive purposes only and does not constitute endorsement by the U.S. Geological Survey.

Site

Measurements were made in a well approximately 27 km southeast of Palmdale, Calif. and 3.7 km northeast of the San Andreas fault (Fig. 1). The well was drilled to a depth of 260 m in quartz monzonite of Cretaceous age (Noble, 1954). Elevation of the drill site is 1085 m above sea level. At the time of drilling the water table was encountered at a depth of 25.9 m and subsequently rose to a depth of 9.1 m.

A brief operational note: The well was drilled with a downhole air hammer by a commercial drilling company at a cost of approximately $4000; the measurements described here were made by a crew of three in approximately one week.

RESULTS

Natural Fracture Distribution

The borehole televiewer survey showed the well to be highly fractured. Fig. 2 presents data over a 14-m interval that contains numerous fractures (indicated by the dark, or nonreflecting, sinusoidal signatures); the diameter of the well is 14 cm, and magnetic declination is 15° E.

Strikes and dips of interpretable fractures (those for which the sinusoidal fracture signature can be analyzed) in the well are presented in Figures 3 and 4. The lower hemisphere stereographic projection of fracture poles (Fig. 3) emphasizes strike and dip information (using various symbols to represent depth). The plot of fracture azimuth vs. depth (Fig. 4) also contains dip, width, and descriptive information. Because each method of presentation has distinct advantages and disadvantages, both figures are given. Interesting features of the fracture distibution are:

(1) Strikes are distributed fairly uniformly but appear clustered in the northeast quadrant at depths of about 25 to 50 m (symbol A, Fig. 3) and in the northwest quadrant of about 100 to 150 m (symbol C);

(2) Fractures are predominately concentrated above 150 m;

(3) The upper 20 m is remarkably unfractured, although fracture identification within this interval is hampered by poor resolution;

(4) Most fractures dip fairly steeply; mostly between 45° and 75°.

In Situ Stress

Approximately 3 m of unfractured rock is required to make a single measurement with the equipment used. Measurements were attempted over five intervals (considered to be unfractured) at depths of 56, 149, 167, 230, and 256 m. Measurements at the highest and lowest intervals were clearly unsuccessful, and preexisting fractures were apparently opened. Plots of pressure and flow vs. time for the other three sets of measurements are presented in Fig. 5. Computation of downhole pressure from uncorrected surface pressure (as plotted) is performed by adding the appropriate hydrostatic head (15.0, 16.8, or 23.2 bars, respectively) and subtracting an

appropriate pressure during pumping to correct for the gradient between the pressure transducer and the wellhead. Interpretation was actually made on data (not reproducible) from a downhole pressure recorders that did not require these corrections.

As seen in Fig. 5, the least horizontal compressive stress, S_h, is greater than the lithostat and is determined from the pumping pressure and instantaneous shut-in pressure (ISIP) (Zoback and Pollard, 1978). A flattening of the decay rate at about the lithostat (minus the hydrostatic head) indicates that the vertical fracture at the wellbore rotated into a horizontal plane as it propagated away; S_h is measurable within 2 bars. At 230 m the ISIP does not agree with the pumping pressure, which indicates little fracture propagation immediately after initiation. The maximum horizontal compressive stress is calculated from the minimum principal compressive stress, and the zero-strength breakdown pressure, as in eq. 1. The reasonably consistent calculated values of tensile strength (Table I) are, in part, evidence that the method is reliable. The values for stress listed in Table I and shown in Fig. 6 are believed to be accurate to within 6 bars.

As presented in Table I and Fig. 6, the measurements at 149 and 167 m are in good agreement; the measurement at 230 m, however, shows an abrupt increase in stress with depth during a postfracturing

TABLE I

Summary of Stress Measurements

Depth (m)	S_h (bars)	S_H (bars)	T (bars)	S (bars)	τ Azimuth (bars) (Quality)
149	50±2	88±6	96	39.7	19±4 N.93°E. (poor)
167	51±2	89±6	92	44.5	19±4 N.83°E. (poor)
230	83±2	88±6	79	61.2	29±4 N.14°W. (excellent)

televiewer survey (Fig. 7) and also a distinct difference in the azimuth of S_H. The direction of horizontal compression indicated by this hydraulic fracture is N.140° ± 5°W.

Fracture Permeability

The effective permeability of the fracture system shown in Fig. 2 was determined by isolating the interval from 26.5 to 38.7 m and observing the decay of the applied pressure pulse. The term "effective permeability" is used because this 12.2-m interval is considered a uniform isotropic medium rather than almost impermeable, fractured rock containing fractures. The calculated effective permeability therefore represents flow properties over the interval as a whole.

Fig. 8 shows the decay of the pressure pulse plotted as normalized pressure vs. the logarithm of time and compared to type curves prepared by Cooper and others (1967). A reasonably good match is found for a storage coefficient, α, of 10^{-1}; had curves for larger α been available, a slightly better fit could have been achieved. Storage coefficient of the fracture system is basically how much the fracture system stores (per unit surface area) for a unit change in pressure; the data match the type curves at a time of 16 s. With the appropriate dimensions, this corresponds to an effective permeability of approximately 2.5 darcies.

DISCUSSION

In Situ Stress

The state of stress to depths of 230 m is highly compressional. In areas of strike slip motion along vertical faults one would expect the vertical stress to be intermediate in magnitude between the two principal horizontal stresses. The manner in which these stresses change at greater depth is of considerable interest and deserves further investigation.

The significant change in stress magnitude and direction between 149, 167, and 230 m is interpreted to demonstrate that extensive fracturing has decoupled the upper 200 m or so of rock from the tectonic stress field. This interpretation is supported by the fact that the direction of horizontal compression at the two upper points is approximately east-west, the same as determined by Sbar and others (1978) using surface-measurement techniques. The determination of N.140°W. at 230 m, however, is consistent with geodetic measurements (Savage and Prescott, 1978), the vector of relative plate motion (Minster and others, 1974), earthquake focal mechanisms (Fuis and others, 1977), and Holocene geologic deformation (D. Burke, oral commun.). The increase in the magnitude of the principal stresses seems to corroborate this interpretation.

Although slightly west of north horizontal compression and high east-west compression (compared to vertical stress) are consistent with thrust faulting in the Transverse Ranges (and especially with ground breakage associated with the 1971 San Fernando, Calif. earthquake), it is not consistent with

strike-slip motion on the San Andreas fault, which strikes approximately N.65°W. in this area. It is interesting to speculate whether precursors of the next 1857-type earthquake in the area will be a counterclockwise rotation of the stress field or a marked decrease in the magnitude of this east-west compressive stress.

The shear stress at 230 m, which we can define simply as $(S_H - S_h)/2$, is 29±4 bars. This value is significantly lower than measurements at similar depths in wells farther from the fault (Zoback, unpub. data, 1978) and may provide evidence to corroborate heat flow data which suggest that the average frictional strength of the San Andreas fault to a depth of about 20 km is only several hundred bars (Lachenbruch and Sass, 1973).

Natural Fractures

Many of the fractures observed in this well were probably formed as the original granitic intrusion cooled; others are possibly due to uplift and weathering. Nevertheless, the absence of intense fracturing near the surface and the fact that no surface-dominated fracture pattern was observed suggests other mechanisms of fracture formation. For example, shear motion may be concentrated both in thrust planes striking west northwest-east southeast and dipping about 30°, and in nearly vertical planes striking subparallel and conjugate to the San Andreas fault. A possible case might be made for the existence of a horizontal set of fractures (Fig. 3) but a vertical well does not sufficiently sample vertical fractures to indicate the presence of these fracture sets.

Fracture Permeability

The effective permeability of about 2.5 darcies measured over the highly fractured, shallow interval investigated indicates an extremely permeable material that is probably not characteristic of the rock mass as a whole. Estimates based on various earthquake phenomena are about two orders of magnitude lower. Only measurements over more representative intervals, as well as measurements at greater depths, will help determine whether fluid flow-related processes are likely.

CONCLUSIONS

The measurements reported here illustrate how a great deal of information on the physical state of materials at depth can be gathered through an integrated series of borehole measurements. In the region surrounding the well in which the measurements were made the crust is apparently decoupled from the tectonic stress field to a depth of about 200 m. The least compressive stress at 230 m is the vertical component of stress, and the direction of maximum horizontal compression is N.140° ± 5°W.; shear stress at this depth is 29±4 bars, somewhat less than estimates made at similar depths in wells farther from the San Andreas fault. The effective permeability over a highly fractured, near-surface interval may be estimated at approximately 2.5 darcies.

REFERENCES

Bredehoeft, J. D., R. G. Wolff, W. S. Keys, and E. Shuter, 1976, Hydraulic fracturing to determine the regional in-situ stress field, Piceance Basin, Colorado, Geol. Soc. Amer. Bull., v. 87, 250-258.

Cooper, H. H., Jr., J. C. Bredehoeft, and I. S. Papadopulos, 1967, Response for a finite-diameter well to an instantaneous change of water, Water Resour. Res., v. 3, no. 1, 263-269.

Fuis, G. S., M. E. Friedman, and J. A. Hileman, 1977, Preliminary catalog of earthquakes in southern California, July 1974-September 1976, U.S. Geol. Surv. Open-File Rpt. 77-181, 107 p.

Haimson, B. C., 1973, Earthquake related stresses at Rangely, Colorado: in New Horizons in Rock Mechanics, Proc. 14th Symp. Rock Mech., Eds. Hardy and Stefanho, ASCE, New York, 689-708.

Hanks, T. C., 1977, Earthquake stress drops, ambient tectonic stresses and stresses that drive plate motions, Pure Appl. Geophys., v. 115, no. 1/2, 441-458.

Hubbert, M. K., and D. G. Willis, 1957, Mechanics of hydraulic fracturing, Pet. Trans. AIME, v. 210, 153-168.

Lachenbruch, A. H., and J. H. Sass, 1973, Thermo-mechanical aspects of the San Andreas fault system: in Proc. Conf. Tectonic Probl. San Andreas Fault System, R. L. Kovack and A. Nur, Stanford Univ. Press, Stanford, Calif., 192-205.

Minster, J. B., T. H. Jordan, P. Molnar, and E. Harnis, 1974, Numerical modelling of instantaneous plate tectonics, Geophys. J. Roy. Astr. Soc., v. 36, 541-576.

Noble, L. F., 1954, The San Andreas fault zone from Soledad Pass to Cajon Pass, California, Calif. Div. Mines Bull. 170, 37-48.

Savage, J. C., and W. H. Prescott, 1978, Geodimeter measurements of strain during the southern California uplift, Science, in press.

Sbar, M. L., T. Engelder, R. Plumb, and S. Marshak, 1978, Stress pattern near the San Andreas fault, Palmdale, California from near surface in-situ measurements, Jour. Geophys. Res., in press.

Sbar, M. L., T. Engelder, and T. Tullis, 1978, Near surface in situ stress measurements along the 1857 break of the San Andreas fault, in Measurement of Stress and Strain Phenomena Related to Earthquake Prediction, U.S.G.S. Open File Report, this issue.

Zoback, M. D., F. Rummel, R. Jung, H. J. Alheid, and C. B. Raleigh, 1977, Laboratory hydraulic fracturing experiments in intact and pre-fractured rock. Int. Jour. Rock Mech. Mining Sci. Geomech. Abstr., v. 14, 49-58.

Zoback, M. D., J. H. Healy, J. C. Roller, G. S. Gohn, and B. B. Higgins, 1978, Normal faulting and in situ stress in the South Carolina coastal plain near Charleston, Geology, v. 6, 147-152.

Zoback, M. D., and D. D. Pollard, 1978, Hydraulic fracture propagation and the interpretation of pressure-time records for in-situ stress determinations, in 19th U.S. Symp. Rock Mech., Ed. Y. S. Kim, 14-22.

Figure captions

Fig. 1 Location of well (+) in which measurements were made.

Fig. 2 Borehole televiewer records from depth of 26 to 40 m. Azimuth and dip indicated on records are not corrected for magnetic declination (15° E.). Interpretation of fractures for which sinusoidal signature can be distinguished is shown to right of records, along with computed strikes and dips.

Fig. 3 Lower hemisphere projection of fracture poles from well. Various symbols represent depth ranges as follows: A=0 to 50 m, B=51 to 100 m, C=101 to 150 m, D=151 to 200 m, and E=201 to 260 m.

Fig. 4 Plot of fracture strike and dip vs. depth. Size of symbol represents estimated fracture width.

Fig. 5 Plots of uncorrected surface pressure (see text) and flow rate vs. time.

Fig. 6 Plot of maximum and minimum horizontal compressive stresses, S_H, and S_h vs. depth. Lithostat at a density of 2.7 g/cm^3 is shown for reference.

Fig. 7 Posthydraulic-fracturing televiewer record from 229-m-deep fracture which indicates that S_H is at an azimuth of N.140°W.

Fig. 8 Plot of normalized pressure vs. logarithm of time. Curve from Cooper and others (1967) for a storage coefficient, α, of 10^{-1}. Curves match at 16 s.


36°
35°
34°
33°
115°
116°
117°
118°
119°
120°
121°
SAN ANDREAS
PALMDALE
LOS ANGELES
N
0 50 100 Km

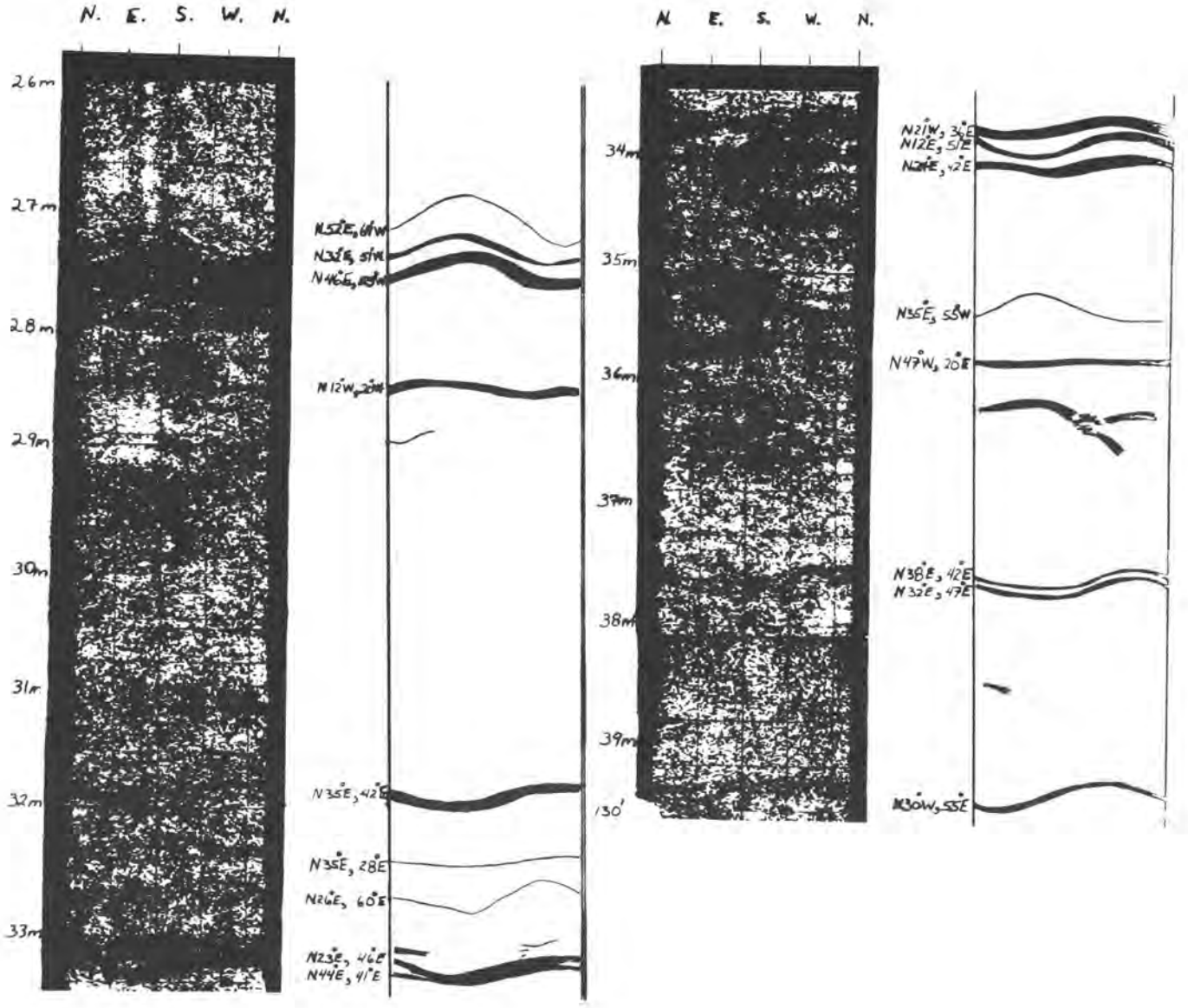
N. E. S. W. N.
26m
27m
28m
29m
30m
31m
32m
33m
N52E, 68W
N35E, 51W
N46E, 83W
N12W, 20W
N35E, 42E
N35E, 28E
N26E, 60E
N23E, 46E
N44E, 41°E
N. E. S. W. N.
34m
35m
36m
37m
38m
39m
130'
N21W, 34E
N12E, 51E
N24E, 42E
N35E, 55W
N47W, 20E
N38E, 42E
N32E, 47E
N30W, 55E

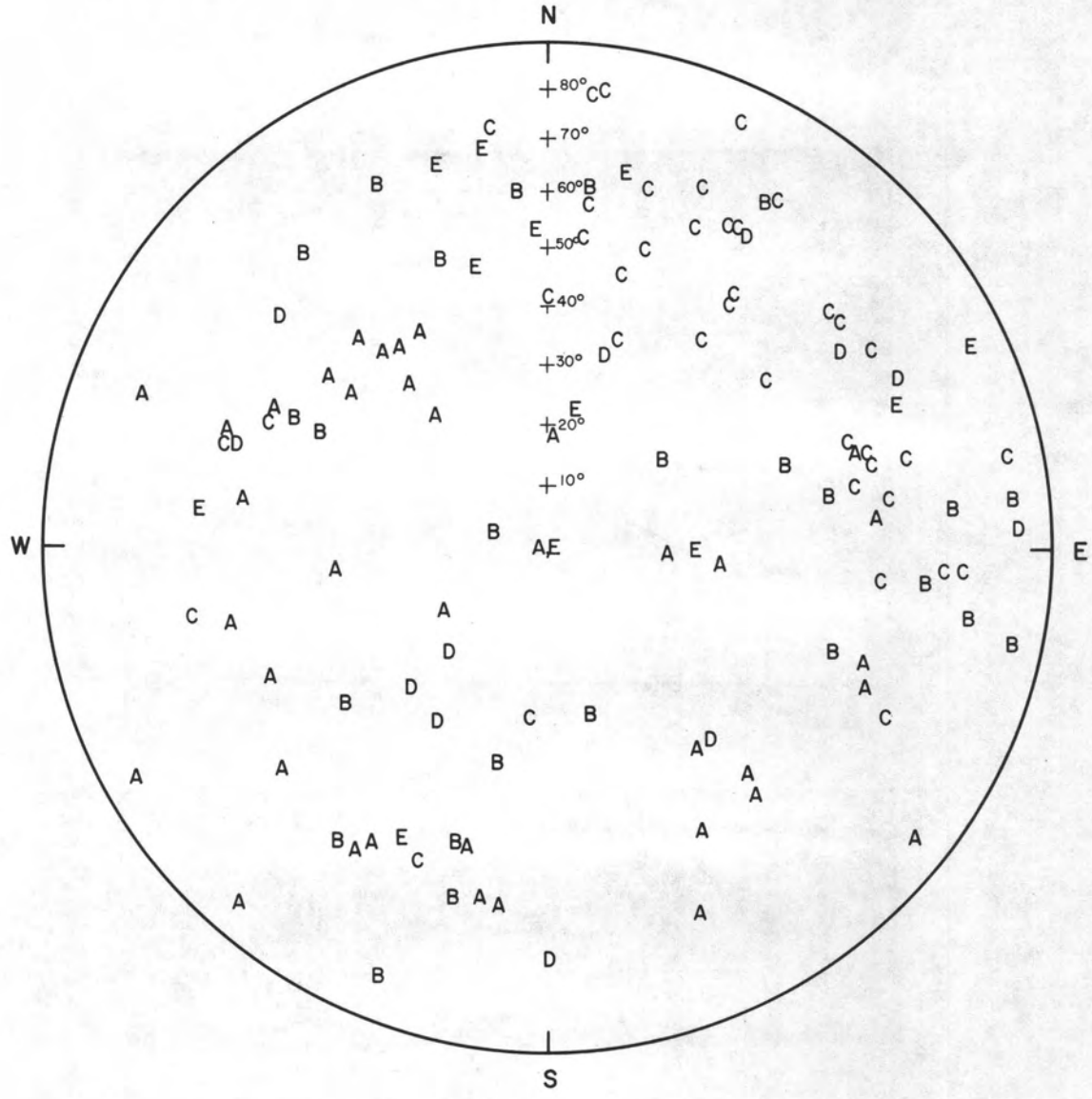
N
W
E
S
80°
70°
60°
50°
40°
30°
20°
10°

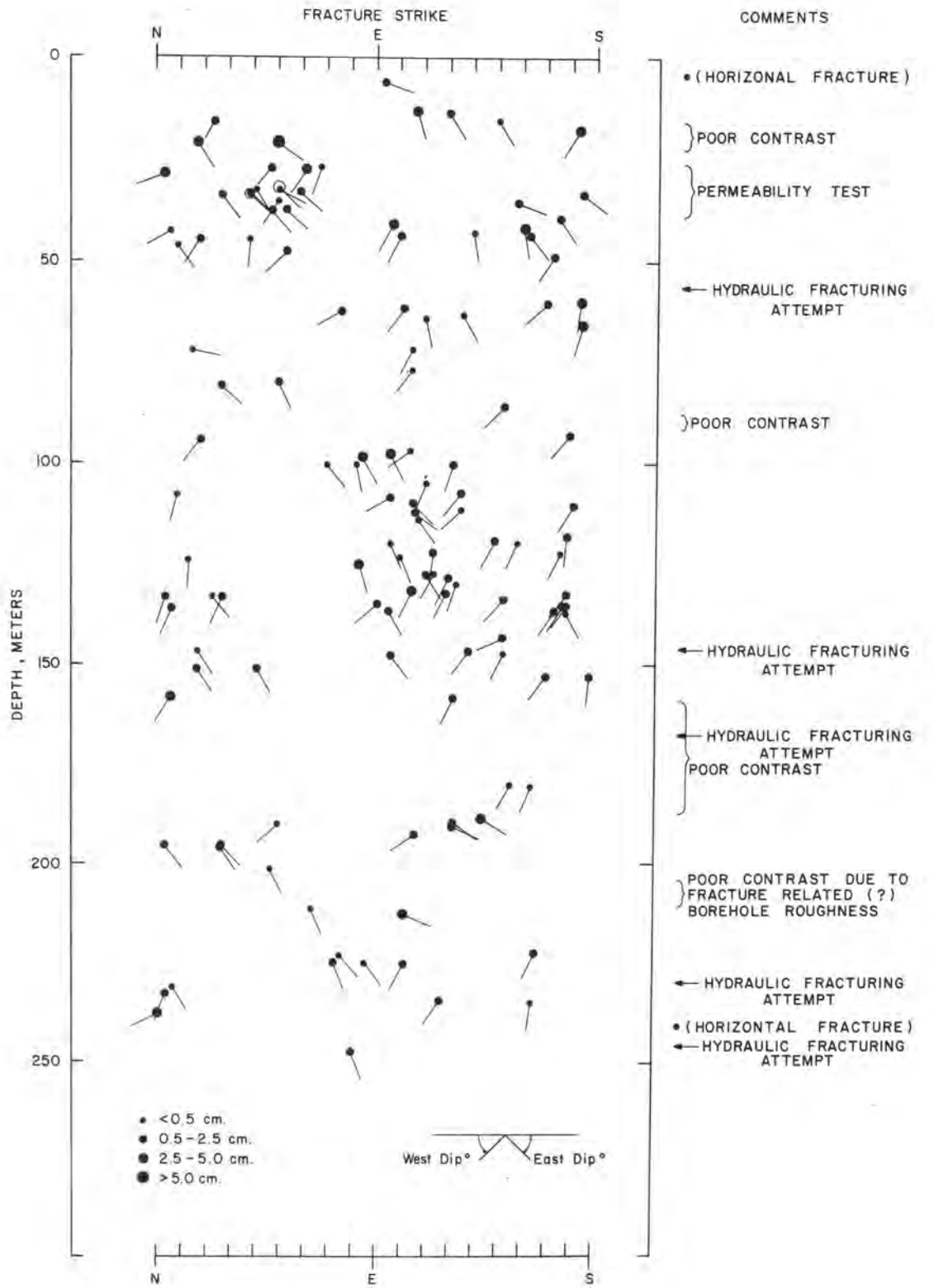
FRACTURE STRIKE
N
E
S
COMMENTS
0
50
100
150
200
250
DEPTH, METERS
• (HORIZONAL FRACTURE)
POOR CONTRAST
PERMEABILITY TEST
HYDRAULIC FRACTURING ATTEMPT
POOR CONTRAST
HYDRAULIC FRACTURING ATTEMPT
HYDRAULIC FRACTURING ATTEMPT
POOR CONTRAST
POOR CONTRAST DUE TO FRACTURE RELATED (?) BOREHOLE ROUGHNESS
HYDRAULIC FRACTURING ATTEMPT
• (HORIZONTAL FRACTURE)
HYDRAULIC FRACTURING ATTEMPT
• <0.5 cm.
• 0.5 - 2.5 cm.
• 2.5 - 5.0 cm.
• >5.0 cm.
West Dip°
East Dip°
N
E
S

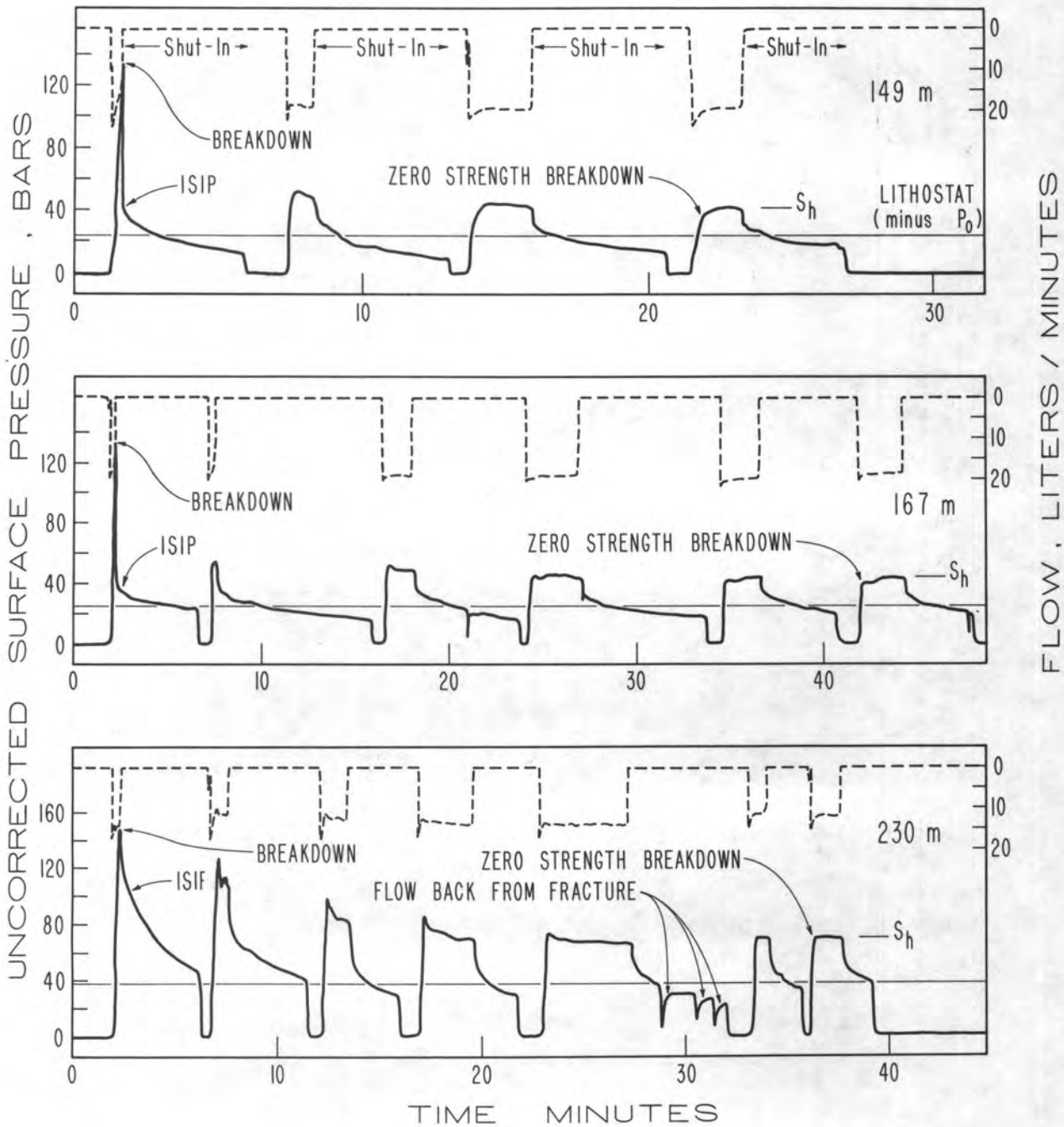
Shut-In
Shut-In
Shut-In
Shut-In
149 m
BREAKDOWN
ISIP
ZERO STRENGTH BREAKDOWN
S_h
LITHOSTAT
(minus P_0)
167 m
BREAKDOWN
ISIP
ZERO STRENGTH BREAKDOWN
S_h
230 m
BREAKDOWN
ISIP
ZERO STRENGTH BREAKDOWN
FLOW BACK FROM FRACTURE
S_h
UNCORRECTED SURFACE PRESSURE, BARS
FLOW, LITERS / MINUTES
TIME MINUTES

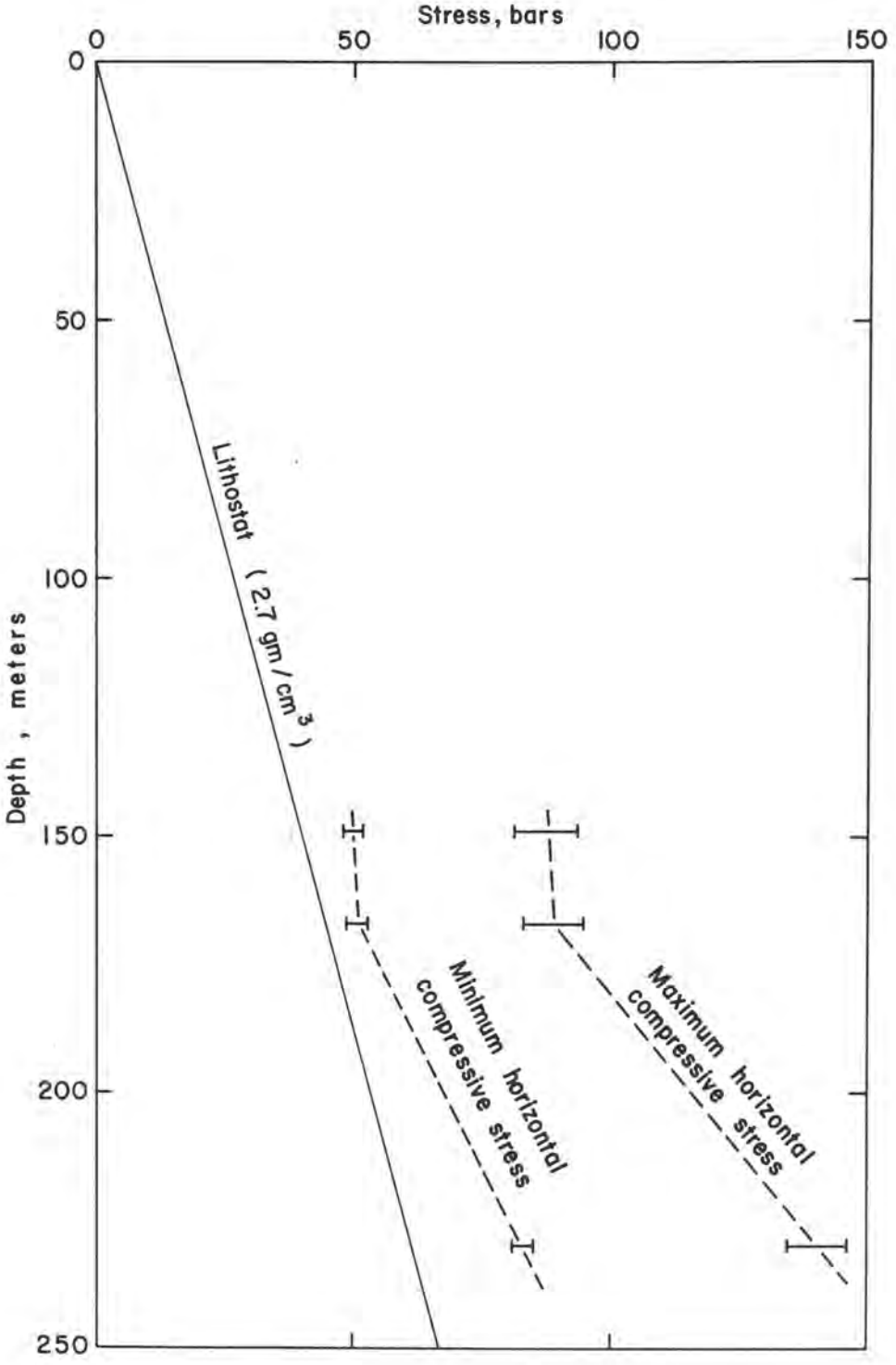
Stress, bars
0
50
100
150
Depth , meters
0
50
100
150
200
250
Lithostat (2.7 gm / cm³)
Minimum horizontal compressive stress
Maximum horizontal compressive stress

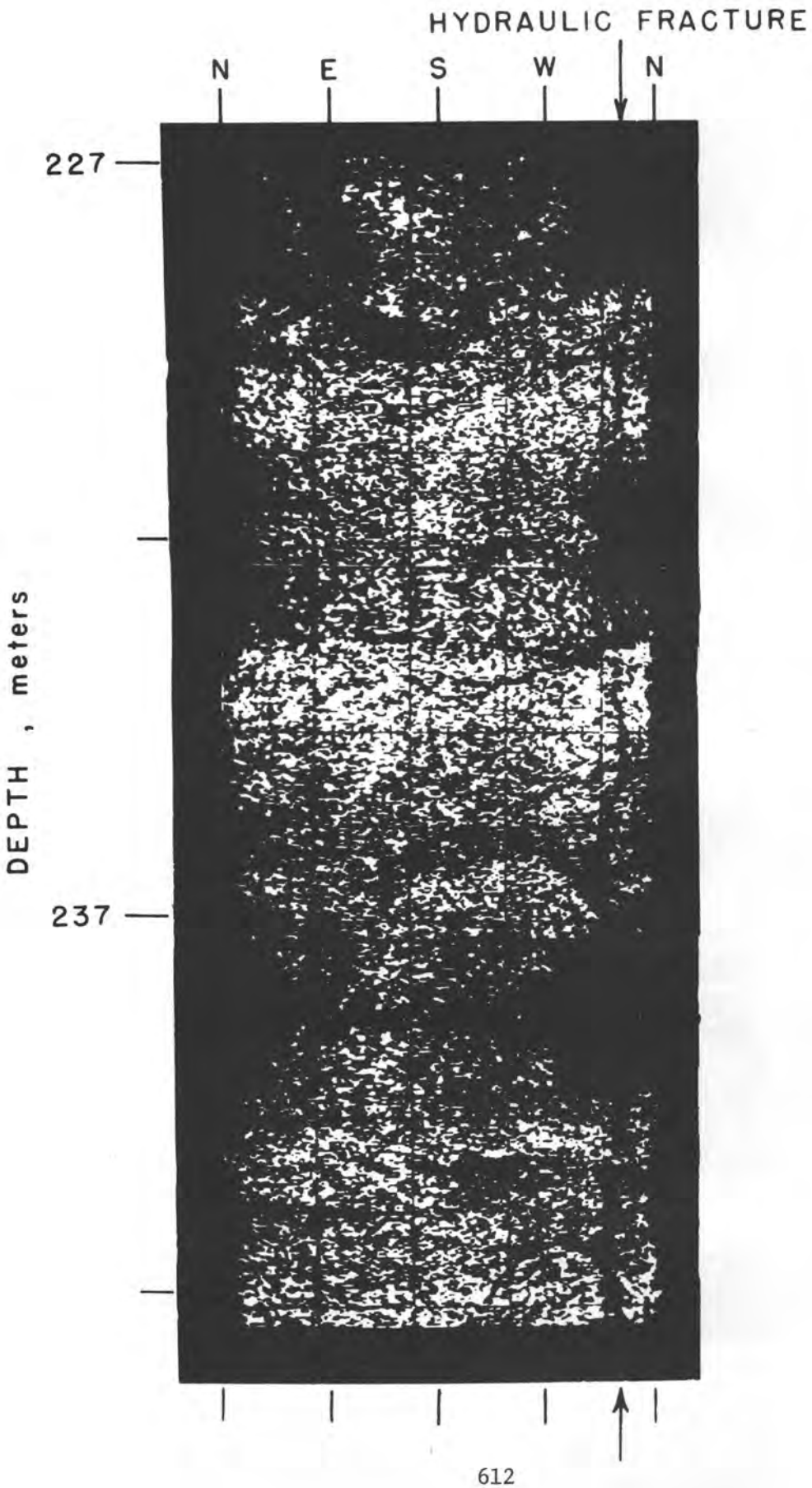
HYDRAULIC FRACTURE
N
E
S
W
N
227
237
DEPTH , meters

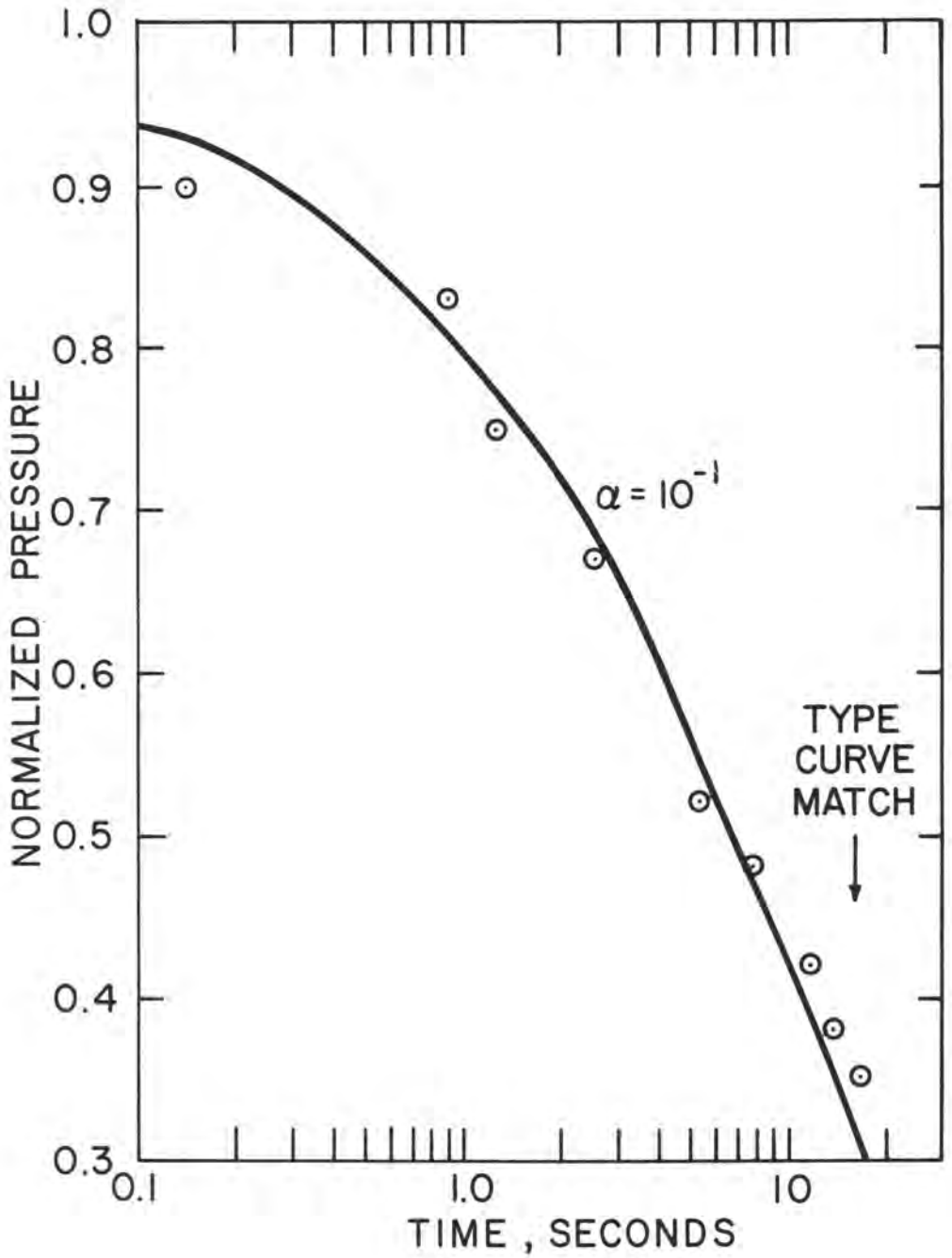
1.0
0.9
0.8
0.7
0.6
0.5
0.4
0.3
NORMALIZED PRESSURE
$\alpha = 10^{-1}$
TYPE
CURVE
MATCH
0.1
1.0
10
TIME , SECONDS

SUMMARY
Part I

I should give a strong admonition to all readers of this part of the summary. You must read all comments following Part I if you wish to acquire a proper flavor of the Conference. There was no time at this conference for recording views and comments of participants as at previous conferences. Therefore, I proposed that I would write a Summary and others would comment on it. As will be seen, the Summary is designed to solicit comments. I may or may not actually believe all statements in the Summary. All statements certainly are supportable by statements made at the conference. Some are, of course, contrary to some assertions and it is hoped that such contrary views will be expressed in comments by others. It will then be up to the reader to form his own opinions of what the situation really is.

The most extensive and acrimonious discussions at the Conference were triggered by discussions of utility of the Kinemetrics tiltmeters. At one end of the spectrum were comments by John Berger to the effect that installations at Pinon Flat Observatory of Kinemetrics tiltmeters at a spacing of 10 meters demonstrated unequivocally complete incoherence in resultant signals, thus demonstrating uselessness of the instruments whether due to ground or equipment noise level. I think it fair to say that few if any felt he had made his point, the reason being that we had already heard a series of papers discussing the problems associated with installation of these tiltmeters. Much of this is described in the papers but the core of the problem appears to be that the long pipe (1 meter) in which the instrument is mounted tends to bend under small environmental perturbations of temperature or any other ground condition unless the greatest care is taken in installation. Thus, Sean Morrissey, who has apparently worked harder at debugging installation procedures than anyone else (including the USGS), finds that environmental noise is drastically reduced if the top half of the one-meter pipe is not packed with anything at all! The general view of most practitioners, these views not always being supported by facts presented at the Conference, are that the instruments themselves are highly stable. Bilham asserted he had performed a test of a locked-together pair, though he presented no data and the literature is still free of any data demonstrating noise level of the instrument-electronics package. Environmental noise is always a problem and no one has yet demonstrated that two tiltmeters "properly installed" and at a separation of ten meters will track each other. Hopefully, we will have a near-definitive demonstration when CIRES receives data from the new installations in the Aleutians in December. The USGS asserted that they had largely solved installation problems and knew all about what Morrissey was discovering. However, as usual, there was a minimum of data presented to support their views. Bill Stuart, when attempting to apply his F_2 precursory detector to a significant fraction of USGS tiltmeter data in order to evaluate false alarm, detection and surprise levels, found that data of only 2 of the many USGS instruments were in a form where such an investigation could be performed. It is, of course, true that the USGS instruments, extensive as they are, have been near only one M5+ earthquake and apparently got definite premonitory tilt signals on three instruments.

Bilham made the pitch for abandoning all Kinemetric tiltmeters and replacing them with long base line tiltmeters. He described the Lamont one-fluid instrument and presented data demonstrating its immunity from a variety of problems plaguing point tiltmeters. The Lamont meter has the one disadvantage that every element of the entire line of the meter must be very nearly horizontal. This limitation is quite severe and is the reason for development of a two-fluid tiltmeter. It certainly appears that there is a real need for deployment of some long-baseline tiltmeters in California but I don't think Bilham made his case for abandoning the Kinemetrics meter.

A truly grave problem relative to tiltmeters (or any strain-measuring device) as an instrument for detection of premonitory signals of earthquakes came into focus via two separate but related discussions. Selwyn Sacks pointed out the extremely low amplitude strain signals expected from even reasonably large earthquakes. At epicentral distances comparable to fault-lengths, strains of order 10^{-6} are expected, at twice fault-length 10^{-7}, at 5 times fault-length 10^{-8}. If these estimates are valid, very few strain measurements will have adequately low noise (instrumental or environmental) to be useful at sites other than in or very near fault zones. To compound this problem, the inelastic character of the San Andreas Fault zone, the demonstrated (at least to me) fact that the San Andreas Fault is a very low stress system (see below), and the distinct possibility that all major faults function similarly (high pore pressure leading to low confining stress with rate of subduction being conditioned entirely by rate of delivery of crust to zone by body forces and/or basal shear stress) imply that Sack's estimates of distances may be excessive. The only ways out of this problem are: (a) if all above is true, observations must be in fault-zones which means prediction of subduction earthquakes may be very difficult if there are no seismic precursors; (b) all above is not true, the possible way for this being a highly heterogeneous world with numerous or occasional "soft spots". The Chinese data discussed in Tanaka's paper, as well as the observations and conclusions of Keilis-Borok and collaborators (see Volume VI of this series) suggest the possibility of grossly heterogeneous behavior of the crust, the problem of this approach being the difficulty of specification of the epicenter and of the time-scale to the earthquake.

The major cause for continued enthusiasm about long range predictors is the continuing flow of stories about such signals being important elements of successful predictions in China. It may be important to note that collection of extensive and continuous reports of personally (rather than instrumentally) observed abnormal phenomena appear to play a far greater role in Chinese predictions than appeared at first reports (R. Wallace, personal communication).

Only Kumar of N.G.S. was present to discuss data of level lines, the practitioners of this art within O.E.S. refusing to attend or to give us a manuscript. Kumar made a strong point as regards level lines run over mountainous

terrain, as were several of the lines run in Southern California last winter. None of such loops closed to normally stated specifications for first order leveling. Kumar reported that his associates at N.G.S. told him that no such loops ever close. The low elevation loops all closed nicely. The worst closure error is 21 centimeters. Kumar suggests that all of this results from lack of parallelism and distortion of geopotential surfaces, leading to the integral of Δh not being zero no matter what care is taken in observations. He will be able to check quality of observations of the non-closing loops as g values were obtained at all stations and the integral of $g \Delta h$ should close. The implications of his statements are that failure of loops to close cannot be intepreted as uplift during observations, "errors" in closure on such loops are not to be distributed, and changes in Δh are best observed along profiles with no effort being expended on closing loops having large elevation changes as results will only be confusing (can check data quality by $g \Delta h$). It wasn't clear whether the geopotential problem is resolvable by evaluation of terrain effects and/or regionally observable gravity profiles.

Some years ago, it was decided to commence gravity observations with the intent of evaluating the capability to detect elevation changes via this technique. It appears the problems are somewhat greater than expected for more reasons than expected. In the first place, the standard deviation of relative gravity values estimated by double observations with two instruments appears to be 10 or so μgals (see Fett's profiles), thus rendering 20 μgal changes observed on an annual basis of uncertain significance. The pages of data obtained by Fett and included in roceedings (see notes preceding the charts explaining how to interpret them) indicate that monthly observations can yield data clearly establishing changes of 20 μgals and less over periods of a few months. I would suggest that annual observations of an extended network of gravity stations are of far less use and interpretability than are profiles observed on a monthly basis. The second and unexpected problem is that 20 - 30 μgal changes seem to occur on a period of months, probably without associated elevation or water level change. Thus, the changes at C_1 on Fett's C profile (changes at C_1 relative to Hemet Base) exceed 25 μgals in a period of 5 months. A magnitude 4+ earthquake occurred essentially under C_1 on July 4 and the gravity value has decreased since. This certainly isn't due to a change in water-level. I can't guarantee it is not related to an elevation change but other reports of gravity changes unrelated to elevation or water-level change (Tangshan earthquake - 150 μgals) suggest existence of stress- induced density change at depth. Maybe by serendipity we have stumbled upon a winner.

Noise levels in short base line or point measurements, inability to economically measure strains over lengths of kilometers, need for elevation estimates at times of determination of gravity, etc., etc., indicate need for a magic instrument that can rapidly and accurately determine all vector components of specific line segments for routine monitoring. This system should involve little or no man-power, field installations should be simple and inexpensive. For transport while profiling, the instruments should be small and durable. The phenomenal fact seems to be that, with diligent effort at persuasion of D.O.D., we could have such a magical capability coming to pass around 1985. C. Councilman

captivated the entire group with his report on capabilities of long base line VLBI and the state-of-the-art capability inherent in the MITES interferometry technique developed at MIT. It is pointless for me to elaborate further here. His text gives the essential details. Suffice it to say that they have demonstrated 3 cm. rms error of multiple determinations of the Haystack-Owens Valley (4000 km) line without the use of radiometry and British investigators have rms errors of about one millimeter along a 1.5 kilometer line, again without resort to radiometry. The one problem is that the requisite transmitters are not now planned for the G.P.S. satellites. Councilman was asked to consider whether we might get a useful capability from existant satellite-borne transmitters and a somewhat changed receiver. If time permits, a response will be forthcoming.

Another aspect of the EHRP is measurement of state of stress or changes in state of stress. As regards state of stress, Sbar reported on door-stopper measurements in Southern California, tried to make the case that he could separate residual and active stress, and suggested that his data indicated a definite pattern of active stress related to the San Andreas Fault. None of his arguments were particularly convincing. Engelder presented data from the Northeast U.S. which suggested that the door-stopper technique of overcoring is severely contaminated by residual stress. Clark said that Sbar's data looked like his comparably obtained data in central U.S., i.e., reproducibility of stress values in small areas but highly divergent and uninterpretable values over distances of 10 or more kilometers. Finally, Zoback gave results of hydrofracing at a variety of depths (10 or so meters to 250 or more meters depths) in several wells in Southern California. He found near-surface stresses near the fault similar to those suggested by Sbar (main compression nearly east-west) but stresses below 200 or so meters to be nearly north-south. He suggested some kind of decoupling at around 200 meters with deep values of stress direction being those of active stress. The only problem with this interpretation is that J. Logan, when analysing the hydrofrac data of_____oilfield, concluded that the hydrofrac measurements were related to residual stress rather than to active stress. More work,men.

Accepting Zoback's intrepretation, the stress values he found at depth were extremely interesting, 20 bar shear stress within 2 kilometers of the San Andreas Fault and 50 bar shear stress at 15 kilometers and greater, thus implying a very weak fault zone. This result has, of course, strong implications for the mechanics of the San Andreas Fault. Slater gave results which are best interpreted to imply the same thing. The data are based on use of the 2-frequency laser distance measuring device in the Hollister area. He finds that near-surface creep events extend throughout the seismic zone in a matter of weeks. In other works, the step in strain seen on creepmeters or along short lines crossing the fault as a creep event are seen at distances of several kilometers from the fault within a matter of weeks. Wayne Thatcher, in work not reported at the Conference, has found annual rate of movement of points 30 kilometers west of the San Andreas Fault (along the creeping part of the fault) relative to points just east of the fault to be equal to the rate of creep on the fault. Slater's and Thatcher's analysis establish that, along the creeping part of the fault, rigid block motion is operative. Vibroseis results by McEvilly (also not given at the Conference) show very low velocities at several kilometers depth near the fault. It is my conclusion that all of this implies very low to vanishing stress throughout the "seismic" zone along the creeping section of the fault and the only model we have for this is high pore pressure. Finally, I would guess that the struck parts of the fault are comparatively minor perturbations on the slipping portion, i.e. low stress as indi-

cated by Zoback. All of this is extremely important if true but makes prediction harder than expected.

The only paper that addressed detection of changes in stress was that by Clark. He thinks he is seeing stress changes of a bar or more over periods of several months in very shallow holes. How this is possible if near-surface over-coring door-stopper measurements are reporting only residual stress is not obvious. A real degree of confusion seems to exist. Items suggesting that Clark's measurements are valid measures of changes in ambient stress are; (a) the fact that most of the changes show north-south compression in agreement with other data; and (b) that the gauge in the Palmdale area is showing dilatation in all horizontal directions in recent months while the Lytle Base station of Fett has shown a decrease of about 20 μgals in gravity (relative to Hemet Base), suggesting a decrease in horizontal compression leading to a decrease in mass under the station(?) Since the gauges used by Clark are inexpensive and apparently adequate to measure actually occurring levels of change in ambient stress, an expanded program of deployment at shallow depth seems warranted.

Little new was presented on electrical and magnetic techniques for detection of precursory anomalies. Madden continued his campaign against even feasibility of there being detectable changes in resistivity. His arguments, based as they are on credible intergranular and crack patterns in otherwise homogeneous rocks, are no doubt valid. However, the possibility exists (at least conceptually) of massive dilatation in the fault-zone. Unfortunately, F. Morrison of UCB failed to make his promised appearance, either in person or text, so no presentation of his analysis, based on such a hypothesis could be presented. As Madden pointed out, existence of a self-potential anomaly would imply a new pressure drive or a new pressure sink, thus possibly implying massive dilatation in the fault-zone. Madden asserted that no self-potential anomalies have ever been seen. The attached figure indicates two possible self-potential anomalies recorded in Central California. What do you think of these, Ted?

Work by Kuckes and Coleman is only beginning and the results presented by Johnson (magnetic anomaly for Thanksgiving Day earthquake and magnetic effects at ends of creeping zone) have been presented previously and so require no comment here.

A few other papers were presented which will make interesting reading but have little to offer to the sort of summary here written.

JFE

COMMENTS ON JACK EVERNDEN'S SUMMARY OF THE USGS CONFERENCE ON GROUND STRAIN PHENOMENA RELATED TO EARTHQUAKE PREDICTION

September 1978

by Roger Bilham

On the whole Jack Evernden's summary is a reasonably accurate review of the meeting, but since it was written to provoke I cannot allow some of his weaker assertions to remain in print without at least mild protest. I restrict myself to the first two pages of his summary.

Small tiltmeters

A 2 m vertical tube placed in a hole in the ground will respond to all wavelengths of tilt (i.e., rotation about horizontal axes) with wavelengths longer than about 2 m. A significant point that Berger makes is that no one knows what the wave number/frequency spectrum for tilt noise is, but both he, USGS, and our group present data indicating that there is considerable incoherence for instruments spaced between 10 m and 200 m apart at virtually all frequencies. The problem appears to be then, that very short wavelength noise (less than 10 m) is generated near the surface and that in order to attenuate this, instruments must either be buried at depths greater than the horizontal wavelength of the noise or instruments must be sufficiently long to average out the short wavelength noise. Morrisey has chosen to meet the noise half-way by systematically improving the instrument installation. Thus he finds not unsurprisingly that an instrument supported at depth (3 m) and only by its lower half appears to be less noisy by an order of magnitude than a conventional installation. It is well known that surface installations are noisy ($> 10^{-6}$/year) and that deep observatory installations are quiet ($< 10^{-7}$/year). Improvements to the installation method of shallow borehole tiltmeters (< 5 m) are only worthwhile if we make the assumption that surface tilt

noise has its maximum energy for wavelengths that are less than about 5 m. If this is not a valid assumption, then a correspondingly deeper installation with a short instrument or a surface installation of a very long instrument must be used to improve the signal-to-noise ratio.

Would we recognize an earthquake precursor on noisy data? The question was asked at the meeting. I think the answer is a discouraging no. Without exceptional coherence between an array of instruments the precursor is likely to be missed. So far I have not seen any coherence for frequencies other than the microseismic band.

Short tiltmeter instrument performance

Both USGS (Johnston) and Lamont (Bilham and Murphy, USGS G371 final report - see enclosed excerpts) have conducted studies of the instrument stability by suspending Kinemetrics tiltmeters from a free vertical pendulum. In our test two instruments were strapped back to back on the pendulum and the *difference* in their electrical outputs plotted as a function of tilt. The test revealed non-linearity outside a range of $\pm$ 4 x 10^{-6} rad. A long free-hanging test with both outputs recorded gave good tracking stability (10^{-7} per month) and a short length of the data showed identical performance (Fig. 1).

Long tiltmeters

Clearly short instruments are ideal for looking at short wavelength signals. Long instruments are intended to more closely monitor long-wavelength tectonic signals. We describe one of several instrument designs

which can do the job and one that we assert is inherently more stable, noise-free, and accurate than others designs. Its disadvantage is that it requires a horizontal piece of ground on which to install it. Fortunately, many such locations exist in the form of contour lines on maps; the instrument does not have to be installed on an exactly straight line. The inconvenience of surface levelness does exist but it should not be forgotten that the half-filled tube tiltmeter we describe is a surface instrument that attains a noise level of about 10^{-7} radians for periods greater than a day. We believe this could be improved by at least an order of magnitude by shallow burial and improved end mounts. The best borehole installation has barely attained our existing stability.

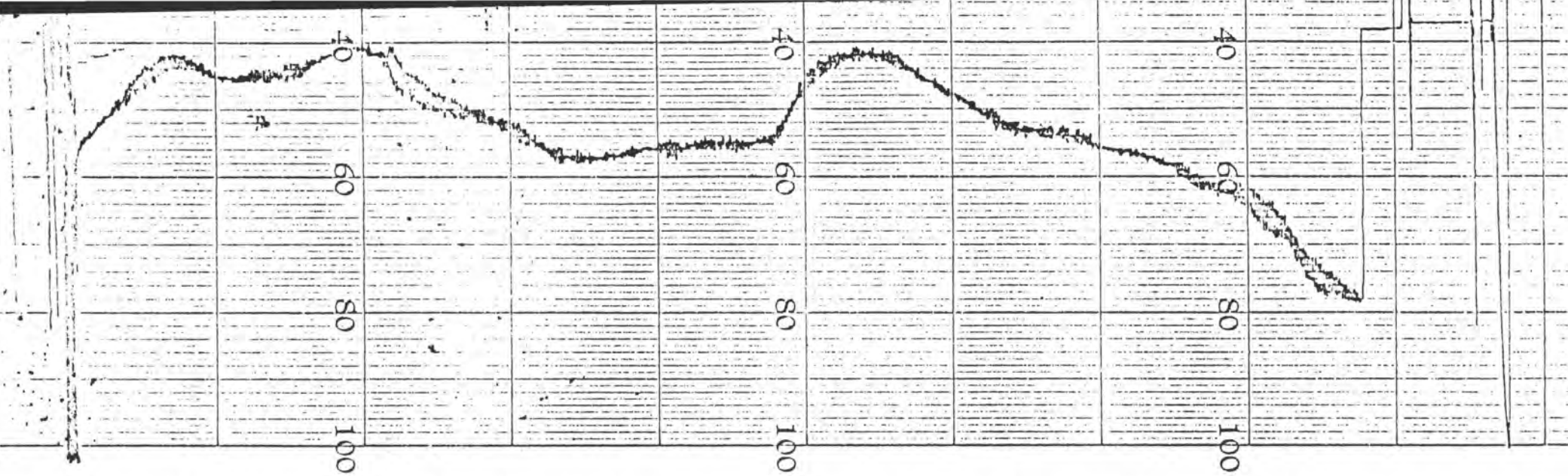

Figure 1. One day of data taken from the long free-hanging test of two back to back Kinemetrics tiltmeters at Ogdensburg Seismic Observatory.

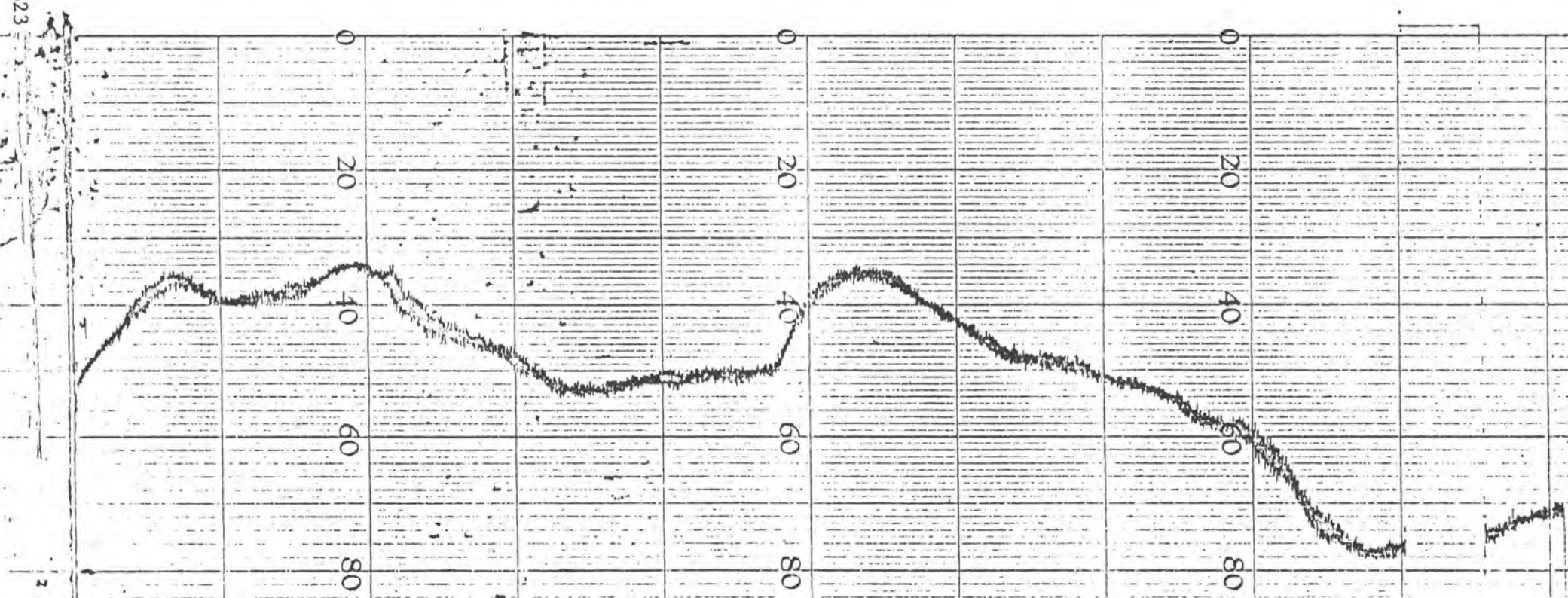

REVIEW OF GROUND STRAIN MEASUREMENTS CONFERENCE

Bruce R. Clark, Leighton and Associates

The Measurements Conference afforded a good opportunity for the participants to assess the state-of-the-art in measurement instrumentation. With a few exceptions, the instruments and installation techniques need more seasoning and the data are still fairly messy. It is encouraging that we are getting measurements of apparent ground phenomena by several different types of instruments. Unfortunately, we are not yet able to interpret what we are measuring very intelligently.

By most measures, this is where the Earthquake Hazards Research Program ought to be. The first great push was to develop instrumentation which was able to measure the ground phenomena hypothesized. And indeed, new instruments and deployment philosophies have appeared. While the tiltmeters seem to defy our best efforts to install them, we are witnessing real innovations in long baseline strain and displacement measurements, the first attempts to monitor small ground stress changes over long periods of time, a concerted effort to improve the accuracy of gravity measurements, and attempts to design specific experiments that would detect tectonically-generated electromagnetic fields.

Since deployment of instruments began in earnest there have been no earthquakes near the California stations large enough to provide the kind of signals we hope to detect. However, even without real signals, we can see that some of the data are dirty enough to send instrument designers and builders back to the drawing boards. In some cases the problems might be insurmountable. We are probably going to have to live with noise levels of at least 10 microgals in the repeat gravity surveys, and unless the revised tiltmeter emplacement methods really do give consistently quiet stations, much of the high tiltmeter sensitivity is going to be wasted. Long-baseline measurements, particularly distance measurements, are showing impressive levels of sensitivity but noise from moving benchmarks and ground surface effects from rainfall or temperature render the last digit or so useless. At the other end of the spectrum, in situ absolute stress, and even stress-monitoring instrumentation may be an order of magnitude too low in sensitivity. Effects are being seen but they might be from non-tectonic causes.

Clearly the real science is just beginning. Now we must establish the difference between signal and noise even though non-earthquake generated signals might be very small indeed. Yet we can't stop and wait for a great earthquake to check out the instruments. Satisfactory field checks depend upon recording coherent signals by multiple instruments at nearby sites. To date this coherence has not been successfully demonstrated, with the exception of a few possible examples in the vast tiltmeter net and some believable creepmeter events. However, Zoback's analysis of the shallow vs. deep in situ stress measurements suggests that the near-surface ground measurements may not relate directly to deeper movements. If vertical coupling is poor, then we might have lots of problems with coherence between scattered surface stations. This noise-evaluation stage is clearly the next important task facing the measurements group.

Finally we have to consider the relation of the signals to models. The two groups are simply not ready for each other yet. When we cannot distinguish signal from noise, we cannot use the data to construct models. It might be better to work in relative isolation for a while longer until we believe in some measurements than to encumber the models with data which are tenuous at best. Don't place too much faith in Evernden's analysis of the low stress system in the San Andreas fault. He has overdriven the data. Of course, so have Clark and many others. I came away from the Conference with a strong skepticism for fault zone movement models based on the present quality of field data. Even levelling data were challenged during the meeting.

In general, the Conference reinforced my belief that we still have a long way to go. Yet the improvement of instrumentation as a whole was impressive, and we've made great progress in establishing field networks. It seems highly unlikely to me that the precursors of a great earthquake today along the San Andreas would not be recorded by more than one type of highly sensitive ground-strain measuring instrument . . . unless, of course, precursors just don't exist.

Comments on Jack Evernden's Summary of the U.S.G.S. Conference on Earth Strain

TERRY ENGELDER

Lamont-Doherty Geological Observatory of Columbia University, Palisades, New York 10964

I found the Summary of the Conference on Earth Strain as colorful as the Conference. This summary will undoubtedly not clear the confusion about earth strain on the part of those geophysicists who did not attend the Conference on Earth Strain. There still exists a great confusion among the experts and Evernden's summary makes this confusion quite clear.

My specific interest in residual strain in rocks was triggered by Evernden's comment on my paper. I will restrict my comments to the significance of residual strain.

The summary suggests that the doorstopper measurement is "severely contaminated by residual stress". This is one way of stating that near surface overcoring measurements, particularly those using bonded strain gauges, are sensitive to strains which bear no relationship to present boundary loads. However, this summary statement "severely contaminated by" should not imply that residual strains have nothing to do with present tectonic forces or that they are absent at depth in the crust. Two important factors suggest that residual strains must be considered when dealing with questions concerning the mechanisms of earthquake generation. Firstly, the orientation of deep hydraulic fractures might be influenced by residual strains, and secondly, some areas of the crust, like California, may have a maximum residual strain in the same orientation as the maximum tectonic stress.

Experiments in the Wattenberg gas field north of Denver, Colorado show that hydraulic fracture orientation correlates with either a rock fabric or residual strain [*Smith et al.*, 1978; *Logan and Teufel*, 1978]. Admittedly this gas field may be in an area of exceptionally low tectonic stresses in which case some other rock property would control hydraulic fracture orientation. However, it was shown that the rock subject to a massive hydraulic fracturing contains a fracture anisotropy due either to a rock fabric or residual strain. In the geologic setting of the Wattenberg gas field the hydraulic fracture followed the fracture anisotropy of the sandstone. It was also significant that the orientation of the hydraulic fracture varied across the gas field.

Few experiments on measuring residual strain have been attempted in California. The most notable is *Hoskins et al.* [1972] who showed that the residual strains in Sonoma County, California were oriented with the maximum

principal compression north-south. This is about the orientation for tectonic stresses associated with the right lateral San Andreas fault. Another experiment showing a strong correlation between residual strains and "tectonic" stress is the Rangely Experiment [*de la Cruz and Raleigh*, 1972]. In the cases where residual strains and tectonic stresses have the same orientation, it is going to be difficult to assess the role of residual strain in earthquake generation.

It is a mistake to think that an understanding of residual strains will be of little use in earthquake prediction. Residual strains may very well add to other stresses causing earthquakes but in no way do they "contaminate".

REFERENCES

de la Cruz, R. V., and C. B. Raleigh, Absolute stress measurements at the Rangely anticline, northwestern Colorado, *Int. J. Rock Mech. Min. Sci.*, *9*, 625-634, 1972.

Hoskins, E. R., J. E. Russell, K. Beck, and D. Mohrman, *In situ* and laboratory measurements of residual strain in the Coast Ranges north of San Francisco Bay, *EOS*, *53*, 1117, 1972.

Logan, J. M., and L. W. Teufel, The prediction of massive hydraulic fracturing from analysis of oriented cores, *19th U. S. Rock Mech. Symp.*, p. 340-344, Stateline, Nevada, 1978.

Smith, M. B., G. B. Holman, C. R. Fast, and R. J. Covlin, The azimuth of deep, penetrating fractures in the Wattenberg Field, *J. Petrol. Tech.*, *266*, 185-193, 1978.

Comments on summary of "Conference on Measurements of Stress and Strain Pertinent to Earthquake Prediction" by J. F. Evernden

Robert C. Jachens
U.S. Geological Survey
345 Middlefield Road
Menlo Park, CA. 94025

As pointed out in the summary, uncertainties in the measurement of relative gravity with available instruments limit the magnitude of temporal gravity anomalies that can be resolved with confidence. The specific causes of the scatter in the data are not known but the uncertainties appear to result from the manner in which individual gravimeters respond to non-gravitational influences. One way to increase the measurement precision is to repeat surveys at frequent intervals, such as the monthly surveys being conducted by Fett. Another approach might be to employ more than two gravimeters during each survey. An advantage in the use of more than two gravimeters would be a reduction of the influence of systematic errors peculiar to individual instruments.

In order to assess the ability of the gravity method to detect precursors to large earthquakes, the temporal behavior of the gravity field prior to a number of large earthquakes should be studied. This will require some knowledge of the location of impending large earthquakes. If the locations of such earthquakes are believed to be known quite precisely, then repeat gravity surveys over detailed profiles probably would give the best results. If, however, the locations of impending earthquakes are known only in general terms, then surveys of regional networks would be most likely to yield the desired information given constraints imposed by time and funding.

Comments on Summary of "Conference on Measurements of Stress and Strain Pertinent to Earthquake Prediction" by J. F. Evernden

M. J. Johnston
U.S. Geological Survey
345 Middlefield Road
Menlo Park, A 94025

COMMENTS ON EHRP CONFERENCE

The conference was unfortunately too short in time and too broad in content to allow clarification, or at least discussion of the problems facing those of us trying to understand the behavior of crustal materials around active faults.

The questions at issue regarding the measurement of deformation, stress and other parameters along active faults fall into three main groups; 1) Data Quality, 2) Measurement Limitations for each Measurement System and 3) Possible Relationships Between Observations and Known Fault Activity (earthquakes, fault slip, etc.). Regarding deformation measurements, the most important of these questions, in my view, are summarized in Table 1. Similar sets can be determined for each of the other measurement techniques.

Many of these issues are exceedingly complex. However, from data presented, or available but not presented due to lack of time, at least some of these issues can be resolved for each of the particular measurement systems. The main conclusions that are apparent concerning the general state of deformation measurements are:

1) The primary poorly understood features of the data are of site and installation origin, not of instrument origin.
2) Most instruments apparently can reliably monitor short period geophysical information (i.e. < 1 day) including earth tides, local earthquakes and teleseisms, creep events, etc.
3) The secular rates for short baseline instruments ($\sim$10m) do not agree with geodetically determined rates (i.e. averaged over 20 Km) nor, at one location with rates determined over an 800 m baseline. Furthermore rates determined with an 800 m baseline instrument do not agree with the geodetically determined rates. It is apparent that

some of this is due to installation instabilities, some due to higher strain rates near faults and some due to sampling in different parts of wave number space.

4) Pressure, temperature and rainfall effects can sometimes seriously contaminate the data but do not explain the primary characteristics of the data.

5) The noise spectrum appears higher for short baseline instruments near the earth's surface than for longer baseline instruments. It varies with position along faults and distance from them.

6) The wave number spectrum appears also to vary with position and distance from faults. Some power at high wave number is due to installation generated signals. Coherence between instruments as a function of frequency is therefore also a function of position and distance from faults.

TABLE 1.

QUESTIONS AT ISSUE WITH CONTINUOUS DEFORMATION MEASUREMENTS NEAR ACTIVE FAULTS

A. DATA QUALITY

a. **Indications from Passive Tests or Questions**

(1) Use of known signals

Are earth tides ($\sim 5 \times 10^{-8}$) observed?
Are they contaminated?
Are teleseismic waves ($\sim 10^{-8}$) observed?
Are creep-related strains and tilts observed?

(2) What are the secular rates?

Are they believable?
Do they agree with independent measurements?
If not, do we know why not?

(3) Spurious signals

Are pressure, temperature, rainfall effects observed?

b. **Indications from Active Tests**

(1) What is the likelihood that observed tilts/strains are not generated in the earth? How can this be determined?

(2) Are near-surface installations significantly noisier than deeper installations? Is this true at all periods?

(3) What is the coherence between adjacent instruments?

(4) How does noise/signal change with increasing baseline?

(5) Is noise/signal higher near active faults than at a distance from them. What are strain amplification effects likely to be?

B. MEASUREMENT LIMITATIONS

What is the apparent noise spectrum.
Is this stable with time?
Does it vary with position? e.g. along, near and far from active faults?
What is noise?
What is the wave-number spectrum?
Does it vary with time or position?

C. RELATION TO EARTHQUAKES AND/OR FAULT SLIP

Can objective tests be defined?
Do we have any convincing results?
Is there any definitive experiment that could, in the absence of significant earthquakes, clarify these issues?

A. F. Kuckes

These three days of meetings showed that there are indications of observable crustal changes before even magnitude 4 earthquakes though essentially all of our observations have been severely contaminated by extraneous effects. The need for continued monitoring of large regions of the fault with admittedly marginal instruments was appreciated. However, the urgent need for systematic work to improve our methods by an order of magnitude was apparent.

I was encouraged about the potential of induction methods which directly measure change in the electrical conductivity and thus stress change at the 2-8 km depths where the primary energy release is. The experiments of Madden showed that the required sensitivity and stability are not greatly beyond the results he presented.

The need for developing more stable geodetic monuments which respond to more than just very local movements was particularly apparent. The potential of satellite VLBI in conjunction with a set of geodetic monuments which are more stable than those we have at present, seems particularly important to me.

Comments on Carmel Conference on Stress and Strain Studies for Earthquake Prediction

by Ted Madden

Stress and strains are of course basic to earthquake phenomena and their study a must for earthquake prediction. Progress is slow, however, and we still have a long hard road ahead of us. I think the conference showed us that the bold gamble to study strain effects by deploying a large number of easily installed tilt meters has not worked, because of the erratic nature of the near surface behavior, and that continued attempts to salvage the installations by playing with the tamping or the length of piping will not be productive. The same applies to continued efforts at interpreting the signals of these instruments. Even the 100 meter type instruments will probably face some of the same difficulties if deployed in this environment. We saw dramatic evidence that point measurements in drill holes can give very stable results, but I doubt if anyone knows yet how deep is deep enough in California. The hope for surface strain measurements lies I believe in much longer base line measurements. Multifrequency line of sight measurements have shown they can do the job, but a large number of installations are required for any kind of coverage with continuous monitoring. VLBI measurements on quasar sources come close, but I think the systems are too cumbersome for this problem and their accuracy not

good enough for following short term phenomena. Interferometer measurements on satellite sources seem to hold the best promise, but we may have to wait to see what they can really accomplish.

Physical property changes as a tool in earthquake prediction have also yet to prove themselves. My own contribution to this conference was to try and show that past measurements have not been made at a high enough sensitivity to be meaningful. I discussed only electrical properties, but I believe the same is true in all the other studies. On the other hand I am still optimistic that large scale measurements will find a low enough environmental noise level to allow in principle the detection of meaningful variations.

Stress measurements are less well understood at this moment and we obviously need more experience. The preliminary hydrofracturing results are intriquing, but it may be too soon to comment on the data. I don't see how these point measurements can avoid the problems of the near surface that plague the strain measurements, however, and I think they will have to go deep.

My biggest disappointment at this meeting was a feeling that we have learned very little about the phenomena we are trying to study. Only one paper provided any data from which we could learn something about stress or strain behavior (Hollister optical ranging experiment), but the nonuniqueness of the interpretation was a frustration. This is a good measure, I am afraid,

of our rate of progress, but then I don't think we are working on an easy problem.

have had discouraging results, and we have been more inclined to blame the instrument or abandon the method rather than to continue to examine all aspects of the systems in question and modify, re-install, or do whatever is necessary to the instruments or installation method until they do agree over short distances. No one proposed any cogent reasons why measurements of strain, tilt, resistivity, magnetics, etc., should not be coherent over small distances. Even the closure errors of gravity, leveling, and geodimetry were much larger than desirable, and in some cases data were unhesitatingly used from benchmarks of known instability.

An obvious drawback to redundant installations is that less "coverage" of a given earthquake zone is afforded with the available funding. The inclination is to try to have an instrument "near" any earthquake of major significance. Unfortunately, if we are to believe the accepted precursor interval estimates, we need two years of unquestionable data for the precursor interval of a magnitude 6 earthquake, and a reference period of similar duration, prior to the anomalous period. So going after the "major" quakes requires more time than the program reasonably can allow for the achievement of reliable results. In essence, we can gain much more by concentrating our efforts in areas of a more intense background of smaller quakes, and first verifying that what we propose to do will work, before we try to cover every active fault system with widely separated instruments.

We must conclude that we are apparently not as close to earthquake prediction by these methods as we had hoped. We are agreed, though, on a common assumption that, as with all non-quantum physical processes, earthquakes as an event are a process in time and space, and that although the generation of elastic waves is a dramatic portion of that process, it must have beginning and ending phases that are of the same intent and scope as the elastic energy release, and these phases should eventually be detectable by the application of current and future technologies. And we must proceed with an open-mindedness toward precursory information, realizing that most likely no one method or data base will provide sufficient information for prediction, but a complex interrelationship of phenomena, many possibly yet unknown and unexplored, will most likely produce our first confident earthquake predictions.

Sean-Thomas Morrissey
Saint Louis University
25 September 1978

Comments on the Summary - C. E. Mortensen

In response to Dr. Evernden's comments in his summary of this conference, particularly regarding tiltmeter measurements, I should like to provide my own characterization of these discussions. It appears to me that there exist roughly three classes of practitioners of shallow-borehole, short-baseline tilt and strain measurement. There are those who, as a result of early failures, imagine that the problems associated with such measurements cannot be solved. Others believe that the problems are not worth solving, while the third group is actively working to solve the problems. I am not aware of anyone actively working in the field who believes that the problems are largely solved, and it was certainly not my intent to convey such an illusion, as even a cursory reading of my paper will show. I suppose that I number myself among the third group for basically four reasons. The first reason is the immense amount of personal energy invested in this project. This I freely admit and make no apologies for, recognizing that taking pride in one's work is a natural and necessary human condition. Of course, it is important that this condition not interfere with scientific objectivity--important negative results must be duly reported, and a certain basic skepticism is probably healthy. The second reason involves what I feel are important results regarding the fault mechanics of creep events (Johnston, et. al., 1976; Mortensen, et. al., 1977) and early encouraging, though poorly understood, observations near the times of some local earthquakes (for example, Mortensen and Johnston, 1976). These observations tend to verify the substantial theoretical reasons for monitoring crustal deformation along active faults. The third reason involves the progress that is being made experimentally in improving signal-to-noise ratio and in understanding the sources of spurious signals. The final and most fundamental reason for counting myself in the third group, is that proof or disproof of the validity of this type of experiment will only result from the work of observers in the third group.

Of course, members of the first and second groups consider that members of the third group are merely beating a dead horse. It seems to me that as long as progress toward some well defined goal is being made the horse is not dead. Various details of such progress can be found in several of the papers in this volume. This is not to suggest that the first group does not serve an important function. Indeed, their persistent outspoken skepticism is an important inducement for the third group to maintain focus in its work and to recognize when no further progress can be made.

Continuous monitoring of crustal deformation using large networks of highly sensitive instruments is an extremely difficult and multifaceted task. I am very skeptical that any one experiment will be definitive for more than one question, as implied by Dr. Evernden, or that a definitive test under one

set of conditions will equally well provide the answer under a different set of conditions. I am sure Mr. Morrissey did not intend such a broad extrapolation of his results. The idea that a quick, straightforward solution to all problems will be forthcoming seems almost characteristic of observers not facing the difficulties, which I suppose is true in most fields. In the U.S.G.S. experiment I believe that some very important preliminary work was neglected due to a naive hope, on several levels, that the problems would not be as severe as they have proven to be. That work is now being undertaken. This is not to imply lack of validity in any of our early work, but merely to suggest, in response to Dr. Evernden's implication regarding the relative amounts of energy applied to particular problems by various principal investigators, that we could be further along in some areas if a more methodical approach had been adopted in the past. Indeed, if a quick, definitive, and complete solution is still expected after studying these papers, then perhaps I should reevaluate my affiliation with group three.

References

Johnston, M. J. S., S. McHugh, and R. O. Burford, On simultaneous tilt and creep observations on the San Andreas fault, Nature, 260, 691-693, 1976.

Mortensen, C. E., R. C. Lee, and R. O. Burford, Observations of creep-related tilt, strain, and water-level changes on the central San Andreas fault, Bull. Seism. Soc. Amer., 67, 641-649, 1977.

Mortensen, C. E. and M. J. S. Johnston, Anomalous tilt preceding the Hollister Earthquake of November 28, 1974, Jour. of Geophys. Res., 81, 3561-3566, 1976.

Larry Slater

During this 3-day conference much of the discussion focused on two topics; first, the relative merits of long and short-baseline instruments and second, the very large magnitude and spacial extent of some "precursory" deformation phenomina.

The long-term stability of some short-baseline instruments, particularly the shallow-borehole tiltmeter, appears to be so poor that future wide-spread use of the current technique seems unwise. The problems of site selection and installation must be more vigorously attacked because unless close tiltmeter pairs demonstrate the ability to track long-term tilts in the near future it will become increasingly difficult for many to place any confidence in the data. Sean Morrissey presented some encouraging preliminary data collected from tiltmeters he recently installed. Morrissey suggests that much of the current long-term stability problem may be considerably reduced by new installation techniques.

I would like to see an increased emphasis put on the deployment of several different types of instrumentation, both short and long-baseline instruments, within a small area for intensive coverage and comparison of the data.

Tanaka's paper and to some extent, several other papers identifying earthquake "precursors" prompted the observation that these precursors are much larger and

detected at much greater distances than expected from most model predictions. I agree with some of the other conference attendees that many of these models may be inappropriate when applied to very low frequency phenomina in the hetrogeneous crust of the earth. I would also suggest that some of the "precursors" observed in central California may be due to large scale, deep aseismic fault slip before the earthquake. The typical small central California earthquake may, therefore, be an incidental response to the larger creep episode.

If these precursors are due to large scale, deep aseismic slip which, may or may not, produce a small earthquake I suggest that we have to be very cautious in predicting a specific seismic event. It might be more appropriate to consider an advisory of increased seismic risk.

Reply to comments on "The Prediction of Massive Hydraulic Fracturing from Analysis of Oriented Cores" by Mark D. Zoback

by

John M. Logan and L. W. Teufel

It appears that the basic element of discussion is exactly what parameter or parameters control the direction of a propagating hydraulic fracture.

We believe that attempts to measure the tectonic stress field through hydraulic fracturing or similar techniques, simply measure the in-situ condition. This condition is composed of a superposition of the active stress field and the condition of the rock. The later is influenced by fabric elements such as dimensional alignment of grains or crystals, preferred orientation of microfractures, macrofractures, and residual elastic strain. Depending upon the situation any one of these factors and the active stress may control the in-situ condition or it may reflect an interaction of all parameters. From our point of view, it is important that we do not believe that one can a priori infer which parameter is the most significant, and thus is being reflected by the measurement. We agree that in some areas you can argue, and maybe convincingly, that the tectonic stress field will dominate the measurement, but we are uncomfortable with an unequivocal statement of this type to cover all situations. One can also argue, as we have done in this paper, that the tectonic stress field is either very close in uniform in the horizontal plane, or that it coincides with the anisotropic condition of the rock, which is in turn controlled by the residual strain state.

Although we have long been interested in the influence of residual strain on fracture propagation (see Friedman and Logan, 1970; Friedman,

1972), this just happens to be the parameter that emerged from this study. It potentially could have been any number of others, including macrofractures. We do believe, however, that it is significant that we have had such a strong correlation with residual strain in this and in a similar study in the Spindle Field, Colorado (Smith, Logan and Wood, 1978). Another notable correlation of the orientation of the stresses inferred from hydraulic fracturing and residual strain is found at Rangely anticline (Raleigh, Healy, and Bredehoeft, 1972; Friedman, 1972, personnal communication). Here the situation is ambiguous as the measurements of residual and in situ strains show similar orientations. That this not always is the case is shown by the work of Swolfs, Handin, and Pratt (1974), where they conclude that in one location near Cedar City, Utah that the in-situ and residual strain conditions are not coincident. It would be interesting to investigate this location with hydraulic fracturing to observe the results. One reason we believe that residual strain may be an important factor in controlling hydraulic fracturing is that given by M. Zoback, whose work has suggested that stress differences of as small as 10 bars may control the direction of fracture propagation. This, combined with residual strain measurements that indicate that such stress differences are not rare and may contribute to the fracturing process (Friedman, 1972), all argue that it is a parameter that should be considered when making hydraulic fracture determinations.

We do not want to overemphasize residual strain, it is only one of parameters that may contribute to the in situ condition of the rocks. Clearly, the influence of pre-existing fractures on the propagating fracture has received considerable attention (Daneshy, 1964; Abou-Sayed, Brechtel, Clifton, 1978) and it may prove to be the most important rock

property that must be considered. This discussion has been merely to emphasize the point that we believe that hydraulic fracturing results have to be used cautiously in inferring the condition of stress. We do believe that with complimentary core studies, the level of confidence in what is actually being measured can be raised to a suitable level, but without the studies we would have to be doubtful.

REFERENCES

Abou-Sayed, A. S., C. E. Brechtel, and R. J. Clifton, 1978, In situ stress determination by hydrofracturing: A fracture mechanics approach, J. Geophys. Res., 83, 2851-2862.

Daneshy, A. A., 1974, Hydraulic fracture propagation in the presence of planes of weakness, Soc. Pet. Eng. paper no. 4852, Spring European Meeting, Amsterdam.

Friedman, M., 1972, Residual elastic strain in rocks, Tectonophysics, 15, 297-330.

Friedman, M. and J. M. Logan, 1970, The influence of residual elastic strain on the orientation of experimental fractures in three quartzose sandstones, J. Geophys. Res., 75, 387-405.

Raleigh, C. B., J. H. Healy, and J. D. Bredehoeft, 1972, Faulting and crustal stress at Rangely, Colorado in Flow and Fracture of Rocks, eds. H. C. Heard, I. Y. Borg, N. L. Carter, C. B. Raleigh, Mon. 16, Am. Geophys. Union, 275-284.

Smith, M. B., J. Logan, and M. D. Wood, 1978, In situ determination of hydraulic fracture geometry--Spindle Field, Energy Technology Conference and Exhibition, Am. Soc. Mech. Eng., Nov. 5-9, 1978, Houston, TX.

Swolfs, H., J. Handin, and H. R. Pratt, 1974, Field measurements of residual strain in granitic rock masses, Proc. of Third Int. Soc. Rock Mech. Congress, II-A, 563-568.

Comments on "The Prediction of Massive Hydraulic Fracturing from Analysis of Oriented Cores" by J. M. Logan and L. W. Teufil

by Mark D. Zoback

Although I am in basic agreement with the authors that microstructure and residual strain can influence hydraulic fracture and, presumably, dike orientations, I do not think this effect is usually comparable to the effect of the applied tectonic stress field. As they state, the tectonic stress field at the Wattenberg field may be anomalous because of uniform stress in the horizontal plane and/or close to the directions implied by the residual strain. I strongly believe that studies, on all scales, demonstrate that the tectonic stress field is the dominant factor in controlling hydraulic fracture and dike orientations.

Examples of this are as follows: Bezalel Haimson has made measurements in various rock types and has found regional conformity of hydraulic fracture orientations (that are consistent with focal plane mechanisms) in the circum-Great Lake area. As Terry Engelder has shown, this regional conformity exists despite residual strain and petrofabric effects which dominate the behavior of overcoring stress measurements. Regional conformity of hydrofrac measurements in different rock types has also been found in Southwest Texas (by Zemanek and others), in the Mojave Desert (my own work), and excellent correlations between hydrofrac orientations and geologic data has been found in the Basin and Range Province and on the Colorado Plateau (the work of Mary Lou Zoback). With respect to dike patterns, I think the work of Nakamura has clearly shown the dominance of the stress field effect, and Pollard and his colleagues have shown that the influence of the stress field can be modelled analytically and excellently reproduce observed phenomena. A recent study of Delaney and Pollard shows no consistency between natural joint and fracture orientations and the direction of intruded dikes. Finally, on the laboratory scale, work done by Fritz Rummel and myself on many samples of crystalline and sedimentary rocks shows that even minimal applied stress (about 10 bars) is always sufficient to control the direction of hydraulic fracture orientation. Thus, while effects due to petrofabric and residual strain are important (especially to near surface measurements) they are usually secondary processes to the stress effect under most conditions.

GPO 689-035